Hydrocarbon Generation and Alteration in the Vienna Basin

PhD thesis

Dipl.-Ing. Bernhard J. Rupprecht BSc.

Supervisor:

Univ.-Prof. Dr. Reinhard F. Sachsenhofer

Department of Applied Geosciences and Geophysics

Chair of Petroleum Geology

Montanuniversitaet Leoben

Leoben, 2017

Affidavit

I declare in lieu of oath, that I wrote this thesis and performed the associated research myself, using only literature cited in this volume.

_____

Dipl.-Ing. Bernhard Rupprecht, BSc.

„Glaube mir, ich habe es erfahren, du wirst ein Mehreres in den Wäldern finden als in den Büchern; Bäume und Steine werden dich lehren, was kein Lehrmeister dir zu hören gibt“

Bernhard von Clairvaux, Brief an Heinrich Murdach

Danksagung

Mein erster Dank sei meinem Doktorvater Herrn Professor Reinhard Sachsenhofer für die Betreuung dieser Arbeit gewidmet. Seine Hilfe trug ganz wesentlich zum Fortschritt und dem Erfolg der vorliegenden Arbeit bei.

Der nächste Dank sei namentlich an Friedrich Kucher und Clemens Zach sowie dem Team der OMV ausgesprochen. Ohne die Unterstützung bei der Probenahme, im Kernhaus, der Beprobung von Öl- und Gassonden, Messung von Gasproben und Recherchen im Archiv wäre diese Arbeit nicht zustande gekommen.

Ausgesprochen gerne möchte ich mich bei Doris Groß und Reinhard Gratzer für die unermüdliche Unterstützung, für das ständige Motivieren und das zur Verfügung stehen als Diskussionspartner bedanken. Ich möchte mich außerdem für eure Freundschaft recht herzlich bedanken.

Dank gebührt auch Achim Bechtel, Christoph Walkner, Madalina-Elena Kallanxhi und Sabine Feuchter für die Unterstützung im Geochemie- und Isotopenlabor, für die Messungen mittels ICP-QQQ-MS, für die Hilfe bei der Untersuchung des Nannoplanktons und für die Unterstützung beim Herstellen diverser Schliffe und für viele aufmunternde Worte.

Das Unmögliche möglich machen sind sicher angebrachte Worte für die ich mich bei Frau Ursula Schmid bedanken möchte. So vieles wäre ohne die Unterstützung nicht möglich gewesen.

Für die gemeinsame, unvergessliche Zeit am Lehrstuhl möchte ich mich bei David Misch, Marie-Lousie Grundtner, Lukasz Pytlak, Susanne Strobl und Magdalena Pupp bedanken. Auch möchte ich mich bei meinen Tutoren in der Erdölgeologieübung, Marko, Irene und Javad für die unkomplizierte Zusammenarbeit und ihre Hilfe bedanken.

Meiner Schwester Christina sei ein Dank dafür ausgesprochen, ein Vorbild zum Nachahmen zu sein und für alles was wir je miteinader unternommen haben.

Der letzte Dank soll sich nun an dieser Stelle an meine Eltern Eva und Martin richten. Es ist gut zu wissen, dass ihr immer für mich da gewesen seid und sein werdet. Ohne eure Unterstützung wäre das alles so nicht möglich gewesen.

Abstract

The Vienna Basin, located in Central Europe, is a mature hydrocarbon province. It hosts hydrocarbons in sandstone and carbonate rocks of autochthonous units, the Calcareous Alps, in turbiditic sandstones of the Flysch Zone, in a high number of transgressive and regressive Miocene sandstone reservoirs, as well as in sandstones of the Molasse zone. The most important source rocks are Upper Jurassic marlstones (Mikulov Fm.) and marly limestones (Falkenstein Fm.) with a total thickness of more than 1500 m. They form part of the autochthonous succession underlying the Alpine nappes and the Miocene fill of the Vienna Basin. In addition, the Mikulov Formation has been considered a potential shale gas play.

Study aims include the determination of the depositional environment of the main Upper Jurassic source rock, the evaluation of lateral and vertical variations of its source potential, the assessment of possible additional source rocks with a Middle Jurassic age, oil/gas-source rock correlations, and the description and quantification of hydrocarbon migration and alteration. In order to reach the aims, 212 rock samples, 86 oil samples and 69 gas samples have been investigated.

Borehole Staatz 1 has been selected as a key well for the study of the vertical variability of the source potential of the Upper Jurassic source rocks. Samples have been investigated using organic geochemical, petrographical and mineralogical techniques. Additional samples from other boreholes are used to evaluate lateral trends. Deltaic sediments (Lower Quarzarenite Member) and prodelta shales (Lower Shale Member) of the Middle Jurassic Gresten Formation are potential secondary sources for hydrocarbons in the Vienna Basin area and are therefore also included in the present study.

The Falkenstein and Mikulov formations in Staatz 1 contain up to 2.5 wt.% TOC and a type III to II kerogen. The organic matter is dominated by algal material. Nevertheless, HI values are relative low (<400 mgHC/gTOC), a result of organic matter degradation in a dysoxic environment. Both formations hold a fair to good petroleum potential. Whereas vertical variations are minor, limited data from the deep overmature samples suggest that the original TOC contents may have increased basinwards. Based on TOC contents (typically <2.0 wt.%) and the very deep position of the maturity cut-off values for shale oil (~4000 m) and shale gas (~5000 m)

production, the potential for the economic production of unconventional petroleum is limited. Hence, previous estimates of the shale gas potential seem too optimistic. The Lower Quarzarenite Member of the Middle Jurassic Gresten Formation hosts a moderate oil potential, while the Lower Shale Member is a poor source rock. An active, but minor petroleum system could be identified within the Lower Quartzarenite Member (Lower Quartzarenite Member – Doggerian (.) PS).

The majority of the investigated oils have been generated from the Mikulov and Falkenstein formations. Oil has been generated at peak oil maturity (0-8-0.9 %Rr), gas was generated at higher maturity (1.1-1.6 %Rr). Microbial gas prevails in fields located along the southeastern High (east of Vienna) and in the Molasse zone.

Biodegradation affects oil down to a depth of approximately 2000 m. Biodegradation reaches rank 4 of the Biomarker Biodegradation Scale (BBDS). Apart from reservoir temperature, both the tectonic position of reservoirs and trap type, influence the degree of biodegradation. Reservoirs in the hangingwall of major faults and oils in transgressive sands are more prone to biodegradation than reservoirs in the footwall and oils in turbiditic sands in structural-stratigraphic traps. Anaerobic biodegradation results in the formation of isotopically heavy CO_2 and isoptically light (secondary) microbial methane.

Hydrocarbons in deep reservoirs within the Calcareous Alps are affected by thermochemical sulphate reduction (TSR). While TSR-affected gas is rich in H_2S and CO_2, oil is characterized by increased DBT/Ph ratios. In contact with clastic rocks, H_2S is removed by pyrite precipitation, whereas DBT/Ph ratios remain high. Hence, high DBT/Ph ratios may be used as proxy for TSR, which affected oils before they charged clastic reservoirs. Stable sulphur isotope signatures confirm Upper Triassic anhydrites as the main sulphur source for H_2S.

Oils contain different quantities of benzocarbazoles, which can be used to determine the migration distances from the active source rocks. Although a general agreement exists between estimates based on benzocarbazoles and geological evidence, more detailed information about the timing of tectonic events is needed to refine these estimates.

Kurzfassung

Das Wiener Becken ist ein Sedimentbecken in Zentraleuropa mit einer mehr als 100-jährigen Kohenwasserstoffexplorationsgeschichte. Heute werden Öl und Gas in den autochthononen Einheiten, den nördlichen Kalkalpen, den Turbiditen der Flysch Zone, in zahlreichen transgressiven und regressiven miozänen Sandsteinen und in der Molassezone gefördert. Die wichtigsten Muttergesteine sind oberjurassische Mergel (Mikulov-Fm.) und mergelige Kalke (Falkenstein Fm.) in den authochthonen Einheiten, welche eine kombinierte Mächtigkeit von 1500 m erreichen. Der Mikulov Mergel wurde auch als potentielles Schiefergas-Play erachtet.

Die Ziele der Studie beinhalten die Bestimmung des Ablagerungsmilieus der oberjurassischen Muttergesteine und der vertikalen und lateralen Variabilität ihres Muttergesteinspotentials. Zusätzlich soll das Muttergesteinspotential mitteljurassischer Einheiten bestimmt werden, Öl und Gas mit einzelnen Muttergesteinen korreliert werden und Prozesse der Kohlenwasserstoffmigration und -alteration beschrieben werden.

Hierfür wurden 212 Gesteinsproben, 86 Ölproben und 69 Gasproben untersucht. Bohrung Staatz 1 wurde als Schlüsselbohrung für die Untersuchung der vertikalen Variabilität des Muttergesteinspotentials des Oberjura ausgewählt. Proben dieser Bohrung wurden organisch-geochemisch, petrographisch und mineralogisch untersucht. Zusätzlich wurden Oberjura-Proben weiterer Bohrungen, sowie Deltasedimente (Untere Quartzarenitserie) und Prodelta Tone (Untere Tonsteinserie) der mitteljurasssichen Gresten-Formation untersucht.

Die Falkenstein-Formation und die Mikulov-Formation in der Bohrung Staatz 1 enthalten maximal 2.5% TOC und Typ II bis III Kerogen. Das organische Material besteht zu einem guten Teil aus Algen. Der für solches Kerogen ungewöhnlich niedrige Wasserststoff Index (<400 mgHC/gTOC) kann of Abbau in einem dysoxischen Mileu zurückgeführt werden. Beide Formationen weisen ein durchschnittliches („fair“) bis gutes Muttergesteinspotential auf. Die vertikale Variabilität des Muttergesteinspotentials in der Bohrung Staatz 1 ist gering. Die (wenigen) Daten anderer Bohrungen weisen darauf hin, dass der ursprüngliche TOC-Gehalt gegen die Beckenmitte hin zugenommen hat. Aufgrund der trotz allem geringen TOC-Gehalte und der großen Tiefenlage jener Maturitätsbereiche, die für

Schieferöl- oder Schiefergasproduktion geeignet sind, ist das Potenzial für die ökonomische Produktion von Schieferöl/-gas limitiert. Die Untere Tonsteinserie ist ein schlechtes Muttergestein. Hingegen weist die Untere Quartzareniteserie ein durchschnittliches Potential zur Ölgenese auf und konnte als aktives Muttergestein des Untere Quartzareniteserie - Dogger (.) Kohlenwasserstoffsystems bestätigt werden.

Die Mehrzahl der untersuchten Öle wurde im Mikulov Mergel und der Falkenstein-Formation während der Hauptphase der Ölbildung (0.8-0.9%Rr) generiert. Thermogenes Gas wurde in einem Stadium erhöhter thermischer Reife (1.1-1.6%Rr) gebildet. Mikrobiell gebildetes Gas überwiegt in den Feldern der südöstlichen Hochzone (östlich Wien) und der Molassezone.

Biodegradation betrifft Öle in Lagerstätten bis zu 2000m Teufe. Die Biodegradation erreicht die Stufe 4 der Biomarker-Biodegradations-Skala. In seichten Lagerstätten wird der Grad der Degradation durch die tektonische Position der Lagerstätte sowie den Fallentyp kontrolliert: Felder im Hangenden einer Störung und in transgressiven Sanden sind anfälliger für Biodegradation als Felder in deren Liegenden und mit turbiditischen Reservoirgesteinen. Bei der anaeroben Biodegradation entsteht isotopisch schweres CO_2 und isotopisch leichtes Methan.

Kohlenwasserstoffe in tiefliegenden kalkalpinen Lagerstätten, sind von thermo-chemischer Sulphatreduktion (TSR) betroffen. Gas, welches aus diesen Lagerstätten gefördert wird ist reich an H_2S und CO_2, wohingegen Öle durch ein erhöhtes DBT/Ph Verhältnis gekennzeichnet sind. In Relieflagerstätten mit Kontakt zu klastischen Sedimenten wird H_2S durch Reaktion mit Eisen als Pyrit ausgefällt, während das DBT/Ph Verhältnis hoch bleibt. Hohe DBT/Ph Verhältnisse können daher als Marker für TSR-beeinflusste Öle in klastischen Sedmenten verwendet werden. Als Schwefel-quelle konnten mittels Untersuchung der stabilen Schwefelisotope Anhydrite der Opponitz-Formation (Obertrias) identifiziert werden.

Benzocarbazole erlauben die Migrationsdistanzen von Ölen abzuschätzen. Generell konnte eine gute Übereinstimmung von Abschätzungen basierend auf Benzocarbazol-Proxies und der geologischen Situation beobachtet werden. Trotzdem sind für die Verifizierung der Ergebnisse genauere Studien über die Versenkungsgeschichte nötig.

Content

1. Introduction

The Vienna Basin is a major hydrocarbon province in central Europe (Fig. 1). The main source rock in the Vienna Basin is the Upper Jurassic Mikulov Formation (Ladwein, 1988). Reservoirs in siliciclastic rocks (Badenian) in the Miocene basin are most important. However, oil and gas are found in various Miocene aged stratigraphic units and also in the Alpine basement.

Since the first discoveries of oil and gas, more than 3700 wells have been drilled and exploration is still ongoing. Reinterpretations of the tectonic evolution of the basin, the emerging of new, so-called unconventional plays, more and more sophisticated exploration and production, as well as high economic risks have shown the need for a detailed reevaluation of hydrocarbon source rocks and related oil and gas.

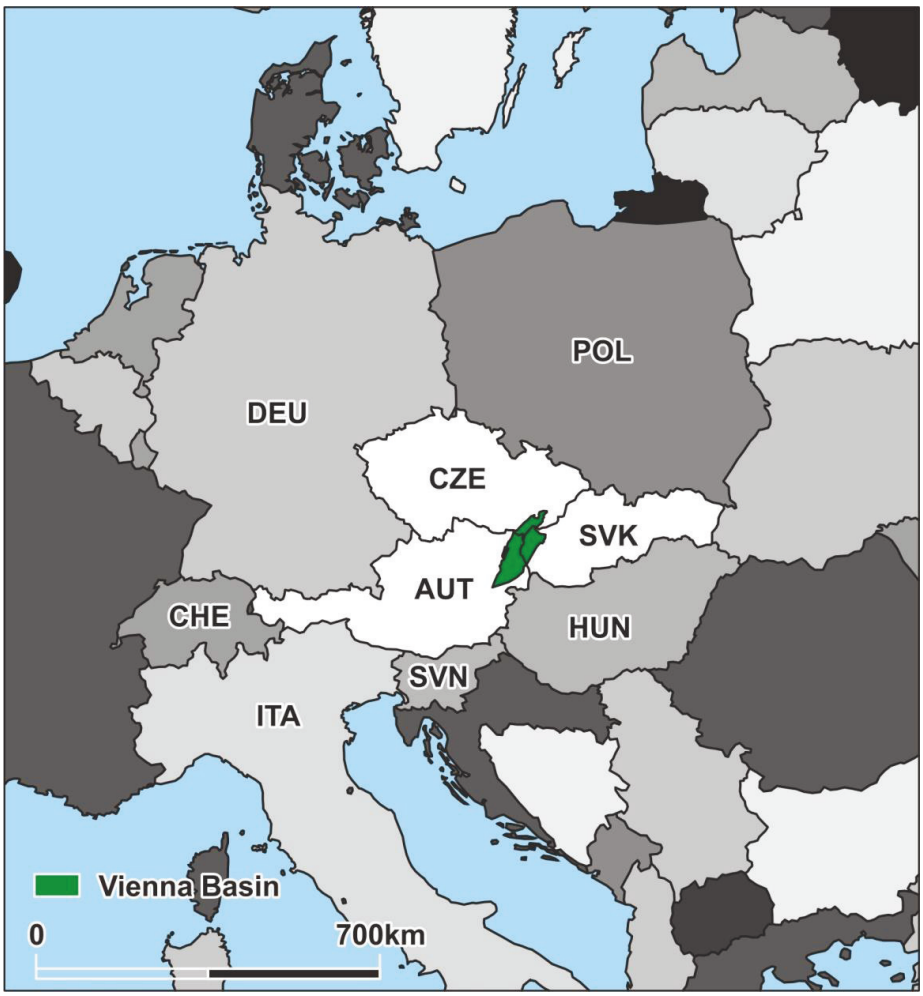

Fig. 1: Political map of Europe with position of the Vienna Basin. Area codes according to ISO 3166 Alpha 3:2016 are used.

In recent years, unconventional shale gas plays have been explored in Europe, so far with little success. While hopes were also high for shale gas production in Austria (Langanger, 2008), protests of residents caused very strict governmental regulations on fracking techniques. The main target for shale gas exploration in Austria is the Mikulov Formation. However, its ability to serve as a shale gas reservoir has yet to be proven (Schulz et al., 2010).

Whereas the Mikulov Formation is clearly the most important source rock in the Austrian part of the Vienna Basin area, additional source rocks may occur in the Middle Jurassic Gresten Formation. However, till now only the lower member of this formation has been studied properly (Sachsenhofer et al., 2006).

Petroleum production is strongly controlled by reservoir properties, but also by the physical and chemical properties of oil and gas. Obviously, production is significantly more challenging for high viscous, biodegraded oils or if highly toxic gaseous compounds, like H_2S, occur within the reservoir.

Aims:

This study focuses on the conventional and unconventional potential of the Mikulov-Badenian Petroleum System of the Vienna Basin:

(I) Evaluation of the hydrocarbon and shale gas/oil potential of proven and potential Middle and Upper Jurassic source rocks
(II) Reconstruction of the depositional environment of Upper Jurassic source rocks
(III) Oil/gas-source correlations
(IV) Evaluation of the extent of biodegradation and its controls
(V) Understanding the interaction between crude oil and sulphate in deeply buried, hot carbonate reservoirs.

1.1 A brief exploration history of the Vienna Basin

Although natural gas accumulations have been encountered during construction work in Vienna in 1844 and 1906 (Pois, 1933 and refrences therein), hydrocarbon exploration in the Vienna Basin literally took an exploding start in 1913: Ján Medlen had discovered that flammable gases were emerging from a pond named “Kde voda vrie” (“Where the water cooks”) near his farm in Gbely (Hungary, today Slovakia) (Pois, 1933). He used simple drilling tools to (Fig. 2) find gas and cook outdoors, a technique he previously learned in Pennsylvania (Pois, 1933).

Fig. 2: Jan Medlen (1910) drills for gas. From Pois (1933).

For rainy days and cold winter times, he improvised a pipeline to supply his property with gas for cooking and heating. Briefly after finishing the pipeline, his farm blew up with a roaring sound. Fortunately nobody was harmed. However, the explosion triggered the drilling of the first exploration well, which was spudded in October 1913 (Pois, 1933). Already on the 10.1.1914 the first wild cat borehole in Gbely encountered an oil reservoir at 164 m depth, marking the first production of hydrocarbons from the northern Vienna Basin (Friedl, 1956 and refrences therein).

Within the southern Vienna Basin (S of the Markgrafneusiedl fault), the first gas accumulations were discovered during coal exploration between 1919 and 1921. Near Maria-Lanzendorf a well encountered oil impregnated rocks and hugh amounts

of gas in a depth of about 600 m; the gas erupted with a rate of up to 10.000 m^3/d for several months (Pois, 1933).

The first hydrocarbons in the Alpine nappes benath the Vienna Basin were discovered on the 30.8.1930 in the well Windisch Baumgarten 1a at 729 m depth, located in the Zistersdorf Unit of the Flysch nappes (Friedl, 1933). Well Windisch Baumgarten 1a holds the honor to be the first successful well ever to be drilled in Lower Austria.

Central Europe's biggest oil field, the giant Matzen field, was discovered in 1949. Shortly afterwards the Zwerndorf field was detected in 1952 (Friedl, 1956).

More advanced drilling techniques allowed the spudding of ever deeper boreholes and in 1959 the first reservoir within the Calcareous Alps, Aderklaa, had been discovered (Sommer, 1993). At time of drilling, Europe's deepest well was sunk as Zistersdorf 2a, with a total depth of 8553 m (Wessely, 2000).

1.2 Conventional and unconventional hydrocarbons

Ever since on the 27.08.1859 a well drilled by Edwin L. Drake encountered oil in sandstones near Titusville, hydrocarbons have been produced from sedimentary rocks with reasonable porosity and permeability, thus becoming the overall standard of petroleum production. This conventional production technique is aimed on hydrocarbons which have been generated in source rocks, migrated to reservoir rocks and became trapped in suitable structures, from where they can be produced without extensive well stimulation.

The energy price peak of the late 2000´s has triggered an intensive search for additional, unconventional hydrocarbon resources. These include

(I) Shale gas/oil from thermally mature or overmature organic matter rich rocks
(II) Coal seam gas (coal bed methane; CBM)
(III) Tight oil/gas from low permeable sandstones
(IV) Oil sands from seeped natural petroleum and
(V) Oil shales containing thermally immature organic matter, which can be transformed into hydrocarbons by pyrolysis (Fig. 3).

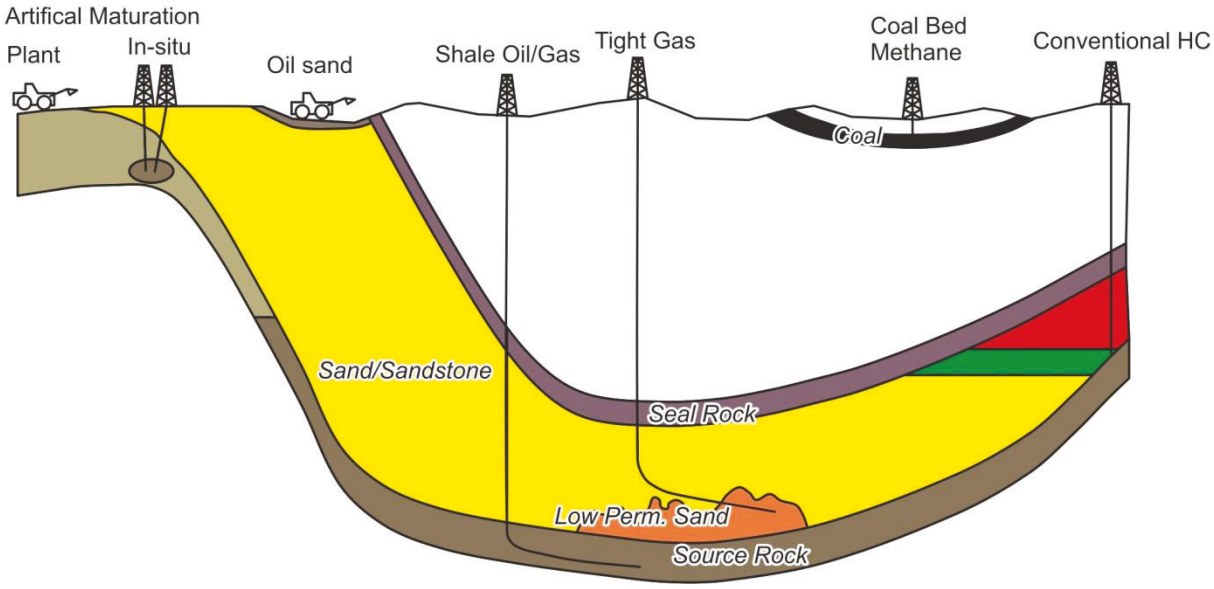

Fig. 3: Schematic sketch of different conventional and unconventional hydrocarbon deposits (modified from Andruleit et al., 2010).

Ad (I): Shale gas/oil is currently the most widely developed unconventional hydrocarbon source. In order to liberate and produce gas and oil trapped in impermeable thermally mature or overmature source rocks, artificial permeability has to be produced via hydrofracking.

Ad (II): Coal seam gas or coal bed methane applies the same technique to liberate methane from coal seams. To desorbe methane from the organic matter, efforts have to be taken to reduce the pore pressure. In addition, CO_2 can be injected to exploit the stronger adsorption of CO_2 to organic matter and to liberate additional methane (Özgen Karacan et al., 2009).

Ad (III): Thight oil and tight gas reservoirs are produced using hydrofracking since the 1970´s (Law and Spencer, 1993). Actually hydrofracking was initially invented to produce these very low permeable sandstones.

Ad (IV): Oil sands are natural oil seeps. Natural tar has been used at least since 70.000 BC by humans (Boëda et al., 2008). Typically, sever degraded oils are produced by surface mining of sand and cleaning the sand of oil. Today, these deposits are the biggest unconventional oil reserves in production. The Athabasca tar sands in Canada represent the biggest oil sand deposit. However production is

accompanied by deforestation in sensible tundra regions and is therefore massively criticized.

Ad (V): Oil generated artificially by pyrolytic processes has been exploited in minor quantities for centuries (e.g.in Scotland). Great quantities were produced in Germany during WW II. Today, China and Estonia are the largest oil shale producers. In contrast to tradional mining techniques, in situ maturation (Shell In-Situ Conversion Process ®, ExxonMobil Electrofrac ®) is probably the latest approach to produce unconventional hydrocarbons. It is very energy intensive and exhaled gases from production represent a significant disadvantage of this technique (Bartis et al., 2005, Symington et al., 2010).

1.3 Upper Jurassic source rocks

Petroleum systems with Upper Jurassic source rocks contain 25% of the world´s discovered oil and gas reserves (Klemme, 1994). Upper Jurassic source rocks source mainly petroleum basins on land (80%) and minor petroleum systems off shore (20%) (Klemme, 1994).

Table 1: Biggest 14 petroleum systems with Upper Jurassic source rocks (modified from Klemme, 1994).

Petroleum System	**Basin**	**Location**
Hanifa-Arab (!)	Arabian	Middle East
Bazhenov-Neocomian (!)	West Sibiria	Sibiria
“Hot Shale”-Brent (!)	Northwest Europe	North Sea
Smackover-Tamman (!)	Gulf of Mexico	North America
Khodzipaik-Shatlyk (?)	Amu Darya	Central Asia
J3 “Black Shales”-J3 to K2 (.)	Caspian	Central Asia
Lam-Amla’ah (!)	Yemen	Middle East
Vaca Muerta-Sierras Blancas (!)	Neuquen	South America
Maril-Toro (.)	Greater Papua	Oceania
Dingo-Wandalia	Northwestern shelf	Australia
“Hot Shale”-Hibernia (!)	Jeane d’Arc	North America
Verril Canyon-Mic Mac (!)	Scotia Shelf	North America
Mikulov-Badenian (!)	“Vienna”	Central Europe
Flamingo-Plover (.)	Vulcan Graben	Australia

The 14 biggest petroleum systems (Table 1) of Upper Jurassic age can be grouped into a southern North Gondwana realm, a Tethyan realm (including the Vienna Basin), a Boreal realm and a Pacific realm (Klemme and Ulmishek, 1991). The Tethyan group has the greatest recovery per unit area of mature source rock (Klemme, 1994).

1.4 Evaluation of source potential and unconventional hydrocarbons

The most important parameters to evaluate source rocks for conventional hydrocarbons are (I) the amout of organic matter, (II) the type of organic matter and (III) the its thermal maturity (e.g. Peters, 1986).

Additional parameters are necessary to characterize a shale gas play. Nevertheless, the traditional source rock requirements are still valid (Jarvie et al., 2007, Jarvie, 2012). Effective well stimulation is important as shales are tight. High content of brittle minerals enhance the result of such operations (Hester and Harrison, 2015, Rybacki et al., 2014). Finally a certain lateral extent and a minimum thickness are required (Jarvie et al., 2007, Charpentier and Cook, 2011). Table 2 summarizes the agreed parameters and their minimum values for a shale gas target. These parameters should be supplemented by experimental adsorption isotherm data for a final assessment of the gas potential.

Table 2: Required minimum values for a successful shale gas/oil play (Jarvie et al., 2007, Jarvie, 2012, Hester and Harrison, 2015, Rybacki et al., 2014, Charpentier and Cook, 2011).

Parameter	**Minimum value**
TOC content	2%
Thermal maturity (Vitrinite reflectance)	1.2% / 0.8% (for shale gas/ shale oil)
Kerogen kinetics (Transformation ratio)	0.78
Brittleness	40% quartz
Thickness	20m

1.5 Hydrocarbon generation and migration

Thermogenic hydrocarbons are formed in organic matter rich, fine grained sedimentary rocks, which are called source rocks. When these rocks are affected by thermal stress during burial, the primary organic matter (kerogen) will be broken down. During this process liquid and gaseous hydrocarbons will be formed (e.g. Horsfield, 1989) (Fig. 4). During this transformation process the hydrocarbons are expelled from the source rock into permeable carrier beds.

Due to buoyancy, the hydrocarbons migrate in carrier beds into updip positions and eventually become trapped in appropriate geological structures. The accumulated hydrocarbons carry chemical signatures characteristic for the source rock. Therefore, the comparison of the chemical composition of source rock extracts and oils may allow correlating accumulated oils with their source rock (e.g. Alexander et al., 1992).

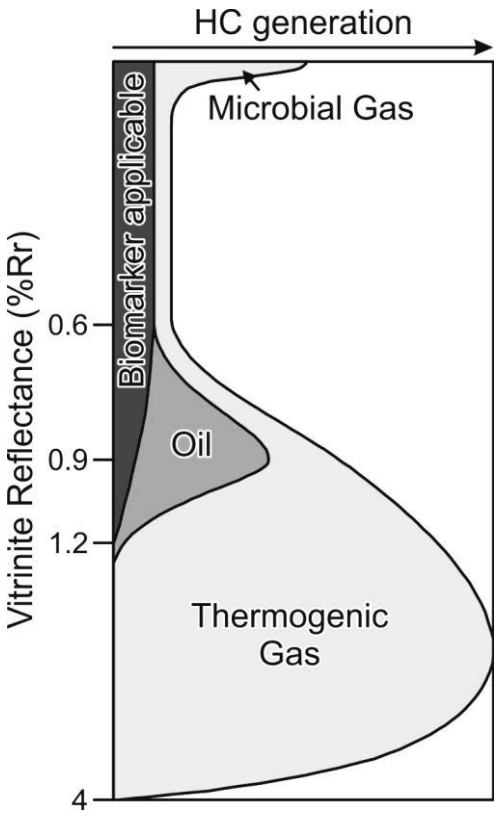

Fig. 4: Maturity range for the generation of different hydrocarbons (modified from McCarthy et al., 2011)

1.6 Hydrocarbon alteration

From the moment of expulsion from the source rock till the moment of production, hydrocarbons may be subjected to processes which change their chemical and physical properties. These processes can be classified into 4 groups:

(I) Biodegradation, where the alteration is performed by microbes

(II) Water washing, where mainly light and more polar compounds are removed by solution in water

(III) Mixing with other hydrocarbons (the term “deasphalting” is normally used only for mixing with gases of different source) which changes the solubility of long chained compounds in crude oils

(IV) Thermal alteration of crude oils under elevated temperatures. Processes may require additional reactants like SO_4^{2-} (i.e. thermochemical sulphate reduction) or directly decompose oil (cracking).

Kuo (1994) studied water washing of crude oils and compiled a list of changes of chemical and physical properties caused by different alteration processes (Table 3).

Biodegradation and thermochemical sulphate reduction are relevant for the Vienna Basin and, therefore discussed in some more detail.

Table 3: Changes in properties of crude oils through different alteration processes (from Kuo, 1994 and refrences therein).

Property	Water washing	Biodegradation	Deaspalting	Maturation
API gravity	Decreased	Decreased	Decreased	Increased
Metal content	Decreased	Increased	Increased	Decreased
Sulphur content	Decreased	Increased	Increased	Decreased
C_{6-15} content	Decreased	Decreased	Decreased	Increased
Gas-to-oil ratio	Decreased	Decreased	Decreased	Increased
C_{15+} composition	Aromatics decreased	Saturates decreased	Asphaltenes increased	Asphaltenes and NSOs decreased
C_{31}/C_{19}, pristane/nC_{17}, phytane/nC_{18}	Increased	Increased	Unchanged	Decreased
Carbon isotopic composition	NSO fraction lighter	Saturated fraction heavier, Asphaltenes lighter	Aromatic fraction lighter	Asphaltene fraction heavier
C_{15}/C_{16} bicyclic alkanes	Increased	Increased	Unchanged	Increased
Rearranged/8β (H) C_{15} bicyclic alkanes	Increased	Decreased	Unchanged	Increased
Terpanes	Diterpanes decrease relative to triterpanes	Diterpanes increase relative to triterpanes	Unchanged	Diterpanes increase relative to triterpanes
Steranes	C_{27} steranes decrease relative to C_{30} hopane	Decrease when severly degraded	Unchanged	Unchanged
Triaromatic steranes	C_{20} and C_{21} increase relative to C_{27} and C_{28}	C_{20} and C_{21} increase relative to C_{27} and C_{28}	Unchanged	C_{20} and C_{21} increase at the expense of C_{27} and C_{28}
Methylphenantrene index (MPI)	Increased	Decreased	Decreased	Increased
DBT/MDBT	Decreased	Decreased	Increased	Increased
PHEN/MPH	Decreased	Decreased	Increased	Decreased

DBT: Dibenzothiophene, MDBT: Methyldibenzothiophenes, PHEN: Phenantrene, MPH: Methylphenantrenes

1.6.1 Biodegradation

Biodegradation of hydrocarbons is the alteration of crude oils and gases by living organisms (e.g. Milner et al., 1977, Connan, 1984, Palmer, 1993, Blanc and Connan, 1994). Microorganisms oxidize the compounds within the oils and gases to generate energy for living. Biodegradation is a process observed worldwide and the amount of biodegraded oil is may be larger than the amount of undegraded oils (Tissot and Welte, 1984). To degrade hydrocarbons, the reservoirs have to support microbial activity. The microbes need sufficient amounts of metabolic electron acceptors (oxygen, nitrate, sulphate, iron) and nutrients (phosphorus, trace metals) (Peters et

al, 2005). Permeability in the rocks must be suitable for nutrient and bacterial transport via water (Jenneman et al., 1985, Brooks et al., 1985, Frederickson et al., 1997, Krumholz, 2000, Wenger and Isaksen 2002). Temperatures within the reservoir have to support life and must not exceed 80°C (e.g. Shi et al., 1982, Wilhelms et al., 2001) which typically corresponds to reservoir depth shallower than 2000 m. Formation water salinity may not exceed 150 parts per thousand (Wenger and Isaksen, 2002). With the exception of reservoirs, which suffer from bacterial sulphate reduction, H_2S must not be present at any given point during degradation (Peters et al., 2005).

Hydrocarbons are degraded by microbes via two major and one minor pathway:

(I) Aerobic degradation, which is the breakdown of hydrocarbons in the presence of oxygen into CO_2 and H_2O. If favorable conditions are prevailing, huge amounts of oil can be degraded in short periods (e.g. Connan, 1984, Blanc and Connan, 1994).

(II) Anaerobic degradation is the destruction of oil and gas without oxygen and sulphate into CH_4, CO_2 and H_2O. Larter et al. (2000) suggested that “anaerobic biodegradation is slower than aerobic biodegradation” and Yamane et al. (1997) found that aerobic degradation is ten times faster than anaerobic biodegradation in a laboratory study.

(III) Sulphate reduction is the degradation of hydrocarbons via anaerobic microbes using sulphate as the reductant. Beside CH_4 and CO_2 significant amounts of H_2S (up to 5%) are produced (Peters et al., 2005).

1.6.2 Thermochemical sulphate reduction

Hydrogensulphide in natural gases may originate from

(I) thermal decomposition of kerogen (very rare observed)

(II) bacterial sulphate reduction (BSR) of primary organic matter or crude oil

(III) thermochemical sulphate reduction (TSR) of hydrocarbons.

TSR is the abiotic reaction between hydrocarbons and dissolved sulphate in reservoirs under elevated temperatures (Orr, 1974/1977). Research focused mainly on four areas: (I) the Nisku Formation in the Western Canadian Sedimentary Basin, (II) the sour gas fields of western Canada, (III) the Smackover Formation in the southeastern Mississippi Salt Basin, and (IV) the Khuff Formation in the Persian Gulf Realm (Machel, 2001 and refrences therein). Smaller systems are described in the Tarim basin in China (Cai et al., 2001) and the Big Piney-La Barge field in the Green River Basin (King et al., 2014).

Typically the source of the sulphate is either gypsum or anhydrite. If sulphate reduction occurs directly within the sulphate-source formation up to 20% of the produced gas can be H_2S (Nisku and Khuff formations, Machel, 2001; Worden and Smalley, 1996).

Machel et al. (1995) presented a series of individual reactions that can occur during TSR, where they present an unbalanced TSR reaction equation (1):

1) Crude Oil => light crude oil + H_2S + CH_4 (+polysulphides).

This reaction is only possible under elevated temperatures (above 100°C) and in the presence of minor clay, which acts as a catatalyst (Machel 1987, 1989, Goldstein and Aizenshtat, 1994). The resulting polysulphides act as an additional catalyst, increasing the speed of the reaction before been consumed in a later stage (Machel, et al., 1995). Maybe an intermediate stage S_3^- ion speeds up the reaction even more (Truche et al., 2014). A more realistic equation (2) has also presented by Machel et al. (1995):

2) Hydrocarbons +SO_4^{2-} => lighter hydrocarbons + solid bitumen + HCO_3^- + HS^-.

In general, the pH-conditions are low during TSR, as sulphuric acid is generated as a byproduct via reaction 3:

3) H_2S + SO_4^{2-} + $2H^+$ => S + $2H_2SO_4$ + $2H_2O$.

Sulphuric acid is a strong acid and therfore formally displaces (double displacement reaction) the weak acids HCO_3^- and HS^-, formed during reaction 2. Both,

hydrocarbonic acid and hydrogen sulphide spontaneously decompose to CO_2 and H_2S immedatly after their dislacement.

In general, most authors agree that TSR occurs in the temperature range between 120°C and 140°C (Worden et al., 1995 and refrences therein, Worden and Smalley, 1996, Nöth, 1997 and refrences therein), although TSR has been observed from 100°C up to 180°C (Fig. 5) (Machel, 2001).

Depending on the temperature of the reservoir, which is affected by TSR, a varying strong isotopic composition fractionation can be observed in the resulting hydrocarbons and gases. This kinetic sulphur isotope fractionation equation (Kiyosu and Krouse, 1990) has been used to calculate the temperature during TSR (Burnie, 1979) and to determine the sulphate source for TSR (Amrani et al., 2012).

Hydrogen sulphide is only stable in metal-ion free reservoirs. As soon as such ions are available reaction 4 leads to the formation of sulphides (Me^{2-} = metal-ion):

$$4)\ Me^{2-} + 2S^{+} \Rightarrow MeS_2\downarrow.$$

Iron is the most common sulphide-forming metal ion available in geological settings. The sulphide of iron (pyrite) has a very small solubility constant and therfore immidiatly precipitates from the solution. Consequently, H_2S is not found in siliciclastic reservoirs.

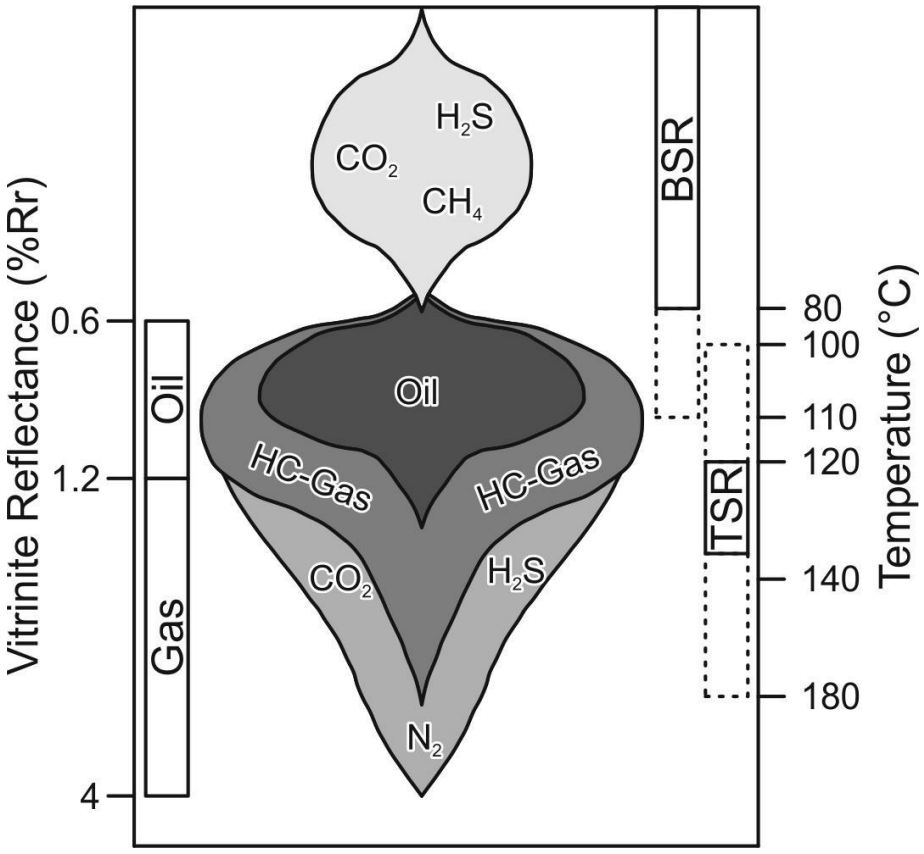

Fig. 5: Maturity and temperature ranges for HC-generation as well as bacterial sulphate reduction and thermochemical sulphate reduction (modified from Machel, 2001).

2. Geology of the Vienna Basin area

The Miocene Vienna Basin is located at the Alpine-Carpathian transition zone and is shared between Austria, the Czech Republic and Slovakia. The sediments of the Vienna Basin were deposited on allochthonous Alpine units (Waschberg Zone, Flysch Zone, Calcareous Alps, Central Carpathians), which in return overthrusted autochthonous basement units (Bohemian Massif and its sedimentary cover) during the Alpine Orogeny.

In the following the geological units are discussed from base to top, separately for autochthonous units, allochthonous Alpine units and the Miocene basin fill. Traditionally, these tectonic units are called 3rd floor, 2nd floor and 1st floor, respectively (Wessely, 1993).

2.1 Autochtonous Units (3rd floor)

The autochtonous units consist of crystalline basement, local Permo-Carboniferous graben sediments, which are preserved west of the Vienna Basin area, Middle Jurassic syn-rift sediments (Gresten Formation) overlain by Callovian to Maastrichtian post-rift sediments and Oligocene-Miocene molasse deposits (Elias and Wessely, 1992). A subcrop map of the Pre-Cenozoic units is provided in Fig. 5.

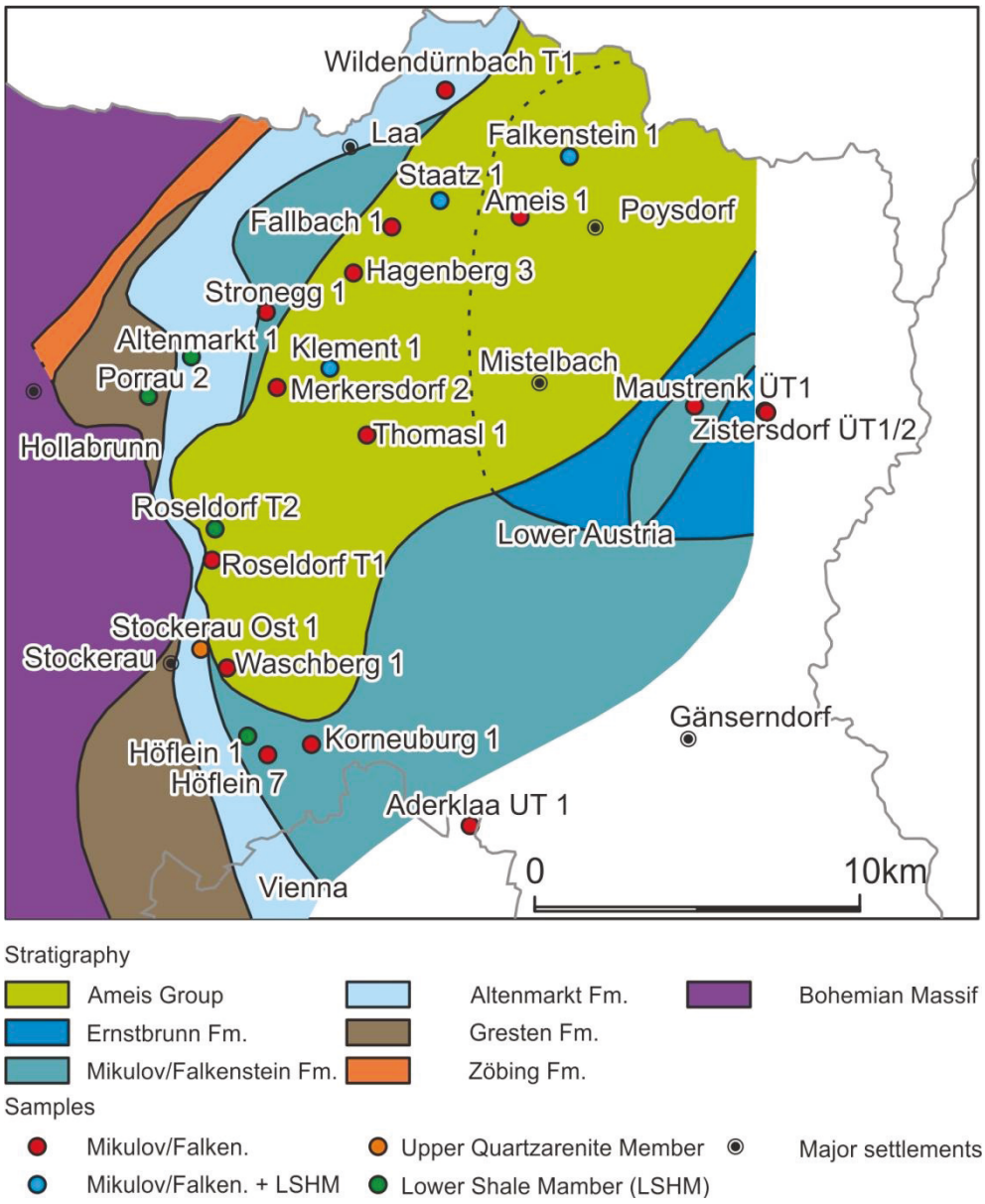

Fig. 6: Subcrop map of the pre-Cenozoic autochthonous units in the Vienna Basin area. Location of sampled wells and sampled intervals are marked (modified from Wagner and Wessely, 1992).

2.1.1 Autochthonous Mesozoic

The Gresten Formation has been deposited in halfgrabens during the Middle Jurassic rifting phase of the later Penninic Ocean (Fig. 7). The Gresten Formation is subdivided from base to top into Lower Quartzarenite Member, Lower Shale Member, Upper Quartzarenite Member and Upper Shale Member.

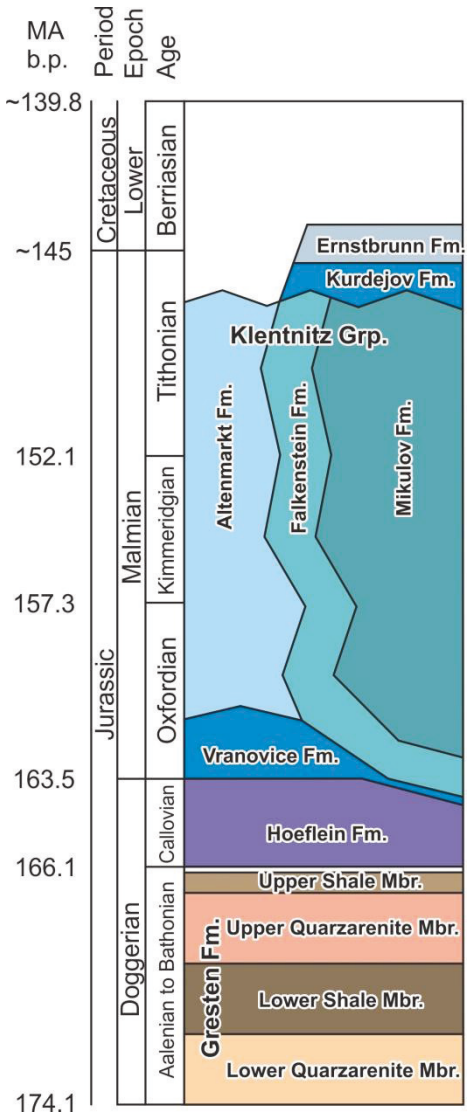

Fig. 7: Jurassic stratigraphy and formations of the Bohemian shelf. This succession now forms the deepest, autochthonous unit in the Vienna Basin area (mod. from Elias and Wessely, 1992).

The Gresten Formation is unconformably overlain by postrift sediments, starting with dolomitic sandstones with chert nodules (Höflein Formation; e.g. Wessely, 2006; Picha et al, 2006). After the establishment of stable marine conditions, a carbonate depositional system evolved. The lowermost unit of this package is the uniform Oxfordian Vranovice Formation composed of dolostones and limestones without clastic input (Wessely, 2006, Picha et al, 2006). The Klentnitz Group (sensu Wessely, 2006) represents a more differentiated carbonate depositional system (Fig. 7). A carbonate ramp evolved in the western part of the basin, whereas marly rocks have been deposited in the deeper eastern part. Traditionally three formations are differentiated within the Klentnitz Group: The Altenmarkt Formation includes shallow water carbonates, the Falkenstein Formation represents a transitional facies and the Mikluov Formation comprises deeper marine marlstones. The carbonate rocks of the Klentnitz Group grade upwards into dark, sandy dolomitic limestones of the Kurdejov Formation. Sedimentation in the Jurassic period ended with deposition of a limestone

succession, which ranges into the Berriasian (Ernstbrunn Formation). Due to major regression and Cretaceous erosion, the upper age limit of the Ernstbrunn Formation is unknown. Cretaceous rocks within the autochthonous unit of the Vienna Basin consist of a sandy-marly (Ameis Group) and a shaly-marly succession (Poysdorf Group; Wessely, 2006).

Petroleum geological relevance: The main source rock in the Vienna Basin area is the Malmian Mikulov Formation (Ladwein, 1988). Some potential for oil is also found within algae-rich coals of the Lower Quartzarenite Member of the Gresten Formation (Sachsenhofer et al., 2006).

The biggest reservoir within the autochthonous units, the Höflein field, is located within the Höflein Formation. From this reservoir wet gas and gas condensate are produced (Malzer and Brix, 1993). Relative small reservoirs in the Lower Quartzarenite Member have been exploited in the Hagenberg and Klement fields (Kreutzer, 1993).

2.1.2 Autochthonous Molasse

Upper Eocene to Upper Miocene Molasse sediments were deposited in front of the Alpine nappes. Sedimentation started with deposition of Eocene (?) (Moosbierbaum Fm.) and Eocene to Oligocene conglomerates (Zistersdorf Molasse; Wessely, 2006). The age of the Moosbierbaum Formation remains unclear, as it is barren of any fossils (Freilinger, 1963). Little is known about the Zistersdorf Molasse, which has only been encountered in well Zisterdorf ÜT2 (Wessely, 2006). Egerian deposits are represented by the sands of the Linz-Melk Formation deposited in a proximal position to the shoreline (Roetzl and Krenmayer, 2002). Within deeper settings the “Älterer Schlier” had been deposited during the Late Egerian. Eggenburgian rocks consist mainly of marls with minor sand lenses and contain glauconite (“Glauconite Sands”), a rich foraminifera fauna (“Foraminifera Facies”) or fish remains (“Fish Facies”). The Eggenburgian to Ottnangian “Sandstreifenschlier” is overlain by sands and silts of the “Oncaphora beds”, which have been deposited in a deep water, turbiditic environment (Hamilton, 1997, Wessely, 2006). In Karpatian times the fully marine shaly marls of the Laa Formation werde deposited in deeper parts of the basin.

Sediments deposited during or after the Badenian play only a minor role and are found mainly in the area of Hollabrunn (Wessely, 2006).

Petroleum geological relevance: Hydrocarbon reservoirs are located within the Oligo-Miocene Linz-Melk Formation (Stockerau Nord) and the Oligocene Oncophora beds (Altprerau, Neuprerau, Pottenhofen, Neuruppersdorf, Wildendürnbach, Merkersdorf).

2.2 Alpine Nappes (2nd floor)

The allochthonous units (2nd floor) comprise different tectonic nappes (Waschberg Zone, Flysch Zone, Calcareous Alps, Carpathians). The thrusting of these nappes onto the autochthonous series started in Paleogene time and lasted until the late Karpatian (Beidinger and Decker, 2014). A subcrop map of the allochthonous units in the Vienna Basin area are shown in Fig. 10.

2.2.1 Waschberg Zone

The Waschberg zone (Zdanice zone in the Czech Republic) is subdivided into two subunits, the „Outer Zone“ and the „Inner Zone“ (Grill, 1953). The Outer Zone consists of sediments of Ottnangian age, which are thrusted onto autochtonous molasse sediments along the Senninger Thrust Fault (Wessely, 2006). The “Roseldorf zone” in the south comprises slightly deformed sediments of Egerian to Karpatian age, whereas Ottnangian Oncaphora beds prevail in the north (Grill, 1953, Wessely, 2000). The Inner Zone comprises Eocene and Oligocene sediments as well as “cliffs”, tectonic imbricates with Upper Jurassic and Cretaceous rocks (Fig. 8). Latest research suggests, that the Inner Zone is thrusted onto the Roseldorf zone alonge multiple faults rather than one large (Fuchs et al., 2001).

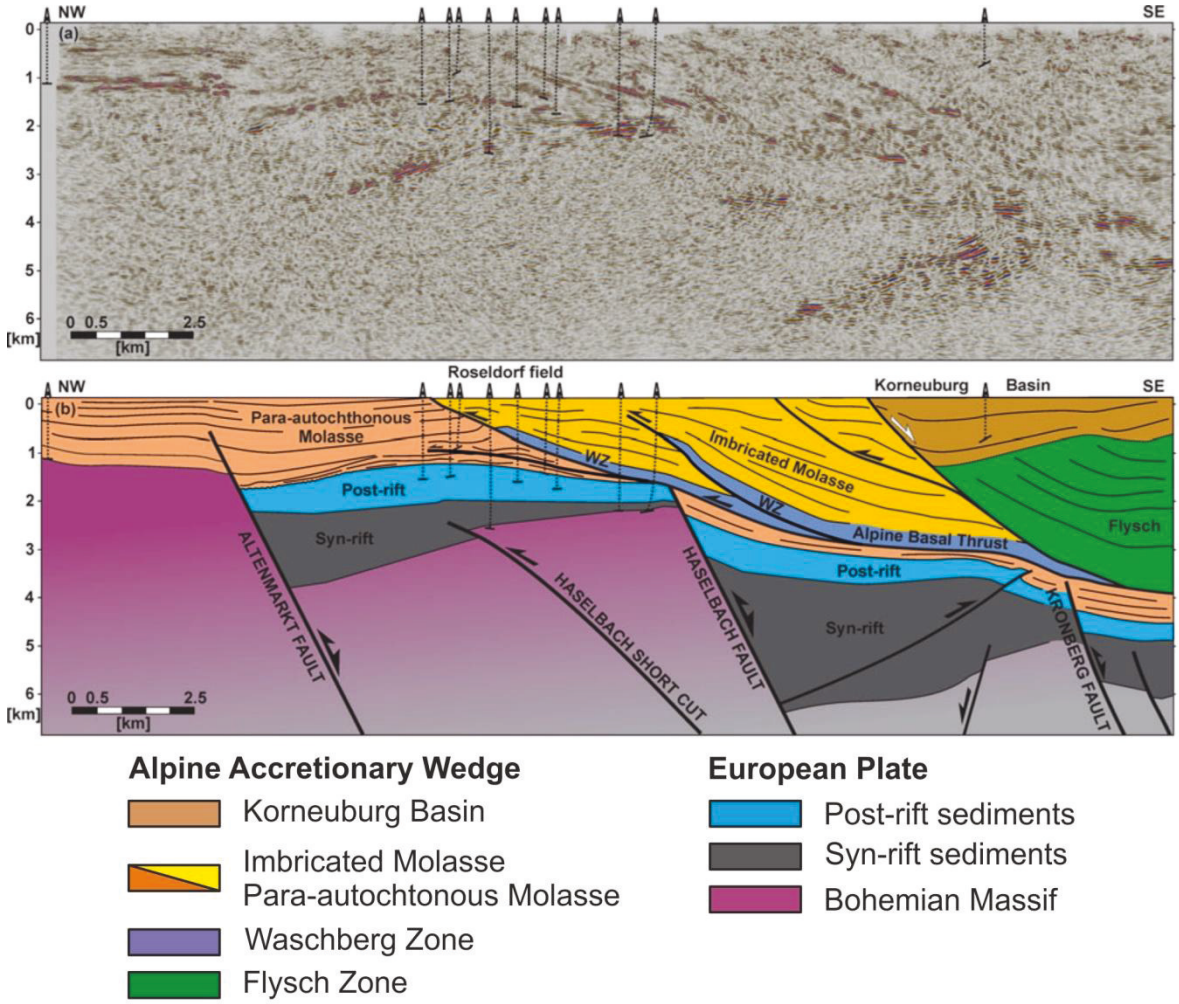

Fig. 8: Cross-section through the Roseldorf field displaying the geometry of the Waschberg Zone. Modified from Granado et al. (2016).

Petroleum geological relevance: The Oligocene Ottenthal Formation and the overlying Thomasl Formation in the Inner Zone may act as source rocks (e.g. Kratochvil and Ladwein, 1984).

Hydrocarbon fields within the Outer Zone (Roseldorf, Stockerau Ost) produce from Egerian, Ottnangian and Eggenburgian sandstones (Kreutzer, 1993). Within the Inner Zone hydrocarbons were produced from Eggenburgian reservoirs (Waschberg and Ameis fields; Kreutzer, 1993).

2.2.2 Flysch Zone

The sediments of the Flysch zone were deposited between the Late Jurassic and the Eocene in a deep water turbiditic system (Faupl, 1996 and references therein; Fig. 9) and consist mainly of sandstones, shales and marls. The Flysch zone benath the Vienna Basin comprises three tectonic units including from base to top the lower Raca-Greifenstein nappe system, the Kahlenberg nappe and the upper Laab nappe.

The sediments of the Raca-Greifenstein nappe comprise turbiditic glauconite sandstones and marls deposited in varying distance to land (Wessely, 1993). The Harrersdorf unit in the area between Steinberg and Zistersdorf represents a very distal Eocene facies and may be part of the Raca nappe (Wessely, 1993, 2006). The Greifenstein nappe overlies the Raca nappe and is further subdivided into the Gösting and the Zistersdorf units. Both units can be correlated from the Zistersdorf area as far as Höflein (Rammel, 1989).

The Kahlenberg nappe is called Niedersulz unit in the basement of the Vienna Basin, where it comprises Upper Cretaceous turbidites. However, the full sedimentary succession cannot be constructed based on the available well data (Wessely, 2006).

The Upper Cretaceous sediments of the Laab nappe contain mainly turbiditic sandstones as well as some synsedimentary basalt and colored clay layers (Wessely, 1993). This indicates volcanic activity during the Late Cretaceous in the Penninic realm (Wessely, 1993).

Petroleum geological relevance: Reservoirs in the Flysch zone are found in the Paleocene “Glauconite Sandstone” and the Eocene “Steinberg-Flysch” of the Harrersdorf unit. However, the reservoir quality of these turbiditic sandstones is generally moderate (average porosity: 7%, average permeability: 7 mD; Glantschnig and Kroell, 1997).

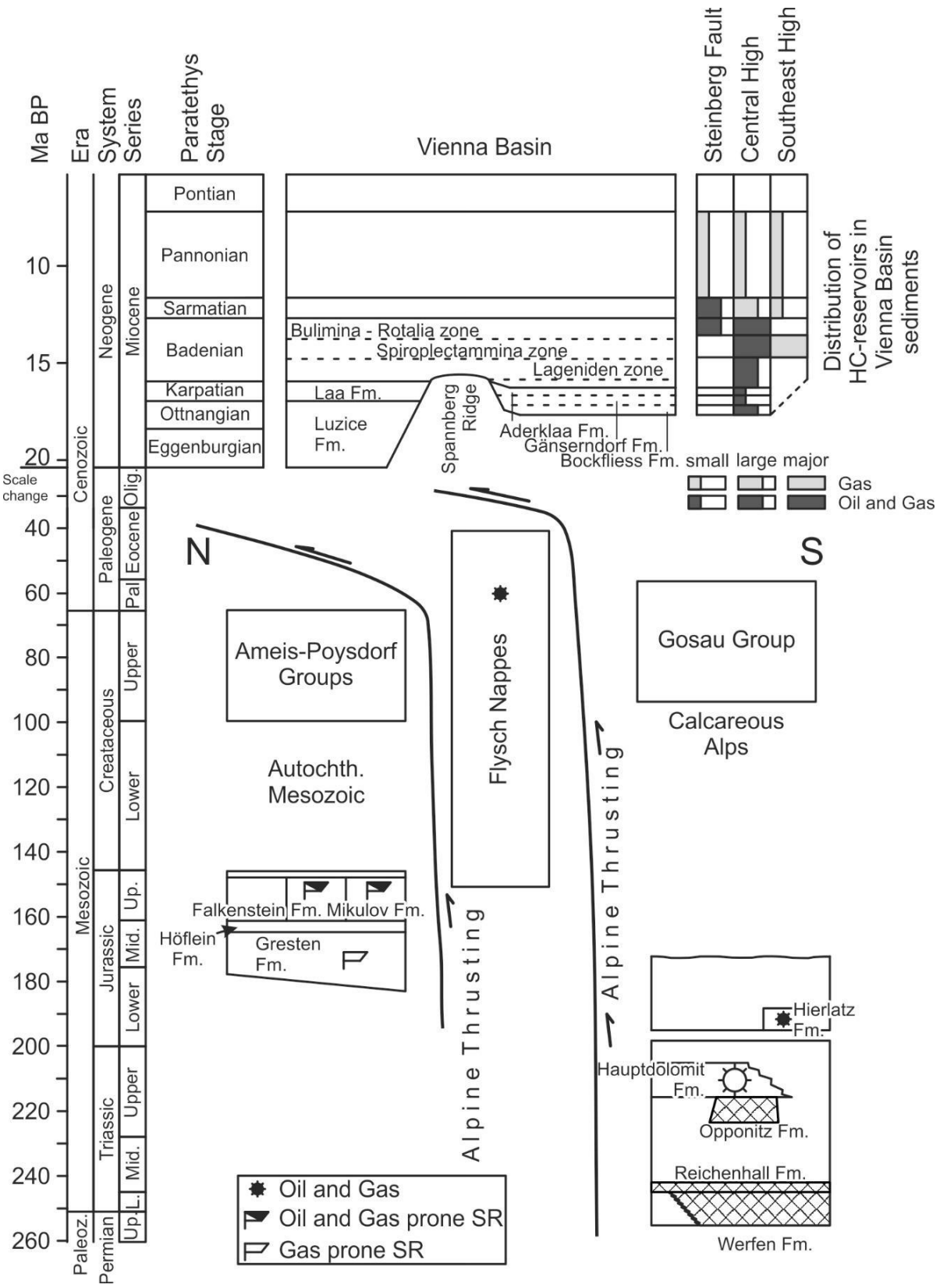

Fig. 9: Simplified stratigraphic chart of the Vienna Basin and underlying units. Note that the Alpine nappes were thrusted onto the autochtonous units before the deposition of the Vienna Basin sediments. Highlighted are potential source rocks and reservoir rocks. Compiled from: Piller et al. (2004), Kreutzer (1993) and Wessely (1993).

2.2.3 Northern Calcareous Alps and Carpathian nappes

The sediments assembled in this unit were deposited between the Late Permian and the Middle Paleocene (Fig. 9). Due to Alpine thrusting three nappes/ nappe systems are present in the floor of the Vienna Basin. From bottom to top these are the Frankenfels-Lunz nappe system of the Bajuvaric domain, the Göller nappe of the Tirolic domain and an unclassified nappe of the Juvavic domain (Wessely, 1993). The latter may be an equivalent of the Juvavic Schneeberg nappe and/or of Carpathian nappes (Wessely, 2006). In any case, the latter does not contain HC-reservoirs.

The general stratigraphy of the Calcareous Alps is quite complex and a detailed discussion is beyond the aim of this chapter. Therefore the following discussion focuses on reservoir formations and sulphate-bearing formations in the Frankenfels-Lunz nappe system and the Göller nappe.

Petroleum geological relevance: Major hydrocarbon reservoirs are found within the Hauptdolomite Formation (Figs. 9, 10). This Norian to Rhaetan formation was deposited in a lagoonal setting. Within the Frankenfels-Lunz nappe in the Vienna Basin area, the Hauptdolomit is very heterogenous in clay content and grain size and even contains some sand layers (Wessely, 2006). Within the Göller nappe, the Hauptdolomite is more homogenous, less shaly, less sandy and more laminated than in the Frankenfels-Lunz nappe (Wessely, 2006). Additonaly some stromatolithes occur within the Hauptdolomite of the Göller nappe (Wessely, 2006).

Minor hydrocarbon reservoirs are also found in the Sinemurian Hierlatz-Limestone Formation. It is mainly a crinoide-breccia with significant occurrence of brachiopods. Fine-grained varieties contain significant amounts of sponge spiculae.

Sulphate rocks occur in the Permoskythian Werfen Formation, the Anisian Reichenhall Formation and the Karnian to Norian Opponitz Formation, which were deposited in shallow marine settings. The Werfen and Reichenhall formations contain gypsum, anhydrite and halite, whereas halite is absent in the Opponitz Formation.

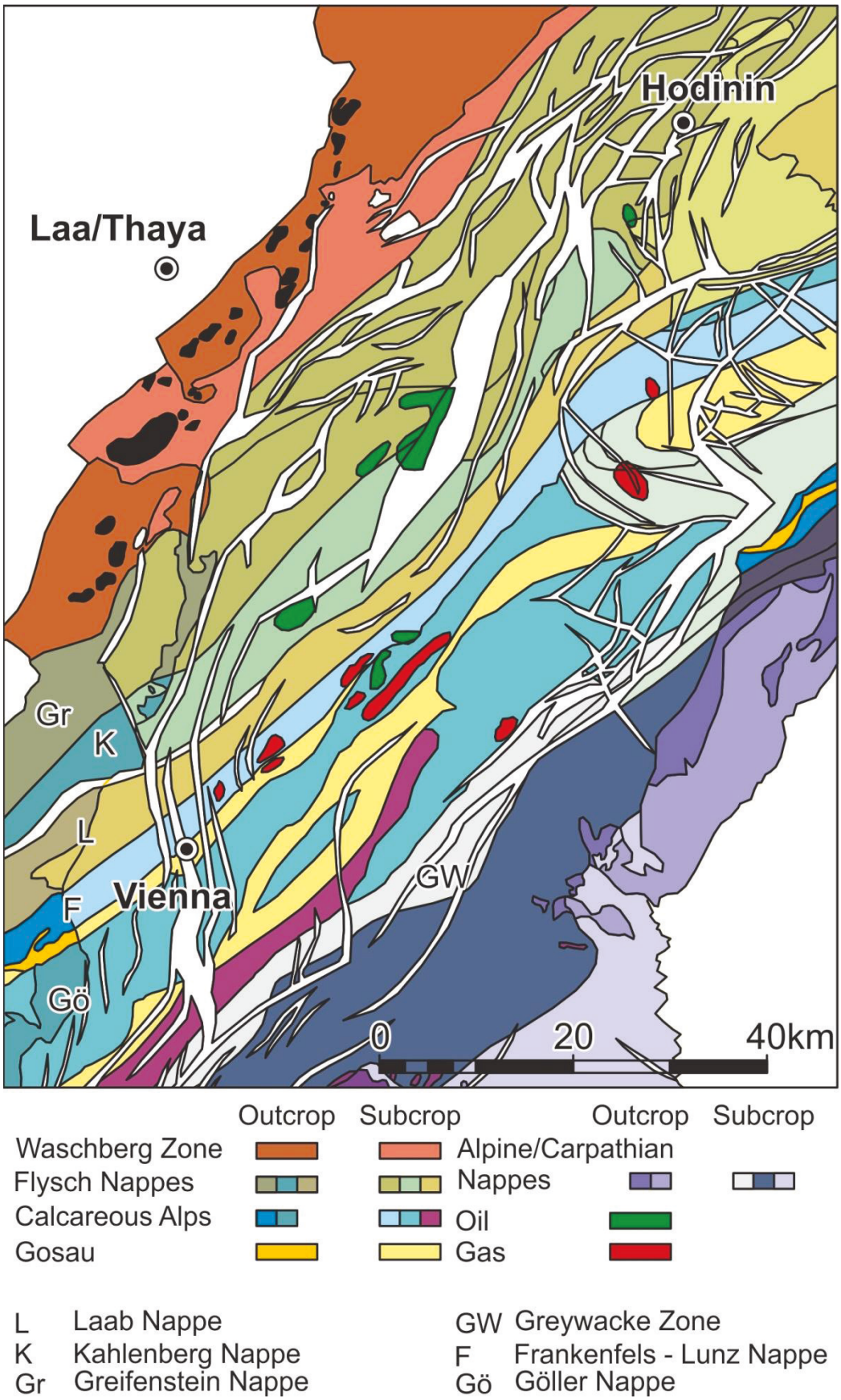

Fig. 10: Subcrop map of the Vienna Basin with oil and gas fields in allochthonous units. Modified from Arzmüller et al. (2006).

2.3 Vienna Basin (1st floor)

The Miocene basin fill comprises sediments of a piggy-back stage (proto-Vienna Basin, early Miocene) and a pull-apart stage (neo-Vienna Basin, middle to late Miocene; Steininger et al, 1986). These sediments host the largest HC fields within the area (Fig .11). In Miocene time, the Vienna Basin formed part of the Central Paratethys.

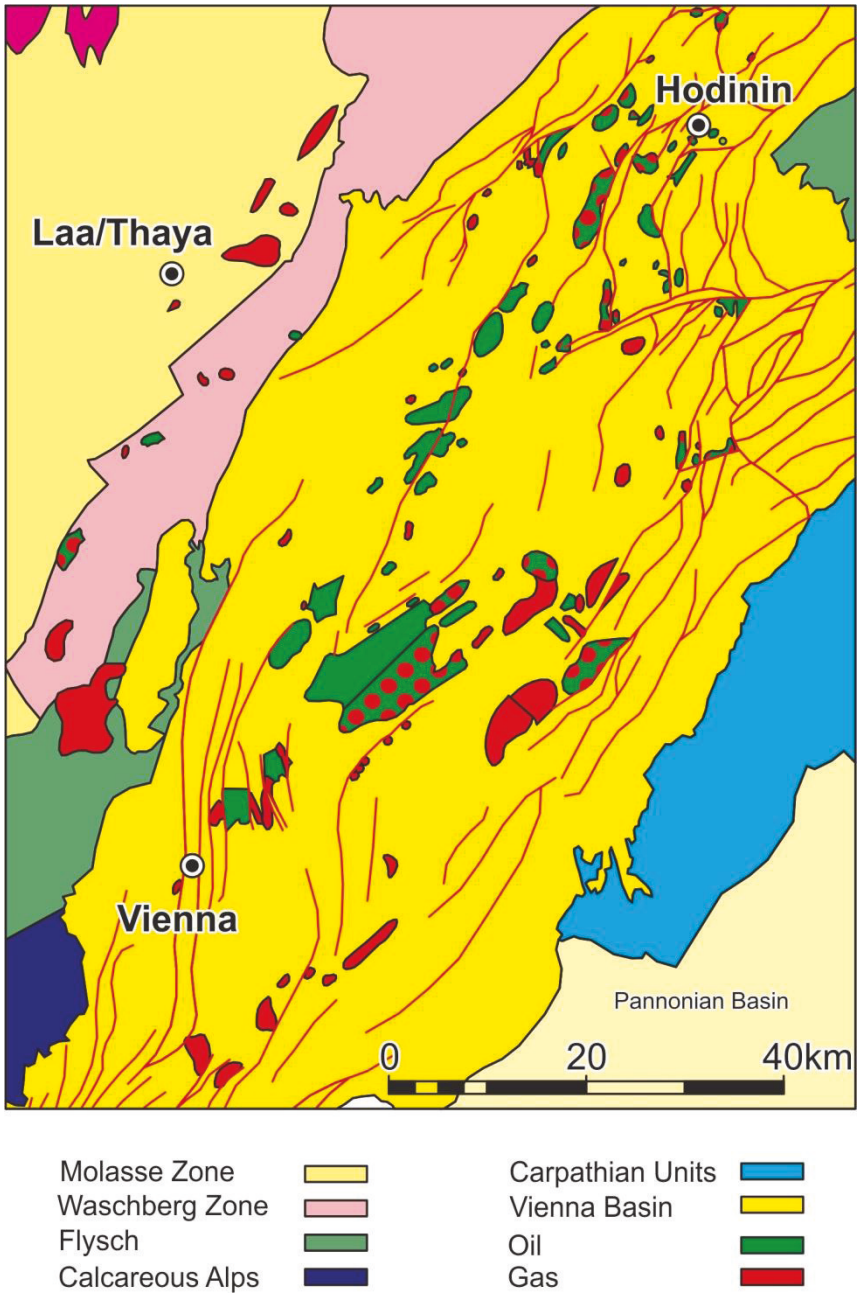

Fig.11: Oil and gas fields in the Vienna Basin plotted onto the surface geology of the area. Modified from Arzmüller et al. (2006).

2.3.1 Proto Vienna Basin

Since the Middle Paleogene, Alpine nappes overthrusted onto autochthonous units and Eocene Molasse sediments. However, between Eggenburgian and Karpatian times, sedimentation also took place on top of the Alpine nappes. Those sediments were transported together with the Alpine nappes and a piggy-back basin developed (Proto Vienna Basin). The highly active tectonic setting caused the creation of sediments with varying thickness due to synsedimentary faulting, block tilting and internal thrusting (Wessely, 2006).

Within the Proto Vienna Basin the sedimentary record is split by the Spannberg Flysch ridge (Fig. 14). North of this structure, fine-grained shaly marls were deposited (Luschitz Fm.). During the Karpatian continued marine ingressions resulted in deposition of the marly, sandy Laa Formation (Fig. 14). South of the Spannberg Flysch ridge, deposition commenced with the Bockfließ Formation, a unit comprising limestone sands, breccias and conglomerates from the beginning erosion of the Calcareous Alps. Above an unconformity the marls and sandstones of the Gänserndorf Formation were deposited during the Karpatian. Sedimentation in the Karpatian ended with the deposition of the Aderklaa Formation, a fossil-bearing (ostracodes, congerias, hydrobiidias and snails) marl.

Petroleum geological relevance: Reservoirs within the Proto Vienna Basin are mainly found in the Bockfliess Formation (Aderklaa, Schönkirchen, Matzen, Gänserndorf). Minor reservoirs and oil shows also occur in the Gänserndorf and Aderklaa formations.

2.3.2 Neo-Vienna Basin

At the end of the Karpatian, overthrusting of the Alpine nappes significantly slowed down. The dominating tectonic regime changed to a pull-apart setting caused by differential movements between the northward moving Carpathian nappes and the already fixed Alpine nappes. Sedimentation was controlled by major faults (Steinberg Fault [Fig.13], Leopoldsdorf Fault, Markgrafneusiedl Fault), sea level variations and the progradation of deltas into the basin (Fig 15).

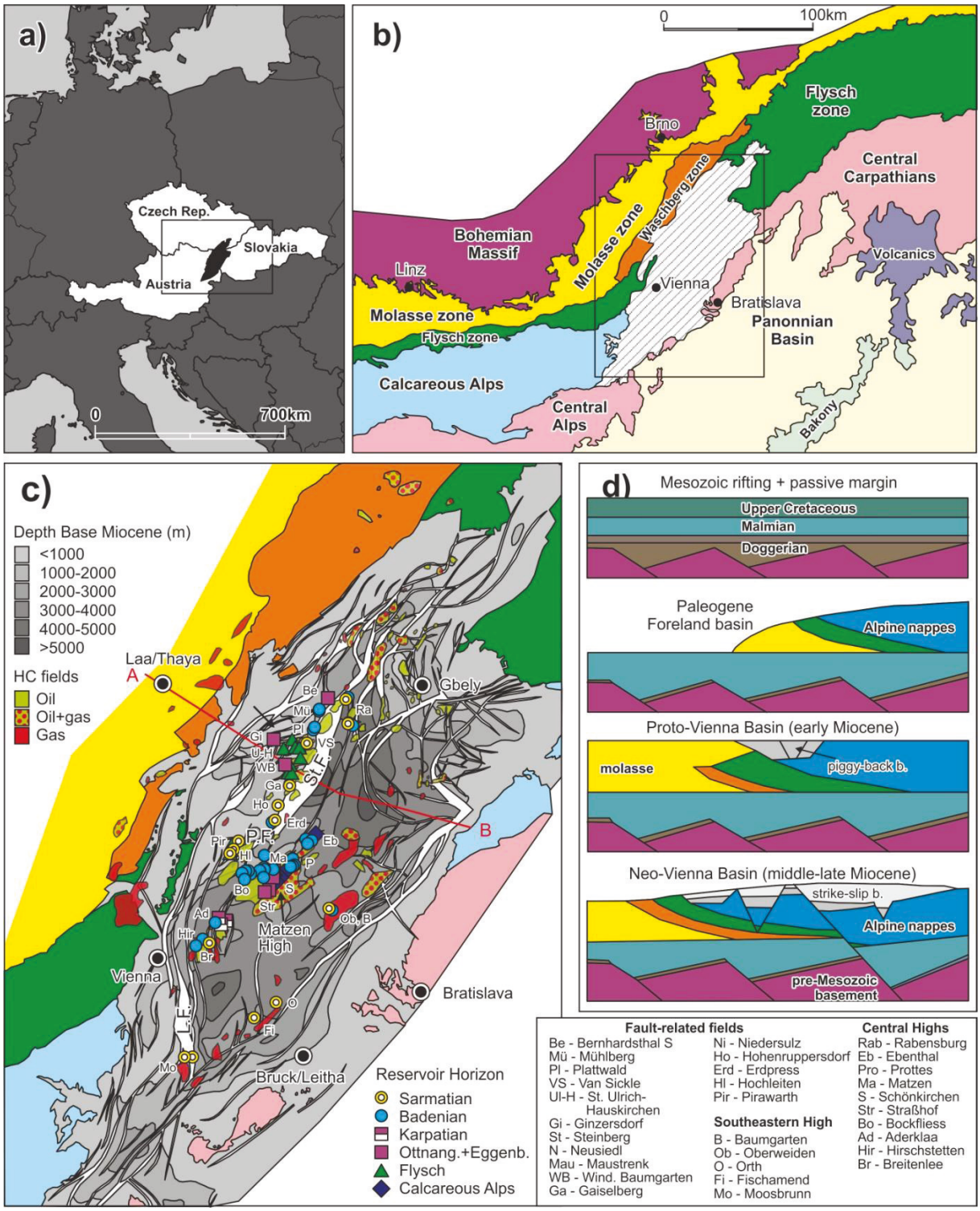

Fig.12: a) Location of the Vienna Basin in Europe, b) regional geology of central Europe (modified Wessely, 2000) and c) structure map of the Vienna basin and surounding tectonic units with location of sampled wells (compiled from Wessely et al., 1993, Kröll and Wessely, 1993 and Arzmüller et al., 2006). d) Main evolutionary stages of the Vienna Basin area (modified from Seifert, 1996). L.F. Leopolsdorf Fault; St.F.: Steinberg Fault, P.F.: Pirawarth Fault

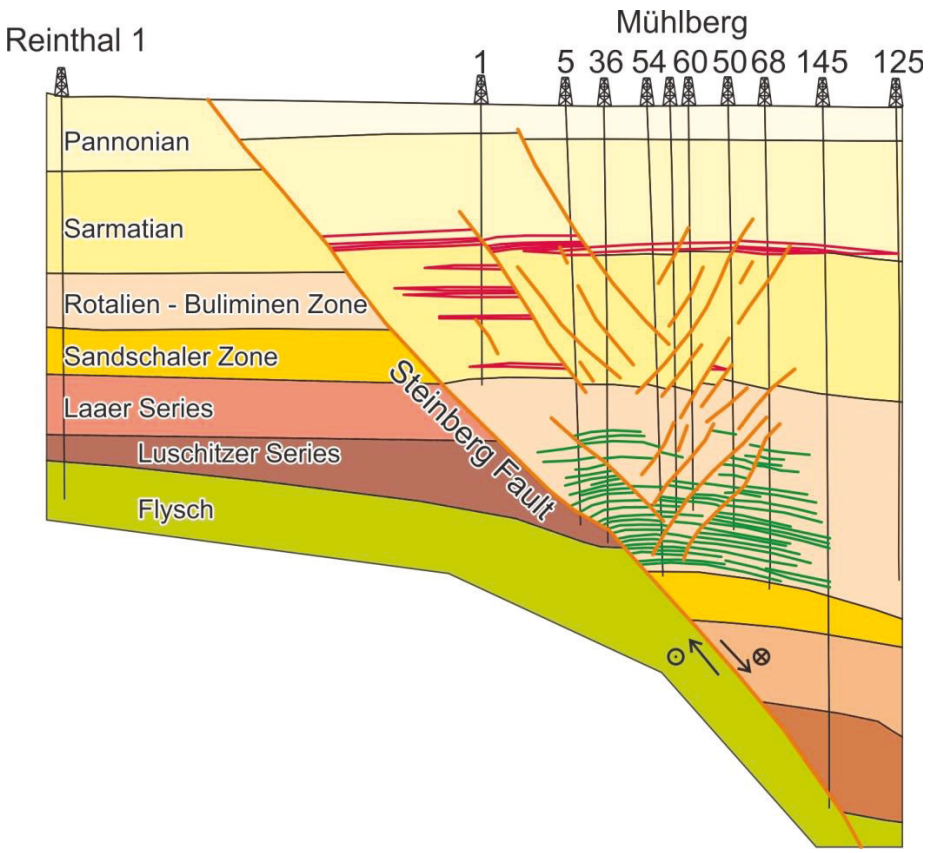

Fig. 13: Cross section through the Mühlberg Field. The main tectonic feature in the area is the Steinberg Fault. Modified from Kreutzer (1993).

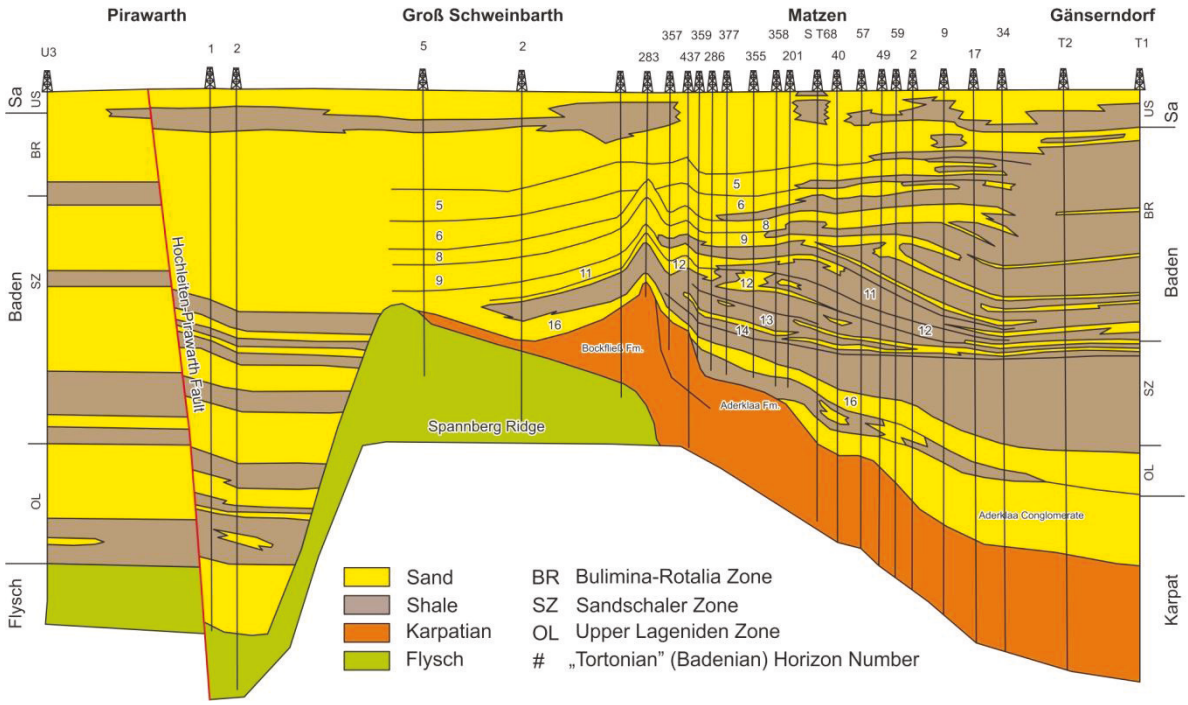

Fig. 14: Cross section through the Spannberg ridge beneath the giant Matzen field. The main tectonic features in the area are the Spanberg Ridge and the Hochleiten-Pirawarth Fault. Modified from Kreutzer (1993).

South of the Spannberg Flysch ridge, the first sedimentary record is the fluvial Aderklaa-Conglomerate Formation, comprising debris from the Alps and the Carpathians (Fig. 14). It is overlain by the transgressive 16th TH sand horizon.

North of the ridge, the main Badenian sedimentary input into the basin was delivered by rivers from the west. These fluvial and deltaic sediments filled up all accommodation space north of the Spannberg Flysch ridge. Further sediment input caused sediment shedding into the southern part of the basin. The further sedimentary succession was mainly dominated by transgressive and regressive cycles (Wessely, 2006 and refrences therein). Stratigraphic units within the Badenian succession are defined by the occurrence of foraminifers (Lageniden zone, Spiroplectammina zone (Sandschaler zone), Bulimina-Rotalia zone, Fig. 9).

At the Badenian-Sarmatian boundary the Paratethys became isolated from the open ocean, causing a faunal change (Popov et al., 2004). Whereas Paratethyan sediments often show an increase in salinity during the early Sarmatian, the fauna within the Vienna Basin realm displays normal marine salinity (Piller and Harzhauser, 2005). Rivers continued to transport siliciclastic material into the basin.

At the Sarmatian-Pannonian boundary the Vienna and Pannonian Basin were isolated from the open sea (Popov et al., 2004). During the early Pannonian brakish conditions prevailed, while the main sedimentary input did not change. A major regression of the sea caused a rapid fill of deep areas with fresh water sediments. Subsequently upper Pannonian sediments were deposited in a lacustrine setting. If Pontian sediments have been deposited is still unclear (Wessely, 2006).

Petroleum geological relevance: The main reservoirs in the Vienna Basin are located within Badenian sands, with the most important 16th TH and 9th TH horizons. Important reservoirs horizons are also found within Sarmatian sands. Gas can be found in Pannonian sediments.

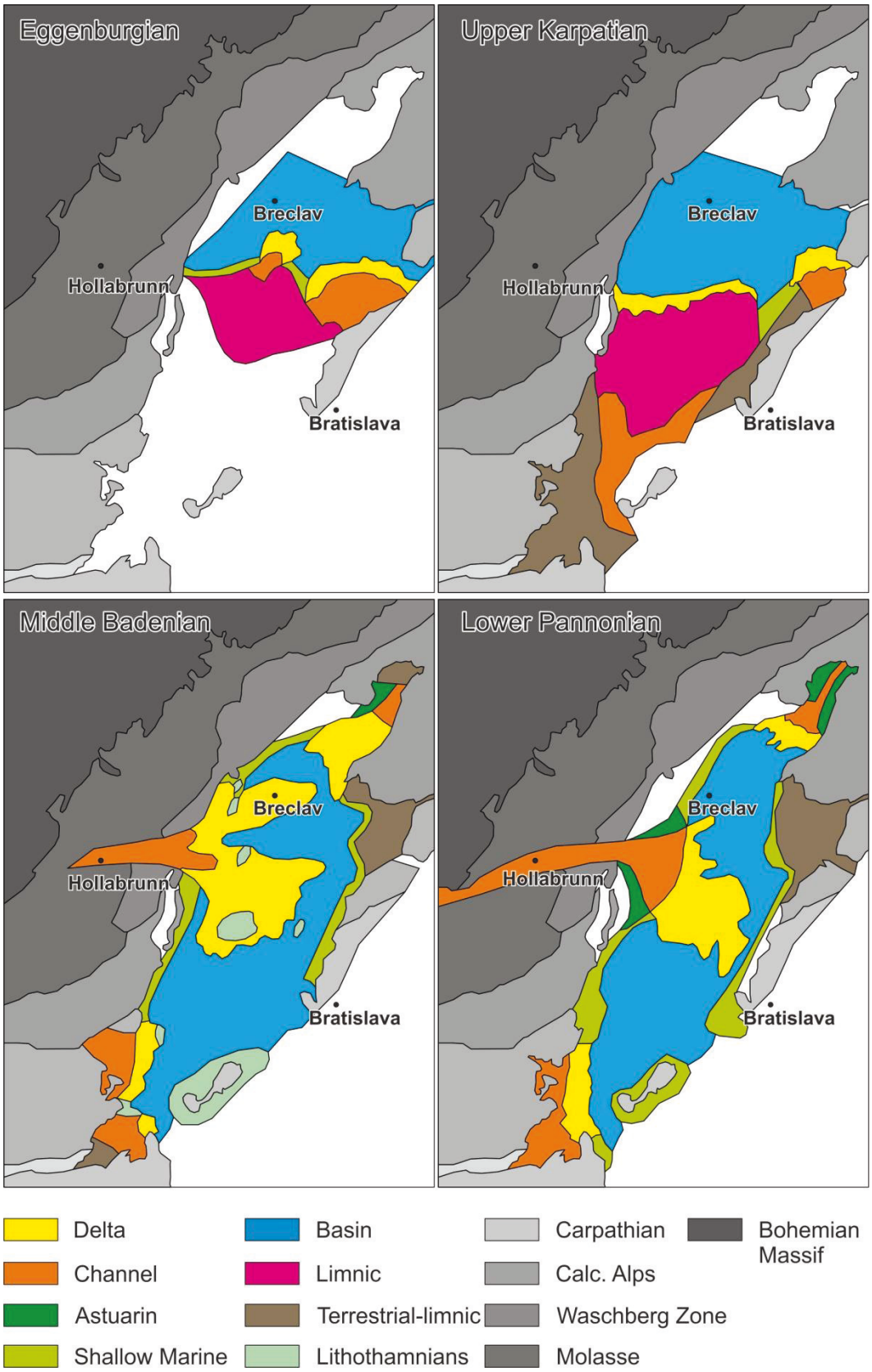

Fig. 15: Facies variation over time within the Vienna Basin. Modified from: Jiricek (1985) and Jiricek and Seifert (1990).

3. Samples

212 rock samples, 3 oil stained samples, 86 oil samples and 69 gas samples have been investigated. Each core sample was taken representative for 10-15 cm of thickness. The depth of all rock samples is referred to as measured depth (MD) below surface.

Wells sampled for oil and gas are grouped according to production fields. With the exception of oil samples from fields Aderklaa, Gbely, Hodonín, Holíč, Kierling, Lanžhot, Maustrenk, Mühlberg, Neusiedl and Windisch-Baumgarten, which were sampled from the archive of the Austrian Geological Survey, all samples have been provided by OMV. The depth of all oil and gas samples is refered to as true vertical depth (TVD) below sea level.

An overview of sample details and all analytical techniques applied can be found in Appendix I.

Rock Samples

Gresten Formation

Lower Quarzarenite Member

Porrau	212 Samples

Lower Shale Member

Altenmarkt 1	18 Samples
Falkenstein 1	6 Samples
Hagenberg 3	9 Samples
Höflein 1	10 Samples
Klement 1	8 Samples
Porrau 2	30 Samples
Roseldorf Tief 2	8 Samples
Staatz 1	1 Sample

Upper Quarzarenite Member

Stockerau Ost 1	22 Samples

Falkenstein Formation

Falkenstein 1	2 Samples
Klement 1	2 Samples
Staatz 1	7 Samples
Stronegg 1	2 Samples
Waschberg 1	2 Samples
Wildendürnbach K4	2 Samples

Mikulov Formation

Aderklaa UT 1a	1 Sample
Ameis 1	6 Samples
Falkenstein 1	9 Samples
Fallbach 1	1 Sample
Höflein 7a	2 Samples
Klement 1	2 Samples
Korneuburg T1	2 Samples
Maustrenk UT 1a	2 Samples
Merkersdorf 2	1 Sample
Roseldorf T1	1 Sample
Staatz 1	38 Samples
Stronegg 1	2 Samples
Thomasl 1	4 Samples
Wildendürnbach T1	1 Sample
Zistersdorf UT 1	8 Samples
Zistersdorf UT 2a	5 Samples

Oil Samples (Field: Well#)

Aderklaa: 3, 4, 34
Bockfliess: 1, 24, 33, 35, 37, 43, 205
Ebenthal: 5, 15, 17a, 20
Erdpress: 4, 17a, 24
Gbely: 2, H6
Hodonín: 1, 3, 4
Hochleiten: 15, 24, 31, 60, 65, 66, 67
Höflein: 1, 3, 4, 6, 8, 9, 10, 12
Hohenruppersdorf: 42
Holíč: 4
Kierling: 1, 2
Lanžhot: 15, 30
Maustrenk: 29
Matzen: 91, 115, 116, 286, 322, 390y, H 703b
Mühlberg: 15
Neusiedl: 1, 3
Pirawarth: U10
Prottes: 26, 27, 29, 98, 104, T S 3b
Rabensburg: 11, N3, U4
Roseldorf: 2
Schönkirchen: 267, T12, T29a, T38, T32, T42, T62, T64, T69, T90a
St. Ulrich: 65, 92, 213a
Steinberg: 11, 21
Stockerau Ost: 1, 16
Van Sickle: 29
Windisch-Baumgarten: 1

Oil Stained Samples

Mank 1 (157.8 m; Molasse)
Urmansau 1 (152.1 m Calacareous Alps)
Urmansau 1 (758.4 m Calacareous Alps)

Gas Samples (Field: Well#)

Aderklaa: 98a
Baumgarten: 1
Bockfliess: 1, 24, 33, 35, 37, 43, 205
Breitenlee: 15, 17
Ebenthal: T1
Erdpress: 4, 17a, 24
Fischamend: 6
Ginzersdorf: 4
Hauskirchen: 86
Hirschstetten: 7a
Hochleiten: 15, 24, 60, 65, 66, 67
Höflein: 1, 4, 6, 8, 9, 10, 12
Hohenruppersdorf: 42
Matzen: 115, 116, 286, 322, H703b
Moosbrunn Ost: 1
Moosbrunn West: 1
Niedersulz: 12a
Oberweiden West: 1
Orth: 2
Prottes: 27, 29
Rabensburg: 12, 13, 14, W4
Roseldorf: 4, 6, 20, T2
Schönkirchen: T32, T42, T62, T64, T90a
St. Ulrich: 65, 92, 213
Steinberg: 21
Stockerau Ost: 7, 13, 16
Van Sickle: 29
Wildendürnbach: 5, 10, 16

4. Methods

Bulk Geochemistry - Total carbon (TC), total sulphur (S), as well as total organic carbon (TOC) contents were determined using an Eltra Helios Double Dual Range C/S-Analyzer. All determinations refer to a dry powdered sample in mass-%. To determine the amount of TC and S, 100 to 120 mg of the samples were burnt at 1350°C in a pure oxygen atmosphere. To determine TOC, the same amount of sample was heated to about 100°C and treated twice with 50% phosphoric acid to remove inorganic carbon. Each sample was measured in duplicate. The difference between TC and TOC is the total inorganic carbon (TIC). TIC contents were used to calculate calcite equivalent percentages (calcite-eq) using the formula TIC*8.34.

Rock Eval Pyrolysis - Pyrolysis was carried out using a "Rock Eval 6 classic" instrument (Vinci Technologies) in combination with the "Rockplus" Software. The weight of the powdered sample was about 80 mg. The measurements were performed in duplicate. Two peaks were recoreded. The S1 peak (mgHC/gRock) records hydrocarbons volatilized at 300°C and represents free or adsorbed hydrocarbons that were present in the rock before pyrolysis. The S2 peak (mgHC/gRock) is produced during gradual heating from 300 to 650°C by thermal breakdown of kerogen and from heavy extractible compounds such as resins and asphaltenes. S1 and S2 were used to calculated

Hydrogen Index (HI) (Espitalie et al., 1977):

$$HI = \frac{S_2}{TOC} * 100.$$

Production Index (PI) (Espitalie et al., 1977):

$$PI = \frac{S_1}{S_1 + S_2}.$$

As a maturation indicator, the temperature of maximum hydrocarbon generation (Tmax) was measured.

Pyrolysis Gas chromatography - Pyrolysis gas chromatography was performed using the Quantum MSSV-2 Thermal Analysis System®. Six extracted samples were heated in a flow of helium, and products released over the temperature range 300-

600°C (40K/min) were focussed using a cryogenic trap, and then analysed using a 50m x 0.32mm BP-1 capillary column equipped with a flame ionisation detector. The GC oven temperature was programmed from 40°C to 320°C at 8°C/minute. Boiling ranges (C1, C2-C5, C6-C14, C15+) and individual compounds (n-alkenes, n-alkanes, alkylaromatic hydrocarbons, phenols and alkylthiophenes) were quantified by external standardisation using n-butane. Response factors for all compounds were assumed the same, except for methane whose response factor was 1.1. The pyrograms can be found in Appendix VI.

Organic petrology and thin section microscopy - For organic petrological investigations 50 polished blocks were prepared and mean random vitrinite reflectance (%Rr) was determined using a Leica microscope and following established procedures (Taylor et al., 1998). Maceral composition was assessed semi-quantitatively using white-light and blue-light irradiation. For microfacies analysis, 26 thin sections were prepared. The composition of the samples was assessed on a Leica DM 4500P microscope with transmitted, unpolarized white light. Selected polished blocks were carbon-coated for electron microprobe analyses, performed with a Superprobe JEOL JXA 8200 electron microprobe in high vacuum mode. Energy dispersive (EDX) spectra were used for identification of mineral phases.

Mineralogy - Preparation of 28 samples for XRD-measurements included hand-milling to a grain size of ~10 µm. Two different types of mounts were used for analysis: For determination of the bulk mineralogy and for semi-quantitative analysis, sideward-filled powder mounts with nearly random particle-orientation were used. In addition, five oriented powder mounts were applied for clay mineralogical analyses. For preparation of oriented powder mounts, 0.085 g of air-dried powder was mixed with 0.045 g of deionized water, and the obtained paste was smeared to a glass sample holder. Each oriented mount was measured in untreated condition, after solvation with ethylene glycol, and after thermal treatment (350°C and 550°C, 2 h). Quantitative interpretation was done according to Schultz (1964). All mineral amounts are given as wt.%. The relative error is estimated as 5%.

Calcareous nannofossils - Calcareous nannofossils from eight samples were investigated by Madalina-Elena Kallanxhi. Smear slides were prepared using

standard techniques (Bown and Young, 1998) and investigated under a light microscope Leica DM 4500P (1000 x magnification), in parallel light and crossed nicols. The relative abundance of nannofossils was considered as follows: C - common (1 specimen / 2 - 10 FOV [field of view]), F - few (1 specimen / 11 - 20 FOV), R - rare (1 specimen / 21 - 50 FOV), VR - very rare (1 specimen / 50 - 100 FOV), P - present (1 specimen in more than 100 FOV or per sample). Additionally, 100 FOV were investigated for rarer taxa. The nannofossil preservation (Roth and Thierstein, 1972) was assessed as: M – moderate (dissolution and overgrowth are present, ~25% of the specimens cannot be identified at species level) and P - poor (the majority of the specimens cannot be identified at species level due to occurrence of dissolution, fragmentation, and/or overgrowth). Pictures of nannofossils were captured under cross-polarized light (XPL) with a Leica DFC420 camera.

Gas-Chromatography-Flame Ionization Detector - The whole oils were analysed using a gas chromatograph equipped with a 50 m HP-PONA fused silica column (i.d. 0.2 mm; 0.5 µm film thickness) and coupled to a FID (GC-FID system). The oven temperature was programmed to 32°C for 5 minutes and then heated up to 310° C at 2.5°C min−1, followed by an isothermal period of 30 min. He was used as carrier gas. Water liquid sample were injected pure with a split ratio of 150. Non-water liquid samples were diluted in C_2S and injected splitless. The injector temperature was set to 300°C. Data were processed using a ThermoFisher data system. Individual compounds were identified on the basis of retention time. All chromatograms can be found in Appendix VIII.

Gas-Chromatography-Mass Spectroscopy - For organic geochemical analysis of source rock samples, representative aliquots of 49 selected samples were extracted for ca. 1 h using dichloromethane (DCM) in a Dionex ASE 200 accelerated solvent extractor at 75° C and 50 bar. After evaporation to 0.5 ml in a Zymark TurboVap 500 closed cell concentrator, asphaltenes were precipitated from a hexane:DCM solution (80:1) and separated using centrifugation. Oil stained rocks samples were crushed and the rock chips were washed using DCM. The following procedure was the same as for source rock extracts. Oil samples (ca. 50 mg) were directly diluted with the hexane:DCM (80:1) mixture and the insoluble asphaltenes were separated by centrifugation. The hexane-soluble fractions were separated into NSO compounds,

saturated hydrocarbons and aromatic hydrocarbons using medium pressure liquid chromatography (MPLC) with a Köhnen-Willsch instrument (Radke et al., 1980).

The saturated and aromatic hydrocarbon fractions were analysed using a gas chromatograph equipped with a 30 m DB-5MS fused silica column (i.d. 0.25 mm; 0.25 µm film thickness) and coupled to a ThermoFisher ISQ quadropole mass spectrometer (GC–MS system). The oven temperature was programmed from 70° C to 300° C at 4° C min−1, followed by an isothermal period of 15 min. He was used as carrier gas. The sample was injected with a split ratio of 10, with the injector temperature at 275° C. The spectrometer was operated in the EI (electron ionization) mode over a scan range from m/z 50 to 650 (0.7 s total scan). Data were processed using a ThermoFisher data system. Individual compounds were identified on the basis of retention time in the total ion current (TIC) chromatogram and comparison of the mass spectra with published data. Proportions (%) and absolute concentrations of different compound groups in the saturated and aromatic hydrocarbon fractions were calculated using peak areas in the TIC chromatograms vs. internal standards (deuterated n-tetracosane and 1,1'-binaphthyl, respectively) or by integration of peak areas in appropriate mass chromatograms using response factors to correct for the intensity of the fragment ion used for quantification of the total ion abundance. Concentrations were normalised to TOC.

The low polarity nitrogen, sulphur and oxygen (NSO) compounds fraction containing the carbazole derivatives was isolated according to the polarity–affinity liquid chromatography method of Willsch et al. (1997). The low polarity NSO compounds were analysed on a gas chromatograph equipped with the same column as described above and coupled to a Finnigan MAT GCQ ion trap mass spectrometer. The oven temperature was programmed as follows: 60 °C for 2 min then ramped to 180 °C at 20 °C/min, kept isothermal for 1 min, increased to 310 °C at 4 °C/min and held at the final temperature for 10 min. Helium was used as carrier gas. The sample was injected splitless at 275 °C. The mass spectrometer was operated in the EI (electron impact) mode. Carbazoles were detected in selective ion monitoring (SIM) mode, scanning for the following ions: m/z 167 (carbazole), m/z 181 (methylcarbazoles), m/z 195 (C2-carbazoles), m/z 209 (C3-carbazoles), m/z 217 (benzocarbazoles) and m/z 243 (phenylcarbazole). Mass spectra were recorded at a scan rate 0.7 scans/s. Data were processed with a ThermoFisher data system.

Identification of alkylated carbazoles was achieved following the elution orders provided by Nakazawa et al. (1981) and Bowler et al. (1997). The quantitative amounts were determined relative to 9-phenylcarbazole as an internal standard. No corrections were made for specific response factors of individual compounds.

The medium polarity NSO compounds were derivatised with BSTFA [N,O-bis(trimethyl-silyl)trifluoroacetamide, Fluka] for 1 h at 80°C to form trimethylsilyl ethers. They were analysed using a gas chromatograph equipped with a 30 m DB-5MS fused silica column (i.d. 0.25 mm; 0.25 µm film thickness) and coupled to a ThermoFisher ISQ quadropole mass spectrometer (GC–MS system). The oven temperature was programmed from 70° C to 300° C at 4° C min−1, followed by an isothermal period of 15 min. He was used as carrier gas. The sample was injected with a split ratio of 10, with the injector temperature at 275° C. The spectrometer was operated in the EI (electron ionization) mode over a scan range from m/z 50 to 650 (0.7 s total scan). Data were processed using a ThermoFisher data system. Individual compounds were identified on the basis of retention time in the total ion current (TIC) chromatogram and comparison of the mass spectra with published data. Proportions (%) and absolute concentrations of different compound groups in the saturated and aromatic hydrocarbon fractions were calculated using peak areas in the TIC chromatograms vs. internal standards (deuterated n-tetracosane and 1,1'-binaphthyl, respectively) or by integration of peak areas in appropriate mass chromatograms using response factors to correct for the intensity of the fragment ion used for quantification of the total ion abundance. Concentrations were normalised to TOC. All chromatograms can be found in Appendix VIII.

Gas composition

HC gases, N_2, O_2 and CO_2: The natural gas analyses were performed using an Agilent 7890 gas chromatograph using a three column switching/backflush arrangement for the determination of nitrogen, oxygen, carbon dioxide and hydrocarbons from C1 to C6+. The oven was programmed at 90°C isothermal with helium as carrier gas. The sample loop volume was 1ml, directl injected. The columns used were 15 ft.; 1/8 in.; 25% DC 200 silicone oil on P-AW 80/100 mesh; 10 ft.; HayeSep Q 80/100 mesh and 10 ft. Molecular Sieve 13X; 45/60 mesh. Quantification was performed by TCD and FID. For calibration external gas

standards, provided by SIAD, at different concentrations, were used.

Sulphur compounds: The sulphur compounds were determined using an Agilent 7890 gas chromatograph coupled to a sulphur chemiluminescence detector (SCD). The GC was equipped with a CP-PoraBOND Q (25 m x 0,53 mm I.D x 10 μm) and a 0.05ml gas injection loop. Helium was used as carrier gas; injection was performed splitless for samples with low H_2S concentration and with split (50 ml/min splitflow) for samples with high concentrations of H_2S. The oven was held at 50°C for 3min and programmed at 25°C/min to 200°C 10min isothermal. The calibration gases were provided by SIAD at different concentrations.

Stable Isotope Ratios – Isotopic Ratio Mass Spectrometry

Carbon, hydrogen: For bulk carbon isotope analyses of the TOC, powdered samples were treated with hydrochloric acid to remove inorganic carbon. Decarbonated bulk rock samples and saturated and aromatic hydrocarbon fractions of rock extracts and oils were placed into tin foil boats and combusted using an elemental analyzer (Flash EA 1112) at 1020°C in an excess of oxygen. The resulting CO_2, separated by column chromatography, was analysed online by a ThermoFisher DELTA-V isotope ratio mass spectrometer. The $^{13}C/^{12}C$ isotope ratios of the CO_2 were compared with the corresponding ratio in a monitoring gas, calibrated against the Vienna-Pee Dee Belemnite (V-PDB) standard by the NBS-19 reference material. Stable isotope ratios are reported in delta notation ($\delta^{13}C$) relative to the V-PDB standard ($\delta^{13}C$ = [($^{13}C/^{12}C$) sample/($^{13}C/^{12}C$)standard − 1]). Delta notation is expressed in parts per thousand or per mil (‰).The reproducibility of the total analytical procedure is in the range of 0.1–0.2‰.

The n-alkanes were separated from branched/cyclic hydrocarbons by an improved 5 Å molecular sieve method (Grice et al., 2008) for the analysis of stable carbon and hydrogen isotope ratios on individual n-alkanes and isoprenoids. Stable C isotope measurements were made using a Trace GC-ultra gas chromatograph attached to the ThermoFisher Delta-V isotope ratio mass spectrometer (irMS) via a combustion and high temperature reduction interface, respectively (GC Isolink, ThermoFisher). The GC coupled to the irMS was equipped with a 30 m DB-5MS fused silica capillary column (i.d. 0.25 mm; 0.25 lm film thickness). The oven temperature was programmed from 70–300 °C at a rate of 4 °C/min followed by an isothermal period

of 15 min. Helium was used as carrier gas. The sample was not split and was injected at 275 °C. For calibration, a CO_2 standard gas was injected at the beginning and at the end of each analysis. Isotopic compositions are reported in the δ notation relative to the V-PDB (for C) standard. Analytical reproducibility (0.2‰ for $\delta^{13}C$) was controlled by repeated measurements of n-alkane standard mixes.

Measurements of stable C and H isotope composition of hydrocarbon gases were carried out using a Trace GC-ultra gas chromatograph attached to the ThermoFisher Delta-V isotope ratio mass spectrometer (IRMS) via a combustion and high temperature reduction interface, respectively (GC Isolink, ThermoFisher) (Hilkert et al., 1999). The GC coupled to the IRMS was equipped with a 25 m PoraPlot capillary column (i.d. 0.32 mm; 0.10 µm film thickness). The oven temperature was programmed from 30–180 °C at a rate of 5 °C/min followed by an isothermal period of 5 min. Helium was used as carrier gas. For calibration, a CO_2 or H_2 in-house standard gas was injected at the beginning and at the end of each analysis. Analytical reproducibility was controlled by repeated measurements of a calibration gas. $^2H/^1H$ and $^{13}C/^{12}C$ relative ratios are expressed relative to V-SMOW and V-PDB respectively (Coplen, 1995).

Sulphur: H_2S from natural gas was precipitated by washing the gas in a saturated solution of cadmium acetate. The precipitated cadmium sulphide was washed with distilled water, dried and sent to Stefano Bernasconi (ETH Zürich). At ETH Zürich the samples were wrapped in tin capsules with V_2O_5 and converted to SO_2 in a ThermoFisher Flash-EA 1112 coupled with a Conflo IV interface to a ThermoFisher Delta V isotope ratio mass spectrometer (IRMS). Isotope ratios are reported in the conventional δ-notation with respect to V-CDT (Vienna Canyon Diablo Troilite). The method was calibrated with the reference materials IAEA –S-1 (δ34S = -0.3), IAEA –S-2 (δ34S = +22.67), IAEA –S-3 (δ34S = -32.55) Reproducibility of the measurements based on the repeated measurement of an internal standard is better than 0.2‰.

ICP-QQQ-MS - 16 oil samples have been selected together with extracts from two rock samples (Staatz 1, 2825.7; Zistersdorf ÜT 1, 5602.7) to determine concentrations of the following trace elements: Mg, P, S, K, Ti, V, Cr, Mn, Fe, Co, Ni,

Cu, Zn, AS, Se, Rb, Sr, Ag, Cd, Ba, Re, Pb, U). The samples have been measured by C. Walkner at the chair of chemistry of the Montanuniversitaet Leoben.

The samples were digested using concentrated HNO_3 and 30% H_2O_2 applying the method described by Ricard et al. (2011). After the digestion the samples were diluted to decrease the acid concentration. Measurements were performed using the method described by Walkner et al. (2016) appling a Agilent 8800 Triple Quadrupole ICP-MS equipped with a MicroMist nebulizer, a Peltier-cooled Scott-type spray chamber and nickel sampler and skimmer cones. O_2 and NH_3 were used as collision/reaction gases.

5. Hydrocarbon Source Rocks

Bulk geochemical parameters are listed Appendix II, while mineralogical and maceral compositions are summarized in Appendices III and IV.

5.1 Results

5.1.1 Upper Jurassic source rocks (Mikulov Fm., Falkenstein fm.)

Borehole Staatz 1 was selected as a key well for the Upper Jurassic source rocks, because 25 cores representing the Falkenstein and Mikulov formations (1950-3100 m) were available for investigations. Results from other boreholes are reported for comparison.

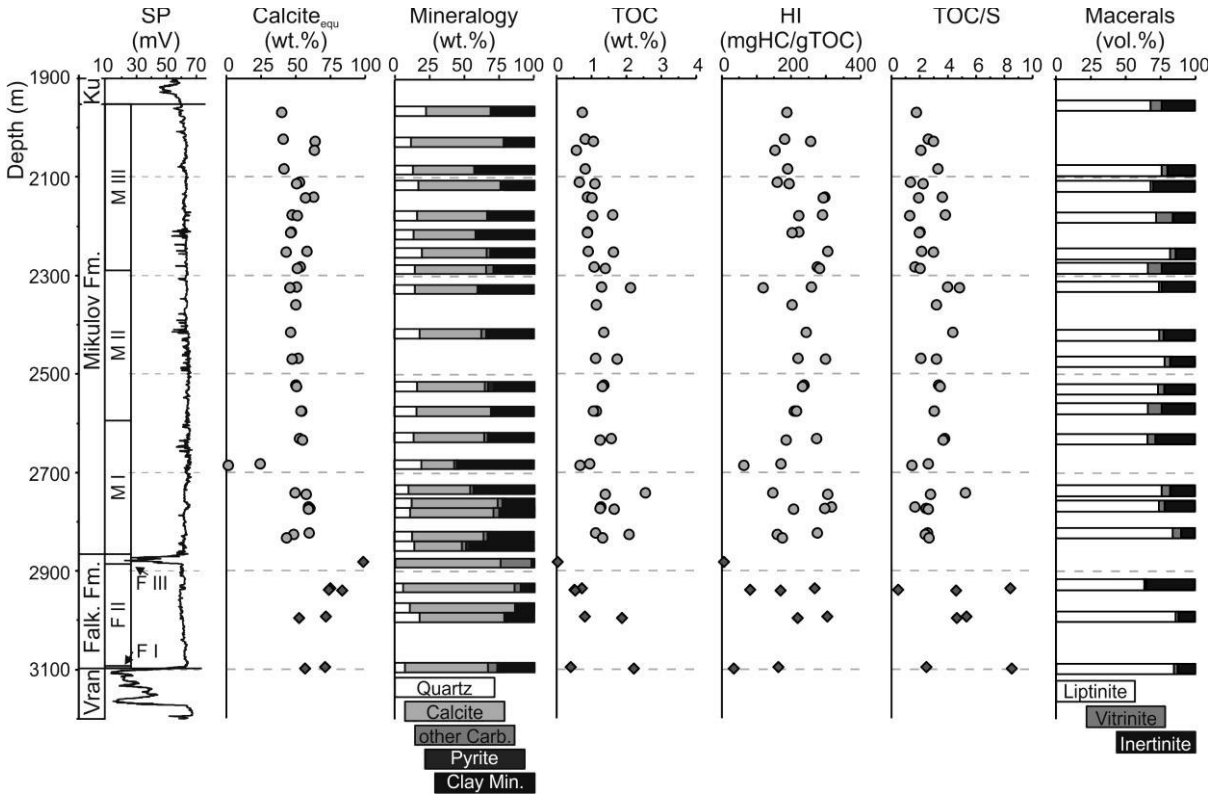

Fig. 16: Vertical variation of bulk geochemical, mineralogical and organic petrological data from the Falkenstein and Mikulov formations in well Staatz 1. SP – Spontaneous potential, Calcite$_{equ.}$ - Calcite equivalent, TOC – Total organic carbon, HI – Hydrogen Index, S – Total sulphur.

5.1.1.1 Lithology

The Falkenstein Formation in borehole Staatz 1 (2848-3098 m) is composed of marls and marly limestones and includes a calciturbidite near its top. Based on thin section microscopy, the Falkenstein Formation is subdivided into three layers (F1-3).

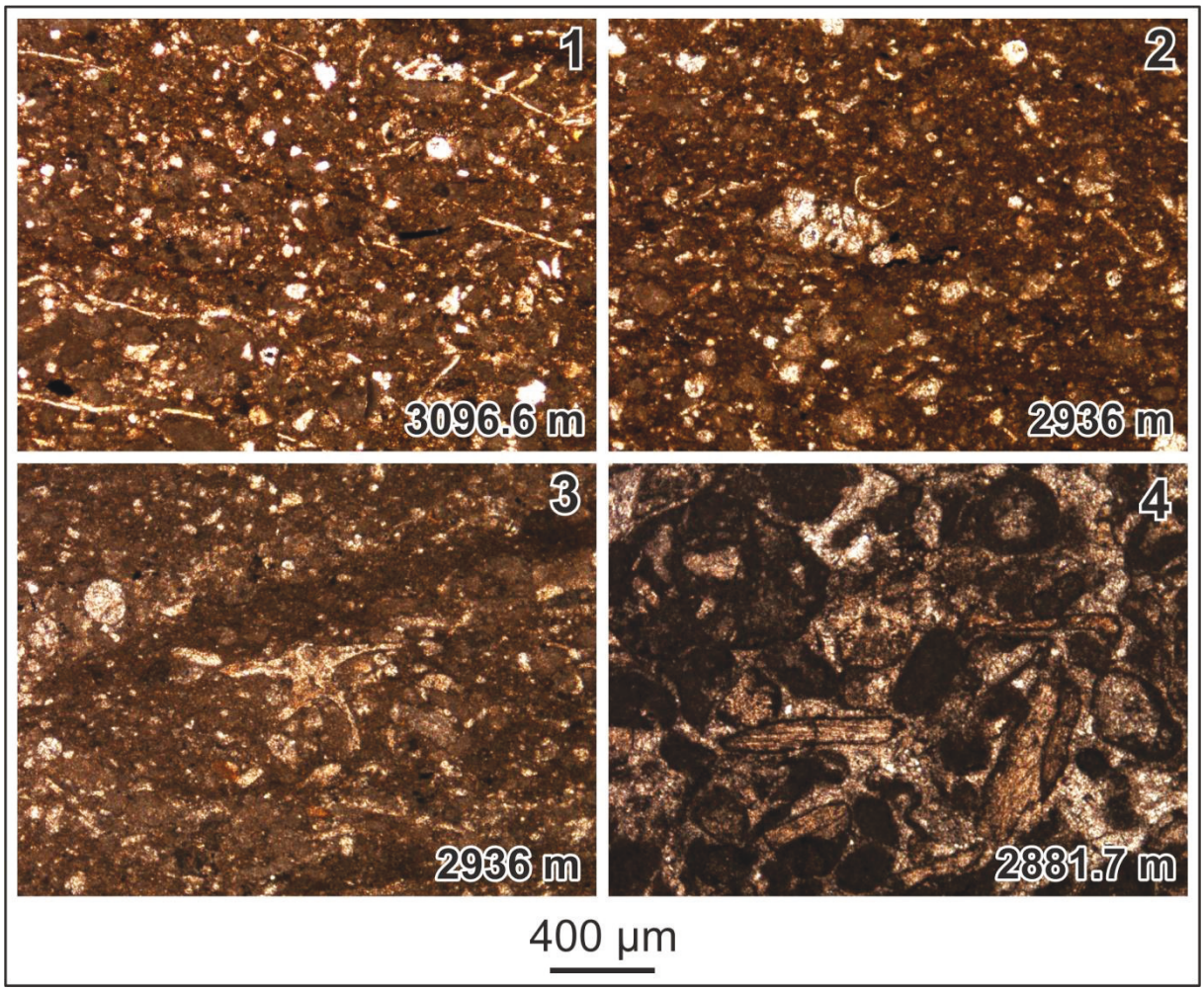

Fig. 17:Thin section photomicrographs from the Falkenstein Formation. All photomicrographs are from Staatz 1. 1- Clayey micritic and organic-rich limestone with recrystallized radiolarians, quartz clasts and *Bositra* shells, bioturbated in layer F1. The occurrence of Bositra shells indicates at least a latest Middle Jurassic age of this part of the succession (compare Fig. 7). 2- Textularid formanifera in a bioturbated clayey and organic-rich marly limestone in layer F2. Beside some recrystallized limestone fragments broken shell fragments occur. Micrite clasts occur commonly. 3- Clayey micritic and organic-rich limestone with *Saccocoma* sp. indicating a late Oxfordian to Kimmeridgian age for layer F2 of the succession. 4- Calcareous resediment with components from the westward adjacent shallow-water carbonate ?platform of layer F3. Most components have a micritic envelope.

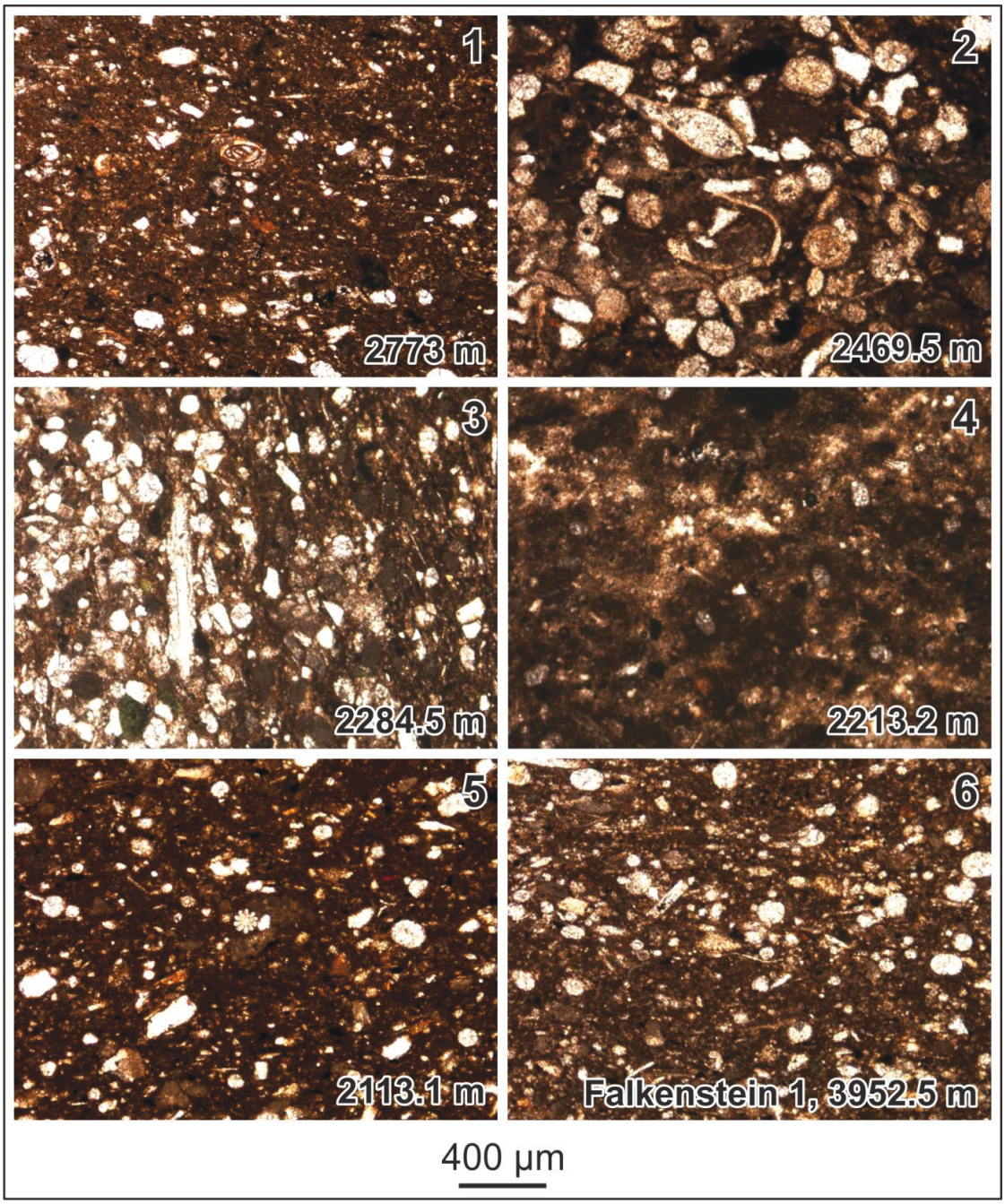

Fig. 17: Thin section photomicrographs from the Mikulov Formation from Staatz 1. 1- Clayey micritic and organic-rich marlstone with quartz clasts, few spicules and a benthic foraminifera in layer M1. 2- Recrystallized organisms with a micritic infill. The shape of the recrystallized parts of these organisms is oriented all in the same direction indicating a sessile organism in layer M2. 3- Graded turbiditic layer with quartz, carbonate and glauconite clasts. This microphotograph is clockwise 90° rotated. 4- Cloudy fabric of a micritic marly limestone with few quartz clasts, slightly silicified. 5- Bioturbated organic-rich clayey wackestone. Fragments of echinoderms beside quartz grains and recrystallized calcite clasts indicating provenance of the clasts from the continental hinterland and shallower depositional realm. 6- Clayey slightly silicified spicula- and radiolaria-bearing wackestone with rare shell fragments.

The base of the Falkenstein Formation (layer F1) is formed by a thin layer with alternations of bioturbated and non-bioturbated wackestones. It is composed from micrite, clay and abundant fossils, comprising crinoidea, calcitic recrystallized siliceous sponge needles and Bositra sp. (Fig. 17-1) indicating a latest Middle Jurassic age. According to XRD investigations, the clay content of the basal layer F1 is about 25 wt.%. Minor amounts of quartz and Fe-rich dolomite (or Mg-rich ankerite) are also present.

The main part of the Falkenstein Formation (layer F2) is characterized by a lower input of detrital material (clay minerals < 20 %) and a smaller average grain size. Beside sponge spicules, radiolarians and foraminifera occur in layer F2. Bioturbation is not observed. Saccocoma sp. at a depth of 2936 m (Fig. 17-2-3) indicates at least a ?late Oxfordian-?Kimmeridgian age for the succession.

Layer F3 represents the calciturbidite near the top of the Falkenstein Formation. It contains rounded micritic material derived from shallow water environments and occasionally some foraminifera. The dolomite percentage in F3 (~20 wt.%) is higher than in any other layer Evidence for calcite solution and incrustation is observed near the top of this layer (Fig. 17-4).

The overlying Mikulov Formation (2848-1950 m) comprises marls and a thin shale layer. Similar to the Falkenstein Formation, it is subdivided into three layers (M1-3). Layer M1 is dominated by significant amounts of clay and mud, which have been deposited together with fine detrital material of biogenic origin. A shale layer occurs in the upper part of layer M1 and is characterized by abundant kaolinite (Fig. 16). Glauconite is present in minor amounts in all thin sections. It is dominated by dark green peletoidal shapes and subordinate light green detrital grains. Foraminifera (Fig. 18-1) and serpulide worms are present, but deep bioturbation is missing. This fits with dysoxic conditions. Apart from foraminifera, the fossil record comprises radiolarians, bryozoa, some crinoids, calcitic recrystallized sponge needles and thick shelled bivalvia. In the upper part of this section crinoids tend to get bigger and shells are incrusted, which may record the formation of a hard ground (Fig. 18-2). Rocks with an identical facies in well Falkenstein 1 (3952 m, see Fig. 18-6) have been dated as Tithonian based on ammonites (*L. Krystyn* in Wessely, 2006).

Layer M2 differs from M1 by a bigger size of fossils (Fig. 18-8-9), which include some deep water corals, echinoidea spikes and remains of holothurian. Larger benthic fossils support the formation of hard grounds.

The upper part of the Mikulov Formation (layer M3) contains a significant amount of quartz grains. Consequently the carbonate content is typically lower than in underlying layers. The fossil record has a low diversity and includes sponge needles, deep water? corals and the remains of echinodermata. The sample at 2213.2 m depth is strongly silicified (Fig. 18-5). Within this section some semi-lithified slides and bioturbation structures can be found. The top of layer V is formed by a turbidite.

Carbonate minerals form the main constituent of the Mikulov Formation. Electron microprobe images reveal that apart from fossils (round, homogenous grains), diagenetic carbonate phases (angular, zoned grains) contribute significantly to the total carbonate content. The core zone of diagenetic carbonate is often iron-free dolomite, whereas the middle and outer zones are formed by iron-rich dolomite and iron- and magnesium-rich calcite, respectively (Fig. 19).

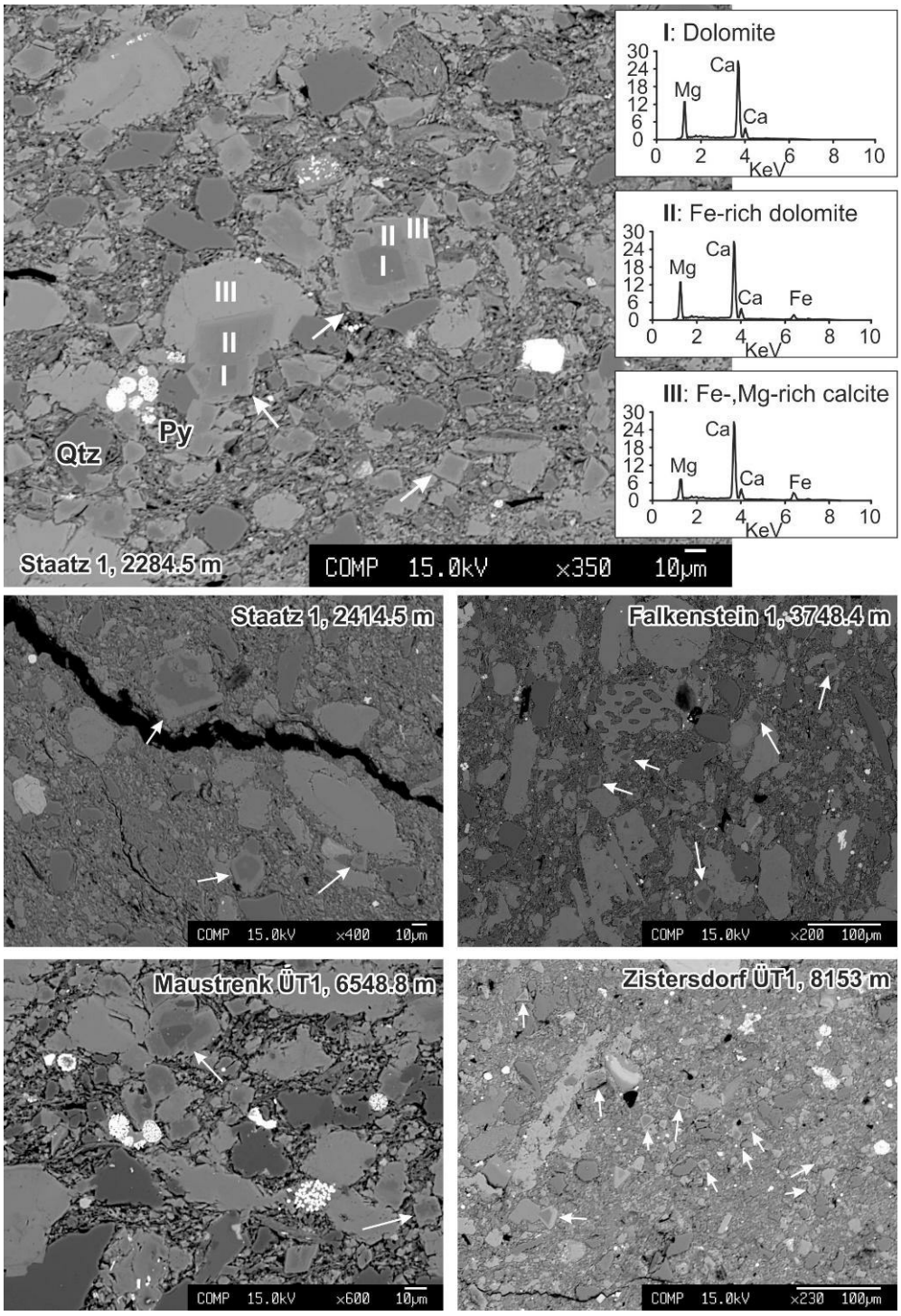

Fig. 19: EDX images displaying angular, zoned carbonate grains (arrows). EDX spectra (X-axis: absorbed energy, Y-axis: cps) identify the carbonate phases in sample Staatz 1 (2284.5 m) as dolomite (I), Fe-rich dolomite (II) and Fe-, Mg-rich calcite (III). Similar grains are found in all samples from Staatz 1 (2284.5 m, 2414.5 m), Falkenstein 1 (3748.4 m), Maustrenk ÜT1 (6548.8 m) and Zisterdorf ÜT1 (8153 m).

5.1.1.2 Calcareous Nannoplankton

Calcareous nannoplankton was determined for samples from Staatz 1 in order to provide additional age constraints. The calcareous nannofossil assemblages (Fig. 20) contain moderate to poorly preserved specimens, with very low diversity and abundance. A total number of 14 species were identified. The assemblages are dominated by species belonging to the Watznaueriaceae and Nannoconaceae families, which in alphabetical order are: *Cyclagelosphaera deflandrei*, *C. cf. jiangii*, *C. margerelii*, *Lotharingius contractus*, *L. velatus*, *Lotharingius* sp*., Nannoconus* sp., *Watznaueria barnesiae*, *W. britannica*, *W. communis*, *W. fossacincta*, *W. manivitae*, *W. ovata* and *Watznaueria* sp.

Regarding the calcareous nannofossils biostratigraphy, the main problem is related to the lack of nannofossil index species characteristic for the investigated interval. The most abundant species are the long-ranging taxa *W. britannica* (Fig. 20-5, 15), *W. barnesiae* (Fig. 20-13), *C. margerelii* (Fig. 20-1, 2, 15, 21), followed by *L. contractus* (Fig. 20-3, 4, 6, 9-10, 11-12, 23) and *W. communis (*Fig. 20-24), all with their first occurrence (FO) in the lower stages of the lower Middle Jurassic. Many of the specimens, due to poor preservation, were identified only at genus level and were placed under the *Watznaueria* sp. description. Less abundant, but present in all investigated samples are *Lotharingius* sp. (Fig. 20-7, 20), *W. fossacincta* (Fig. 20-19) and *W. manivitae* (Fig. 20-18). Very rare appearances have the following species: *C. deflandrei* (Fig. 20-17), *C. cf. jiangii* (Fig. 20-8), *W. ovata, L. velatus* (Fig. 20-22) and *Nannoconus* sp. (Fig. 20-14).

Correlation of the investigated material to the boreal (Germany, Great Britain, northern France) calcareous nannofossil zones and subzones of Bown and Cooper (1998) is not very precise, due to the absence of index species for the interval Oxfordian – Tithonian. The lithostratigraphical succession, based on the existing literature, spans the interval belonging to the standard nannofossil zones NJ14 (*Stephanolithion bigotii maximum* Zone, late Callovian) to NJ17 (*Stephanolithion atmetos*, middle Tithonian). The samples at 2996.5 and 2938.2 m depth (layer F2) yield the highest amount of nannofossils. The assemblage from sample 2996.5 m might suggest a late Callovian age, which fits with the occurrence of Bositra in this sample.

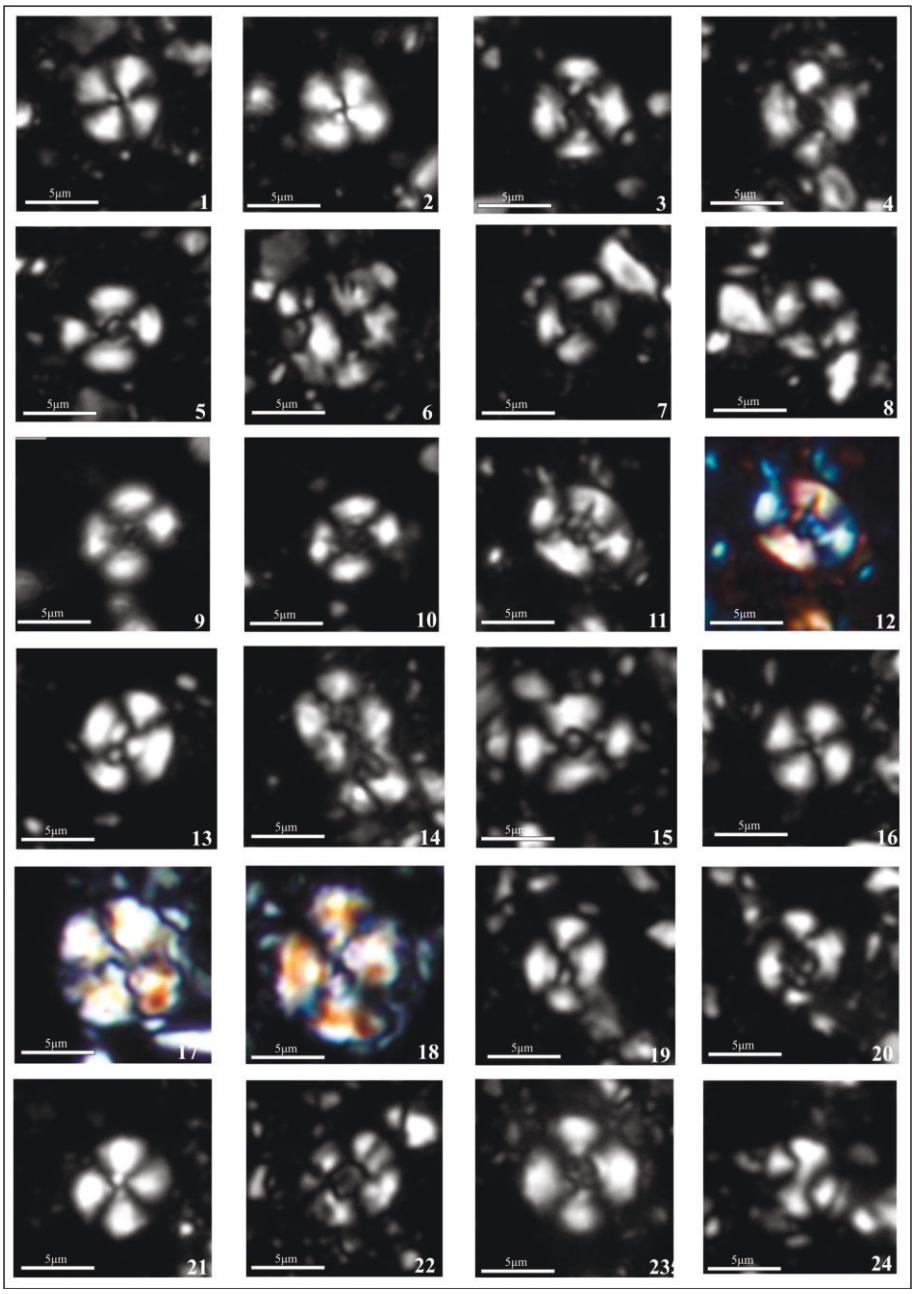

Fig. 20: Calcareous nannoplankton in well Staatz 1. All pictures have been taken in cross-polarized light. A gypsum plate has been used for pictures 12, 17, 18.

1,2- *Cyclagelosphaera margerelii* (2026.5 m); 3,4,6- *Lotharingius contractus* (2026.5m); 5- *Watznaueria britannica* (2026.5 m); 7- *Lotharingius* sp. (2026.5 m); 8- *Cyclagelosphaera cf. jiangii* (2938.2 m); 9,10- *Lotharingius contractus* (2469.5 m); 11,12- *Lotharingius contractus* (2938.2 m); 13- *Watznaueria barnesiae* (2996.5 m); 14- *Nannoconus sp.* (2996.5 m); 15- *Watznaueria britannica* (2996.5 m); 16- *Cyclagelosphaera margerelii* (2996.5 m); 17- *Cyclagelosphaera deflandrei* (2938.2 m); 18- *Watznaueria manivitiae* (2996.5 m); 19- *Watznaueria fossacincta* (2996.5 m); 20- *Lotharingius sp*. (2996.5 m); 21- *Cyclagelosphaera margerelii* (2938.2 m); 22- *Lotharingius velatus* (2996.5 m); 23- *Lotharingius contractus* (2996.5 m); 24- *Watznaueria communis* (2938.2 m).

5.1.1.3 Bulk geochemical parameters

Average T_{max} values of both, the Falkenstein and the Mikulov formations are 431°C, indicating that the organic matter is immature. TOC contents range from 0.3 to 2.2 wt.% in the Falkenstein Formation (average: 0.9 wt.%) and from 0.6 to 2.5 wt.% in the Mikulov Formation (average: 1.2 wt.%). In the upper part of the Mikulov Formation (layer M3) TOC contents decrease slightly upwards (Fig. 16). HI values range from 34 to 473 mgHC/gTOC, indicating the presence of type III to II kerogen. Although average HI values are slightly lower in the Falkenstein Formation (177 mgHC/gTOC) than in the Mikulov Formation (230 mgHC/gTOC), no clear vertical trends are visible. The average TOC/S ratio is 3.1, close to the value of 2.8, which is characteristic for normal marine environments (Berner and Raiswell, 1984).

Similar TOC contents are observed for the Falkenstein (0.5-1.9 wt.%; average 1.2 wt.%) and Mikulov formations (0.4-3.3 wt.%; average 1.5 wt.%) in other wells. Relatively high HI values (300-400 mgHC/gTOC) are observed in Falkenstein Formation from boreholes Waschberg 1, Wildendürnbach K4 and Falkenstein 1 (Appendix II). In contrast, obviously HI is significantly reduced (0-170 mgHC/gTOC, Fig. 21) in samples from deep wells (Aderklaa UT1, Maustrenk ÜT1a, Zistersdorf ÜT1/2a), which recovered overmature Mikulov Formation from depths exceeding 5500 m. It is worth noting that these rocks, despite of their high maturity, partly contain higher TOC contents (up to 3.3 wt. %) than shallow samples from the western part of the study area. Clearly the original TOC was even higher. Although only few samples from great depth have been analyzed, this may imply an eastward increase in original TOC contents.

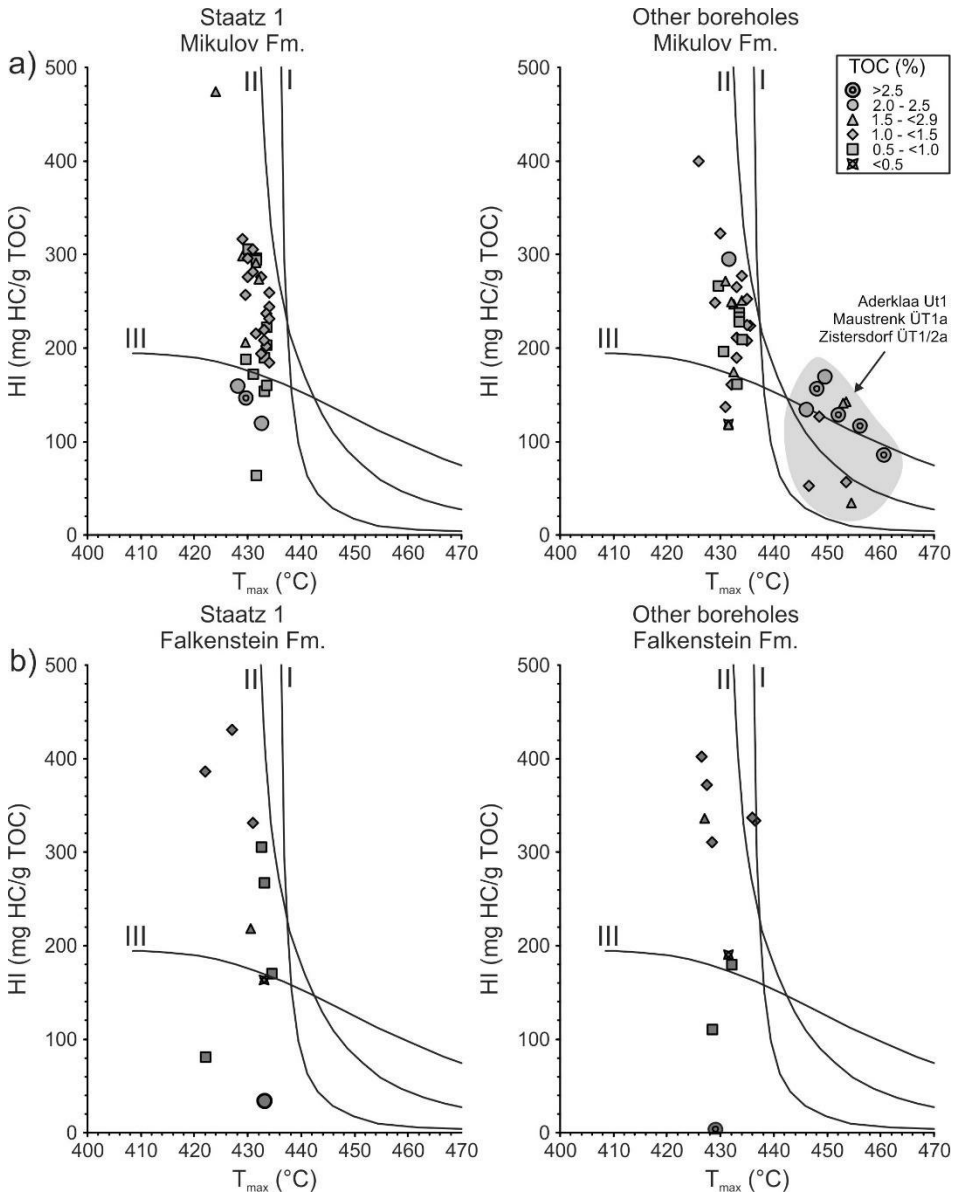

Fig. 21: Plot of Hydrogen Index (HI) versus Tmax (according to Espitalie et al., 1984) outlining the kerogen-type and source potential. a) Mikulov Formation in key well Staatz 1 and in other borehole. HI values of deeply buried Aderklaa, Maustrenk and Zistersdorf samples are reduced due to increased maturity. b) Falkenstein Formation in key well Staatz 1 and in other borehole.

5.1.1.4 Organic petrology

Samples from the Falkenstein Formation and the Mikulov Formation consist of a mixture of liptinites (66-86 vol.%), inertinites (10-35 vol.%) and minor vitrinite (1-12% vol.%, Fig.22). Liptinites macerals include lamalginite and minor telalginite (Fig. 23). Similar maceral compositions were also determined by Gerslova (2015) for the Mikulov Formation in the Czech part of the basin. Rare vitrinite particles are often

rounded and display elevated reflectivity (~0.9 %Rr), suggesting that these grains are of detrital origin. Therefore, it was impossible to measure vitrinite reflectance of an indigenous vitrinite population in Staatz 1 (and other boreholes with immature Malmian rocks).

Vitrinite reflectance of overmature samples from deep wells increases from 1.46%Rr at 5600 m to 2.53%Rr at 8500 m.

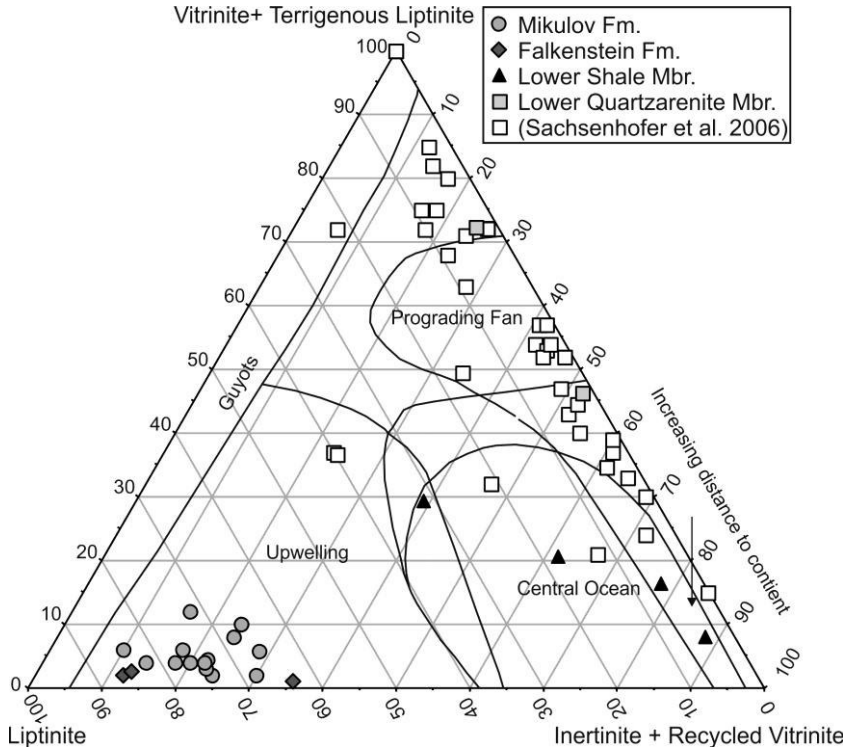

Fig. 22: Distribution of vitrinite, liptinite, and inertinite macerals superimposed with typical compositions for different sedimentary environments defined by Littke and Sachsenhofer (1994). Samples of the Mikulov and Falkenstein formations plot in the area of coastal upwelling and samples from the Gresten Formation into the position of prograding fans. Data from the Lower Quartzarenite Member is from this study and Sachsenhofer et al. (2006).

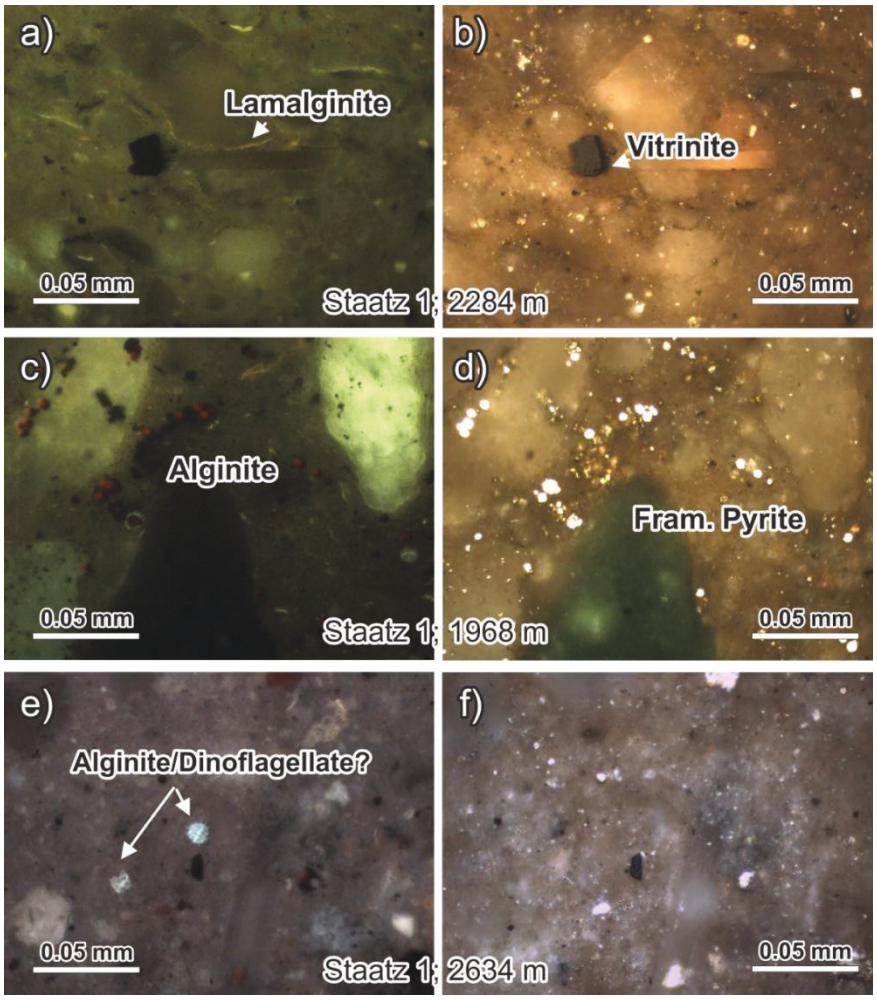

Fig. 23: Blue and white light photomicrographs of the Mikulov Formation from well Staatz 1 (a, b: 2284 m; c, d: 1968 m; e, f: 2634 m). The organic matter is dominated by different liptinite macerals. Subrounded vitrinite grains reaveal their reworked origin.

5.1.1.5 Extractable organic matter

Eight samples from the Falkenstein Formation and 41 samples from the Mikulov Formation are included in the present study (Appendix VII). Typical gas chromatograms of immature and (over-)mature Mikulov Formation are shown in Fig. 24. Typical fingerprints of steranes (m/z = 217+218) and hopanes (m/z = 191) are presented in Fig. 25.

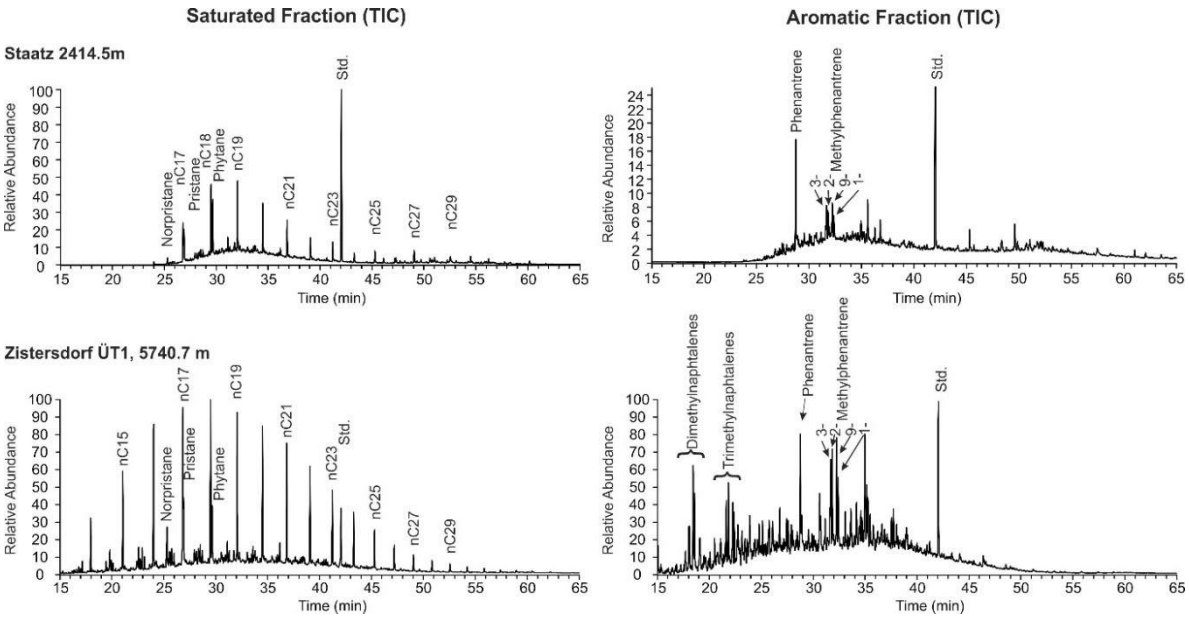

Fig. 24: Gas chromatograms of the saturated and aromatic hydrocarbon fractions of immature (Staatz 1, 2414.5 m) and (over)mature (Zistersdorf ÜT1, 5740.7 m) Mikulov Formation. Std – standard

Biomarker data for well Staatz 1 are plotted versus depth in Fig. 26. As both formations yielded similar results, the Falkenstein and Mikulov formations are discussed together.

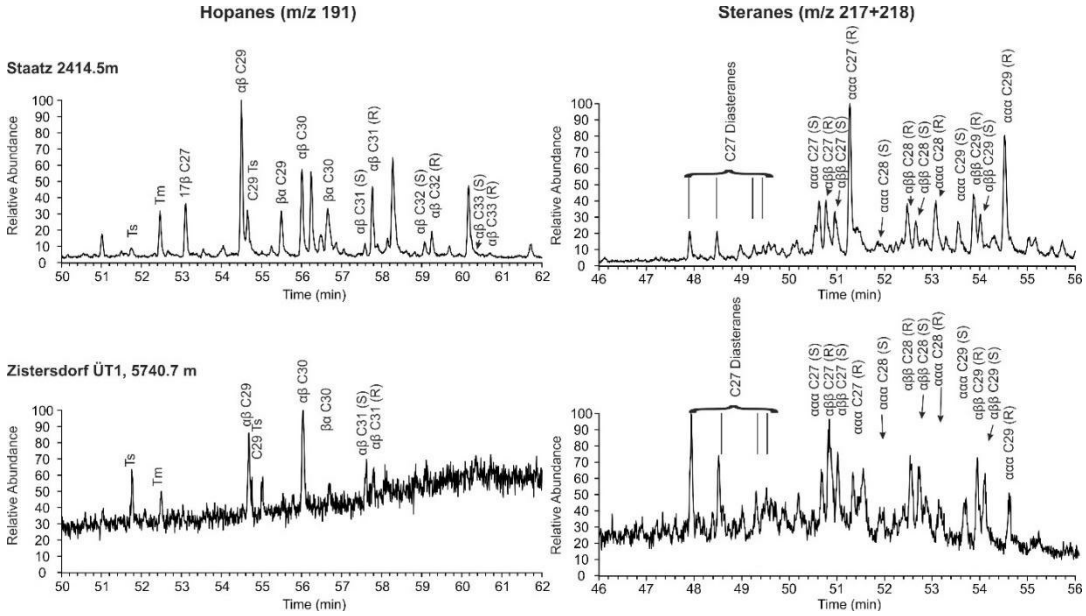

Fig. 25: Hopanes and steranes patterns of immature (Staatz 1, 2414.5 m) and (over)mature (Zistersdorf ÜT1, 5740.7 m) Mikulov Formation.

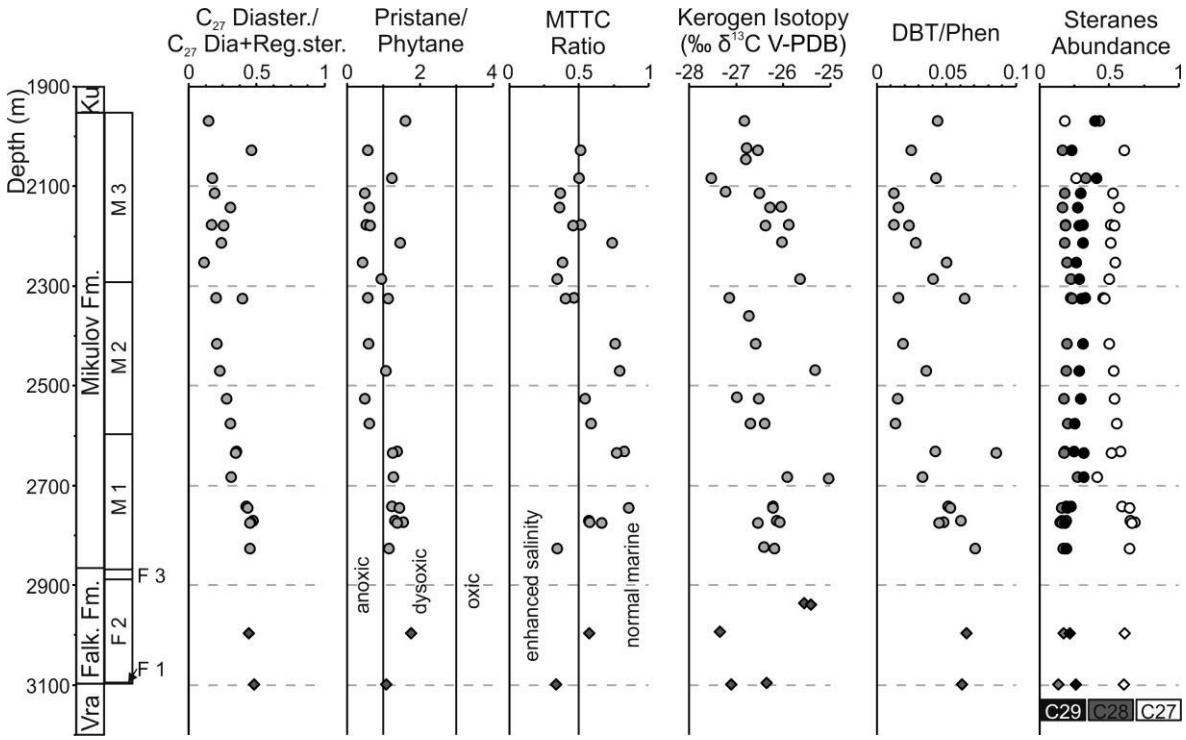

Fig. 26: Vertical variation of biomarker ratios, abundance of C_{27}, C_{28} and C_{29} steranes and stable carbon isotope ratios of kerogen in well Staatz 1. C_{27} Diaster - C_{27} diasteranes; Reg. - C_{27} regular steranes; MTTC ratio - ratio of 5,7,8-trimethylchroman/total MTTC; DBT – dibenzothiophene; Phen - phenantrene.

Straight chain alkanes, isoprenoids – The saturated hydrocarbon fractions of Malmian samples in well Staatz 1 are dominated by n-alkanes ranging up to C_{36}. The highest abundance (40-85%) is found within the C_{15-19} group, which are interpreted as remains of algae (Cranwell, 1977). The second most abundant group (10-40%) are the C_{21-25} alkanes which derive from aquatic macrophytes (Ficken et al., 2000). Long-chain alkanes (C_{26-36}) make up less than 20 % of the alkanes series. Odd-numbered n-alkanes are dominating over even-numbered ones. This also applies for immature samples from other boreholes. In contrast, samples with increased thermal maturity from wells Zistersdorf ÜT1/2a and Maustrenk ÜT1 display a balanced equilibrium (carbon preference index [CPI] = 1.09-1.13, Bryan and Evans, 1961).

Isoprenoids, including pristane (Pr) and phytane (Ph), are present within all samples. Pristane/phytane (Pr/Ph) ratios are commonly used as a redox indicator. According to Didyk et al. (1978), Pr/Ph ratios <1.0 indicate anaerobic conditions whereas values >1.0 reflect suboxic to oxic environments. Pr/Ph ratios in the Falkenstein and Mikulov formations ranging from 0.4 to 2.0 and suggest that the Falkenstein Formation in well

Staatz 1 was deposited under dysoxic conditions. Dysoxic conditions also prevailed during deposition of layer M1 of the Mikulov Formation. In contrast, layers M2 and M3 of the Mikulov Formation were deposited in anoxic conditions.

The Pr/nC_{17} and Ph/nC_{18} ratios of immature samples of the Falkenstein and Mikulov formations are, typically for immature samples (Connan and Cassou, 1980), higher than 1.0 (Fig. 27). Samples displaying lower values originate from deeply buried, thermally higher mature samples from Aderklaa UT1, Falkenstein 1, Maustrenk ÜT1, Zistersdorf ÜT1/2/2a.

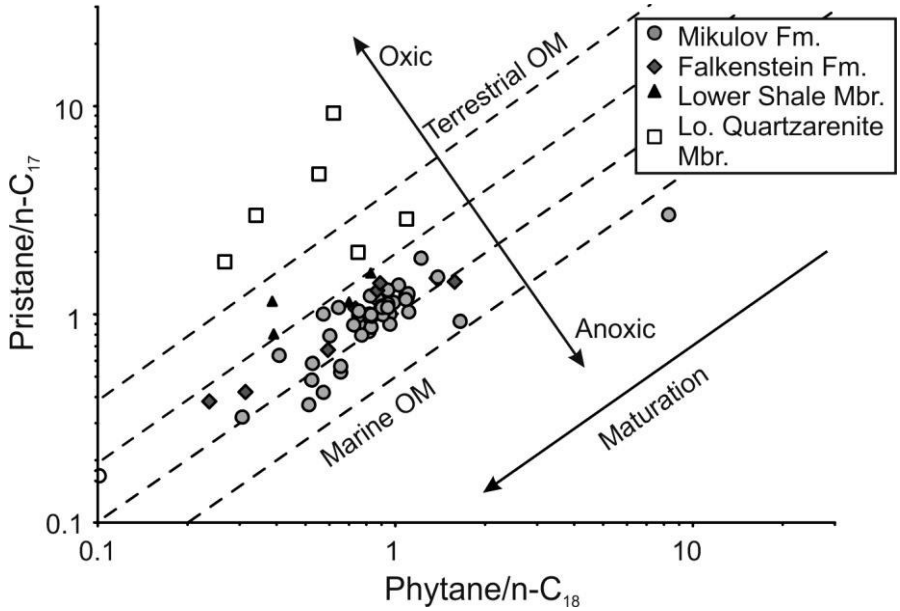

Fig. 27: Crossplot of the phytane/nC_{18} ratio versus the pristane/nC_{17} ratio (according to Connan and Cassou, 1980). Data of the Lower Quartzarenite Member is from Sachsenhofer et al. (2006).

Steroids - Except samples from well Zistersdorf and Maustrenk, which originate from more than 5500 m depth, all samples display a dominance of 5α,14α,17α(H) steranes over 5α,14β,17β(H) steranes.

In samples from well Staatz 1, C_{27} steranes are typically more abundant (30-60 %) than C_{29} (20-40%) and C_{28} (15-30 %) steranes (Figs. 26, 28). These values suggest a higher input of algal organic matter than of higher land plants (Volkman, 1986). The relative amounts of C_{28} and C_{29} steranes show similar vertical trends within the Falkenstin and Mikulov Formation, in well Staatz 1, whereas C_{27} percentages trends are reversed. The ratio between C_{28} and C_{29} steranes range from 0.68 to 1.16 and,

therefore, are in the range of typical Jurassic source rocks (Grantham and Wakefield, 1988). The previous observations also apply for immature Malmian samples from other boreholes.

C_{27} Diasteranes are present in varying concentrations. Because the diasteranes/steranes ratio shows a positive relation with carbonate contents in well Staatz 1 (Fig. 29), the increase in content relative to C_{27} steranes with depth in this well (Fig. 26) is most probably due to variations in clay content and the clay catalytic effect (Sieskind et al., 1979).

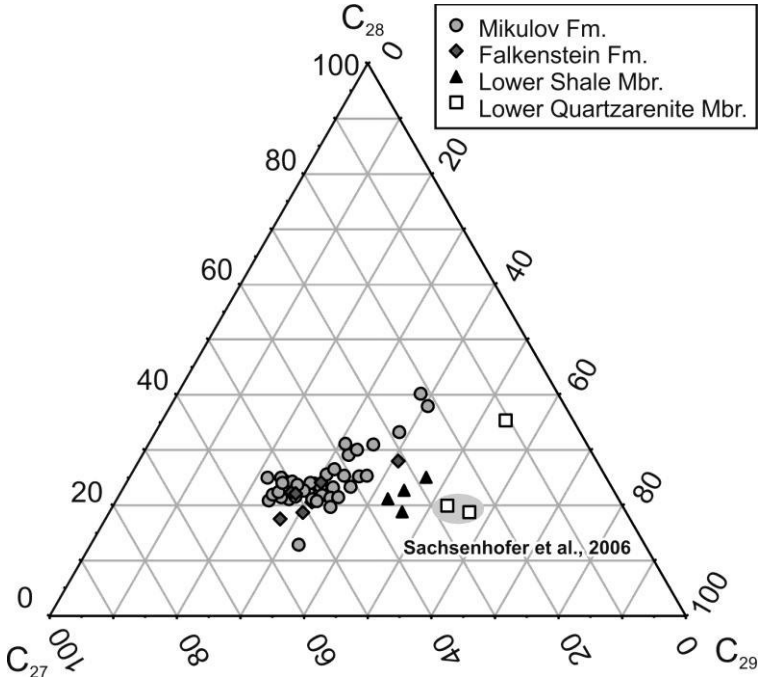

Fig. 28: Distribution of C_{27}-, C_{28}-, and C_{29}-steranes. The Lower Quartzarenite Member, the Lower Shale Member and the Mikulov and Falkenstein formations plot in different fields. Data of the Lower Quartzarenite Member is from this study and Sachsenhofer et al. (2006).

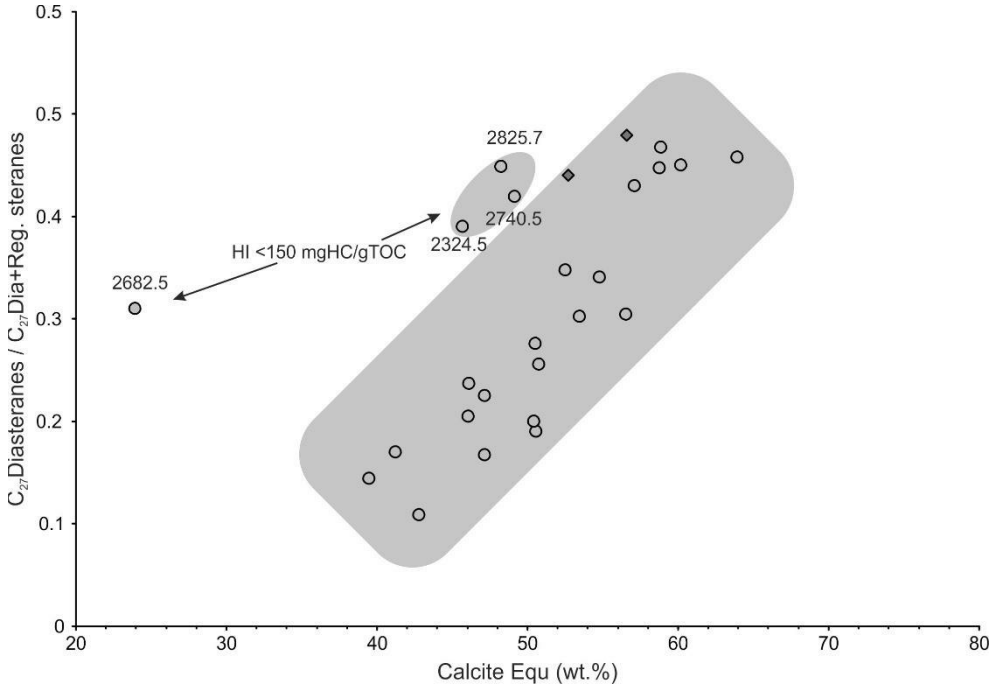

Fig. 29: Cross-plot of carbonate content (calcite equivalents) versus the ratio of the C_{27}-diasteranes and the sum of C_{27} (dia- and regular steranes). The plot indicates an increased clay catalytic effect for low-carbonte samples. Samples with a very low HI (<150 mgHC/g TOC) do not follow this trend.

The S/(S+R) isomers ratio of C_{29} steranes is a maturity parameter. It ranges from 0.15 to 0.25 in Staatz 1 without a clear depth trend. The equilibrium value of 0.55, corresponding to a vitrinite reflectance of ~0.8%Rr (Mackenzie and Maxwell, 1981), is reached at about at ~5000 m depth (Fig. 38).

Hopanoides – Hopanes occur in minor amounts within all Malmian samples. According to Peters et al. (2005), the ratio of the αβC_{31}R hopane against the αβ C_{30} hopane is a useful parameter to differentiate marine (>0.25) and lacustrine (<0.25) environments of deposition. As expected, marine values (>0.49) are observed both for the Falkenstein and Mikulov formations. High steroids/hopanoids ratios (>0.4) indicate a marine, algal-dominated organic facies (Mackenzie, 1984). Gammacerane, a highly specific marker for salinity stratification (Sinninghe Damsté et al., 1995), has not been detected.

The S/(S+R) isomers ratio of C_{31} hopanes is a maturity parameter for samples with low maturity. In Staatz 1 the ratios vary between 0.1 and 0.2 above 2300 m depth and increases downwards to 0.4 at ~3000 m depth. The equilibrium value of 0.60, corresponding to a vitrinite reflectance of ~0.55 %Rr (Mackenzie and Maxwell, 1981), is reached in boreholes in the Vienna Basin are at about ~4000 m depth (Fig. 38).

The ratio of trisnorneohopane/(trisnorneohopane+trisnorhopane) (Ts/(Ts+Tm) shows little variation above 4500 m depth and increases significantly in deeply buried, overmature samples from wells Zistersdorf and Maustrenk.

Polycyclic aromatic hydrocarbons (PAHs) – Significant amounts of mono-, di-, and trimethylated naphthalenes could be detected in mature and overmature Malmian samples from wells Zistersdorf ÜT1 and Maustrenk ÜT1 (Fig. 24). In contrast, these compounds are rare in immature samples (<4000 m).

Phenanthrene and methylphenanthrenes could be found in all samples <6000 m depth. These compounds derive from a variety of non-specific precursors such as steroids and triterpenoids (Tissot and Welte, 1984). According to Radke and Welte (1983) the ratio between phenanthrene (Phen) and different methylated phenanthrenes (MP) is called Methylphenanthrene Index (MPI=$\frac{3MP+2MP}{Phen+9MP+1MP}$) and can be used as maturity parameter for rock extracts and crude oils. An empirical relationship was established for type III kerogen between MPI and vitrinite reflectance (calculated vitrinite reflectance, R_c) ($R_c = 0.6 * MPI + 0.4$), which is valid for the maturity interval between 0.55 and 1.35 %Rr (Radke et al., 1983). MPI values of shallow samples (< 4000 m depth) vary between 0.28 and 0.66 without depth trend, but increase downwards from 0.72 to 0.94 in the depth interval between 5600 and 6550 m. The R_c values (0.83 – 0.96 %R_c) are lower than measured vitrinite reflectance values.

The dibenzothiophene/phenanthrene (DBT/Ph) ratio assesses the availability of reduced sulphur for incorporation into organic matter (Hughes et al., 1995). In general the ratio in Malmian rock extracts is low (<0.2). The DBT/Ph ratios in Staatz 1 vary between 0.01 and 0.10. They decrease upwards in layer M1 and the lower part of layer M3 and are generally very low in layer M2.

Chromans – Although the origin of methylated 2-methyl-2-(trimethyltridecyl) chromans (MTTCs) is not clear (Sinninghe Damsté et al., 1993, Barakat and Rullkötter, 1997, Li et al., 1995), the concentration ratio of trimethylated MTTC to all MTTCs (Sinninghe Damsté et al., 1993) has widely been used for salinity reconstructions (Sinninghe Damsté et al., 1993, Barakat and Rullkötter, 1997). MTTC ratios of samples from well Staatz 1 range from 0.35 to 0.85. The vertical variation of MTTC ratios (Fig. 26) suggests that the upper part of layer M1 and the lower part of

layer M2 (2800-2350 m depth) was deposited under less saline conditions than the rest of the Malmian succession.

5.1.1.6 Stable Carbon isotope ratio

Stable carbon isotope ratios have been acquired from both, the kerogen as well as aliphatic and aromatic extract fractions. The stable carbon isotope ratios of the aliphatic and aromatic fraction have been used to distinguish marine and non-marine environments (Sofer, 1984). The $\delta^{13}C$ values range between -28.7 and -28.2‰ for the aliphatic fraction and between -25.2 and -28.6‰ for the aromatic fraction for the Falkenstein Formation and between -27.4 and -30.3‰ for the aliphatic fraction and between -25.3 and -28.8‰ for the aromatic fraction for the Mikulov Formation. A non-marine depositional environment for samples from the Mikulov Formation, suggested by Fig. 30, can be excluded.

The isotopic composition of kerogen is influenced by ^{13}C-content of the environment, isotope effects associated with assimilation of carbon, isotope effects during metabolism, cellular carbon budget and post deposition processes (Hayes, 1993, 2001). $\delta^{13}C$ values of the Falkenstein and Mikulov formations in well Staatz 1 show a wide scatter between -23.5 and -27.5‰ (Fig. 30, Appendix XI). The kerogen in layer M3 gets isotopically lighter from base to top.

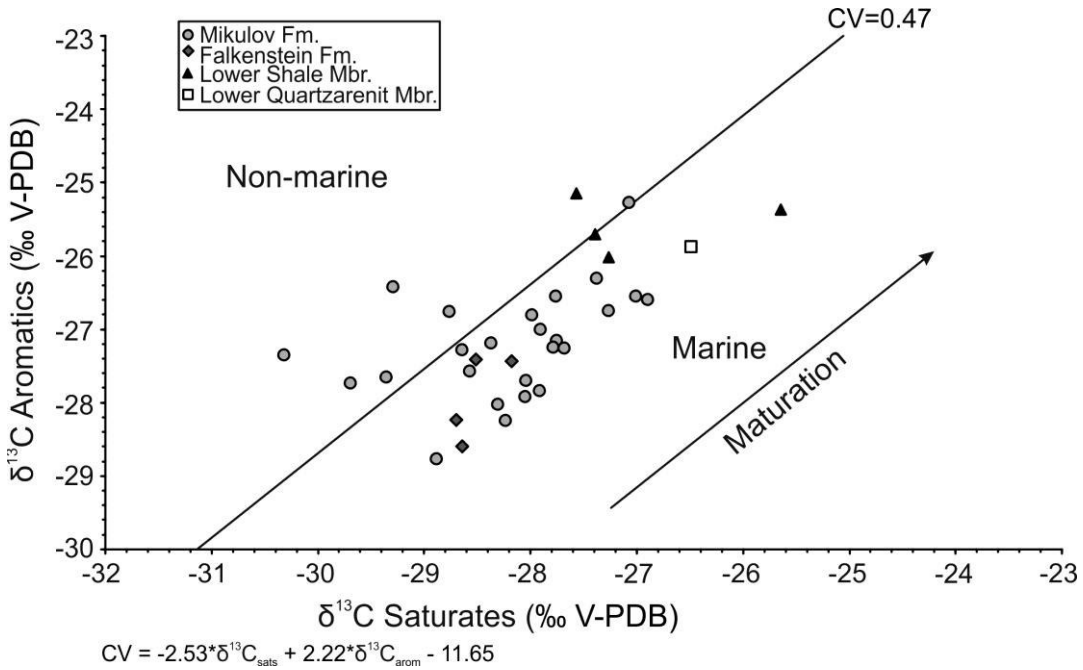

Fig. 30: Cross-plot of the stable carbon isotope ratio of the aliphatic and aromatic fraction (according to Sofer, 1984).

The compound specific stable carbon isotope ratio has been determined only from extracts originating from mature samples (Maustrenk ÜT1, 6546.7m and 6548.8m, Zisterdorf ÜT1, 5602.7m and 5740.7m). The maximum intensity signal for single compounds was obtained for n-alkanes in the range of nC_{17} up to nC_{22} (Fig. 31). In general it can be seen, that $\delta^{13}C$ values increase with decreasing chain length, which is reported as typical behavior of marine source rocks (Bjoroy et al., 1994).

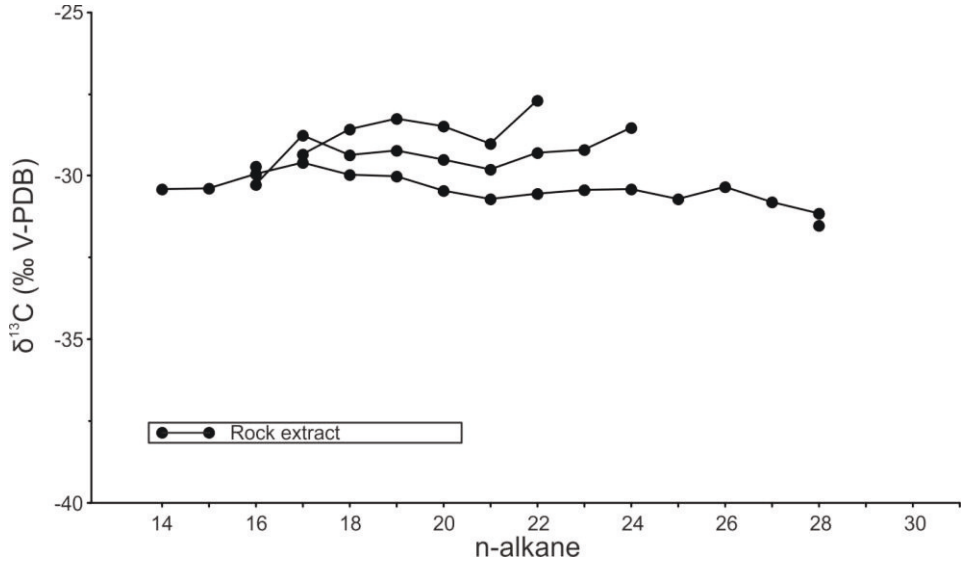

Fig. 31: Stable carbon isotope ratios of individual n-alkanes from source rocks extracts (Mikulov Fm.).

Interestingly, no increasingly negative $\delta^{13}C$ values from C_{21} upwards are observed, which would indicate a marine source (Murry et al., 1994). However this samples are overmature and probably therefore displaying too positive values.

5.1.1.7 Pyrolysis Gas Chromatography

One sample from the Falkenstein Formation and nine samples from the Mikulov Formation were selected for Py-GC measurements. Results from one additional sample from the Lower Shale Member are also presented in this section.

Based on the distribution of compound chain lengths (Horsfield, 1989), samples from the Mikulov and Falkenstein formations will generate low wax paraffinic-naphthenic-aromatic mixed oil (Fig. 32), whereas the sample from the Lower Shale Member will generate gas (or condensate). The triangular diagram contrasting nC_9, o-xylene and 2,3-dimethyl-thiophene (Eglinton et al., 1990) shows that all samples will generate hydrocarbons with low sulphur contents (Appendix V).

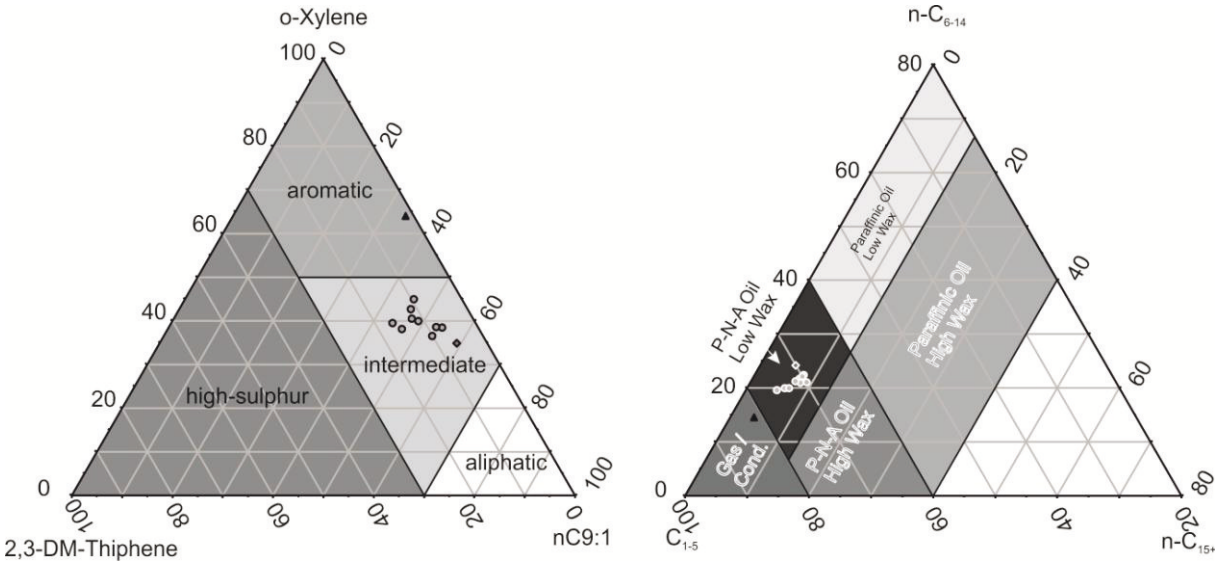

Fig. 32: Ternary diagrams illustrating the results from pyrolysis GC measurements: kerogen type characterization (according to Eglinton et al., 1990) and petroleum type characterization (according to Horsfield, 1989).

5.1.1.8 Trace element concentration

The trace element concentrations of two rock extracts have been measured to compare the results from immature,mature source rocks and oils. Interestingly, the trace element concentration is nearly a magnitude smaller in the mature sample Zisterdorf ÜT1 (5602.7 m MD) than compared to the immature sample from Staatz 1 (2825.7 m MD) (see Appendix X). Copper concentrations are not listed for the rock samples. This is due to the fact, that copper was used during the extraction to catch any elemental sulphur. Therefore the sulphur content refers to only chemically bound sulphur.

5.1.2 Gresten Formation

Coals and bituminous shales of the Lower Quartzarenite Member have been investigated by Sachsenhofer et al. (2006). Hence, main focus is put here on the Lower Shale Member and the Upper Quartzarenite Member. A few samples from the Lower Quartzarenite Member are included in the present study.

5.1.2.1 Bulk geochemical parameters and organic petrology

Tmax values of nine samples from the **Lower Quartzarenite Member** in borehole Porrau 2 are low (~420°C), indicating that the organic matter is immature. Coaly samples are characterized by TOC contents up to 27 wt.% and HI values up to 150 mgHC/gTOC indicating the presence of type III kerogen. The kerogen classification is supported by macerals assemblages dominated by vitrinite (46-72 vol.%.) and inertinite (52-26 vol.%; Figs. 22 and 35-e, f). Liptinite is rare. Similar maceral compositions have also been described by Sachsenhofer et al. (2006). TOC/S ratios exceed 2.8 significantly, which agrees with the non-marine depositional environment (Berner and Raiswell, 1984) of the Lower Quartzarenite Member.

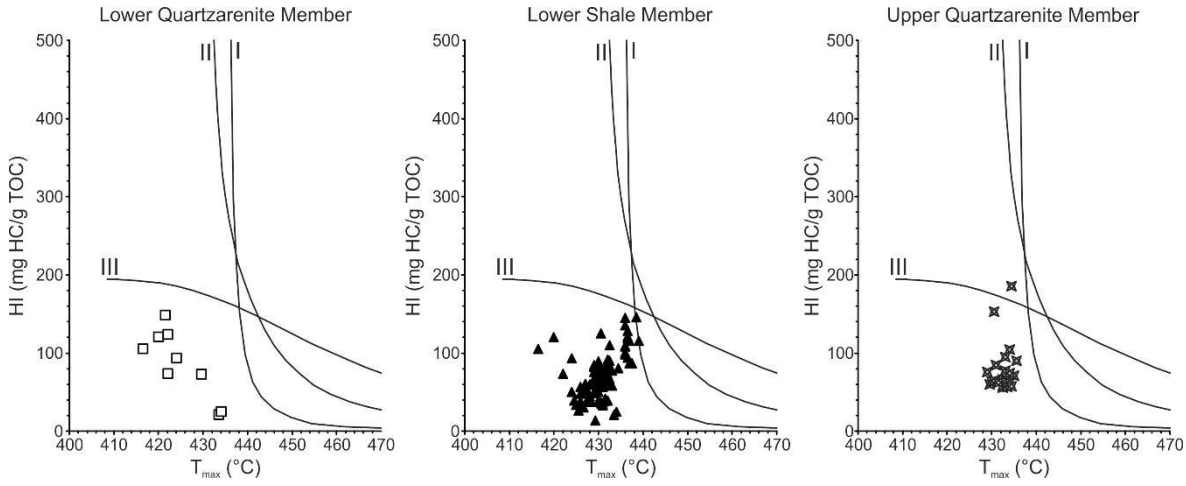

Fig. 33: Plot of Hydrogen Index versus Tmax (according to Espitalie et al., 1984) outlining the kerogen-type and source potential of different members of the Gresten Formation.

The **Lower Shale Member** has been investigated using a total of 107 cores samples from boreholes Porrau 2 (Fig. 34), Altenmarkt 1, Falkenstein 1, Hagenberg 3, Höflein 1, Roseldorf Tief 2, and Klement 1, Staatz 1. With the exception of samples from Falkenstein 1 (4490 - 4500 m depth), which are marginally mature (Tmax: 436-439 °C), all samples are immature (Tmax: <435 °C). TOC contents vary between 0.5 and 2.5 wt.% (average 1.6 wt.%). HI values (9 - 148 mg HC/g TOC) indicate a mixture of type III and IV kerogen (Fig. 33). Maceral composition of four samples from well Porrau 2 has been quantified and shows that low HI values are due to abundant inertinite macerals (62 - 88 vol.%) and 8 to 20 vol.% of vitrinite (Fig. 22 and 36-c, d), which based on elevated reflectance values (0.6-1.3 %Rr) is redeposited. Liptinite macerals (mainly liptodetrinite) are rare. The S content is generally moderate with a values between 0.2 and 2.8 wt.% (av. 1.3 wt.%).

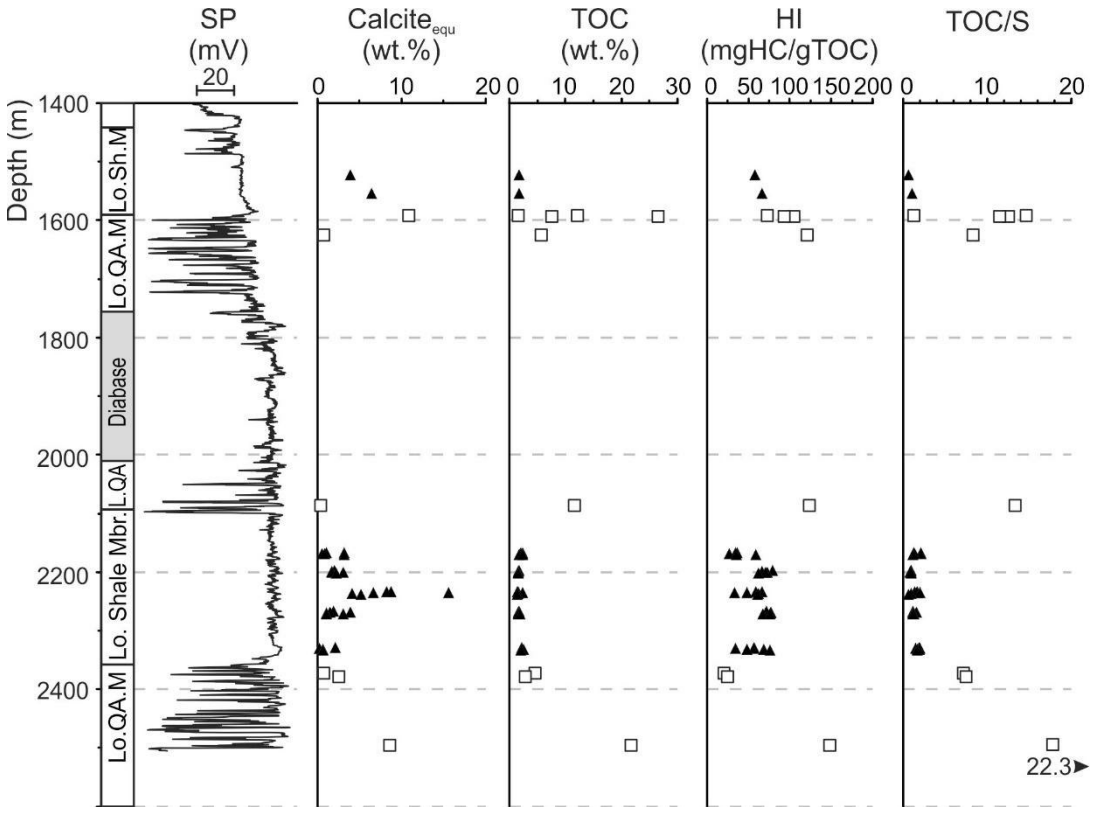

Fig. 34: Vertical variation of bulk parameters of the Lower Quartzarenite Member (L.QA.M) and the Lower Shale Member of the Gresten Formation in well Porrau 2. SP – Spontaneous potential, TOC –Total organic carbon, HI –Hydrogen Index, Calcite$_{equ.}$ - calcite equivalent, S - total sulphur. Stratigraphy is taken from Wessely (2006).

The **Upper Quartzarenite Member** was studied in well Stockerau Ost 1 using five samples from two cores (3828 - 3833 m; 4208 - 4212 m) and 16 cutting samples representing shaly intervals interlayering with deltaic sandstones. A coal layer, at least 20 cm thick, occurs at the base of the lower core. The TOC content of a coal sample is 80 wt.%. In the rest of the samples the TOC content varies between 1.0 and 2.6 wt.% and decreases upwards (Fig. 35). The HI values (56 - 185 mgHC/g TOC) indicate the presence of type III kerogen (Fig. 33). The coal sample consists mainly of vitrinite (72 vol.%) and inertinite (26 vol.%). Liptinite macerals (incl. exsudatinite) are rare (<2 vol.%) (Fig. 36-a, b). The presence of exsudatinite indicates early oil generation, which agrees with a measured vitrinite reflectance of 0.67 %Rr of the sample from 4211 m depth. Low TOC/S ratios of shale samples (~1) agree with the postulated marine environment and indicate oxygen-depleted conditions.

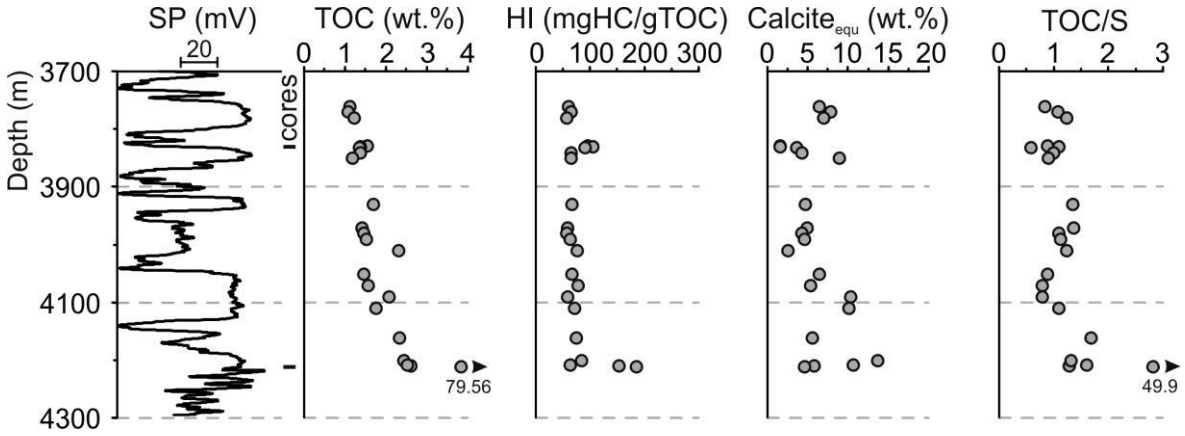

Fig. 35: Vertical variation of bulk parameters of the lower part of the Upper Quartzarenite Member (Gresten Fm.) in well Stockerau Ost 1. The position of two cores is marked. SP – Spontaneous potential, TOC –Total organic Carbon, HI –Hydrogen Index, Calciteequ. -Calcite equivalents, TOC/S –TOC content versus total sulphur.

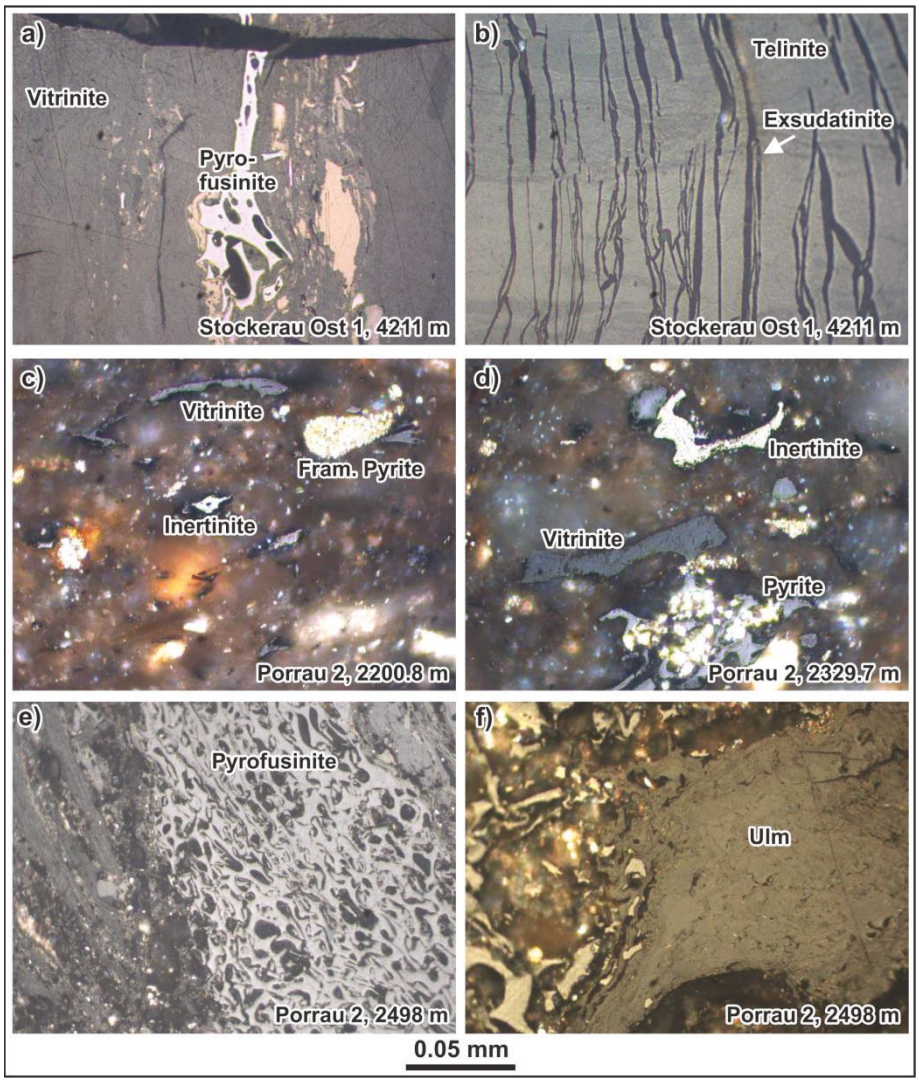

Fig. 36: Photomicrographs of samples from the Gresten Formation. (a,b) Upper Quartzarenite Member (Stockerau Ost 1, 4211 m), (c,d) Lower Shale Member, (e,f) Lower Quartzarenite Member.

5.1.2.2 Extractable organic matter

Biomarkers of a coal sample from the Lower Quartzarenite Member and four samples from the Lower Shale Member (Fig. 37 and 38) have been studied. Some biomarker proxies are plotted in Figs. 27, 28 and 30.

Pr/Ph ratios (1.7-2.9) in the Lower Shale Member suggest dysoxic (to oxic) environments and are higher than in the Falkenstein and Mikulov formations. This difference is also visible in a cross-plot of Pr/nC_{17} versus Ph/nC_{18} (Fig. 27).

In comparison to the Falkenstein and Mikulov formations, the Lower Shale Member is enriched in C_{29} steranes (40-50 %) and depleted in C_{27} steranes (30-40 %, Fig. 28). This reflects the different organic matter input as C_{27} steranes are primarily produced by algae, whereas C_{29} steranes are a product of land plants (Volkman, 1986). In line with this interpretation, the coal sample from the Lower Quartzarenite Member contains an even higher percentage of C_{29} steranes. Within the sterane triangle, samples from and the Falkenstein/Mikulov formations, the Lower Shale Member and the Upper Quartzarenite Member form distinct groups (Fig. 29). A high amount of terrestrial organic matter in samples from the Gresten Formation is also reflected by significant amounts of fluoranthen, pyren, benz(a)anthracen, chrysen, benzfluoranthracen, benz(e) and (a)pyren, perylen and benz(ghi)perylen, which form during wildfires and microbial mediated diagenetic processes (Killops and Killops, 1993, Alexander et al., 1992).

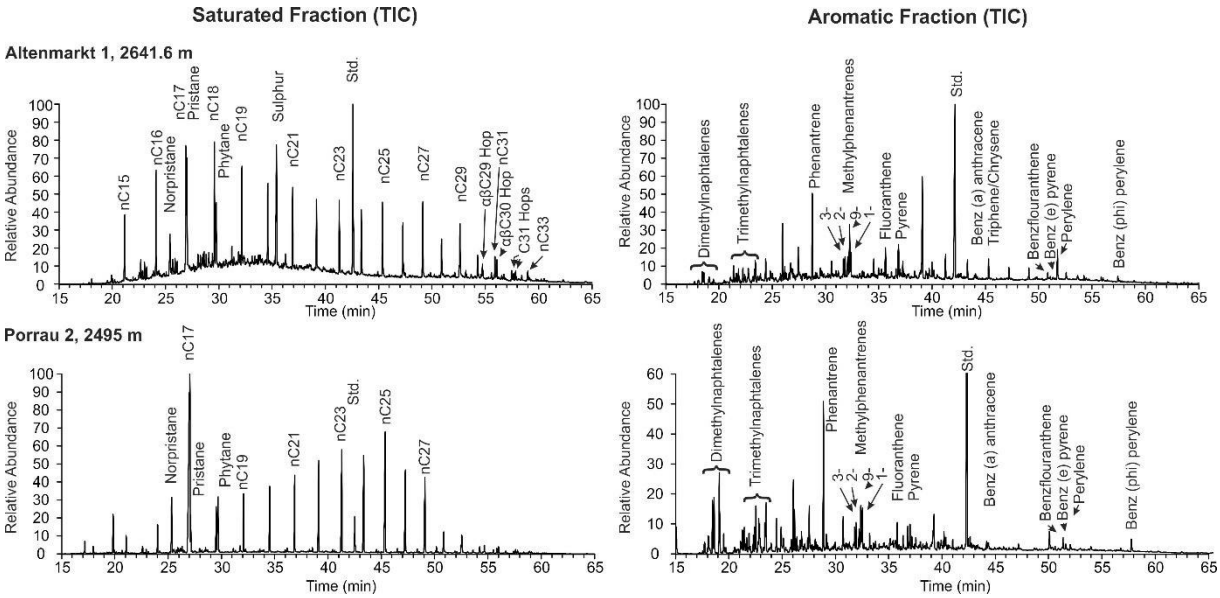

Fig. 37: Gas chromatograms of the saturated and aromatic hydrocarbon fractions of immature sample from the Lower Shale Member (Altenmarkt 1, 2641 m) and a coal sample from the Lower Quartzarenite Member (Porrau 2, 2495 m). Std – standard.

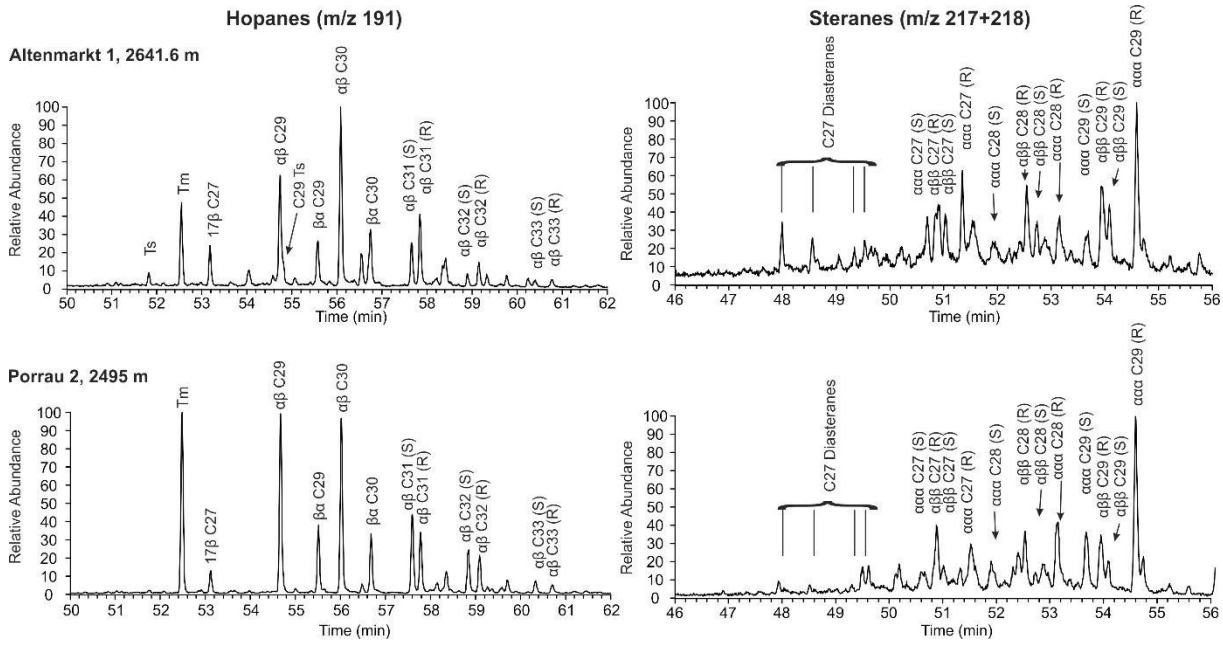

Fig. 38: Hopanes and steranes patterns of immature samples from the Lower Shale Member (Altenmarkt 1, 2641 m). Left column: hopanes (m/z = 191) and the Lower Quartzarenite Member (Porrau 2, 2495 m).

5.2 Discussion

5.2.1 Maturity

Vitrinite reflectance data from deep wells show a linear trend from 1.46 %Rr at 5600 m to 2.53 %Rr at 8500 m (Fig. 38). Although a data gap exists between 4500 and 5600 m depth, the presented parameters are in agreement with the position of the oil window (4000-6000 m) according to Ladwein (1988). Peak oil maturity (~0.85 %Rr), which is typically required for shale oil production, is reached at a depth of about 4500 m and maturity for shale gas production (1.3 %Rr) at a depth of about 5500 m (Fig. 26).

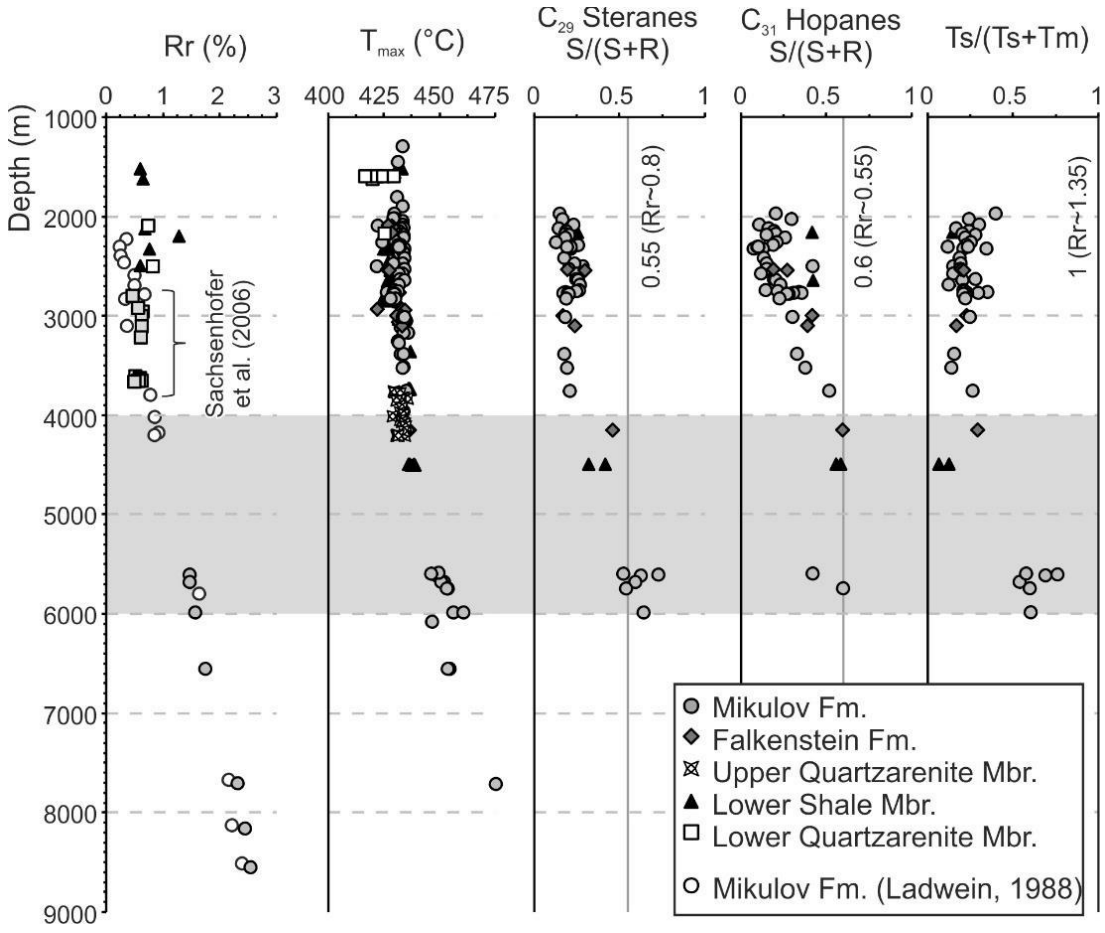

Fig. 39: Depth plot of different maturity parameters in the autochthonous units in the Vienna Basin area. Rr - random vitrinite reflectance, T_{max} - temperature of maximum HC-generation from Rock Eval pyrolysis, Ts – trisnorhopane; Tm -Trisnorneohopane. This plot contains data from the present study, Ladwein (1988) and Sachsenhofer et al. (2006).

5.2.2 Depositional environment of the Falkenstein and Mikulov formations

The vertical variations of bulk parameters (Fig. 16), biomarker and isotope ratios for the key well Staatz 1 (Fig. 26) are used together with the microfacies of different layers to determine the depositional environment of the Falkenstein and Mikulov formations.

The Falkenstein Formation (layers F1-3) overlies carbonate rocks of the Vranovice Formation. It is composed of marl and marly limestone deposited on a deeper shelf. The average TOC is 1.0 wt.%. The microfacies of layer F1 suggests deposition under restricted conditions. Because limestones with a filament facies are wide-spread in Middle Jurassic deposits (e.g. Flügel, 2004 and references therein), but rare in post-Callovian deposits, the onset of deposition of the Falkenstein Formation may have occurred as early as late Callovian time (see also Elias and Wessely, 1990), an age assignment, which is also supported by nannoplankton data. The occurrence of siliceous sponges suggests a water depth larger than 50 m (Flügel, 2004 and references therein) and a change to stable, open marine conditions. The presence of benthic foraminifera indicates oxic conditions in the water column. According to Pr/Ph ratios, dysoxic conditions prevailed within the sediments. This interpretation is supported by alternations of bioturbated and non-bioturbated wackestones in layer F1 and non-bioturbated wackestones in layer F2. MTTC ratios suggest normal to slightly enhanced salinity. High percentages of aquatic liptinite macerals and steranes abundances prove that the organic matter is mainly of aquatic origin. The relative low HI values are interpreted to reflect high levels of marine organic matter degradation, although inertinite maceral percentages are partly also high. *Saccocoma* sp. in the upper part of layer F2 (Fig. 17-3) indicates a Kimmeridgian or Tithonian age (Müller, 1978, Brodacki, 2006). The top of the Falkenstein Formation in Staatz 1 is formed by a calciturbidite (layer F3) with low TOC content.

The transition from the Falkenstein and Mikulov formations is characterized by a significant decrease in grain size and the occurrence of turbidite layers indicating further deepening of the environment. The Mikulov Formation is subdivided into layers M1 to M3. Layer M1 is attributed to the Tithonian based on an ammonite found in well Falkenstein 1 (3952 m). In this layer serpulide worms are present, whereas deep bioturbation is missing. This observation agrees with Pr/Ph ratios slightly >1, which indicate dysoxic conditions. Pr/Ph ratios, which are typically <1 indicate that

anoxic conditions prevailed during deposition of layers M2 and M3. TOC/S ratios significantly below 2.8 in layer M3 may be a consequence of the anoxic conditions (Berner and Raiswell, 1984). However, TOC/S ratios are not strongly reduced in layer M2. Remnants of sessile fossils indicate that anoxic conditions prevailed only within the pore space. Whereas carbonate contents are typically in the order of 50 wt.%, rocks with significantly lower carbonate contents occur at 2682.5 m depth (layer M1). TOC contents and HI of this layer are also reduced, while clay minerals (illite, kaolinite) are abundant. Kaolinite is derived from the crystalline basement of the Bohemian Massif. Although maceral data are not available, a HI below 50 mgHC/gTOC and high percentages of C_{29} steranes indicate a high proportion of land plants, which were transported together with the clay minerals into the basin. The average TOC and HI in M1 and M2 are 1.4 wt.% and 220 mgHC/gTOC. MTTC ratios suggest that salinity may have been slightly enhanced during deposition of layer M3 (Fig. 26). Layer M3 is further characterized by the presence of detrital quartz grains (Fig. 18), which may indicate a decrease in water depth. An upward decrease in TOC contents in M3 (average 1.0 wt.%; Fig. 16) may be a result of dilution by detrital minerals. Even more detrital quartz is found in the overlying Kurdějov (arenite) Formation. Similar to the Falkenstein Formation, maceral and biomarker data prove an aquatic origin of the organic matter, whereas relative low HI values reflect high levels of organic matter degradation. The zonation of authigenic carbonate minerals (Fig. 19) shows that organic matter degradation probably commenced within the water column, but continued in the uppermost sediment layer: (i) During denitrification, alkaline conditions resulted in the precipitation of euhedral dolomite crystals. (ii) In the absence of high Mn concentrations, Fe reduction (Piper and Calvert, 2009) became the main reducing process for organic matter degradation after consumption of all nitrate. Fe reduction occurred around the chemocline and resulted in liberation of Fe, which became incorporated into Fe-bearing dolomite forming rims around older dolomite grains (Canfield et al., 1993, Morse et al., 2007, Sanchez-Roman et al., 2007, 2009). (iii) When Fe was consumed, bacterial sulphate reduction (BSR, Baily et al. 1973, Jobson et al., 1979) further degraded the organic matter. However, low dibenzothiophene/phenatrene (DBT/Phen) ratios show that the extent of BSR was limited. Moreover, the amount of framboidal pyrite (Vairavamurthy and Schoonen, 1995) is minor.

Tari et al. (2011) suggested that the Mikulov Formation has been deposited in a setting with coastal upwelling. Golonka and Krobicki (2001) also proposed coastal upwelling during Malmain time along the southern European margin. Typical features of upwelling zones are high bioproductivity rates and oxygen depleted conditions below the photic zone. Sediments underlying upwelling areas include high TOC contents (2-20 wt.%), high biogenic silica (5- 70 wt.%) and elevated phosphorous contents (0.2- >1.0 wt.%; Littke and Sachsenhofer, 1994 and references therein). High amounts of radiolarians and siliceous sponges, now largely replaced by calcite, prove high original silica contents. Furthermore, maceral assemblages plot nicely into the field for coastal upwelling according to Littke and Sachsenhofer (1994; Fig. 22). Relative low TOC contents (typically <3 wt.%) may indicate a setting similar to the recent Northwest African shelf, where sediments are not particularly enriched in organic carbon (Littke et al., 1997). Low HI values (<350 mgHC/gTOC) are due to organic matter oxidation within the water column. Relative low HI values are found in many upwelling areas (Littke et al., 1997) and may result from the absence of strictly anoxic conditions. However, in the present case, poor organic matter preservation may also result from a relative shallow proximal position. Actually, TOC data from deep, overmature wells representing distal depositional settings indicate a basinward increase in organic matter. Rosenfeld et al. (1994), Pennington and Chavez (2000) and Schneider et al. (2005) reported an increase of salinity during coastal upwelling. Hence, slightly enhanced salinity during deposition of layer M3 may result from upwelling.

5.2.3 Source Rock Potential of the Falkenstein and Mikulov formations

Based on TOC contents and the classification of Peters (1986), the majority of the samples has a good petroleum potential (Fig. 40). However, based on Rock-Eval data (generative potential: S_1+S_2), the Falkenstein and Mikulov formations hold only a fair (to good) potential to generate oil. According to Py-GC results, both formations will generate low wax paraffinic-naphthenic-aromatic oil with low sulphur contents.

Whereas only a small proportion of studied samples from Austrian boreholes are classified as “good” based on their generative potential, about 20 % of the samples from the Czech part fall into this category, despite of similar TOC contents (see data

in Gerslova et al., 2015). Although analytical problems (e.g. cuttings contaminated with oil-based mud) cannot be completely excluded, this may indicate an increase in HI towards the NE.

The Source Potential Index (SPI = thickness*(S_1+S_2)*bulk density/1000) integrates source rock richness and thickness (Demaison and Huizinga, 1994). It represents the maximum quantity of hydrocarbon generated within a column of source rock under 1 m² of surface area. Density was measured for five rock samples using the Archimedes´ principle. The average density for immature samples from the Falkenstein and Mikulov formations is 2.67 and 2.62 g/cm³, respectively. The subtle difference may reflect the higher carbonate content in the Falkenstein Formation. The Falkenstein Formation in well Staatz 1 is 250 m thick, the thickness of the Mikulov Formation is 898 m. The average generation potential for both formations in well Staatz 1 is 1.20 and 2.85 gHC/gRock, respectively. Applying these input data, the SPI for the Falkenstein and Mikulov formations in well Staatz 1 is calculated as 0.8 and 6.7 t_{HC}/m². Consequently the total SPI of Malmian source rock interval is in the order of 7.5 t_{HC}/m². According Demaison and Huizinga (1994), this classifies the fault-controlled Vienna Basin, which is dominated by vertical migration, as “normally charged”.

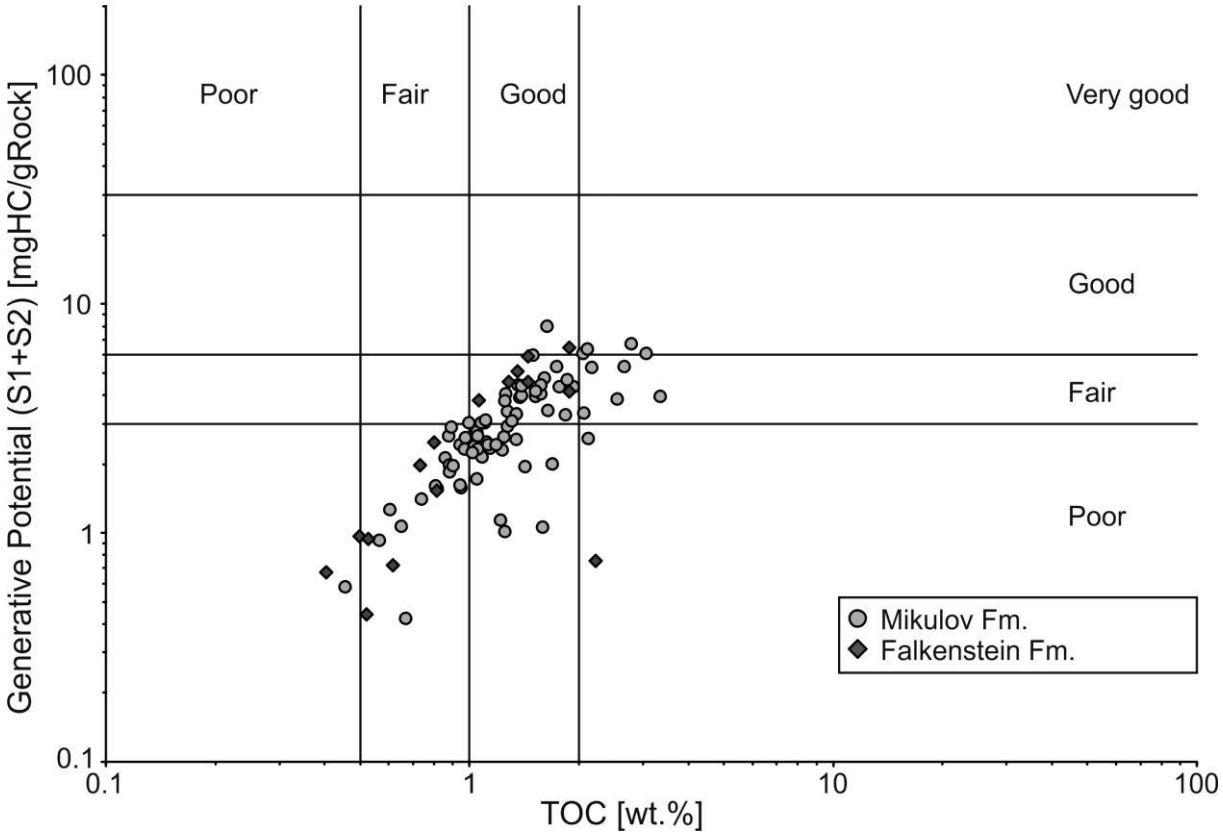

Fig. 40: Plot of TOC content versus the Generative Potential (Peters and Cassa, 1994) outlining that the Mikulov and Falkenstein Formation is a fair to good source rock.

Further, it has to be noted that most rock samples are from the western part of the study area (see Fig. 6), where the Falkenstein and Mikulov formations are immature (to marginal mature). These rocks represent a relative proximal paleogeographic position. Hence, an eastward increase in TOC contents to the basin center cannot be excluded. Unfortunately, only a limited number of overmature samples are available from this part of the basin (wells Aderklaa UT 1a, Maustrenk ÜT 1a, Zistersdorf ÜT 2a). Their present-day TOC contents range from 0.7 to 2.7 wt.%. The original TOC was certainly higher, but cannot be reconstructed because of tiny S_1 and S_2 peaks. The original TOC, however, can be estimated for Mikulov Formation in a tectonic imbricate drilled at ~5600 m depth in well Zistersdorf ÜT 1. The average TOC and HI of these rocks are 2.7 wt.% and 150 mgHC/gTOC, respectively, at a maturity level of about 1.5 %Rr (Fig. 39). A reconstruction of the initial TOC content gives values between 3.4 to 3.9 wt.% (method described in Peters et al., 2005). Nevertheless, more samples would be necessary to (dis-)prove the model of an eastward increasing TOC content.

5.2.4 Shale Gas/Oil Potential of the Falkenstein and Mikulov formations

The following prerequisites for the presence of a successful unconventional shale gas/oil play are widely accepted (e.g. Jarvie, 2012, Charpentier and Cook, 2011, Andrews, 2013 cum ref.): TOC content >2.0%, thickness >20 m, presence of kerogen type I, II or IIS. For shale gas, the maturity should be in the range of 1.2-3.5 %Rr, whereas lower maturity (>0.8 %Rr) is appropriate for shale oil. In order to enable hydraulic fracturing, a low percentage of ductile minerals is preferential (Fig 41a). Moreover, because of increasing drilling costs and increasing lithostatic pressure, the depth should not be greater than 5000 m. Similar parameters have been used by Uffmann et al. (2012) to delineate fields where commercial gas production can be achieved (Fig. 41b). In the following the Upper Jurassic samples are discussed accordingly.

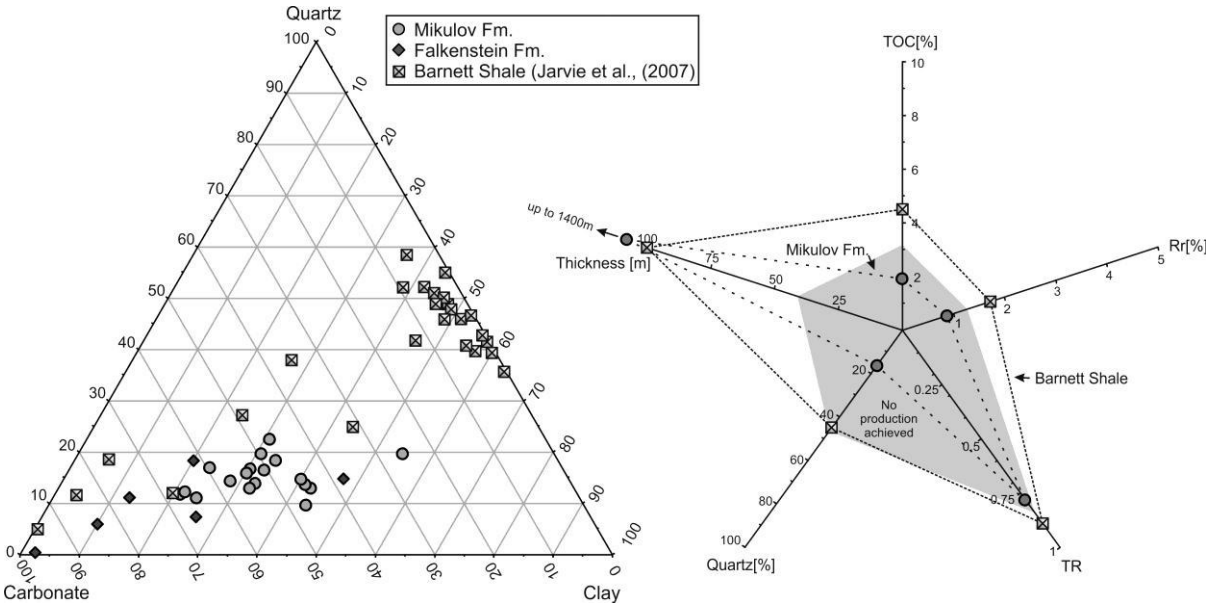

Fig. 41: a) Mineralogical distribution of quartz, carbonates and clay in the Falkenstein and Mikulov formations. b) Spider-diagram displaying TOC content, vitrinite reflectance (%Rr), transformation ratio (according to Peters et al., 2006), quartz content and thickness of the Mikulov and Falkenstein formations. The area of non-productivity is highlighted by grey shading (modified from Uffmann et al., 2012). Data from the Barnett Shale (Jarvie et al., 2007) are shown for comparison in a) and b).

Organic matter richness – The average TOC of 87 immature samples is 1.2 wt.% and only six samples (two from the Falkenstein Formation, four samples from the Mikulov Formation) exceed slightly the threshold value of 2.0 wt.%. In contrast, TOC data from 16 samples from the deeper part of the study area (>5600 m) suggest an eastward increase in TOC towards the basin centre.

Organic matter type – The Malmian succession contains a type II kerogen with a relative low HI (<400 mgHC/gTOC). The presence of labile type II-S kerogen can be excluded.

Thickness - The extraordinary thickness of the Mikulov Formation (several hundreds of metres) is the greatest advantage of this formation. Moreover, the rock parameters are relative uniform. This implies that even with vertical wells a feasible length of production wells can be achieved.

Thermal maturity – Fig. 39 shows that the Vienna Basin area is characterized by low maturity gradients. Consequently, 0.8 %Rr are reached only at 4000 m depth (according to vitrinite reflectance data of Ladwein, 1988) or even at greater depth (T_{max} and biomarker data provided in this study). A vitrinite reflectance of 1.2 %Rr is reached at ~5000 m depth, considered a cut-off value for economic shale gas production. In Fig. 41b a vitrinite reflectance of 1.0 %Rr (~4800 m depth) is shown. Similar to vitrinite reflectance, the TR (0.75; Fig. 41b has been calculated for 4800 m depth using the approach of Peters et al. (2006).

Mineralogy - The application of hydraulic stimulation techniques for the production of shale gas /shale oil depends on different factors including mineralogy. Expandable clay minerals are detrimental, whereas brittle minerals like quartz and calcite contents are critical. According to Schicker (2011), the Mikulov Formation is characterized by a low amount of expandable smectite (0.3 – 3.8 %) at 4500 m depth. In the spider-diagram in Fig. 41b the Falkenstein and Mikulov formations plot into the non-productive field. This is mainly because quartz is considered the main phase controlling brittleness. Hence, the geomechanical properties of the carbonate-rich Malmian rocks should be investigated in future.

Summarizing, it is obvious that the Mikulov Formation presents a poor shale oil/shale gas potential where it is at shallow depth (<4000 m). The organic matter richness may increase eastwards. However, in this area the Mikulov Formation rapidly gains

uneconomic depths. Hence, we conclude that the shale oil/ shale gas potential has been overestimated in the past.

5.2.5 Source Rock Potential of the Gresten Group

The chemical composition of hydrocarbons in the Klement, Roseldorf and Höflein fields (see Fig. 6 for location of boreholes in these fields) differs from the composition in most other fields. Consequently, several authors (e.g.) assumed an additional source rocks. Therefore the petroleum potential of the Gresten Group is discussed in the following.

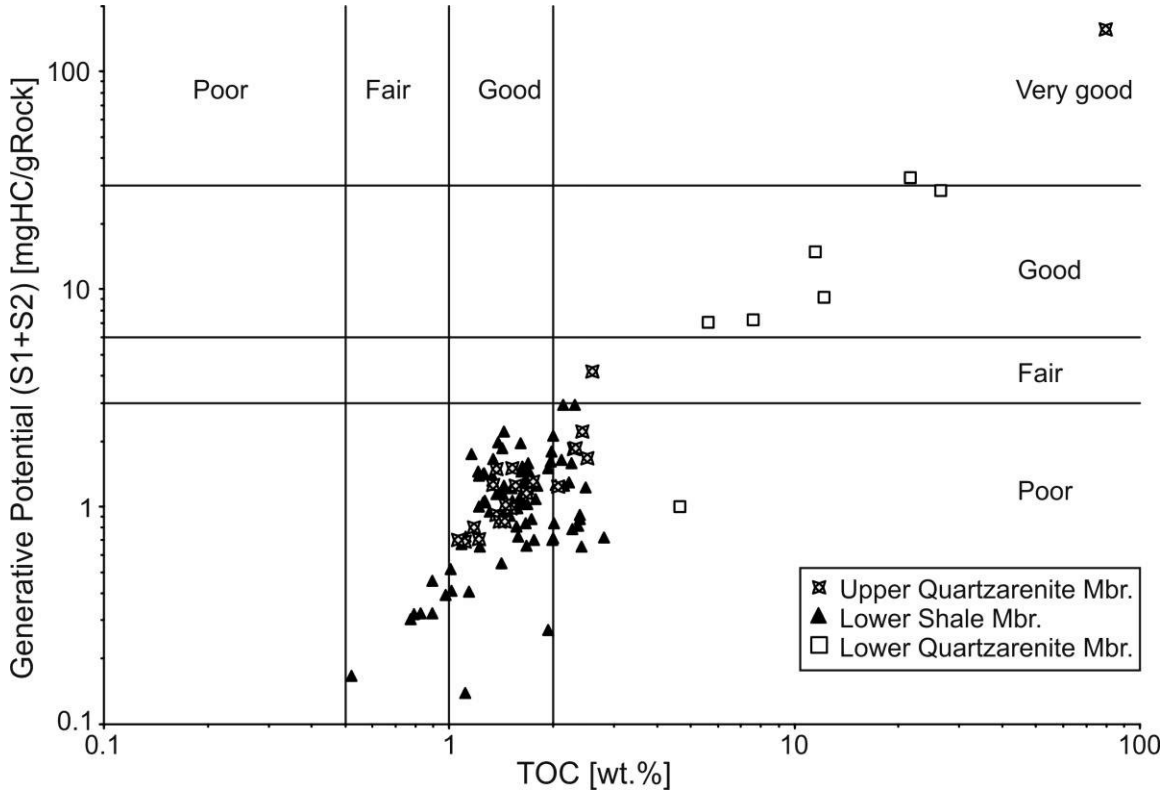

Fig. 41: Plot of TOC content versus the Generative Potential (Peters and Cassa, 1994) outlining that only coaly layers within the Lower Quartzarenite Member and the Upper Quartzarenite Member display a significant hydrocarbon potential.

Lower Quartzarenite Member - The petroleum potential of the Quartzarenite Member has been studied by Sachsenhofer et al. (2006). Therefore only few coaly samples have been included in the present project (Fig. 34). The new results support the previous ones, which showed that despite high inertinite contents, coal within the LQM has a significant oil potential. In addition bituminous shales contain a Type III–II kerogen and generate high wax paraffinic oil when reaching oil window maturity (Sachsenhofer et al., 2006).

Lower Shale Member - The generative potential of the prodelta shales from the Lower Shale Member is poor (Fig. 42), despite of TOC contents ranging from 0.5 to 2.5 wt.%. The poor source rock quality is due to high percentages of inertinite (40-90 vol.%) and vitrinite (10-50 vol.%) macerals (Fig. 22). Relative high Pr/Ph ratios (1.7-2.9) suggest that oxic degradation further decreased the organic matter quality. The Gresten Formation has been deposited in halfgrabens. Hence it is characterized by largely varying paleo-water depth. Although the studied samples are disappointing, it cannot be excluded that better source rocks have been deposited in former depocentres, which have not been drilled yet.

Upper Quartzarenite Member - TOC contents in shales from the Upper Quartzarenite Member in Stockerau Ost 1 decrease upwards from 3.0 to 1.0 wt.%. Low HI values show that these rocks have a poor to fair gas potential. Coaly layers near the base of the member have a good gas potential.

6. Hydrocarbons in the Austrian part of the Vienna Basin and in Alpine Nappes

The majority of the produced hydrocarbon in Austria originates from reservoirs within the Vienna Basin area. The outstanding relevance of these deposits justifies a detailed investigation of their origin and alteration.

6.1 Results

6.1.1 Oils

6.1.1.1 Biomarkers

Straight chain alkanes, isoprenoids – The relative amounts of n- and iso-alkanes differ greatly depending on depth and degree of biodegradation. n-Alkanes are typically missing in oils from shallow reservoirs (< 1600 m true vertical depth subsea; TVD_{ss}; Fig. 43a). However, some fields located within the Flysch Zone (Neusiedl, St. Ulrich, Steinberg, Pirawarth) contain abundant n-alkanes (Fig. 43b), although the amount of short-chain n-alkanes may be depleted.

Oils from Miocene reservoirs below 1600 m depth (TVD_{ss}) are characterized by FID traces with unimodal n-alkane distributions and maximum intensities at nC_{15} or nC_{17} (e.g. Ebenthal 17a; Fig. 43c). A bimodal distribution of n-alkanes with peak intensities at $nC_{15\text{-}17}$ and nC_7 is observed in Ebenthal 20 (Badenian reservoir), Schönkirchen T12 (Ottnangian reservoir) and Neusiedl 3 (Flysch reservoir; Fig. 43b). The biomodal distribution may indicate mixing of crude oil with high mature condensates. Unimodal n-alkane distributions with maximum intensities in the range of nC_7 to nC_9 are observed in condensates in the Aderklaa Field (Fig. 43d), both in Badenian and Karpatian reservoirs. In oils from Karpatian reservoirs long-chain n-alkanes ($>nC_{21}$) occur in trace amounts only, whereas in all other non-degraded oils with Miocene or Flysch reservoirs n-alkanes are present up to nC_{33}.

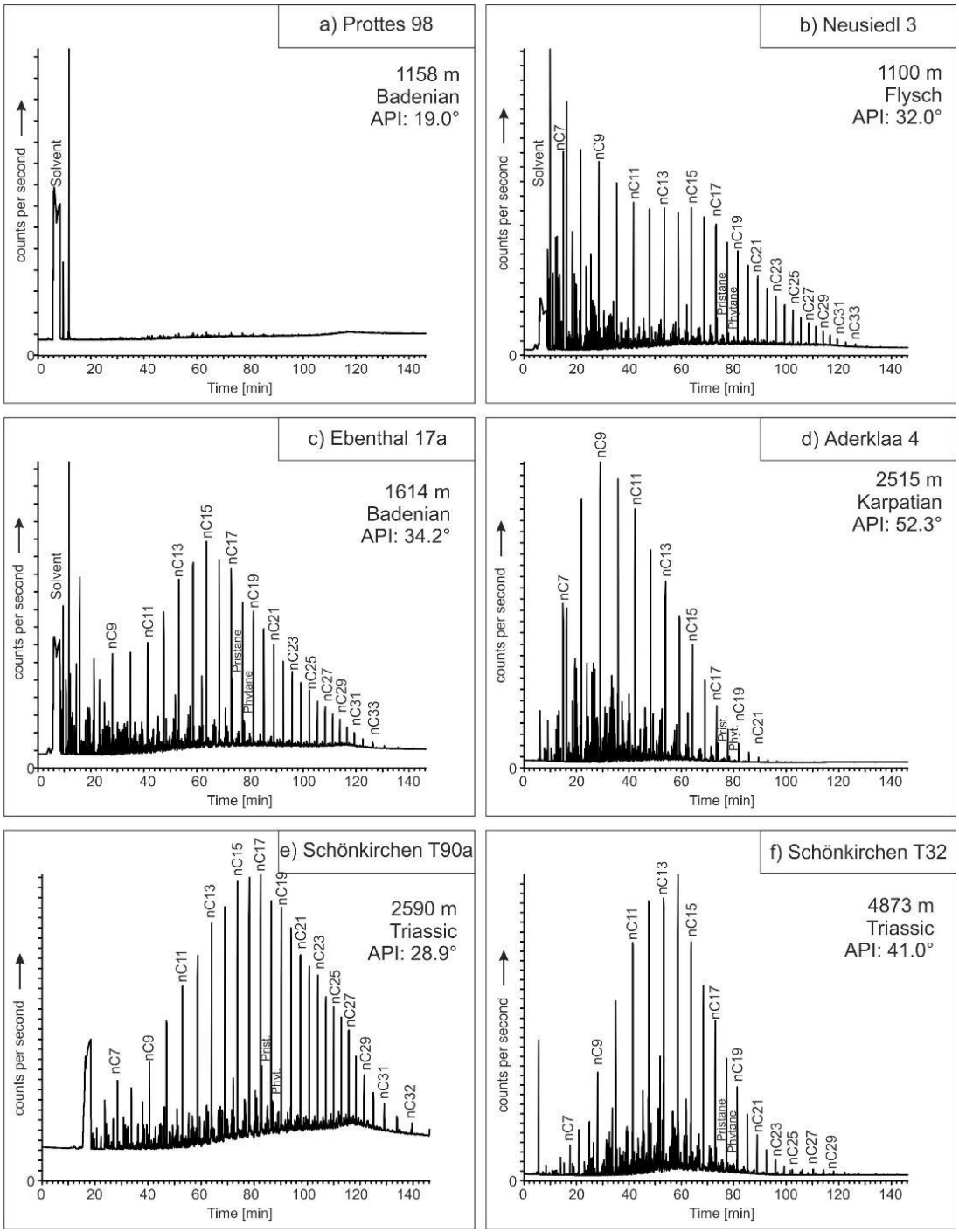

Fig. 43: FID traces of oils from different depth and different reservoir units. Depth is given in true vertical depth, subsea.

Based on n-alkanes distributions, oils produced from the Calcareous Alps can be subdivided into two groups. One group (i) consists of oils from relative shallow reservoirs (2540 - 2805 m) with unimodal n-alkane distribution and maximum intensities between $nC_{15\text{-}17}$, similar to most oils with Miocene reservoirs (Fig. 43e). The other group (ii) comprises oils from deep reservoirs (Schönkirchen T32, T42,

T62; 4167-5390 m) and is characterized by unimodal n-alkane patterns with a maximum at nC_{11-14} (Fig. 43f). The carbon preference index (CPI; Bryan and Evans, 1961) of undegraded samples is close to equilibrium (0.99-1.03).

The Pr/Ph ratio is an indicator for eh-conditions of the source rock during deposition (Didyk et al., 1978). Pr/Ph ratios of Vienna Basin oils (1.0-2.9) fall into the range characteristic for dysoxic environments (1.0-3.0 according to Didyk et al., 1978). The Pr/nC_{17} and Ph/nC_{18} ratios increase with progressive degradation and decrease with increasing maturity. Many oils from shallow Middle Miocene (Badenian, Sarmatian) reservoirs are characterized by high Pr/nC_{17} and Ph/nC_{18} ratios (>>1) indicating advanced biodegradation. Pr/nC_{17} and Ph/nC_{18} ratios around ~1 are observed in non-biodegraded oils from shallow flysch reservoirs and decrease generally with reservoir depth. The smallest ratios are observed in deep group (ii) oil from the Calcareous Alps (Fig. 44).

Steroids and hopanoides – Samples from lower Miocene reservoirs in wells Aderklaa 3 and 4 and deep group (ii) samples from the Calcareous Alps do not contain any steranes and hopanes. All other samples are dominated by 14β, 17β(H) steranes over 5α, 14α, 17α(H) steranes isomers. The relative abundance of C_{27} steranes (31-53 %), C_{28} steranes (12-40 %) and C_{29} steranes (27-43 %) varies, but the ternary steranes diagram shows that most samples plot into a narrow cluster (Fig. 45). Variations in the ratio of C_{27}-diasteranes to the sum of C_{27}-diasteranes and C_{27}-steranes (Miocene: 0.27-0.61; Flysch: 0.37-0.60; group (i) Calcareous Alps: 0.36-0.54) probably reflect different clay contents in the source rock and the clay catalytic effect (Sieskind et al., 1979). The C_{28}/C_{29} steranes ratio increases through geological time and thus gives some information on the age of the source rocks (Grantham & Wakefield, 1988). The observed values (0.5-1.0) agree with a Mesozoic age of the source rock.

Hopanes occur in minor amounts. All samples with hopanes are characterized by $\alpha\beta C_{31}R$ hopane / $\alpha\beta C_{30}$ hopane ratios exceeding 0.4 and high steranes/hopanes ratios (>0.4) suggesting an algal-dominated marine source rock (Mackenzie, 1984; Peters et al. (2005). Oleanane has not been detected in any of the oil samples, but has been described in samples from the Czech Republic by Francu et al. (1996).

All samples display 20S/(20S+20R) isomer ratios for C_{29} steranes and 22S/(22S+22R) isomer ratios for C_{31} hopanes, which are close to the equilibrium values of 0.55 and 0.60, respectively (Mackenzie and Maxwell, 1981). The Ts/(Ts+Tm) ratio varies between 0.36 and 0.74.

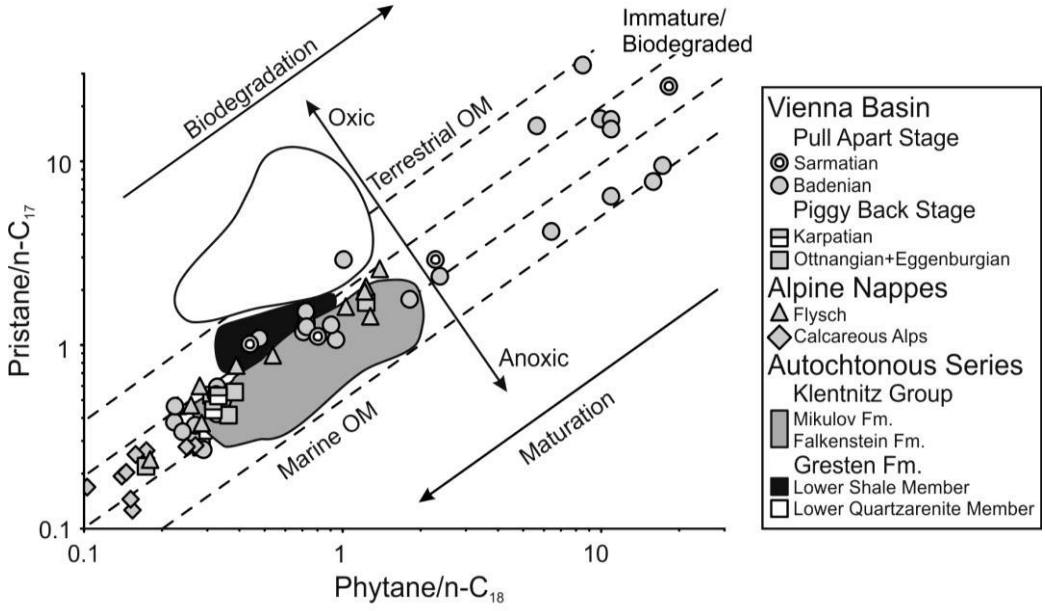

Fig. 44: Crossplot of phytane/nC_{18} and pristane/nC_{17} ratios (according to Connan and Cassou, 1980).

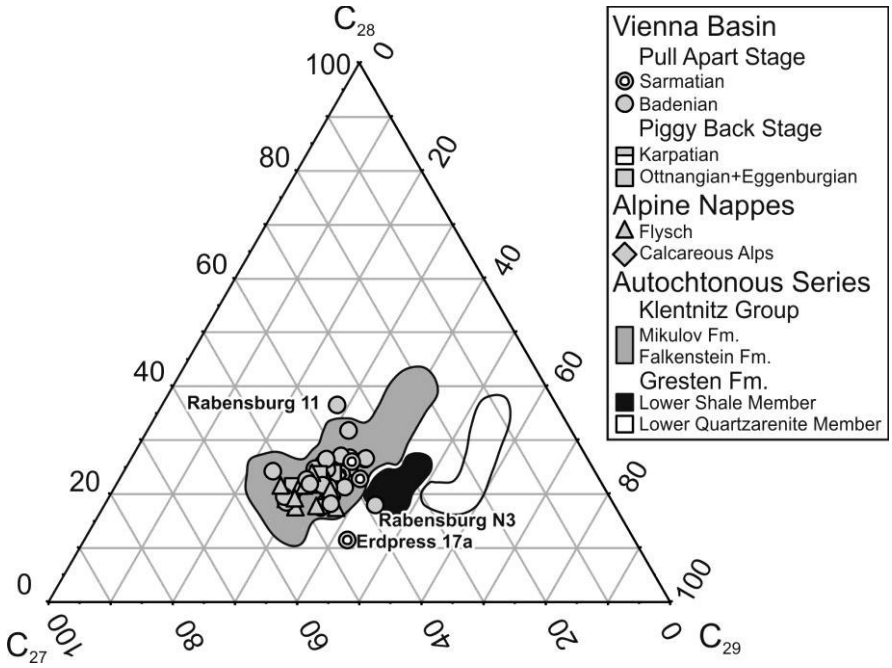

Fig. 45: Ternary diagram showing the distribution of C_{27}-, C_{28}-, and C_{29}-steranes.

Polycyclic aromatic hydrocarbons - Two major contributing compound groups could be identified within the samples. The first group is formed from mono-, di-, tri-, and tetramethylated naphthalenes which are present in high quantities within all investigated samples. The second group consists of phenanthrene and methylphenanthrenes. These compounds derive from a variety of non-specific precursor compounds such as steroids and triterpenoids (Tissot and Welte, 1984). The ratio between phenanthrene and different methylated phenanthrenes is called methylphenanthrene index (MPI; Radke and Welte, 1983) and can be used as a maturity parameter. MPI values typically range from 0.43 to 1.11, but is very low (0.30) in the strongly degraded Van Sickle 29 oil. This may reflect the differential removal of phenathrenes and methylphenanthrenen during degradation.

Polycyclic aromatic hydrocarbons (PAHs) with more than 3 rings are generally missing. Only in oils from the Neusiedl, Pirawarth and Rabensburg fields, fluoranthene and pyrene are present. The lack of other PAHs suggests that these compounds are not derived from terrestrial organic matter (Killops and Killops, 1993), but products of thermal ("pyrolytic") processes (e.g. Venkatesan, 1988, Jiang et al., 2000). As the Neusiedl, Pirawarth and Rabensburg samples display a bimodal n-alkane distribution (e.g. Fig. 43b), the presence of fluoranthene and pyrene argues for the mixing of crude oil with a high maturity condensate.

The relative concentration of dibenzothiophene (DBT) and alkylated dibenzothiophenes in nearly all Miocene and Flysch reservoirs as well as group (i) oils of the Calcareous Alps is low and does not exceed a ratio 0.5. In contrast DBT is significantly enriched in samples from Karpatian reservoirs in wells Aderklaa 3 and 4 (2.0-2.3) as well as group (ii) oils from the Calcareous Alps (Strasshof T [0.9-1.1] and Schönkirchen T32, T42 and T62 [1.8-1.9])

6.1.1.2 Stable carbon isotope ratio

6.1.1.2.1 Stable carbon isotope ratio of bulk fractions

Stable carbon isotope ratios of the aliphatic and aromatic fraction have been used to distinguish marine and non-marine source rocks and for oil-source correlation (Sofer, 1984; Fig. 46). $\delta^{13}C$ values range from -23.2 to -27.5 ‰ in the aliphatic fraction and from -23.7 to -26.2 ‰ in the aromatic fraction of samples from Miocene and Flysch reservoirs (Appendix XI). Group (i) oils of the Calcareous Alps are comparable to Miocene and Flysch oils or slightly lighter ($\delta^{13}C_{sat}$: -26.1 to -28.3 ‰; $\delta^{13}C_{aro}$: -24.6 to -26.6 ‰). In contrast, group (ii) oils are significantly heavier ($\delta^{13}C_{sat}$: -24.4 to -25.4 ‰; $\delta^{13}C_{aro}$: -23.4 to -23.9 ‰).

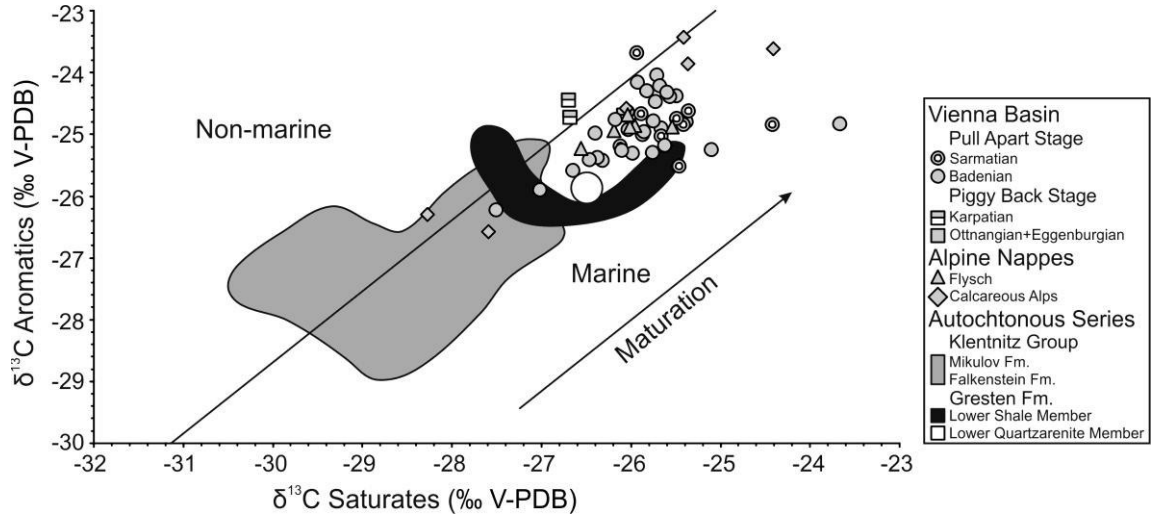

Fig. 46: Crossplot of the stable carbon isotope ratio of the aliphatic and aromatic fraction (according to Sofer, 1984).

6.1.1.2.2 Compound specific stable carbon isotope ratio

The maximum intensity signal for single compounds was obtained for n-alkanes in the range of nC_{17} up to nC_{22}. In general it can be seen, that $\delta^{13}C$ values increase with decreasing chain length, which is reported as typical behavior of numerous oils (Bjoroy et al., 1994).

Increasingly negative $\delta^{13}C$ values from C_{21} upwards are consistent with marine sources (Murry et al., 1994). The slightly lower $\delta^{13}C$ values of odd carbon numbered homologues in the nC_{24-32} range could be interpreted as either contribution of leaf lipids or algae (Collister et al., 1994).

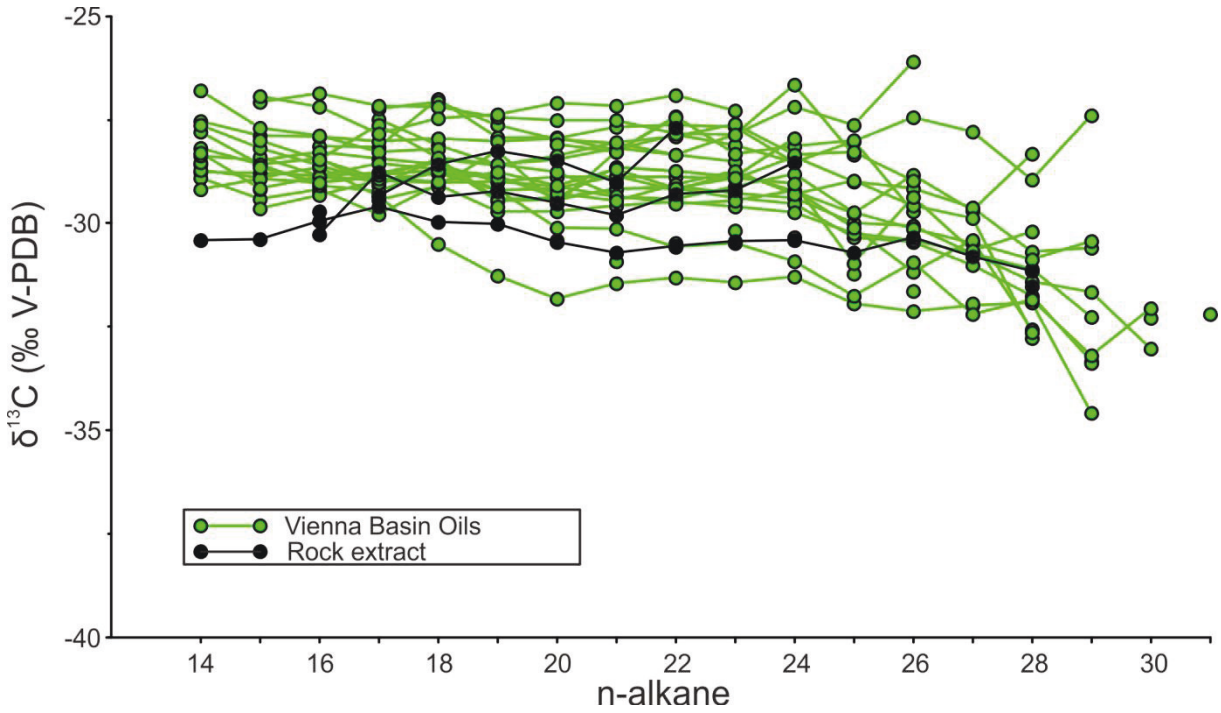

Fig. 47: Stable carbon isotope ratio of individual n-alkanes from oils in the Austrian part of the Vienna Basin.

Obvious more negative stable isotope data from Schönkirchen T29 and Ebenthal 20 can not be explained. Other wells producing from the same reservoir and compartment (Schönkirchen T12, T38, T69; Ebenthal 5, 15, 17a) follow inconspicuously the general trend.

6.1.1.3 Trace element concentration

Mg, P, K, Ti, Rb, Sr (lithophile elements) - Lithophile elements are present in mineral particles or in emulsified water (Filby, 1994). Walkner et al. (2016) used a cross plot of K (indicative of emulsified water) and Al (indicative of entrained clay minerals) to determine the origin of lithophile elements in oils from the Alpine

Foreland basin. As Al has not been detected, Ti is used as an indicator for clay minerals in Vienna basin oils. This is justified by the strong correlation between Al and Ti (Walkner et al., 2016). Fig. 48 reveals that samples from wells Bockfliess 1, Matzen 390 and Prottes 26 contain some clay, whereas the sample from well Schönkirchen T29a may contain some water.

Mn, Fe, Cu, Zn - Elements of this group correlate strongly with each other. We interprete the occurrence of this elements as metal flakes from abrasion within the metallic well completion during production.

As, Se - Although Se and As can substitute S, no correlation can be found with S in the present sample set. As the overall concentration of the elements is low and in sediments Se is only enriched in clay minerals (Malisa, 2001), it can be proposed that the clay minerals found in the Falkenstein Formation and the Mikulov Formation are depleted in Se and As.

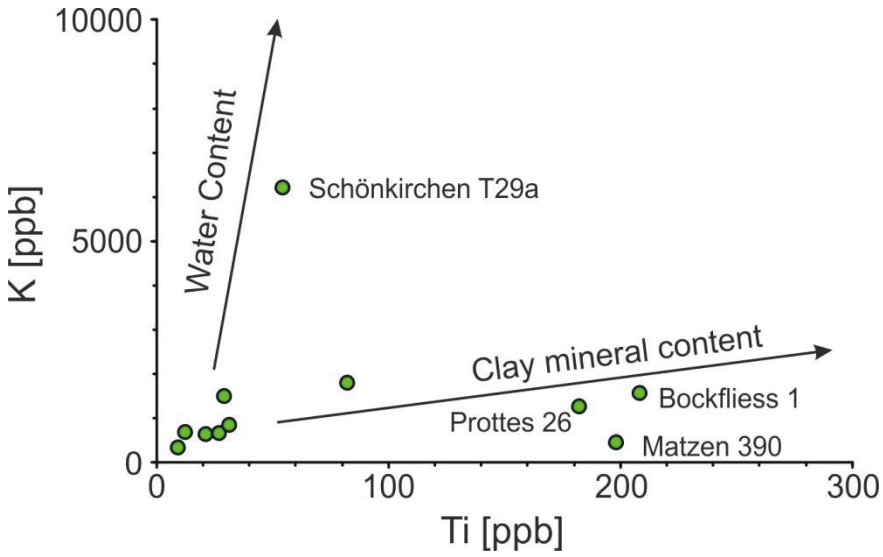

Fig. 48: Titanium versus potassium content in oil samples from the Vienna Basin (according to Walkner et al., 2016). The sample from Schönkirchen T29a contains emulsified formation water whereas samples from Prottes, Matzen and Bockfliess contain some dispersed clay particles.

Ag, Cd, Ba, Re, Pb, U - Some potential for the description of the depositional environment has been proposed for Ba and Cd (Mongenot, 1996). However Ba and Cd concentrations in Vienna basin oils are very low. The Pb-U and Re-Os isotope

systems are routinely used for exploiting ages in all kinds of geological applications (Selby and Creaser, 2005, Selby et al., 2007, Dreyfus et al., 2007, Ortega et al., 2012, Finlay et al., 2012, Lillis and Selby, 2013, Rooney et al., 2012). However Os could not be detected. Moreover, the concentrations of Re, Pb and U are so low, that age dating does not seem feasible.

6.1.2 Gas

6.1.2.1 Molecular composition

Gas samples contain varying amounts of hydrocarbon and non-hydrocarbon gases (Appendix IX). The dominant compounds in gases from Miocene and Flysch reservoirs are methane (C_1: 76.3-99.6 vol.%) and ethane (C_2: up to 7.0 vol.%). Higher hydrocarbon gases are found in minor concentrations. Gas dryness, defined by the $C_1/(C_2+C_3)$ ratio (Bernard et al., 1978) ranges from 12 (Hochleiten 60) to 3300 (Fischamend 6). There is a general trend with increasing dryness in shallow reservoirs, but Flysch reservoirs often contain a wetter gas than Miocene reservoirs from the same depth (Fig. 49). Non-hydrocarbon gas compounds are dominated by CO_2 and nitrogen N_2. Maximum CO_2 contents are observed in the St. Ulrich-Hauskirchen (Flysch) and Hochleiten (Sarmatian) fields. However, CO_2 and N_2 contents in these fields are probably affected by CO_2 and N_2 injection during the late 1990´s and early 2000´s (Kroell and Glantschnig, 1997, Potsch et al., 2004) and, therefore, are not considered further. CO_2 and N_2 contents in the remaining fields range from 0.05 to 6.6 vol.% and from 0.03 to 1.05 vol.%, respectively. Most samples are free of hydrogen sulphide (H_2S: max 300 mg/m³).

Based on H_2S and CO_2 contents, gases in the Calcareous Alps are subdivided into two groups. Group (1) gas is nearly free of H_2S (<26 mg/m³) and contains similar amounts of CO_2 (1.6-6.2 vol.%), N_2 (0.4-0.5 vol.%) and hydrocarbon gases (C_1: 90.1-94.0 vol.%, C_2: 1.8-2.7 vol.%) than gases from Miocene and Flysch reservoirs. The $C_1/(C_2+C_3)$ ratio (26-36) classifies group (1) gases as wet. In contrast, group (2) gases are rich in H_2S (~2%) and CO_2 (~13 vol.%). The contents of methane (83.0-88.9 vol.%), ethane (0.5-0.7 vol.%) and higher hydrocarbons show that they are slightly drier ($C_1/(C_2+C_3)$: 92-159) than group (1) gases.

The i-/n-C_4 and the C_2/C_3 ratio are proxies for gas degradation as microbes preferably consume n-alkanes and C_3 (Jones et al., 2008, Brown, 2011, Milkov, 2011, Larter and di Primio, 2005). Consequently it is not surprising, that i-/n-C_4 and C_2/C_3 ratios are often high for gases in the shallow reservoirs (<1600 m subsea; Fig. 49). i-/n-C_4 ratios in gases from Flysch reservoirs are relatively low (0.7-1.7), despite of shallow depth (< 1050 m).

6.1.2.2 Isotopic composition

The stable carbon ($\delta^{13}C$) and hydrogen (δD) isotopic compositions of hydrocarbons scatter widely. $\delta^{13}C$ ratios in methane range from -24.0 to -62.9 ‰ and show an upward decreasing trend within Miocene and Flysch reservoirs. This suggests mixing of thermogenic gas with increasing amounts of isotopically light microbial methane. In contrast to methane, $\delta^{13}C$ of C_2 (-14.4 to -27.4 ‰), C_3 (-12.2 to -23.9 ‰), i-C_4 (-20.4 to -24.4 ‰) and n-C_4 (-19.8 to -24.6 ‰) vary less significantly.

Methane from the Calcareous Alps is isotopically relatively heavy compared to gas in Miocene and Flysch reservoirs. Within the Calcareous Alps group (1) gases are lighter (-33.0 to -34.2 ‰) than group (2) gases (-26.4 to -29.8 ‰). In contrast, C_2 (-20.6 to -26.8 ‰), C_3 (-22.1 to -25.6 ‰), i-C_4 (-22.7 to -23.4 ‰) and n-C_4 (-22.7 to -25.2 ‰) show similar or slightly lighter $\delta^{13}C$ values than gas in Miocene and Flysch reservoirs.

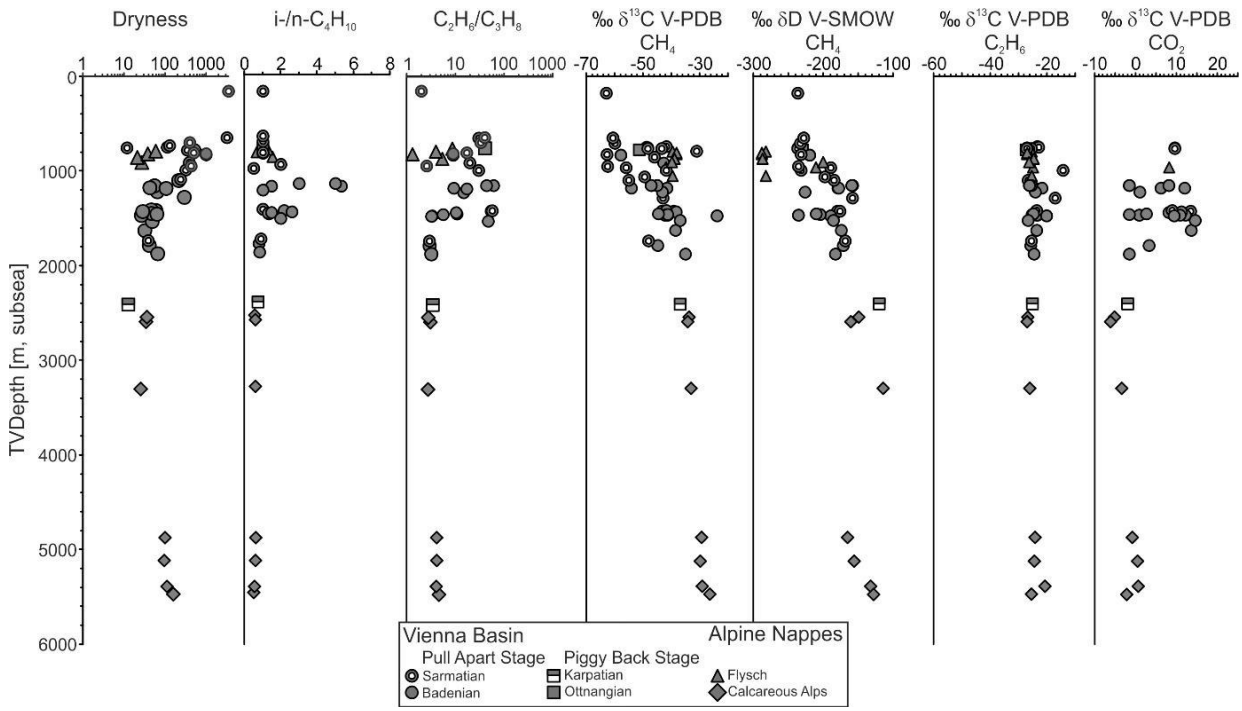

Fig. 49: Vertical variation of different properties of hydrocarbon and non-hydrocarbon gases.

δD ratios of methane in samples recovered from Miocene and Flysch reservoirs typically range from -159 to -237 ‰, but methane with isotopically light hydrogen (-282 to -288 ‰) occurs in the St. Ulrich-Hauskirchen Flysch field (Fig. 50). Isotopically heavy hydrogen (-120 ‰) is observed in a Karpatian reservoir (Aderklaa 98; Fig. 49). Methane in the Calcareous Alps has relative heavy hydrogen (-114 to -165 ‰ δD). In contrast to $\delta^{13}C$, δD values in group (1) and (2) gases are similar.

The $\delta^{13}C$ ratios of CO_2 in samples from Miocene and Flysch reservoirs range from -1.9 ‰ to +14.5 ‰ (up to +23.5 ‰ in the St. Ulrich-Hauskirchen and Hochleiten fields affected by CO_2 injection). Gases in the Calcareous Alps can be distinguished regarding their stable carbon isotope ratio of CO_2. Group (1) gases range from -6.1 to -3.3 ‰ $\delta^{13}C$ and group (2) gases from -2.2 to +0.6 ‰ $\delta^{13}C$.

Stable sulphur isotope ratios ($\delta^{34}S$) have been determined for H_2S-rich group (2) gases from the Calcareous Alps. The measured $\delta^{34}S$ values (+15.6 to + 16.0 ‰) are in good accordance with data from Ladwein (1982).

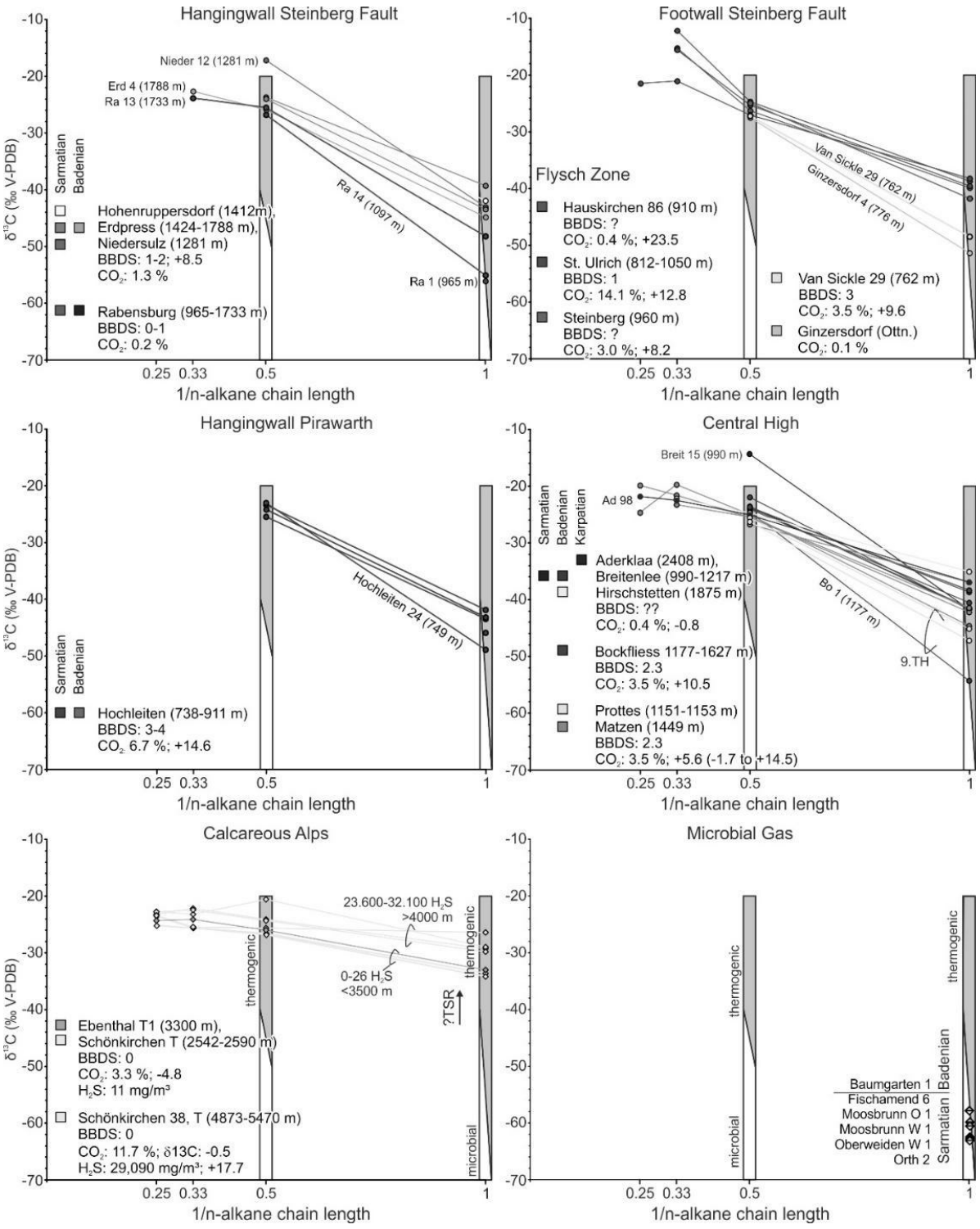

Fig. 50: Natural gas plots (Chung et al., 1988) showing the stable carbon isotope ratio of individual hydrocarbons as a function of their carbon number. The gases are grouped according to their tectonic position in the Vienna Basin.

6.2 Discussion

6.2.1 Oil Maturity

Oil maturity is assessed using MPI-1 values, isomerization ratios of C_{29} steranes and C_{31} hopanes as well as Ts/(Ts+Tm) ratios.

MPI-1 values range from 0.30 to 1.11. However, when oils with heavy biodegradation (BBDS stages 3 and 4; see below) are neglected, MPI-1 values are restricted to the range between 0.42 and 1.11. The equation Rc = 0.60 MPI-1 + 0.40 Radke and Welte (1983) has been used to calculate vitrinite reflectance. Fig. 51 shows that calculated vitrinite reflectance increases slightly from 0.8 %Rr at 1000 m depth to 1.0 %Rr at 5000 m depth. Relative low maturity is found for oils from the Ebenthal Field (0.65-0.70 %Rr) and some Matzen oils with slight biodegradation. For oil fields located along the Pirawarth-Steinberg Fault System, there is also a trend with northward decreasing maturity between the Hochleiten Field (0.90 %Rc) and the Bernhardsthal-Rabensburg area (~0.75 %Rc).

The MPI derived maturity estimates are supported by biomarker isomerization ratios. Both, the 22S/(22S+22R) ratio of C_{31} hopanes and the 20S/(20S+20R) ratio of C_{29} steranes are generally close to the thermal equilibrium (0.6 and 0.55, respectively; Fig. 51), showing that the maturity of the source rocks is at least 0.8 %Rr (Mackenzie, 1984, Mackenzie and Maxwell, 1981). Sterane isomerization values around 0.5 are found only along the northern sector of the Steinberg Fault and in the Ebenthal Field.

Ts/(Ts+Tm) ratios (0.36 - 0.74) support a slightly enhanced maturity of the deep samples from the Calcareous Alps (0.69-0.74) and the relative low maturity of the northern part of the study area (0.36-0.52).

A comparison of maturity trends observed in oil and rock samples (Fig. 51) suggests that main oil generation occurred at about 5 km depth. This indicates significant vertical migration distances. Because downward migration is highly unlikely, the relative low maturity of oil in deeply buried reservoirs in the Calcareous Alps may indicate filling of the reservoir before it reached its present-day depth during Late Miocene time. Oils below 4 km depth are affected by TSR (see below). Therefore, alternatively an influence of TSR on the MPI ratio cannot be excluded.

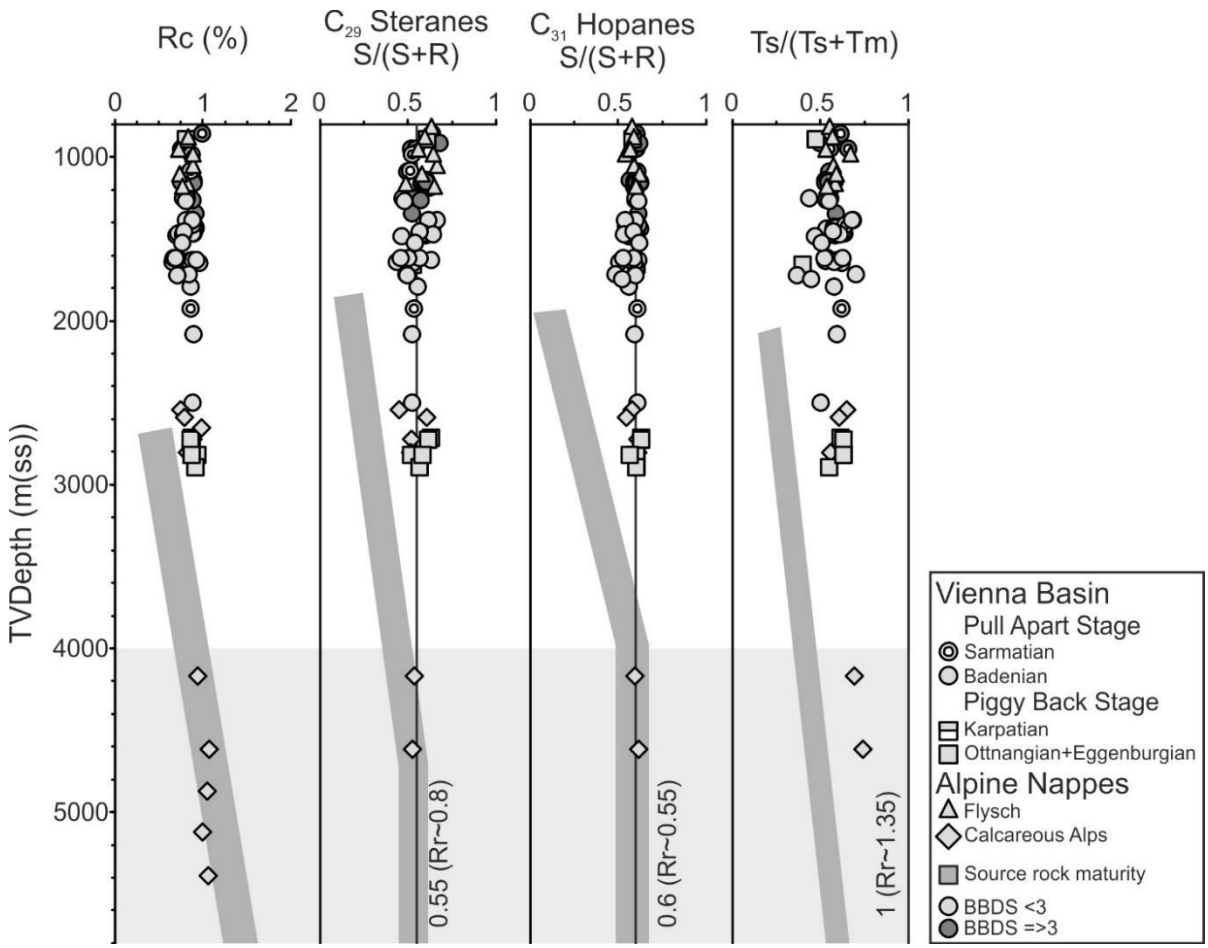

Fig. 51: Different maturity parameters from oil samples against depth. Only samples undegraded, slight and moderate degraded samples are plotted. The oils have been generated at peak oil maturity (~0.8-0.9 %Rr). The depth of the oil window starts at approximately 4000 m depth (Ladwein, 1988).

6.2.2 Oil-source rock correlation and oil families

The most likely source rocks for hydrocarbons in the Vienna Basin area are the Upper Jurassic Mikulov and Falkenstein formations (Ladwein, 1988, Gerslova et al., 2015, Chapter 5). However, the Middle Jurassic Gresten Formation may host additional sources rocks (Kratochvil and Ladwein, 1984, Ladwein, 1988, Sachsenhofer et al., 2006).

In the following, standard parameters and diagrams are used for the correlation of studied oil samples with potential source rocks using source rock data from Sachsenhofer et al. (2006) and Chapter 5. The position of oil samples in the Pr/nC_{17} versus Ph/nC_{18} cross plot (Connan and Cassou. 1980; Fig. 45) is in agreement with

an Upper Jurassic source (Falkenstein Fm., Mikulov Fm.). Differences between oil and rock samples reflect maturation and biodegradation effects. In contrast, the Quartzarenite Member of the Gresten Formation can be excluded as a main contributor to oil accumulations in the Vienna Basin (Fig. 45). An Upper Jurassic source is also supported by the steranes triangular diagram (Fig. 46), which excludes the Lower Shale Member and the Quartzarenite Member of the Gresten Formation as significant oil source. The Sofer plot ($\delta^{13}C_{ali}$ vs $\delta^{13}C_{aro}$; Sofer, 1984) is another correlation tool for oils and source rocks (Fig. 49). The investigated oils show a slightly heavier isotope signature than immature source rocks. The observed increase of about 3 ‰ is typically observed during maturation (Galimov, 1980, Sassen et al., 1988, Claypool and Mancini, 1989).

Considering the above correlation plots, the poor source rock quality of the Lower Shale Member (Chapter 5) and the absence of oleanane, a biomarker typical for oils with a Late Cretaceous or younger age, it is highly probable that oils in the Austrian part of the Vienna Basin have been generated from the Upper Jurassic Mikulov and Falkenstein formations.

Nevertheless, subtle differences in oil facies, probably reflecting regional variations in the source rocks can be distinguished. For example, DBT/Phen ratios reach maxima (0.22-0.30) in Miocene reservoirs along the northern segment of the Steinberg Fault (Van Sickle, Plattwald, Mühlberg, Bernhardsthal S; Fig. 52-a). In contrast DBT/Phen ratios in other Miocene and Flysch reservoirs along the Steinberg Fault are typically below 0.2. Very high DBT/Phen ratios in the Calcareous Alps and overlying Lower Miocene sediments (0.28-2.30) are due to hydrocarbon alteration and will be discussed below.

Despite a significant variation, steranes/hopanes ratios also show a slight dependency on geographic position (Fig. 52-b). Low values (<0.5) prevail in northern fields (Van Sickle, Bernhardsthal S, Rabensburg), whereas high values (>0.6) dominate along the Pirawarth Faults System and in the Central High (e.g.Aderklaa, Matzen, Schönkirchen, Ebenthal).

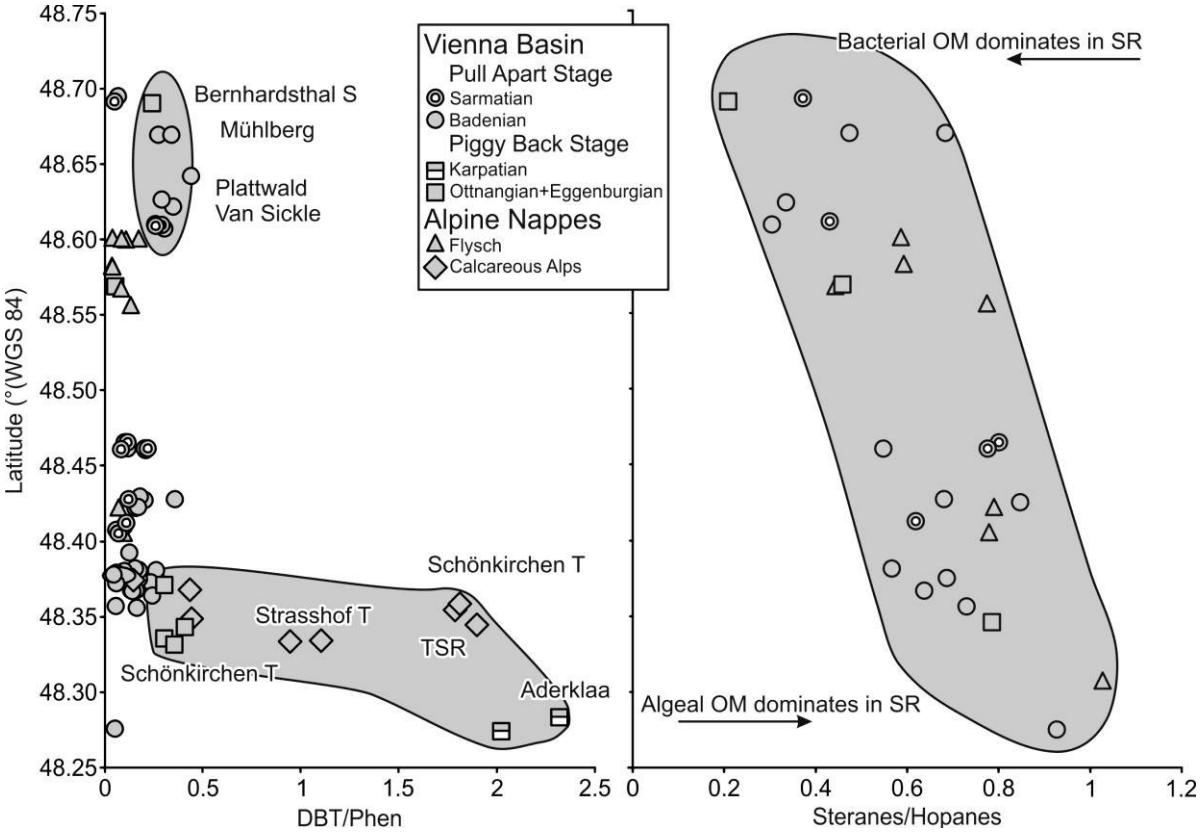

Fig. 52: a) Variation of the Dibenzothiophene/Phenantrene (DBT/Phen) ratio as a function of geographical latitude. High ratios are observed in reservoirs within and above the Calcareous Alps. Slightly elevated ratios are also observed along the northern segment of the Steinberg Fault. b) Cross-plot of the average Sterane/Hopane ratio of oils from different fields against their respective latitude. The slight decrease towards northern fields may be caused by changing input of organic matter.

6.2.3 Microbial and thermogenic gas

Carbon isotope ratios of methane and gas composition show that both, microbial and thermogenic gas occur in the Vienna Basin (Fig. 53). Dry ($C_1/(C_2+C_3)$ >400) and isotopically light ($\delta^{13}C_1$: -57.9 to -62.9 ‰) gas, interpreted as microbial in origin, prevails along the southeastern margin of the Vienna Basin in Sarmatian (Moosbrunn West, Moosbrunn Ost, Fischamend, Orth, Oberweiden) and Badenian (Baumgarten) reservoirs.

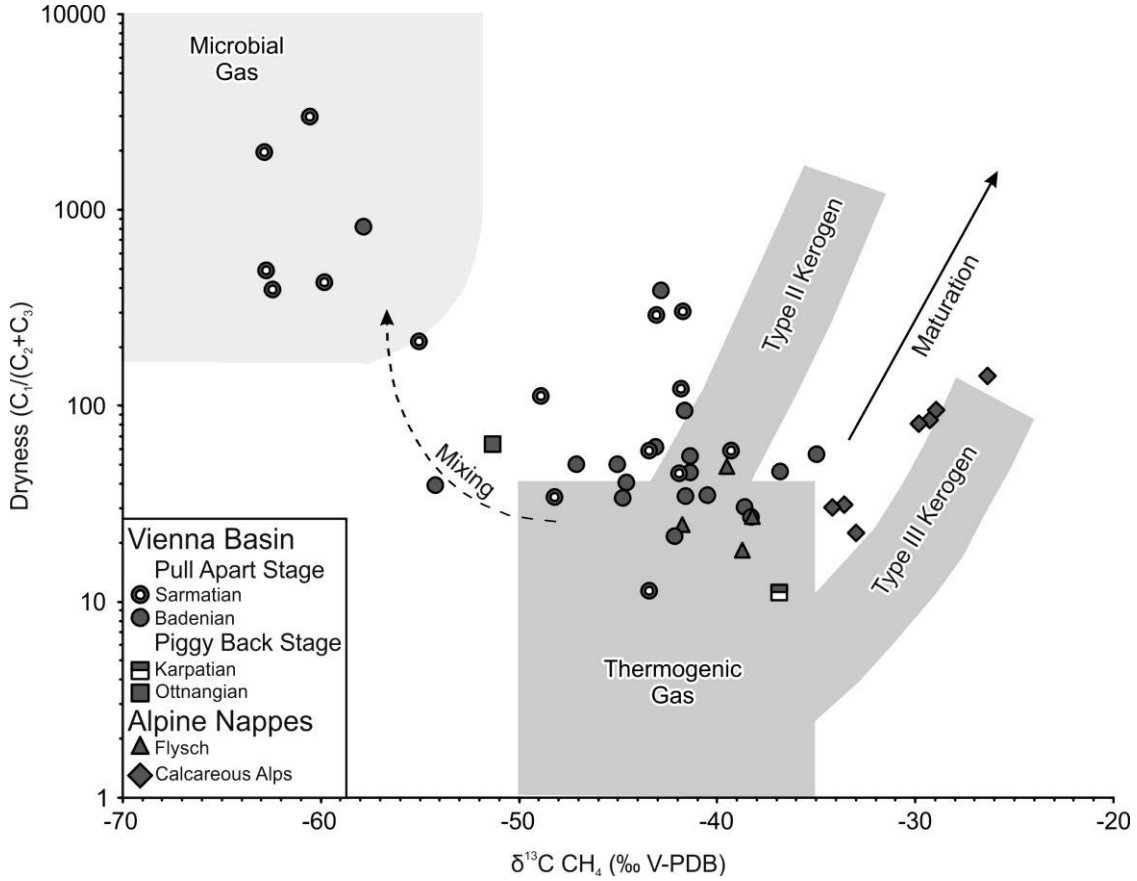

Fig. 53: Genetic classification of gas from the Vienna Basin (mod. from Bernard et al., 1978, Whiticar and Suess, 1990)

With few exceptions, all other gases in Miocene and Flysch reservoirs are wet (<150) and range in $\delta^{13}C_1$ from -35.0 to -55.1. These gases are classified as thermogenic in origin, although they may include varying proportions of primary or secondary microbial methane.

The composition of thermogenic gases is influenced by biodegradation and TSR, but also by EOR (enhanced oil recovery) measures. For example gas the St. Ulrich-Hauskirchen and Hochleiten fields is affected by CO_2 injection. Moreover, traces of H_2S (up to 390 ppm) in Miocene reservoirs are interpreted as contaminations produced by bacteria transported into the sediment by anthropogenic activity (Ladwein, 1982).

In addition to anthropogenic activity, biodegradation of thermogenic hydrocarbons further complicates the interpretation of the origin of the gases. Upward decreasing dryness (e.g. ~500 in Hochleiten 67), i-/n-C_4 and C_2/C_3 ratios (Fig. 51) reflect biodegradation of thermogenic gas in shallow Miocene reservoirs. Isotopically heavy

propane in the St. Ulrich-Hauskirchen Field (Fig. 52-a) are additional consequences of gas degradation. Isotopically light methane and isotopically heavy CO_2 are end-products of anoxic hydrocarbon degradation (Milkov, 2011). Therefore, the observed upward decreasing $\delta^{13}C$ values of methane and upward increasing $\delta^{13}C$ values of CO_2 (Fig. 51) reflect increasing proportions of secondary microbial methane.

Gas in deep and hot carbonate reservoirs within the Calcareous Alps (>4000 m) contain high amounts of CO_2 (1.6-13.2 vol.%) and H_2S (up to 2.6 vol.%). Their origin will be discussed with the context of TSR in one of the following sections.

6.2.4 Gas maturity

Models developed by Berner and Farber (1996) have been applied to estimate the maturity of source rocks during gas generation. Based on isotope data from the Mikulov Formation (Chapter 5), the maturation trend line for a kerogen with -26‰ $\delta^{13}C$ was used in Fig. 54. It is obvious from Fig. 54a that the methane-ethane plot is affected by the presence of microbial methane. As contributions of microbial ethane and propane are very low (e.g. Oremland et al., 1988), more reliable results can be expected from a plot of $\delta^{13}C$ of ethane versus propane (Fig. 54b). According to this plot gas was generated between 1.1 and 1.6 %Rr. This interval is higher than biomarker-derived oil maturities (0.7-0.9 %Rr). As a result of biodegradation, gas from the St. Ulrich field contains isotopically heavy propane and, therefore, plots outside the trend line.

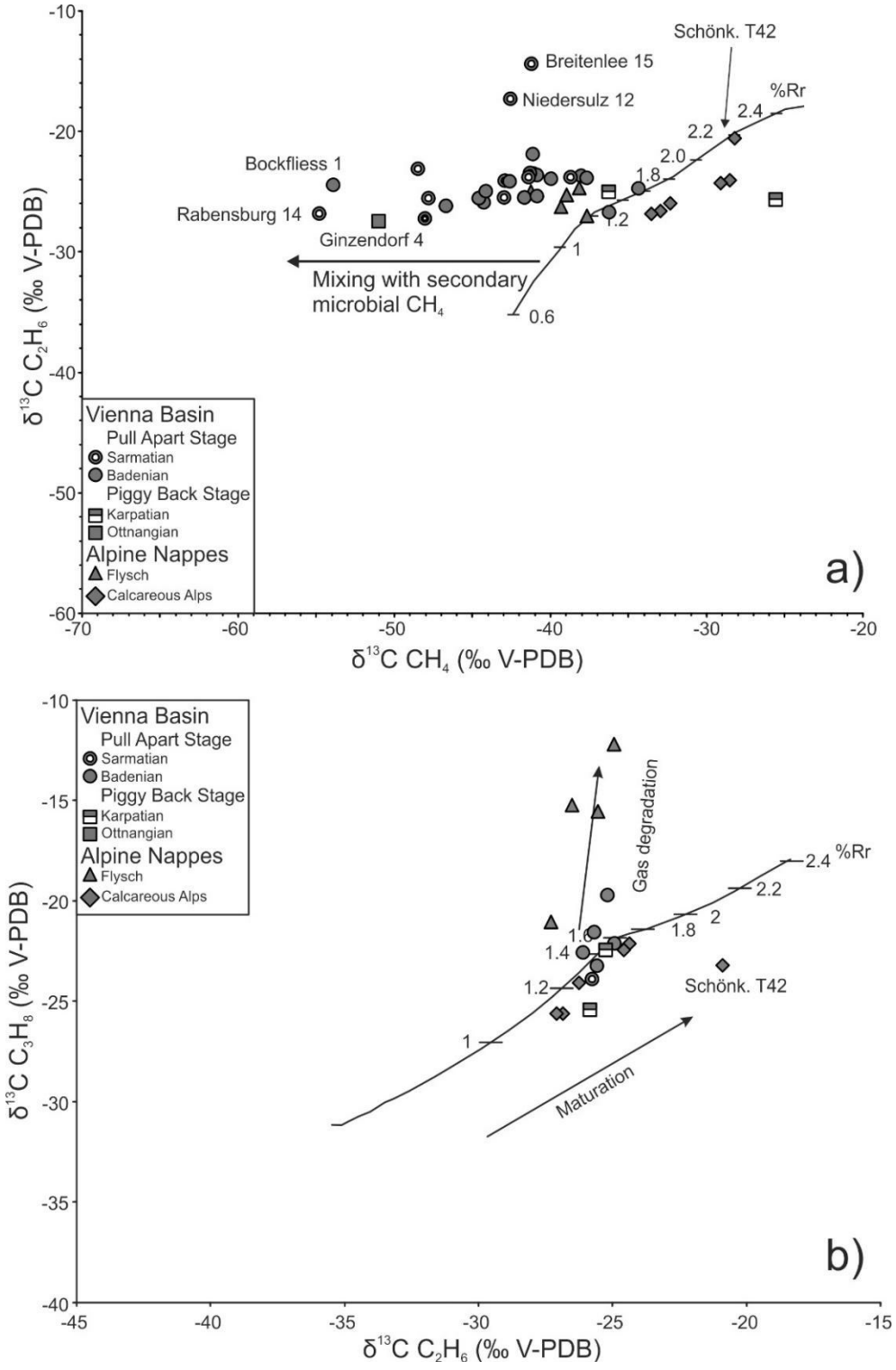

Fig. 54: Maturity characterization of the gases based on the $\delta^{13}C$ of the couples (a) methane-ethane and (b) ethane-propane. Curves indicating maturity of source rocks (-26 ‰ V-PDB) during gas generation expressed in vitrinite reflectance scale are calculated after Berner and Faber (1996)

6.2.5 Biodegradation

Degradation of petroleum by living microorganisms is called biodegradation (Milner et al., 1977, Connan, 1984, Palmer, 1993, Blanc and Connan, 1994). Petroleum quality and volume is significantly decreased with increasing biodegradation. Based on the differential resistivity of different compound classes, different stages of biodegradation have been defined (Alexander et. al., 1983, Moldowan et al., 1992, Wenger and Isaksen, 2002). In this study the biomarker biodegradation scale (BBDS) of Peters et al. (2005) is used to describe the extent of biodegradation. The chemical composition of Vienna Basin oils with different degrees of biodegradation is shown in Fig. 55.

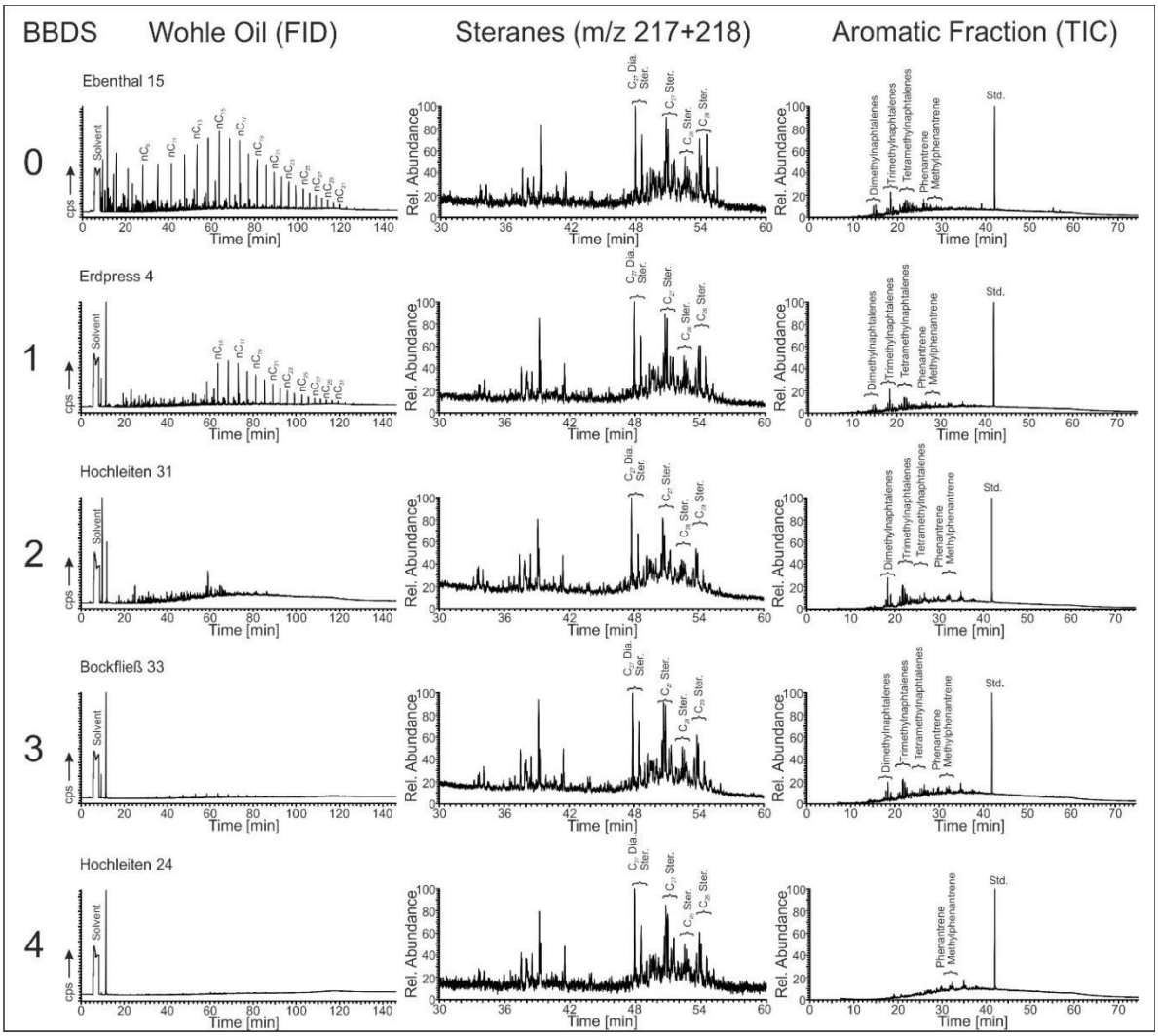

Fig. 55: Variation of the chemical composition of oils with increasing ranks of biodegradation (BBDS - biomarker biodegradation scale). Displayed are the FID-trace of the whole oil, the sterane pattern (m/z 217+218) and the aromatic fraction (TIC-MS trace).

- Undegraded oils (**rank 0**) contain n-alkanes from nC_6 up to nC_{40} with a peak around nC_{15-16}. The mass compounds within the aromatic oil fraction are alkylated napthalenes.
- Slightly biodegraded oils (**rank 1**) are characterized by a significant loss of short chain n-alkanes and the BTEX (benzene, toluene, ethylbenzene, xylene) compounds.
- Moderately biodegraded oils (**rank 2**) have lost nearly all n-alkanes and BTEX-compounds which corresponds to at least 35 vol.% of the original oil volume.
- Heavy biodegradation (**rank 3**) is characterized by a complete loss of n-alkanes and BTEX-compounds. The concentration of isoprenoids is significantly reduced.
- Severe biodegradation (**rank 4**) is characterized by the onset of degradation of cyclic saturated compounds and a near complete loss of all alkylated napthalenes.

The presence of hopanes and the absence of nor-hopanes in all oil samples indicate that stage rank 5 is not reached in the Vienna Basin.

Wenger and Isaksen (2002) and Peters et al. (2005) emphasized that the transition from slight to moderate degradation is gradual. Indeed a rank 1.5 was introduced for four samples (Maustrenk 29, St. Ulrich 213, Steinberg 11, Windisch Baumgarten 1).

The rank of biodegradation clearly controls oil gravity (Fig. 56-a). The observed wide variation of API gravity in rank 0 oils (23.7-52.5°) is due to TSR in deep reservoirs and will be discussed in a later section. API gravity of oil with severe biodegradation is <19°.

6.2.5.1 Controls on biodegradation

There is an obvious relationship between the extent of biodegradation, reservoir temperature (Fig. 56-b) and reservoir depth (Fig. 56-c). As expected, oil degradation is restricted to temperatures up to 80°C (Connan, 1984, Palmer, 1993, Blanc and Connan, 1994, Shi et al., 1982), corresponding to a depth of about 3 km in the Vienna Basin.

Because of the strong relation between biodegradation and API gravity in the Vienna Basin (Fig. 56-a), the latter can be used as a proxy for oil degradation. In Fig. 57 oil gravity is plotted versus depth for different tectonic settings. It shows a strong relation between reservoir depth and oil degradation and that oils in hangingwall reservoirs along the Pirawarth and the Steinberg faults are more heavily degraded than oils in footwall reservoirs. Because biodegradation is dependent on the availability of formation water providing nutrients for microbial activity (Peters et al., 2005), this indicates that fluids circulate more easily through the major faults into hanging wall reservoirs than into footwall reservoirs, which are often formed by low permeable turbidite sands (5-10 mD; Glantschnig and Kroell, 1997) within the Flysch Zone.

Oils above the Matzen High (Bockfliess, Matzen, Prottes) are heavily degraded, but oils from similar depths in the Ebenthal Field, located at its northeastern margin, are not. Probably this reflects an influence of sandstone facies and trap type. Studied oils from the Bockfliess, Matzen and Prottes fields are produced from transgressive sands (9^{th} and 16^{th} TH) with high porosity and permeability. In contrast, oil in the Ebenthal Field is produced from turbiditic sands (15^{th} TH) forming a structural-stratigraphic trap near their shale out (Kreutzer, 1993, Hamilton et al., 2000). This suggests that differences in the degree of biodegradation are again related to sandstone permeability and the availability of nutrients for microbial activity. Apparently this is restricted in the Ebenthal field. Similar controls were described by Brooks et al. (1988) in Western Canadian oil deposits, where oil in fine-grained sandstone is less susceptible to biodegradation than oil trapped in coarse-grained sandstone.

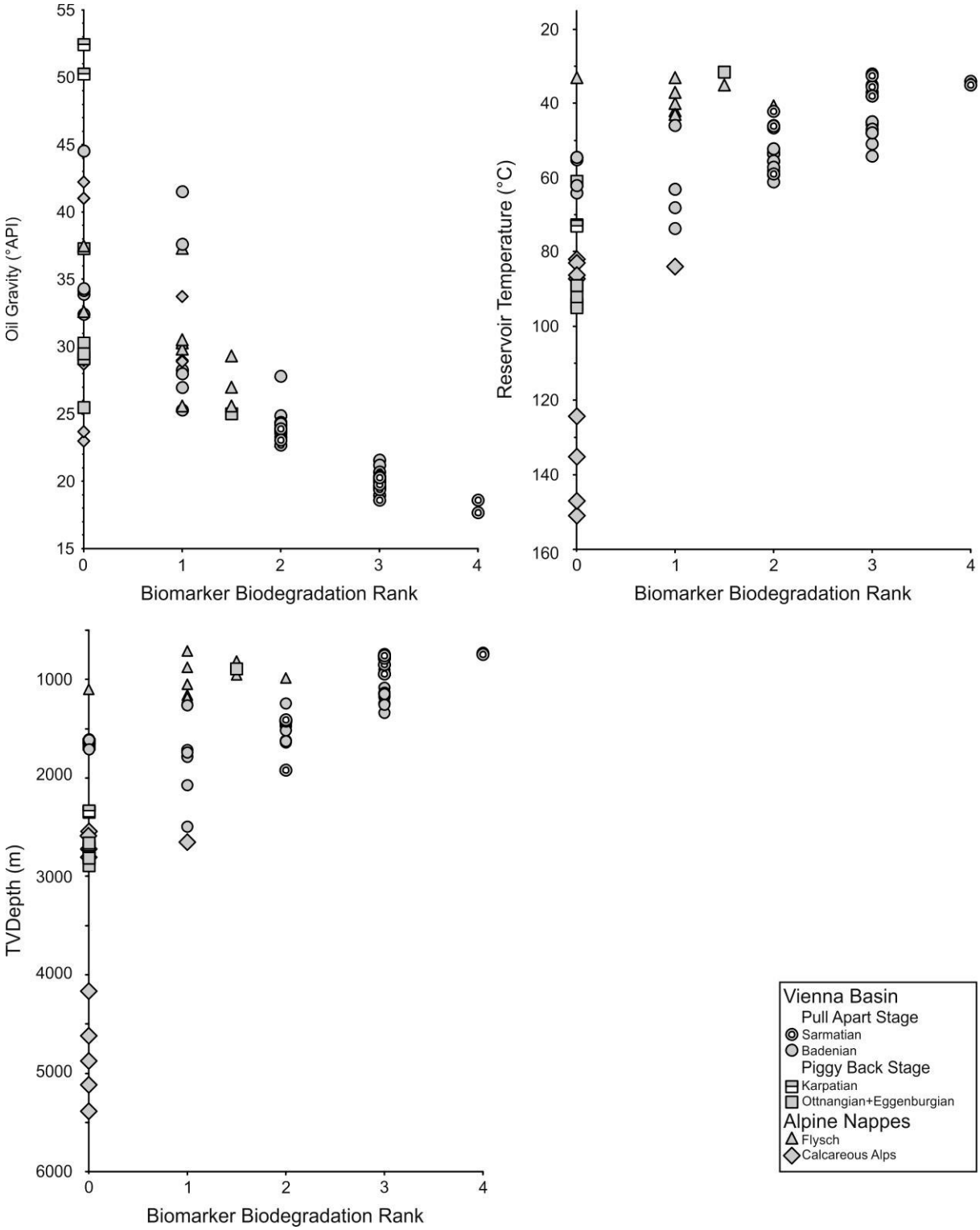

Fig. 56: Variability of the extent of biodegradation against temperature and depth. Reservoir temperatures were estimated using data from Leutner (1990). Due to data gaps, not all reservoir temperatures could be estimated. Clearly different factors control the amount of biodegradation in Flysch- and Miocene reservoirs.

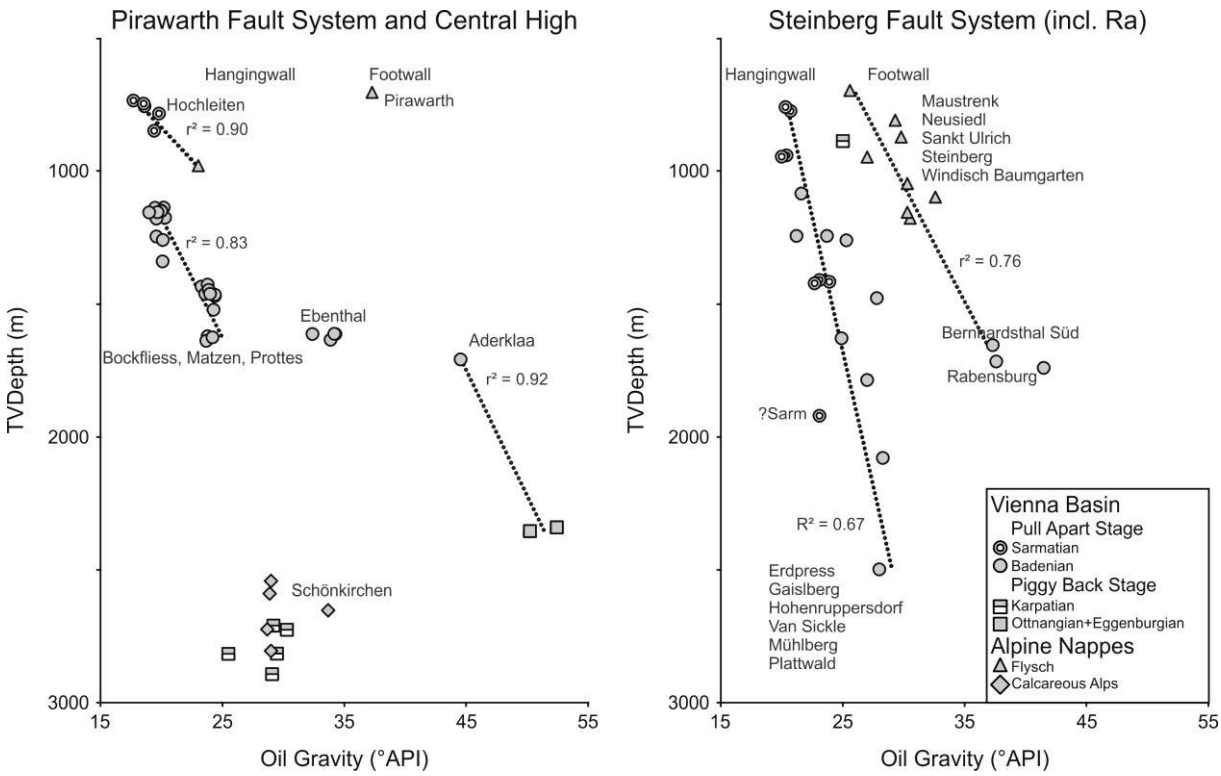

Fig. 57: Gravity versus depth for oils in Flysch and Miocene reservoirs in the Vienna Basin. The plot shows that gravity decreases with depth, but at different rates in different units.

6.2.5.2 Biodegradation and gas composition

The i-/n-C_4 and the C_2/C_3 ratio are proxies for gas degradation as microbes preferably consume n-alkanes and C_3 (Jones et al., 2008; Brown, 2011; Milkov, 2011; Larter and di Primio, 2005). Products of anaerobic biodegradation are secondary microbial methane and isotopically heavy CO_2 (Milkov, 2011). Consequently high i-/n-C_4 and C_2/C_3 ratios in shallow gases (<1600 m subsea; Fig. 49) reflect biodegradation. Moreover anaerobic biodegradation is supported by the presence of isotopically light methane and isotopically heavy CO_2 in many shallow reservoirs.

As an example, gas from Badenian reservoirs in the Bockfliess Field, associated with heavily biodegraded oil (rank 3), is characterized by -54 ‰ $\delta^{13}C_1$ and +6 ‰ $\delta^{13}C_{CO2}$. Methane with negative $\delta^{13}C_1$ values (-49 to -42 ‰) is also associated with severely biodegraded oil (rank 4) in the Hausleiten Field. Unfortunately, $\delta^{13}C_{CO2}$ values (+8 to +18 ‰) are probably influenced by CO_2 flooding in 2003 (Potsch et al., 2004).

The presence of isotopically heavy (residual) C_3 in the St. Ulrich Field (Fig. 50), producing from shallow (<1050 m) Flysch reservoirs in the footwall of the Steinberg Fault, may be another argument for microbial degradation. However, relatively low i-/n-C_4 ratios (0.7 - 1.7) and the presence of only slightly biodegraded oils (rank 1) argue against major degradation. High percentages of isotopically heavy CO_2 (+9 to +16 ‰) in this field are probably due to EOR measurements.

6.2.5.3 Biodegradation and trace element concentration

Ni, V, and Co may replace Mg within porphyrin complexes, which are created from chlorophyll (Sundararaman et al., 1988a, 1988b). Porphyrines show no evidence of destruction during biodegradation (Sundararaman and Hwang, 1993). So these elements become concentrated during biodegradation due to removal of mass compounds. To test this hypothesis concentrations of Ni (585 - 9920 ppb), V (9 - 58 ppb), Co (13 - 104 ppb) and S (78 - 2620 ppm) are plotted versus API gravity in Fig. 58. Indeed, (with the exception of the V concentration of a slightly degraded oil sample) there is a strong correlation between trace element concentrations and gravity. There is also a strong correlation between sulphur contents and biodegradation, but sulphur can also be enriched by sulphate reduction (Cai et al., 2001).

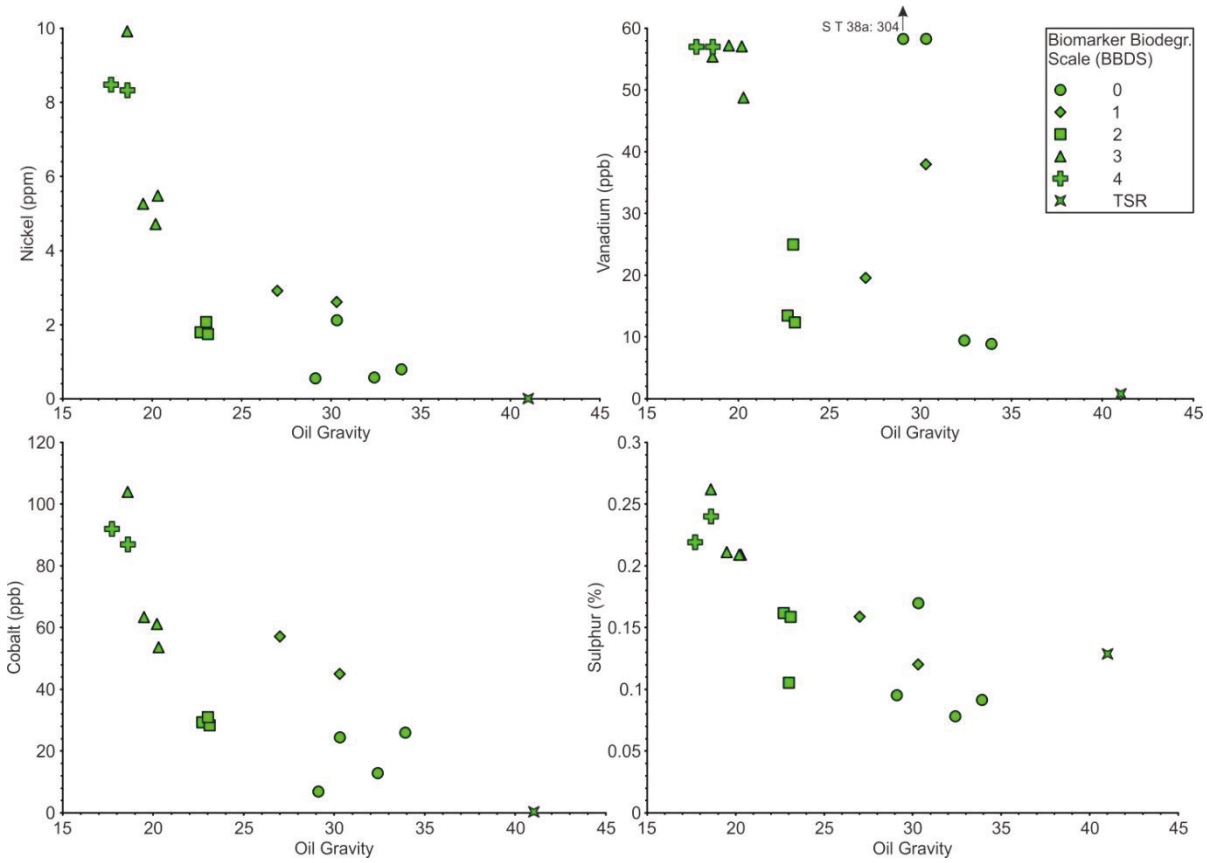

Fig. 58: Variation of trace element concentration against oil density. BBDS acc. Peters et al. (2005). Strongly degraded oils are characterized by high density (low API°) and an enrichment of trace elements.

6.2.6 Thermochemical sulphate reduction

Thermochemical sulphate reduction (TSR) is the abiotic reaction of sulphate ions with organic matter to methane and hydrogen sulphide (H_2S). It is a widely recognized alteration process in carbonate reservoirs (Orr, 1974, Krouse, 1977, Cai et al., 2001; King et al., 2012). The lower thermal limit is controversial, but in the order of 100 to 140°C (Worden et al., 1995; Machel, 1998; 2001).

6.2.6.1 Distribution and characteristics of TSR affected (H_2S-rich) gases

Gas from reservoirs in the Flysch Zone and the Miocene basin fill is largely free of H_2S. In contrast, gases produced from the Lunz-Frankenfels and Göller nappes in the Calcareous Alps are typically rich in H_2S.

The most important gas fields in the Calcareous Alps are the Aderklaa (Fig. 59a), Straßhof Tief and Schönkirchen Tief (Fig. 59b) fields. Reservoirs are mainly dolomitic rocks in different tectonic units within the Lunz-Frankfels nappe (from NW to SE: “Reyersorf Anticline” (relief trap), “Perchtoldsdorf Trend” (internal trap), Aderklaa and Schönkirchen ÜT Trends; internal trap). In Schönkirchen oil and gas are also produced from the Göller nappe (relief trap; Fig. 59b). Apart from the above fields, H_2S rich gas was also produced from the Hirschstetten Field (Lunz-Frankenfels Nappe). The Baumgarten Field is partly located in the Göller nappe from where it produced gas with low H_2S contents.

Only a limited number of gas samples from the Calcareous Alps was available for the present study (Schönkirchen ÜT [5470-4873 m] and Göller nappe [2805-2542 m], Ebenthal Tief [3300 m]). Therefore H_2S contents of these samples are supplemented by gas data (average values for specific depth intervals) from the OMV archive in Fig. 60. In these plots the data are differentiated according to gas fields (Aderklaa, Straßhof Tief, Schönkirchen Tief) and tectonic units within these fields. Average gas composition data are displayed for the most important reservoirs in Fig. 59.

In the Aderklaa Field gas from the Reyersorf Anticline (2550-2900 m) contains a wet gas ($C_1/[C_2+C_3]$: <50) with low H_2S (~0.3 %) and CO_2 (<2 %) contents. A slightly higher H_2S content (1.1 %) is observed in a single, slightly deeper sample from borehole Ad 80 (~3000 m). Gas from the Perchtoldsdorf Trend contains significantly higher H_2S (~1.7 %) and CO_2 (~3.5 %) contents and is slightly more dry (~200) despite of similar depth (2670-2870 m). Even higher H_2S (~3.0 %), but similar CO_2 (3.0-5.4 %) contents are recorded in gas from the Aderklaa ÜT Trend (3080-3190 m), which is the driest gas (~300) in the Calcareous Alps.

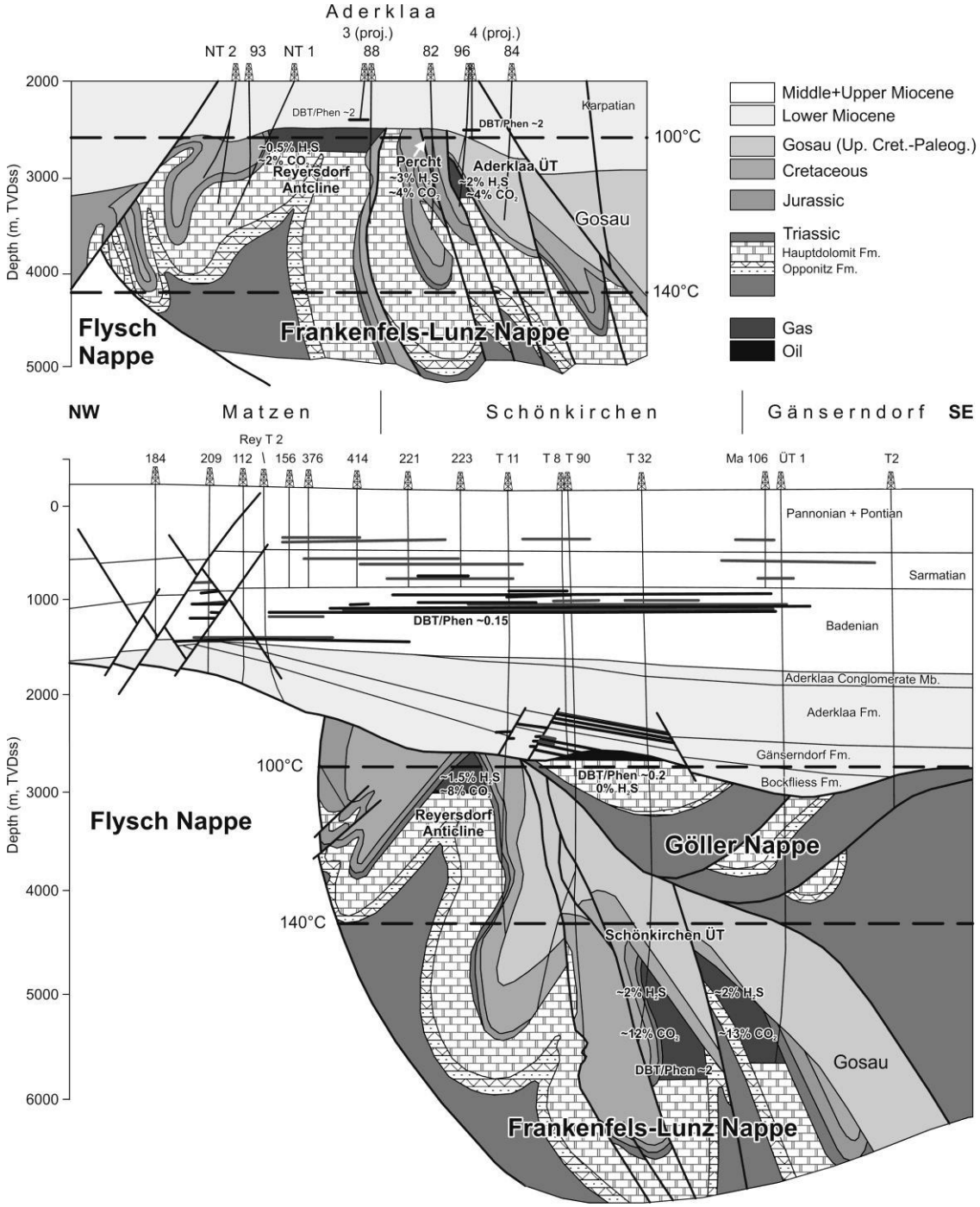

Fig. 59: Cross-section through the a) Aderklaa and b) Schönkirchen fields. Average gas composition, DBT/Ph (dibenzothiophene/phenanthrene) ratios in oils and the 100°C as well as the 140°C isotherms are shown. Modified from Wessely, 1993 and Wessely and Gohs, 1993.

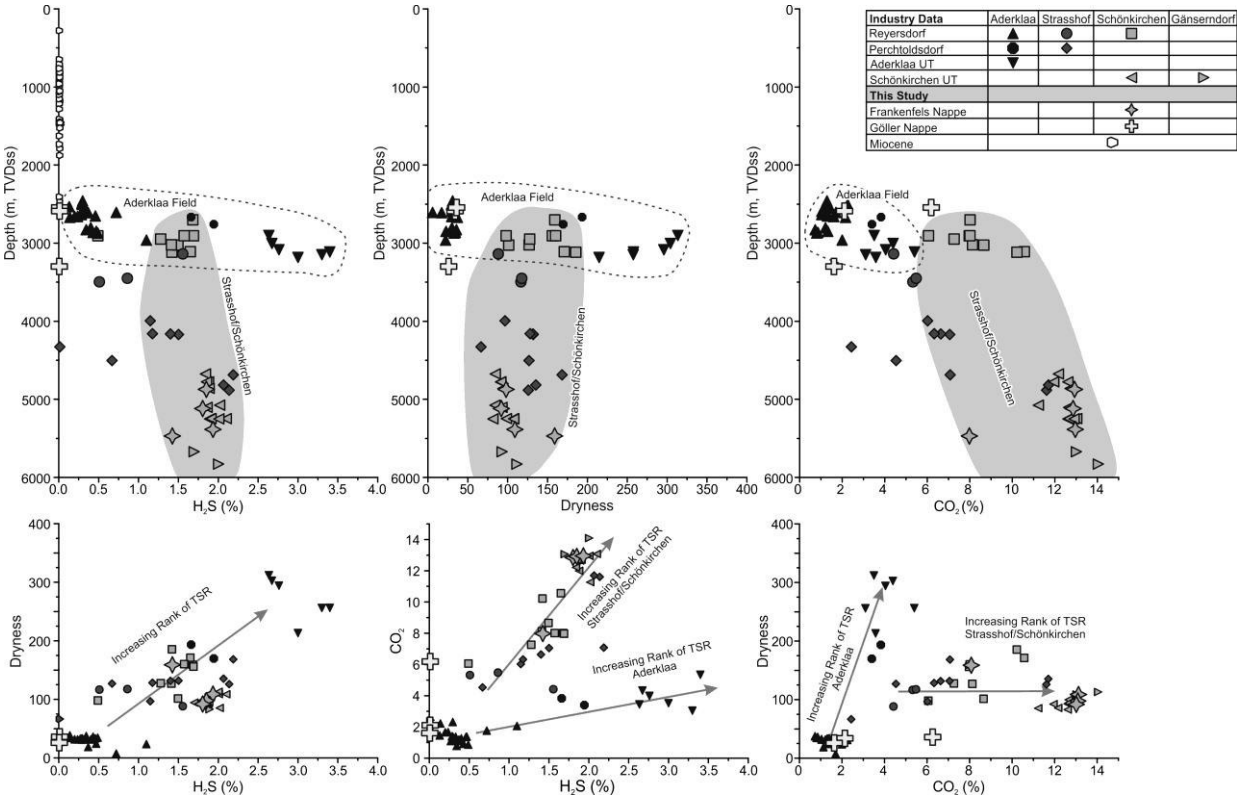

Fig. 57: a) Plots of H_2S contents, dryness and CO_2 contents of gases in the Calcareous Alps versus depth (data from the OMV archive). b) Cross-plots of H_2S contents, CO_2 contents and dryness. The data points are labelled according to hydrocarbon field and tectonic unit.

In the Straßhof Field gas with varying H_2S contents (0.5-1.6 %) was encountered in the Reyersorf Anticline (3100-3500 m), whereas gas from the Perchtoldsdorf Trend, typically contains 1.2-2.2 % H_2S, although two samples (Str T11; ~4300 m; 0.0 %; Str T5a, ~4500 m; 0.7 %) are poor in H_2S. CO2 contents range from 2 to 12 % and are positively correlated with H_2S contents (r^2=0.76).

In the Schönkirchen Field (Fig. 59b) H_2S contents in gas from the Reyersorf Anticline (2900-3120 m) typically is about 1.5 % with the exception of a single relative shallow sample from well S T 53 (0.5 %). CO_2 contents are about 8 %. Higher H_2S (~2.0 %) and CO_2 contents up to 13 % are determined in deep gases from the Schönkirchen ÜT Trend (4500-6000 m).

Notably gas associated with oil produced from a relief structure within the Göller Nappe (~2500 m depth) contains traces of H_2S only. Similarly gas with low H_2S

contents (~0.2 %) was produced from the Göller Nappe in the Baumgarten Field (2560 m depth).

Overall there is a positive relation between H_2S contents and dryness (Fig. 60; r^2=0.66), confirming that TSR causes gas drying (e.g. Sassen et al., 1987; Worden and Smalley, 1995; Nöth, 1997). H_2S is also positively correlated with CO_2. However, different trends are observed for the Aderklaa Field, which contains relative low amounts of CO_2 (r^2=0.80; CO_2 = 1.03% H_2S+1.04) and the Straßhof and Schönkirchen fields, rich in CO_2 (r^2=0.61; CO_2 = 4.94% H_2S+1.74). Similar differences in H_2S/CO_2 ratios have been described by Machel et al. (1995) in Western Canada and by Worden and Smalley (1996) in Abu Dhabi and probably reflect that the H_2S/CO_2 ratio originally formed is variable and/or result from later selective removal of H_2S/CO_2 (Machel, 2001).

Gases from the Calcareous Alps are isotopically heavy ($\delta^{13}C$ -26 to -34‰; Figs. 50, 53). Based on these isotope data, Schoell (1984) proposed a coaly source for gas in the Calcareous Alps. However, coaly rocks (e.g. Carnian Lunz Beds) are thin and probably not able to generate huge amounts of gas. Alternatively, we assume that the heavy isotope signature, especially of deep H_2S rich gases from the Schönkirchen ÜT Trend (-26 to -30‰ $\delta^{13}C_1$), is the combined effect of elevated maturity and TSR (Chung et al., 1988; Machel et al., 1995).

6.2.6.2 Origin of sulphur

Stable sulphur isotope ratios ($\delta^{34}S$) of H_2S and sulphate rocks can be used to determine the sulphur source, although temperature-dependent kinetic isotope fractionation during TSR (up to -20 ‰) is sometimes observed (Harrison and Thode, 1957; Husain, 1967; Husain and Krouse, 1978; Kiyosu, 1980; Kiyosu and Krouse, 1990). However, if sulphate is faster consumed by TSR than it can be dissolved from the source formation, no fractionation will be observed, because all sulphate will be consumed. This is true, even if additional sulphate becomes available after TSR (Machel et al., 1995). Stable sulphur isotope ratios of H_2S and sulphate rocks within the Calcareous Alps are listed in Table 4 and Appendix XI respectively. Assuming that all sulphate has been consumed, we argue for a single sulphur source for TSR in the Frankenfels-Lunz nappe, namely anhydrites in the Upper Triassic (Carnian)

Opponitz Formation, which are widespread in this nappe. Following Ladwein (1982), the source for (minor) H_2S in the Baumgarten Field, located within the Göller nappe, may be the Permian part of the Werfen Formation.

Table 4: Stable sulphur isotope ratios of anhydrates with the Calcareous Alps in the subsurface of the Vienna Basin (Ladwein, 1982).

Opponitz Fm. (Frankenfels-Lunz Nappe):	14.5-17.5 ‰ $\delta^{34}S$
Reichenhall Fm. (Ötscher Nappe):	23.5-24.5 ‰ $\delta^{34}S$
Werfen Fm. (Triassic/Ötscher Nappe):	24.0-27.5 ‰ $\delta^{34}S$
Werfen Fm. (Permian/Ötscher Nappe):	10.5-13.0 ‰ $\delta^{34}S$

6.2.6.3 Distribution and characteristics of TSR affected (S-rich) oils

Oils from the Calcareous Alps, which coexists with H_2S-rich gas, are typically lighter (>40° API) than unaltered oils (Straßhof?), and consist mainly of n-alkanes (peaking at nC_{10-12}) and alkylated naphtalenes, but lack complex biomarkers (e.g. steranes; Fig. 61). The TSR affected oils are characterized by high organic-bound sulphur contents (e.g. dibenzothiphene; Fig. 61) and thus strongly elevated dibenzothiophene /phenantrene (DBT/Ph) ratios (Fig. 62). The sulphur content of oil from Schönkirchen Tief 62 (5119.25 m; Fig. 59) is 0.13 wt.%. This value is relative high, if the low oil density (41°API) is considered. Relative high sulphur contents (up to 0.8 wt.%) have also been reported from Schönkirchen Tief oils by Ladwein (1982) and are known from other TSR oils (Amrani et al., 2012; Truche et al., 2014).

In the Straßhof-Schönkirchen area, both DBT/Ph ratio (Fig. 61) and H_2S contents increase with increasing depth. DBT/Ph ratios of oil from the relief structure within the Göller Nappe (~2550 m depth; Fig. 59b) is only 0.4, but still higher than in most Miocene reservoirs (Fig. 62). Similar DBT/Ph ratios in Miocene reservoirs are only observed in oils accumulated in Oligocene carbonate debris along the flanks of the buried hill (2710-2815 m).

The only oils from Miocene reservoirs with very high DBT/Ph ratios (~2) are found in clastic Lower Miocene (Karpatian) reservoirs in the Aderklaa Field (Ad 3, 4; ~2350 m; Figs. 59a, 62), although gas from these reservoirs are free of H_2S (Ladwein, 1982). Based on the very high DBT/Ph ratios, these oils are considered as TSR affected, thus indicating upward migration of TSR oils from the Calcareous Alps (e.g. Aderklaa

ÜT trend) into the Lower Miocene succession. Whereas H_2S was lost, probably by pyrite precipitation, organic bound sulphur has not been removed. Thus, high DBT/Ph ratios may be used as proxies for TSR in hydrocarbon deposits where H_2S is missing.

This finding has major implications for the understanding of hydrocarbon migration. Whereas former models (e.g. Ladwein et al., 1988) assumed that oil generation occurred after deposition of the Miocene basin fill, Rainer (oral comm.) showed that oil generation probably ended before Miocene time. This implies that hydrocarbons, which are now found in Miocene reservoirs, must have been temporarily stored elsewhere. Internal traps within the Calcareous Alps are a likely site for this temporal storage. However, as the majority of oils in Miocene reservoirs is not affected by TSR, this makes models necessary which prohibited TSR (e.g. reservoir temperature <100°C, restricted sulphate availability).

Pr/Ph ratios in the Ad 3 and 4 samples are relative high, but still within the variability of other oil samples from Miocene reservoirs (Fig. 62). Nevertheless, we speculate that the ratios are increased due to evaporative fractionation occurring during upward migration through rocks with low permeability (Machel et al., 1995).

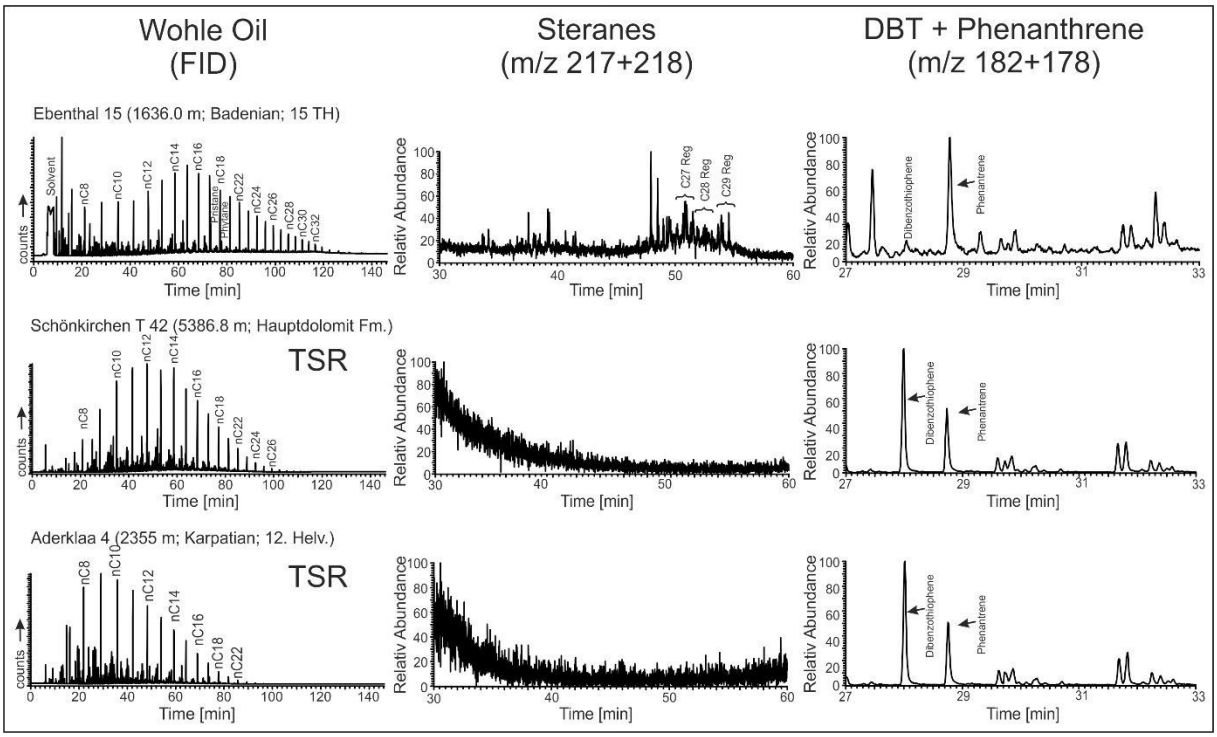

Fig. 61: FID-traces of whole oils, steranes (m/z 217 and 218) and mass trace (m/z 182+178) to detect dibenzothiophene (DBT) and phenathrene. Oils Schönkrchen T42 and Aderklaa 4 suffered thermochemical sulphate reduction (TSR). The unaltered Ebenthal oil is shown for comparison.

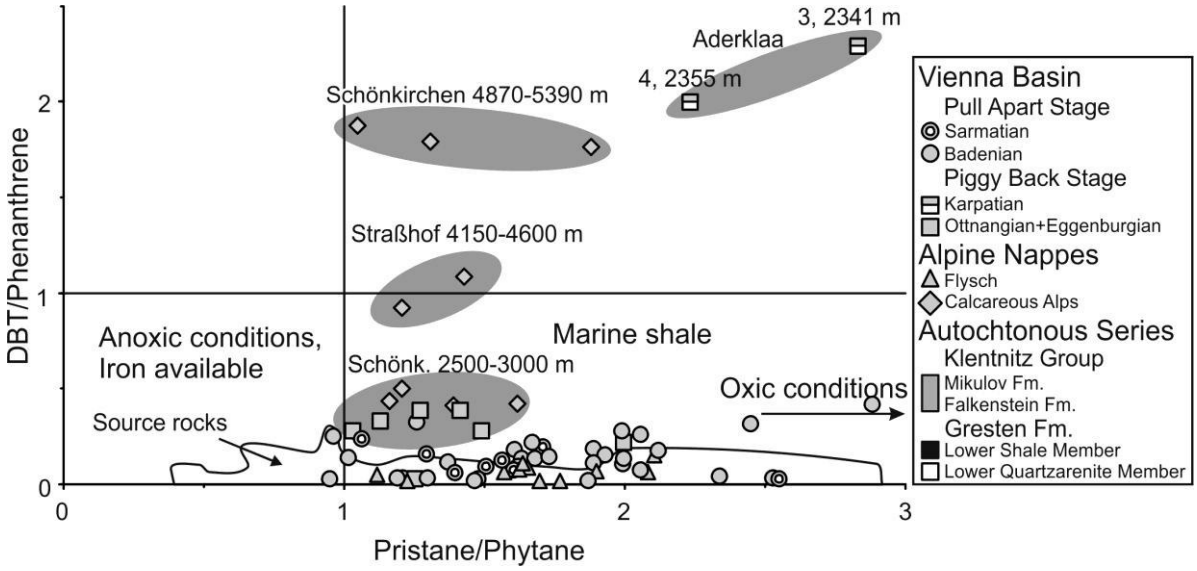

Fig. 62: Cross plot of Pristane/Phytane and Dibenzothiophene(DBT)/Phenantrene ratios. TSR affected oils are highlighted by grey shading.

6.2.6.4 Factors controlling TSR gas and oil in the Vienna Basin

Fig. 60 shows that neither H_2S content nor dryness of gases in the Calcareous Alps follow a simple depth trend. Moreover high H_2S contents occur in shallow reservoirs with temperatures around or slightly above 100°C. Although TSR can start at 100°C (Machel, 2001), most authors assume that TSR requires significantly higher temperatures (>140°C; e.g. Nöth, 1997; Worden et al., 1995; Machel, 2001).

Therefore, low H_2S contents in the shallow Reyersdorf Anticline in the Aderklaa Field may reflect the fact that significant TSR was hindered by low formation temperatures (~100°C). On the other hand, high H_2S contents in the Perchtoldsdorf and Aderklaa ÜT trends may be explained by upward migration of relative dry, H_2S-rich gas from deeper and hotter parts of the Lunz-Frankenfels nappe. Perhaps upward migration was caused by the significant increase in volume of gaseous products, which occurs during TSR (Machel, 2001), and which may have triggered spilling from pre-existing deeper traps.

An alternative scenario is that low H_2S contents in the Reyersdorf Anticline in the Aderklaa Field are caused by pyrite precipitation resulting in a loss of H_2S. This assumption is inspired by the fact that the Reyersdorf Anticline forms a relief trap with extensive contact to overlying Lower Miocene siliciclastic seal rocks. The same explanation could be used to explain the observed low H_2S contents in associated gas from the buried hill structure in the Göller nappe. Indeed, elevated DBT/Ph ratios (Fig. 62) indicate that the oil is slightly enriched in sulphur. However, TSR probably played probably a minor role. Moreover, gas in the Reyersdorf Anticline in the Aderklaa Field is wet and low in CO_2. Hence we assume that the hydrocarbons were affected by insignificant TSR, because of low temperatures.

7. Oils in the Czech and Slovak part of the Vienna Basin

Oils from the Czech Republic and Slovakia have been sampled in the archive of the Austrian Geological Survey. As these samples were stored during WWII, they are labelled with German names. In this thesis the Czech/Slovac names are used

Göding – Hodonín
Lanzhot – Lanžhot
Egbel – Gbely
Holitsch – Holíč.

Unfortunately no information about the reservoir horizon, depth, density or the well position was available.

7.1 Results

7.1.1 Biomarkers

Straight chain alkanes, isoprenoids - Most samples are characterized by unimodal n-alkane distributions with a maximum intensity in the range of nC_{16-19}. The Gbely 2 oil display a shift in maximum intensity in direction of longer n-alkanes, whereas n-alkanes are absent in Hodonín 1. Bimodal distributions of n-alkanes are observed in samples from fields Lanžhot and Holíč. The characteristics of these oils argue for a mixing of crude oil with high maturity condensates.

The carbon preference index (CPI; Bryan and Evans, 1961) of undegraded samples is close to equilibrium (0.99-1.03). Slightly degraded samples show a dominance of odd numbered n-alkanes (~1.2).

The Pr/Ph ratios typically range from 1.53 to 2.2. Only in Gbely H6 the Pr/Ph ratio is 5.0.

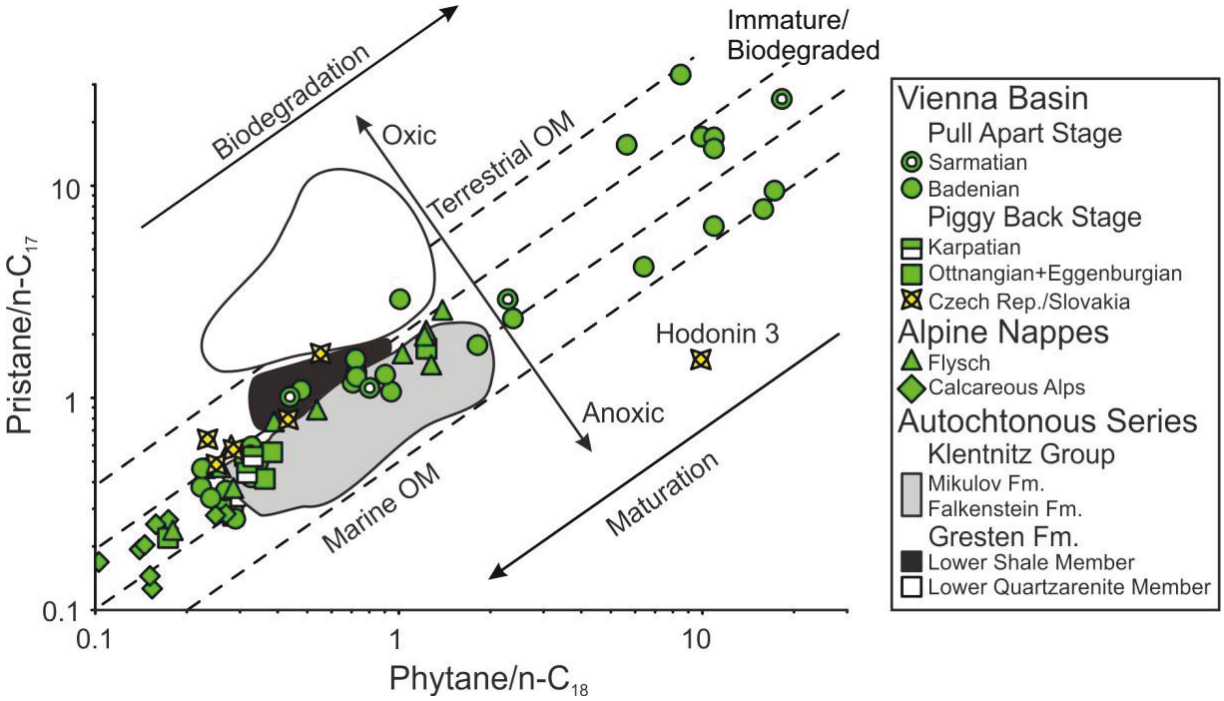

Fig. 63: Cross-plot of the Phytane/nC_{18} and Pristane/nC_{17} ratios (Connan and Cassou, 1980). Oils from the Czech Republic and Slovakia correlate to oils from Austria and to the Mikulov Formation The sample from well Hodonin 3 suffers from a biodegradation which had already removed nC_{18} completely, but some nC_{17} remains.

Because isoprenoids are more resistant towards biodegradation than n-alkanes, the Pr/nC_{17} ratio and the Ph/nC_{18} ratio increase during biodegradation. Hence, the cross plot of Pr/nC_{17} versus Ph/nC_{18} reveal that all samples are mature, but that the sample from well Hodonín 3 suffered from slight biodegradation (Fig. 63). Samples Gbely 2 and Hodonín 1 are not plotted because of the absence of nC_{17}.

Steroids - All samples are dominated by 14β, 17β(H) steranes over 5α, 14α, 17α(H) steranes isomers. The relative abundance of C_{27} steranes (31-48 %), C_{28} steranes (21-40 %) and C_{29} steranes (29-43 %) varies significantly, but the ternary steranes diagram shows that, with the exception of Gbely H6, most samples plot into a narrow cluster (Fig. 64).

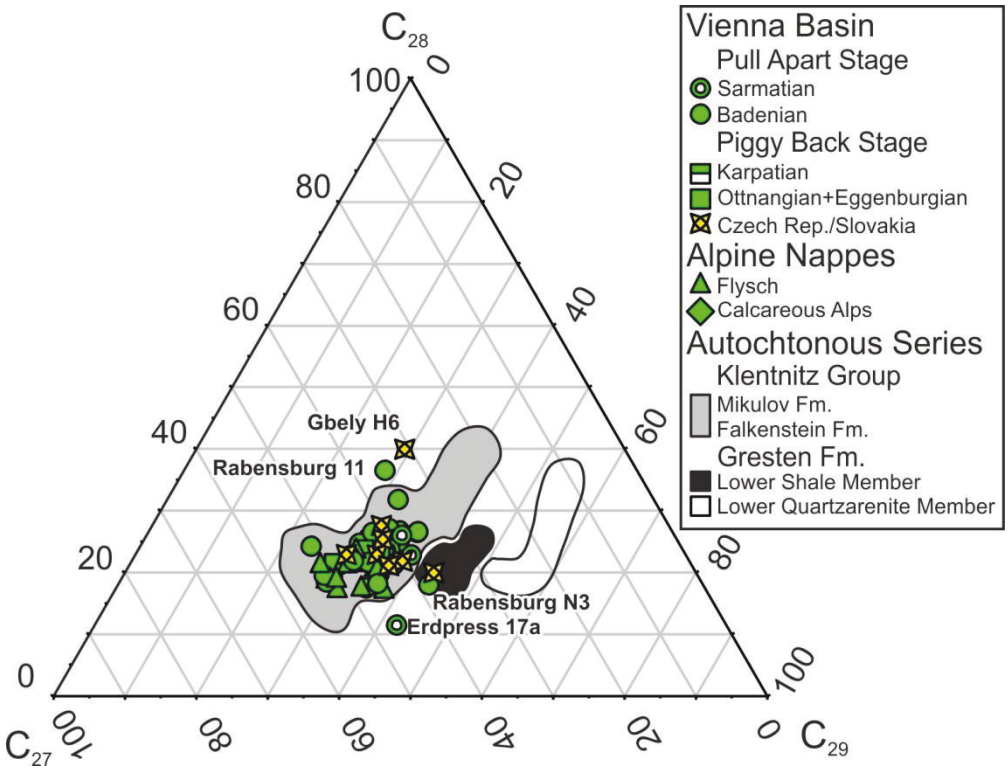

Fig. 64: Sterane triangle indicating the origin of the oils from Austria, the Czech Republic and Slovakia originate from the Mikulov Formation.

The observed C_{28}/C_{29} steranes ratios (0.5-1.0; Fig. 32) agree with an assumed Mesozoic age (Grantham and Wakefield, 1988). Lower values (argueing for Paleozoic source rocks) are found in biodegraded samples Gbely 2 and Hodonín 1. Gbely H6 shows a very high C_{28}/C_{29} steranes ratio, which would fit with a Cenozoic source rock.

The 20S/(20S + 20R) ratio of the C_{29} steranes varies between 0.46 and 0.67. This is close to the equilibrium value (0.55), which is reached at 0.8 %Rr (Mackenzie and Maxwell, 1981).

Hopanoides - Hopanes occur (in minor) amounts within all samples. The steranes/hopanes ratio reflects the ratio between eucariotes (mainly algae) and procariotes (microbial biomass) and varies significantly between 0.3 and 0.6.

Oleanane, a biomarker typical for oils with a Late Cretaceous or younger age, has not been detected in any of the oil samples.

The ratio of 22S/(22S + 22R) isomers of the C_{31} hopanes is close to the equilibrium of 0.6 showing that the maturity of the source rocks is at least 0.6 %Rr. The Ts/(Ts+Tm) ratio suggests peak oil maturity (~0.9 %Rr).

Polycyclic aromatic hydrocarbons - Mono-, di-, tri-, and tetramethylated naphthalens are present in high quantities within the samples together with phenanthrene and methylphenanthrenes. MPI values range from 0.47 (Hodonín 3) to 0.89 (Hodonín 4). Gbely H6 yields a lower value (0.13).

In the fields Holíč and Lanžhot, PAHs, which are interpreted as products of thermal ("pyrolytic") processes (fluoranthene, pyrene), are present. This argues for the mixing of crude oil with a high maturity condensate. All other samples do not contain these compounds (or any other PAHs with more than 3 rings). This argues against input from a source rock with a high amount of terrestrial organic matter (Killops and Killops, 1993).

7.1.2 Stable carbon isotope ratios

$\delta^{13}C$ values of the aliphatic fraction range from -24.6 to -25.5 ‰ and for the aromatic fraction from -24.7 to -27.5 ‰ (Fig. 65).

Compound specific stable carbon isotope ratios of a single, slightly degraded oil could be gained (Fig. 66). The maximum intensity signal for single compounds was obtained for n-alkanes in the range of nC_{17} up to nC_{22}.

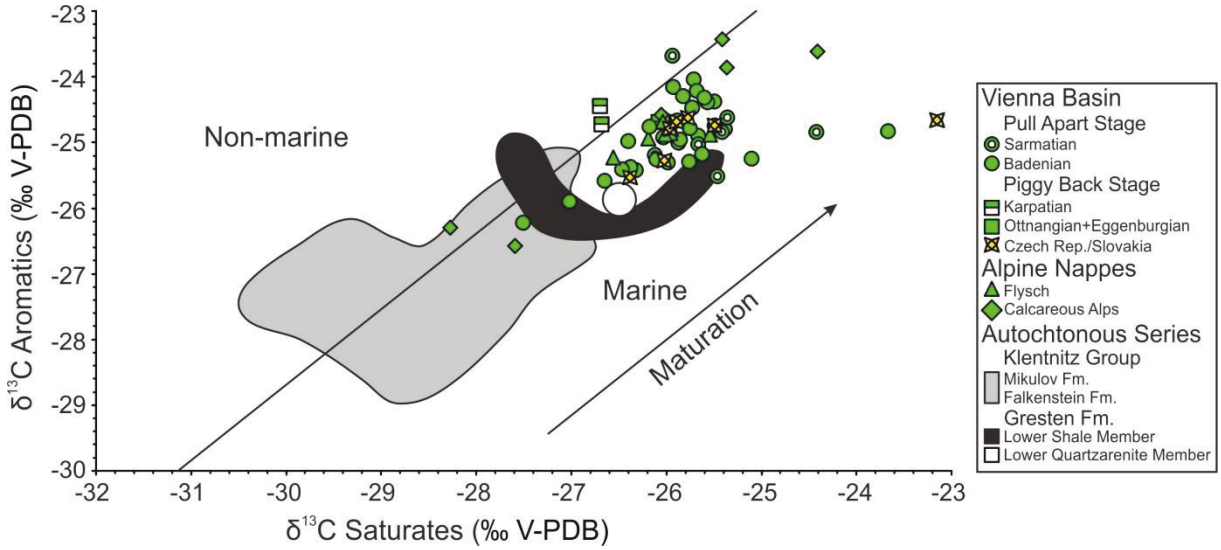

Fig. 65: Cross-plot of the stable carbon isotope ratio of the aliphatic and aromatic fraction (according to Sofer, 1984).

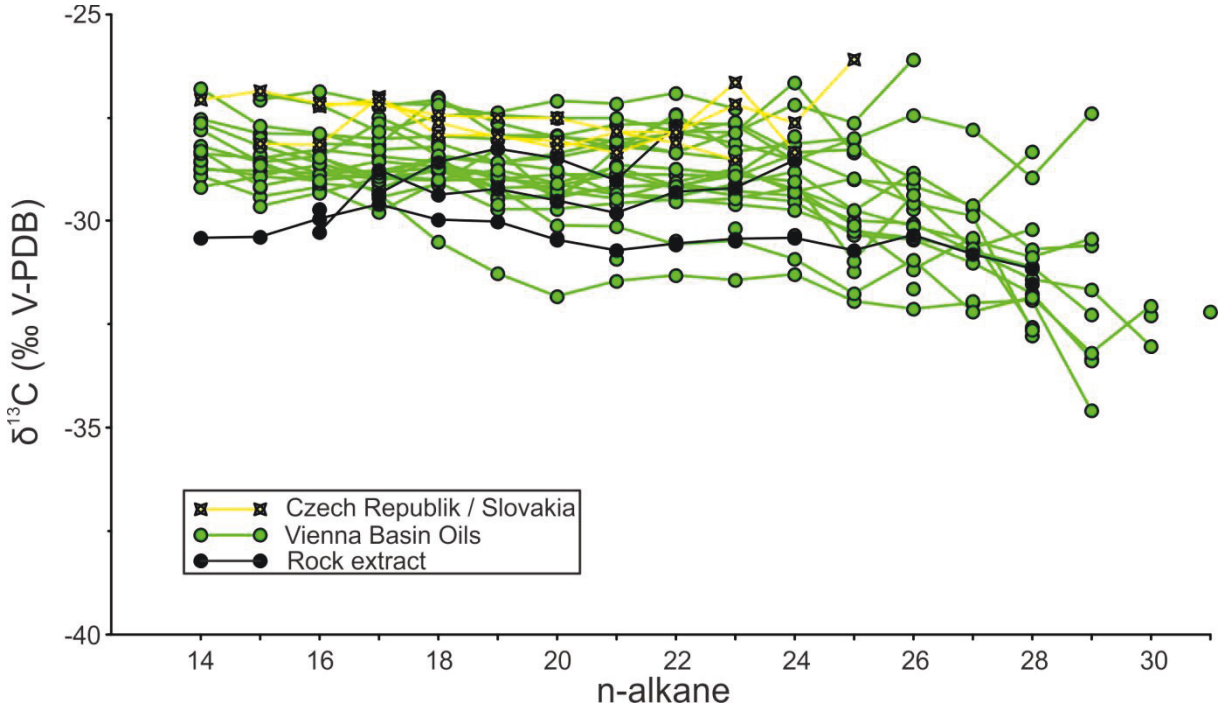

Fig. 66: Stable carbon isotope ratio of the individual n-alkanes from the oils of the Austrian part of the Vienna Basin.

7.2 Discussion

7.2.1 Oil Source Correlation

Overall all oils from the Czech Republik and Slovakia follow the general biomarker trends established for oils in the Austrian part of the basin. From the position of the data points within Figs. 63-66 it seems that these oils have also been generated from the Mikulov Formation. Furthermore, in contrast to Francu et al. (1996), oleanane has not been detected in any sample, suggesting a pre-Cenozoic source rock. Sterane- and hopane isomerization as well as the MPI ratio suggest generation of the oils at peak oil maturity. Hence, the Czech and Slovak oils have been generated from the same source rock and in the same depth interval as oils accumulated in the Austrian part of the basin.

Unfortunatly the exact location, structural position or reservoir horizons of the Czech and Slovak samples are unknown. Therefore, no real correlation regarding the DBT/Phen ratio is possible with oils from Austria. Anyhow, the recorded sterane/ hopane ratios (0.3-0.6) fit to the northern position of the oils (compare Fig. 52).

Sample Gbely H6 displays a very high C_{28}/C_{29} sterane ratio (which may argue for a Cenozoic source) as well as other unique properties. However, as this was the only sample, which was stored in a glass bottle sealed by a cork for more than 70 years, an influence of oxic degradation during sample storage cannot be excluded.

7.2.2 Biodegradation

The degree of biodegradation within the sample set from the Czech Republic varies. Undegraded oils (BBDS rank 0) are produced from Lanzhot and Holic, slight degraded oils (BBDS rank 1) were found in wells Hodonin 3 and 4, moderate degradation (BBDS rank 2) is recognized in the Gbely field. A severe degraded sample (BBDS rank 4) originates from well Hodonin 1.

Oxic degradation caused by insufficient sealing of the sample container of Gbely H6 may have had a significant impact on the composition.

8. Hydrocarbons in the surroundings of the Vienna Basin

Oil samples from six fields located along the western margin of the Vienna Basin have been investigated. The fields are producing hydrocarbons from different stratigraphic units:

- Klement: sandy interval within the autochtonous Lower Quartzarenite Member
- Höflein: dolomitic sandstones of the autochtonous Höflein Formation
- Kierling: sandstones in the Flysch zone
- Stockerau Ost: sandstones in the Molasse zone (Linz-Melk Fm.)
- Roseldorf: sandy Oncaphora Beds (Waschberg zone).

Visually the oils can be subdivided into four groups: a black oil group (Roseldorf; Kierling), a gas condensate group (Höflein, Stockerau Ost), a group of mixed black oil and condensate (oil rim in Höflein) and the light oil from Klement, which was archived in 1931, when 500 l of oil were produced from a planned water well (Waagen, 1931).

A thin rim of black oil is present at the oil-water contact (OWC) of the Höflein field. This rim constitutes a major production problem, as the condensate-oil mixture blocks all production equipment (F. Kucher, personal information). Samples of this rim have been gatherd from wells Höflein 9 (2633.6 m) and 12 (2670.3 m).

In addition gases from four fields have been investigated:

- Höflein: dolomitic sandstones of the autochtonous Höflein Formation
- Stockerau Ost: sandstones in the Molasse zone (Linz-Melk Fm.)
- Wildendürnbach: sandstones in the Molasse zone (Oncophora Beds)
- Roseldorf: sandy Oncaphora Beds (Waschberg zone).

8.1 Results

8.1.1 Liquid hydrocarbons

8.1.1.1 Biomarkers

Straight chain alkanes, isoprenoids - Oils from Roseldorf are characterized by unimodal n-alkane distributions and have similar Pr/Ph (0.95-1.29) as well as Pr/nC_{17} and Phy/nC_{18} ratios than unaltered oils from the Vienna Basin (Fig. 67). In contrast the Kierling oil displays a bimodal n-alkane distribution, but the Pr/Phy ratio (1.75-2.08) and Pr/nC_{17} and Ph/nC_{18} ratios are similar.

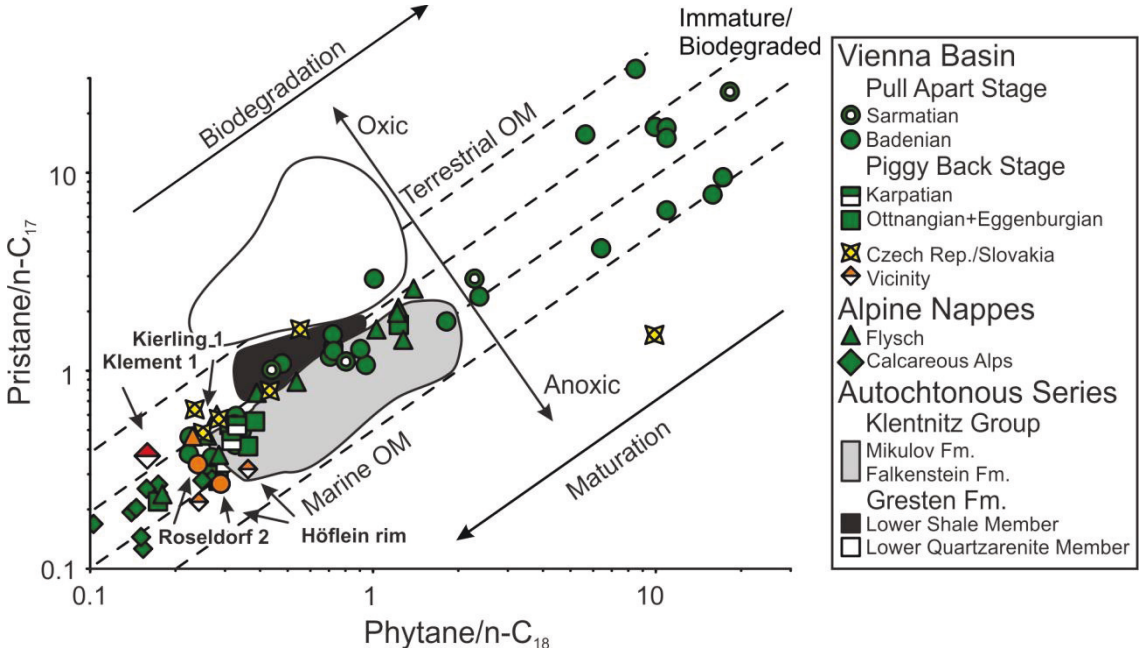

Fig. 67: Cross-plot of the Pythane/nC_{18} and Pristane/nC_{17} ratios (Connan and Cassou, 1980). Oils from the vicinity of the Vienna Basin are hardly influenced by biodegradation.

A unimodal n-alkane distribution is observed in the gas condensate samples (Höflein 3, 4, 6, 8, 10, Stockerau Ost 1, 16; Fig. 74) and the oil rim samples (Höflein 9, 12). In GC-FID measurements even n-butane could be detected and the maximum intensity at n-hexane, clearly indicates a retrograde gas condensate. In pure condensate samples the longest detected n-alkane is nC_{13}. The input of the black oil for the oil rim is so low, that no bimodale alkane distribution can be observed.

The Klement oil (Fig. 74) displays a unimodal n-alkane distribution peaking at nC_{12} and is characterized by a slight odd-numbered alkane preference (Fig. 69-a). Within

the whole sample set, the sample from Klement has the highest Pr/Ph ratio of 2.35 (Fig. 69-b. The Pr/nC_{17} ratio is 0.36 and the Ph/nC_{18} ratio is 0.16, respectivley.

Steroids - With the exception of the pure gas condensates, all samples are dominated by 14β, 17β(H) steranes over 5α, 14α, 17α(H) steranes isomers.

Within the black oil group, the relative percentages of C_{27} steranes (52 %), C_{28} steranes (18-24 %) and C_{29} steranes (24-31 %) vary, but they also plot into the narrow cluster defined by Vienna Basin oils in the ternary steranes diagram. Similar as for oils from Vienna Basin reservoirs, C_{28}/C_{29} sterane (0.7-1.0) ratios are in agreement with a Mesozoic source rock. The 20S/(20S + 20R) ratio of the C_{29} steranes varies between 0.58 and 0.66. This is close to the equilibrium composition (0.55), which is reached at 0.8 %Rr (Mackenzie and Maxwell, 1981).

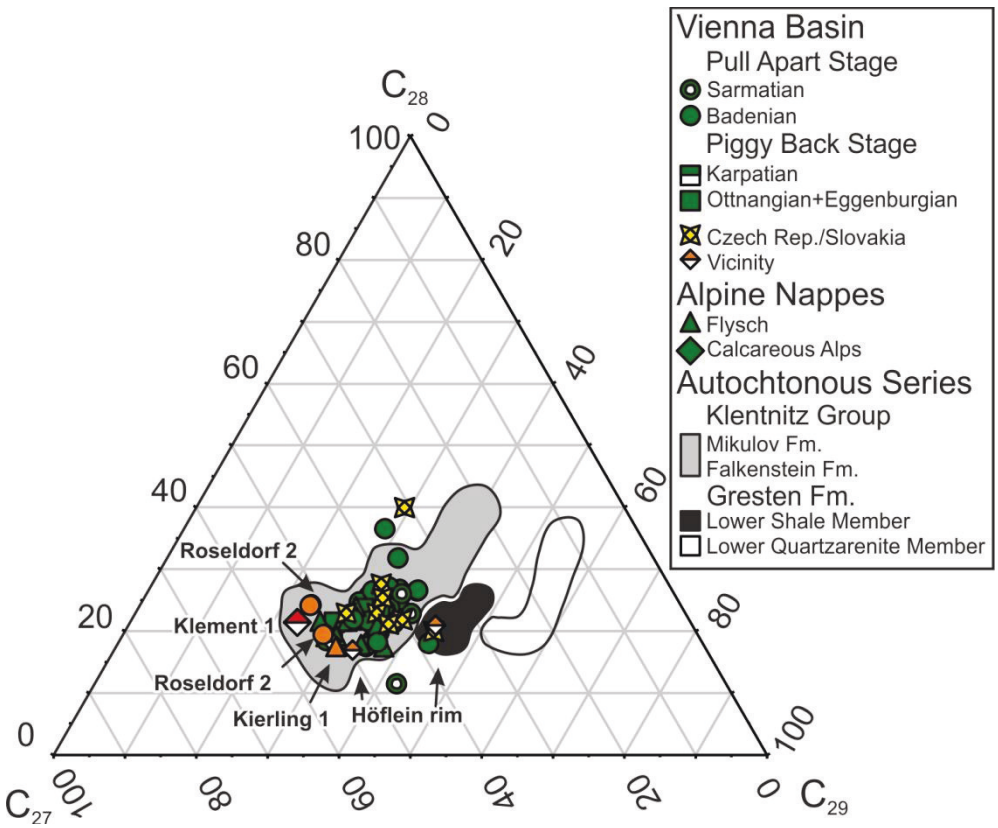

Fig. 68: Distribution of the sterane content of oils from the vicinity of the Vienna Basin. The oils fall into the cluster of all other oils.

Sterane data from Höflein black oil (C_{27} steranes [36-50 %], C_{28} steranes [17-21 %], C_{29} steranes [33-43 %], C_{28}/C_{29} steranes ratio [0.26], S/(S+R) C_{29} sterane ratio [0.6]) also fit with results from Vienna Basin oils (Fig. 68). A slight deviation of one of the samples may be caused by mixing with gas condensate.

The concentration of steranes in the Klement sample is very low. However the distribution of C_{27} steranes (55%), C_{28} steranes (21%) and C_{29} steranes (23%) is similar to other oils from the area. The ratio of the 20S/(20S + 20R) steranes is 0.47.

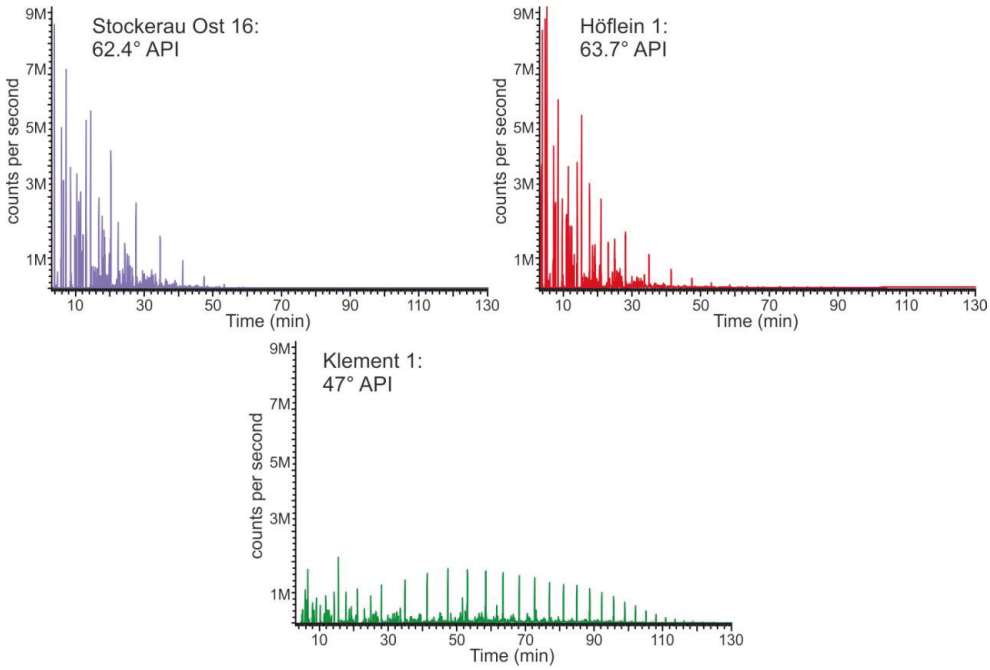

Fig. 69: Comparison of the FID-traces from Stockerau Ost 16, Höflein 1, and Klement 1. Note the significant different chemical composition of the two samples from the hydrocarbon of the Höflein Group and the Klement oil.

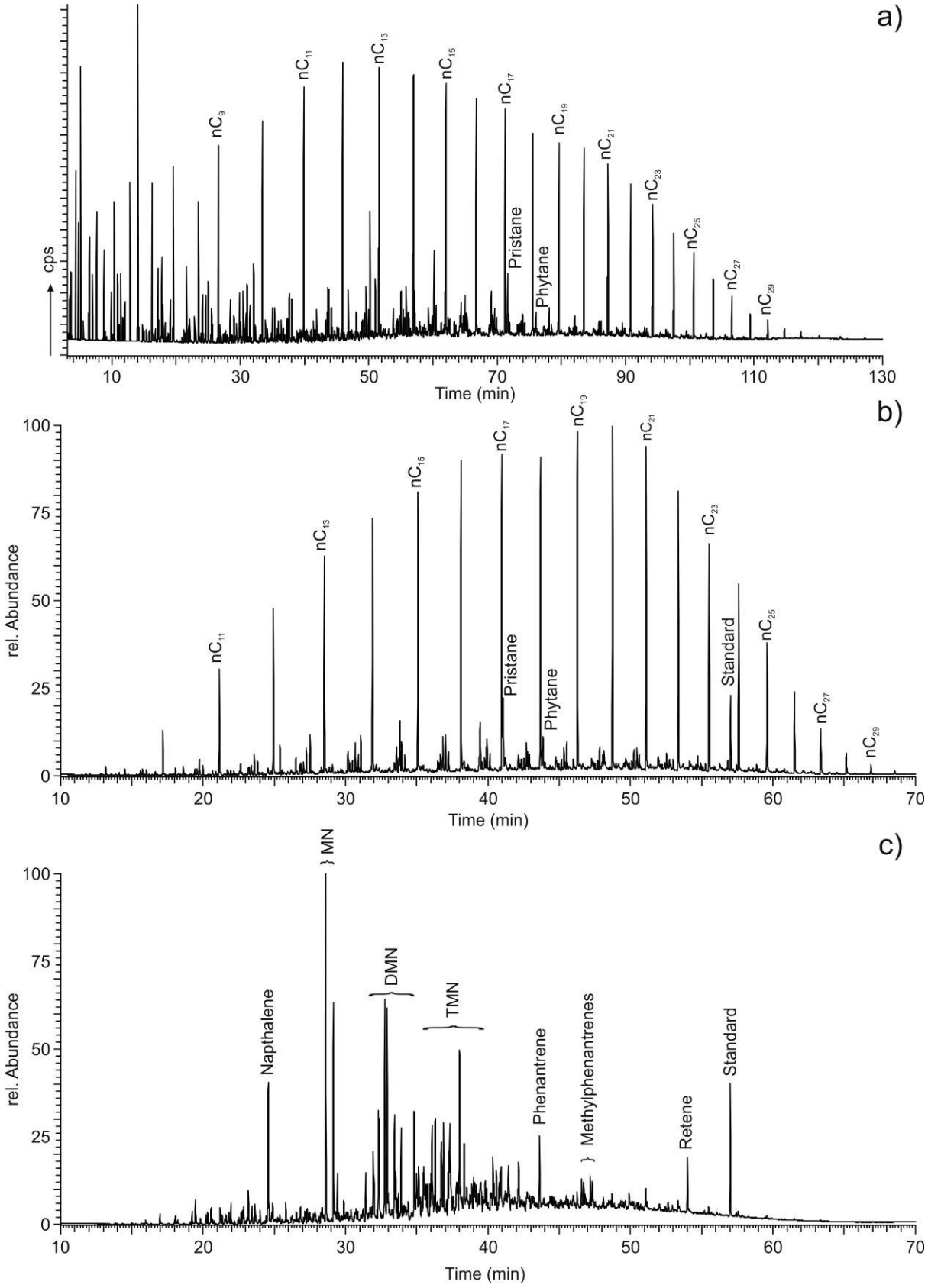

Fig. 70: Chromatogramms from the sample Klement 1: a) FID-trace b) TIC-trace of the aromatic fraction c) TIC trace of the aromatic fraction. Note the significant content of retene.

Hopanoides - In the black oil group, hopanes occur (in minor) amounts in all samples. The steranes/hopanes ratio is above one, displaying a significant higher amount of algae than bacteria in the source rock. Oleanane has not been detected. The 22S/(22S + 22R) isomers ratio of the C_{31} hopanes points out a source rock maturity of at least 0.6 %Rr (equilibrium ratio), wereas the Ts/(Ts+Tm) ratio indicates a maturity close to peak oil maturity.

The same is true for the black oil rim in field Höflein, however the organic matter in the source rock is more equally formed by algae and bacteria (steranes/hopanes ratio: 0.7).

Polycyclic aromatic hydrocarbons - Alkylated napthalenes as well as phenantrene and methylphenantrenes are present in significant quantities. The MPI suggests peak oil maturity (~0.90 %Rr) for black oils from Roseldorf and Kierling, but a lower maturity (~0.75 %Rr) for the Klement oil.

No PAHs with 3 or more rings were detected, indicating no or negligible input from a terrestrial source rock in samples from Roseldorf, Kierling, Stockerau Ost and Höflein (Killops and Killops, 1993). In contrast, the Klement oil contains retene in significant amounts (Fig. 70-c), which is a marker for the input of conifers into the source rock (Simonite, 1986; Alexander et el., 1988, a, b). So far, the Klement oil is the only oil sample from the Austrian part of the Vienna Basin area, which contains a biological marker arguing for a mature source rock with a strong terrestrial influence.

8.1.2 Stable carbon isotope ratios

8.1.2.1 Stable carbon isotope ratio of bulk fractions

Similar results are obtained for oils from the black oil group (aliphatic fraction: -25.6 to -26.1 ‰; aromatic fraction: -24.3 to -24.9 ‰) and the black oil rim in Höflein (aliphatic fraction: -25.5 to -26.7 ‰; aromatic fraction: -24.1 to -25 ‰ (Fig. 71).

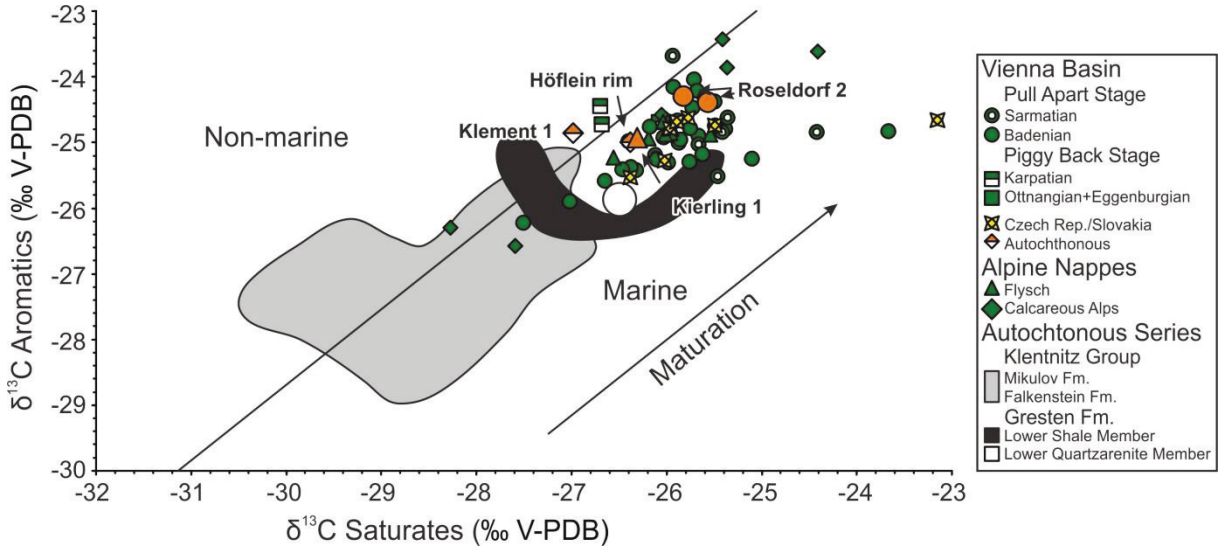

Fig. 71: Cross-plot of the stable carbon isotope ratio of the aliphatic and aromatic fraction (according to Sofer, 1984).

8.1.2.2 Compound specific stable carbon isotope ratio

To avoid the potential hazards of overloading and destroying the IsoLink® oxidation oven of the GC-IRMS system, no gas condensate sample (Höflein, Stockerau Ost) has been subjected to this measurement. Therefore, only n-alkane profiles of samples Klement and Roseldorf were obtained.

The maximum intensity signal for single compounds was obtained for n-alkanes in the range of nC_{17} up to nC_{22}. The Klement oil displays increase $\delta^{13}C$ values with decreasing chain length (Fig. 72), which is reported as typical behavior of numerous oils (Bjoroy et al., 1994). However the drop is significantly less steep in the sample from Klement. In the Roseldorf sample the isotopes get slightly heavier between nC_{14} and nC_{22} and lighter between nC_{22} and nC_{25}.

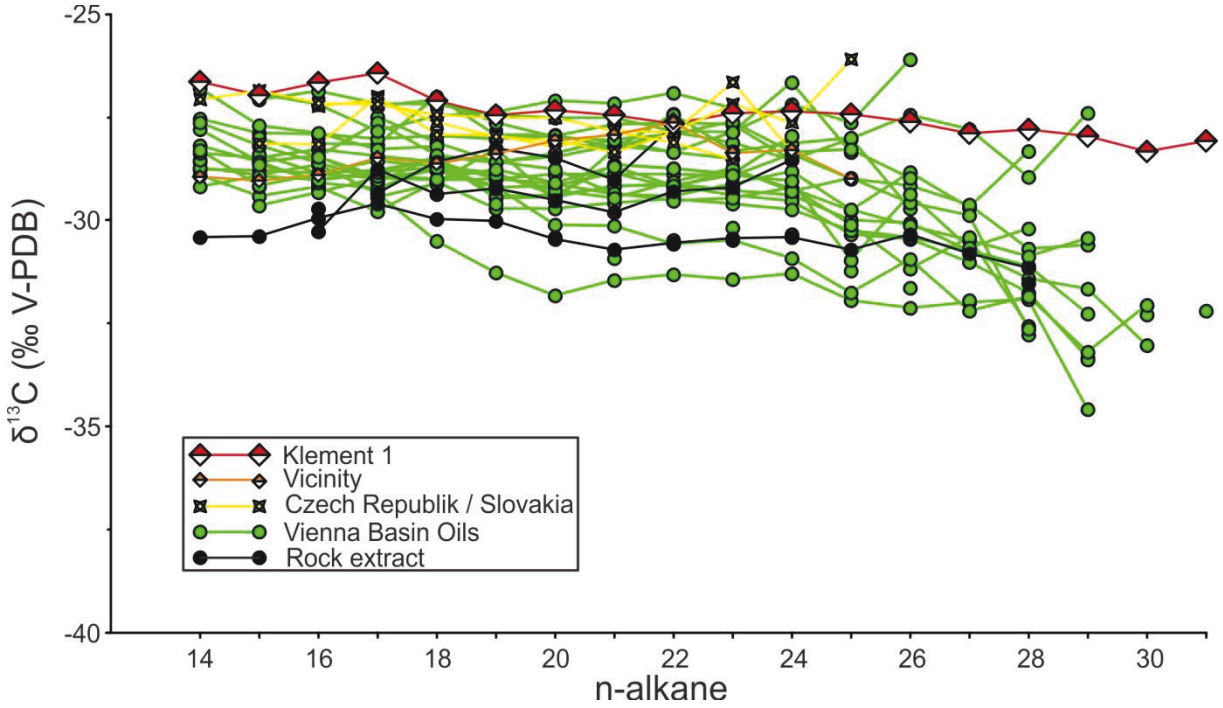

Fig. 72: Compound specific stable carbon isotope ratio of n-alkanes from all investigated samples.

8.1.2 Gas

8.1.2.1 Molecular composition

Gas samples contain varying amounts of hydrocarbon and non-hydrocarbon gases. The dominant compound in all samples is methane (C_1: 70.22-99.50 vol.%). Ethane is present in significant concentrations in the Höflein and Stockerau Ost fields (C_2: 3.70-5.63 vol.%) but only in minor amounts in the Roseldorf and Wildendürnbach fields (0.13-0.37 vol.%). Whereas higher hydrocarbon gases have been detected only at detection limits in gases from Roseldorf and Wildendürnbach, propane (C_3: 0.30-2.57 vol.%), butanes (iC_4+nC_4: 0.44-1.90 vol.%), pentanes (iC_5+nC_5: 0.24-0.46 vol.%) and higher hydrocarbons (C_{6+}: 0.14-0.37 vol.%) have been detected in significant amounts in Höflein and Stockerau Ost. Non-hydrocarbon gases are dominated by carbon dioxide (CO_2: up to 18.78 vol.% in Höflein, up to 1.0 vol.% in Stockerau Ost, at detection limit in Roseldorf and Wildendürnbach). Nitrogen is present in moderate concentrations in Höflein and Stockerau Ost (N_2: 1.00-3.46 vol.%) and in minor concenterations in Roseldorf and Wildendürnbach (0.19-0.34 vol.%).

Gas dryness ($C_1/(C_2+C_3)$, Bernard et al., 1978) ranges from 9 (Höflein) to 711 (Wildendürnbach).

The i-/n-C_4 ratio is below 1 (0.76-0.82) in samples from Höflein and in Stockerau Ost 16. In contrast, ratios for samples from wells Stockerau Ost 7 and 13 exceed 1 significantly (1.75-1.94) indicating gas degradation. As expected, the average C_2/C_3 ratio is smaller in Höflein and Stockerau Ost 16 (avg. 2.2) than in the degraded Stockerau Ost 7 and 13 samples (avg. 12.6).

8.1.2.2 Isotopic composition

The stable carbon ($\delta^{13}C$) and hydrogen (δD) isotopic ratios of hydrocarbons scatter widely. $\delta^{13}C$ ratios in methane range from -56.4 to -61.7 ‰ in samples from reservoirs from the Molasse Zone. This suggests a microbial origin of methane. In contrast the stable carbon isotope ratio of C_1 in samples from Höflein and Stockerau Ost ranges between -37.4 and -46.7 ‰, typical for thermogenic gas.

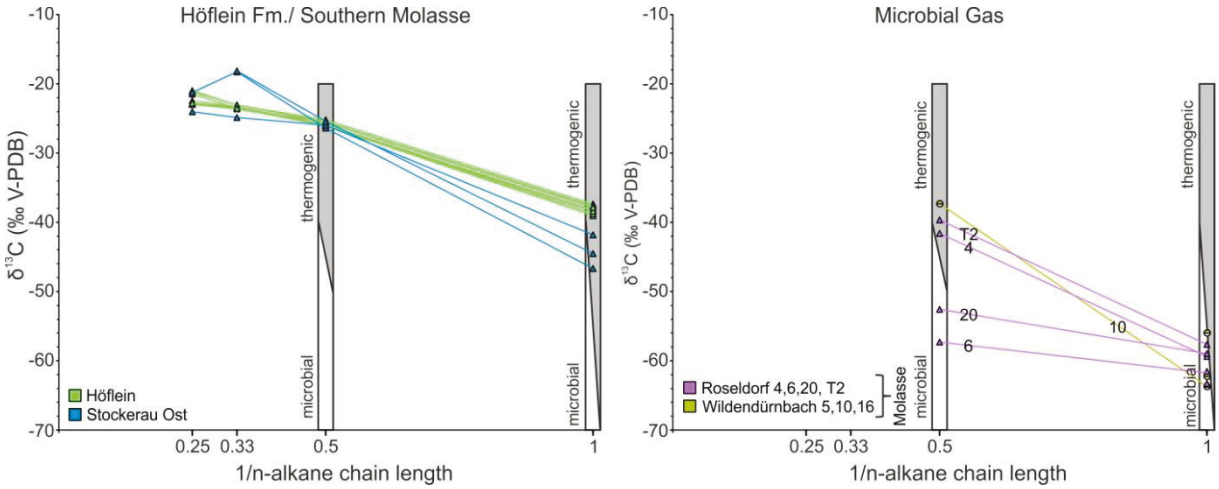

Fig. 73: Natural gas plot (Chung et al., 1988) for gases from Höflein and Stockerau Ost fields and Roseldorf and Wildendürnbach fields.

The same observations may be made on the $\delta^{13}C$ ratio of ethane: C_2 is relatively light in samples from Roseldorf and Wildendürnbach (-37.3 to -57.3 ‰) and relatively heavy in Höflein and Stockerau Ost (-25.2 to -26 ‰).

Propane displays a stable carbon isotope ratio of about -23.5 ‰ in Höflein and Stockerau Ost 16 whereas in Stockerau Ost 7 and 13 propane is significantly heavier (-18.3 ‰). $\delta^{13}C$ ratios of iC_4 (-22.6 to -25.7 ‰) and nC_4 (-21 to -24.1 ‰) are the similar in Höflein and Stockerau Ost (Fig. 73).

δD ratios of methane range from -128.1 to -181.1 ‰ whereby no lateral trend between the samples is identifiable. The δD ratio of ethane lies between -59.6 and -115.7 ‰ for samples from field Stockerau Ost and between -168.4 and -187.2 ‰ for samples from field Höflein. This is spectacular, because the δD ratio of methane is typically always more negative than that of ethane (e.g. Schoell, 1980; Dai, 1990; Lewan, 1993, 1997; Schimmelmann et al., 2001; Schimmelmann et al., 2004; Yoneyama et al., 2002, Radke et al., 2005; Tang et al., 2005; Ni et al., 2011). According to my knowledge, the Höflein field is the only field described in literature, where hydrogen in methane is heavier than in ethane.

CO_2 displays light $\delta^{13}C$ ratios values between -7 (Höflein) and -3 ‰ (Stockerau Ost) indicating its thermal origin (Golding et al., 2013 and refrences therein).

8.2 Discussion

8.2.1 Oil-source correlation

With the exception of the Klement oil, black oils in the vicinity of the Vienna Basin (Roseldorf, Kierling, oil rim in the Höflein field) are probably generated from Mikulov Formation as the sterane and hopane patterns match with the patterns in rock extracts from the Mikulov Formation and in Vienna Basin oils (Figs. 67, 68). The same is true for stable carbon isotope ratios of individual compounds and of hydrocarbon fractions (Figs. 71, 72). However, all samples (Höflein, Kierling and probably also very weak in Roseldorf) display mixing with a very light hydrocarbon phase. The presence of condensate is indicated by a bimodal n-alkane distribution with maximum concentrations of nC_{8-11} and nC_{15}. In terms of biodegradation the oils are undegraded.

In contrast, the Klement oil probably has a different source, as the occurrence of retene points to a terrestrial influenced source rock (Otto et al., 1997). Relative heavy stable carbon isotope ratios of alkanes with chain length nC_{21+} also support the presence of a source rock with terrestrial organic matter (Murry et al., 1994).

The source rock for the gas condensates in the Höflein and Stockerau Ost fields remains debatable, because of the lack of biomarkers and isoprenoids. Investigations on an evaporatic concentrate (10:1) show that traces of alkanes occur up to nC_{24}, but higher biomarkers were also absent. Sachsenhofer et al. (2006) speculated that the source may be the Lower Quartzarenite Member of the Gresten Formation.

8.2.2 Microbial versus thermogenic gas

Natural gas produced from Wildendürnbach and Roseldorf is dry (231-711) and isotopically light ($\delta^{13}C_1$: -56.4 to -63.7‰) suggesting that the gas is of primary microbial origin. Furthermore, also ethane carries a microbial isotopic signature in both deposits.

In contrast, gases recovered from Höflein and Stockerau Ost are wet and isotope ratios suggest a thermal origin. However, both fields differ in CO_2 contens (Höflein: 16-19%, Stockerau Ost: <1%) and $\delta^{13}C$ values of methane (Höflein: -37 to -39‰;

Stockerau Ost: -41 to -48‰) and propane (Höflein: -23‰; Stockerau Ost: -25 to -18‰). Because biodegradation results in lighter methane and heavier propane, the observed differences in isotopic values may indicate a higher degree of biodegradadition in the Stockerau Ost field. Indeed the shallow Stockerau Ost reservoir (~2000 m) is cooler and more susceptible to biodegradation than the deeper Höflein reservoir (~2600 m).

8.2.3 Arguments for mixing of hydrocarbons generated from the Mikulov Formation and the Lower Quartzarenite Member

The results of the investigation of the Kierling and Klement oils and of cutting samples from the Upper Quartzarenite Member (well Stockerau Ost 1) forces a reinterpretation of established petroleum system models for the western vicinity of the Vienna Basin.

Migration direction: Sachenhofer et al. (2006) suggested that the condensate within the Höflein field has migrated into the reservoir via southward migration from depocenters of the Gresten Formation in the northeast of Stockerau. However a condensate component is also found in the Kierling oil sample. The local geological setting (Fig. 74) will not allow condensate to migrate into the Kierling reservoir via southward migration. North- to northestward migration of hydrocarbons generated in the area of the city of Vienna seems more likely. Such an active source kitchen within the Gresten Formation could also charge the reservoirs in Höflein and Stockerau Ost via migration alonge thrust planes and Egerian sandstones.

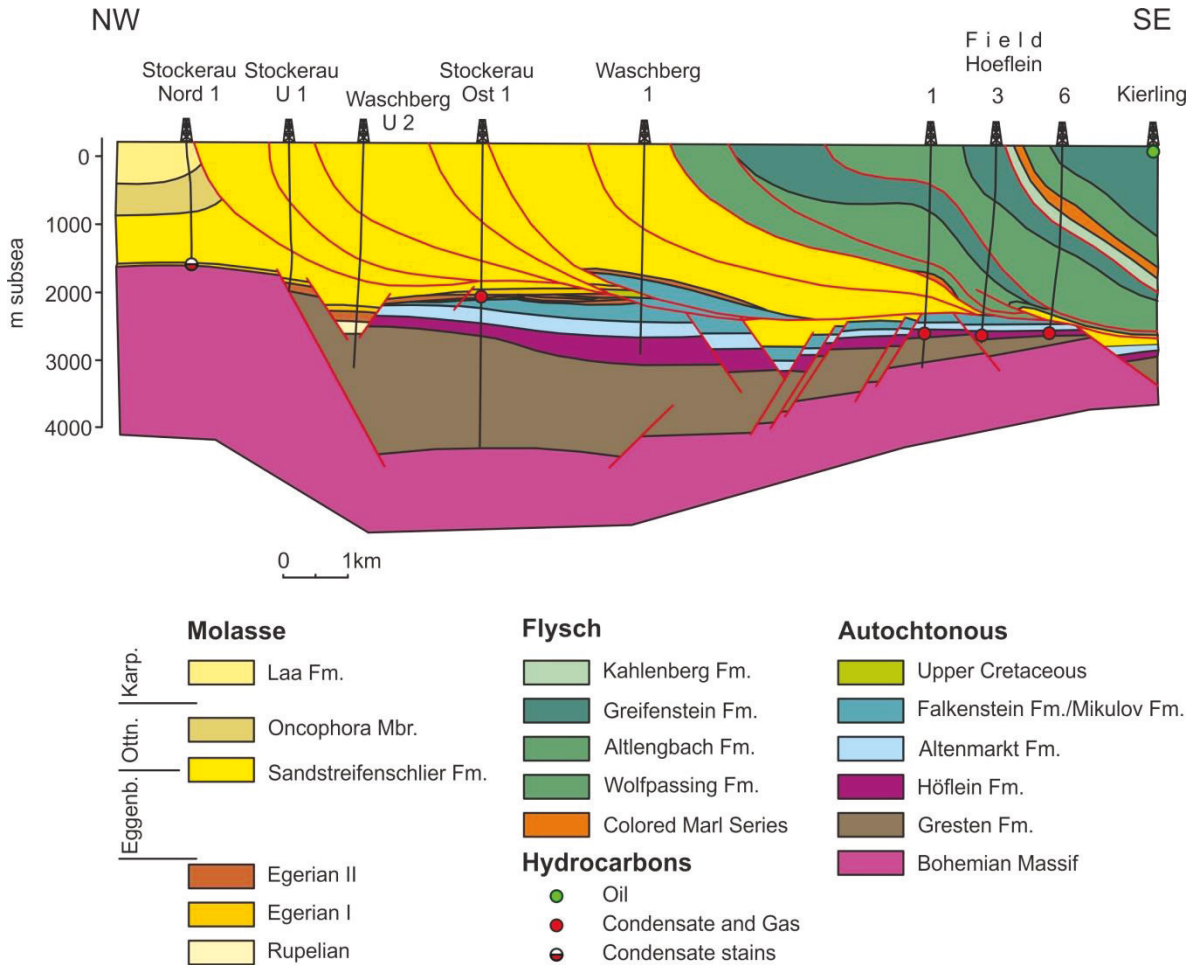

Fig. 74: Cross section through the Korneuburg Basin. Compiled and modified from Kreutzer (1993) and Wessely (1993).

Source rocks: The hydrocarbons within the Höflein, Stockerau Ost and Klement fields are different from the rest of the Vienna Basin. Several authors considered this as a strong indication for a second active source rock (Kratochvil and Ladwein, 1984, Sachenhofer et al., 2006). Indeed the biomarker composition of the Klement oil indicates argues for a source rock with a strong terrestrial influence, which is not the Mikulov Formation. In contrast, a Mikulov/Falkenstein source is likely for the black oils in Höflein, Kierling and Roseldorf. As mentioned above, the Lower Quartzarenite Member is a potential source for the gas condensate in Höflein and Stockerau Ost.

Considering a north- to northeastward migration and mixing of Mikulov oil with condensates, active source rocks have to be postulated in the area of Vienna. Within this area both, the Mikulov Formation and a probable better source facies within the Lower Quartzarenite Member reach oil windw maturity and generate oil (Mikulov Fm.)

and gas condensate (Lower Quartzarenite Mbr.). These hydrocarbon phase migrate updip and get mixed. This model implies the presence of an active Lower Quartzarenite Member - Doggerian (.) Petroleum System.

Gas condensate: Gas condensate found within the Höflein and Stockerau Ost reservoirs could originate from two fundamenatly different proceses: evaporative fractionation and generation from a humic, early mature source.

Evaporative fractionation is observed in tight reservoirs and occurs along tight fault planes (Silverman, 1965; Thompson, 1987; Thompson, 1988). Hydrocarbons affected by evaporitc fractionation are retrograde condensates and very wet gases (Thompson and Kennicutt, 1990). Gas generated from a humic source would display similar properties, but can be rich in isotopically light (-5 to -10‰) CO_2 (Hunt, 1996). Consequently the gas condensate in the Höflein field comprising huge amounts of isotopically light CO_2 (-6.7 to -7.4‰) supports an origin from the coaly Lower Quartzarenite Member.

9. Oils from Urmannsau and Mank

During the 1960s, a series of exploration wells were drilled in the western part of Lower Austria, mainly to explore the hydrocarbon potential of the Molasse Zone and of the Calcareous Alps. Well Urmannsau 1 (Fig. 75) was located near an oil seep in the Calcareous Alps, which was used in medieval times by monks of the nearby monastery Gaming (Ruttner, 1963, Wessely, 2006). No commercial deposits were encountered during this campaign, but oil impregnations were found in a molasse core from Mank 1 and two cores from Urmannsau 1 from the Calcareous Alps (Fig. 75). These oil stains are investigated in the present study in order to determine whether the oil has been generated from Mesozoic or Cenozoic source rocks.

Fig. 75: Map showing the position of the boreholes Mank 1 and Urmannsau 1.

9.1 Results

Straight chain alkanes, isoprenoids - Oil samples are characterized by unimodal n-alkane distribution with a maximum intensity in the range of nC_{18-19}. The Pr/Ph ratios range from 0.70 to 0.93 indicating an anoxic environment of deposition (Didyk et al., 1978). Pr/nC_{17} (0.56 – 0.95) and Ph/nC_{18} (0.55 – 0.73) ratios are low and indicate that the samples did not suffer from advanced biodegradation.

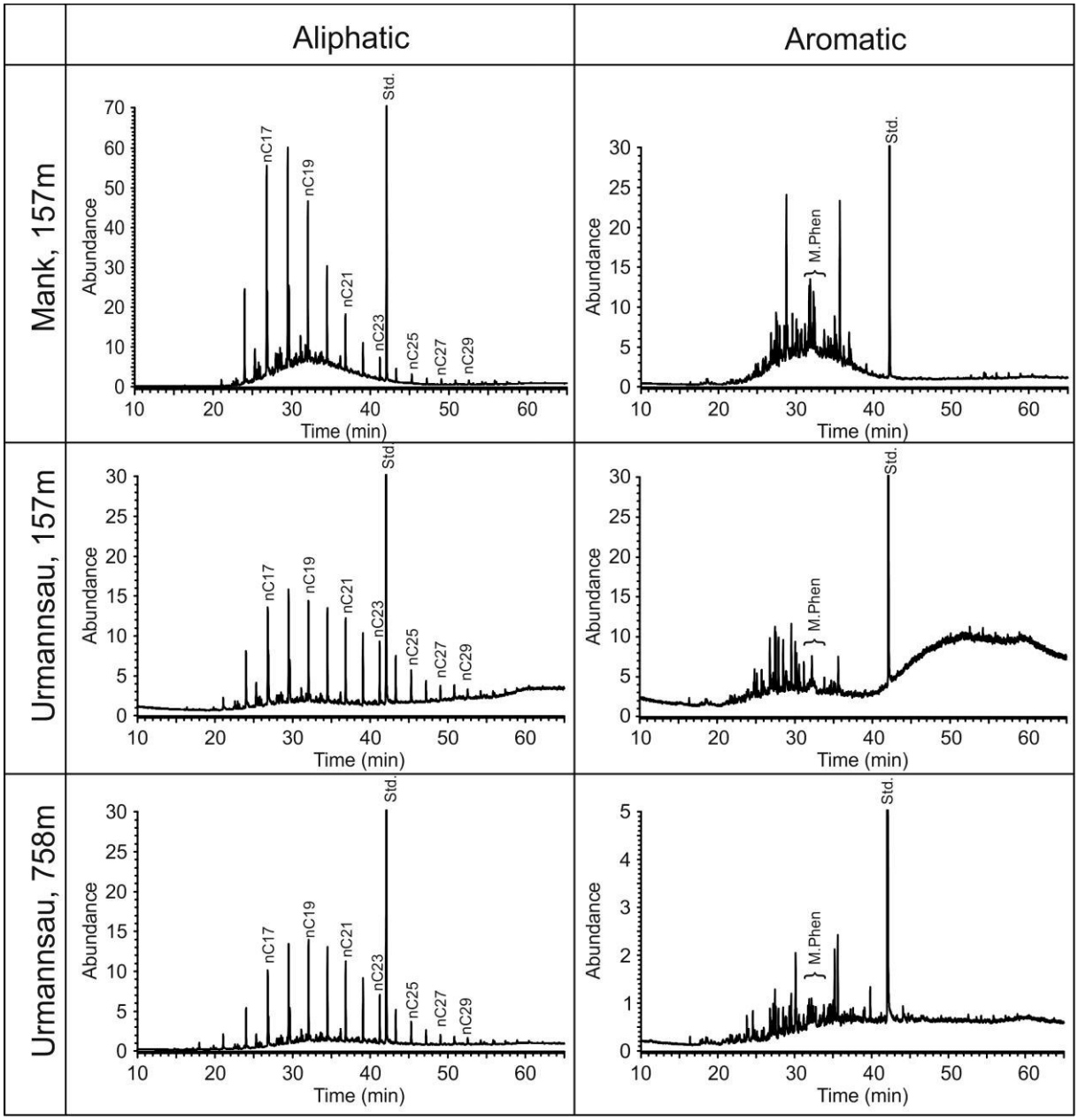

Fig.76: TIC-traces of the aliphatic and aromatic fraction of oil stains from boreholes Mank 1 and Urmannsau 1.

Steroids - All samples are dominated by 14β, 17β(H) steranes over 5α, 14α, 17α(H) steranes isomers. The relative abundance of C_{27} steranes (31-41 %), C_{28} steranes (23-40 %) and C_{29} steranes (29-36 %) varies significantly. The observed C_{28}/C_{29} steranes ratios (0.5-1.0) agree with a Mesozoic source rock (Grantham and Wakefield, 1988). The 20S/(20S + 20R) ratio of the C_{29} steranes varies between 0.60 and 0.68 for samples from Urmansau. This is close to the equilibrium composition (0.55), which is reached at 0.8 %Rr (Mackenzie and Maxwell, 1981). In contrast, the ratio from the sample from Mank 1 is significantly lower (0.24), pointing out an early oil maturity.

Hopanoides - Hopanes occur (in minor) amounts within all samples. Oleanane has not been detected. The 22S/(22S + 22R) isomers ratio of the C_{31} hopanes for samples from Urmansau 1 is close to the equilibrium value of 0.6 showing that the maturity of the source rocks is at least 0.6 %Rr. The Ts/(Ts+Tm) ratio (0.57 – 0.63) suggests peak oil maturity (~0.9 %Rr). The (22S/(22S + 22R) ratio of the sample from Mank 1 (0.52) indicates an early oil window maturity, which is in agreement with a Ts/(Ts+Tm) ratio of 0.33.

Polycyclic aromatic hydrocarbons - Mono-, di-, tri-, and tetramethylated naphthalens are present in unusual low quantities within the samples. Phenanthrene and methylphenanthrenes are also present in very small quantities. Therefore it cannot be excluded, that the content of aromatic compounds are reduced due to 50 years of core storage.

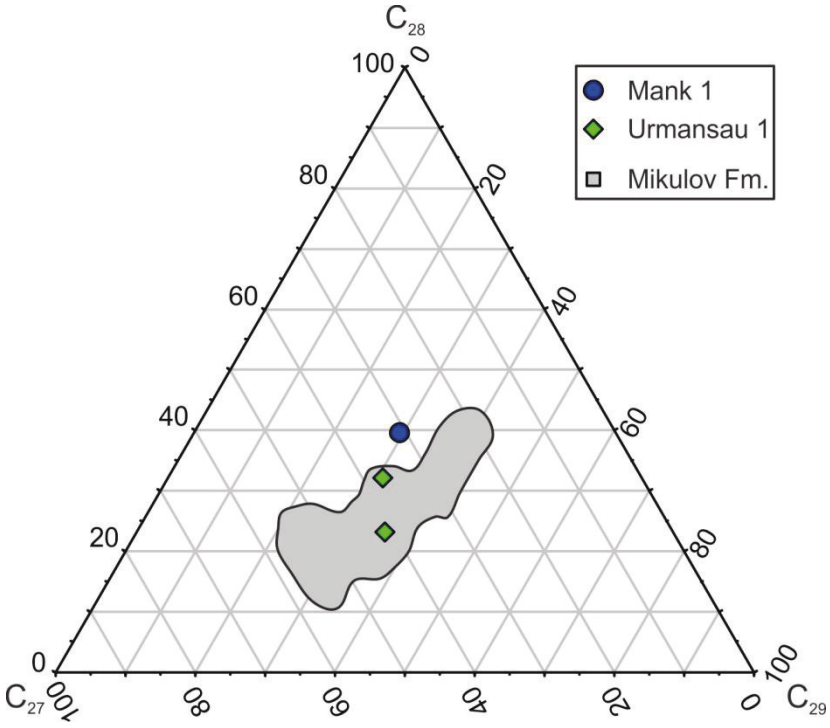

Fig. 77: Distribution of the sterane content of oils stains from Mank and Urmansau.

Stable carbon isotope ratios – $\delta^{13}C$ of the aliphatic hydrocarbon fractions from all samples are -28.5‰. $\delta^{13}C$ values of the aromatic fractions range from -26.5 to –17.5 ‰.

9.2 Discussion

The biomarker patterns from oil stains in Mank 1 and Urmannsau 1 are characterized by abundant n-alkanes proving that the oils are not biodegraded despite of their shallow depth. Although the sterane as well as the hopane pattern show a low signal to noise ratio, they allow for a number of significant findings:

The absence of oleanane and the C_{28}/C_{29} sterane ratio suggest a Mesozoic source rock. The ternary steranes diagram (Fig. 77) shows that this source rock is not the authochthonous Mikulov Formation, which s geological reasonable, as the Mikulov Formation extends westwards only to the Höflein area. Consequently a Mesozoic source located within the Northern Calcareous Alps has to bee assumed. Oil generated from organic matter-rich Mesozoic rocks in the Calcareous Alps has also been proven by Gratzer et al. (2015) in Upper Austria. Important to note that the isotopic composition of the oil stains is heavier ($\delta 13C_{sat}$: -28.5 ‰; $\delta 13C_{aro}$: -26.5 ‰) than from oils in the Alpine Foreland Basin in Upper Austria, which have been generated from Lower Oligocene source rocks (Gratzer et al., 2011). This is an additional argument against a Cenozoic source rock.

The observed different maturity of the Mank and Urmannsau samples may be explained by a varying burial depth of the source and, therefore, different thermal stress with increasing temperatures in southward direction.

10. Migration within the Mikulov-Badenian Petroleum Sytem (!)

Benzocarbazoles, a part of the NSO fraction, are generated during thermal maturation of organic matter. A maximum yield is achieved near peak oil maturity at 0.88 %Rr (Clegg et al., 1997). However, Bennett et al. (2002) and Bechtel et al. (2013) reported no significant variation of benzocarbazole content in a maturity range between 0.76 %Rr and 0.88 %Rr in the North Sea petroleum realm and the Alpine Foreland Basin. Furthermore, Hallmann et al. (2007) found out that the distribution of benzocarbazoles is not controlled by lithology and organic facies.

Both, the concentration of benzocarbazoles as well as their composition changes with increasing migration distance. However the exact process is still unclear. Larter et al. (1996) proposed that benzocarbazoles are adsorbed from crude oil by dispersed organic matter and clay minerals, but they stated that this only works under water-saturated conditions. Based on experiments, Bennet et al. (2002) argued benzocarbazoles are removed by water and that they are then attached to clay minerals. In any case, benzocarbazoles are often used to estimate migration distances of crude oils (Li et al., 1997, 1998, Clegg et al., 1998, Terken and Frewin, 2000, Bechtel et al., 2013).

The overall removal of benzocarbazoles with increasing migration distance is expressed by the Reservoir-Source Fraction Parameter (RSFP, Bennett et al., 2002), whereas an increased removal of benz(a)carbazole compared to benz(c)carbazole is expressed by the Benzocarbazole-Ratio (BCR, Larter et al., 1996). The stronger depletion of benz(a)carbazole may be caused by a stronger interaction with clay minerals (Larter et al., 1996).

Investigations on benzocarbazoles were conduted in order to test their applicability as a migration proxy within the Vienna Basin and to try to validate established hydrocarbon migration models.

The deepest non-overmature samples from the Mikulov, displaying a maturity between 0.68 and 0.71 %Rr in well Falkenstein 1, are considered to contain the maximum benzocarbazole concentrations in the Vienna Basin. Therefore, the carbazole concentration in the extract from rock sample Falkenstein (4148 m) has been used to calculate the RSFP. In Fig. 78, the RSFP of the samples (0.0426 –

0.2271) is plotted against the BCR of the samples (0.5298 - 0.5943). As expected, both parameters show a positive correlation.

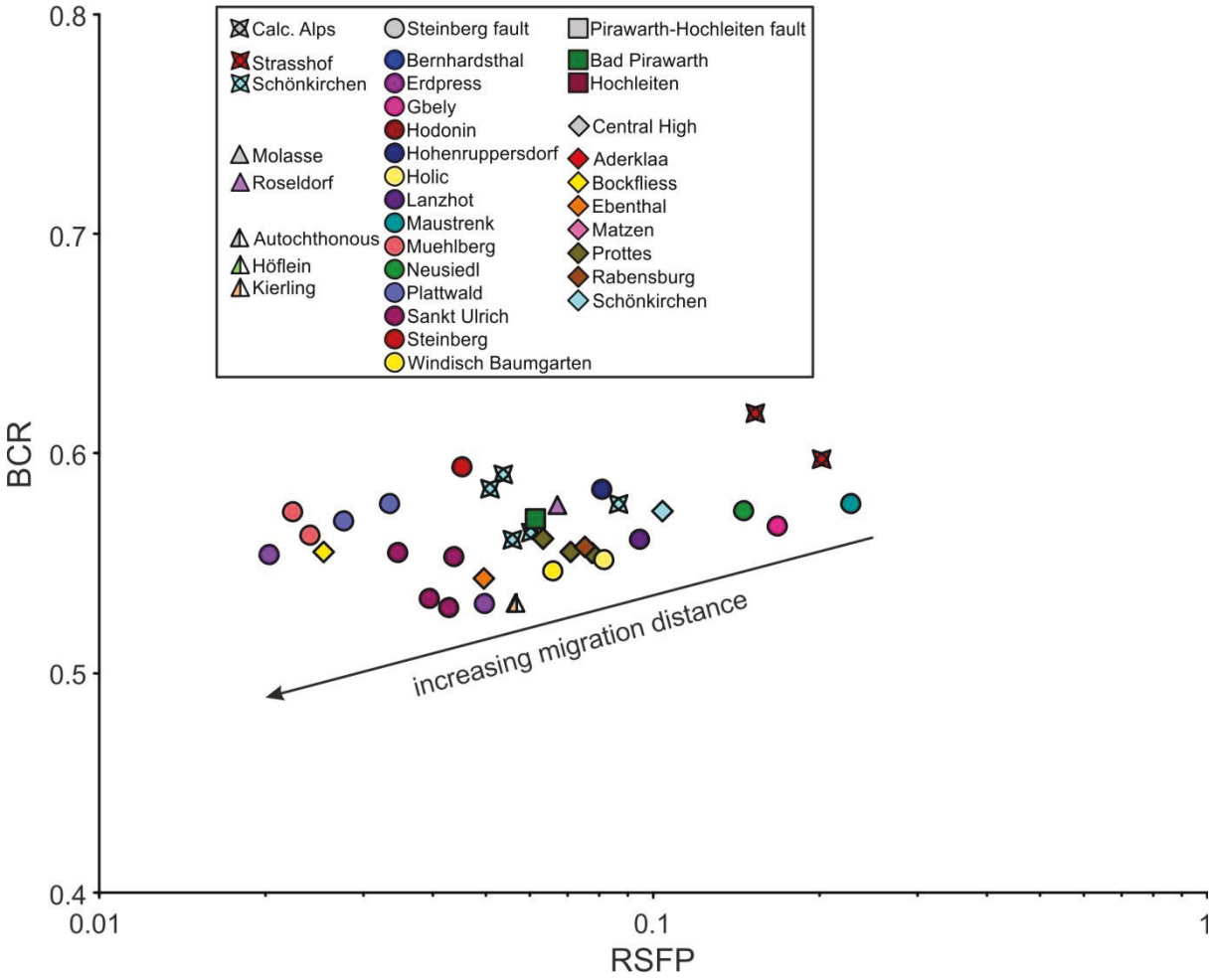

Fig.78: Crossplott of the Reservoir-Source fraction parameter (RSFP, Bennett et al., 2002) against Benzocarbazol ratio(BCR, Larter et al. 1996) (according to Bechtel et al., 2013) of oils from the Vienna Basin. Decreasing RSFP and BSR values point out the increasing migration distances.

In Fig. 79 the RSFP, which shows a greater variability than the BCR, is plotted against the vertical migration distance, defined as the difference between the reservoir depth and the estimated generation depth derived from the maturity indicated by the MPI and the maturity depth trend shown in Fig. 39. In general there is a good fit. Partly the observed scatter in Fig. 79 may be caused by the fact that any lateral migration is neglected in the estimated migration distance.

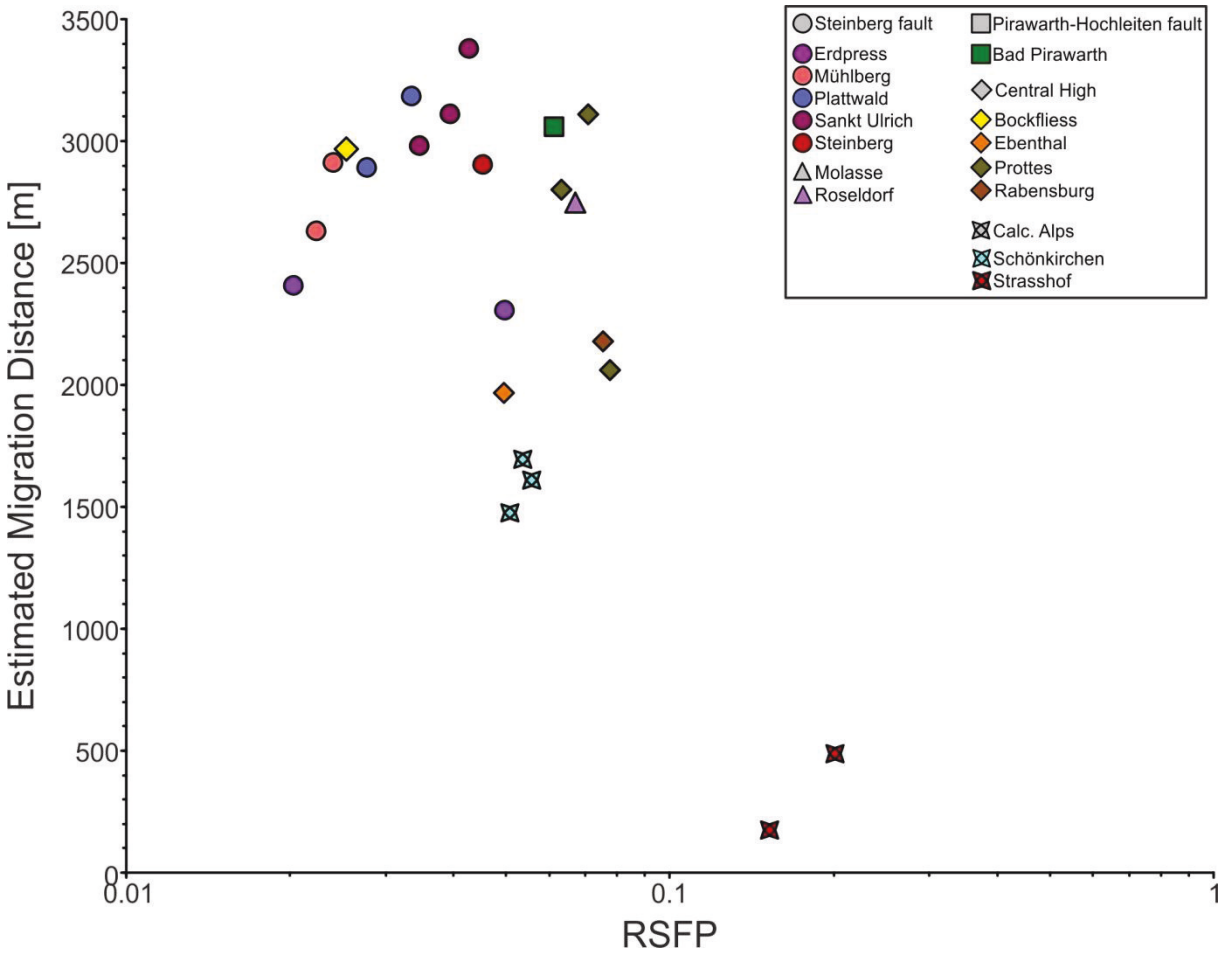

Fig. 79: RSFP (Bennett et al., 2002) against an estimated migration distance (derived from the present day oil window depth and the reservoir depth) displaying increasing migration distances with decreasing RSFP values.

It is likely that fields located at the Steinberg and Pirawarth-Hochleiten Fault systems were charged via migration along these faults. Fields in the Central High zone were probably charged with oil, which migrated along the basal overthrust of the Calcareous Alps.

Note, that the estimated vertical migration distance does not take into account the multi-stage migration suggested by the latest thermal models (Rainer, T., pers. comm.) and, therefore, may display significant deviation from the real migration distances. This thermal model (Fig. 80) suggests that the Mikulov Formation generated all oil already during overthrusting by the Alpine Nappes, long before the Miocene reservoirs have been deposited. If this (unpublished) thermal basin model is correct, it has also to be considered that huge quantities of oil have been stored

within the Calcareous Alps, and migrated later upwards into Miocene sediments. Within this context it is remarkable that oils, which suffered TSR within Calcareous Alps (e.g. Aderklaa 3, 4) are found in Karpatian reservoir rocks. On the other hand, all other oils from Miocene reservoirs do not show any indications for TSR. However, as these oils may have escaped from the Calcareous Alps before temperatures needed for TSR (>100°C) have been reached, this is not a final argument against the above model.

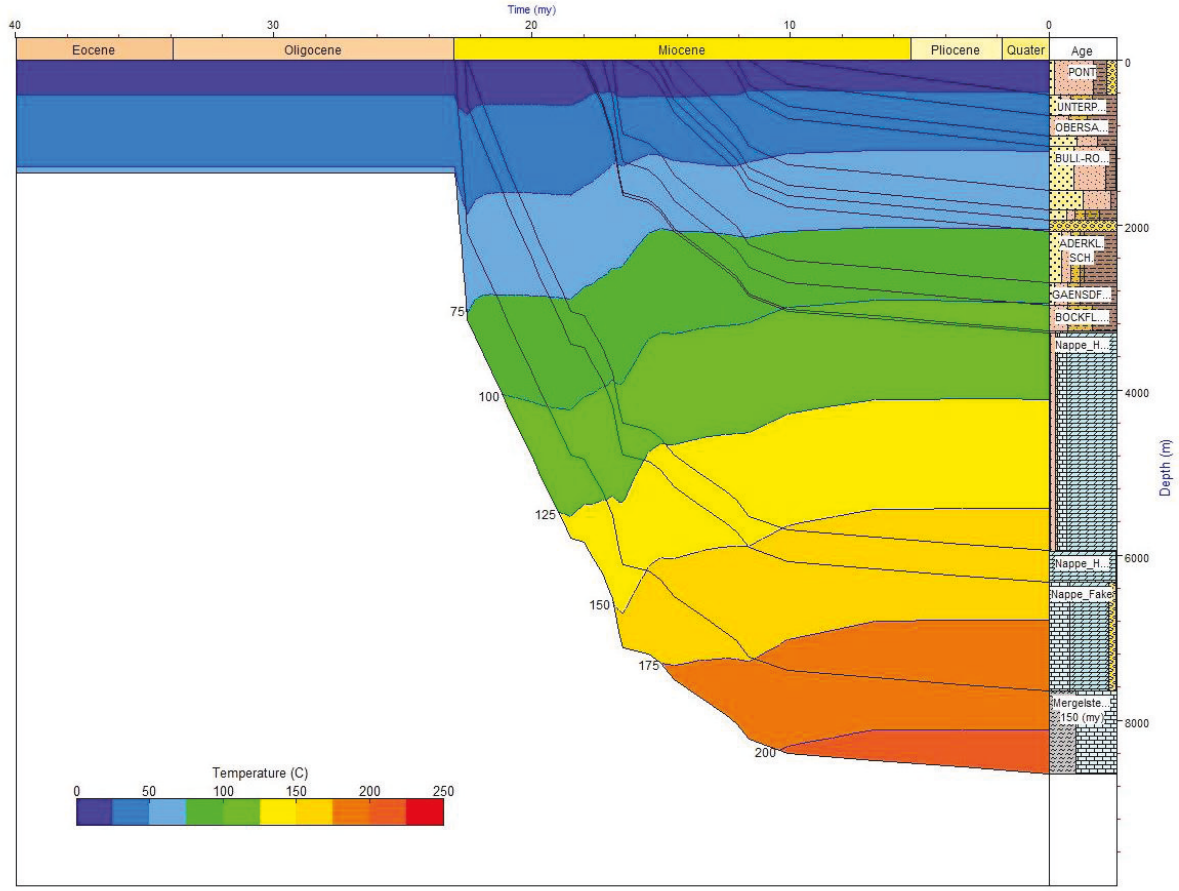

Fig. 80: Thermal history for well Gänserndorf ÜT1 kindly provided by Rainer T.

Hydrocarbons in Autochtounous Mesozoic sediments and the Molasse zone (e.g. Höflein, Stocker Ost) may have been charged by migration along basal flysch overthrusts. Because the hydrocarbons are very light it is possible that they experienced evaporative fractionation. Evaporative fractionation is observed in tight reservoirs and along tight fault planes (Silverman, 1965; Thompson, 1987; Thompson, 1988).

11. Conclusions

In the following the main study results are summarized separately for source rocks, hydrocarbons within and outside the Vienna Basin.

Source Rocks

The Upper Jurassic basinal marls of the Mikulov Formation, more than 1000 thick, interfinger with slope deposits of the Falkenstein Formation. According to previous studies, the organic matter-rich succession has been deposited on an open marine shelf under the influence of upwelling (Tari et al., 2011, Golonka and Krobicki, 2001). Langanger (2008) postulated a significant shale gas potential for the Mikulov Formations, which is the main source for conventional oil and gas in the Vienna Basin (Ladwein, 1988). The present study uses borehole Staatz 1 as a key well and yields important additional insights into depositional environment and source rock potential:

- Based on microfacies analysis, both the Falkenstein and Mikulov formations are subdivided into 3 layers (F1-3; M1-3). The upper part of the Mikulov Formation (M-3) is characterized by an increase in detrital input.
- Differences in the microfacies of layers F1 to M3 in combination with the vertical variability of biomarker parameters argue against tectonic multiplication of the succession. Consequently, the high thickness can be considered as original.
- In borehole Staatz 1 TOC contents vary between 0.3 and 2.2 wt.% in the Falkenstein Formation and between 0.6 and 2.5 wt% in the Mikulov Formation. Limited data from deep wells in the deep overmature central part of the basin suggest that the original TOC contents may have increased basinwards.
- The Falkenstein and Mikulov formations contain type III-II kerogen to type II kerogen. Petrographically the organic matter is dominated by aquatic liptinite macerals (alginite, liptodetrinite). The observed relative low HI values (<400 mgHC/gTOC) in immature sediments are explained by organic matter degradation in a dysoxic environment.
- Bulk parameters, organic matter composition and biomarker ratios agree with a coastal upwelling setting, which is not particularly enriched in organic

carbon, like the Northwest African shelf (comp. Littke and Sachsenhofer, 1994).

- Both, the Falkenstein and the Mikulov Formation may be considered as fair to good source rocks for conventional hydrocarbons. Within the oil window, they will produce paraffinic-naphtenic-aromatic low wax oil with low sulphur content.
- Based on TOC contents (typically <2.0 wt.%) and the very deep position of the maturity cut-off values for shale oil (0.8 %Rr; ~4000 m) and shale gas production (1.2 %Rr; ~5000 m), the shale oil/shale gas potential of both formations is limited, despite of their great thickness. Quartz contents considered to increase fraccability are low. However, geochmechanical data from the carbonate-rich rocks are missing. In any case, previous estimates of the shale gas potential seem too optimistic.
- The syn-rift deposits of the Middle Jurassic Gresten Formation host a moderate oil potential in its lower part (deltaic Lower Quarzarenite Member). In contrast, prodelta shales of its middle part (Lower Shale Member) are poor source rocks according to the classification of Peters (1986).

Hydrocarbons in the Austrian part of the Vienna Basin

The present study of oil and gas samples from the Alpine nappes and the Neogene fill of the Vienna Basin in Austria support some traditional ideas, but also contributes important new insights into the petroleum system of the Vienna Basin region:

- The only significant source rocks for hydrocarbons in the Austrian sector of the basin are the Upper Jurassic Mikulov and Falkenstein formations. Oil was generated at about a maturity of 0.7 to 1.0 %Rr. Thermogenic gas was generated at higher maturity (1.1-1.6 %Rr). Apart from thermogenic gas, also microbial gas exists and prevails in fields located in southern and southeastern positions.
- The molecular composition of oil and gas are strongly controlled by biodegradation, which affects oil and gas down to approximately 2000 m depth. Biodegradation reaches rank 4 of the BBDS (Wenger and Isaksen, 2002; Peters et al., 2005) and is strongly related to oil gravity. It is more efficient in traps located in the hangingwall of major faults than in the footwall. Moreover, biodegradation is retarded in low permeable turbiditic sandstone

reservoirs (15th TH; Flysch Zone). The amount of CO2 and its isotopic composition has to be evaluated critically, because of past EOR measures. Nevertheless the light isotopy of methane in some shallow deposits together with elevated contents of isotopically heavy CO_2 suggests the presence of secondary microbial gas in some shallow reservoirs.

- TSR is an important alteration process for hydrocarbons in the Calcareous Alps. It is reflected by gases with high H_2S and CO2 contents, as well as by oils with high DBT/Ph ratios. When TSR affected hydrocarbons are in contact with clastic reservoirs, H2S is removed by pyrite precipitation, whereas the DBT/Ph ratios remain constant. Hence, DBT/Ph ratios may be used as proxy for TSR, which affected oils before they charged clastic reservoirs. Stable sulphur isotope signatures of H2S confirm anhydrites from the Lunz-Frankenfels nappes system as the main sulphur source.

Hydrocarbons in the Czech Republik and Slovakia

- Oils from the Czech Republik and Slovakia originate from the same source rock as oils in Austria, namely the Mikulov Formation. They are slight to moderate biodegraded and fit areal trends (e.g. sterane/hopane ratio).

Hydrocarbons in the vicinity of the Vienna Basin (Autochtounous Mesozoic, Waschberg Zone, Molasse Zone)

In the vicinity of the Vienna Basin Mikulov-sourced oils are mixed with a light condensate of unknown origin. The condensates may originate either from coaly source rocks or have been affected by evaporative fractionation.

- The oil from Klement 1 contains land plant biomarkers and suggests an active, previous unknown petroleum system: the Lower Quartzarenite Member – Lower Quartzarenite Member (!) petroleum system.
- The condensate from the Stockerau Ost field is slightly biodegraded.
- Microbial gas is produced from reservoirs in the Molasse Zone (Roseldorf, Wildendürnbach).

Oil stains from Mank and Urmannsau

- Oil stains encountered in the Calcareous Alps (Urmannsau) and in the Alpine Foreland Basin SW of St. Pölten (Mank) are sourced from organic matter-rich rocks within the northen Calcareous Alps.

Hydrocarbon migration within the Vienna Basin

- The investigation of benzocarbazoles reveals differing (vertical) migration distances. Benzocarbazole-based estimates of migration distances correlate well with estimates, based on maturity trends of source rocks and the maturity of oil samples. However this approach, does not consider the latest basin models, which suggest a multi-stage migration history.

12. References

Alexander, R., Kagi, R.I., Woodhouse, G.W., Volkman, J.K., 1983. The geochemistry of some biodegraded Australian oils. Australian Petroleum Exploration Association Journal, 23, 53-63.

Alexander, R., Kagi, R.I., Toh, E., van Bronswijk, W., 1988. The use of aromatic hydrocarbons for assessment of thermal histories in sediments. In: Purcell, P.G., Purcell, R.R. (eds.). The North West Shelf, Australia: Proceedings of the Petroleum Exploration Society of Australia, Perth. Petroleum Exploration Society of Australia, Perth, Australia, 55-62.

Alexander, R., Larcher, A.V., Kagi, R.I., Price, P.L., 1988. An oil-source correlation study using age specific plant-derived aromatic biomarkers. In: Moldowan, M.J., Albrecht, P., Philip, P.R. (eds.). Biological Markers in Sediments and Petroleum. Prentic-Hall, Englewood Cliffs, NJ., 201-221.

Alexander, R., Larcher, A.V., Kagi, R.I., Prince, P.L., 1992. An oil-source correlation study using age specific plant-derived aromatic biomarkers. in: Moldowan, M.J., Albrecht, P., Philips, P.R. (eds.). Biological Markers in Sediments and Petroleum, Prentice-Hall, Englewood Cliffs, NJ., 201-221.

Andrews, I.J., 2013. The Carboniferous Bowland Shale Gas Study: Geology and Resource Estimation. British Geological Survey for Department of Energy and Climate Change, London, UK.

Amrani, A., Deev, A., Sessions, A.L., Tang, Y., Adkins, J.F., Hill, R.J., Moldowan, J.M., Wei, Z., 2012. The sulfur-isotopic compositions of benzothiophenes and dibenzothiophenes as a proxy for thermochemical sulfate reduction. Geochimica et Cosmochimica Acta, 84, 152-164.

Andruleit, H., Babies, H.G., Cramer, B., Messner, J., Rempl, H., Schlömer, S., Schmidt, S., 2010. Nicht-konventionelles Erdgas: Weltweite Ressourcen und Entwicklungen eines „Hoffnungsträgers“ unter den fossilen Energierohstoffen. Erdöl, Erdgas, Kohle, 126 (7/8), 277-282.

Arzmüller, G., Buchta, S., Ralbovky, E., Wessely, G., 2006. The Vienna Basin. In Golonka, J., Picha, F.J. (eds.). The Carpathinas and their foreland: Geology and hydrocarbon resources. AAPG Memoir 84, 191-204.

Baily, N.J.L., Jobson, A.M., Rogers, M.A., 1973. Bacterial degradation of crude oil: comparison of field and experimental data. Chemical Geology, 11, 203-221.

Barakat, A.O., Rullkötter, J., 1997. A comparative study of molecular paleosalinity indicators: chromans, tocopherols and C20 isoprenoid thiophenes in Miocene lake sediments (Nördlinger Ries, Southern Germany). Aquatic Geochemistry, 3, 169–190.

Bartis, J.T., La Tourrette, T., Dixon, L., Peterson, D.J., Cecchine, G., 2005. Oil Shale Development in the United States. RAND Corporation monograph series # MG 414.

Bechtel, A., Gratzer, R., Linzer, H-G., Sachsenhofer, R.F., 2013. Influence of migration distance, maturity and facies on the stable isotopic composition of alkanes and on carbazole distributions in oils and source rocks of the Alpine Foreland Basin of Austria. Organic Geochemistry, 62, 74-85.

Beidinger, A., Decker, K., 2014. Quantifying EarlyMiocene in-sequence and out-of-sequence thrusting at the Alpine-Carpathian junction. Tectonics, 33, 222–c52.

Bennett, B., Chen, M., Brincat, D., Gelin, F.J.P., Larter, S.R., 2002. Fractionation of bezocarbazoles between source rocks and petroleums. Organic Geochemistry, 33, 345-559.

Bernard, B.B., Brooks, J.M. Sackett, W.M., 1978. Light hydrocarbons in recent Texas continental shelf and slope sediments. Journal of Geophysical Research, 83, 4053-4061.
Berner, R.A., Raiswell, R., 1984. C/S method for distinguishing freshwater from marine sedimentary rocks. Geology, 12, 365–368.
Berner, U., Faber, E., 1987. Maturity related mixing model for methane, ethane and propane, based on carbon isotopes. Organic Geochemistry, 13, 67-72.
Berner, U., Faber, E., 1996. Empirical carbon isotope/maturity relationships for gases from algal kerogens and terrigenous organic matter, based on dry, open-system pyrolysis. Organic Geochemistry, 24, 947-95.
Bjorøy, M., Hall, P.B., Moe, R.P., 1994. Stable carbon isotope variation of n-alkanes in central graben oils. Organic Geochemistry, 22, 355–381.
Blanc, P., Connan, J., 1994. Preservation, degradation and destruction of trapped oil. In Magoon, L.B., Dow, W.G. (eds.). The Petroleum System – From Source to Trap. AAPG, Tulsa, OK.
Boëda, E., Bonilauri, S., Connan, J., Jarvie, D., Mercier, N., Tobey, M., Valladas, H., Al Sakhel, H., 2008. New Evidence for Significant Use of Bitumen in Middle Palaeolithic Technical Systems at Umm el Tlel (Sysria) around 70,000 BP. Paléorient, 34, 67-83.
Bown, P.R., Cooper, M.K.E., 1998. Jurassic. in: Bown, P.R. (ed.). Calcareous nannofossil biostratigraphy. Kluwer Academic Publications, Dordrecht, 33-85.
Bown, P.R., Young, J.R. 1998. Techniques. in: Bown, P.R. (ed.). Calcareous nannofossil biostratigraphy. Kluwer Academic Publications, Dordrecht, 16-28.
Bowler, B.F.L., Larter, S.R., Clegg, H., Wilkes, H., Horsfield, B., Li, M., 1997. Dimethylcarbazoles in crude oils: comment on liquid chromatographic separation schemes for pyrrole and pyridine nitrogen aromatic heterocycle fractions from crude oils suitable for rapid characterisation of geochemical samples. Analytical Chemistry, 69, 3128–3129.
Brodacki, M., 2006. Functional anatomy and mode of life of the latest Jurassic crinoid Saccocoma. Acta palaentologica polonica, 51, 261-270.
Brooks, P.W., Fowler, M.G., Macqueen, R.W., 1988. Biological marker and conventional organic geochemistry of oil sands/heavy oils, Western Canada Basin. Organic Geochemistry, 12, 519-538.
Brown, A., 2011. Identification of source carbon for microbial methane in unconventional gas reservoirs. AAPG Bulletin, 95, 1321-1338.
Bryan, E.E., Evans, E.D., 1961. Distribution of n-paraffins as a clue to recognition of source beds. Geochimica et Cosmochimica Acta, 22, 2–15.
Burnie, S.W., 1979. A sulphure and carbon isotope study of hydrocarbons from Devonian of Alberta, Canada. Unpublished PhD Thesis, University of Alberta, Edmonton.
Canfield, D.E., Jørgensen, B.B., Fossing, H., Glud, R., Gundersen, J., Ramsing, N.B., Thamdrup, B., Hansen, J.W., Nielsen, L.P., Hall, P.O.J., 1993. Pathways of Organic-Carbon Oxidation in 3 Continental-Margin Sediments. Marine Geology, 113, 27-40.
Cai, C., Hu, W., Worden, R.H., 2001. Thermochemical sulphate reduction in Cambro-Ordovician carbonates in Central Tarim. Marine and Petroleum Geology, 18, 729-741.
Charpentier, R.R., Cook, T.A., 2011 USGS Methodology for Assessing Continuous Petroleum Resources. US Geological Survey Poen-File Report 2011-1167

Chung, H.M.; Gormly, J.R. Squires, R.M.; 1988. Origin of gaseous hydrocarbons in subsurface environments: Theoretical considerations of carbon isotope distribution. Chemical Geology, 71, 97-104.
Claypool, G.E., Mancini, E.A., 1989. Geochemical relationships of petroleum in Mesozoic reservoirs to carbonate source rocks in Jurassic Smackover Formation, southwest Alabama. AAPG Bulletin, 73, 904-924.
Clegg, H., Wilkes, H., Horsfield, B., 1997. Carbazole distributions in carbonate and clastic source rocks. Geochimica et Cosmochimica Acta, 61, 5335–5345.
Clegg, H., Wilkes, H., Oldenburg, T.B.P., Santamaria-Orozco, D., Horsfield, B., 1998. Influence of maturity on carbazole and benzocarbazole distributions in crude oils and source rocks from the Sonda de Campeche, Gulf of Mexico. Organic Geochemistry 29, 183–194.
Collister, J.W., Rieley, G., Stern, B., Eglinton, G., Fry, B., 1994. Compound-specific d13C analysis of leaf lipids from plants with differing carbon dioxide metabolism. Organic Geochemistry, 21, 619–627.
Connan, J., Cassou, A.M., 1980. Properties of gases and petroleum lipids derived from terrestrial kerogen at various maturation levels. Geochimica et Cosmochimica Acta, 44, 1-23.
Connan, J., 1984. Biodegradation of crude oils in reservoirs. In: Brooks, J., Welte, D.H. (eds.). Advances in Petroleum Geochemistry, Vol. 1, Academic Press, London.
Coplen, T.B., 1995: New IUPAC guidelines for the reporting of stable hydrogen, carbon, and oxygen isotope-ratio data. Journal of Research of the National Institute of Standards and Technology, 10, 285.
Cranwell, P.A., 1977. Organic geochemistry of CamLoch (Sutherland) sediments. Chemical Geology, 20, 205-221.
Dai, J., 1990. Characteristics of hydrogen isotopes of paraffinic gas in China. Petroleum Exploration and Development, 17, 27-32.
Demaison, G., Huizinga, B.J., 1991. Genetic classification of petroleum systems. AAPG Bulletin, 75, 1626-1643.
Didyk, B.M, Simoneit, B.R.T,Brassell, S.C., G. Eglinton, 1978. Organic geochemical indicators of palaeoenvironmental conditions of sedimentation. Nature, 272, 216–222.
Dreyfus, S., Pecheyran, C., Lienemann, C.P., Magnier, C., Prinzhofer, A., Donard, O.F.X., 2007. Determination of lead isotope ratios in crude oils with Q-ICP/MS. Journal of Analytical Atomic Spectrometry, 22, 351-360.
Eglinton, T.I., Sinninghe Damsté, J.S., Kohnen, M.E.L., de Leeuw, J.W., 1990. Rapid estimation of the organic sulphur content of kerogens, coals and asphaltenes by pyrolysis-gas chromatography. Fuel, 69, 1394-1404.
Elias, M., Wessely, G., 1990. The autochthonous Mesozoic on the eastern flank of the Bohemian Massif – an object of mutal geological effort between Astria and CSSR. in: Petranek, J. (reviewer), Thrity years of geological cooperation between Austria and Czechoslovakia. Ustredni ustav geologicky, 78-83.
Espitalie, J., La Porte, J.L., Madec, M., Marquis, F., Leplat, P., Paulet, J., Boutefeu, A., 1977. Methode rapide de characterisation des roches meres de leir potential petrolier et de leur degree dèvolution. Revue de lÍnsitute Francais du Pétrol, 32, 23-42.
Faupl, P., 1996. Exkursion 2A. Tiefwassersedimente und tektonischer Bau der Flyschzone des Wienerwaldes. In: Exkursionsführer Sediment 96,11. Sedimentologietreffen, Wien.

Ficken, K.J., Li, B, Swain, D.L., Eglinton, G., 2000. An n-alkane proxy for the sedimentary input of submerged/floating freshwater aquatic macrophytes. Organic Geochemistry, 31, 745–749.
Filby, R.H.; 1994. in: Parnell, J. (ed.). Geofluids: Origin, Migration and Evolution of Fluids in Sedimentary Basins, 203-219.
Finlay, A.J., Selby, D., Osborne, M.J., 2012. Re-Os geochronology and fingerprinting of United Kingdom Atlantic margin oil: Temporal implications for regional petroleum systems. Geology, 39, 475-478.
Flügel, E., 2004. Microfacies of carbonate rocks: analysis, interpretation and application. Springer, Berlin.
Francu, J., Radke, M., Schafer, R.G., Poelchau, H.S., Caslavsly, J., Bohacek, Z., 1996. Oil-oil and oil-source rock correlation in the northern Vienna basin and adjacent Carpathian Flysch Zone (Czech and Slovak area). In: Wessely, G., Liebl, W. (eds.). Oil and gas in Alpidic thrustbelt and basins of Central and Eastern Europe. EAGE Special Publication 5. Geological Society, London, 343-353.
Frederickson, J.K., McKinley, J.P., Bjornstad, B.N., 1997. Pore-size constraints on the activity and survival of subsurface bacteria in a Late Cretaceous shale-sandstone sequence, northwestern New Mexico. Geomicrobiology Journal, 14, 183-202.
Freilinger, G., 1963. Das Konglomerat von Moosbierbaum (Basis der Molasse) und die Granodiorite des Molasseuntergrundes SW von Tulln. Unpublished PhD Thesis, University of Vienna.
Friedl, K., 1933. Die Erschließung von Erdöl und Erdgas im österreichischen Anteil des Wiener Bekkens. Internationale Zeitschrift für Bohrtechnik, Erdölbergbau und Geologie, 41, 6, 48-54.
Friedl, K., 1956. Erdölgewinnung in Österreich: Gestern-heute-morgen. Neue Technik und Wirtschaft, 10, 2, 73-86.
Fuchs, R., Hamrsmid, B., Kuffner, T., Peschl, R., Rögl, F., Sauer, R., Schreiber, O.S., 2001. Mid Oligocene Thomasl formation (Waschberg Unit, Lower Austria) – micropaleontology and stratigraphic correlation. In: Piller, W.E., Rasser, M.W. (eds.). Paleogene of the Eastern Alps, Österreichische Akademie der Wissenschaften – Schriftereihe Erdwissenschaftliche Kommentare, 14, 255-290.
Galimov, E.M., 1980. C13/C12 in kerogen. In: Durand, B. (ed.). Kerogen, insoluble Organic Matter from Sedimentary Rocks. Edition Technip. Paris.
Gerslova, E., Opletal, V., Sykorova, I., Sedlakova, I., Gersl, M., 2015. A geochemical and petrographical characterization of organic matter in the Jurassic Mikulov Marls from the Czech Republic. International Journal of Coal Geology, 141-142, 42-50.
Glantschnig, J., Kroell, E., 1997. Injection of Nitrogen for Improved Oil recovery: A successful case study. 15th World Petroleum Congress, 12-17 Oktober 1997, Beijing.
Golding, S.D., Boreham, C.J., Esterle, J.S., 2013. Stable isotope geochemistry of coal bed and shale gas and related production waters: A review. International Journal of Coal Geology, 120, 24-40.
Goldstein, T.P., Aizenshat, J.D., 1994. Thermochemical sulfate reduction – a review. Journal of Thermal Analysis, 42, 241-290.
Golonka, J., Krobicki, M., 2001. Upwelling regime in the Carpathian Tethys: a Jurassic-Cretaceous palaeogeographic and paleoclimatic perspective. Geological Quarterly, 45, 15-32.

Granado, P., Thöny, W., Carrera, N., Gratzer, O., Strauss, P., Munoz, J.A., 2016. Basemnet-involved reactivation in foreland fold-and-thrust belts: the Alpine-Carpathian Junction (Austria). Geological Magazine, 153, 5-6, 1110-1135.

Grantham, P.J., Wakefield, L.L., 1988. Variations in the sterane carbon number distributions of marine source rock derived crude oils through geological time. Organic Geochemistry, 12, 61-73.

Gratzer, R., Bechtel, A., Sachsenhofer, R.F., Linzer, H.-G., Reischenbacher, D., Schulz, H.-M., 2011. Oil-oil and oil-source rock correlations in the Alpine Foreland Basin of Austria: Insights from biomarker and stable carbon isotope studies. Marine and Petroleum Geology, 28, 1171-1186.

Gratzer, R., Sachsenhofer, R.F., Bechtel, A., Gawlick, H.-J., 2015. Geogenic versus Anthropogenic: Hydrocarbons in the Spoil from the Falkenstein and Spering Tunnels (A9 Phyrn Autobahn, Austris). Geomechanics and tunneling, 8, 356-363.

Grice, K., de Mesmay, R., Glucina, A., Wang, S., 2008. An improved and rapid 5A molecular sieve method for gas chromatography isotope ratio mass spectrometry of n-alkanes (C8–C30+). Organic Geochemistry, 39, 284–288.

Grill, R., 1953. Der Flysch, die Waschbergzone und das Jungtertiär um Ernstbrunn (Niederösterreich). Jahrbuch der Geologischen Bundesanstalt, 96, 65-116.

Hallmann, C.O.E., Arouri, K.R., McKirdy, D.M., Schwark, L., 2007. Temporal resolution of an oil charging history – a case study of residual oil benzocarbazoles from the Gidgealpa field. Organic Geochemistry, 38, 1516–1536.

Hamilton, W., 1997. Die Oncaphoraschichten im Bereich Altprerau – Wildendürnbach. Exkursionsführer der Österreichischen Geologische Gesellschaft, 17: Das Land um Laa/Thaya, Verlag der Geologischen Bundesanstalt, Wien.

Hamilton, W., Wagner, L., Wessely, G., 2000. Oil and Gas in Austria. Mitteilungen der Österreichischen Geologischen Gesellschaft, 92, 235-262.

Harrison, A.G., Thode, H.G.; 1957. The kinetic isotope effect in the chemical reduction of sulfate. Trans. Farady Soc., 53, 1-4.

Hayes, J.M., 1993. Factors controlling 13C content of sedimentary organic compounds: principale and evidence. Marine Geology 113, 111-125.

Hayes, J.M., 2001. Fractionation of carbon and hydrogen isotopes in biosynthetic processes. in: Vally, J.W., Cole, D.R. (eds.). Stable isotope geochemistry. Reviews in mineralogy and geochemistry, 43, 225-277.

Hester, R.E., Harrison, R.M., 2015. Issues in Environmental Science and Technology. Vol. 39 – Fracking. Royal Society of Chemistry. Cambridge.

Hilkert, A.W., Douthitt, C.B., Schlüter, H.J., and Brand, W.A., 1999. Isotope ratio monitoring gas chromatography/mass spectrometry of D/H by high temperature conversion isotope ratio mass spectrometry. Rapid Communications in Mass Spectrometry, 13, 1226-1230.

Horsfield, B., 1989. Practical criteria for classifying kerogens: some observations from pyrolysis-gas chromatography. Geochimica et Cosmochimica Acta, 53, 891-901.

Hughes, W.B., Holba, A.G., Dzou, L.I.P., 1995. The ratio of dibenzothiophene to phenatrene and pristane to phytane as indicators of depositional environment and lithology of petroleum source rocks. Geochimica et Cosmochimica Acta, 59, 3581-3598.

Hunt, J.M., 1996. Petroleum Geochemistry and Geology. W.H Freeman & Co., New York.

Husain, S.A., 1967. Sulphur isotopes and limestone lithification. J Geol. Soc. London, 133, 637-660.
Husain, S.A., Krouse, H.R., 1978. Sulphur isotope effects during the reaction of sulphate with hydrogen sulphide. In: Robinson, B.W. (ed.). Stable isotopes in the earth sciences. Department of Scientific and Industrial Research Bulletin, 220, 207-210.
ISO/IEC stage 3166-1:2016; Country Codes, 2017-05-25, International Organization for Standardization, Geneva, Switzerland.
Jarvie, D.M., 2012. Shale resource systems for oil and gas: Part 1 – Shale-gas resource systems. In Breyer, J.A. (ed.). Shale reservoirs – Giant resources for the 21st century. AAPG Memoir, 97, 69-87.
Jarvie, D.M., Hill, R.J., Ruble, T.E., Pollastro, R.M., 2007. Unconventional shale-gas systems: the Mississippian Barnett Shale of north-central Texas as one model for thermogenic shale-gas assessment. AAPG Bulletin, 91, 4, 475-499.
Jenneman, G.E., Mcinerney, M.J., Knapp, R.M., 1985. Microbial penetration through nutrient saturated Berea sandstone. Applied and Environmental Microbiology, 50, 383-391.
Jiang, C.; Alexander, R., Kagi, R.I., Murray, A.P., 2000. Origin of perylene in ancient sediments and its geological signifcance. Organic Geochemistry, 31, 1545-1559.
Jiricek, R., 1985. Deltovy vyvoj spodniho Panonu v jizni casti videnske panve – Zemni plyn a nafta. Rocnik, 31, 161-186.
Jiricek, R., Seifert, P., 1990. Paleogeography of the Neogene in the Vienna Basin and the adjacent part of the foredeep. In: Minarikova, D., Lobitzer, H. (eds.). 30 Years of geological cooperation between Austria and Czechoslovakia, Verlag der Geologischen Bundesanstalt, Wien, 89-105.
Jobson, A.M., Cook, F.D., Westlake, D.W.S., 1979. Interaction of aerobic and anaerobic bacteria in petroleum biodegradation. Chemical Geology, 24, 355-365.
Jones, D.M.; Head, et al., 2008. Crude-oil biodegradation via methanogenesis in subsurface petroleum reservoirs. Nature, 451, 176-181.
Killops, S.D., Killops, V.J., 1993. An Introduction to Organic Geochemistry. Longman Group, England.
King, H.E., Walters, C.C., Horn, W.C., Zimmer, M., Heines, M.H., Lamberti, W.A., Kliewer, C., Pottorf, R.J., Macleod, G., 2014. Sulfate isotope analysis of bitumen and pyrite associated with thermal sulfate reduction in reservoir carbonates at the Big Piney-La Barge production complex. Geochimica et Cosmochimica Acta, 134, 210-220.
Kiyosu, Y., 1980. Chemical reduction and sulfur isotope effects of sulfate by organic matter under hydrothermal conditions. Chemical Geology, 30, 47-56.
Kiyosu, Y., Krouse, H.R., 1990. The role of organic acid in the abiogenic reduction of sulfate and sulfur isotope effect. Geochemistry Journal, 24, 21-27.
Klemme, H.D., 1994. Petroleum Systems of the World Involving Upper Jurassic Source Rocks. in: Magoon, L.B., Dow, W.G. (eds.). The petroleum system – from source to trap, AAPG Memoir 60, Tulsa, OK.
Klemme, H.D., Ulmishek, G.F., 1991. Effective petroleum source rocks of the world-stratigraphic distribution and controlling factors. AAPG Bulletin, 75, 12, 1809-1851.
Kratochvil, H., Ladwein, H.W., 1984. Die Muttergesteine der Kohlenwasserstofflagerstätten im Wiener Becken und ihre Bedeutung für zukünftige Exploration (The Vienna Basin hydrocarbon source rocks and their importance for future exploration. Erdöl Erdgas, 100, 3, 107-115.

Kreutzer, N., 1993. Die ÖMV-Gas- und Öllagerstätten der nieder- und oberösterreichischen Molassezone. In: Brix, F. and Schultz, O. (eds.). Erdöl und Erdgas in Österreich, Verlag des NHM Wien und F.Berger, Horn.

Krumholz, L.R., 2000. Microbial communities in the deep subsurface. Hydrogeology Journal, 8, 4-10.

Kuo, L.C., 1994. An experimental study of crude oil alteration in reservoir rocks by water washing. Organic Geochemistry, 21, 5, 465-479.

Kröll, A., Wessely, G., 1993. Wiener Becken und angrenzende Gebiete – Strukturkarte – Basis der tertiären Beckenfüllung. Geologischen Karte herausgegeben von der Geologischen Bundesanstalt, Wien.

Ladwein, H.W., 1982. Versuch einer Migrationsanalyse im Wiener Becken und die darausfolgende Verteilung von Erdöl- und Erdgasfeldern. Unpublished internal OMV report.

Ladwein, H.W., 1982. Bericht über H2S-Verbreitung und Herkunft in Lagerstätten der ÖMV-AG und mögliches H2S-Auftreten bei künftigen Explorationszielen. Unpublished internal OMV report.

Ladwein, H.W., 1988. Organic Geochemistry of Vienna Basin: Model for Hydrocarbon Generation in Overthrust Belts. AAPG Bulletin, Vol 72, 586-599.

Langanger, H. 2008. Exploration and Production. OMV Capital Markets Day 2008, London. World Wide Web Address: http://www.omv.com/SecurityServlet/secure?cid=1225986876259&lang=de&swa_site=wps.vp.com&swa_nav=OMV+Holding%7C%7CInvestor+Relations%7C%7CEvents%7C%7CCapital+Markets+Day+2008%7C%7C&swa_pid=6_B_QFO+%5BCONTENT_NODE%3A3096224743844344%5D&swa_lang=de.

Larter, S.R., Bowler, B., Li, M., Chen, M., Brincat, D., Bennett, B., Noke, K., Donohoe, P., Simmons, D., Kohen, M., Allan, J., Telnaes, N., Horstad, I., 1996. Benzocarbazoles as molecular indicators of secondary oil migration distance. Nature, 383, 593-597.

Larter, S., Koopmans, M.P., Head, I., 2000. Biodegradation rates assessed geologically in a heavy oilfield – implications for a deep, slow (Largo) biosphere. GeoCanada 2000 – The Millenium Geoscience Summit, Calgary, Alberta.

Larter, S.R., di Primo, R., 2005. Effects of biodegradation on oil and gas field PVT properties and the origin of oil rimmed gas accumulations. Organic Geochemistry, 36, 299-310.

Law, B.E., Spencer, C.W., 1993. Gas in Thight Reservoirs – An Emerging Major Source of Energy. In: Howell, D.G. (ed.). The Future of Energy Gases – U.S. Geological Survey Professional Paper 1570, 1993.

Leutner, M., 1990. Die Temperaturverteilung im Neogen des Wiener Beckens und dessen Untergrund. Unpublished Master Thesis, Montanuniversitaet Leoben.

Lewan, M.D., 1993. Laboratory Simulation of Petroleum Formation. in Engel, M.H., Macko, S.A. (eds.). 1993. Organic Geochemistry- Principles and Applications. New York, Plenum Press, 419-422.

Lewan, M.D., 1997. Experiments on the role of water in petroleum formation. Geochimica et Cosmochimica Acta, 61, 3691-3723.

Li, M., Larter, S.R., Taylor, P., Jones, D.M., Bowler, B., Bjorøy, M., 1995. Biomarkers or not biomarkers? A new hypothesis for the origin of pristane involving derivation from methyltrimethyltridecylchromans (MTTCs) formed during early diagenesis from chlorophyll and alkylphenols. Organic Geochemistry, 23, 159–167.

Li, M., Yao, H., Stasuik, L.D., Fowler, M.G., Larter, S.R., 1997. Effect of maturity and petroleum expulsion on pyrrolic nitrogen compound yields and distributions in

Duvernay Formation petroleum source rocks in Central Alberta, Canada. Organic Geochemistry, 26, 731–744.
Li, M., Yao, H., Fowler, M.G., Stasuik, L.D., 1998. Geochemical constraints on models for secondary petroleum migration along the Upper Devonian Rimbey–Meadowbrook reef trend in central Alberta, Canada. Organic Geochemistry, 29, 163–182.
Lillis, P.G., Selby, D., 2013. Re-Os geochronology and fingerprinting of United Kingdom Atlantic margin oil: Temporal implications for regional petroleum systems. Geochimica et Cosmochimica Acta, 118, 312-330.
Littke, R, Sachsenhofer, R.F., 1994. Organic petrology of deep sea sediments: a compilation of results from the Ocean Drilling Program and the Deep Sea Drilling Project. Energy and Fuels, 8, 1498-1512.
Littke, R., Baker, D.R., Rullkötter, J., 1997. Deposition of Petroleum Source Rocks. in: Welte, D.H., Horsfield, B., Baker, D.R. (eds.). Petroleum and Basin Evolution, Springer, 273-333.
Machel, H.G., 1989. Relationships between sulphate reduction and oxidation of organic compounds to carbonate diagenesis, hydrocarbon accumulations, salt domes, and metal sulphide deposits. Carbonates and Evaporites, 4, 137-151.
Machel, H.G., 2001. Bacterial and thermochemical sulfate reduction in diagenetic settings – old and new insights. Sedimentary Geology, 140, 143-175.
Machel, H.G., Krouse, H.R., Sassen, R., 1995. Products and distinguishing criteria of bacterial and thermochemical sulfate reduction. Applied Geochemistry, 10, 373-389.
Mackenzie, A.S., 1984. Application of biological markers in petroleum geochemistry. in: Brooks, J., Welte, D.H. (eds.). Advances in Petroleum Geochemistry. Academic Press, London, 115-214.
Mackenzie, A.S., Maxwell, J.R.¸1981. Assessment of thermal maturation in sedimentary rocks by molecular measurements. in: Brooks, J. (ed.). Organic Maturation Studies and Fossil Fuel Exploration, Academic Press, London, 239-254.
Malisa, E.P., 2001. The Behavoir of Selenium in Geological Processes. Environmental Geochemistry and Health, 2, 137-158.
McCarthy, K., Rojas, K., Niemann, M., Palmowski, D., Peters, K., Stankiewicz, A., 2011. Basic Petroleum Geochemistry for Source Rock Evaluation. Schlumberger Oilfield Review, 23 (2), 32-43.
Milkov, A.V., 2011. Worldwide distribution and significance of secondary microbial methane formed during petroleum biodegradation in conventional reservoirs. Organic Geochemistry, 42, 184-207.
Moldowan, J.M., Lee, C.Y., Sundararaman, P., 1992. Source correlation and maturity assessment of selected oils and rocks from the Central Adriatic Basin (Italy and Yugoslavia). In: Moldowan, J.M., Albrecht, P., Philips, R.P. (eds.). Biological Markers in Sediments and Petroleum. Prentice Hall, Englewoods Cliffs, NJ, 307-401.
Mongenot, T., Tribovillard, N.P., Desprairies, A., Lallier-Verges, E., Laggoun-Defarge, F., 1996. Trace elements as palaeoenvironmental markers in strongly mature hydrocarbon source rocks: the Cretaceous La Luna Formation of Venezuela. Sedimentary Geology, 103, 1447-1456.
Morse, J.W., Arvidson, R.S., Lüttge, A., 2007. Calcium carbonate formation and dissolution. Chemical Reviews, 107, 342-381.
Malzer, O., Brix, F. 1993. Muttergesteine, Speichergesteine; Migration und Lagerstättenbildung in Der Molassezone und deren sedimentärem Untergrund.

In: Brix, F., Schultz, O. (eds.). Erdöl und Erdgas in Österreich, Verlag des NHM Wien und F.Berger, Horn.
Milner, C.W.D., Rogers, M.A., Evans, C.R., 1977. Petroleum transformations in reservoirs. Journal of Geochemical Exploration, 7, 101-153.
Müller, A.M., 1978. Lehrbuch der Paläozoologie Band II Invertebraten Teil 3 Arthropoda 2 – Hemichordata. Gustav Fischer Verlag, Jena.
Murray, A.P., Summons, R.E., Boreham, C.J., Dowling, L.M., 1994. Biomarker and n-alkane isotope profiles for tertiary oils: relationship to source rock depositional setting. Organic Geochemistry 22, 521–542.
Nakazawa, T., Kuroki, M., Tsunashima, Y., 1981: The chemistry of carbazoles IX. Substituent effect in the gas liquid chromatography of methylcarbazoles. Journal of Chromatography, 211 (388), 391.
Ni, Y., Ma, Q., Ellis, G.S., Dai, J., Katz, B., Zhang, S., Tang, Y., 2011. Fundamental studies on kinetic isotope effect (KIE) of hydrogen isotope fractionation in natural gas systems. Geochimica et Cosmochimica Acta, 75, 2696- 2707.
Nöth, S., 1997. High H2S content and other effects of thermochemical sulfate reduction in deeply buried carbonate reservoirs: a review. Geologische Rundschau, 86, 275-287.
Oremland, R.S., Whiticar, M.J., Strohmaier, F.E., Kiene, R.P., 1988. Bacterial ethane formation from reduced, ethylated sulfur compounds in anoxic sediments. Geochimica et Cosmochimica Acta, 52, 1895-1904.
Orr, W.L., 1974. Changes in sulfur content and isotopic ratios of sulfur during petroleum maturation-study of Big Horn Paleozoic oils. AAPG Bulletin, 58, 2295-2318.
Orr, W.L., 1977. Geologic and geochemical controls on the distribution of hydrogen sulfide in natural gas. In Campo, R., Goni., J. (eds.). Advances in Organic Geochemistry 1975. Enadimsa, Madrid.
Ortega. G.S., Pecheyran, C, Berail, S., Donard, O.F.X., 2012. A fit-for purpose procedure for lead isotopic ratio determination in crude oil, asphaltene and kerogen samples by MC-ICPMS. Journal of Analytical Atomic Spectrometry, 27, 1447-1456.
Otto, A., Walther, H. & Püttmann, W. 1997. Sesqui- and diterpenoid biomarkers in Taxodium-rich Oligocene oxbow lake clays, Weisselster basin, Germany. Organic Geochemistry, 26, 105–115.
Özgen Karacan, C., Larsen, J.W., Esterle, J,S., 2009. CO2 Sequestration in Coals and Enhanced Coalbed Methane Recovery. International Journal of Coal Geology, 77, 1.
Palmer, S.E., 1993. Effect of biodegradation and water washing on crude oil composition. In Engel, M.H., Macko, S.A. (eds.). Organic Geochemistry. Plenum Press, New York.
Pennington, J.T., Chavez, F.P., 2000. Seasonal fluctuations of temperature, salinity, nitrate, chlorophyll and primary production at station H3/M1 over 1989-1996 in Monterey Bay, California. Deep-Sea Research II, 47, 947-973.
Peters, K.E., 1986. Guidelines for evaluating petroleum source rocks using programmed pyrolysis. AAPG Bulletin, 70, 318-329.
Peters, K.E., Cassa, M.R., 1994. Applied source rock geochemistry. in: Magoon, L.B., Dow, W.G. (eds.). The Petroleum System - from Source to Trap. AAPG Memoir 60, 93-120.
Peters, K.E., Walters, C.C., Moldowan, J.M., 2005. The Biomarker Guide – Second edition. Cambridge University Press, Cambridge.

Picha, F.J., Zdenek, S., Oldrich, K., 2006. Geology and hydrocarbon resources of the Outer Western Carpathians and their foreland, Czech Republic. in: Golonka, J., Picha, F.J. (eds.). The Carpathians and their foreland: Geology and hydrocarbon resources. AAPG Memoir 84, 49 – 175.

Piller, W.E., Egger, H., Erhart, C.W., Gross, M., Harzhauser, M., Hubmann, B., van Husen, D., Krenmayer, H.-G., Krystyn, L., Lein, R., Lukeneder, A., Mandl, G.W., Rögl, F., Roetzel, R., Rupp, C., Schnabel, W., Schönlaub, H.P., Summesberger, H., Wagreich, M., Wessely, G., 2004. Die stratigraphischer Tabelle von Österreich 2004.

Piller, W.E., Harzhauser, M., 2005. The myth of the brackish Sarmatian Sea. Terra Nova, 17, 450-455.

Piper, D.Z., Calvert, S.E., 2009. A marine biogeochemical perspective on black shale deposition. Earth Science Reviews, 95, 63-96.

Pois, A., 1933. Zur Geschichte der Erdöl- und Erdgasfunde in Österreich. Petroleum, 29, 1-13.

Popv, S.V., Rögl, F., Rozanov, A.Y., Steininger, F.F., Shcherba, I.G., Kovac, M., 2004. Lithological-Paleogeographic maps of the Paratethys, E. Schweizerbart´sche Verlagsbuchhandlung (Nägele u. Obermiller), Stuttgart. 19-30.

Potsch, K., Ramberger, R., Glantschnig, J., Baumgarthuber, S., Gößnitzer, F., 2004. Gas Injection Pilot in the Hochleiten Field. SPE/DOE Symposium on Improved Oil Recovery, 17-21.04.2004. Tulsa.

Radke, J, Bechtel, A., Gaupp, R., Püttmann, W., Schwark, L., Sachse, D., Gleixner, G., 2005. Correlation between hydrogen isotope ratios of lipid biomarkers and sediment maturity. Geochimica et Cosmochimica Acta, 69, 5517–5530.

Radke, M., Welte, D.H., 1983. The methylphenanthrene index (MPI): a maturity parameter based on aromatic hydrocarbons. in: Bjoroy, M. (ed.). Advances in Organic Geochemistry, Wiley, Chichester, 504-512.

Radke, M., Willsch, H., Welte, D.H., 1980. Preparative hydrocarbon group type determination by automated medium pressure liquid chromatography. Anal. Chem., 52, 406–411.

Rammel, M., 1989. Zur Kenntnis der Flyschzone im Untergrund des Wiener Beckens. Die Glaukonitsandsteinserie. Unpublished PhD Thesis, Universität Wien

Ricard, E., Pécheyran, C., Sanabria Ortega, G., Prinzhofer, A., Donard, O.X., 2011. Direct analysis of trace elements in crude oils by high-repetition-rate femtosecond laser ablation coupled to ICPMS detection. Analytical and Bioanalytical Chemistry 399, 2153-2165.

Roetzl, R., Krenmayer, H.G., 2002. Exkursion in die Niederösterreichische Molassezone südlich der Donau. Molassetreffen 2002, Verlag der Geologischen Bundesanstalt, Wien.

Rooney, M.A., Selby, D., Lewan, M.D., Lillis, P.G., Houzay, J.P., 2012. Re-Os geochronology and fingerprinting of United Kingdom Atlantic margin oil: Temporal implications for regional petroleum systems. Geochimica et Cosmochimica Acta, 77, 275-291.

Rosenfeld, L.K., Schwing, F.B., Garfield, N., Tracy, D.E., 1994. Bifurcated flow from an upwelling center: a cold water source for Monterey Bay. Continental Shelf Research, 14, 931-964.

Roth, P. H., Thierstein, H. 1972. Calcareous nannoplankton, Leg 14 of the Deep Sea Drilling Project. in: Hayes, D.E., Pimm, A.C. & al. (eds.), Initial Reports of the Deep Sea Drilling Project, Washington, 14, 421-485.

Ruttner, A.W., 1963. Das Fenster von Urmannsau und seine tektonische Stellung. Verhandlung der Geologischen Bundesanstalt, 1/2, 6-16.
Rybacki, E., Reinicke, A., Meier, T., Makasi, M., Dresen, G., 2014. What controls the strenght and brittleness of shale rocks? Geophysical Research Abstracts, 16, EGU 2014-1877.
Sachsenhofer, R.F., Bechtel, A., Kuffner, T., Rainer, T., Gratzer, R., Sauer, R., Sperl, H., 2006. Depositional environment and source potential of Jurassic coal-bearing sediments (Gresten Formation, Höflein gas/condensate field, Austria). Petroleum Geoscience, 2006, 99-114.
Sánchez-Román, M., Rivadeneyra, M.A., McKenzie, J.A., 2007. Carbonate and phosphate precipitation by halophilic bacteria: influence of Ca2+ and Mg2+ ions. FEMS Microbiology Ecology, 61, 273-284.
Sánchez-Román, M., McKenzie, J.A., de Luca Rebello Wagener, A., Rivadeneyra, M.A., Vasconcelos, C., 2009. Presence of sulfate does not inhibit low-temperature dolomite precipitation. Earth and Planetary Science Letters, 285, 131-139.
Sassen, R., 1988. Geochemical and carbon isotopic studies of crude oil destruction, bitumen precipitation, and sulfate reduction in the deep Smackover formation. Organic Geochemistry, 12, 351-361.
Schicker, A., 2011. Clay mineralogy and diagenesis of Malmian marlstones. Vienna Basin, unpublished PhD Thesis, University of Vienna.
Schimmelmann, A., Boudou, J-P., Lewan, M.D., Wintsch, R.P., 2001. Experimental controls on D/H and 13C/12C ratios of kerogen, bitumen and oil during hydrous pyrolysis. Organic Geochemistry, 32, 1009-1018.
Schimmelmann, A., Sessions, A.L, Boreham, C.J., Edwards, D.S., Logan, G.A., Summons, R.E., 2004. D/H ratios in terrestrially sourced petroleum systems. Organic Geochemistry, 35, 1169-1195.
Schneider, N., Di Lorenzo, E., Niiler, P.P., 2005. Salinity Variations in the Southern California Current. Journal of physical oceanography, 35, 1421-1436.
Schulz, H.-M., Horsfield, B., Sachsenhofer, R.F., 2010. Shale gas in Europe: a regional overview and current research activities. In: Vining, B.A., Pickering, S.C. (eds.). Petroleum Geology: from Mature Basins to New Frontiers-Proceedings of the 7th Petroleum Geology Conference. Geological Society, London, 1079-1085.
Schultz, L.G., 1964. Quantitative interpretation of mineralogical composition from X-ray and chemical data for the Pierre Shale. Geol. Surv. Prof. Pap. 391-C, 31.
Schoell, M., 1984. Wasserstoff- und Kohlenstoffisotope organischer Substanzen, Erdölen und Erdgasen. Geologisches Jahrbuch Reihe D, 67, 136-140.
Seifert, P., 1996. Sedimentary-tectonic development and Austrian hydrocarbon potential of the Vienna Basin. in: Wessely, G., Liebl, W. (eds.). Oil and gas in Alpidic thrustbelt and basins of Central and Eastern Europe. EAGE Special Pub., 5. Geological Society, London, 331-341.
Selby, D., Creaser, R.A., 2005. Direct Radiometric Dating of Hydrocarbon Deposits Using Rhenium-Osmium Isotopes. Science, 308, 1293-1295.
Selby, D., Creaser, R.A., Fowler; M.A., 2007. Re–Os elemental and isotopic systematics in crude oils. Geochimicha et Cosmochimica Acta, 71, 378-386.
Sieskind, O., Joly, G., Albrecht, P., 1979. Simulation of the geochemical transformations of sterols: superacid effect of clay minerals. Geochimica et Cosmochimica Acta, 43, 1675–1679.
Sinninghe Damsté, J.S., Keely, B.J., Betts, S.E., Baas, M., Maxwell, J.R., de Leeuw, J.W., 1993. Variations in abundances and distributions of isoprenoid chromans

and long-chain alkylbenzenes in sediments of the Mulhouse Basin: a molecular sedimentary record of palaeosalinity. Organic Geochemistry, 20, 1201–1215.
Sinninghe Damsté, J.S., Kenig, F., Koopmans, M.P., et al., 1995. Evidence for gammacerane as an indicator of water-colum stratification. Geochimica et Cosmochimica Acta, 59, 1895-1890.
Shi, J.Y., Mackenzie, A.S., Alexander, R., 1982. A biological marker investgation of petroleums and shales from Shengli oilfield, the People´s Republic of China. Chemical Geology, 35, 1-31.
Silverman, S.R., 1965. Migration and segregation of oil and gas. In: Young, A.; Galley, G.E. (eds.). Fluids in Subsurface Environments. Vol. 4 , AAPG, Tulsa, OK.
Simonite, B.R.T., 1986. Cyclic terpenoids of the geospere. In: Johns, R.B. (ed.). Biological Markers in the Sedimentary Record, Elsevier, NY., 43-99.
Sofer, V., 1984. Stable carbon isotope composition of crude oil, application to source depositional environment and petroleum alteration. AAPG Bulletin, 68, 31-49.
Sommer, D., 1993. Zur Geschichte des Kohlenwasserstoffbergbaues in Österreich. In Brix, F., Schultz, O. (eds.). 1993. Erdöl und Erdgas in Österreich, Verlag des NHM, Wien und F. Berger, Horn. 387-395.
Steininger, F.F., Wessely, G., Rögl, F., Wagner, L., 1986. Tertiary sedimentary history and tectonic evolution of the eastern Alpine foredeep. Giornale Geol., 3; 48, 285-297.
Sundararaman, P., Biggs, W.R., Reynolds, J.G., Fetzer, J.C., 1988. Vanadylporphyrins, indicators of kerogen breakdown and generation of petroleum. Geochimica et Cosmochimica Acta; 52, 2337-2341
Sundararaman, P., Moldowan, J.M., Seifert, W.K., 1988. Incorporation of petroporphyrines into biomarker correlation problems. In: Yen, T.F., Moldowan, J.M. (eds.). Geochemical Biomarkers, Harwood Academic Publishers. New York.
Sundararaman, P., Hwang, R.J., 1993. Effect of biodegadation on vanadylporphyrin distribution. Geochimica et Casmochimiva Acta, 57, 2283-2290.
Symington, W.A., Olgaard, D.L., Otten, G.A., Phillips, T.C., Thomas, M.M., Yeakel, J.D., 2010. ExxonMobil´s Electrofrac Process for On Situ Oil Shale Conversion. AAPG Annual Convention, San Antonio.
Tang, Y., Huang, Y., Ellis, G.S., Wang, Y., Kralert, P.G., Gillaizeau, B., Ma, Q., Hwang, R., 2005. A kinetic model for thermally induced hydrogen and carbon isotope fractionation of individual n-alkanes in crude oil. Geochimica et Cosmochimica Acta, 69, 4505-4520.
Tari, G., Ciudin, D., Kostner, A., Raileanu, A., Tulucan, A., Vacarescu, G., Vangelov, D., 2011. Play types of the Moesian Platform of Romania and Bulgaria. AAPG Search and Discovery #10311.
Taylor, G.H., Teichmüller, M., Davis, A., Diessel, C.F.K., Littke, R., Robert, P., 1998. Organic Petrology, Gebrüder Borntraeger, Berlin, 704.
Terken, J.M.J., Frewin, N.L., 2000. The Dhahaban petroleum system of Oman. AAPG Bulletin, 84, 523–544.
Thompson, K.F.M., 1987. Fractionated aromatic petroleums and the generation of gas-condensate. Organic Geochemistry, 11, 573-90.
Thompson, K.F.M., 1988. Gas-condensate migration and oil fractionation in deltaic systems. Marine and Petroleum Geology, 5, 237-246.
Thompson, K.F.M., Kennicutt, M.C. II, 1990. Nature and frequenzy of occurrence of non-thermal alteration processes in offshore Gulf of Mexico petroleums. in: Schumacher, D.; Perkins, B.F. (eds.). Gulf Coast Oils and Gases, Society of Economic Paleontologists and Mineralogists, Tulsa, OK.

Tissot, B.P., Welte, D.H., 1984. Petroleum Formation and Occurence. Springer Verlag, New York, NY.
Truche, L., Bazarkina, E.F., Barre, G., Thomassot, E., Berger, G., Dubessy, J., Robert, P., 2014. The role of S3- ion in thermochemical sulphate reduction: Geological and geochemical implications. Earth and Planetary Science Letters, 396, 190-200.
Uffmann, A.K., Littke, R., Rippen, D., 2012. Mineralogy and geochemistry of Mississippian and Lower Pennsylvanian Black Shales at the Northern Margin of the Varsican Mountain Belt (Germany and Belgium). International Journal of Coal Geology, 103, 92-108.
Vairavamurthy, M.A., Schoonen, M.A.A., 1995. Geochemical transformation of sedimentary sulphur. Washington DC., ACS Symposium Series, 612, 16-37.
Venkatesan, M.I., 1988. Occurrence and possible sources of perylene in marine sediments-a review. Marine Chemistry, 25, 1-27.
Volkman, J.K., 1986. A review of sterol markers for marine and terrigenous organic matter. Organic Geochemistry, 9, 83-99.
Waagen, L., 1931. Der neue Oelaufschluss von Kierling bei Wien. Internationale Zeitschrift für Bohrtechnik, Erdölbergbau und Geologie, 39, 89-91.
Wagner, L., Wessely, G., 1992. Molassezone Österreichs – Relief und Tektonik des Untergrundes. Beilage 5. in: Brix, F., Schultz, O. (Eds.), Erdöl und Erdgas in Österreich, Verlag des Naturhistorischen Museums, Wien und F. Berger, Horn.
Walkner, C.; Gratzer, R.; Meisel, T.; Bokhari, S.N.H., 2016: Multi-element analysis of crude oils using ICP-QQQ-MS. Organic Geochemistry, 103, 22-30.
Wenger, L.M., Isaksen, G.H., 2002. Control of hydrocarbobn seepage intensity on level of biodegradation in sea bottom sediments. Organic Geochemistry; 33, 1277-1292.
Wessely, G., 1992. The Calcareous Alps below the Vienna Basin in Austria and their structural and facial development in the Alpine-Carpathian border Zone. Geologica Carpatica, 43, 347-353.
Wessely, G., 1993. Der Untergrund des Wiener Beckens. in: Brix, F. and Schultz, O. (eds.), Erdöl und Erdgas in Österreich. Verlag des NHM Wien und F.Berger, Horn.
Wessely, G., Gohs, G., 1993. Geologischer Schnitt Pirawarth-Matzen-Gänserndorf. In Brix, F., Schultz, O. (eds.). Erdöl und Erdgas in Österreich. Verlag des NHM Wien und F.Berger, Horn.
Wessely, G., 2006. Niederösterreich. Verlag der Geologischen Bundesanstalt, Wien.
Wessely, G., Kröll, A., Jiricek, R, Nemec, F., 1993. Wiener Becken und angrenzende Gebiete – Geologische Einheiten des präneogenen Beckenuntergrundes, Geologische Karte herausgegeben von der Geologischen Bundesanstalt, Wien.
Wessely, G., Gohs, G., 1993. Geologischer Schnitt Pirawarth-Matzen-Gänserndorf. In Brix, F., Schultz, O. (eds.). Erdöl und Erdgas in Österreich. Verlag des NHM Wien und F.Berger, Horn.
Wessely, G., 2000. Sedimente des Wiener Beckens und seiner alpinen und subalpinen Unterlagerung (The Vienna Basin and its alpine and subalpine basement). Mitt. Ges. Geol. Bergbaustud. Österr., Vol. 44, P. 191-214.
Whiticar, M.J. Suess, E., 1990. Hydrothermal hydrocarbon gases in the sediments of the King George Basin, Bransfield Strait, Antarctica. Applied Geochemistry, 5, 135-147.
Wilhelms, A., Larter, S.R., Head, I., 2001. Biodegradation of oil in uplift basins prevented by deep-burial sterilization. Nature, 411, 1034-1037.

Willsch, H.; Clegg, H., Horsfield, B., Radke, M., Wilkes; 1997: Liquid chromatographic separation of sediment, rock, and coal extracts and crude oil into compound classes, Analytical Chemistry 69 (1997) 4203-4209

Worden, R.H., Smalley, P.C., 1996. H2S producing reactions in deep carbonate gas reservoirs: Khuff Formation, Abu Dhabi. Chemical Geology, 133, 157-171.

Worden, R.H., Smalley, P.C., Oxtoby, N.H., 1995. Gas Souring by Thermochemical Sulfate Reduction at 140°C. AAPG Bulletin, 79, 6, 854-863.

Yamane, A., Sakakibara, K., Hosomi, M., Murakami, A., 1997. Microbial degradation of petroleum hydrocarbons in estuarine sediment of Tama River in Tokyo urban area. Water Science and Technology, 35, 69-76.

Yoneyama, Y., Okamura, M., Morinaga, K., Tsubaki, N., 2002. Role of Water in Hydrogenation of Coal without Catalyst Assition. Energy Fuels 16, 48-53.

13 Appendices

Appendix I

Sample overview

Rock Samples

Well	Depth [m]	Stratigraphic Unit	XRD	Thin Section	Nanno Plankton	Bulk Data	Rock Eval	Py-GC	Organic Petrol.	Vitrinite Reflect.	Trace Metals	Bio-marker	NSO	Kerogen	Isotopy Extract	Comp.
Aderklaa UT 1a	6076.5	Mikulov Fm.				x	x									
Altenmarkt 1	2439.5	Lower ShMb.				x	x									
Altenmarkt 1	2457	Lower ShMb.				x	x									
Altenmarkt 1	2459.3	Lower ShMb.				x	x									
Altenmarkt 1	2459.8	Lower ShMb.				x	x									
Altenmarkt 1	2460.2	Lower ShMb.				x	x									
Altenmarkt 1	2460.9	Lower ShMb.				x	x									
Altenmarkt 1	2461.3	Lower ShMb.				x	x									
Altenmarkt 1	2461.8	Lower ShMb.				x	x									
Altenmarkt 1	2538.6	Lower ShMb.				x	x									
Altenmarkt 1	2540.3	Lower ShMb.				x	x									
Altenmarkt 1	2541.9	Lower ShMb.				x	x									
Altenmarkt 1	2542.3	Lower ShMb.				x	x									
Altenmarkt 1	2558.4	Lower ShMb.				x	x									
Altenmarkt 1	2558.6	Lower ShMb.				x	x									
Altenmarkt 1	2638.9	Lower ShMb.				x	x									
Altenmarkt 1	2639	Lower ShMb.				x	x									
Altenmarkt 1	2640.5	Lower ShMb.				x	x					x				
Altenmarkt 1	2641.6	Lower ShMb.				x	x					x			x	
Ameis 1	3043.2	Mikulov Fm.				x	x									
Ameis 1	3045.7	Mikulov Fm.				x	x									
Ameis 1	3113.8	Mikulov Fm.				x	x									
Ameis 1	3115.2	Mikulov Fm.				x	x									
Ameis 1	3167	Mikulov Fm.				x	x									
Ameis 1	3170	Mikulov Fm.				x	x									
Falkenstein 1	3378.7	Mikulov Fm.				x	x	x				x			x	
Falkenstein 1	3380.9	Mikulov Fm.				x	x									
Falkenstein 1	3510	Mikulov Fm.				x	x									
Falkenstein 1	3516	Mikulov Fm.				x	x					x	x		x	
Falkenstein 1	3748.4	Mikulov Fm.				x	x					x			x	
Falkenstein 1	3751.8	Mikulov Fm.				x	x									
Falkenstein 1	3952.5	Mikulov Fm.		x		x	x									
Falkenstein 1	3957.8	Mikulov Fm.		x		x	x									
Falkenstein 1	4147.8	Flknstn. Fm.				x	x									
Falkenstein 1	4150.4	Flknstn. Fm.				x	x					x	x	x	x	
Falkenstein 1	4494.8	Lower ShMb.				x	x									
Falkenstein 1	4495.5	Lower ShMb.				x	x					x			x	
Falkenstein 1	4496.8	Lower ShMb.				x	x									
Falkenstein 1	4498.3	Lower ShMb.				x	x					x			x	

Well	Depth [m]	Stratigraphic Unit	XRD	Thin Section	Nanno Plankton	Bulk Data	Rock Eval	Py-GC	Organic Petrol.	Vitrinite Reflect.	Trace Metals	Bio-marker	NSO	Kerogen	Isotopy Extract	Comp.
Falkenstein 1	4499.5	Lower ShMb.				x	x									
Falkenstein 1	4499.7	Lower ShMb.				x	x									
Fallbach 1	1797.4	Mikulov Fm.				x	x									
Hagenberg 3	3032	Lower ShMb.				x	x									
Hagenberg 3	3032.3	Lower ShMb.				x	x									
Hagenberg 3	3032.8	Lower ShMb.				x	x									
Hagenberg 3	3033.6	Lower ShMb.				x	x									
Hagenberg 3	3034.2	Lower ShMb.				x	x									
Hagenberg 3	3034.8	Lower ShMb.				x	x									
Hagenberg 3	3035.6	Lower ShMb.				x	x									
Hagenberg 3	3036.3	Lower ShMb.				x	x									
Hagenberg 3	3036.7	Lower ShMb.				x	x									
Hoeflein 1	2849.2	Lower ShMb.				x	x									
Hoeflein 1	2849.8	Lower ShMb.				x	x									
Hoeflein 1	2850.7	Lower ShMb.				x	x									
Hoeflein 1	2851.5	Lower ShMb.				x	x									
Hoeflein 1	2852.2	Lower ShMb.				x	x									
Hoeflein 1	2852.8	Lower ShMb.				x	x									
Hoeflein 1	2853.2	Lower ShMb.				x	x									
Hoeflein 1	2853.5	Lower ShMb.				x	x									
Hoeflein 1	2854.2	Lower ShMb.				x	x									
Hoeflein 1	2854.7	Lower ShMb.				x	x									
Hoeflein 7a	2761.5	Mikulov Fm.				x	x	x				x			x	
Hoeflein 7a	2762.2	Mikulov Fm.				x	x					x			x	
Klement 1	2366	Mikulov Fm.				x	x									
Klement 1	2368.3	Mikulov Fm.				x	x									
Klement 1	2760.9	Flknstn. Fm.				x	x									
Klement 1	2764	Flknstn. Fm.				x	x									
Klement 1	3057.9	Flknstn. Fm.				x	x									
Klement 1	3059.2	Flknstn. Fm.				x	x									
Klement 1	3735.5	Lower ShMb.				x	x									
Klement 1	3736.3	Lower ShMb.				x	x									
Klement 1	3736.7	Lower ShMb.				x	x									
Klement 1	3737.2	Lower ShMb.				x	x									
Klement 1	3737.7	Lower ShMb.				x	x									
Klement 1	3738.5	Lower ShMb.				x	x									
Klement 1	3739.1	Lower ShMb.				x	x									
Klement 1	3739.8	Lower ShMb.				x	x									
Korneuburg T1	3253.6	Mikulov Fm.				x	x									
Korneuburg T1	3266.5	Mikulov Fm.				x	x									
Maustrenk ÜT 1a	6546.7	Mikulov Fm.				x	x					x	x		x	x

Well	Depth [m]	Stratigraphic Unit	XRD	Thin Section	Nanno Plankton	Bulk Data	Rock Eval	Py-GC	Organic Petrol.	Vitrinite Reflect.	Trace Metals	Bio-marker	NSO	Kerogen	Isotopy Extract	Comp.
Maustrenk ÜT 1a	6548.8	Mikulov Fm.				x	x			x		x	x		x	x
Merkersdorf 2	1896.8	Mikulov Fm.				x	x									
Porrau 2	1522	Lower ShMb.				x	x		x	x						
Porrau 2	1554	Lower ShMb.				x	x									
Porrau 2	1591.7	Lower QaMb.				x	x									
Porrau 2	1592.2	Lower QaMb.				x	x									
Porrau 2	1592.7	Lower QaMb.				x	x									
Porrau 2	1592.9	Lower QaMb.				x	x									
Porrau 2	1624.8	Lower QaMb.				x	x			x						
Porrau 2	2086.2	Lower QaMb.				x	x			x						
Porrau 2	2120.9	Lower ShMb.				x	x		x	x						
Porrau 2	2166.8	Lower ShMb.				x	x					x			x	
Porrau 2	2167.5	Lower ShMb.				x	x									
Porrau 2	2168.5	Lower ShMb.				x	x									
Porrau 2	2169.1	Lower ShMb.				x	x									
Porrau 2	2170.1	Lower ShMb.				x	x									
Porrau 2	2170.8	Lower ShMb.				x	x									
Porrau 2	2197.5	Lower ShMb.				x	x									
Porrau 2	2198.2	Lower ShMb.				x	x									
Porrau 2	2199.8	Lower ShMb.				x	x									
Porrau 2	2200.8	Lower ShMb.				x	x		x	x						
Porrau 2	2201.5	Lower ShMb.				x	x									
Porrau 2	2233.4	Lower ShMb.				x	x									
Porrau 2	2234.1	Lower ShMb.				x	x									
Porrau 2	2235.1	Lower ShMb.				x	x									
Porrau 2	2235.7	Lower ShMb.				x	x									
Porrau 2	2236.7	Lower ShMb.				x	x									
Porrau 2	2237.4	Lower ShMb.				x	x									
Porrau 2	2267.3	Lower ShMb.				x	x									
Porrau 2	2268	Lower ShMb.				x	x									
Porrau 2	2269	Lower ShMb.				x	x									
Porrau 2	2269.6	Lower ShMb.				x	x									
Porrau 2	2270.6	Lower ShMb.				x	x									
Porrau 2	2271.3	Lower ShMb.				x	x									
Porrau 2	2329	Lower ShMb.				x	x	x	x	x						
Porrau 2	2329.7	Lower ShMb.				x	x									
Porrau 2	2330.7	Lower ShMb.				x	x									
Porrau 2	2331.3	Lower ShMb.				x	x									
Porrau 2	2332.3	Lower ShMb.				x	x									
Porrau 2	2333	Lower ShMb.				x	x									
Porrau 2	2373.2	Lower QaMb.				x	x									

Well	Depth [m]	Stratigraphic Unit	XRD	Thin Section	Nanno Plankton	Bulk Data	Rock Eval	Py-GC	Organic Petrol.	Vitrinite Reflect.	Trace Metals	Bio-marker	NSO	Kerogen	Isotopy Extract	Comp.
Porrau 2	2378	Lower QaMb.				x	x									
Porrau 2	2493	Lower QaMb.				x	x			x						
Porrau 2	2495	Lower QaMb.				x	x		x	x		x			x	
Porrau 2	2497	Lower QaMb.							x	x						
Porrau 2	2498	Lower QaMb.							x	x						
Roseldorf T1	1288.5	Mikulov Fm.				x	x									
Roseldorf Tief 2	2647.1	Lower ShMb.				x	x									
Roseldorf Tief 2	2647.4	Lower ShMb.				x	x									
Roseldorf Tief 2	2648.3	Lower ShMb.				x	x									
Roseldorf Tief 2	2648.9	Lower ShMb.				x	x									
Roseldorf Tief 2	2649.5	Lower ShMb.				x	x									
Roseldorf Tief 2	2650.2	Lower ShMb.				x	x									
Roseldorf Tief 2	2650.9	Lower ShMb.				x	x									
Roseldorf Tief 2	2651.6	Lower ShMb.				x	x									
Staatz 1	1968	Mikulov Fm.	x			x	x		x			x	x	x	x	
Staatz 1	1969.6	Mikulov Fm.				x	x									
Staatz 1	2022.7	Mikulov Fm.				x	x							x		
Staatz 1	2026.5	Mikulov Fm.	x	x	x	x	x					x		x	x	
Staatz 1	2045.5	Mikulov Fm.				x	x							x		
Staatz 1	2083	Mikulov Fm.	x			x	x		x			x		x	x	
Staatz 1	2109.3	Mikulov Fm.				x	x							x		
Staatz 1	2113.1	Mikulov Fm.	x	x		x	x		x			x		x	x	
Staatz 1	2140.5	Mikulov Fm.				x	x							x		
Staatz 1	2141.3	Mikulov Fm.		x		x	x					x		x	x	
Staatz 1	2176.3	Mikulov Fm.	x	x		x	x	x				x		x	x	
Staatz 1	2178	Mikulov Fm.				x	x		x			x		x	x	
Staatz 1	2211.2	Mikulov Fm.				x	x							x		
Staatz 1	2213.2	Mikulov Fm.	x	x	x	x	x					x			x	
Staatz 1	2250.5	Mikulov Fm.				x	x							x		
Staatz 1	2251.5	Mikulov Fm.	x	x		x	x		x			x		x	x	
Staatz 1	2281.8	Mikulov Fm.				x	x									
Staatz 1	2284.5	Mikulov Fm.	x	x	x	x	x		x			x		x	x	
Staatz 1	2322.5	Mikulov Fm.				x	x					x		x	x	
Staatz 1	2324.5	Mikulov Fm.	x	x		x	x	x	x			x			x	
Staatz 1	2356.5	Mikulov Fm.				x	x									
Staatz 1	2359.5	Mikulov Fm.				x	x							x		
Staatz 1	2410.5	Mikulov Fm.				x	x							x		
Staatz 1	2414.5	Mikulov Fm.	x			x	x		x			x	x		x	
Staatz 1	2467.8	Mikulov Fm.				x	x							x		
Staatz 1	2469.5	Mikulov Fm.		x	x	x	x	x	x			x	x		x	
Staatz 1	2522.5	Mikulov Fm.				x	x							x		

Well	Depth [m]	Stratigraphic Unit	XRD	Thin Section	Nanno Plankton	Bulk Data	Rock Eval	Py-GC	Organic Petrol.	Vitrinite Reflect.	Trace Metals	Bio-marker	NSO	Kerogen	Isotopy Extract	Comp.
Staatz 1	2524.5	Mikulov Fm.	x	x		x	x		x			x		x	x	
Staatz 1	2574.5	Mikulov Fm.				x	x							x		
Staatz 1	2575.5	Mikulov Fm.	x	x		x	x		x			x		x	x	
Staatz 1	2576.5	Mikulov Fm.				x	x									
Staatz 1	2630.5	Mikulov Fm.	x	x		x	x					x	x		x	
Staatz 1	2634.5	Mikulov Fm.				x	x		x			x			x	
Staatz 1	2682.5	Mikulov Fm.	x	x		x	x					x	x	x	x	
Staatz 1	2685.5	Mikulov Fm.				x	x					x		x	x	
Staatz 1	2740.5	Mikulov Fm.	x	x		x	x	x						x		
Staatz 1	2743.5	Mikulov Fm.			x	x	x		x			x		x	x	
Staatz 1	2770.2	Mikulov Fm.	x	x		x	x					x	x	x	x	
Staatz 1	2773.5	Mikulov Fm.	x	x		x	x					x	x	x	x	
Staatz 1	2774.5	Mikulov Fm.				x	x		x			x		x	x	
Staatz 1	2822.5	Mikulov Fm.				x	x							x		
Staatz 1	2825.7	Mikulov Fm.	x	x	x	x	x	x	x		x	x		x	x	
Staatz 1	2872.5	Flknstn. Fm.	x	x		x	x									
Staatz 1	2881.7	Flknstn. Fm.	x	x		x	x									
Staatz 1	2936	Flknstn. Fm.	x	x		x	x		x					x		
Staatz 1	2938.2	Flknstn. Fm.			x	x	x							x		
Staatz 1	2940	Flknstn. Fm.				x	x									
Staatz 1	2993.8	Flknstn. Fm.	x	x		x	x							x		
Staatz 1	2996.5	Flknstn. Fm.	x	x	x	x	x		x			x	x		x	
Staatz 1	3096.6	Flknstn. Fm.	x	x		x	x							x		
Staatz 1	3098.5	Flknstn. Fm.				x	x	x	x			x		x	x	
Staatz 1	3213	Flknstn. Fm.				x	x									
Staatz 1	3365	Lower ShMb.				x	x									
Stockerau Ost 1	3760	Upper QaMb.				x	x									
Stockerau Ost 1	3770	Upper QaMb.				x	x									
Stockerau Ost 1	3780	Upper QaMb.				x	x									
Stockerau Ost 1	3829	Upper QaMb.				x	x									
Stockerau Ost 1	3830	Upper QaMb.				x	x									
Stockerau Ost 1	3832	Upper QaMb.				x	x									
Stockerau Ost 1	3840	Upper QaMb.				x	x									
Stockerau Ost 1	3850	Upper QaMb.				x	x									
Stockerau Ost 1	3930	Upper QaMb.				x	x									
Stockerau Ost 1	3970	Upper QaMb.				x	x									
Stockerau Ost 1	3980	Upper QaMb.				x	x									
Stockerau Ost 1	3990	Upper QaMb.				x	x									
Stockerau Ost 1	4010	Upper QaMb.				x	x									
Stockerau Ost 1	4050	Upper QaMb.				x	x									
Stockerau Ost 1	4070	Upper QaMb.				x	x									

Well	Depth [m]	Stratigraphic Unit	XRD	Thin Section	Nanno Plankton	Bulk Data	Rock Eval	Py-GC	Organic Petrol.	Vitrinite Reflect.	Trace Metals	Bio-marker	NSO	Kerogen	Isotopy Extract	Comp.
Stockerau Ost 1	4090	Upper QaMb.				x	x									
Stockerau Ost 1	4110	Upper QaMb.				x	x									
Stockerau Ost 1	4160	Upper QaMb.				x	x									
Stockerau Ost 1	4200	Upper QaMb.				x	x									
Stockerau Ost 1	4207	Upper QaMb.				x	x									
Stockerau Ost 1	4209	Upper QaMb.				x	x									
Stockerau Ost 1	4211	Upper QaMb.				x	x			x						
Stronegg 1	2011.5	Mikulov Fm.				x	x									
Stronegg 1	2013.7	Mikulov Fm.				x	x									
Stronegg 1	2101.6	Flknstn. Fm.				x	x									
Stronegg 1	2107.5	Flknstn. Fm.				x	x									
Thomasl 1	2302.6	Mikulov Fm.				x	x					x			x	
Thomasl 1	2304	Mikulov Fm.				x	x	x				x			x	
Thomasl 1	3006.7	Mikulov Fm.				x	x					x			x	
Thomasl 1	3007.7	Mikulov Fm.				x	x									
Waschberg 1	2536.1	Flknstn. Fm.				x	x					x			x	
Waschberg 1	2538.8	Flknstn. Fm.				x	x					x			x	
Wildendürnbach K4	2083.7	Flknstn. Fm.				x	x									
Wildendürnbach K4	2158.6	Flknstn. Fm.				x	x									
Wildendürnbach T1	1447.5	Mikulov Fm.				x	x	x								
Zistersdorf ÜT 1	5602.7	Mikulov Fm.				x	x			x	x	x	x		x	
Zistersdorf ÜT 1	5605.5	Mikulov Fm.				x	x					x			x	x
Zistersdorf ÜT 1	5670.5	Mikulov Fm.	x			x	x			x		x			x	
Zistersdorf ÜT 1	5674.6	Mikulov Fm.				x	x									
Zistersdorf ÜT 1	5737.3	Mikulov Fm.				x	x									
Zistersdorf ÜT 1	5740.7	Mikulov Fm.				x	x					x				
Zistersdorf ÜT 1	5977.3	Mikulov Fm.				x	x			x		x			x	x
Zistersdorf ÜT 1	5983.7	Mikulov Fm.				x	x									
Zistersdorf ÜT 2a	5586	Mikulov Fm.				x	x									
Zistersdorf ÜT 2a	5587	Mikulov Fm.	x			x	x					x			x	
Zistersdorf ÜT 2a	7704	Mikulov Fm.	x			x	x			x						
Zistersdorf ÜT 2a	8153	Mikulov Fm.				x	x			x						
Zistersdorf ÜT 2a	8544	Mikulov Fm.	x			x	x			x						

Hydrocarbon Samples

Well	Depth [m ss]	Reservoir Age	Type	Trace Metals	GC-FID	Bio-marker	NSO	Isotopy Extract	Isotopy Comp.	S
Aderklaa 3	2351	Karpatian	O		x	x		x		
Aderklaa 4	2515	Karpatian	O		x	x		x		
Aderklaa 34	1715	Badenian	O		x	x	x	x	x	
Aderklaa 98	2408	Karpatian	G						x	
Baumgarten 1	830	Karpatian	G						x	
Bockfliess 1	1177.38	Badenian	O+G	x	x	x		x	x	
Bockfliess 24	1436.21	Badenian	O+G		x	x		x	x	
Bockfliess 33	1181.24	Badenian	O+G		x	x	x	x	x	
Bockfliess 35	1460.64	Badenian	O+G		x	x		x	x	
Bockfliess 37	1463.4	Badenian	O+G		x	x		x	x	
Bockfliess 43	1428.71	Badenian	O+G		x	x		x	x	
Bockfliess 205	1627	Badenian	O+G		x	x		x	x	
Breitenlee 15	990	Sarmatian	G						x	
Breitenlee 17	1217	Badenian	G						x	
Ebenthal 5	1614.4	Badenian	O	x	x	x	x	x	x	
Ebenthal 15	1636	Badenian	O	x	x	x		x	x	
Ebenthal 17a	1614	Badenian	O		x	x		x	x	
Ebenthal 20	1614.4	Badenian	O		x	x		x	x	
Ebenthal Tief 1	3300	Norian	G						x	
Erdpress 4	1787.51	Badenian	O+G	x	x	x	x	x	x	
Erdpress 17a	1424.18	Sarmatian	O+G	x	x	x		x	x	
Erdpress 24	1419.12	Sarmatian	O+G		x	x		x	x	
Fischamend 6	278	Sarmatian	G						x	
Gbely 2			O		x	x		x		
Gbely H6			O		x	x	x	x		
Ginzersdorf 4	776	Ottnangian	G						x	
Hauskirchen 86	910	Flysch	G						x	
Hirschstetten 7a	1875	Badenian	G						x	
Hochleiten 15	737.58	Sarmatian	O+G	x	x	x		x	x	
Hochleiten 24	748.74	Sarmatian	O+G	x	x	x	x	x	x	
Hochleiten 31	982	Flysch	O	x	x	x	x	x		
Hochleiten 60	759.31	Sarmatian	O+G	x	x	x		x	x	
Hochleiten 65	851.09	Sarmatian	O+G		x	x		x	x	
Hochleiten 66	911.32	Badenian	O+G		x	x		x	x	
Hochleiten 67	786.44	Sarmatian	O+G		x	x		x	x	
Hodonin 1			O		x	x	x	x		
Hodonin 3			O		x	x		x		
Hodonin 4			O		x	x		x		
Hoeflein 1	2605.37	Höflein Fm.	G		x				x	
Hoeflein 4	2618.1	Höflein Fm.	G		x				x	
Hoeflein 6	2614.04	Höflein Fm.	O+G		x	x		x	x	
Hoeflein 6	2663	Höflein Fm.	O		x	x		x		
Hoeflein 8	2629.55	Höflein Fm.	G		x				x	
Hoeflein 9	2633.63	Höflein Fm.	O+G		x	x	x	x	x	
Hoeflein 9	2685	Höflein Fm.	O		x	x		x		
Hoeflein 10	2613.33	Höflein Fm.	G		x				x	
Hoeflein 12	2670.29	Höflein Fm.	O+G		x	x		x	x	
Hohenruppersdorf 42	1412.35	Sarmatian	O+G	x	x	x	x	x	x	
Holic 4			O		x	x	x	x	x	
Kierling 1		Flysch	O		x	x	x	x		
Kierling 2		Flysch	O		x	x		x	x	
Klement 1	3539	LQAM	O		x	x		x	x	
Lanzhot 15			O		x	x		x	x	
Lanzhot 30			O		x	x	x	x	x	
Matzen 91	1464	Badenian	O		x	x		x	x	
Matzen 115	1472	Badenian	G		x	x	x	x	x	
Matzen 116	1449	Badenian	G		x	x		x	x	
Matzen 286	1467	Badenian	O+G		x	x		x	x	
Matzen 322	1458	Badenian	O+G		x	x		x	x	

Well	Depth [m ss]	Reservoir Age	Type	Trace Metals	GC-FID	Bio-marker	NSO	Isotopy Extract	Isotopy Comp.	S
Matzen 390	1139.7	Badenian	O	x	x	x	x	x	x	
Matzen H 703b	1523	Badenian	O+G		x	x		x	x	
Maustrenk 29	900	Ottnangian	O		x	x	x	x	x	
Moosbrunn Ost 1	820	Sarmatian	G						x	
Moosbrunn West 1	950	Sarmatian	G						x	
Mühlberg 15	1480	Badenian	O		x	x	x	x		
Neusiedl 1	1180	Flysch	O		x	x		x		
Neusiedl 3	1100	Flysch	O		x	x	x	x		
Niedersulz 12	1281	Sarmatian	G						x	
Oberweiden West 1	647	Sarmatian	G						x	
Orth 2	708	Sarmatian	G						x	
Pirawarth U10	707	Flysch	O		x	x	x	x		
Prottes 26	1140.44	Badenian	O	x	x	x		x		
Prottes 27	1150	Badenian	O+G		x	x	x	x	x	
Prottes 29	1152	Badenian	O+G		x	x		x	x	
Prottes 98	1157.63	Badenian	O		x	x	x	x		
Prottes 104	1156.78	Badenian	O		x	x		x		
Prottes T S 3b	2653	Norian	O		x	x	x	x	x	
Rabensburg 11	1742	Badenian	O		x	x	x	x	x	
Rabensburg 12	964.78	Sarmatian	G						x	
Rabensburg 13	1733.35	Bad.+Sarm.	G						x	
Rabensburg 14	1097.04	Sarmatian	G						x	
Rabensburg N3	1718	Badenian	O		x	x		x	x	
Rabensburg U4		Sarmatian	O		x	x		x	x	
Rabensburg West 4	1062	Sarmatian	G		x	x		x	x	
Roseldorf 2	1383	Ottnangian	O		x	x	x	x		
Roseldorf 2	1383	Ottnangian	O		x	x		x		
Roseldorf 4	532	Ottnangian	G						x	
Roseldorf 6	760	Ottnangian	G						x	
Roseldorf 20	380	Ottnangian	G						x	
Roseldorf Tief 2	500	Ottnangian	G						x	
Sankt Ulrich 65	875	Flysch	O+G		x	x	x	x	x	
Sankt Ulrich 92	1050	Flysch	O+G	x	x	x		x	x	
Sankt Ulrich 213	812	Flysch	O+G		x	x		x	x	
Schoenkirchen 267	1260	Badenian	O		x	x	x	x		
Schoenkirchen T12	2709.73	Ottnangian	O		x	x	x	x	x	
Schoenkirchen T29a	2725.54	Ottnangian	O	x	x	x	x	x	x	
Schoenkirchen T32	4873.01	Upper Cret.	O+G		x	x		x	x	x
Schoenkirchen T38	2726	Ottnangian	O	x	x	x	x	x	x	
Schoenkirchen T38a	2809	Hierlatz Fm.	G						x	
Schoenkirchen T42	5386.79	Upper Cret.	O+G		x	x		x	x	x
Schoenkirchen T62	5119.25	Upper Cret.	O+G	x	x	x		x	x	x
Schoenkirchen T64	2542	Trias	O+G		x	x		x	x	
Schoenkirchen T69	2815	Ottnangian	O		x	x		x	x	
Schoenkirchen T90a	2590	Trias	O+G		x	x		x	x	
Steinberg 11	950	Flysch	O		x	x		x	x	
Steinberg 21	960	Flysch	G				x		x	
Stockerau Ost 7	1980	Egerian	G						x	
Stockerau Ost 13	1792	Egerian	G		x				x	
Stockerau Ost 16	2101	Egerian	O+G		x	x		x	x	
Van Sickle 29	750	Sarmatian	O+G		x	x	x	x	x	
Wildendürnbach 5	540	Ottnangian	G						x	
Wildendürnbach 10	550	Ottnangian	G						x	
Wildendürnbach 16	560	Ottnangian	G						x	
Wind. Baumgarten 1	700	Flysch	O		x	x	x	x	x	
Wind. Baumgarten 1	700	Flysch	O		x	x		x		

Appendix II
Bulk data

n.d. not detected

n.c. not calculated

Well	Depth	Stratigraphic	TOC	S	Calc.equ.	S_1	S_2	HI	T_{max}
	[m]	Unit	[wt.%]	[wt.%]	[wt.%]		[mgHC/gRock]	[mgHC/gTOC]	[°C]
Aderklaa UT 1a	6076.5	Mikulov Fm.	1.25	0.51	39.74	0.37	0.66	52	447
Altenmarkt 1	2439.5	Lower ShMb.	1.31	1.04	2.85	n.m.	n.m.	n.c.	n.m.
Altenmarkt 1	2457	Lower ShMb.	1.46	0.70	1.80	0.02	0.92	63	432
Altenmarkt 1	2459.3	Lower ShMb.	1.58	1.62	0.80	0.02	0.96	61	427
Altenmarkt 1	2459.8	Lower ShMb.	1.22	1.00	1.10	0.02	0.99	81	430
Altenmarkt 1	2460.2	Lower ShMb.	1.01	1.01	0.31	0.01	0.51	50	427
Altenmarkt 1	2460.9	Lower ShMb.	1.12	0.66	0.26	0.01	0.72	64	432
Altenmarkt 1	2461.3	Lower ShMb.	1.46	0.90	0.36	0.02	0.90	62	430
Altenmarkt 1	2461.8	Lower ShMb.	1.44	1.04	0.73	0.03	1.22	85	429
Altenmarkt 1	2538.6	Lower ShMb.	1.43	0.82	4.79	0.02	1.13	79	432
Altenmarkt 1	2540.3	Lower ShMb.	1.35	0.98	2.26	0.02	1.24	91	432
Altenmarkt 1	2541.9	Lower ShMb.	1.08	1.32	1.84	0.02	0.65	60	428
Altenmarkt 1	2542.3	Lower ShMb.	1.25	1.73	1.36	0.02	1.03	82	429
Altenmarkt 1	2558.4	Lower ShMb.	1.31	0.62	1.09	0.02	0.93	71	432
Altenmarkt 1	2558.6	Lower ShMb.	1.50	0.70	2.21	0.02	0.98	65	432
Altenmarkt 1	2638.9	Lower ShMb.	2.31	1.60	0.91	0.05	2.90	125	431
Altenmarkt 1	2639	Lower ShMb.	1.98	1.15	2.82	0.03	1.77	89	430
Altenmarkt 1	2640.5	Lower ShMb.	1.97	1.74	4.30	0.03	1.59	81	430
Altenmarkt 1	2641.6	Lower ShMb.	2.03	2.28	6.17	0.03	1.23	60	431
Ameis 1	3043.2	Mikulov Fm.	1.24	0.41	44.83	0.06	2.59	208	435
Ameis 1	3045.7	Mikulov Fm.	1.37	0.44	46.09	0.13	3.79	277	434
Ameis 1	3113.8	Mikulov Fm.	1.51	0.46	51.96	0.24	3.74	247	433
Ameis 1	3115.2	Mikulov Fm.	1.57	0.40	39.84	0.15	3.94	251	434
Ameis 1	3167	Mikulov Fm.	1.27	0.50	37.69	0.12	2.83	223	436
Ameis 1	3170	Mikulov Fm.	1.85	0.48	33.87	0.20	4.36	236	434
Falkenstein 1	3378.7	Mikulov Fm.	1.83	0.39	40.82	0.09	3.20	175	433
Falkenstein 1	3380.9	Mikulov Fm.	0.94	0.22	62.91	0.21	2.23	237	434
Falkenstein 1	3510	Mikulov Fm.	0.85	0.27	58.60	0.16	1.99	233	434
Falkenstein 1	3516	Mikulov Fm.	1.10	0.55	54.28	0.13	2.92	265	433
Falkenstein 1	3748.4	Mikulov Fm.	1.04	0.28	56.87	0.11	2.64	252	435
Falkenstein 1	3751.8	Mikulov Fm.	1.05	0.30	55.57	0.16	2.36	225	435
Falkenstein 1	3952.5	Mikulov Fm.	0.96	0.30	59.10	0.14	2.20	228	434
Falkenstein 1	4147.8	Flknstn. Fm.	1.06	0.13	68.48	0.25	3.55	334	437
Falkenstein 1	4150.4	Flknstn. Fm.	1.28	0.52	54.02	0.26	4.32	336	436
Falkenstein 1	4494.8	Lower ShMb.	1.44	1.06	1.44	0.12	2.10	146	439
Falkenstein 1	4495.5	Lower ShMb.	2.00	0.87	0.44	0.16	1.96	98	436
Falkenstein 1	4496.8	Lower ShMb.	1.42	1.60	0.45	0.14	1.72	121	437
Falkenstein 1	4498.3	Lower ShMb.	2.14	2.02	0.40	0.18	2.75	128	437
Falkenstein 1	4499.5	Lower ShMb.	1.69	2.00	1.38	0.11	1.48	87	438
Falkenstein 1	4499.7	Lower ShMb.	1.61	1.34	1.35	0.10	1.87	116	439
Fallbach 1	1797.4	Mikulov Fm.	0.60	0.36	59.31	0.10	1.18	196	431
Hagenberg 3	3032	Lower ShMb.	1.26	1.63	3.09	0.05	1.39	110	433
Hagenberg 3	3032.3	Lower ShMb.	1.67	2.19	4.49	0.07	1.44	86	432
Hagenberg 3	3032.8	Lower ShMb.	1.51	1.54	6.35	0.05	1.18	78	432
Hagenberg 3	3033.6	Lower ShMb.	1.37	1.53	4.14	0.09	1.06	77	433
Hagenberg 3	3034.2	Lower ShMb.	1.27	1.84	4.25	0.04	1.03	81	432
Hagenberg 3	3034.8	Lower ShMb.	1.63	2.17	6.94	0.07	1.47	90	433
Hagenberg 3	3035.6	Lower ShMb.	1.80	2.37	3.28	0.05	1.20	67	433
Hagenberg 3	3036.3	Lower ShMb.	1.71	2.44	2.69	0.04	1.39	81	435
Hagenberg 3	3036.7	Lower ShMb.	1.72	2.47	5.96	0.05	1.36	79	433
Hoeflein 1	2849.2	Lower ShMb.	1.02	1.90	0.00	0.01	0.40	39	425
Hoeflein 1	2849.8	Lower ShMb.	0.89	2.85	0.00	0.01	0.45	50	424
Hoeflein 1	2850.7	Lower ShMb.	1.23	2.02	0.00	0.01	0.65	52	428
Hoeflein 1	2851.5	Lower ShMb.	1.42	1.99	0.00	0.01	0.54	38	426
Hoeflein 1	2852.2	Lower ShMb.	1.56	2.20	0.00	0.02	0.79	51	430
Hoeflein 1	2852.8	Lower ShMb.	1.68	2.09	0.00	0.02	0.65	38	428
Hoeflein 1	2853.2	Lower ShMb.	1.76	2.30	0.00	0.01	0.70	40	428
Hoeflein 1	2853.5	Lower ShMb.	1.59	1.78	0.00	0.02	0.71	45	428
Hoeflein 1	2854.2	Lower ShMb.	1.73	2.39	0.00	0.02	0.86	50	429
Hoeflein 1	2854.7	Lower ShMb.	2.02	1.59	0.00	0.01	0.83	41	432
Hoeflein 7a	2761.5	Mikulov Fm.	1.49	0.60	50.92	0.07	5.94	399	426

Well	Depth	Stratigraphic	TOC	S	Calc.equ.	S_1	S_2	HI	T_{max}
	[m]	Unit	[wt.%]	[wt.%]	[wt.%]		[mgHC/gRock]	[mgHC/gTOC]	[°C]
Hoeflein 7a	2762.2	Mikulov Fm.	1.36	0.46	50.79	0.07	4.38	322	430
Klement 1	2366	Mikulov Fm.	0.45	0.18	66.12	0.05	0.54	119	432
Klement 1	2368.3	Mikulov Fm.	1.05	0.43	50.86	0.05	1.69	161	432
Klement 1	2764	Flknstn. Fm.	0.81	0.25	59.97	0.08	1.46	179	432
Klement 1	3059.2	Flknstn. Fm.	0.50	0.35	62.78	0.02	0.95	191	432
Klement 1	3735.5	Lower ShMb.	1.33	0.58	0.94	0.06	1.26	94	437
Klement 1	3736.3	Lower ShMb.	1.34	1.31	4.42	0.05	1.34	100	436
Klement 1	3736.7	Lower ShMb.	1.34	1.16	5.23	0.06	1.60	119	437
Klement 1	3737.2	Lower ShMb.	1.26	0.97	5.29	0.05	1.37	109	436
Klement 1	3737.7	Lower ShMb.	1.21	0.50	4.56	0.05	1.40	116	437
Klement 1	3738.5	Lower ShMb.	1.22	0.74	6.42	0.05	1.34	109	436
Klement 1	3739.1	Lower ShMb.	1.16	0.65	8.34	0.06	1.69	145	436
Klement 1	3739.8	Lower ShMb.	1.39	1.56	3.23	0.09	1.89	136	436
Korneuburg T1	3253.6	Mikulov Fm.	1.41	0.26	53.44	0.02	1.94	137	431
Korneuburg T1	3266.5	Mikulov Fm.	1.68	0.29	48.72	0.03	1.99	118	432
Maustrenk ÜT 1a	6546.7	Mikulov Fm.	1.58	0.19	45.39	0.53	0.54	34	455
Maustrenk ÜT 1a	6548.8	Mikulov Fm.	1.21	0.29	42.46	0.46	0.69	57	454
Merkersdorf 2	1896.8	Mikulov Fm.	0.95	0.51	49.75	0.06	1.52	161	433
Porrau 2	1522	Lower ShMb.	1.78	2.70	3.93	0.05	1.04	58	433
Porrau 2	1554	Lower ShMb.	1.69	1.59	6.44	0.07	1.13	67	430
Porrau 2	1591.7	Lower QaMb.	1.65	1.33	10.80	0.08	1.21	73	430
Porrau 2	1592.2	Lower QaMb.	12.17	0.83	0.00	0.32	8.89	73	422
Porrau 2	1592.7	Lower QaMb.	26.54	2.32	0.00	0.59	27.91	105	417
Porrau 2	1592.9	Lower QaMb.	7.58	0.61	0.00	0.13	7.08	93	424
Porrau 2	1624.8	Lower QaMb.	5.62	0.68	0.75	0.25	6.78	120	420
Porrau 2	2086.2	Lower QaMb.	11.47	0.86	0.32	0.74	14.14	123	422
Porrau 2	2166.8	Lower ShMb.	1.99	1.62	1.06	0.02	0.68	34	426
Porrau 2	2167.5	Lower ShMb.	2.39	1.12	3.20	0.04	0.88	37	431
Porrau 2	2168.5	Lower ShMb.	2.41	1.14	0.58	0.02	0.64	26	426
Porrau 2	2169.1	Lower ShMb.	2.00	1.48	0.85	0.03	0.69	35	426
Porrau 2	2170.1	Lower ShMb.	1.68	1.41	3.19	0.04	0.99	59	431
Porrau 2	2170.8	Lower ShMb.	2.39	n.m.	n.c	0.03	0.85	36	426
Porrau 2	2197.5	Lower ShMb.	1.70	1.74	2.04	0.07	1.34	79	431
Porrau 2	2198.2	Lower ShMb.	1.60	1.91	1.67	0.03	1.07	67	432
Porrau 2	2199.8	Lower ShMb.	1.67	1.68	1.67	0.03	1.22	73	432
Porrau 2	2200.8	Lower ShMb.	1.66	2.05	3.02	0.03	1.18	71	430
Porrau 2	2201.5	Lower ShMb.	1.64	1.72	2.20	0.03	1.02	62	431
Porrau 2	2233.4	Lower ShMb.	1.52	0.88	8.20	0.05	1.02	67	429
Porrau 2	2234.1	Lower ShMb.	1.50	1.10	8.70	0.03	0.88	58	430
Porrau 2	2235.1	Lower ShMb.	1.66	1.08	15.60	0.03	0.81	49	429
Porrau 2	2235.7	Lower ShMb.	2.36	1.17	6.63	0.04	0.78	33	431
Porrau 2	2236.7	Lower ShMb.	1.55	1.58	4.17	0.02	0.96	62	432
Porrau 2	2237.4	Lower ShMb.	1.42	2.15	5.15	0.03	0.88	61	430
Porrau 2	2267.3	Lower ShMb.	1.68	1.43	1.87	0.03	1.21	72	432
Porrau 2	2268	Lower ShMb.	1.72	1.42	3.90	0.03	1.33	77	430
Porrau 2	2269	Lower ShMb.	1.63	1.03	1.49	n.m.	n.m.	n.c.	n.m.
Porrau 2	2269.6	Lower ShMb.	1.65	1.39	1.04	0.03	1.27	77	431
Porrau 2	2270.6	Lower ShMb.	1.61	1.26	1.06	0.02	1.08	67	431
Porrau 2	2271.3	Lower ShMb.	1.94	1.62	3.02	0.03	1.48	76	431
Porrau 2	2329	Lower ShMb.	2.15	1.12	2.14	0.03	1.22	56	431
Porrau 2	2329.7	Lower ShMb.	2.23	1.52	0.20	0.03	1.26	57	426
Porrau 2	2330.7	Lower ShMb.	2.27	1.15	0.26	0.02	0.77	34	425
Porrau 2	2331.3	Lower ShMb.	2.49	1.43	0.00	0.03	1.20	48	426
Porrau 2	2332.3	Lower ShMb.	2.26	1.20	0.60	0.04	1.55	68	430
Porrau 2	2333	Lower ShMb.	2.12	1.25	0.65	0.04	1.60	76	429
Porrau 2	2373.2	Lower QaMb.	4.65	0.65	0.70	0.04	0.96	21	434
Porrau 2	2378	Lower QaMb.	2.81	0.38	2.54	0.02	0.70	25	434
Porrau 2	2495	Lower QaMb.	21.60	0.97	8.52	0.70	31.94	148	422
Roseldorf T1	1288.5	Mikulov Fm.	1.34	0.32	43.47	0.03	2.55	190	433
Roseldorf Tief 2	2647.1	Lower ShMb.	0.79	0.41	1.87	0.01	0.31	39	430
Roseldorf Tief 2	2647.4	Lower ShMb.	0.98	0.41	2.71	0.01	0.38	39	432

Well	Depth	Stratigraphic	TOC	S	Calc.equ.	S_1	S_2	HI	T_{max}
	[m]	Unit	[wt.%]	[wt.%]	[wt.%]		[mgHC/gRock]	[mgHC/gTOC]	[°C]
Roseldorf Tief 2	2648.3	Lower ShMb.	1.14	0.51	2.55	0.01	0.40	35	431
Roseldorf Tief 2	2648.9	Lower ShMb.	1.93	0.22	24.36	0.00	0.27	14	429
Roseldorf Tief 2	2649.5	Lower ShMb.	0.89	0.35	2.54	0.01	0.31	35	431
Roseldorf Tief 2	2650.2	Lower ShMb.	0.83	0.67	3.39	0.01	0.31	38	428
Roseldorf Tief 2	2650.9	Lower ShMb.	0.77	0.29	3.88	0.01	0.29	38	431
Roseldorf Tief 2	2651.6	Lower ShMb.	0.52	0.57	9.69	0.01	0.16	30	427
Staatz 1	1968	Mikulov Fm.	0.73	0.42	39.42	0.05	1.37	187	430
Staatz 1	2022.7	Mikulov Fm.	0.81	0.31	40.95	0.10	1.47	181	429
Staatz 1	2026.5	Mikulov Fm.	1.05	0.35	63.91	0.12	2.68	256	430
Staatz 1	2045.5	Mikulov Fm.	0.56	0.28	62.96	0.07	0.86	152	433
Staatz 1	2083	Mikulov Fm.	0.81	0.25	41.21	0.09	1.52	188	433
Staatz 1	2109.3	Mikulov Fm.	0.65	0.49	52.45	0.05	1.03	158	434
Staatz 1	2113.1	Mikulov Fm.	1.08	0.49	50.53	0.07	2.08	193	433
Staatz 1	2140.5	Mikulov Fm.	0.88	0.25	62.62	0.07	2.59	295	432
Staatz 1	2141.3	Mikulov Fm.	0.99	0.52	56.50	0.16	2.90	292	432
Staatz 1	2176.3	Mikulov Fm.	1.60	0.42	47.13	0.12	4.65	290	432
Staatz 1	2178	Mikulov Fm.	1.03	0.80	50.69	0.12	2.28	221	434
Staatz 1	2211.2	Mikulov Fm.	0.88	0.43	46.38	0.05	1.94	220	434
Staatz 1	2213.2	Mikulov Fm.	0.88	0.46	46.06	0.08	1.78	202	434
Staatz 1	2250.5	Mikulov Fm.	0.89	0.43	57.75	0.20	2.71	304	430
Staatz 1	2251.5	Mikulov Fm.	1.63	0.55	42.74	0.32	7.69	473	424
Staatz 1	2281.8	Mikulov Fm.	1.07	0.65	53.01	0.09	2.95	275	433
Staatz 1	2284.5	Mikulov Fm.	1.39	0.69	51.09	0.11	3.90	281	431
Staatz 1	2322.5	Mikulov Fm.	1.27	0.32	50.39	0.13	3.27	258	434
Staatz 1	2324.5	Mikulov Fm.	2.11	0.44	45.65	0.10	2.49	118	433
Staatz 1	2359.5	Mikulov Fm.	1.13	0.36	49.70	0.08	2.28	201	434
Staatz 1	2414.5	Mikulov Fm.	1.34	0.31	46.02	0.09	3.25	243	434
Staatz 1	2467.8	Mikulov Fm.	1.11	0.54	51.31	0.08	2.43	218	433
Staatz 1	2469.5	Mikulov Fm.	1.74	0.55	47.12	0.19	5.16	297	429
Staatz 1	2522.5	Mikulov Fm.	1.34	0.40	49.55	0.16	3.16	236	434
Staatz 1	2524.5	Mikulov Fm.	1.30	0.38	50.50	0.10	3.00	230	434
Staatz 1	2574.5	Mikulov Fm.	1.12	0.37	54.23	0.12	2.32	207	433
Staatz 1	2575.5	Mikulov Fm.	1.05	0.35	53.41	0.07	2.26	215	432
Staatz 1	2630.5	Mikulov Fm.	1.56	0.42	52.48	0.19	4.27	273	432
Staatz 1	2634.5	Mikulov Fm.	1.23	0.34	54.75	0.06	2.25	183	434
Staatz 1	2682.5	Mikulov Fm.	0.94	0.36	23.90	0.03	1.60	170	431
Staatz 1	2685.5	Mikulov Fm.	0.67	0.47	1.05	0.01	0.42	62	432
Staatz 1	2740.5	Mikulov Fm.	2.54	0.49	49.12	0.17	3.69	145	430
Staatz 1	2743.5	Mikulov Fm.	1.39	0.51	57.06	0.18	4.23	304	431
Staatz 1	2770.2	Mikulov Fm.	1.25	0.76	58.84	0.13	3.95	315	429
Staatz 1	2773.5	Mikulov Fm.	1.25	0.52	60.15	0.12	3.67	294	430
Staatz 1	2774.5	Mikulov Fm.	1.63	0.64	58.72	0.11	3.35	205	430
Staatz 1	2822.5	Mikulov Fm.	1.10	0.43	59.47	0.09	3.04	275	430
Staatz 1	2825.7	Mikulov Fm.	2.06	0.86	48.23	0.10	3.25	158	428
Staatz 1	2872.5	Flknstn. Fm.	0.01	n.m.	100.00	n.m.	n.m.	n.c.	n.m.
Staatz 1	2881.7	Flknstn. Fm.	0.33	n.m.	99.00	n.m.	n.m.	n.c.	n.m.
Staatz 1	2936	Flknstn. Fm.	0.73	0.09	74.71	0.03	1.95	267	433
Staatz 1	2938.2	Flknstn. Fm.	0.52	1.07	73.95	0.02	0.42	81	422
Staatz 1	2940	Flknstn. Fm.	0.53	0.12	83.27	0.05	0.90	169	435
Staatz 1	2993.8	Flknstn. Fm.	0.80	0.15	71.48	0.05	2.44	305	433
Staatz 1	2996.5	Flknstn. Fm.	1.88	0.40	52.71	0.06	4.10	218	431
Staatz 1	3096.6	Flknstn. Fm.	0.40	0.16	71.37	0.01	0.66	163	433
Staatz 1	3098.5	Flknstn. Fm.	2.22	0.26	56.60	0.01	0.75	34	433
Staatz 1	3365	Lower ShMb.	1.62	1.82	2.43	0.05	1.41	87	437
Stockerau Ost 1	3760	Upper QaMb.	1.11	1.33	1.48	0.03	0.66	60	430
Stockerau Ost 1	3770	Upper QaMb.	1.06	0.99	1.58	0.03	0.68	64	430
Stockerau Ost 1	3780	Upper QaMb.	1.22	1.00	3.61	0.03	0.69	56	433
Stockerau Ost 1	3829	Upper QaMb.	1.53	1.74	5.70	0.06	1.45	95	433
Stockerau Ost 1	3830	Upper QaMb.	1.37	1.26	4.54	0.06	1.43	105	434
Stockerau Ost 1	3832	Upper QaMb.	1.34	2.35	6.37	0.05	1.22	90	436
Stockerau Ost 1	3840	Upper QaMb.	1.37	1.38	7.79	0.04	0.88	64	433

Well	Depth [m]	Stratigraphic Unit	TOC [wt.%]	S [wt.%]	Calc.equ. [wt.%]	S_1 [mgHC/gRock]	S_2 [mgHC/gRock]	HI [mgHC/gTOC]	T_{max} [°C]
Stockerau Ost 1	3850	Upper QaMb.	1.18	1.32	6.96	0.05	0.76	65	431
Stockerau Ost 1	3930	Upper QaMb.	1.68	1.26	4.27	0.05	1.11	66	433
Stockerau Ost 1	3970	Upper QaMb.	1.40	1.03	8.92	0.04	0.82	58	433
Stockerau Ost 1	3980	Upper QaMb.	1.45	1.34	4.65	0.04	0.82	57	434
Stockerau Ost 1	3990	Upper QaMb.	1.50	1.34	4.91	0.05	0.94	62	434
Stockerau Ost 1	4010	Upper QaMb.	2.30	1.87	4.18	0.09	1.75	76	429
Stockerau Ost 1	4050	Upper QaMb.	1.45	1.65	4.54	0.05	0.97	66	433
Stockerau Ost 1	4070	Upper QaMb.	1.55	1.97	2.51	0.05	1.20	77	433
Stockerau Ost 1	4090	Upper QaMb.	2.07	2.64	6.37	0.05	1.19	58	435
Stockerau Ost 1	4110	Upper QaMb.	1.75	1.62	5.34	0.06	1.25	71	435
Stockerau Ost 1	4160	Upper QaMb.	2.33	1.39	10.30	0.12	1.74	74	434
Stockerau Ost 1	4200	Upper QaMb.	2.43	1.85	10.04	0.17	2.05	84	431
Stockerau Ost 1	4207	Upper QaMb.	2.51	1.57	5.52	0.11	1.56	62	432
Stockerau Ost 1	4209	Upper QaMb.	2.60	2.02	13.59	0.23	3.96	153	431
Stockerau Ost 1	4211	Upper QaMb.	79.57	1.59	10.56	5.36	147.39	185	435
Stronegg 1	2011.5	Mikulov Fm.	0.97	0.20	68.78	0.04	2.59	266	430
Stronegg 1	2013.7	Mikulov Fm.	1.05	0.18	72.67	0.05	2.61	249	429
Stronegg 1	2101.6	Flknstn. Fm.	0.62	0.16	77.08	0.04	0.68	110	429
Stronegg 1	2107.5	Flknstn. Fm.	3.67	0.06	64.97	0.01	0.07	2	429
Thomasl 1	2302.6	Mikulov Fm.	1.85	0.31	36.82	0.08	4.61	249	432
Thomasl 1	2304	Mikulov Fm.	2.11	0.63	31.00	0.17	6.21	295	432
Thomasl 1	3006.7	Mikulov Fm.	1.02	0.46	52.44	0.11	2.14	211	433
Thomasl 1	3007.7	Mikulov Fm.	0.90	0.43	55.29	0.10	1.88	208	434
Waschberg 1	2536.1	Flknstn. Fm.	1.45	0.50	59.35	0.05	5.84	402	427
Waschberg 1	2538.8	Flknstn. Fm.	1.35	0.39	59.55	0.05	5.03	372	428
Wildendürnbach K4	2083.7	Flknstn. Fm.	1.88	0.56	42.93	0.13	6.32	336	427
Wildendürnbach K4	2158.6	Flknstn. Fm.	1.45	0.48	56.76	0.06	4.50	311	429
Wildendürnbach T1	1447.5	Mikulov Fm.	1.52	0.61	53.48	0.06	4.12	271	431
Zistersdorf ÜT 1	5602.7	Mikulov Fm.	2.77	0.84	30.04	2.42	4.33	156	448
Zistersdorf ÜT 1	5605.5	Mikulov Fm.	1.18	0.49	65.35	0.94	1.50	126	449
Zistersdorf ÜT 1	5670.5	Mikulov Fm.	2.66	0.55	33.94	1.93	3.41	128	452
Zistersdorf ÜT 1	5674.6	Mikulov Fm.	2.80	0.50	n.m.	2.03	4.16	149	451
Zistersdorf ÜT 1	5737.3	Mikulov Fm.	1.93	0.06	43.19	1.64	2.74	142	454
Zistersdorf ÜT 1	5740.7	Mikulov Fm.	1.76	0.24	46.62	1.88	2.49	141	453
Zistersdorf ÜT 1	5977.3	Mikulov Fm.	3.05	0.53	30.07	2.59	3.54	116	456
Zistersdorf ÜT 1	5983.7	Mikulov Fm.	3.33	0.79	35.28	1.11	2.85	85	461
Zistersdorf ÜT 2a	5586	Mikulov Fm.	2.04	0.22	43.34	2.67	3.45	169	450
Zistersdorf ÜT 2a	5587	Mikulov Fm.	2.16	1.14	48.36	2.40	2.90	134	446
Zistersdorf ÜT 2a	7704	Mikulov Fm.	2.73	0.63	30.25	n.m.	n.m.	n.c.	n.m.
Zistersdorf ÜT 2a	8153	Mikulov Fm.	0.72	0.35	55.42	n.m.	n.m.	n.c.	n.m.
Zistersdorf ÜT 2a	8544	Mikulov Fm.	0.74	0.44	57.59	n.m.	n.m.	n.c.	n.m.

Appendix III

Organic petrology

Vitrinite reflectance

Well	Depth [m]	Stratigraphic Unit	Liptinite [Vol.%]	Vitrinite [Vol.%]	Inertinite [Vol.%]	Rr [%]	Std. Dev. [-]	n [-]
Maustrenk ÜT 1a	6548.8	Mikulov Fm.	n.m.	n.m.	n.m.	1.73	0.17	30
Porrau 2	1522	Lower ShMb.	31.5	29.3	39.1	0.60	0.03	29
Porrau 2	1624.8	Lower QaMb.	n.m.	n.m.	n.m.	0.66	0.03	31
Porrau 2	2086.2	Lower QaMb.	n.m.	n.m.	n.m.	0.73	0.03	31
Porrau 2	2120.9	Lower ShMb.	5.8	16.3	77.9	0.69	0.03	22
Porrau 2	2200.8	Lower ShMb.	17.6	20.6	61.8	1.28	0.11	31
Porrau 2	2329	Lower ShMb.	4.0	8.0	88.0	0.77	0.05	13
Porrau 2	2493	Lower QaMb.	n.m.	n.m.	n.m.	0.81	0.03	30
Porrau 2	2495	Lower QaMb.	1.4	72.1	26.4	0.82	0.02	30
Porrau 2	2498	Lower QaMb.	1.5	46.2	52.3	0.61	0.01	17
Staatz 1	1968	Mikulov Fm.	68.0	8.0	24.0	n.m.	n.m.	n.m.
Staatz 1	2083	Mikulov Fm.	76.0	4.0	20.0	n.m.	n.m.	n.m.
Staatz 1	2113.1	Mikulov Fm.	68.0	2.0	30.0	n.m.	n.m.	n.m.
Staatz 1	2178	Mikulov Fm.	72.0	12.0	16.0	n.m.	n.m.	n.m.
Staatz 1	2251.5	Mikulov Fm.	82.0	4.0	14.0	n.m.	n.m.	n.m.
Staatz 1	2284.5	Mikulov Fm.	66.0	10.0	24.0	n.m.	n.m.	n.m.
Staatz 1	2324.5	Mikulov Fm.	74.0	2.0	24.0	n.m.	n.m.	n.m.
Staatz 1	2414.5	Mikulov Fm.	74.2	3.1	22.7	n.m.	n.m.	n.m.
Staatz 1	2469.5	Mikulov Fm.	78.0	4.0	18.0	n.m.	n.m.	n.m.
Staatz 1	2524.5	Mikulov Fm.	73.3	4.4	22.2	n.m.	n.m.	n.m.
Staatz 1	2575.5	Mikulov Fm.	66.0	10.0	24.0	n.m.	n.m.	n.m.
Staatz 1	2634.5	Mikulov Fm.	65.7	5.7	28.6	n.m.	n.m.	n.m.
Staatz 1	2743.5	Mikulov Fm.	76.0	6.0	18.0	n.m.	n.m.	n.m.
Staatz 1	2774.5	Mikulov Fm.	74.0	4.0	22.0	n.m.	n.m.	n.m.
Staatz 1	2825.7	Mikulov Fm.	84.0	6.0	10.0	n.m.	n.m.	n.m.
Staatz 1	2936	Flknstn. Fm.	63.4	1.1	35.5	n.m.	n.m.	n.m.
Staatz 1	2996.5	Flknstn. Fm.	86.0	2.0	12.0	n.m.	n.m.	n.m.
Staatz 1	3098.5	Flknstn. Fm.	84.6	2.6	12.8	n.m.	n.m.	n.m.
Stockerau Ost 1	4211	Upper QaMb.	n.m.	n.m.	n.m.	0.67	0.02	42
Zistersdorf ÜT 1	5602.7	Mikulov Fm.	n.m.	n.m.	n.m.	1.46	0.17	30
Zistersdorf ÜT 1	5670.5	Mikulov Fm.	n.m.	n.m.	n.m.	1.47	0.20	19
Zistersdorf ÜT 1	5977.3	Mikulov Fm.	n.m.	n.m.	n.m.	1.56	0.13	30
Zistersdorf ÜT 2a	7704	Mikulov Fm.	n.m.	n.m.	n.m.	2.30	0.19	32
Zistersdorf ÜT 2a	8153	Mikulov Fm.	n.m.	n.m.	n.m.	2.43	0.14	30
Zistersdorf ÜT 2a	8544	Mikulov Fm.	n.m.	n.m.	n.m.	2.54	0.13	30

n.m.	not measurable

Appendix IV
XRD results

n.d. not detected

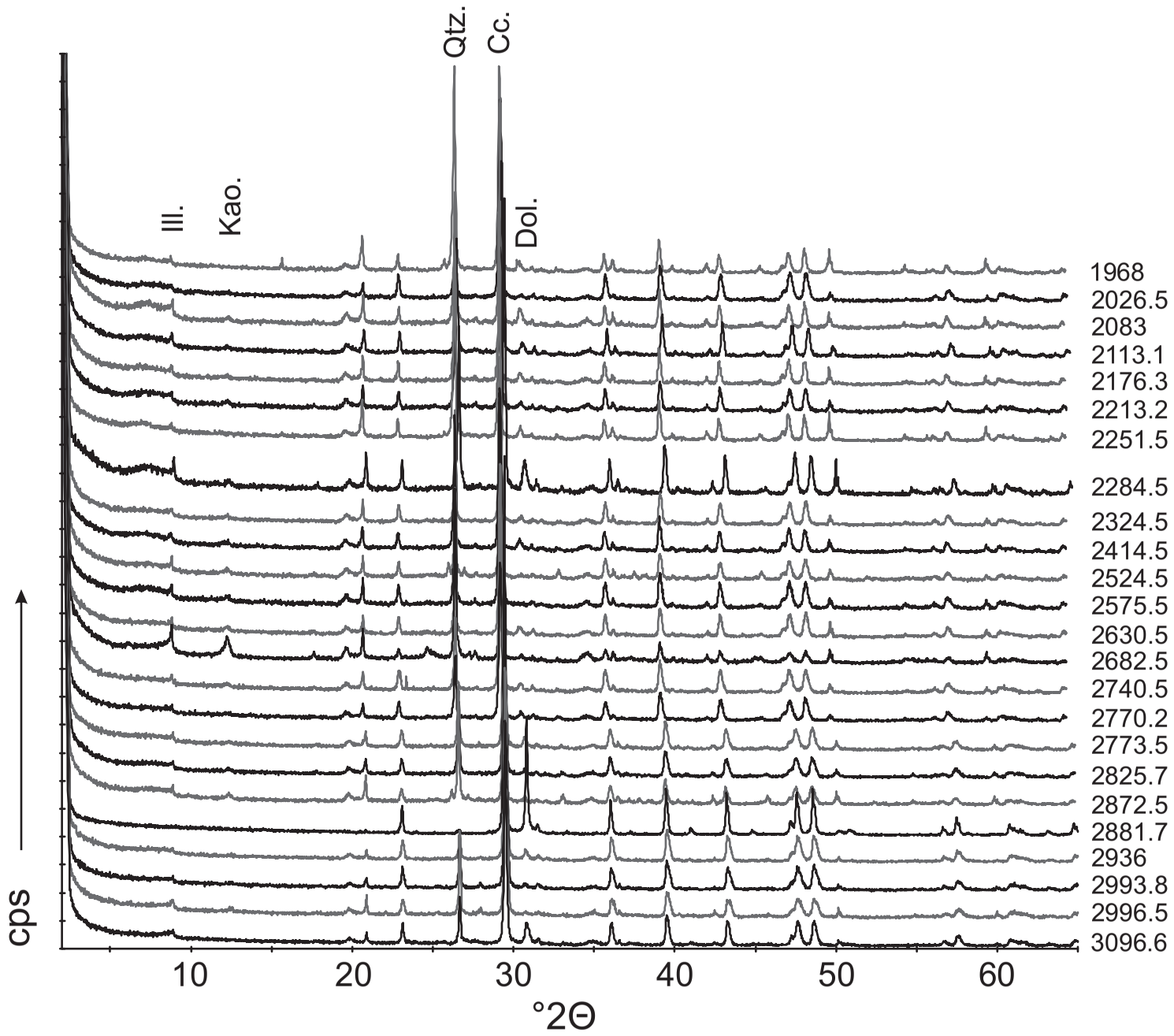
Qtz.
Cc.
Ill.
Kao.
Dol.
1968
2026.5
2083
2113.1
2176.3
2213.2
2251.5
2284.5
2324.5
2414.5
2524.5
2575.5
2630.5
2682.5
2740.5
2770.2
2773.5
2825.7
2872.5
2881.7
2936
2993.8
2996.5
3096.6
cps
10
20
30
40
50
60
°2Θ

Well	Depth [m]	Stratigraphic Unit	Quartz [%]	Calcite [%]	Dolomite [%]	Siderite [%]	Pyrite [%]	Clay min. [%]
Staatz 1	1968	Mikulov Fm.	22.42	46.11	n.d.	n.d.	1.07	30.40
Staatz 1	2026.5	Mikulov Fm.	11.78	66.38	n.d.	n.d.	1.07	20.78
Staatz 1	2083	Mikulov Fm.	12.92	43.87	n.d.	n.d.	1.30	41.91
Staatz 1	2113.1	Mikulov Fm.	16.84	58.66	n.d.	n.d.	1.45	23.05
Staatz 1	2176.3	Mikulov Fm.	16.42	49.98	n.d.	n.d.	1.08	32.52
Staatz 1	2213.2	Mikulov Fm.	13.49	44.24	n.d.	n.d.	1.85	40.42
Staatz 1	2251.5	Mikulov Fm.	19.46	46.28	2.54	n.d.	1.43	30.30
Staatz 1	2284.5	Mikulov Fm.	14.27	50.95	5.40	n.d.	1.66	27.71
Staatz 1	2324.5	Mikulov Fm.	14.73	44.76	n.d.	n.d.	1.08	39.43
Staatz 1	2414.5	Mikulov Fm.	18.31	44.10	3.23	n.d.	0.71	33.65
Staatz 1	2524.5	Mikulov Fm.	16.06	48.20	n.d.	2.30	4.37	29.07
Staatz 1	2575.5	Mikulov Fm.	15.88	53.25	n.d.	n.d.	1.03	29.84
Staatz 1	2630.5	Mikulov Fm.	13.89	50.47	2.41	n.d.	0.97	32.26
Staatz 1	2682.5	Mikulov Fm.	19.49	23.45	1.78	n.d.	1.38	53.90
Staatz 1	2740.5	Mikulov Fm.	9.70	44.18	2.17	n.d.	1.21	42.74
Staatz 1	2770.2	Mikulov Fm.	12.14	61.40	3.38	n.d.	1.87	21.21
Staatz 1	2773.5	Mikulov Fm.	11.05	59.59	3.99	n.d.	1.64	23.73
Staatz 1	2825.7	Mikulov Fm.	12.80	51.17	2.57	n.d.	1.96	31.49
Staatz 1	2872.5	Flknstn. Fm.	14.38	33.99	1.79	1.10	2.86	45.88
Staatz 1	2881.7	Flknstn. Fm.	0.40	75.38	21.83	n.d.	n.d.	2.39
Staatz 1	2936	Flknstn. Fm.	5.95	79.57	4.36	n.d.	n.d.	10.12
Staatz 1	2993.8	Flknstn. Fm.	10.99	74.99	n.d.	n.d.	1.31	12.71
Staatz 1	2996.5	Flknstn. Fm.	18.12	60.51	n.d.	n.d.	1.60	19.77
Staatz 1	3096.6	Flknstn. Fm.	7.29	59.39	6.62	n.d.	0.94	25.75
Zistersdorf ÜT 1	5670.5	Mikulov Fm.	16.14	40.10	9.10	n.d.	1.11	33.54
Zistersdorf ÜT 2a	5587	Mikulov Fm.	12.17	56.17	n.d.	n.d.	1.34	30.31
Zistersdorf ÜT 2a	7700	Mikulov Fm.	27.22	33.17	6.52	n.d.	2.99	30.09
Zistersdorf ÜT 2a	8500	Mikulov Fm.	18.86	51.57	3.09	n.d.	1.03	25.45

Appendix V

Pyrolysis GC: Single compounds and boiling ranges

Well		Falkenstein 1	Hoeflein 7a	Porrau 2	Staatz 1	Staatz 1	Staatz 1
Depth	[m]	3378.7	2761.5	2329	2176.3	2324.5	2469.5
Unit	[-]	Mikulov Fm.	Mikulov Fm.	Lower ShMb.	Mikulov Fm.	Mikulov Fm.	Mikulov Fm.
C1	[µg/g TOC]	11706	17144	6688	19366	8063	17383
C2-C5 Total	[µg/g TOC]	49052	63908	16694	72322	34514	66755
C6-C14 Total	[µg/g TOC]	123546	163599	39368	161822	83032	160719
C15+ Total	[µg/g TOC]	171907	242587	61314	180439	111829	163997
C1-C5 Total	[µg/g TOC]	1112	1208	521	1467	898	1464
C1-C30+ Total	[µg/g TOC]	356212	487238	124063	433949	237438	408855
C6-C14 Resolved	[µg/g TOC]	79701	102556	25243	104151	52308	104039
C15+ Resolved	[µg/g TOC]	21231	28512	6211	20600	11308	24626
C1-C30 Resolved	[µg/g TOC]	161690	212119	54835	216439	106193	212804
C2:1	[µg/g Rock]	0	0	0	0	0	0
C2:0	[µg/g Rock]	244.9	290.6	92.7	348.8	190.8	367.2
nC3:1	[µg/g Rock]	0	0	0	0	0	0
nC3:0	[µg/g Rock]	202.8	242.8	95.6	278.8	166.9	283.9
nC4:1	[µg/g Rock]	120.4	113.2	47	111.9	81.7	123.2
nC4:0	[µg/g Rock]	54.6	66.4	18.6	78.2	50.3	80.8
nC5:1	[µg/g Rock]	43.8	44.5	14	52.9	36.8	54.5
nC5:0	[µg/g Rock]	24.8	30.5	8.1	28.4	17.1	32.7
nC6:1	[µg/g Rock]	48.5	48.9	11.6	54.2	34.8	57.2
nC6:0	[µg/g Rock]	20.3	24.3	6	23.8	13.6	25.9
nC7:1	[µg/g Rock]	35.2	34.1	9.8	40.1	26.6	40.5
nC7:0	[µg/g Rock]	21.5	25.6	6.6	26.6	15	28.7
nC8:1	[µg/g Rock]	25.7	23.9	6.2	26.6	16.7	28.3
nC8:0	[µg/g Rock]	18.3	19.8	5.5	19.8	12.3	21.7
nC9:1	[µg/g Rock]	18.9	18.5	4.2	19.4	12.8	20.9
nC9:0	[µg/g Rock]	12.7	14.4	3.5	14.4	8.2	16.2
nC10:1	[µg/g Rock]	21.4	19.8	4.1	20.9	13.5	22.6
nC10:0	[µg/g Rock]	12.2	13.7	3.2	13.8	8.2	14.8
nC11:1	[µg/g Rock]	17	16.6	3.3	16.3	10.5	17.6
nC11:0	[µg/g Rock]	10.7	12.6	2.7	11.8	6.5	12.5
nC12:1	[µg/g Rock]	29.2	22.9	9.6	27	21	23.8
nC12:0	[µg/g Rock]	10.9	13.8	2.7	12.9	6.9	13.3
nC13:1	[µg/g Rock]	13.2	12.6	2.4	12.7	8.7	13.7
nC13:0	[µg/g Rock]	11.2	12.6	2.9	13.6	7.9	13.1
nC14:1	[µg/g Rock]	18.9	16.3	5.3	14.8	11.4	15.3
nC14:0	[µg/g Rock]	13.6	14.6	3.1	14.9	8.8	14.8
nC15:1	[µg/g Rock]	12.4	11.2	3	9.3	6.9	10.5
nC15:0	[µg/g Rock]	11.8	11.7	2.9	13.6	8.5	14.3
nC16:1	[µg/g Rock]	9.3	10.3	1.2	7.9	5.6	9.5
nC16:0	[µg/g Rock]	9.3	9.6	2.1	10.4	7.1	11.1
nC17:1	[µg/g Rock]	8.1	8.7	2.8	5.9	5.2	8.5
nC17:0	[µg/g Rock]	8.2	9.1	2.2	8.8	6.4	10.1
nC18:1	[µg/g Rock]	5	6.9	0.8	3	2.8	5.6
nC18:0	[µg/g Rock]	7	7.8	1.3	5.1	4.5	8
nC19:1	[µg/g Rock]	4.9	6.7	1.3	2.9	2.6	5.7
nC19:0	[µg/g Rock]	5.5	7.1	1.1	4.6	4	6.6
nC20:1	[µg/g Rock]	3.9	6.5	0.5	2.5	2	4.6
nC20:0	[µg/g Rock]	6	7.6	1.1	5	3.6	6.8
nC21:1	[µg/g Rock]	3.6	5.9	0.4	2	1.7	3.6
nC21:0	[µg/g Rock]	4.4	5.8	0.7	3.3	2.4	4.7
nC22:1	[µg/g Rock]	2.6	4.3	0.7	1.9	1.6	3.2
nC22:0	[µg/g Rock]	3.5	4.7	0.6	2.6	1.9	3.9
nC23:1	[µg/g Rock]	1.6	3	0.4	0.6	0.6	1.6
nC23:0	[µg/g Rock]	3	3.7	0.5	1.9	1.5	3
nC24:1	[µg/g Rock]	1.6	2.8	0.2	0.6	0.5	1.3
nC24:0	[µg/g Rock]	2.7	3.2	0.4	1.5	1.2	2.5
nC25:1	[µg/g Rock]	1	1.8	0.1	0.3	0.3	1

Well		Falkenstein 1	Hoeflein 7a	Porrau 2	Staatz 1	Staatz 1	Staatz 1
Depth	[m]	3378.7	2761.5	2329	2176.3	2324.5	2469.5
Unit	[-]	Mikulov Fm.	Mikulov Fm.	Lower ShMb.	Mikulov Fm.	Mikulov Fm.	Mikulov Fm.
nC25:0	[µg/g Rock]	2	2.6	0.2	0.8	0.7	1.9
nC26:1	[µg/g Rock]	0.9	1.8	0	0.1	0.1	0.7
nC26:0	[µg/g Rock]	1.8	2.5	0.1	0.5	0.5	1.6
nC27:1	[µg/g Rock]	0.6	1.1	0	0	0.1	0.4
nC27:0	[µg/g Rock]	1.5	2	0	0.2	0.3	1.2
nC28:1	[µg/g Rock]	0.5	1	0	0	0	0.3
nC28:0	[µg/g Rock]	0.9	1.4	0	0	0.1	0.7
nC29:1	[µg/g Rock]	0.2	0.8	0	0	0	0.1
nC29:0	[µg/g Rock]	0.8	1.2	0	0	0	0.5
nC30:1	[µg/g Rock]	0	0.4	0	0	0	0
nC30:0	[µg/g Rock]	0.6	0.9	0	0	0	0.2
nC31:1	[µg/g Rock]	0	0.3	0	0	0	0
nC31:0	[µg/g Rock]	0.3	0.7	0	0	0	0.2
nC32:1	[µg/g Rock]	0	0.2	0	0	0	0
nC32:0	[µg/g Rock]	0.1	0.6	0	0	0	0
iC18	[µg/g Rock]	1.1	3.6	0.3	1.6	1.3	1.6
Prist-1-ene	[µg/g Rock]	1.1	3.7	2	1.7	1.4	1.9
Prist-2-ene	[µg/g Rock]	1.5	2.9	0.6	2	1.4	2.5
Benzen	[µg/g Rock]	25.9	20.6	18.6	38.7	23.2	37.2
Toluen	[µg/g Rock]	42.6	39	37.5	62.4	37.6	64.1
et-Benz	[µg/g Rock]	10.1	15.2	4.6	15.8	8.7	15.2
m+p Xylen	[µg/g Rock]	27.4	27.4	17.1	37	21.8	38.1
Styr	[µg/g Rock]	10	9.1	3.7	7.1	2.8	19.1
o-Xyl	[µg/g Rock]	13.4	12.7	7.8	19.2	11.5	19.4
Phenol	[µg/g Rock]	3.1	4.1	1.7	4.8	2.8	5.8
o-Cresol	[µg/g Rock]	2.4	3.5	2.6	3.3	3.3	2.1
m+p Cresol	[µg/g Rock]	1.7	2	0.3	3.2	1.6	2.2
Napht	[µg/g Rock]	7.1	5.6	6.5	8.6	5.2	9
2-m Napth	[µg/g Rock]	10.4	8.9	7.9	13.3	7.7	13.3
1-m Napth	[µg/g Rock]	6.5	4.4	5.1	8.6	4.7	8.3
Tetra m Napth	[µg/g Rock]	3.5	2.4	3	2.8	3.1	3.7
Thiophen	[µg/g Rock]	13.7	15.3	3.4	17.3	11	18.8
2m Thiophen	[µg/g Rock]	6.8	9.3	2.2	14.3	8.3	17.1
3m Thiophen	[µg/g Rock]	9.4	6.8	2.5	11.9	7.9	12.8
2,5 dime Thiophen	[µg/g Rock]	1.4	2.3	0.1	2.8	1.1	3.6
2,3 dime Thiophen	[µg/g Rock]	2.5	3.5	0.2	4.1	4.8	5.1
Sum nC6-nC14	[µg/g Rock]	359.4	365	92.7	383.6	243.4	400.9
Sum nC15+	[µg/g Rock]	125.6	155.9	24.6	95.3	72.7	133.9

Well		Staatz 1	Staatz 1	Staatz 1	Thomasl 1	Wildendürnb. T1
Depth	[m]	2740.5	2825.7	3098.5	2304	1447.5
Unit	[-]	Mikulov Fm.	Mikulov Fm.	Flknstn. Fm.	Mikulov Fm.	Mikulov Fm.
C1	[µg/g TOC]	7398	7455	2062	15641	12645
C2-C5 Total	[µg/g TOC]	30731	33983	13394	57898	56139
C6-C14 Total	[µg/g TOC]	82785	100006	35232	158940	166048
C15+ Total	[µg/g TOC]	107852	117948	59734	188792	179503
C1-C5 Total	[µg/g TOC]	968	854	343	1552	1046
C1-C30+ Total	[µg/g TOC]	228766	259392	110422	421270	414335
C6-C14 Resolved	[µg/g TOC]	49691	61278	21255	102704	106030
C15+ Resolved	[µg/g TOC]	12918	15442	4034	25583	23440
C1-C30 Resolved	[µg/g TOC]	100739	118159	40745	201825	198254
C2:1	[µg/g Rock]	0	0	0	0	0
C2:0	[µg/g Rock]	216.6	186.5	59.4	357.2	228
nC3:1	[µg/g Rock]	0	0	0	0	0
nC3:0	[µg/g Rock]	189	167.7	67.7	277.1	203
nC4:1	[µg/g Rock]	94.8	89.9	44.2	153.4	115.1
nC4:0	[µg/g Rock]	50.7	50.2	19.6	77.1	51.9
nC5:1	[µg/g Rock]	41.2	38.1	16.4	60.9	43.5
nC5:0	[µg/g Rock]	20.7	19.8	6.6	39.2	23.3
nC6:1	[µg/g Rock]	42.9	38.2	16.1	62.1	44.6
nC6:0	[µg/g Rock]	16.6	16.1	4.9	31	18.9
nC7:1	[µg/g Rock]	31	26.9	13	42.8	31.9
nC7:0	[µg/g Rock]	18	17.6	5.3	33	20.3
nC8:1	[µg/g Rock]	21.2	18.8	8.6	31.9	23.4
nC8:0	[µg/g Rock]	14.6	13.7	4.5	27.4	16.7
nC9:1	[µg/g Rock]	16.1	14.5	6.8	23.7	16.3
nC9:0	[µg/g Rock]	10.9	10.2	2.9	19	11
nC10:1	[µg/g Rock]	17.9	15.6	7.3	24.8	18.2
nC10:0	[µg/g Rock]	9.5	9.5	3.2	16.9	10.7
nC11:1	[µg/g Rock]	13.9	12.5	5.6	20.4	14.1
nC11:0	[µg/g Rock]	8.3	8.2	2.6	15	8.9
nC12:1	[µg/g Rock]	20.4	20.8	14.1	27.7	20.5
nC12:0	[µg/g Rock]	9.2	8.4	3.9	16.5	9.5
nC13:1	[µg/g Rock]	12.1	9.4	4.5	15	11.6
nC13:0	[µg/g Rock]	9.3	8.2	3.2	16.5	9.5
nC14:1	[µg/g Rock]	15.5	12.4	8.3	18.5	14.6
nC14:0	[µg/g Rock]	10.7	10.3	3.8	18.5	11.3
nC15:1	[µg/g Rock]	10.2	7.6	4	13.8	10.7
nC15:0	[µg/g Rock]	9.8	9.6	2.8	17.5	10.3
nC16:1	[µg/g Rock]	7.7	7.1	2.6	12.9	8.2
nC16:0	[µg/g Rock]	7	7	1.9	13.5	7.3
nC17:1	[µg/g Rock]	6.8	5.8	2	10.2	7.6
nC17:0	[µg/g Rock]	6.1	6.3	2	11.4	6.4
nC18:1	[µg/g Rock]	4.4	3.8	1.3	6.7	4.4
nC18:0	[µg/g Rock]	5.1	5.5	1.6	9.4	5.2
nC19:1	[µg/g Rock]	4.3	3.9	1.2	6.8	4.5
nC19:0	[µg/g Rock]	4.5	4.6	1.5	7.8	4.4
nC20:1	[µg/g Rock]	3.7	3.3	0.9	6.2	3.8
nC20:0	[µg/g Rock]	4.9	4.9	1.2	8.7	4.9
nC21:1	[µg/g Rock]	3	2.7	1	5.5	3.2
nC21:0	[µg/g Rock]	3.6	3.4	0.8	6.3	3.4
nC22:1	[µg/g Rock]	2.9	2.4	0.7	4.1	2.5
nC22:0	[µg/g Rock]	2.9	2.9	0.7	4.9	2.6
nC23:1	[µg/g Rock]	1.7	1.3	0.3	2.5	1.4
nC23:0	[µg/g Rock]	2.4	2.2	0.5	4.1	2.1
nC24:1	[µg/g Rock]	1.4	1.3	0.2	2.6	1.1
nC24:0	[µg/g Rock]	2.1	2	0.4	3.5	1.7
nC25:1	[µg/g Rock]	1	0.8	0.1	1.6	0.8

Well		Staatz 1	Staatz 1	Staatz 1	Thomasl 1	Wildendürnb. T1
Depth	[m]	2740.5	2825.7	3098.5	2304	1447.5
Unit	[-]	Mikulov Fm.	Mikulov Fm.	Flknstn. Fm.	Mikulov Fm.	Mikulov Fm.
nC25:0	[µg/g Rock]	1.6	1.5	0.3	2.6	1.3
nC26:1	[µg/g Rock]	0.8	0.7	0	1.4	0.8
nC26:0	[µg/g Rock]	1.4	1.2	0.1	2.3	1.2
nC27:1	[µg/g Rock]	0.4	0.3	0	0.8	0.4
nC27:0	[µg/g Rock]	1.1	0.9	0.1	1.8	0.9
nC28:1	[µg/g Rock]	0.4	0.3	0	0.8	0.4
nC28:0	[µg/g Rock]	0.6	0.5	0	1.2	0.6
nC29:1	[µg/g Rock]	0.2	0.1	0	0.5	0.2
nC29:0	[µg/g Rock]	0.4	0.4	0	1.2	0.4
nC30:1	[µg/g Rock]	0.1	0.1	0	0.3	0.1
nC30:0	[µg/g Rock]	0.3	0.2	0	0.7	0.3
nC31:1	[µg/g Rock]	0	0	0	0.2	0.1
nC31:0	[µg/g Rock]	0.2	0.1	0	0.5	0.1
nC32:1	[µg/g Rock]	0	0	0	0.1	0
nC32:0	[µg/g Rock]	0.1	0	0	0.2	0
iC18	[µg/g Rock]	0.9	1.1	0.5	1.7	1.3
Prist-1-ene	[µg/g Rock]	1.1	1	0.3	2	1.1
Prist-2-ene	[µg/g Rock]	1.7	2	0.5	1.9	1.5
Benzen	[µg/g Rock]	24.1	27.9	10.7	31.8	26.8
Toluen	[µg/g Rock]	37.6	35.3	12.7	59.1	44.2
et-Benz	[µg/g Rock]	8.2	8	2.7	15.8	11.3
m+p Xylen	[µg/g Rock]	23.3	23.8	6.7	40.9	28.2
Styr	[µg/g Rock]	9.9	8.5	8.4	19.3	17.1
o-Xyl	[µg/g Rock]	11.7	11.9	4	19.4	14
Phenol	[µg/g Rock]	3	3.7	1.2	5.8	4
o-Cresol	[µg/g Rock]	1.6	1.5	0.4	3.4	2.3
m+p Cresol	[µg/g Rock]	1.3	1.2	0.3	2.4	1.8
Napht	[µg/g Rock]	5.4	6.2	1.4	9	7
2-m Napth	[µg/g Rock]	8.6	8.5	2.2	13.6	12
1-m Napth	[µg/g Rock]	5	4.7	0.9	8.6	6.6
Tetra m Napth	[µg/g Rock]	3.2	3.2	0.8	4.2	3.8
Thiophen	[µg/g Rock]	12.9	13	4.1	21.1	16.4
2m Thiophen	[µg/g Rock]	7.3	12.8	2.7	16.1	17
3m Thiophen	[µg/g Rock]	8.8	10.5	3.3	15.7	11.7
2,5 dime Thiophen	[µg/g Rock]	1.4	3.5	0.1	3.6	4.1
2,3 dime Thiophen	[µg/g Rock]	2.5	4.8	0.7	5.4	4.2
Sum nC6-nC14	[µg/g Rock]	298.1	271.3	118.6	460.7	312
Sum nC15+	[µg/g Rock]	103.1	94.7	28.2	174.6	103.3

Appendix VI

Pyrolysis GC: Chromatograms

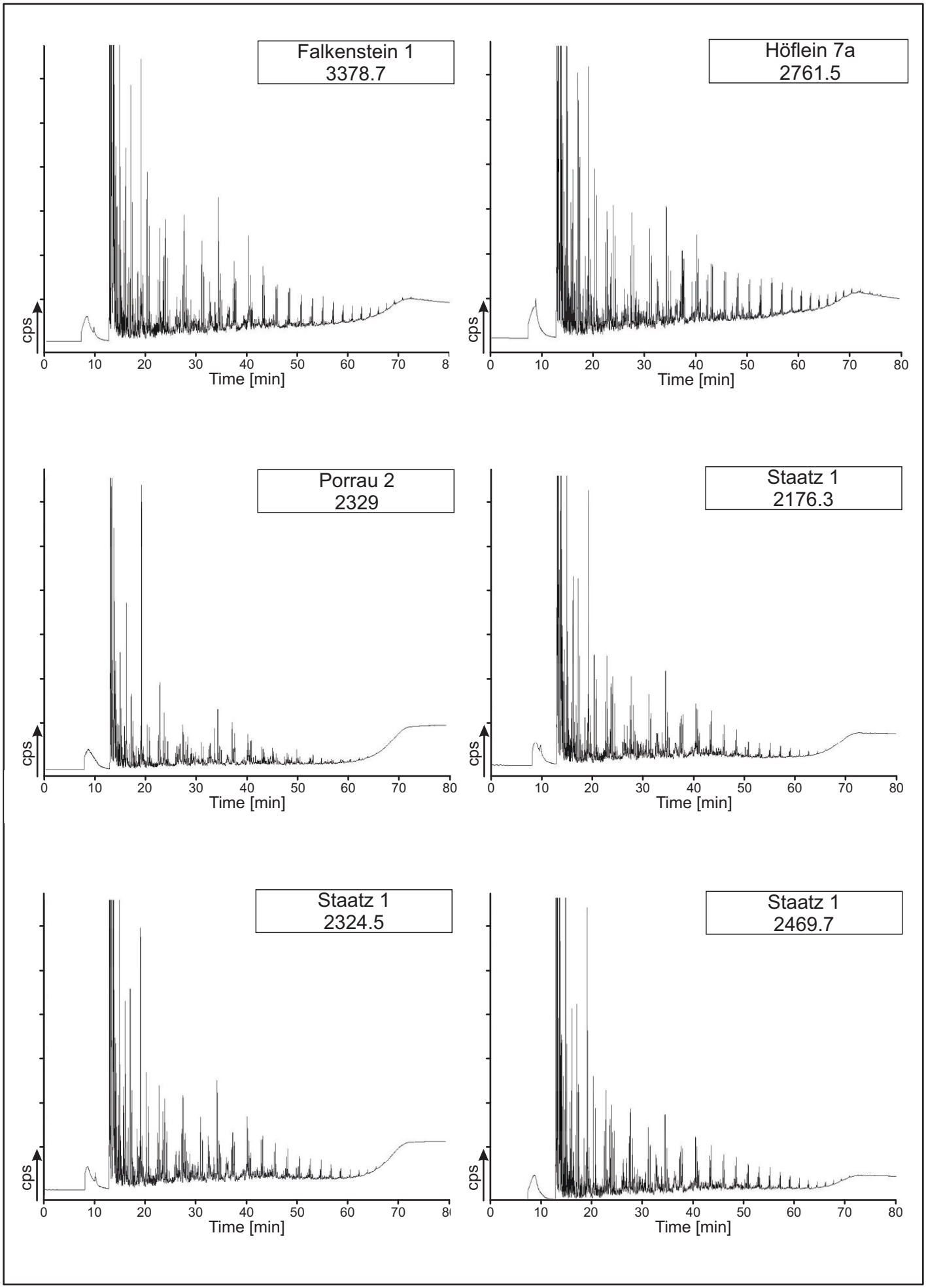
Falkenstein 1
3378.7
Höflein 7a
2761.5
Porrau 2
2329
Staatz 1
2176.3
Staatz 1
2324.5
Staatz 1
2469.7
cps
Time [min]
0
10
20
30
40
50
60
70
80

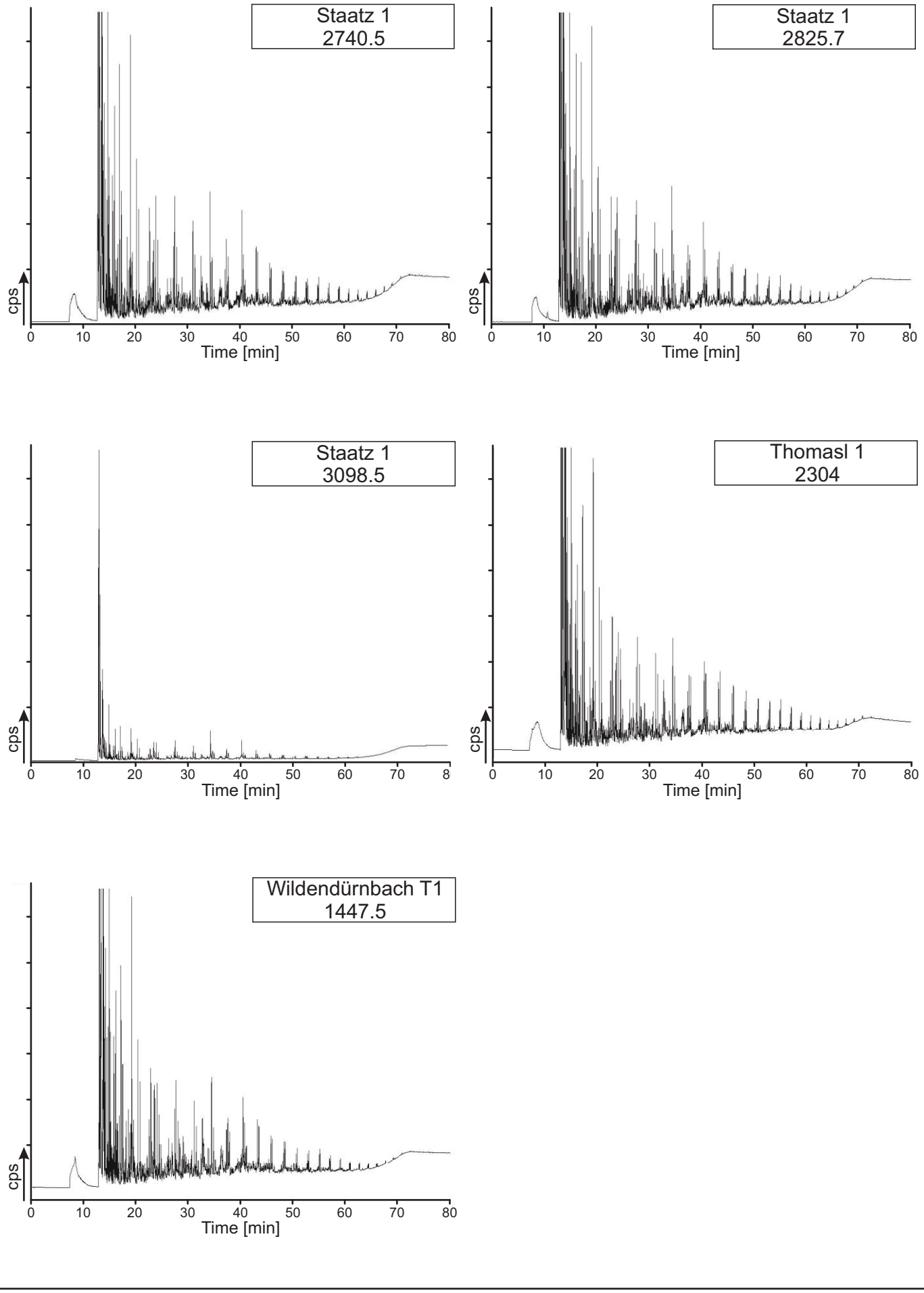
Staatz 1
2740.5
cps
0
10
20
30
40
50
60
70
80
Time [min]
Staatz 1
2825.7
cps
0
10
20
30
40
50
60
70
80
Time [min]
Staatz 1
3098.5
cps
0
10
20
30
40
50
60
70
8
Time [min]
Thomasl 1
2304
cps
0
10
20
30
40
50
60
70
80
Time [min]
Wildendürnbach T1
1447.5
cps
0
10
20
30
40
50
60
70
80
Time [min]

Appendix VII

Biomarkers: concentrations and ratios

EOM Extractable organic matter

Sat Aliphatic fraction

Aro Aromatic fraction

NSO NSO compounds

Asph Asphaltenes

CPI Carbon preference index

RSFP Reservoir-source fraction parameter

BCR Benzocarbazol ratio

BBDS Biomarker biodegradation scale rank

Well	Depth [m]	Stratigraphic Unit	EOM [mg/gTOC]	Sat [% EOM]	Aro [% EOM]	NSO [% EOM]	Asph [% EOM]	CPI [-]	Pr/Phy [-]	Pr/nC_{17} [-]	Ph/nC_{18} [-]	C_{27} Ster/ Ster	C_{28} Ster/ Ster
Altenmarkt 1	2640.5	Lower ShMb.	25.39										
Altenmarkt 1	2641.6	Lower ShMb.	1.96	9.2	9.0	79.7	2.2	1.41	1.75	1.15	0.70	0.33	0.23
Falkenst. 1	3378.7	Mikulov Fm.	10.60	5.4	3.0	84.7	6.9	1.53	1.39	0.83	0.81	0.51	0.24
Falkenst. 1	3516	Mikulov Fm.	39.82	14.4	22.7	52.9	10.0	1.32	1.67	0.99	0.75	0.51	0.25
Falkenst. 1	3748.4	Mikulov Fm.	36.37	11.2	25.6	62.7	0.5	1.25	1.91	1.08	0.64	0.51	0.22
Falkenst. 1	4150.4	Flknstn. Fm.	28.09	18.1	26.1	52.4	3.5	1.08	1.37	0.43	0.31	0.55	0.18
Falkenst. 1	4495.5	Lower ShMb.	34.65	5.7	9.6	84.5	0.1	1.22	2.02	0.80	0.39	0.36	0.21
Falkenst. 1	4498.3	Lower ShMb.	31.08	2.5	6.4	90.9	0.1	1.21	2.87	1.15	0.39	0.35	0.19
Hoeflein 7a	2761.5	Mikulov Fm.	13.59	13.2	7.1	73.6	6.1	1.39	1.04	1.52	1.39	0.50	0.24
Hoeflein 7a	2762.2	Mikulov Fm.	17.68	14.6	12.6	70.4	2.4	1.49	1.31	1.15	0.99	0.52	0.21
Maustr. ÜT 1	6546.7	Mikulov Fm.	63.87	47.2	8.7	42.0	2.1	1.09	1.96	0.64	0.41	1.00	0.00
Maustr. ÜT 1	6548.8	Mikulov Fm.	55.48	52.7	6.7	26.0	14.7	1.06	1.26	0.32	0.30	0.57	0.43
Porrau 2	2166.8	Lower ShMb.	20.65	11.2	0.0	87.9	1.0	1.72	1.55	1.57	0.83	0.28	0.25
Porrau 2	2495	Lower QaMb.	18.88	1.5	3.2	94.9	0.5	1.71	0.46	0.08	1.64	0.11	0.35
Staatz 1	1968	Mikulov Fm.	32.95						1.58	1.87	1.22	0.22	0.40
Staatz 1	2026.5	Mikulov Fm.	37.00	11.9	2.6	79.8	5.7	1.09	0.56	1.22	1.09	0.51	0.22
Staatz 1	2083	Mikulov Fm.	58.15						1.23	1.03	1.11	0.28	0.33
Staatz 1	2113.1	Mikulov Fm.	35.13	6.1	0.3	89.7	3.9		0.48	1.01	0.81	0.46	0.22
Staatz 1	2141.3	Mikulov Fm.	38.49	11.8	0.8	85.7	1.8	1.71	0.59	1.05	0.88	0.48	0.21
Staatz 1	2176.3	Mikulov Fm.	21.89	6.7	0.8	87.8	4.7		0.53		0.87	0.45	0.23
Staatz 1	2178	Mikulov Fm.	43.33	12.0	0.2	87.1	0.7	1.94	0.62	0.90	0.96	0.46	0.23
Staatz 1	2213.2	Mikulov Fm.	48.59	14.5	6.2	52.7	26.6	2.16	1.45	1.19	0.87	0.45	0.22
Staatz 1	2251.5	Mikulov Fm.	47.60	15.5	1.4	81.6	1.5	1.52	0.42	3.01	8.27	0.46	0.24
Staatz 1	2284.5	Mikulov Fm.	38.46	17.3	1.6	79.9	1.3	1.46	0.93	0.89	0.72	0.44	0.26
Staatz 1	2322.5	Mikulov Fm.	36.79	10.9	1.3	87.2	0.6		0.55	1.13	0.94	0.41	0.25
Staatz 1	2324.5	Mikulov Fm.	26.40	33.3	6.4	57.4	2.8	1.55	1.12	0.87	0.83	0.42	0.27
Staatz 1	2414.5	Mikulov Fm.	30.67	5.5	1.0	85.5	8.1	2.21	0.59	1.24	1.09	0.44	0.23
Staatz 1	2469.5	Mikulov Fm.	39.38	14.5	1.9	83.0	0.6	2.18	1.06	1.10	0.90	0.46	0.23
Staatz 1	2524.5	Mikulov Fm.	31.28	10.5	4.4	65.0	20.0		0.48	0.99	0.83	0.46	0.22
Staatz 1	2575.5	Mikulov Fm.	26.02	7.3	4.0	86.5	2.2	1.95	0.61	1.23	0.82	0.47	0.24
Staatz 1	2630.5	Mikulov Fm.	36.27	30.2	16.2	42.0	11.6	1.58	1.36	1.00	0.90	0.49	0.23
Staatz 1	2634.5	Mikulov Fm.	30.62	28.3	9.6	61.4	0.8	1.80	1.23	1.01	0.57	0.45	0.21
Staatz 1	2682.5	Mikulov Fm.	30.61						1.26	0.93	1.65	0.38	0.29
Staatz 1	2740.5	Mikulov Fm.	23.85	29.6	10.8	57.0	2.7	1.66	1.21	1.00	0.83	0.49	0.24
Staatz 1	2743.5	Mikulov Fm.	29.69	17.0	5.6	73.3	4.2	1.57	1.43	1.08	0.90	0.53	0.22
Staatz 1	2770.2	Mikulov Fm.	37.31	14.7	8.2	74.5	2.7	1.05	1.30	1.39	1.02	0.53	0.25
Staatz 1	2773.5	Mikulov Fm.	36.39	19.4	9.5	68.8	2.3	1.06	1.52	1.31	0.94	0.55	0.21
Staatz 1	2774.5	Mikulov Fm.	18.84	17.8	5.6	71.9	4.7	0.99	1.37	1.26	1.10	0.54	0.22
Staatz 1	2825.7	Mikulov Fm.	29.22	23.1	8.6	55.1	13.2	1.18	1.14	1.08	0.94	0.53	0.23
Staatz 1	2996.5	Flknstn. Fm.	18.19	21.4	17.6	59.9	1.1	1.10	1.75	1.31	0.87	0.51	0.22
Staatz 1	3098.5	Flknstn. Fm.	9.70	25.5	15.1	48.1	11.3	1.52	1.08	1.07	0.74	0.51	0.19
Thomasl 1	2302.6	Mikulov Fm.	15.20	14.2	1.7	82.0	2.0	2.31	1.25	1.18	1.08	0.46	0.20
Thomasl 1	2304	Mikulov Fm.	13.62	13.3	3.7	81.0	2.0	3.09	1.44	0.80	0.77	0.44	0.22
Thomasl 1	3006.7	Mikulov Fm.	40.10	15.3	3.9	78.9	1.9	1.44	2.03	1.04	0.75	0.51	0.24
Waschberg 1	2536.1	Flknstn. Fm.	13.31	4.4	11.3	78.3	5.9	2.01	0.78	1.43	1.59	0.50	0.22
Waschberg 1	2538.8	Flknstn. Fm.	2.08	0.0	41.4	0.0	58.6	1.52	0.86	1.41	0.89	0.45	0.24
Zistersd. ÜT 1	5602.7	Mikulov Fm.	165.26	53.6	10.6	21.2	14.6	1.14	0.83	0.53	0.65	0.22	0.38
Zistersd. ÜT 1	5605.5	Mikulov Fm.	76.73	56.0	10.7	27.1	6.1	1.09	1.28	0.59	0.53	0.38	0.31
Zistersd. ÜT 1	5670.5	Mikulov Fm.	103.56	66.0	9.6	19.3	5.0	1.12	0.90	0.37	0.51	0.48	0.21
Zistersd. ÜT 1	5740.7	Mikulov Fm.	188.95	33.6	11.2	54.0	1.3	1.08	0.93	0.48	0.52	0.37	0.30
Zistersd. ÜT 1	5977.3	Mikulov Fm.	126.43	54.5	9.6	35.5	0.4	1.18	0.93	0.57	0.65	0.34	0.31
Zistersd. ÜT 2	5587	Mikulov Fm.	196.39	39.1	11.2	48.8	0.9		0.67	0.42	0.57	0.54	0.13

Well	Depth [m]	C_{29} Ster/ Ster	C_{28}/C_{29} Ster.	Ster C_{27} Dia/ (Dia.+Reg)	C_{29} S/R Ster.	αββ/ααα Steranes	S/(S+R) Steranes	Ster αββ/ (αββ+ααα)	Ster/ Hop.	C_{31} Hop S/(S+R)	Ts/ Ts+Tm
Altenmarkt 1	2640.5										
Altenmarkt 1	2641.6	0.44	0.51	0.35	0.36	0.62	0.27	0.38	0.17	0.42	0.13
Falkenst. 1	3378.7	0.25	0.98	0.47	0.21	0.57	0.17	0.36	0.87	0.32	0.15
Falkenst. 1	3516	0.24	1.05	0.49	0.24	0.54	0.19	0.35	0.87	0.37	0.13
Falkenst. 1	3748.4	0.27	0.82	0.46	0.26	0.40	0.21	0.28	0.69	0.51	0.26
Falkenst. 1	4150.4	0.27	0.64	0.49	0.84	0.44	0.46	0.31	0.40	0.60	0.29
Falkenst. 1	4495.5	0.43	0.50	0.22	0.47	0.45	0.32	0.31	0.22	0.58	0.13
Falkenst. 1	4498.3	0.46	0.41	0.27	0.72	0.50	0.42	0.33	0.15	0.56	0.06
Hoeflein 7a	2761.5	0.26	0.94	0.42	0.21	0.56	0.18	0.36	0.72	0.33	0.35
Hoeflein 7a	2762.2	0.27	0.78	0.45	0.21	0.57	0.17	0.36	0.69	0.35	0.29
Maustr. ÜT 1	6546.7	0.00									
Maustr. ÜT 1	6548.8	0.00									
Porrau 2	2166.8	0.47	0.54	0.57	0.34	0.56	0.26	0.36	0.22	0.42	0.15
Porrau 2	2495	0.54	0.66	0.39	0.40	0.32	0.28	0.24	0.42	0.42	0.15
Staatz 1	1968	0.38	0.91	0.14	0.17	0.55	0.15	0.35	0.74	0.20	0.40
Staatz 1	2026.5	0.28	0.78	0.46	0.20	0.51	0.16	0.34	1.28	0.29	0.24
Staatz 1	2083	0.38	0.74	0.17	0.30	0.70	0.23	0.41	0.42	0.10	0.30
Staatz 1	2113.1	0.32	0.69	0.19	0.17	0.54	0.14	0.35		0.16	0.16
Staatz 1	2141.3	0.31	0.69	0.30	0.22	0.51	0.18	0.34		0.19	0.24
Staatz 1	2176.3	0.33		0.17	0.22	0.46	0.18	0.31		0.20	0.20
Staatz 1	2178	0.31		0.26	0.25	0.52	0.20	0.34		0.15	0.27
Staatz 1	2213.2	0.33	0.68	0.24	0.22	0.46	0.18	0.31		0.25	0.22
Staatz 1	2251.5	0.30	0.81	0.11	0.14	0.35	0.13	0.26	1.24	0.21	0.25
Staatz 1	2284.5	0.31	0.84		0.34	0.61	0.25	0.38		0.19	0.22
Staatz 1	2322.5	0.33	0.76	0.20	0.27	0.51	0.21	0.34		0.12	0.21
Staatz 1	2324.5	0.31	0.85	0.39	0.26	0.65	0.21	0.40		0.07	0.34
Staatz 1	2414.5	0.33	0.71	0.21	0.21	0.59	0.17	0.37		0.13	0.18
Staatz 1	2469.5	0.31	0.76	0.23	0.30	0.65	0.23	0.40		0.15	0.19
Staatz 1	2524.5	0.32	0.69	0.28	0.25	0.58	0.20	0.37		0.15	0.19
Staatz 1	2575.5	0.29	0.84	0.30	0.32	0.69	0.24	0.41		0.12	0.14
Staatz 1	2630.5	0.28	0.80	0.35	0.32	0.63	0.24	0.39		0.19	0.28
Staatz 1	2634.5	0.33	0.64	0.34	0.34	0.62	0.25	0.38		0.20	0.20
Staatz 1	2682.5	0.32	0.76	0.31	0.36	0.67	0.27	0.40	0.51	0.23	0.12
Staatz 1	2740.5	0.27	0.88	0.42	0.35	0.58	0.26	0.37		0.14	0.21
Staatz 1	2743.5	0.26	0.84	0.43	0.32	0.63	0.24	0.39		0.21	0.21
Staatz 1	2770.2	0.22	1.16	0.47	0.24	0.53	0.20	0.35	1.67	0.30	0.23
Staatz 1	2773.5	0.24	0.88	0.45	0.24	0.55	0.19	0.35	1.39	0.28	0.22
Staatz 1	2774.5	0.24	0.92	0.45	0.25	0.55	0.20	0.36	1.55	0.27	0.20
Staatz 1	2825.7	0.25	0.91	0.45	0.23	0.50	0.18	0.33	1.49	0.22	0.22
Staatz 1	2996.5	0.27	0.84	0.44	0.20	0.43	0.17	0.30	0.74	0.42	0.23
Staatz 1	3098.5	0.30	0.61	0.48	0.31	0.52	0.24	0.34	0.38	0.39	0.17
Thomasl 1	2302.6	0.34			0.26	0.55	0.21	0.36		0.09	0.23
Thomasl 1	2304	0.35		0.11	0.23	0.41	0.19	0.29		0.10	0.11
Thomasl 1	3006.7	0.24	0.98	0.41	0.22	0.62	0.18	0.38		0.30	0.24
Waschberg 1	2536.1	0.28	0.80	0.36	0.24	0.60	0.19	0.37	0.88	0.19	0.19
Waschberg 1	2538.8	0.31	0.79	0.35	0.43	0.65	0.30	0.39		0.27	0.21
Zistersd. ÜT 1	5602.7	0.40			2.66		0.73				0.76
Zistersd. ÜT 1	5605.5	0.31			1.66	0.92	0.62	0.48			0.69
Zistersd. ÜT 1	5670.5	0.32			1.44	0.88	0.59	0.47			0.54
Zistersd. ÜT 1	5740.7	0.33	0.91	0.46	1.15	0.79	0.53	0.44		0.60	0.59
Zistersd. ÜT 1	5977.3	0.35			1.75	0.76	0.64	0.43			0.60
Zistersd. ÜT 2	5587	0.33			1.08		0.52			0.42	0.57

Well	Depth [m]	C_{29}Ts C_{29}Ts+Tm	MTTC Ratio	MPI [-]	DBT/ Phen
Altenmarkt 1	2640.5				
Altenmarkt 1	2641.6		0.44	0.28	0.03
Falkenst. 1	3378.7	0.27	0.76	0.45	0.09
Falkenst. 1	3516	0.21	0.70	0.41	0.06
Falkenst. 1	3748.4	0.31	0.44	0.49	0.06
Falkenst. 1	4150.4	0.28		0.52	0.08
Falkenst. 1	4495.5		0.16	0.41	0.05
Falkenst. 1	4498.3		0.30	0.41	0.07
Hoeflein 7a	2761.5	0.36	0.69	0.45	0.10
Hoeflein 7a	2762.2	0.35	0.78	0.43	0.09
Maustr. ÜT 1	6546.7		0.62	0.83	0.07
Maustr. ÜT 1	6548.8			0.94	0.05
Porrau 2	2166.8		0.45	0.33	
Porrau 2	2495		0.11	0.22	0.07
Staatz 1	1968	0.23	0.03	0.45	0.04
Staatz 1	2026.5	0.32	0.51	0.66	0.02
Staatz 1	2083	0.00	0.50	0.39	0.04
Staatz 1	2113.1	0.49	0.36	0.65	0.01
Staatz 1	2141.3	0.55	0.36	0.60	0.02
Staatz 1	2176.3	0.48	0.51	0.47	0.01
Staatz 1	2178	0.48	0.46	0.54	0.02
Staatz 1	2213.2	0.20	0.73	0.28	0.03
Staatz 1	2251.5	0.18	0.38	0.51	0.05
Staatz 1	2284.5	0.50	0.34	0.56	0.04
Staatz 1	2322.5	0.53	0.46	0.57	0.02
Staatz 1	2324.5	0.24	0.40	0.50	0.06
Staatz 1	2414.5	0.46	0.76	0.39	0.02
Staatz 1	2469.5	0.48	0.79	0.40	0.04
Staatz 1	2524.5	0.55	0.54	0.61	0.01
Staatz 1	2575.5	0.52	0.58	0.50	0.01
Staatz 1	2630.5	0.18	0.82	0.41	0.04
Staatz 1	2634.5	0.19	0.77	0.42	0.09
Staatz 1	2682.5	0.00	0.07	0.33	0.03
Staatz 1	2740.5	0.27		0.41	0.05
Staatz 1	2743.5	0.33	0.85	0.36	0.05
Staatz 1	2770.2	0.32	0.57	0.38	0.06
Staatz 1	2773.5	0.33	0.57	0.29	0.05
Staatz 1	2774.5	0.34	0.66	0.32	0.04
Staatz 1	2825.7	0.29	0.34	0.40	0.07
Staatz 1	2996.5	0.26	0.57	0.39	0.06
Staatz 1	3098.5	0.23	0.33	0.39	0.06
Thomasl 1	2302.6	0.40	0.44	0.60	0.09
Thomasl 1	2304	0.44	0.58	0.49	0.09
Thomasl 1	3006.7	0.31	0.56	0.48	0.15
Waschberg 1	2536.1	0.28	0.86	0.51	0.15
Waschberg 1	2538.8	0.23	0.66	0.56	
Zistersd. ÜT 1	5602.7			0.72	0.14
Zistersd. ÜT 1	5605.5		0.43	0.74	0.10
Zistersd. ÜT 1	5670.5			0.75	0.13
Zistersd. ÜT 1	5740.7			0.80	0.16
Zistersd. ÜT 1	5977.3			0.83	0.25
Zistersd. ÜT 2	5587		0.05	0.72	0.18

Well	Depth	Sat	Aro	NSO	Asph	Pr/Phy	Pr/nC$_{17}$	Ph/nC$_{18}$	C$_{27}$ Ster/	C$_{28}$ Ster/	C$_{29}$ Ster/	C$_{28}$/C$_{29}$	Ster C$_{27}$ Dia/	C$_{29}$ S/R	αββ/ααα	S/(S+R)	Ster αββ/	Ster/
	[m ss]	[% EOM]				[-]	[-]	[-]	Ster	Ster	Ster	Ster.	(Dia.+Reg)	Ster.	Ster.	Ster	(αββ+ααα)	Hop.
Aderklaa 3	2351					2.83	0.53	0.33										
Aderklaa 4	2515					2.23	0.45	0.32										
Aderklaa 34	1715	44.7	6.8	48.0	0.4	1.48	0.37	0.27	0.45	0.25	0.30	0.78	0.38	0.96	1.17	0.49	0.54	0.92
Bockfliess 1	1177.4	37.7	22.7	39.4	0.2							0.27	0.53	1.62	1.56	0.62	0.61	0.61
Bockfliess 24	1436.2	44.3	21.4	34.3	0.0	1.63	17.14	9.89				0.40	0.56	1.73	1.53	0.63	0.61	0.66
Bockfliess 33	1181.2	41.1	24.8	34.0	0.1	0.44	1.26	4.88				0.33	0.52	1.59	1.45	0.61	0.59	0.67
Bockfliess 35	1460.6	43.4	24.6	32.2	0.0	1.37	15.68	5.62				0.29	0.50	1.46	1.39	0.59	0.58	0.68
Bockfliess 37	1463.4	22.5	24.4	53.3	0.0	1.99	33.64	8.48				0.29	0.52	1.37	1.24	0.58	0.55	0.65
Bockfliess 43	1428.7	42.3	25.0	32.5	0.1	1.89	15.08	10.86				0.30	0.55	1.61	1.39	0.62	0.58	0.66
Bockfliess 205	1627.0	40.7	20.8	38.7	0.0	1.99	16.96	10.90				0.31	0.54	1.68	1.72	0.63	0.63	0.65
Ebenthal 5	1614.4	52.2	14.3	33.7	0.0	2.12	0.59	0.33	0.45	0.20	0.36	0.33	0.48	1.27	1.42	0.56	0.59	0.91
Ebenthal 15	1636.0	50.5	13.7	35.8	0.0	1.68	0.49	0.34	0.36	0.32	0.32	0.50	0.53	0.77	0.98	0.43	0.49	0.86
Ebenthal 17a	1614.0	51.7	14.6	33.6	0.0	1.93	0.54	0.32	0.36	0.26	0.37	0.41	0.53	0.99	0.94	0.50	0.49	0.83
Ebenthal 20	1614.4	51.0	13.4	35.6	0.0	1.73	0.50	0.34	0.40	0.27	0.33	0.51	0.49	0.84	0.78	0.46	0.44	0.76
Erdpress 4	1787.5	47.3	19.9	32.7	0.1	1.62	0.42	0.32	0.43	0.25	0.32	0.42	0.48	1.23	1.36	0.55	0.58	0.64
Erdpress 17a	1424.2	27.3	23.8	49.0	0.0	1.60		13.64	0.46	0.12	0.42		0.44	1.73	1.54	0.63	0.61	
Erdpress 24	1419.1	46.3	21.9	31.9	0.0	1.50		11.14	0.39	0.23	0.38	0.39	0.56	1.49	1.86	0.60	0.65	0.79
Gbely 2		48.7	22.7	28.2	0.3	1.53		1.59	0.37	0.20	0.43	0.53	0.37	2.46	1.73	0.71	0.63	0.33
Gbely H6		20.4	3.4	76.2	0.0	4.98	1.62	0.55	0.31	0.40	0.29	1.44	0.27	1.40	1.82	0.58	0.64	0.30
Hochleiten 15	737.6	36.9	26.8	35.9	0.4							0.30	0.54	1.51	1.27	0.60	0.56	0.55
Hochleiten 24	748.7	35.5	29.9	34.6	0.0							0.43	0.55	1.89	1.43	0.65	0.59	0.63
Hochleiten 31	982.0	36.3	19.3	44.0	0.4	1.62	1.44	1.28	0.52	0.19	0.29	0.77	0.42	1.82	1.29	0.65	0.56	0.77
Hochleiten 60	759.3	27.1	23.8	49.0	0.1							0.33	0.53	1.36	1.38	0.58	0.58	0.55
Hochleiten 65	851.1	40.4	27.1	32.5	0.1							0.35	0.52	1.74	1.32	0.64	0.57	0.60
Hochleiten 66	911.3	22.9	26.7	50.1	0.2							0.32	0.56	2.10	1.32	0.68	0.57	0.67
Hochleiten 67	786.4	44.3	26.1	29.5	0.1							0.35	0.59	1.76	1.80	0.64	0.64	0.71
Hodonin 1		41.0	26.0	32.9	0.1			1.04	0.43	0.21	0.36	0.58	0.36	4.31	1.59	0.81	0.61	0.46
Hodonin 3		43.5	21.6	34.3	0.6	1.42	1.51	9.92	0.40	0.22	0.38	0.62	0.35	1.73	1.42	0.63	0.59	0.49
Hodonin 4		18.2	6.9	74.5	0.4	2.20	0.79	0.43	0.40	0.28	0.32	0.90	0.34	1.68	1.18	0.63	0.54	0.55
Hoeflein 6	2663.0	41.8	14.6	43.3	0.4													
Hoeflein 9	2633.6					1.01	0.33	0.36	0.36	0.21	0.43	0.26	0.56	1.48	1.65	0.60	0.62	0.71
Hoeflein 9	2685.0	25.8	6.9	66.3	1.0													
Hoeflein 12	2670.3					0.98	0.22	0.24	0.50	0.17	0.33	0.27	0.52	1.49	1.34	0.60	0.57	0.76
HRPD 42	1412.4	43.7	22.3	33.7	0.3	1.39	25.77	18.27				0.39	0.56	1.67	1.31	0.63	0.57	0.77
Holic 4		35.8	11.0	53.2	0.0	2.62	0.64	0.23	0.41	0.25	0.33	0.76	0.39	1.90	1.20	0.65	0.55	0.55
Kierling 1	60.0	35.2	10.6	54.0	0.2	2.08	0.47	0.23	0.52	0.18	0.31	0.72	0.39	1.72	1.52	0.63	0.60	1.02
Kierling 2		41.5	10.2	47.7	0.6	1.75	0.45	0.26	0.52	0.18	0.30	0.73	0.39	1.40	1.51	0.58	0.60	1.06
Klement 1	3539.0					2.35	0.36	0.16	0.55	0.21	0.23	0.91		0.89		0.47	0.50	
Lanzhot 15		50.6	9.5	37.9	2.0	2.12	0.48	0.25	0.48	0.23	0.30	0.74	0.39	1.16	0.97	0.54	0.49	0.57
Lanzhot 30		53.6	9.9	34.3	2.2	2.03	0.57	0.29	0.43	0.23	0.34	0.77	0.40	1.04	1.14	0.51	0.53	0.58
Mank 1	157.0					0.93	0.56	0.55	0.31	0.40	0.29		0.29	0.31	1.56	0.24	0.61	
Matzen 91	1464.0	42.4	20.4	37.2	0.0	1.19	7.78	15.86	0.46	0.18	0.36	0.54	0.37	1.40	1.50	0.58	0.60	0.70
Matzen 115	1472.0	41.1	18.3	40.4	0.3	1.87	6.49	10.86	0.47	0.23	0.30	0.74	0.36	1.45	1.35	0.59	0.57	0.69

Well	Depth	Sat	Aro	NSO	Asph	Pr/Phy	Pr/nC$_{17}$	Ph/nC$_{18}$	C$_{27}$ Ster/	C$_{28}$ Ster/	C$_{29}$ Ster/	C$_{28}$/C$_{29}$	Ster C$_{27}$ Dia/	C$_{29}$ S/R	αββ/ααα	S/(S+R)	Ster αββ/	Ster/
	[m ss]	[% EOM]				[-]	[-]	[-]	Ster	Ster	Ster	Ster.	(Dia.+Reg)	Ster.	Ster.	Ster	(αββ+ααα)	Hop.
Matzen 116	1449.0	41.0	19.6	39.5	0.0	1.93												
Matzen 286	1467.0	36.8	17.5	45.5	0.2	1.46	9.53	17.19	0.47	0.22	0.31	0.71	0.39	1.75	1.42	0.64	0.59	0.71
Matzen 322	1458.0																	
Matzen 390	1139.7	39.0	24.3	36.7	0.0				0.36	0.27	0.37	0.41	0.55	1.49	1.41	0.60	0.59	0.60
Matzen H 703b	1523.0	37.0	20.8	41.9	0.3	1.87												
Maustrenk 29	895.0	42.6	21.5	34.0	2.0	1.25	1.71	1.23	0.45	0.24	0.31	0.75	0.33	1.55	1.26	0.61	0.56	0.45
Mühlberg 15	1480.0	44.7	18.7	35.4	1.3	2.45	2.92	1.00	0.42	0.26	0.31	0.76	0.36	0.86	1.08	0.46	0.52	0.73
Neusiedl 1	1180.0	44.5	11.6	43.8	0.0	1.77	0.47	0.26	0.48	0.21	0.30	0.73	0.40	1.84	1.34	0.65	0.57	0.58
Neusiedl 3	1100.0	44.8	11.4	43.5	0.3	1.23	0.37	0.29	0.44	0.21	0.35	0.68	0.40	1.38	1.52	0.58	0.60	0.59
Pirawarth U10	707.0	39.5	11.1	49.3	0.0	1.12	0.24	0.18	0.46	0.24	0.30	1.01	0.43	2.06	1.78	0.67	0.64	0.78
Prottes 26	1140.4	37.3	23.0	39.3	0.4				0.42	0.21	0.37	0.39	0.53	1.37	1.34	0.58	0.57	0.64
Prottes 27	1150.0	38.6	22.6	38.4	0.4	2.53	1.26	0.72	0.53	0.19	0.29	0.63	0.33	1.49	1.17	0.60	0.54	0.64
Prottes 29	1152.0	37.8	20.5	41.6	0.1	2.05	1.53	0.72	0.45	0.22	0.33	0.69	0.38	1.47	1.51	0.60	0.60	0.67
Prottes 98	1157.6	36.2	24.3	39.3	0.2				0.45	0.23	0.32	0.37	0.52	1.36	1.43	0.58	0.59	0.63
Prottes 104	1156.8	39.7	23.7	36.3	0.3				0.44	0.21	0.34	0.35	0.51	1.37	1.36	0.58	0.58	0.61
Prottes T S 3b	2653.0	57.9	13.2	27.4	1.5													
Rabensburg 11	1742.0	26.9	3.4	69.5	0.1	2.88	0.47	0.22	0.35	0.37	0.28	0.85	0.38	0.19	0.59	0.16	0.37	1.02
Rabensburg N3	1718.0	48.0	12.9	38.9	0.2	2.33	1.09	0.48	0.39	0.18	0.43	0.50	0.34	0.98	1.27	0.49	0.56	0.33
Rabensburg U4		35.9	10.1	53.8	0.2	2.55	1.01	0.44	0.38	0.26	0.36	0.69	0.37	1.34	1.17	0.57	0.54	0.36
Roseldorf 2	1383.0	47.7	12.8	39.4	0.1	0.95	0.27	0.29	0.52	0.24	0.24	1.08	0.41	1.92	1.33	0.66	0.57	1.10
Roseldorf 2	1383.0	48.6	12.5	38.6	0.2	1.29	0.34	0.24	0.52	0.20	0.28	0.89	0.44	1.59	1.48	0.61	0.60	1.10
Sankt Ulrich 65	875.0	43.6	15.3	40.9	0.2	1.90	0.77	0.39	0.48	0.22	0.30	0.72	0.39	1.48	1.36	0.60	0.58	0.66
Sankt Ulrich 92	1050.0	41.9	13.9	44.0	0.1	1.70	0.88	0.54	0.45	0.17	0.37	0.60	0.38	1.97	1.66	0.66	0.62	0.68
Sankt Ulrich 213	812.0	42.2	11.2	46.5	0.1	1.66	1.62	1.03	0.48	0.18	0.34	0.61	0.37	1.74	1.43	0.64	0.59	0.64
Schoenkir. 267	1260.0	36.4	23.6	37.9	2.1	1.21		2.91	0.48	0.18	0.35	0.59	0.38	1.32	1.37	0.57	0.58	0.72
Schoenkir. T12	2709.7	43.5	16.5	39.3	0.7	1.49	0.56	0.38				0.16	0.52	1.70	1.50	0.63	0.60	0.85
Schoenkir. T29a	2725.5	55.6	22.0	21.7	0.6	1.13	0.42	0.36				0.22	0.52	1.57	1.36	0.61	0.58	0.93
Schoenkir. T32	4873.0					1.88	0.20	0.15										
Schoenkir. T38	2892.0	59.8	13.0	26.6	0.7	1.03	0.28	0.28	0.51	0.20	0.29	0.75	0.40	1.29	1.31	0.56	0.57	0.90
Schoenkir. T42	5386.8					1.05	0.13	0.15										
Schoenkir. T62	5119.3					1.31	0.15	0.15										
Schoenkir. T64	2542.0	53.9	16.2	29.0	0.9	1.16	0.28	0.27										
Schoenkir. T69	2815.0	55.9	15.7	25.1	3.3	1.27	0.34	0.26	0.50	0.21	0.29	0.77	0.37	1.38	1.15	0.58	0.53	0.72
Schoenkir. T90a	2590.0	53.1	16.0	30.2	0.7	1.20	0.28	0.25										
Steinberg 11	950.0	41.5	18.4	39.9	0.1	1.57	2.59	1.39	0.49	0.22	0.30	0.69	0.38	1.25	1.02	0.55	0.50	0.43
Stockerau Ost 16	2101.0																	
Urmannsau 1	152.0					0.95	0.73	0.67	0.41	0.23	0.36			2.13	0.78	0.68	0.44	
Urmannsau 1	758.0					0.70	0.53	0.57	0.37	0.32	0.31	1.04	0.39	1.47	0.78	0.60	0.44	0.39
Van Sickle 29	750.0	43.2	22.9	31.9	2.1	1.06		5.90	0.46	0.18	0.35	0.59	0.38	1.63	1.28	0.62	0.56	0.59
Windisch Baum. 1	700.0	48.0	16.1	35.4	0.4	1.64	2.08	1.23	0.52	0.22	0.27	0.82	0.44	1.38	1.00	0.58	0.50	0.77
Windisch Baum. 1	700.0	47.2	17.2	34.0	1.6	1.59	1.96	1.22	0.51	0.19	0.30	0.73	0.34	1.24	0.96	0.55	0.49	0.50

Well	Depth [m ss]	C_{31} Hop S/(S+R)	Ts/ Ts+Tm	C_{29}Ts/ C_{29}Ts+Tm	MPI [-]	DBT/Phen [-]	nC_{17}/ (nC_{17}+nC_{27})	Density [°API]	100x(Tri./ (Tri.+Penta.)Terp.	RSFP [-]	BCR [-]	BBDS
Aderklaa 3	2351					2.30						
Aderklaa 4	2515					2.00		51				
Aderklaa 34	1715	0.48	0.70	0.36	0.72	0.03	0.83	44.6	9.12			0
Bockfliess 1	1177.4	0.60	0.56	0.36	0.73	0.14		20.3				3
Bockfliess 24	1436.2	0.62	0.53	0.32	0.84	0.14		23.3				2
Bockfliess 33	1181.2	0.59	0.56	0.25	0.72	0.14	0.62	19.6				3
Bockfliess 35	1460.6	0.57	0.62	0.33	0.79	0.12	0.63	23.8	10.28			2
Bockfliess 37	1463.4	0.60	0.63	0.41	0.81	0.14	0.58	23.6	12.36			2
Bockfliess 43	1428.7	0.61	0.58	0.35	0.83	0.12		23.8	10.15			2
Bockfliess 205	1627.0	0.57	0.59	0.33	0.86	0.11		24.2				2
Ebenthal 5	1614.4	0.58	0.54	0.35	0.50	0.18	0.77	32.4		0.0495	0.5429	0
Ebenthal 15	1636.0	0.50	0.58	0.25	0.42	0.14	0.79	33.9				0
Ebenthal 17a	1614.0	0.59	0.62	0.31	0.43	0.16	0.79	34.2				0
Ebenthal 20	1614.4	0.53	0.52	0.29	0.47	0.15	0.80	34.3				0
Erdpress 4	1787.5	0.56	0.58	0.33	0.76	0.10	0.84	27		0.0496	0.5319	1
Erdpress 17a	1424.2	0.54	0.53	0.28	0.82	0.08		22.7				2
Erdpress 24	1419.1	0.57	0.61	0.33	0.85	0.10		23.9				2
Gbely 2		0.61	0.41	0.21		0.48			5.45			2
Gbely H6		0.53	0.62	0.26	0.13	0.03	0.97		7.10	0.1669	0.5671	1
Hochleiten 15	737.6	0.60	0.55	0.34	0.84	0.08	0.94	17.7	9.13			4
Hochleiten 24	748.7	0.60	0.50	0.39	0.72	0.04	0.51	18.6	10.99			4
Hochleiten 31	982.0	0.54	0.67	0.35	0.81	0.08		23	9.70			2
Hochleiten 60	759.3	0.60	0.54	0.29	0.76	0.05		18.6	9.05			3
Hochleiten 65	851.1	0.60	0.61	0.31	0.97	0.09		19.4	9.37			3
Hochleiten 66	911.3	0.61	0.49	0.33	1.73	0.34		20.4	14.52			3
Hochleiten 67	786.4	0.61	0.60	0.39	1.07	0.10		19.8	12.59			3
Hodonin 1		0.59	0.57	0.38		0.55			5.95			4
Hodonin 3		0.61	0.55	0.32	0.47	0.06			6.89			1
Hodonin 4		0.57	0.51	0.28	0.89	0.06	0.91		10.23			1
Hoeflein 6	2663.0							41.2				0
Hoeflein 9	2633.6	0.60	0.54	0.39	0.81	0.19	0.00	55.0			0.5500	
Hoeflein 9	2685.0							36.1				0
Hoeflein 12	2670.3	0.61	0.66	0.25	0.73	0.17	0.01	56.2				
HRPD 42	1412.4	0.61	0.64	0.35	0.79	0.06	0.54	23.1	11.65	0.0807	0.5840	2
Holic 4		0.54	0.55	0.20	0.80	0.09	0.85		7.96	0.0813	0.5519	0
Kierling 1	60.0	0.61	0.66	0.43	0.44	0.07	0.82		11.90	0.0565	0.5317	0
Kierling 2		0.52	0.66	0.50	0.45	0.16	0.82		10.03			0
Klement 1	3539.0				0.58			47				0
Lanzhot 15		0.59	0.52	0.26	0.73	0.22	0.78		10.62			0
Lanzhot 30		0.58	0.48	0.28	0.87	0.20	0.72		10.07	0.0944	0.5612	0
Mank 1	157.0	0.52	0.33	0.15	0.60	0.04	0.97					
Matzen 91	1464.0	0.59	0.59	0.36	0.53	0.04		24	7.87			2
Matzen 115	1472.0	0.55	0.58	0.34	0.48	0.02		24.4	5.82			2

Well	Depth [m ss]	C_{31} Hop S/(S+R)	Ts/ Ts+Tm	C_{29}Ts/ C_{29}Ts+Tm	MPI [-]	DBT/Phen [-]	nC_{17}/ (nC_{17}+nC_{27})	Density [°API]	100x(Tri./ (Tri.+Penta.)Terp.	RSFP [-]	BCR [-]	BBDS
Matzen 116	1449.0				0.63			23.9				2
Matzen 286	1467.0	0.53	0.61	0.33	0.61	0.02		24.4	7.03			2
Matzen 322	1458.0							24.1				
Matzen 390	1139.7	0.56	0.52	0.33	0.82	0.15		20.2				3
Matzen H 703b	1523.0				0.60			24.3				2
Maustrenk 29	895.0	0.58	0.47	0.20	0.66	0.03	0.64	25.0	4.87	0.2271	0.5774	1.5
Mühlberg 15	1480.0	0.56	0.46	0.32		0.87	0.83	27.8	8.06			2
Neusiedl 1	1180.0	0.60	0.54	0.28	0.61	0.02	0.75	32.6	6.57			1
Neusiedl 3	1100.0	0.62	0.59	0.29	0.56	0.02	0.69	32	7.72	0.1455	0.5740	1
Pirawarth U10	707.0	0.53	0.66	0.43	0.59	0.05	0.76	37.3	7.91	0.0612	0.5704	0
Prottes 26	1140.4	0.59	0.58	0.33	0.82	0.15		19.5				3
Prottes 27	1150.0	0.62	0.54	0.30	0.58	0.04		20	7.14	0.0632	0.5611	3
Prottes 29	1152.0	0.60	0.57	0.31	0.59	0.08		20	7.07			3
Prottes 98	1157.6	0.62	0.55	0.31	0.82	0.13		19		0.0708	0.5551	3
Prottes 104	1156.8	0.59	0.52	0.29	0.81	0.10		19.7				3
Prottes T S 3b	2653.0				0.98	0.13		33.7		0.0776	0.5544	1
Rabensburg 11	1742.0	0.52	0.45	0.27		0.93	0.91	41.5	10.42	0.0752	0.5576	1
Rabensburg N3	1718.0	0.60	0.36	0.23	0.51	0.05	0.63	37.6	4.80			1
Rabensburg U4		0.59	0.36	0.17	0.57	0.03	0.67		5.64			1
Roseldorf 2	1383.0	0.59	0.68	0.41	0.67	0.03		36.6	9.54	0.0671	0.5767	0
Roseldorf 2	1383.0	0.53	0.68	0.49	0.80	0.04	0.71	36.6	8.35			0
Sankt Ulrich 65	875.0	0.59	0.57	0.35	0.73	0.07	0.80	29.8	7.16	0.0426	0.5298	1
Sankt Ulrich 92	1050.0	0.59	0.57	0.27	0.82	0.02	0.83	30.3	7.30			1
Sankt Ulrich 213	812.0	0.58	0.55	0.32		0.93	0.94	29.3	6.42			1.5
Schoenkir. 267	1260.0	0.59	0.53	0.30	0.80	0.04		20.1	8.54	0.1040	0.5737	3
Schoenkir. T12	2709.7	0.63	0.61	0.31	0.78	0.28	0.73	29.2	11.21	0.0601	0.5640	0
Schoenkir. T29a	2725.5	0.63	0.63	0.40	0.76	0.33	0.72	30.3	13.46	0.0866	0.5769	1
Schoenkir. T32	4873.0				1.08	1.77	1.00	41				
Schoenkir. T38	2892.0	0.60	0.54	0.43	0.86	0.28	0.73	29.1	9.86	0.0557	0.5607	1
Schoenkir. T42	5386.8				1.09	1.88	0.99	42.2				
Schoenkir. T62	5119.3				0.99	1.79	1.00	41				
Schoenkir. T 64	2542.0				0.58	0.44		29				1
Schoenkir. T69	2815.0	0.56	0.63	0.42	0.78	0.39	0.75	29.5	6.50			1
Schoenkir. T 90a	2590.0				0.65	0.50		28.9				1
Steinberg 11	950.0	0.57	0.53	0.33	0.54	0.06	0.66	27	4.99	0.0452	0.5943	1.5
Stockerau Ost 16	2101.0							62.4				
Urmannsau 1	152.0	0.45	0.63		1.00		0.82					
Urmannsau 1	758.0	0.58	0.57	0.17	0.48		0.86					
Van Sickle 29	750.0	0.56	0.56	0.30	0.30	0.24		20.3	5.24	0.0345	0.5550	3
Windisch Baum. 1	700.0	0.56	0.51	0.28	0.72	0.11	0.89	32	15.13	0.0658	0.5469	1.5
Windisch Baum. 1	700.0	0.54	0.48	0.26				32	7.04			1.5

Appendix VIII

Chromatograms

Rocks

Aliphatic Fraction

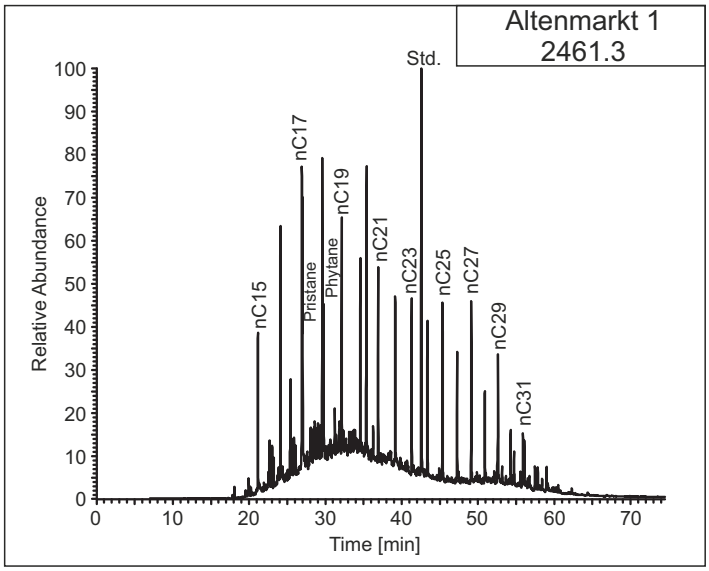
Altenmarkt 1
2461.3
Relative Abundance
Time [min]
nC15
Pristane
nC17
Phytane
nC19
nC21
nC23
Std.
nC25
nC27
nC29
nC31

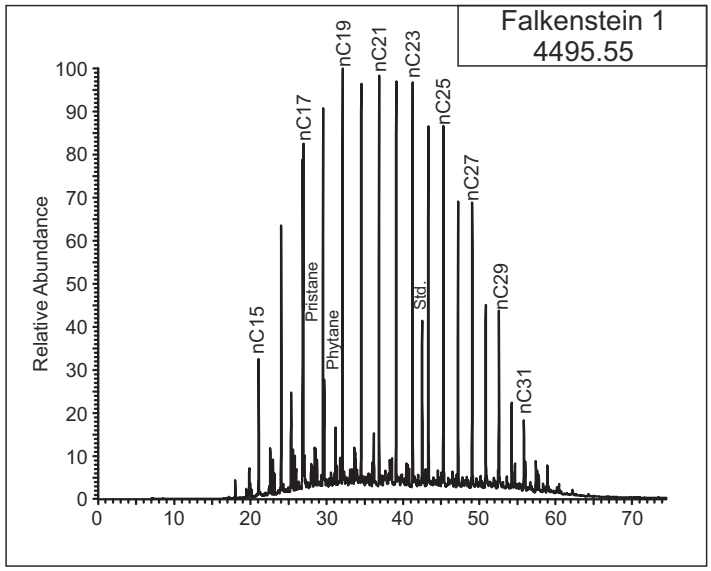
Falkenstein 1
4495.55
Relative Abundance
nC15
nC17
Pristane
Phytane
nC19
nC21
nC23
Std.
nC25
nC27
nC29
nC31

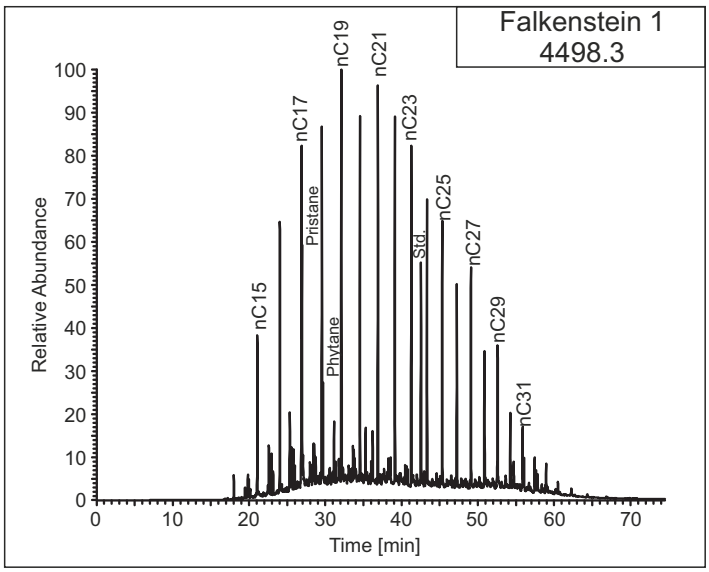
Falkenstein 1
4498.3
Relative Abundance
Time [min]
nC15
nC17
Pristane
Phytane
nC19
nC21
nC23
Std.
nC25
nC27
nC29
nC31

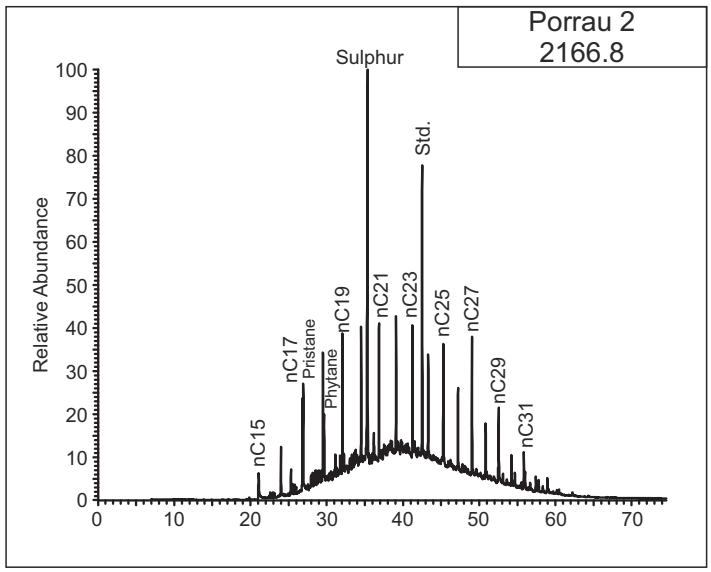
Porrau 2
2166.8
Relative Abundance
Sulphur
Std.
nC15
nC17
Pristane
Phytane
nC19
nC21
nC23
nC25
nC27
nC29
nC31

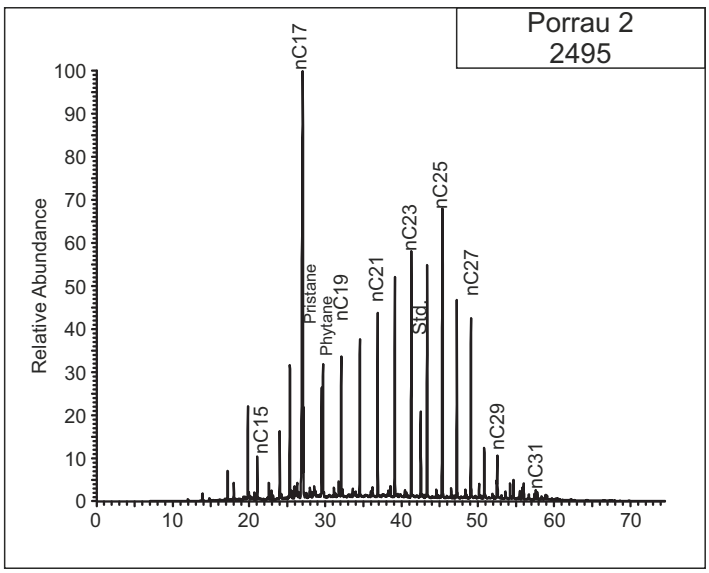
Porrau 2
2495
Relative Abundance
nC15
nC17
Pristane
Phytane
nC19
nC21
Std.
nC23
nC25
nC27
nC29
nC31

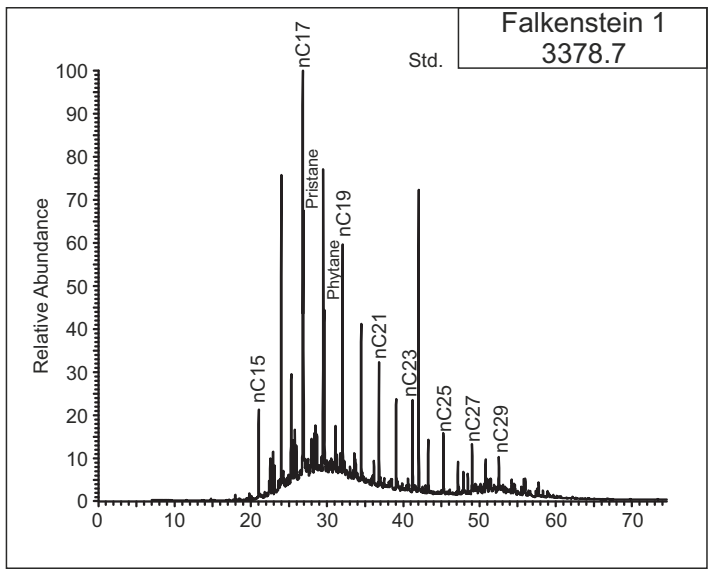
Falkenstein 1
3378.7
Relative Abundance
Std.
nC15
nC17
Pristane
Phytane
nC19
nC21
nC23
nC25
nC27
nC29

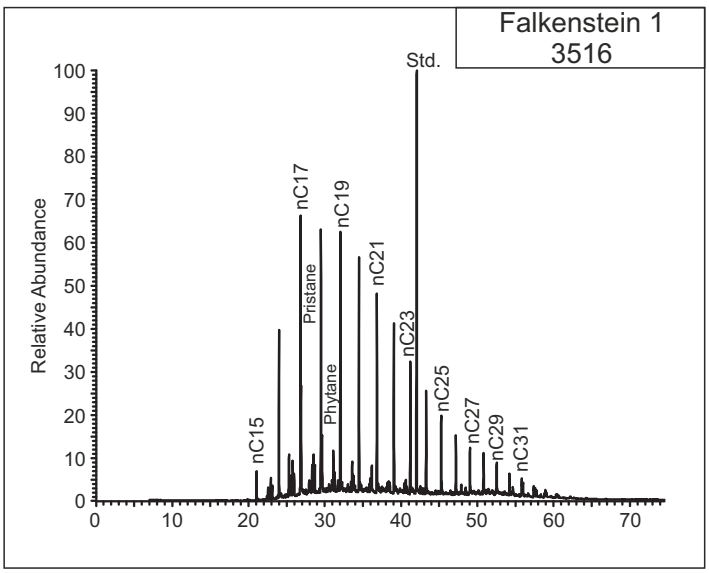
Falkenstein 1
3516
Relative Abundance
Std.
nC15
nC17
Pristane
nC19
Phytane
nC21
nC23
nC25
nC27
nC29
nC31

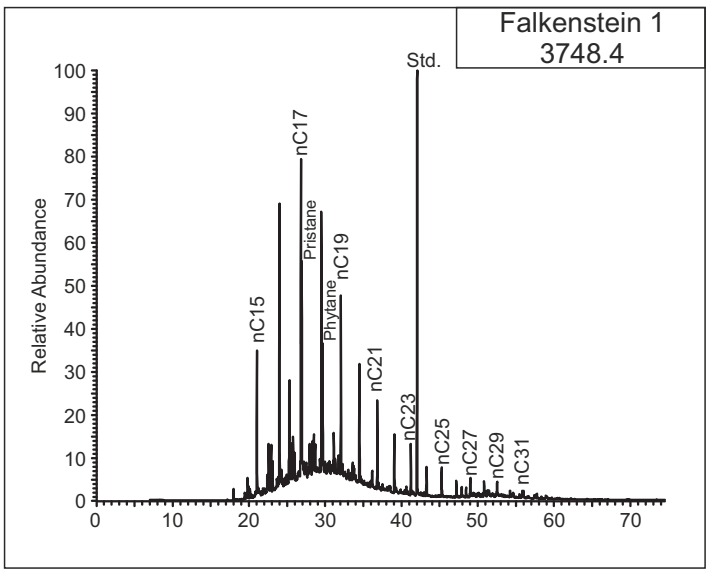
Falkenstein 1
3748.4
Relative Abundance
Std.
nC15
nC17
Pristane
nC19
Phytane
nC21
nC23
nC25
nC27
nC29
nC31

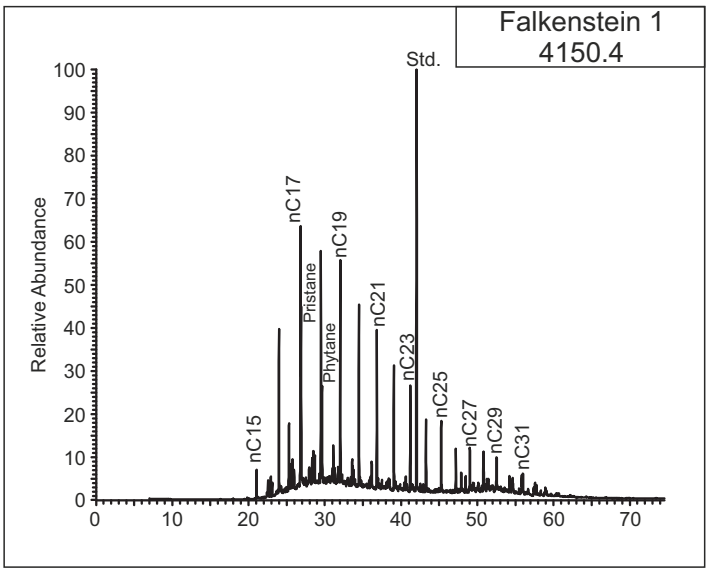
Falkenstein 1
4150.4
Relative Abundance
Std.
nC15
nC17
Pristane
nC19
Phytane
nC21
nC23
nC25
nC27
nC29
nC31

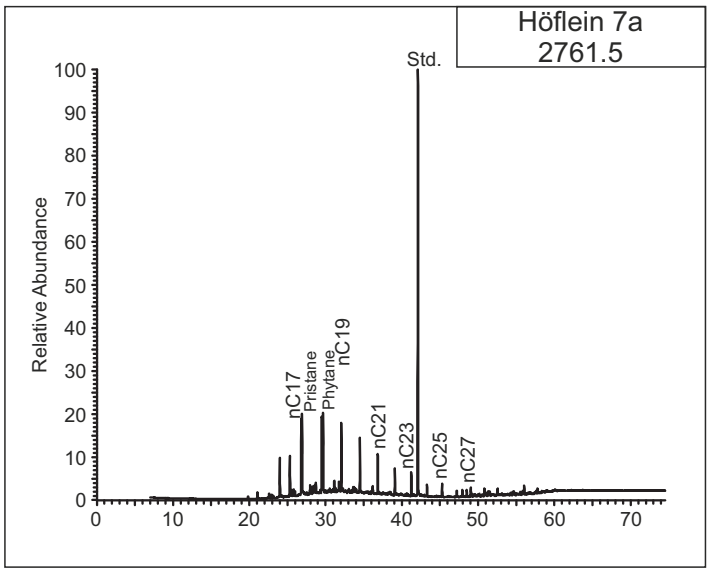
Höflein 7a
2761.5
Relative Abundance
Std.
nC17
Pristane
Phytane
nC19
nC21
nC23
nC25
nC27

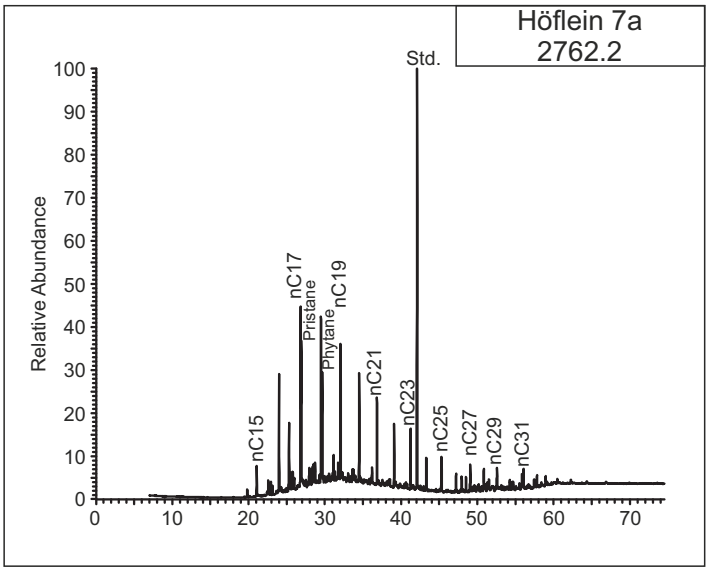
Höflein 7a
2762.2
Relative Abundance
Std.
nC15
nC17
Pristane
Phytane
nC19
nC21
nC23
nC25
nC27
nC29
nC31

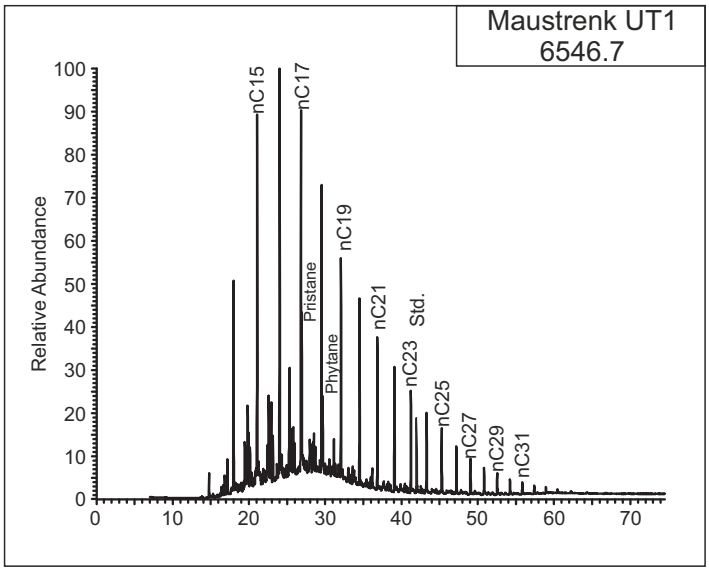
Maustrenk UT1
6546.7
Relative Abundance
nC15
nC17
Pristane
nC19
Phytane
nC21
Std.
nC23
nC25
nC27
nC29
nC31

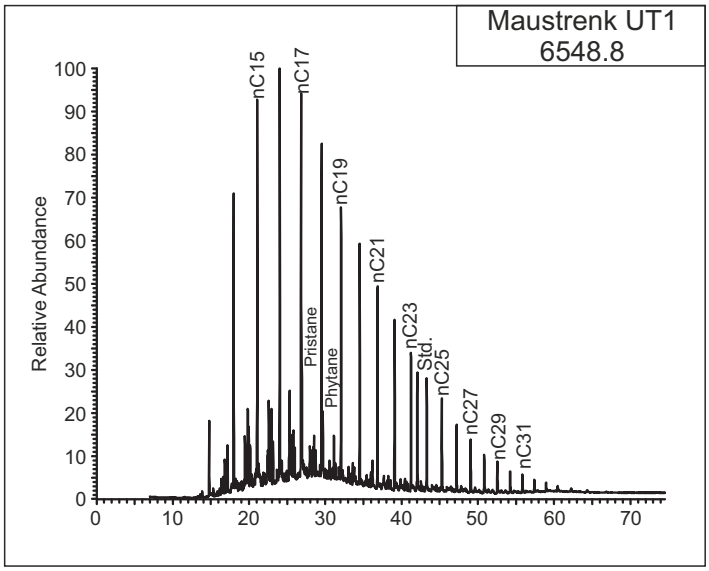
Maustrenk UT1
6548.8
Relative Abundance
nC15
nC17
Pristane
nC19
Phytane
nC21
nC23
Std.
nC25
nC27
nC29
nC31

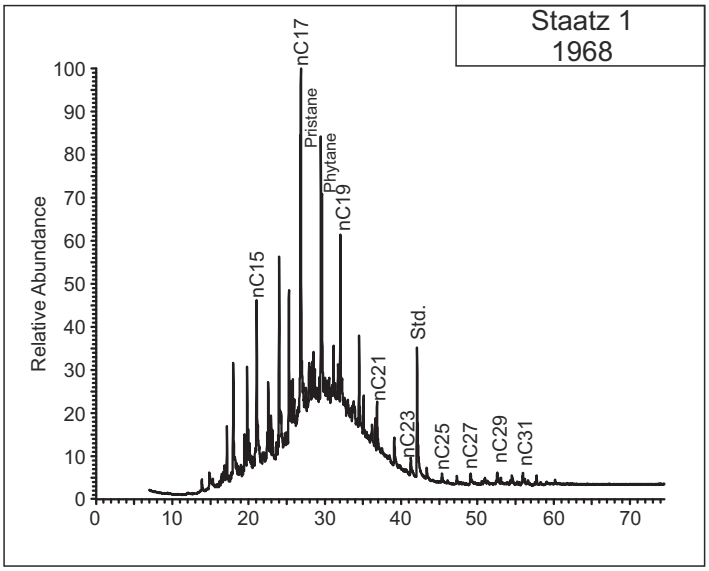
Staatz 1
1968
Relative Abundance
nC15
nC17
Pristane
Phytane
nC19
nC21
nC23
Std.
nC25
nC27
nC29
nC31

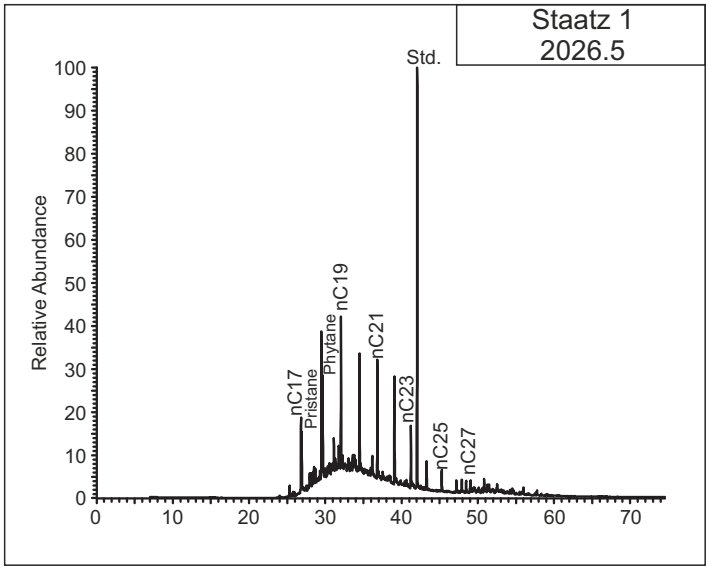
Staatz 1
2026.5
Relative Abundance
nC17
Pristane
Phytane
nC19
nC21
nC23
Std.
nC25
nC27

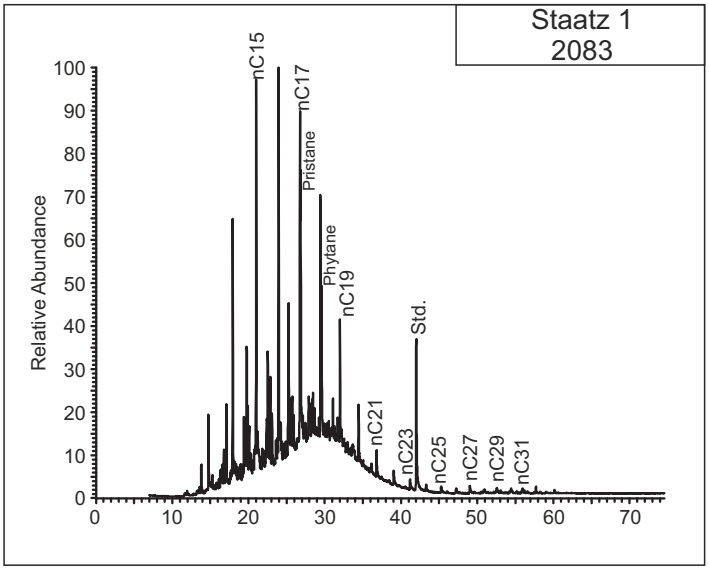
Staatz 1
2083
Relative Abundance
nC15
nC17
Pristane
Phytane
nC19
nC21
nC23
Std.
nC25
nC27
nC29
nC31

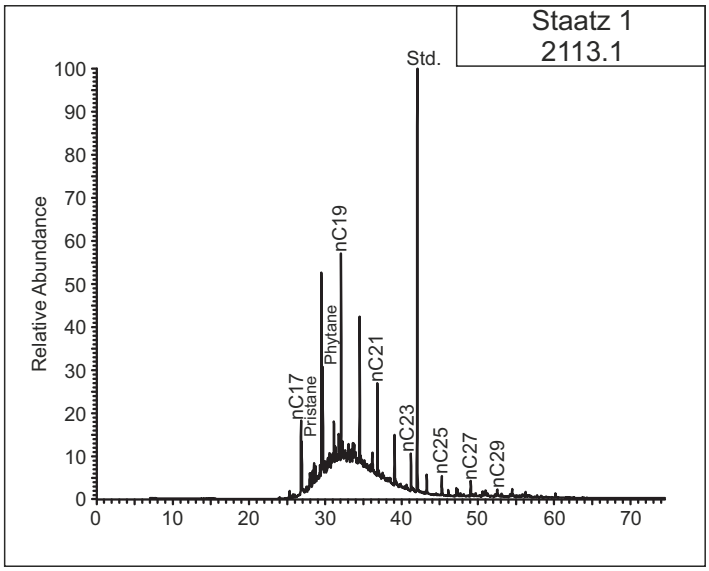
Staatz 1
2113.1
Relative Abundance
nC17
Pristane
Phytane
nC19
nC21
nC23
Std.
nC25
nC27
nC29

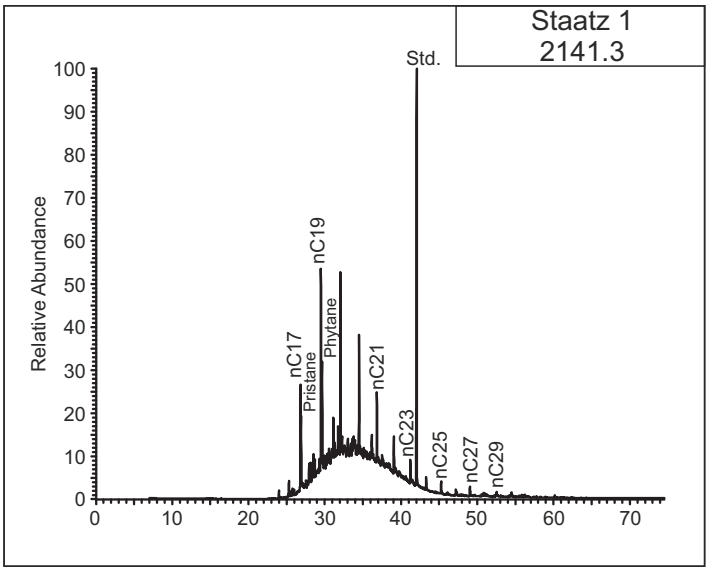
Staatz 1
2141.3
Relative Abundance
nC17
Pristane
Phytane
nC19
nC21
nC23
Std.
nC25
nC27
nC29

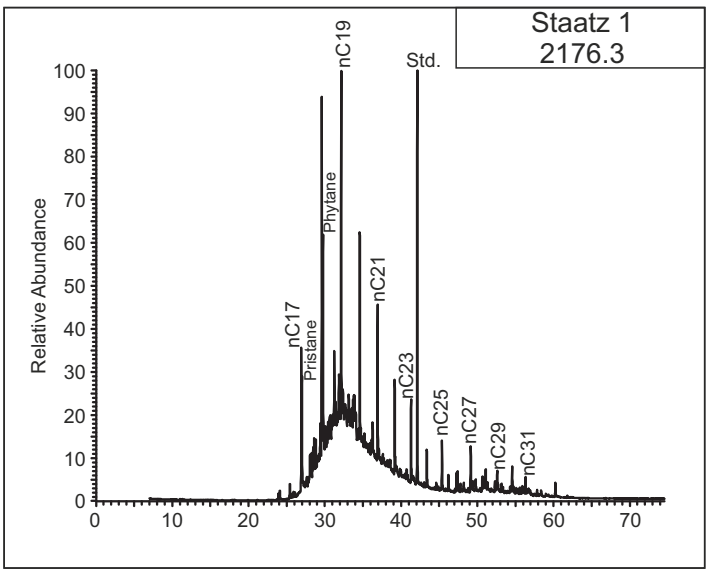
Staatz 1
2176.3
Relative Abundance
nC17
Pristane
Phytane
nC19
nC21
nC23
Std.
nC25
nC27
nC29
nC31

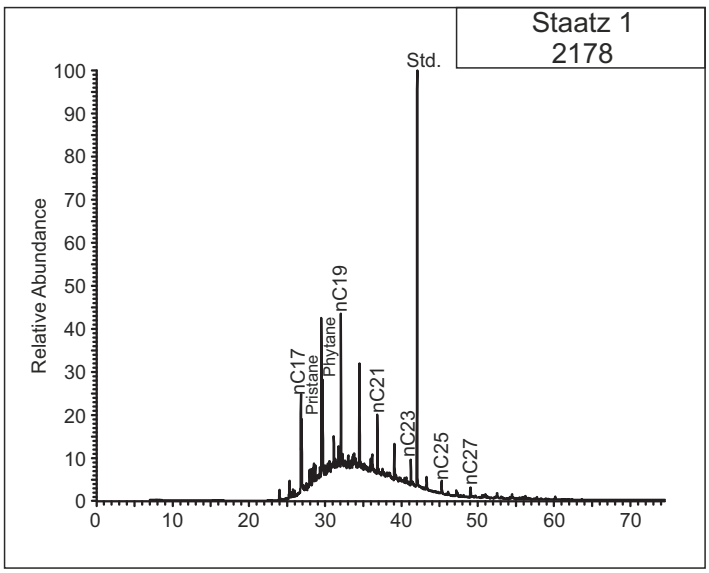
Staatz 1
2178
Relative Abundance
nC17
Pristane
Phytane
nC19
nC21
nC23
Std.
nC25
nC27

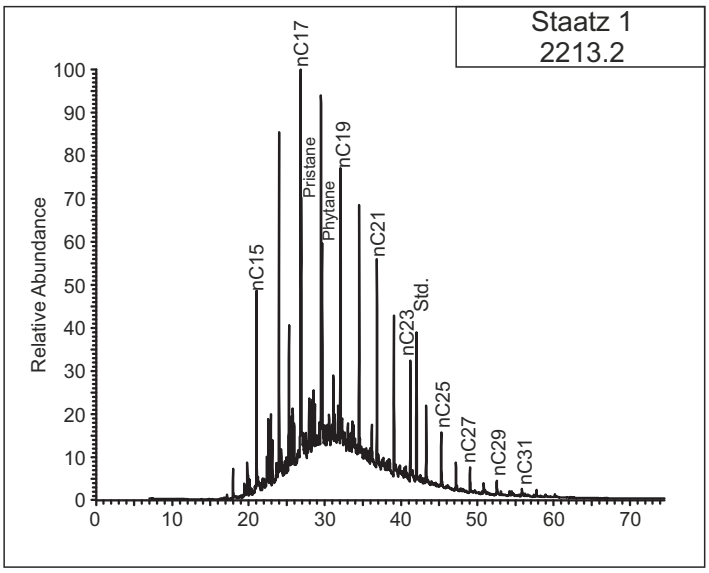
Staatz 1
2213.2
Relative Abundance
nC15
nC17
Pristane
Phytane
nC19
nC21
nC23
Std.
nC25
nC27
nC29
nC31

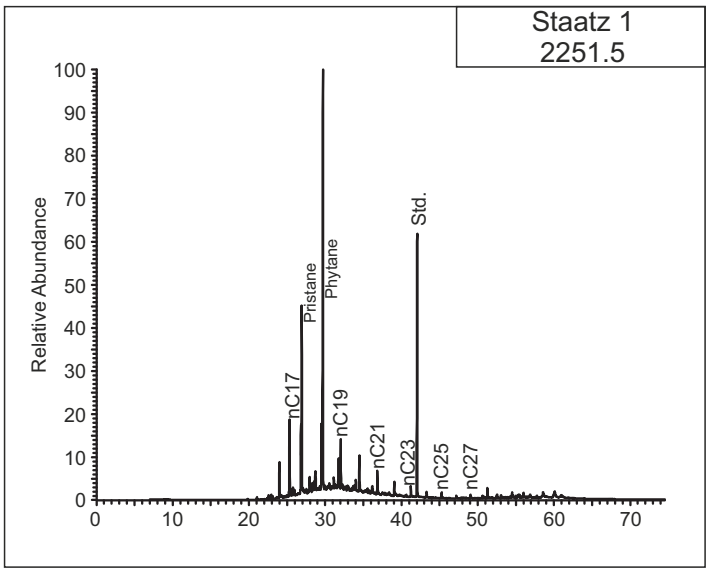
Staatz 1
2251.5
Relative Abundance
nC17
Pristane
Phytane
Std.
nC19
nC21
nC23
nC25
nC27

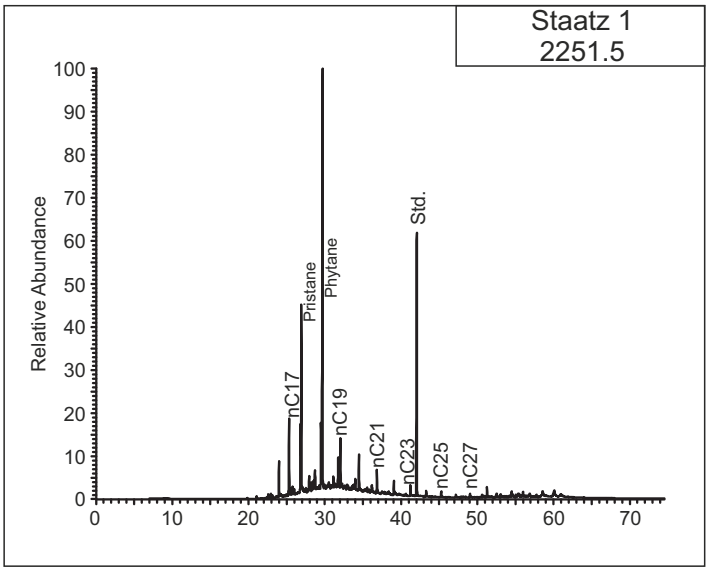
Staatz 1
2251.5
Relative Abundance
nC17
Pristane
Phytane
Std.
nC19
nC21
nC23
nC25
nC27

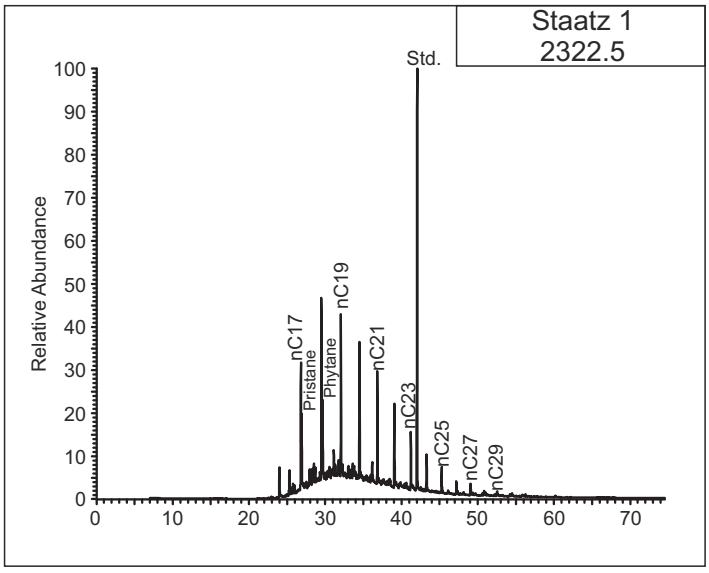
Staatz 1
2322.5
Relative Abundance
nC17
Pristane
Phytane
nC19
Std.
nC21
nC23
nC25
nC27
nC29

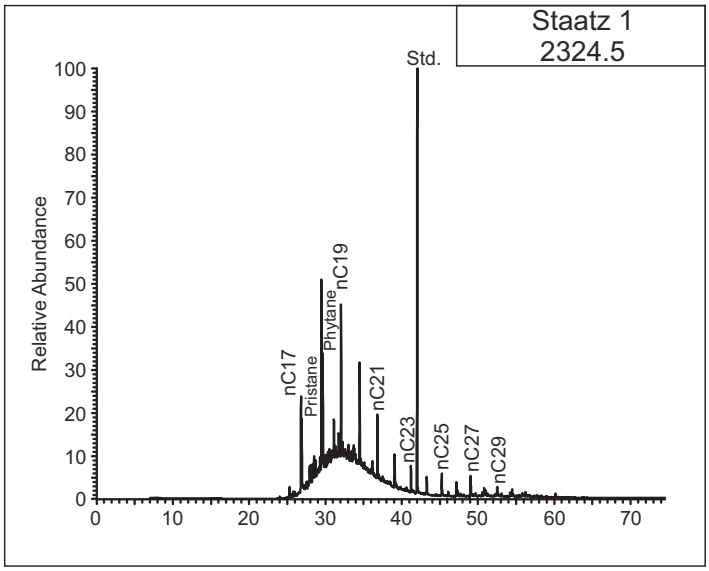
Staatz 1
2324.5
Relative Abundance
Std.
nC17
Pristane
Phytane
nC19
nC21
nC23
nC25
nC27
nC29

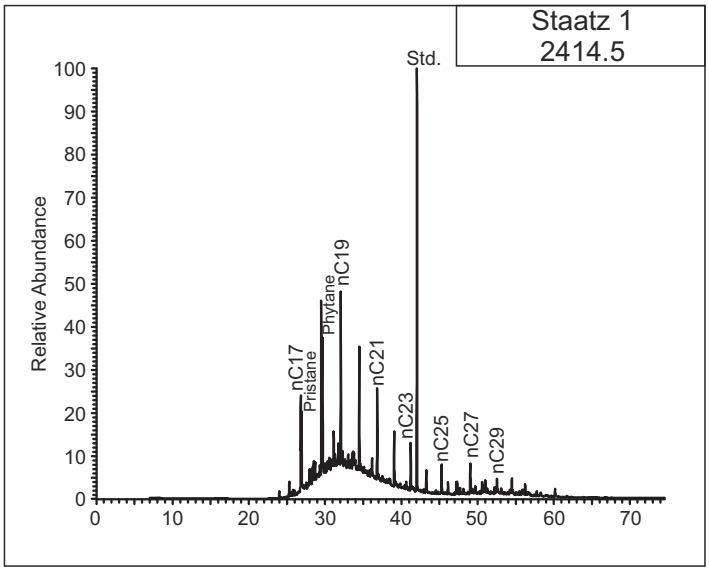
Staatz 1
2414.5
Relative Abundance
Std.
nC17
Pristane
Phytane
nC19
nC21
nC23
nC25
nC27
nC29

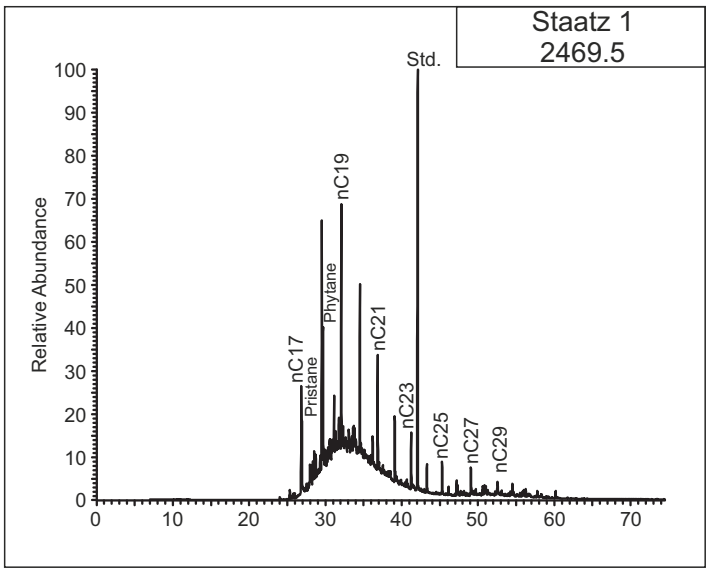
Staatz 1
2469.5
Relative Abundance
Std.
nC17
Pristane
Phytane
nC19
nC21
nC23
nC25
nC27
nC29

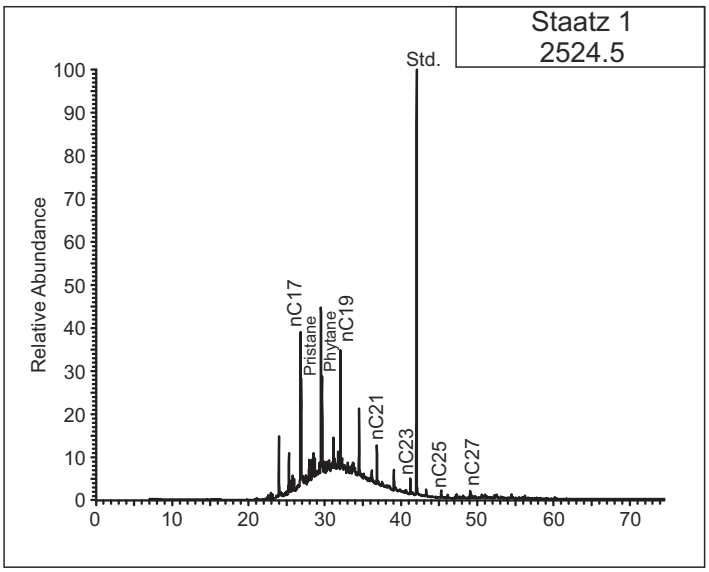
Staatz 1
2524.5
Relative Abundance
Std.
nC17
Pristane
Phytane
nC19
nC21
nC23
nC25
nC27

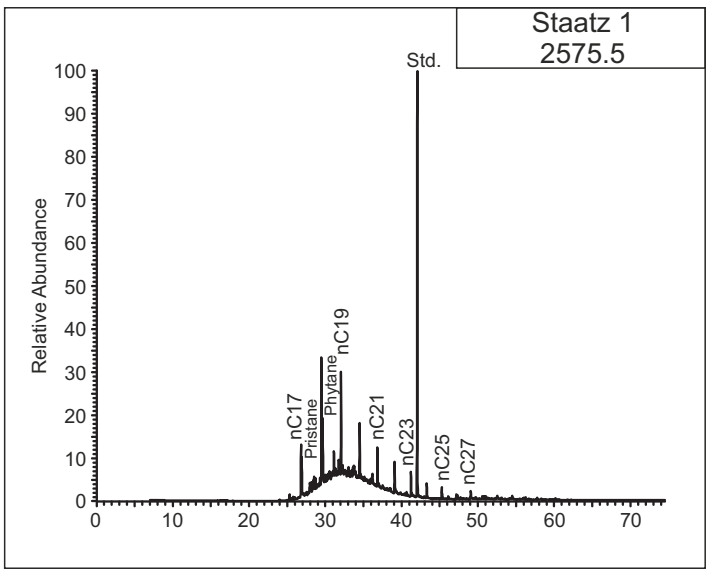
Staatz 1
2575.5
Relative Abundance
Std.
nC17
Pristane
Phytane
nC19
nC21
nC23
nC25
nC27

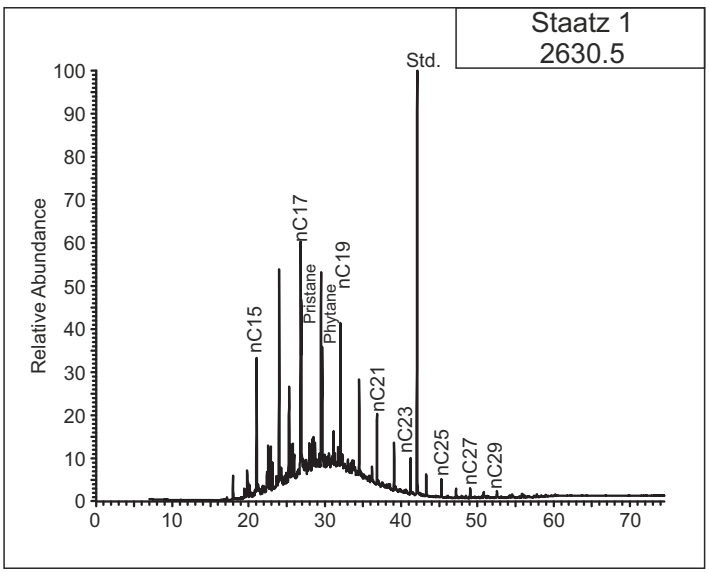
Staatz 1
2630.5
Relative Abundance
Std.
nC15
nC17
Pristane
Phytane
nC19
nC21
nC23
nC25
nC27
nC29

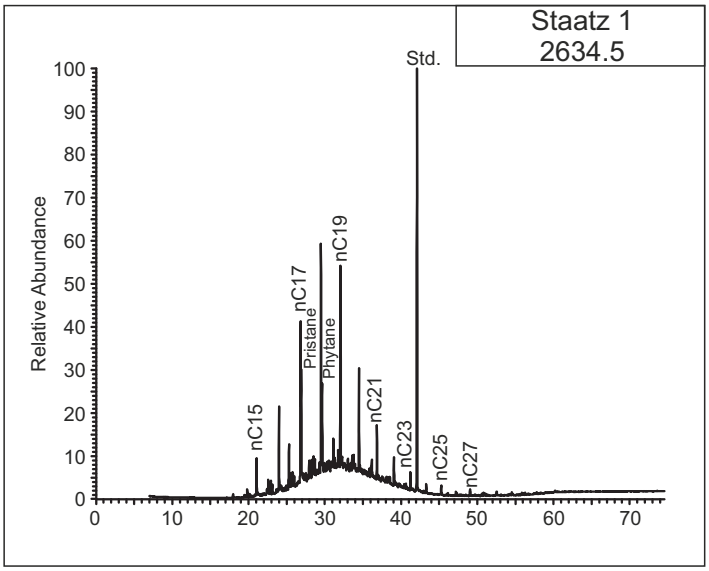
Staatz 1
2634.5
Relative Abundance
nC15
nC17
Pristane
Phytane
nC19
nC21
nC23
Std.
nC25
nC27

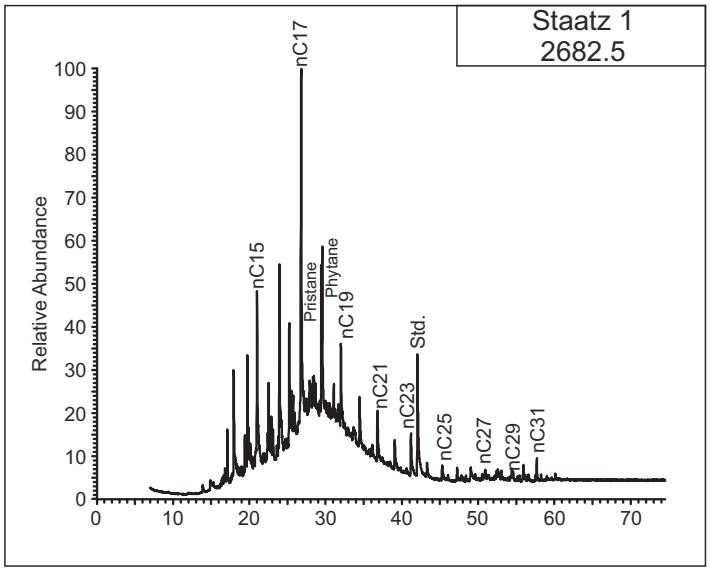
Staatz 1
2682.5
Relative Abundance
nC15
nC17
Pristane
Phytane
nC19
nC21
nC23
Std.
nC25
nC27
nC29
nC31

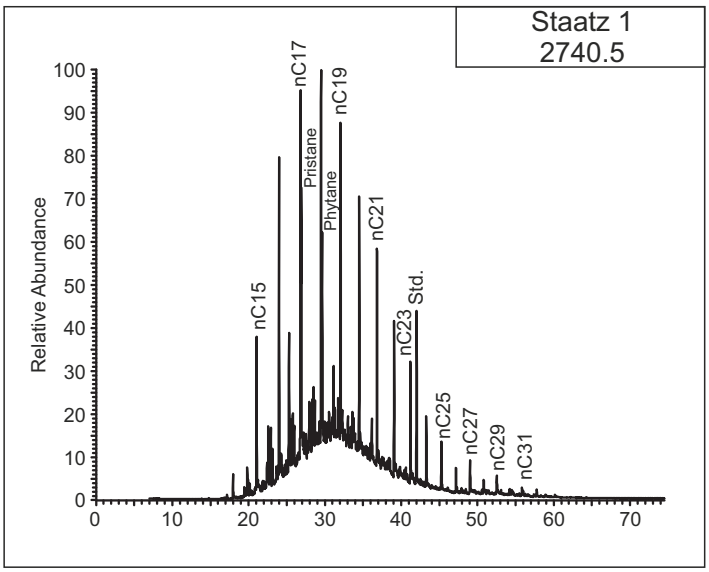
Staatz 1
2740.5
Relative Abundance
nC15
nC17
Pristane
Phytane
nC19
nC21
nC23
Std.
nC25
nC27
nC29
nC31

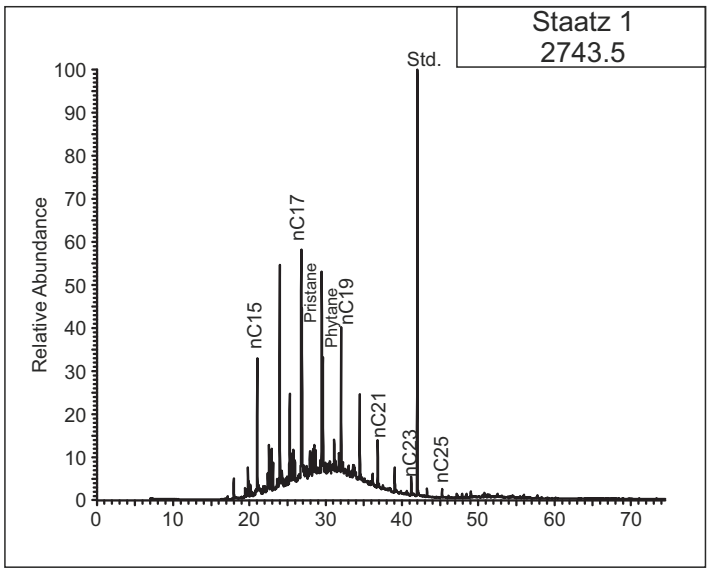
Staatz 1
2743.5
Relative Abundance
nC15
nC17
Pristane
Phytane
nC19
nC21
nC23
Std.
nC25

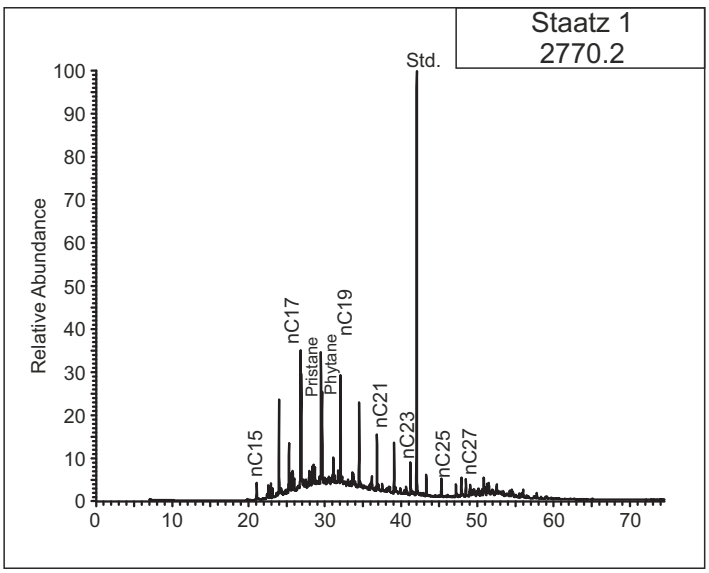
Staatz 1
2770.2
Relative Abundance
nC15
nC17
Pristane
Phytane
nC19
nC21
nC23
Std.
nC25
nC27

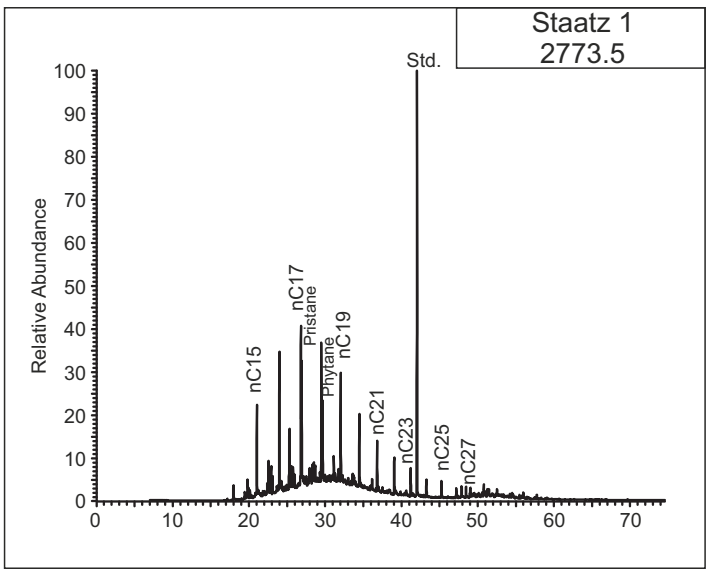
Staatz 1
2773.5
Relative Abundance
nC15
nC17
Pristane
Phytane
nC19
nC21
nC23
Std.
nC25
nC27

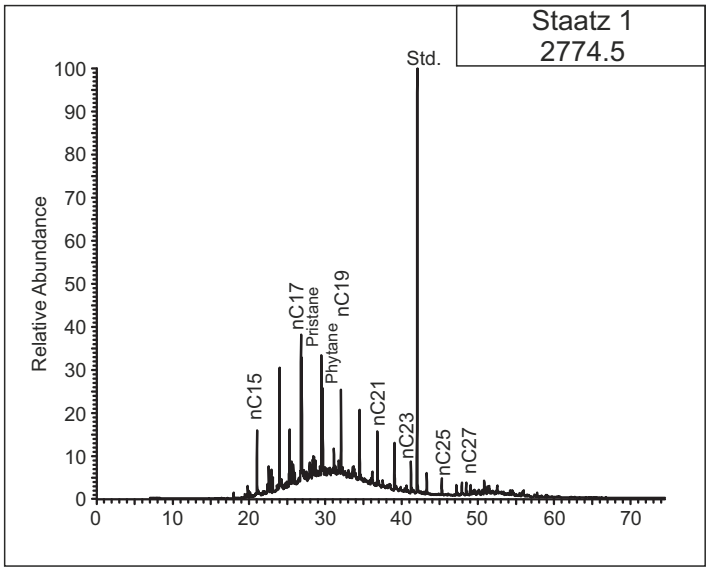
Staatz 1
2774.5
Relative Abundance
nC15
nC17
Pristane
Phytane
nC19
nC21
nC23
Std.
nC25
nC27

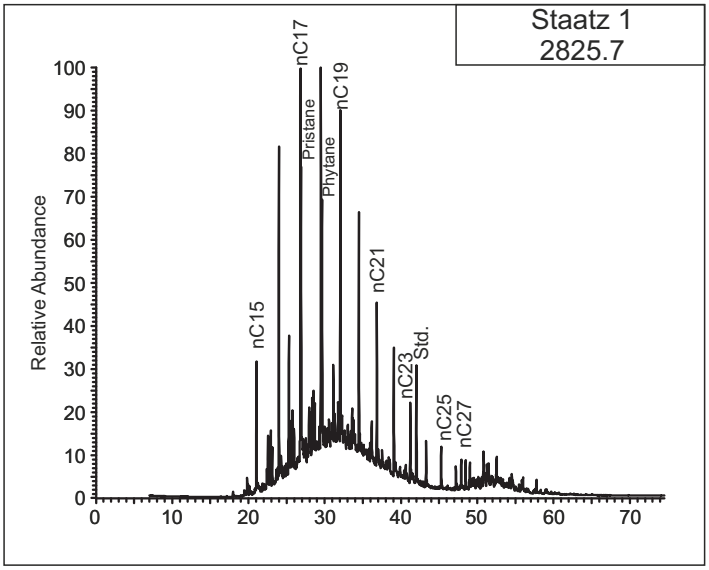
Staatz 1
2825.7
Relative Abundance
nC15
nC17
Pristane
Phytane
nC19
nC21
nC23
Std.
nC25
nC27

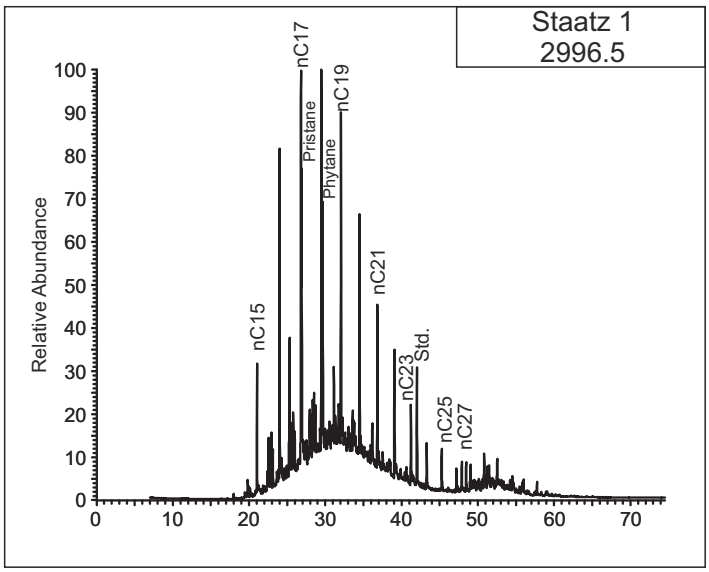
Staatz 1
2996.5
Relative Abundance
nC15
nC17
Pristane
Phytane
nC19
nC21
nC23
Std.
nC25
nC27

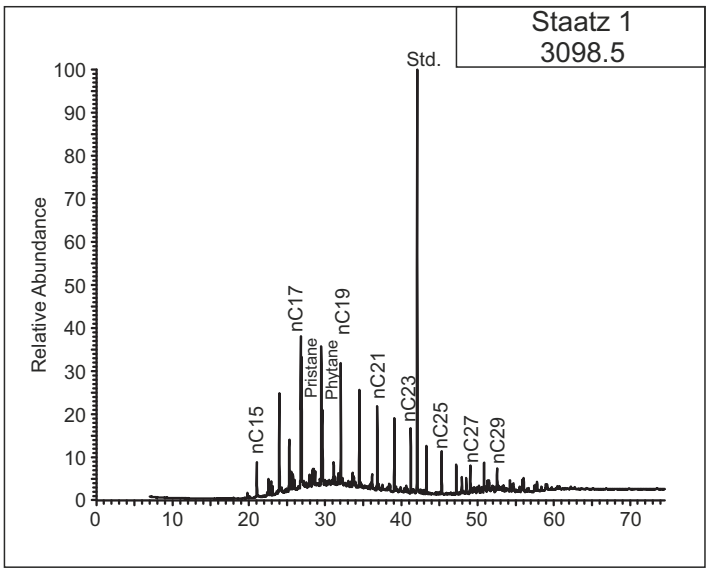
Staatz 1
3098.5
Relative Abundance
nC15
nC17
Pristane
Phytane
nC19
nC21
nC23
Std.
nC25
nC27
nC29

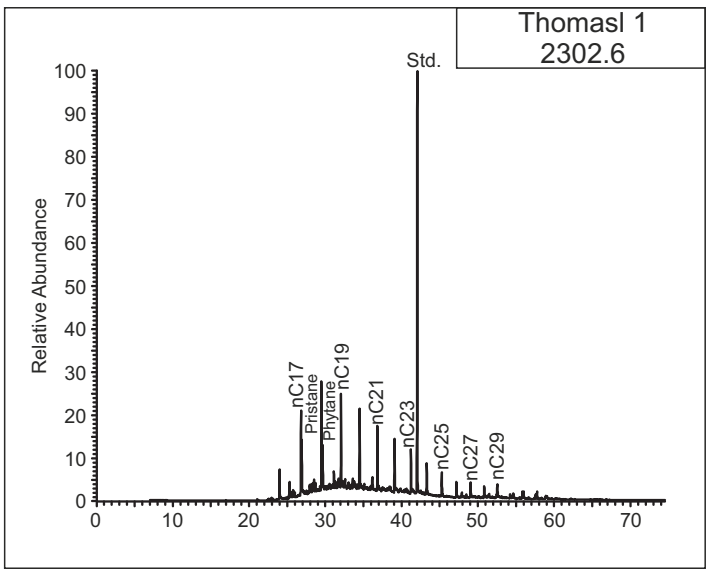
Thomasl 1
2302.6
Relative Abundance
nC17
Pristane
Phytane
nC19
nC21
nC23
Std.
nC25
nC27
nC29

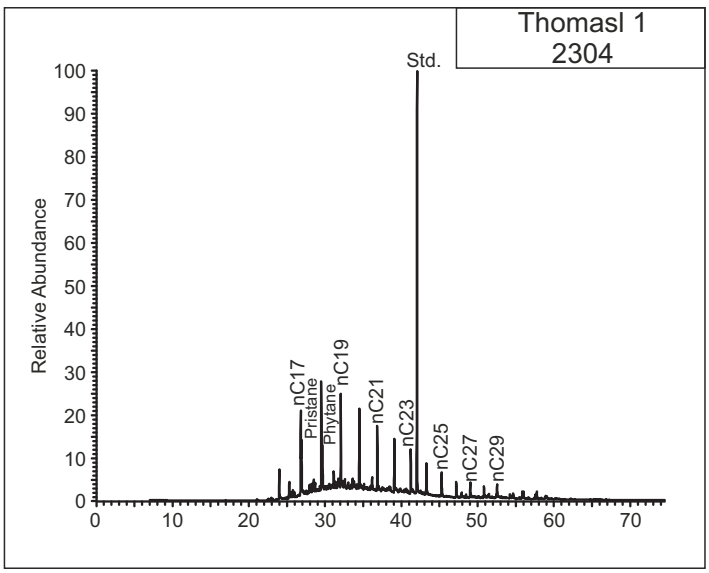
Thomasl 1
2304
Relative Abundance
nC17
Pristane
Phytane
nC19
nC21
nC23
Std.
nC25
nC27
nC29

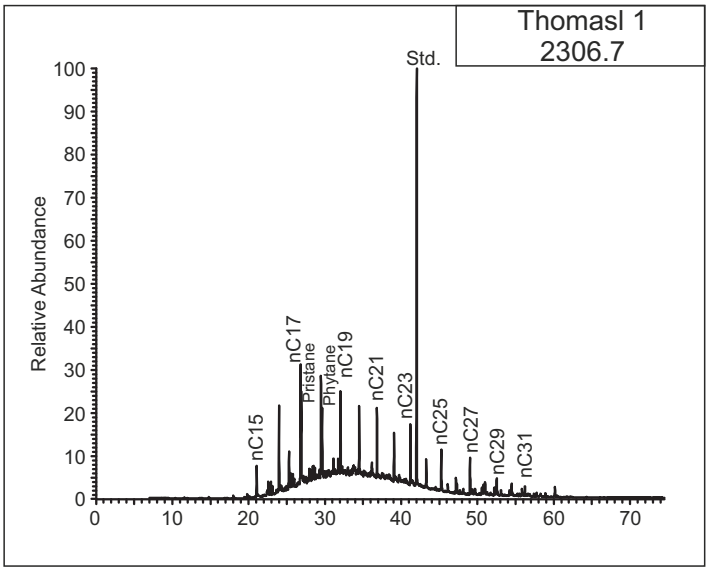
Thomasl 1
2306.7
Relative Abundance
nC15
nC17
Pristane
Phytane
nC19
nC21
nC23
Std.
nC25
nC27
nC29
nC31

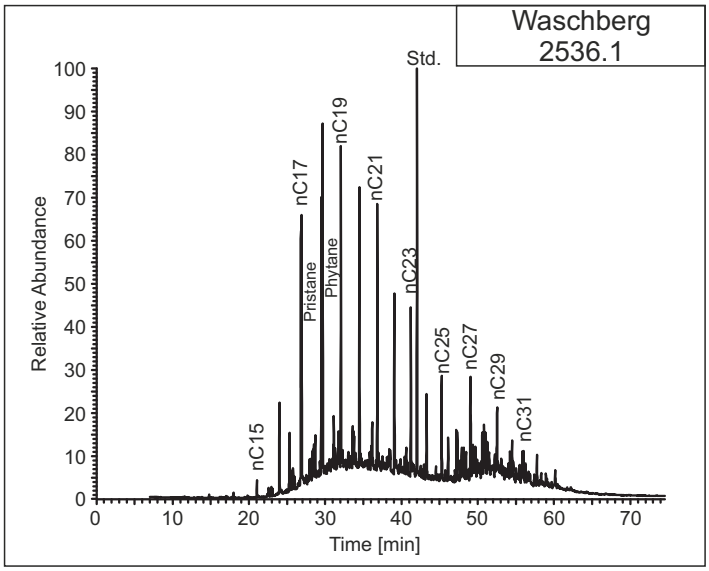
Waschberg
2536.1
Relative Abundance
nC15
nC17
Pristane
Phytane
nC19
nC21
nC23
Std.
nC25
nC27
nC29
nC31
Time [min]

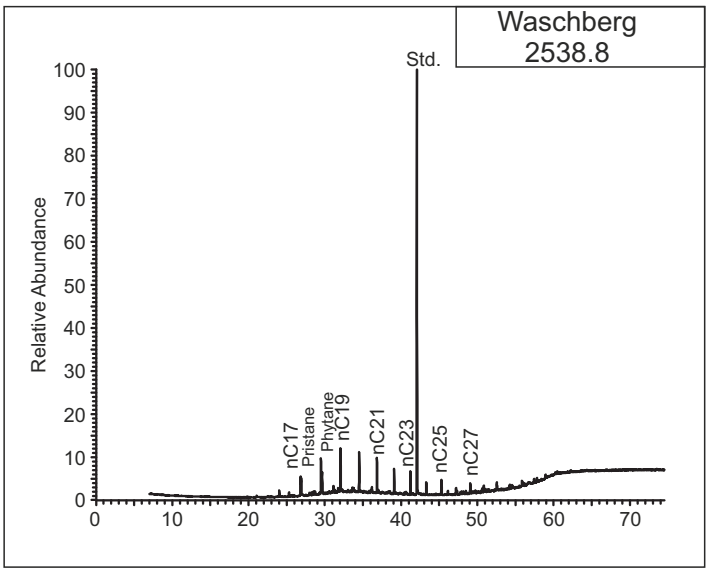
Waschberg
2538.8
Relative Abundance
nC17
Pristane
Phytane
nC19
nC21
nC23
Std.
nC25
nC27

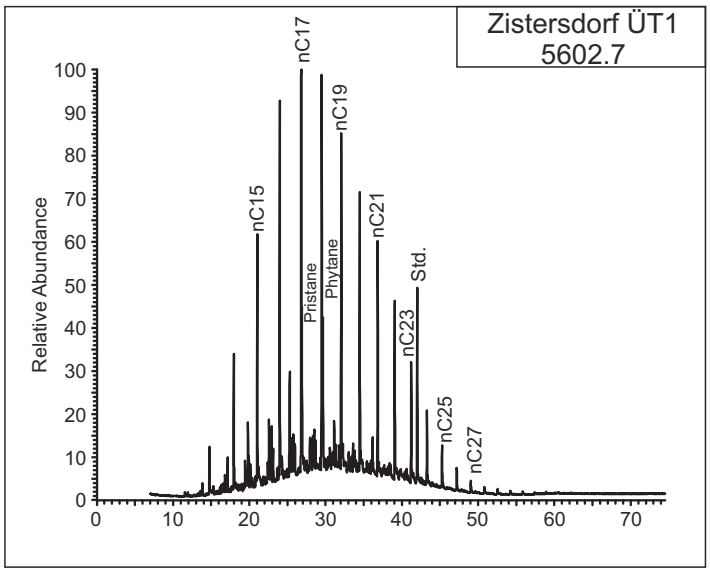
Zistersdorf ÜT1
5602.7
Relative Abundance
nC15
nC17
Pristane
Phytane
nC19
nC21
nC23
Std.
nC25
nC27

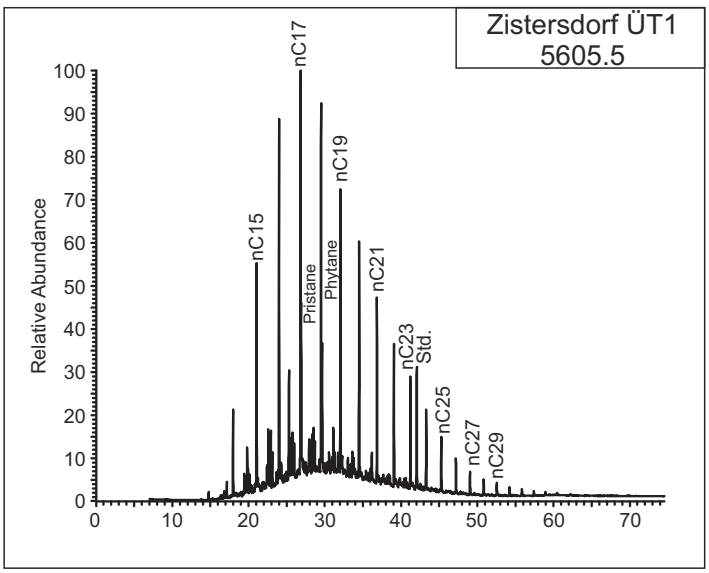
Zistersdorf ÜT1
5605.5
Relative Abundance
nC15
nC17
Pristane
Phytane
nC19
nC21
nC23
Std.
nC25
nC27
nC29

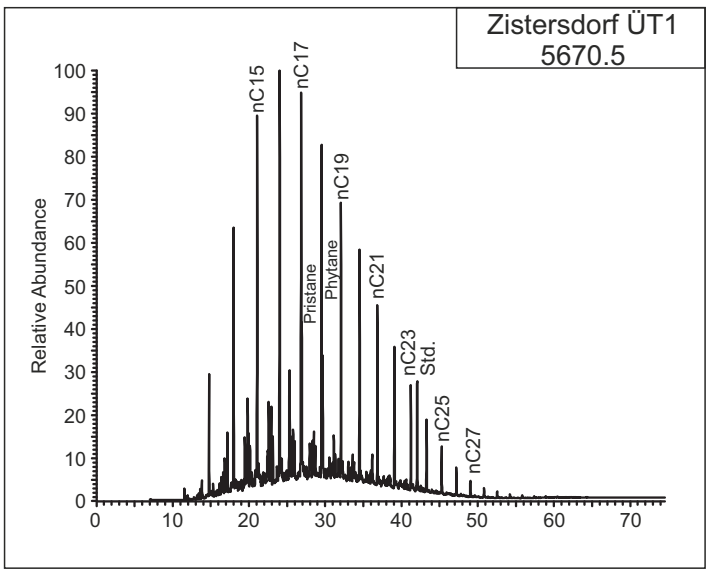
Zistersdorf ÜT1
5670.5
Relative Abundance
nC15
nC17
Pristane
Phytane
nC19
nC21
nC23
Std.
nC25
nC27

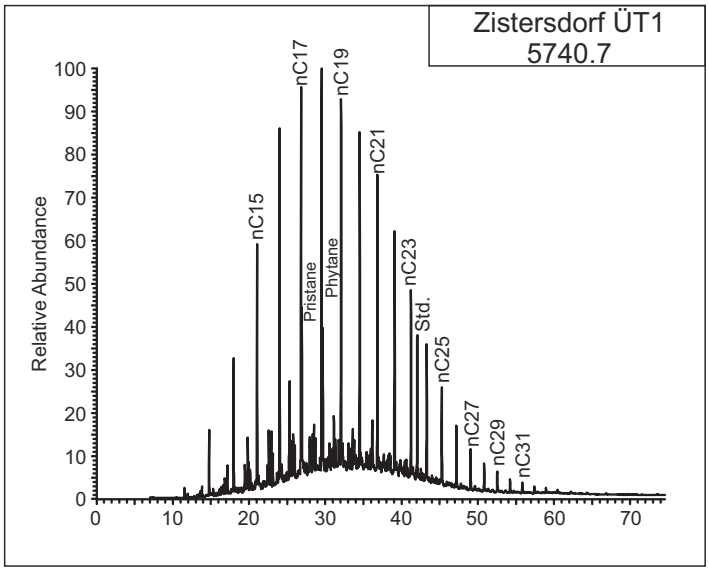
Zistersdorf ÜT1
5740.7
Relative Abundance
nC15
nC17
Pristane
Phytane
nC19
nC21
nC23
Std.
nC25
nC27
nC29
nC31

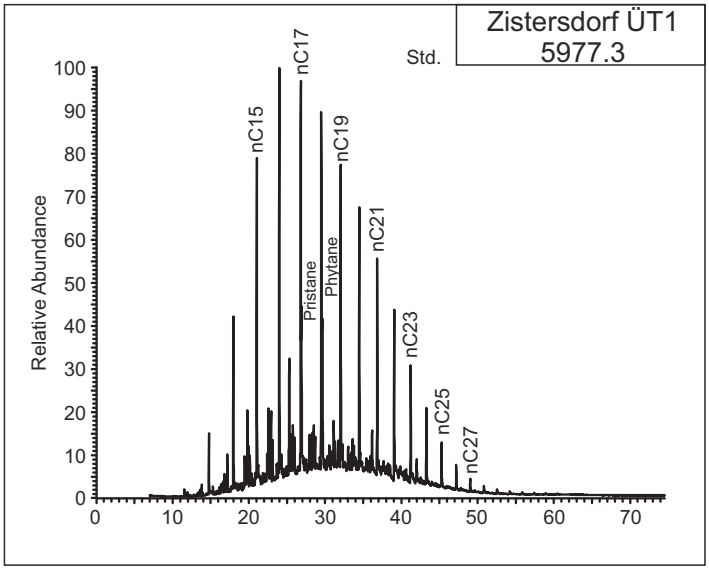
Zistersdorf ÜT1
5977.3
Std.
Relative Abundance
nC15
nC17
Pristane
Phytane
nC19
nC21
nC23
nC25
nC27

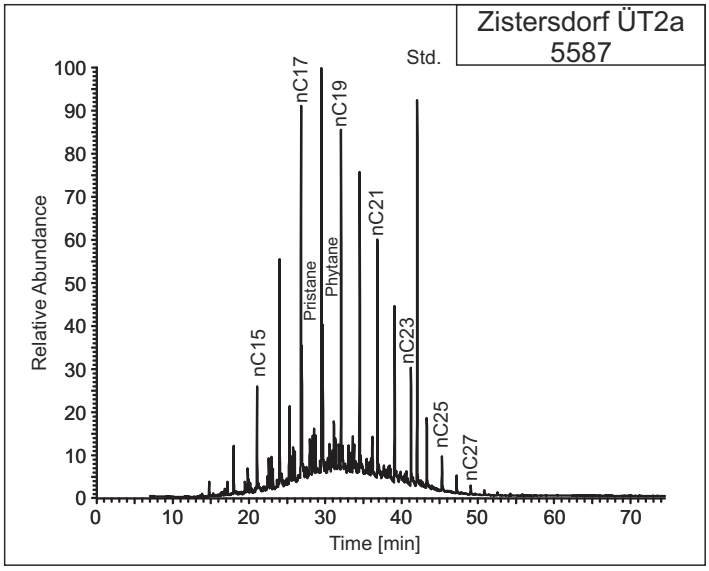
Zistersdorf ÜT2a
5587
Std.
Relative Abundance
nC15
nC17
Pristane
Phytane
nC19
nC21
nC23
nC25
nC27
Time [min]

Rocks

Aromatic Fraction

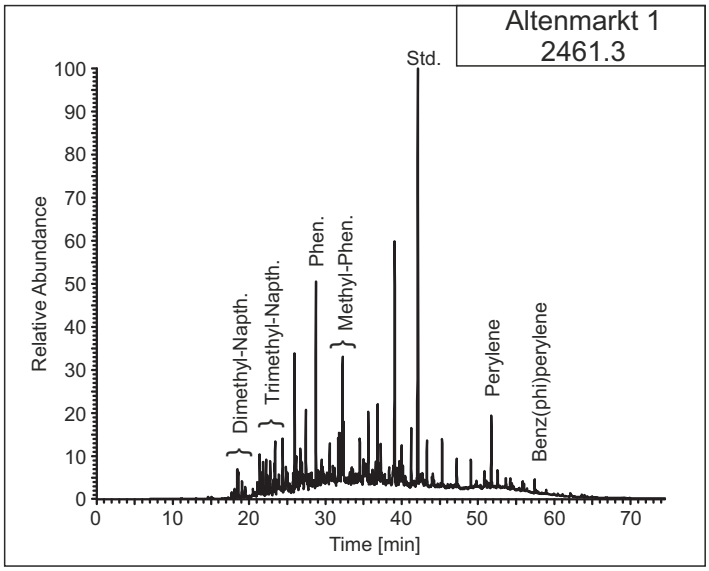
Altenmarkt 1
2461.3
Std.
Dimethyl-Napth.
Trimethyl-Napth.
Phen.
Methyl-Phen.
Perylene
Benz(phi)perylene
Relative Abundance
Time [min]

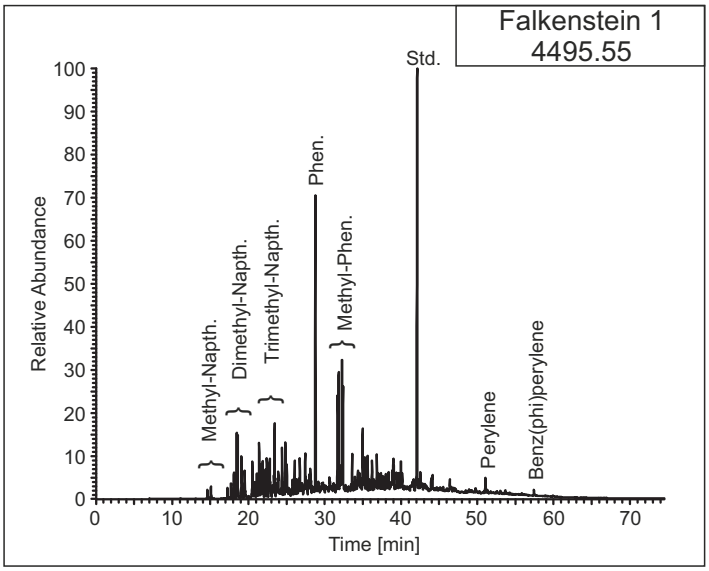
Falkenstein 1
4495.55
Std.
Methyl-Napth.
Dimethyl-Napth.
Trimethyl-Napth.
Phen.
Methyl-Phen.
Perylene
Benz(phi)perylene
Relative Abundance
Time [min]

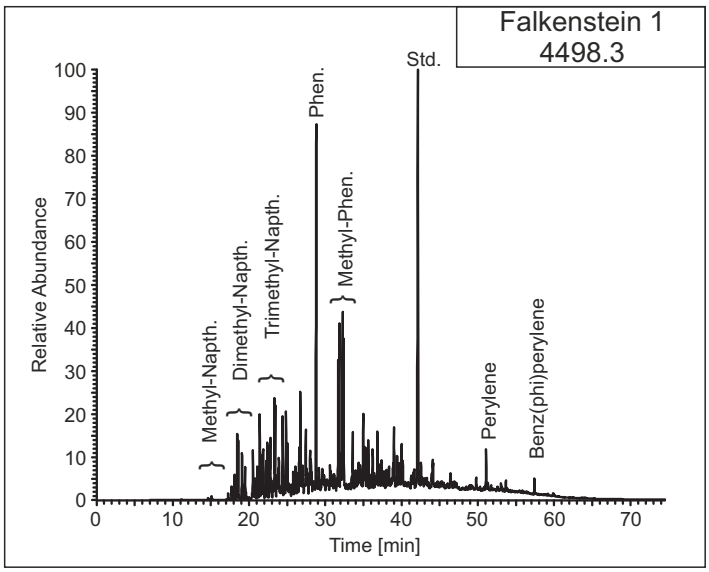
Falkenstein 1
4498.3
Std.
Methyl-Napth.
Dimethyl-Napth.
Trimethyl-Napth.
Phen.
Methyl-Phen.
Perylene
Benz(phi)perylene
Relative Abundance
Time [min]

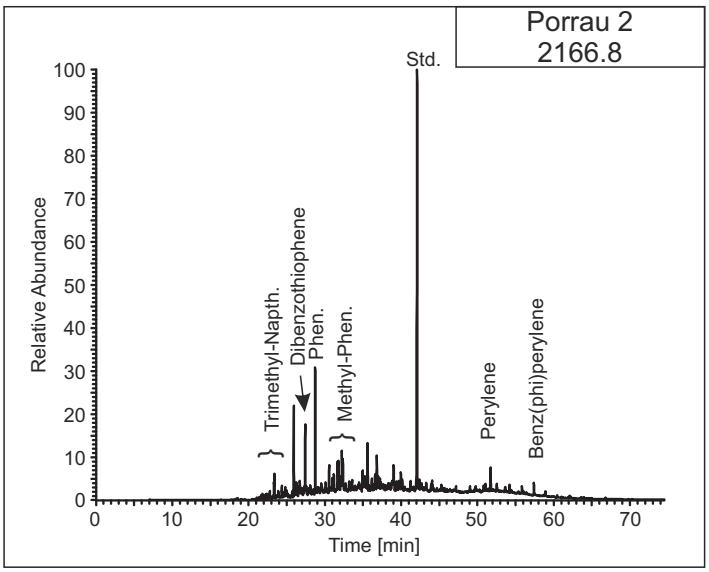
Porrau 2
2166.8
Std.
Trimethyl-Napth.
Dibenzothiophene
Phen.
Methyl-Phen.
Perylene
Benz(phi)perylene
Relative Abundance
Time [min]

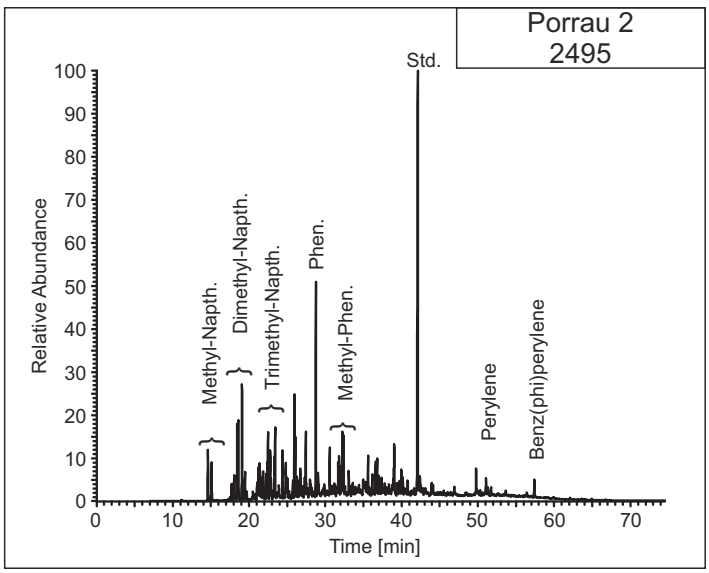
Porrau 2
2495
Std.
Methyl-Napth.
Dimethyl-Napth.
Trimethyl-Napth.
Phen.
Methyl-Phen.
Perylene
Benz(phi)perylene
Relative Abundance
Time [min]

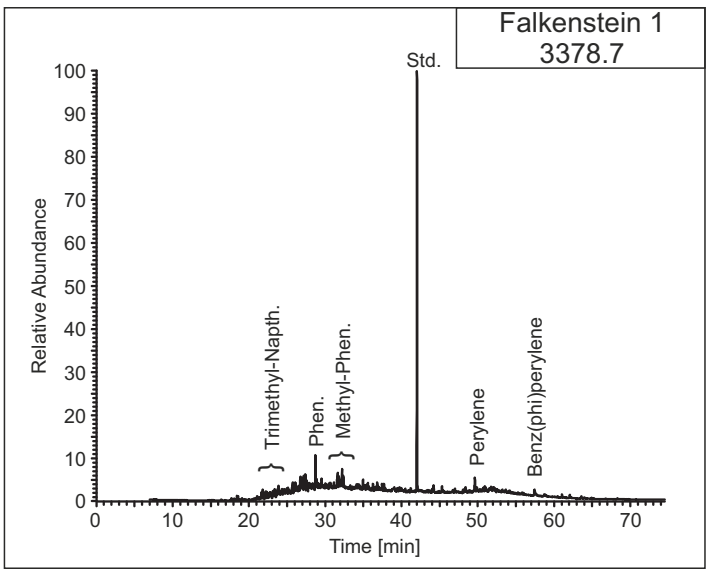
Falkenstein 1
3378.7
Std.
Trimethyl-Napth.
Phen.
Methyl-Phen.
Perylene
Benz(phi)perylene
Relative Abundance
Time [min]

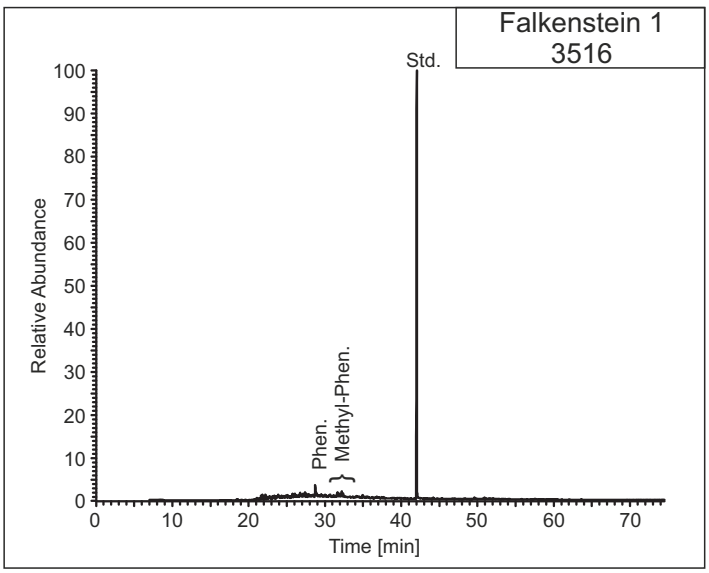
Falkenstein 1
3516
Std.
Phen.
Methyl-Phen.
Relative Abundance
Time [min]

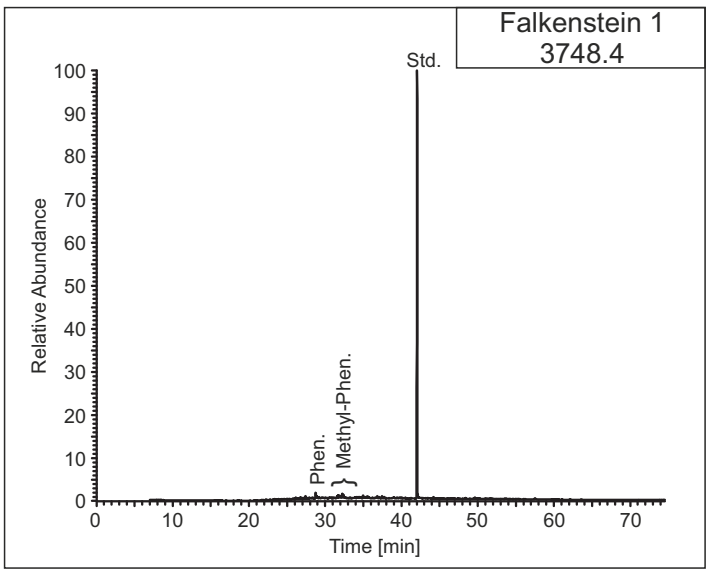
Falkenstein 1
3748.4
Std.
Phen.
Methyl-Phen.
Relative Abundance
Time [min]

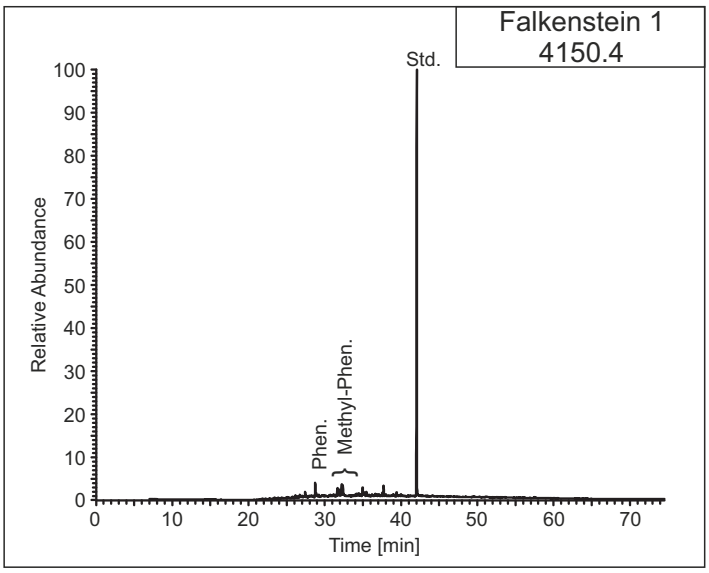
Falkenstein 1
4150.4
Std.
Phen.
Methyl-Phen.
Relative Abundance
Time [min]

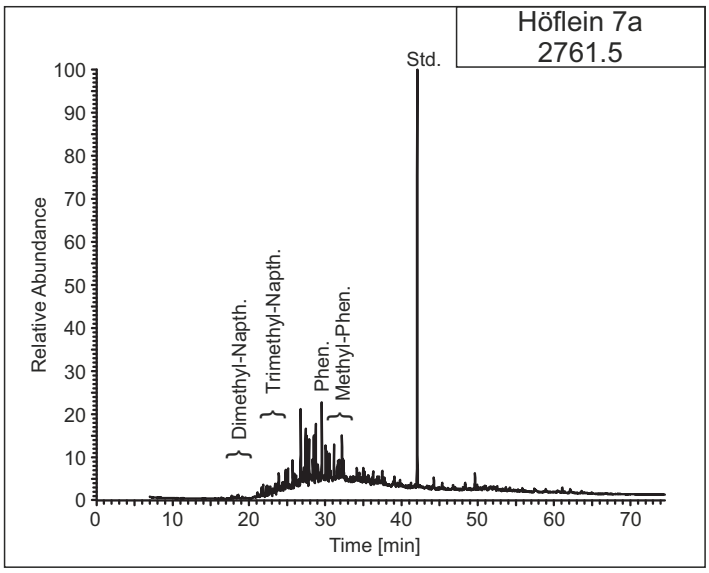
Höflein 7a
2761.5
Std.
Dimethyl-Napth.
Trimethyl-Napth.
Phen.
Methyl-Phen.
Relative Abundance
Time [min]

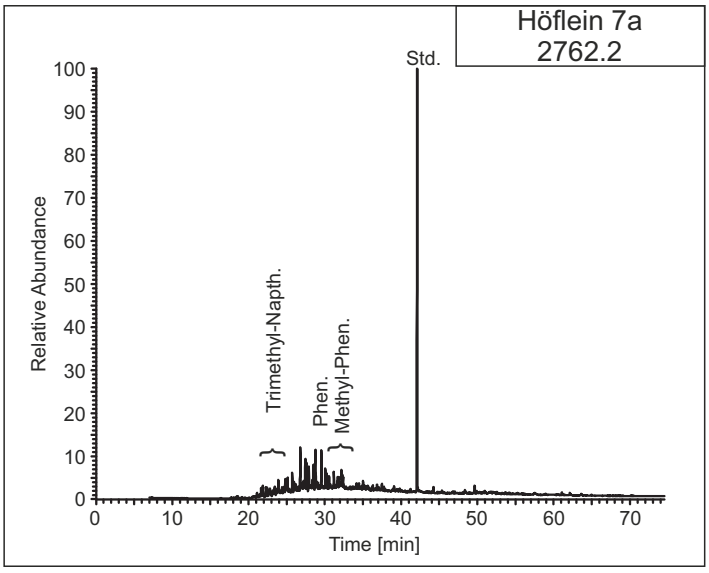
Höflein 7a
2762.2
Std.
Trimethyl-Napth.
Phen.
Methyl-Phen.
Relative Abundance
Time [min]

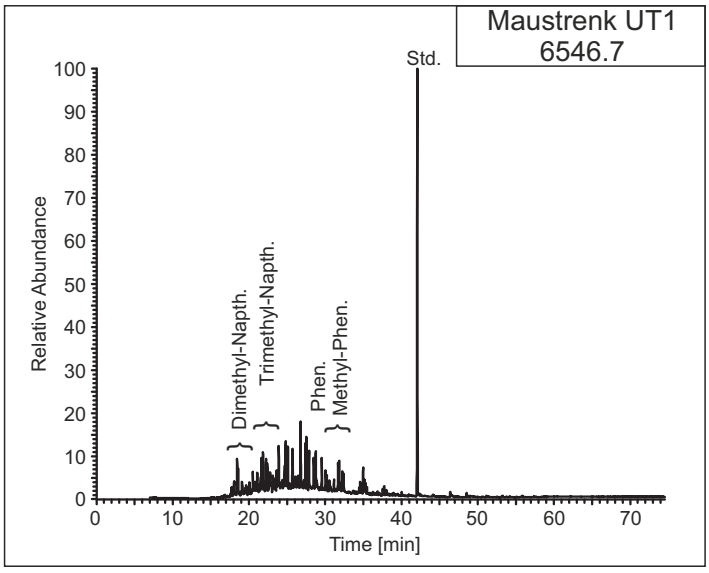
Maustrenk UT1
6546.7
Std.
Dimethyl-Napth.
Trimethyl-Napth.
Phen.
Methyl-Phen.
Relative Abundance
Time [min]

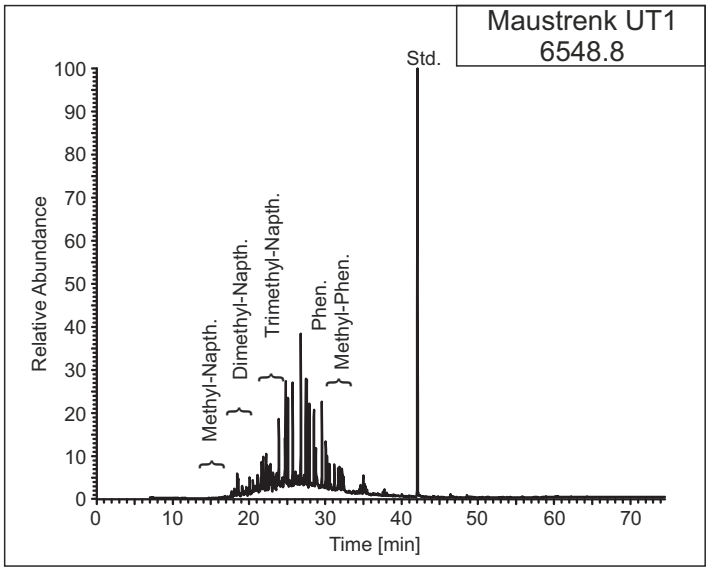
Maustrenk UT1
6548.8
Std.
Methyl-Napth.
Dimethyl-Napth.
Trimethyl-Napth.
Phen.
Methyl-Phen.
Relative Abundance
Time [min]

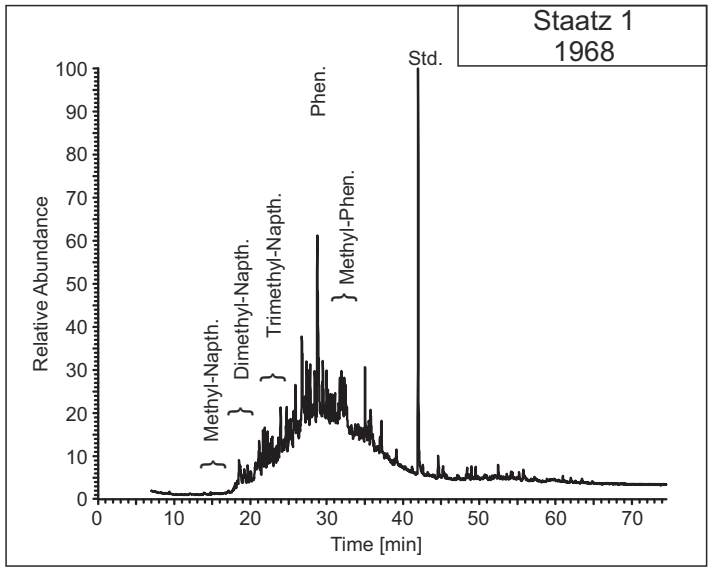
Staatz 1
1968
Std.
Phen.
Methyl-Napth.
Dimethyl-Napth.
Trimethyl-Napth.
Methyl-Phen.
Relative Abundance
Time [min]

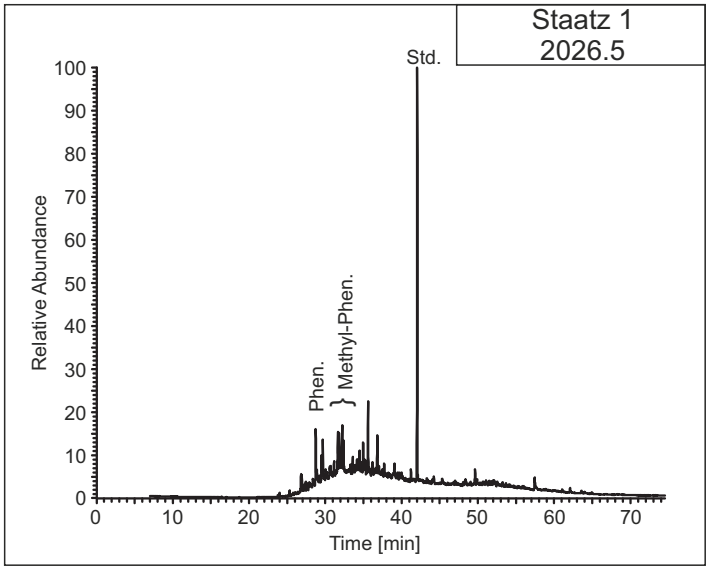
Staatz 1
2026.5
Std.
Phen.
Methyl-Phen.
Relative Abundance
Time [min]

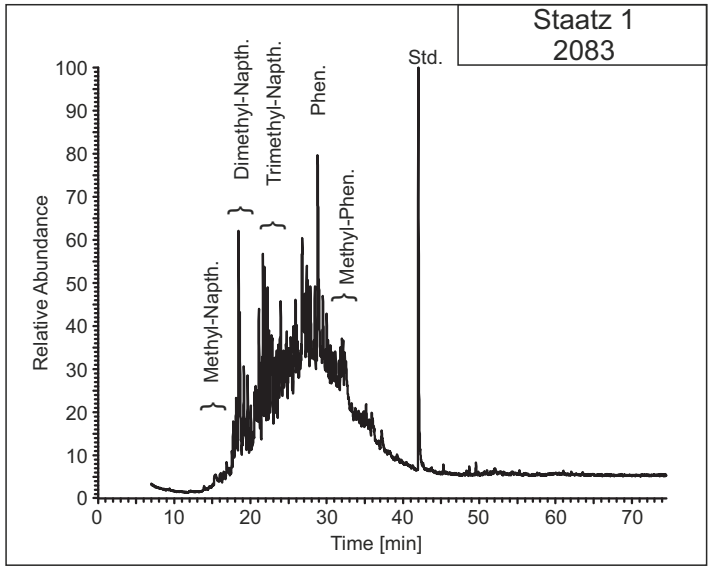
Staatz 1
2083
Std.
Methyl-Napth.
Dimethyl-Napth.
Trimethyl-Napth.
Phen.
Methyl-Phen.
Relative Abundance
Time [min]

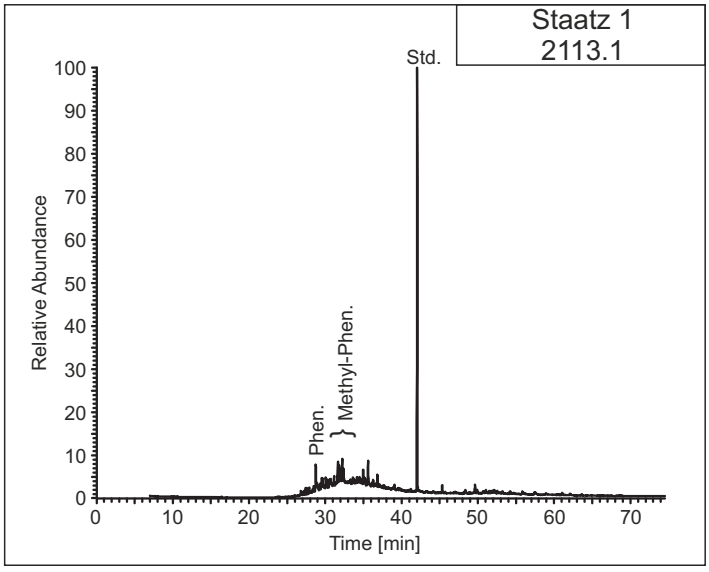
Staatz 1
2113.1
Std.
Phen.
Methyl-Phen.
Relative Abundance
Time [min]

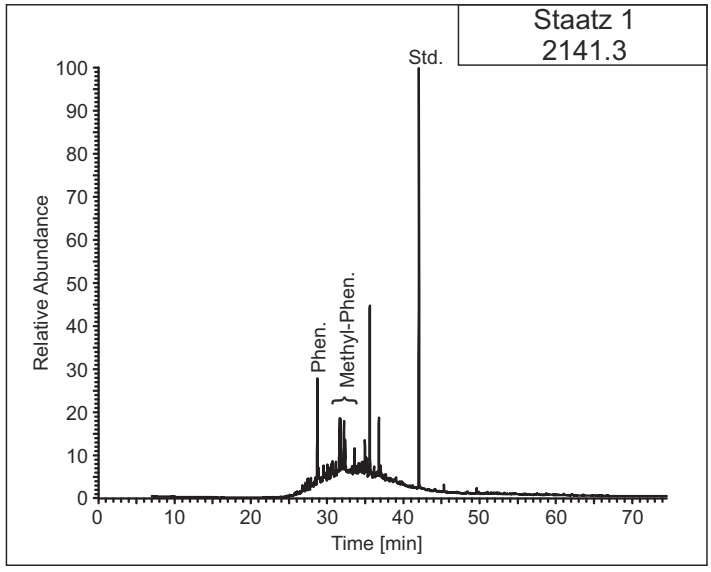
Staatz 1
2141.3
Std.
Phen.
Methyl-Phen.
Relative Abundance
Time [min]

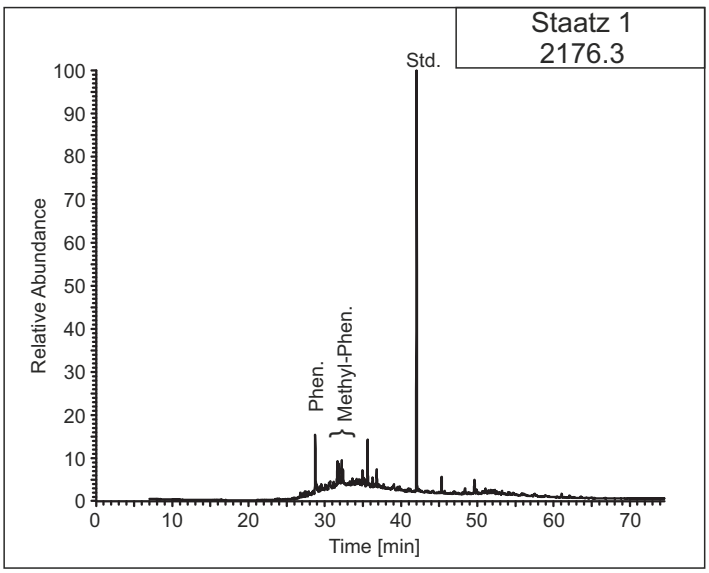
Staatz 1
2176.3
Std.
Phen.
Methyl-Phen.
Relative Abundance
Time [min]

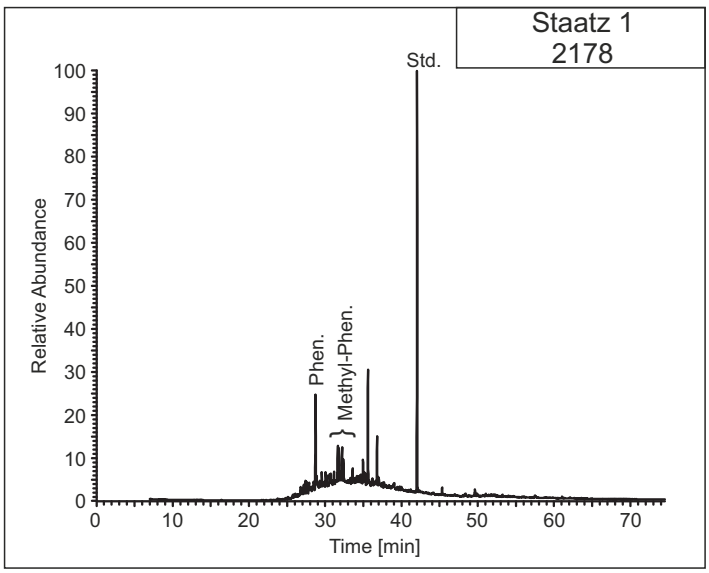
Staatz 1
2178
Std.
Phen.
Methyl-Phen.
Relative Abundance
Time [min]

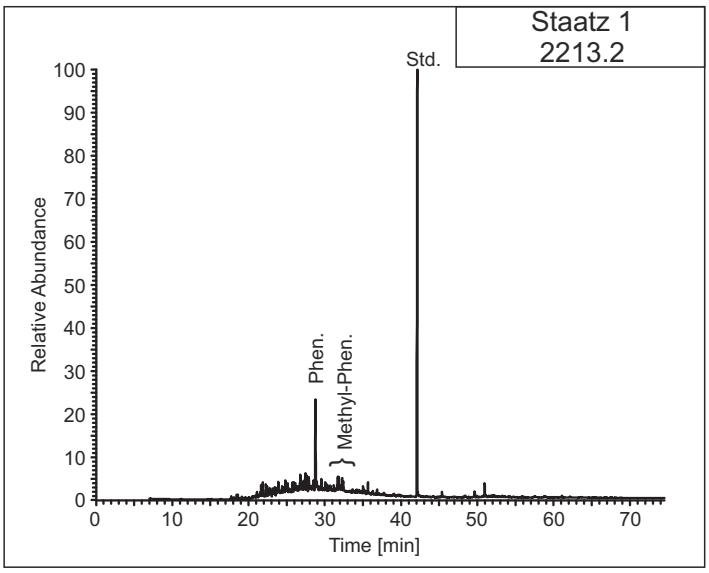
Staatz 1
2213.2
Std.
Phen.
Methyl-Phen.
Relative Abundance
Time [min]

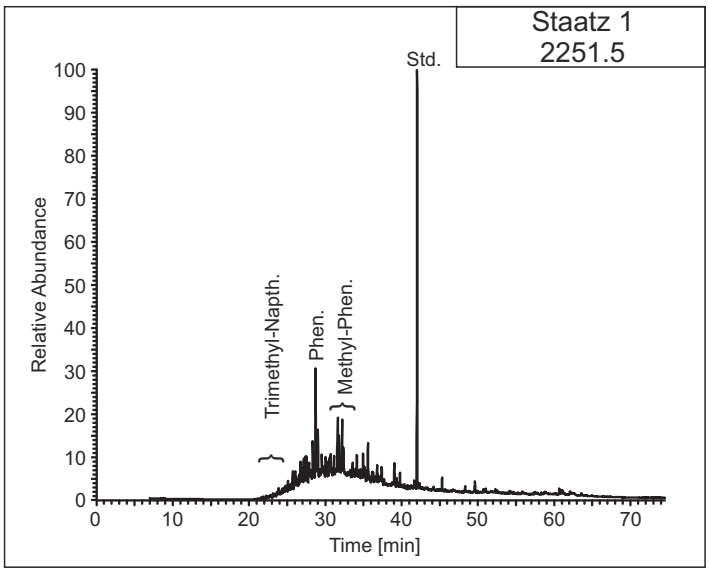
Staatz 1
2251.5
Std.
Trimethyl-Napth.
Phen.
Methyl-Phen.
Relative Abundance
Time [min]

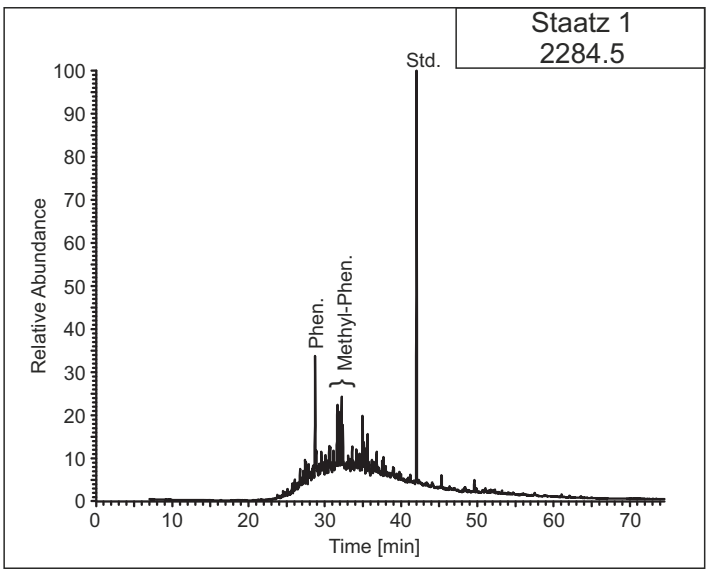
Staatz 1
2284.5
Std.
Phen.
Methyl-Phen.
Relative Abundance
Time [min]

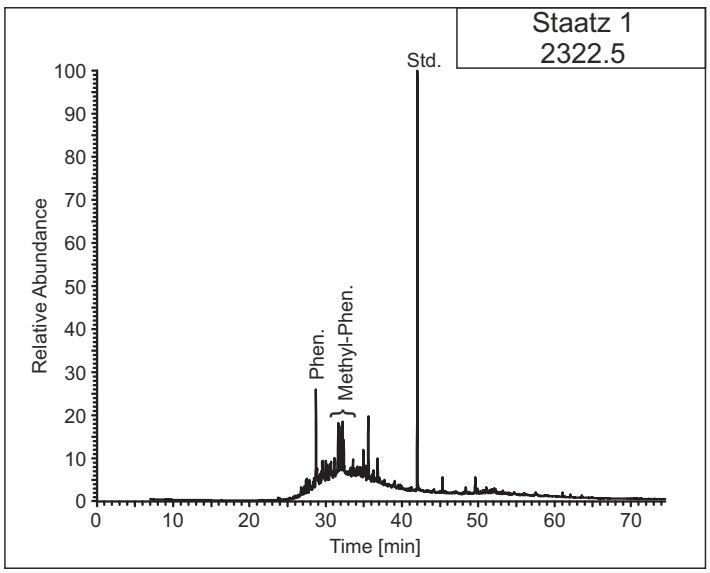
Staatz 1
2322.5
Std.
Phen.
Methyl-Phen.
Relative Abundance
Time [min]

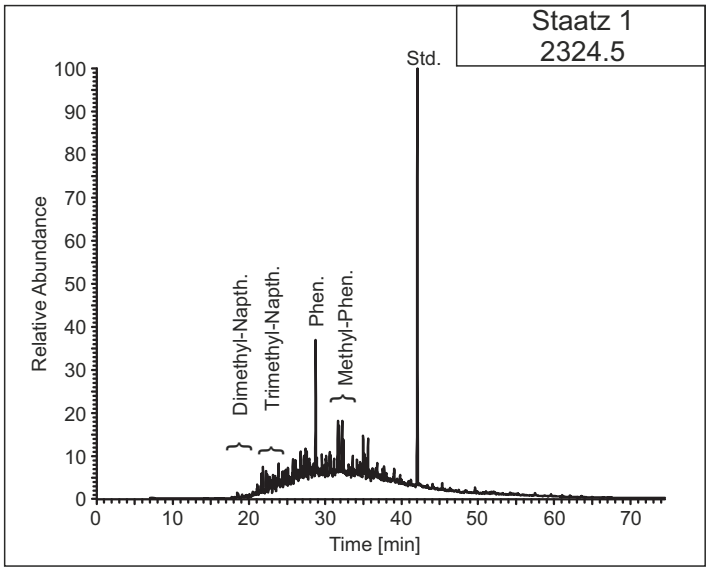
Staatz 1
2324.5
Std.
Dimethyl-Napth.
Trimethyl-Napth.
Phen.
Methyl-Phen.
Relative Abundance
Time [min]

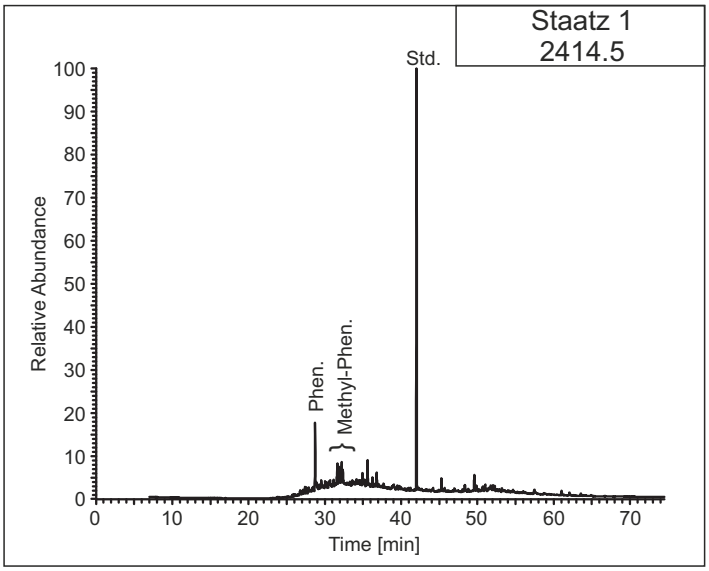
Staatz 1
2414.5
Std.
Phen.
Methyl-Phen.
Relative Abundance
Time [min]

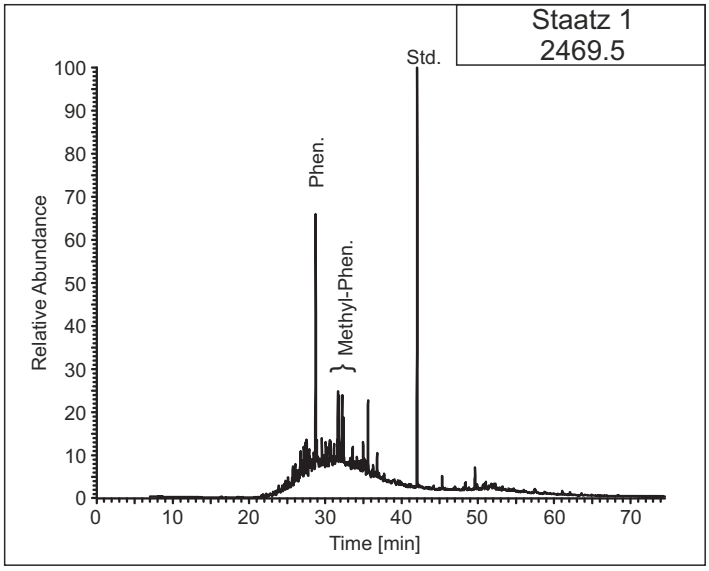
Staatz 1
2469.5
Std.
Phen.
Methyl-Phen.
Relative Abundance
Time [min]

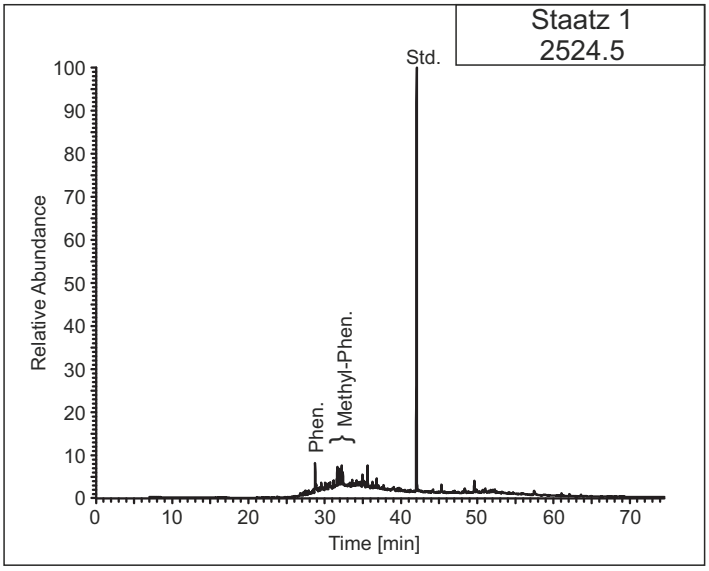
Staatz 1
2524.5
Std.
Phen.
Methyl-Phen.
Relative Abundance
Time [min]

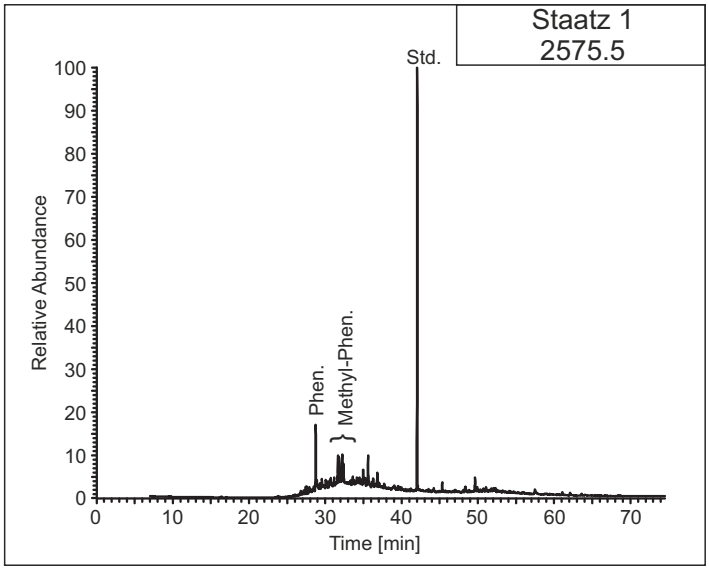
Staatz 1
2575.5
Std.
Phen.
Methyl-Phen.
Relative Abundance
Time [min]

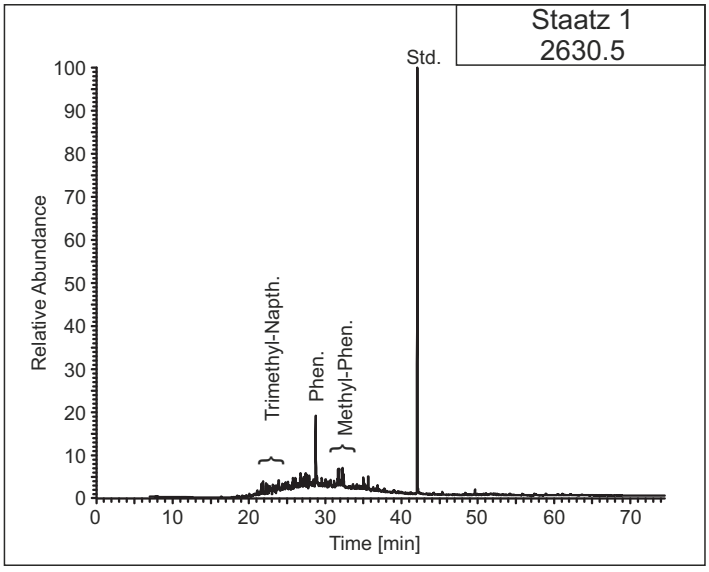
Staatz 1
2630.5
Std.
Trimethyl-Napth.
Phen.
Methyl-Phen.
Relative Abundance
Time [min]

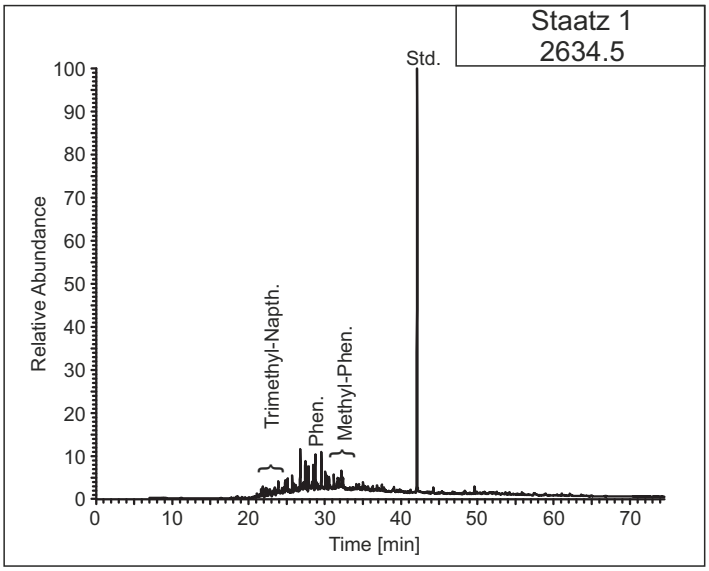
Staatz 1
2634.5
Std.
Trimethyl-Napth.
Phen.
Methyl-Phen.
Relative Abundance
Time [min]

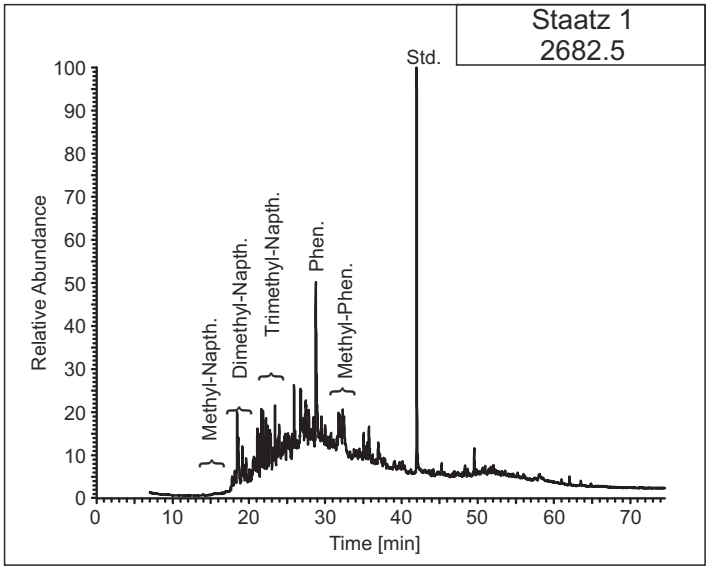
Staatz 1
2682.5
Std.
Methyl-Napth.
Dimethyl-Napth.
Trimethyl-Napth.
Phen.
Methyl-Phen.
Relative Abundance
Time [min]

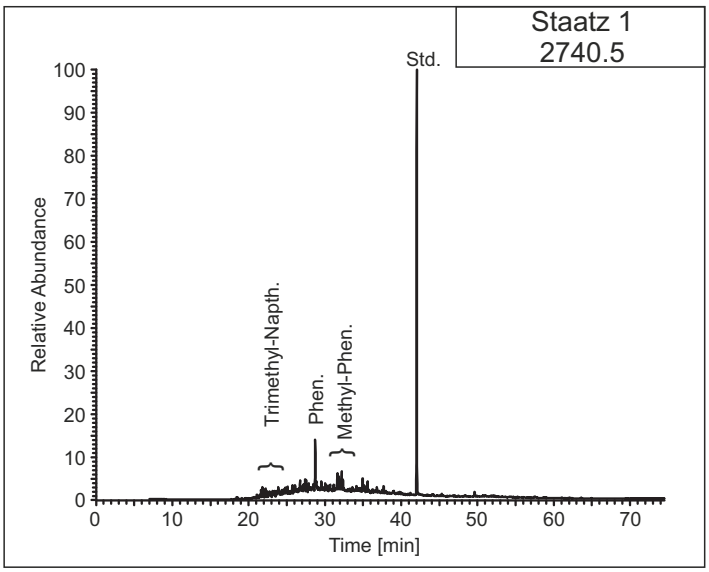
Staatz 1
2740.5
Std.
Trimethyl-Napth.
Phen.
Methyl-Phen.
Relative Abundance
Time [min]

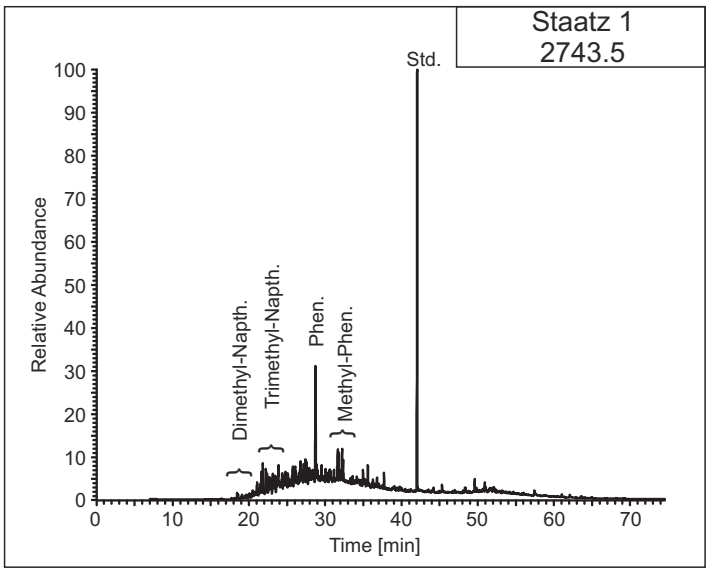
Staatz 1
2743.5
Std.
Dimethyl-Napth.
Trimethyl-Napth.
Phen.
Methyl-Phen.
Relative Abundance
Time [min]

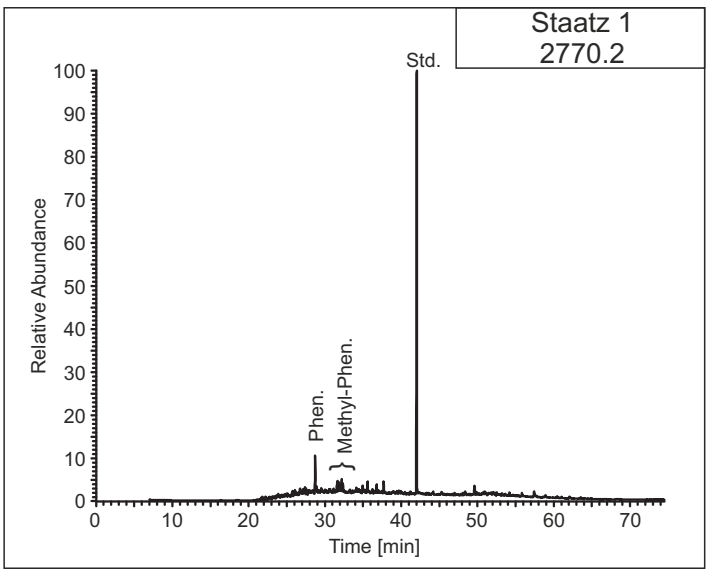
Staatz 1
2770.2
Std.
Phen.
Methyl-Phen.
Relative Abundance
Time [min]

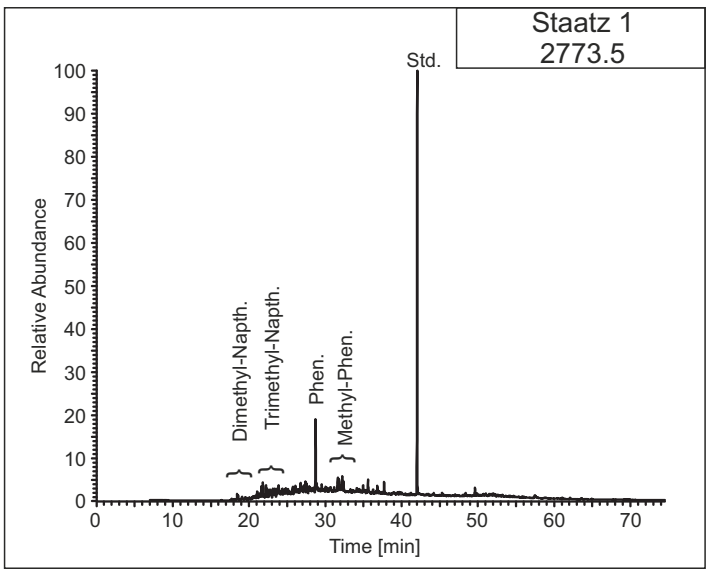
Staatz 1
2773.5
Std.
Dimethyl-Napth.
Trimethyl-Napth.
Phen.
Methyl-Phen.
Relative Abundance
Time [min]

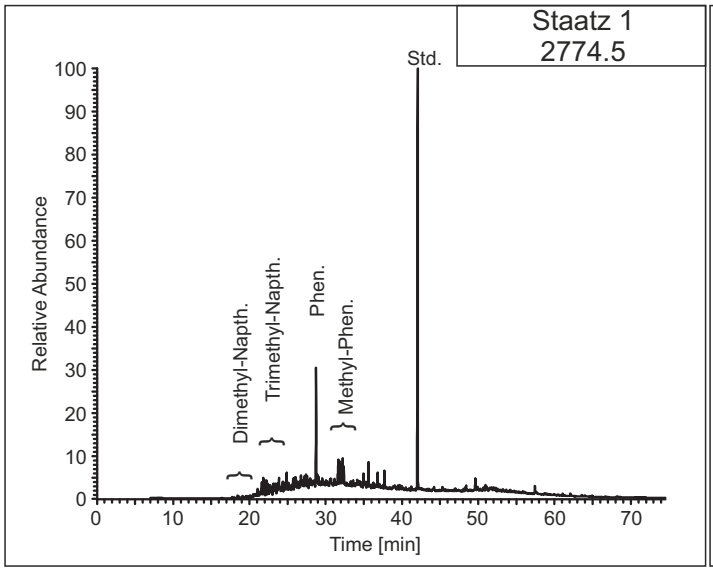
Staatz 1
2774.5
Std.
Dimethyl-Napth.
Trimethyl-Napth.
Phen.
Methyl-Phen.
Relative Abundance
Time [min]

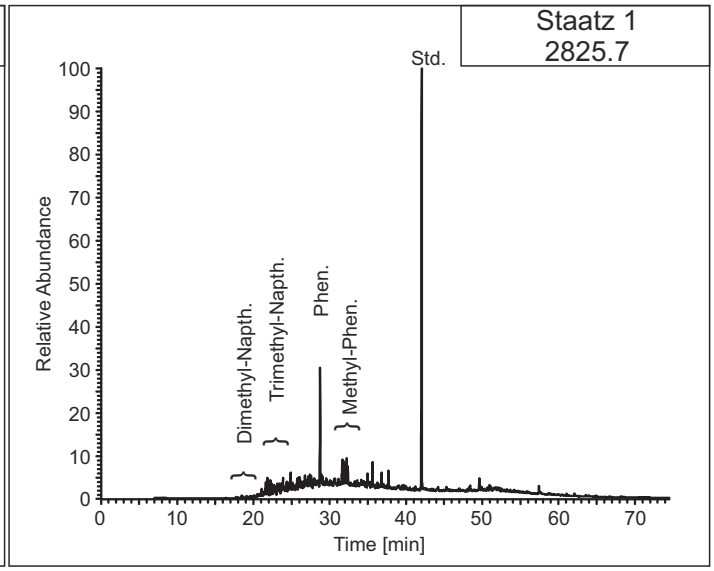
Staatz 1
2825.7
Std.
Dimethyl-Napth.
Trimethyl-Napth.
Phen.
Methyl-Phen.
Relative Abundance
Time [min]

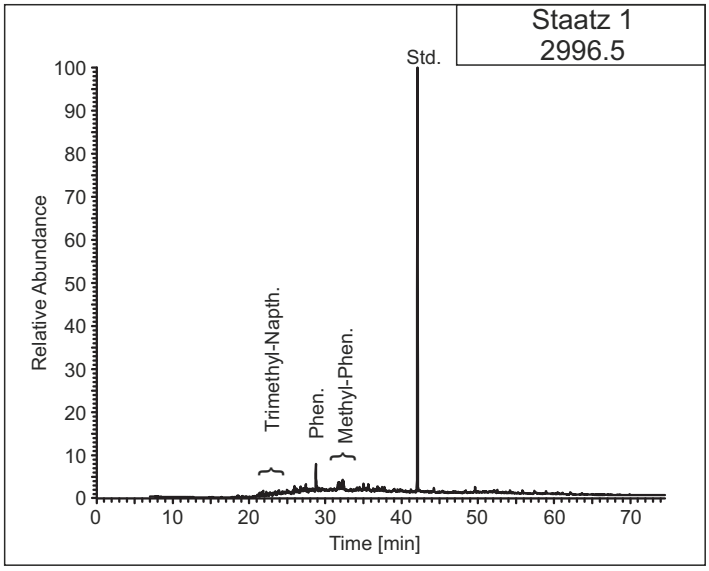
Staatz 1
2996.5
Std.
Trimethyl-Napth.
Phen.
Methyl-Phen.
Relative Abundance
Time [min]

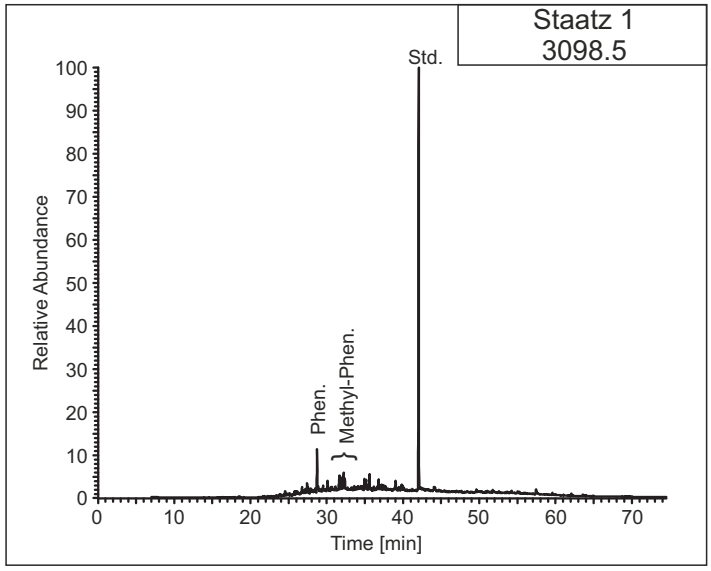
Staatz 1
3098.5
Std.
Phen.
Methyl-Phen.
Relative Abundance
Time [min]

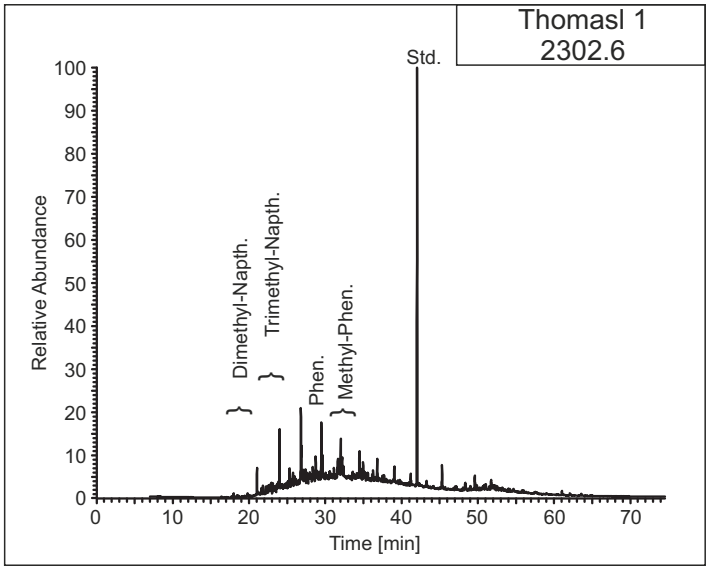
Thomasl 1
2302.6
Std.
Dimethyl-Napth.
Trimethyl-Napth.
Phen.
Methyl-Phen.
Relative Abundance
Time [min]

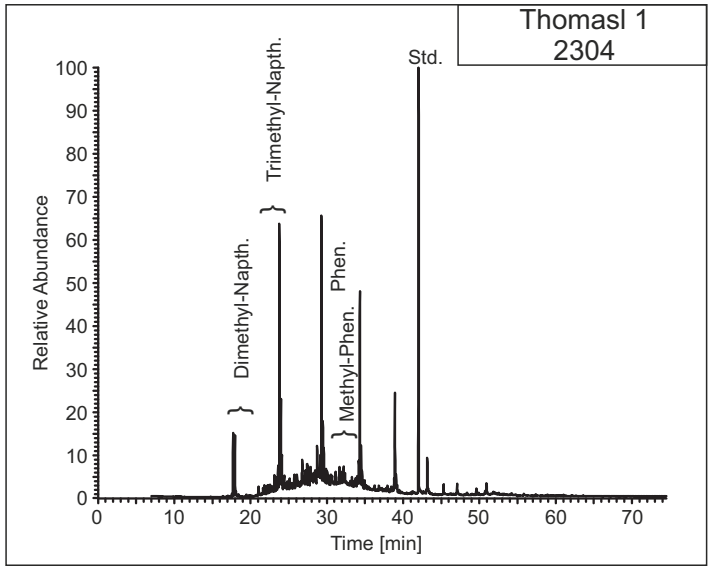
Thomasl 1
2304
Std.
Dimethyl-Napth.
Trimethyl-Napth.
Phen.
Methyl-Phen.
Relative Abundance
Time [min]

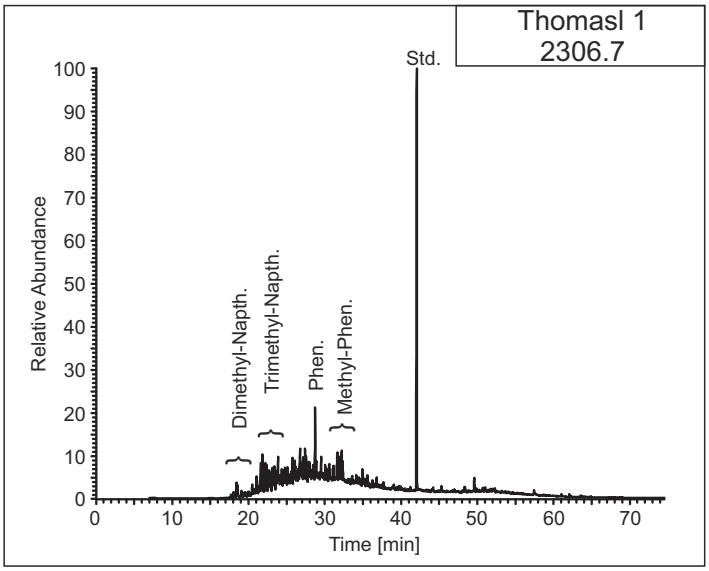
Thomasl 1
2306.7
Std.
Dimethyl-Napth.
Trimethyl-Napth.
Phen.
Methyl-Phen.
Relative Abundance
Time [min]

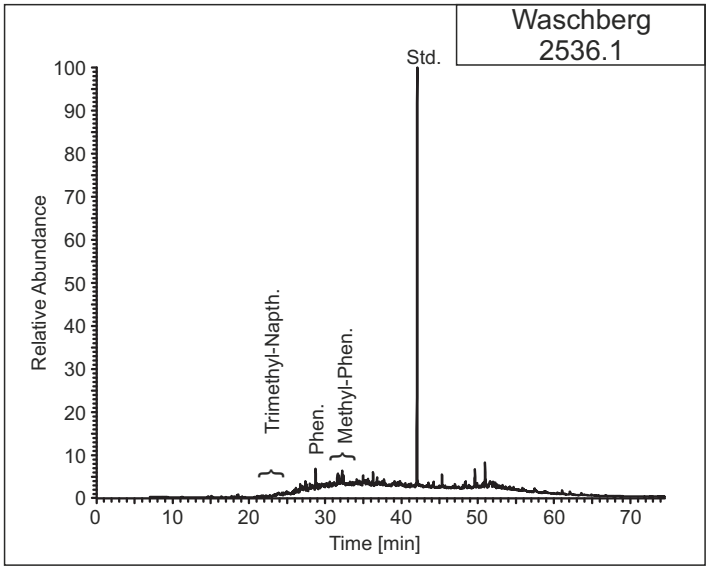
Waschberg
2536.1
Std.
Trimethyl-Napth.
Phen.
Methyl-Phen.
Relative Abundance
Time [min]

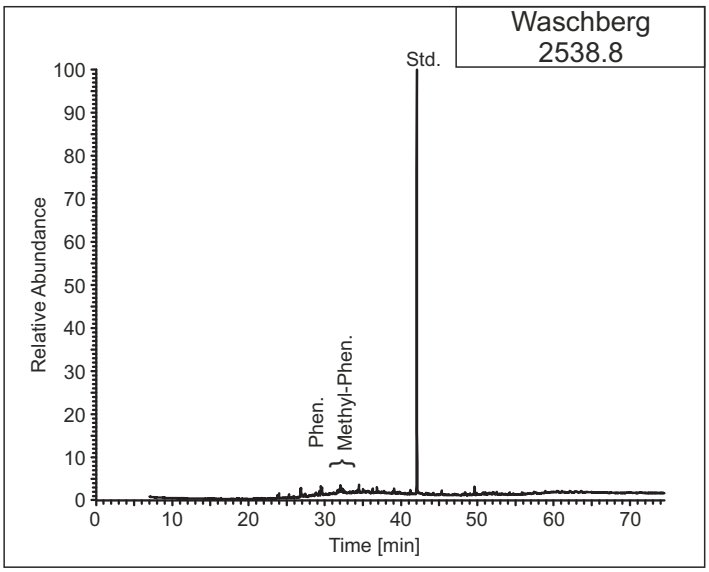
Waschberg
2538.8
Std.
Phen.
Methyl-Phen.
Relative Abundance
Time [min]

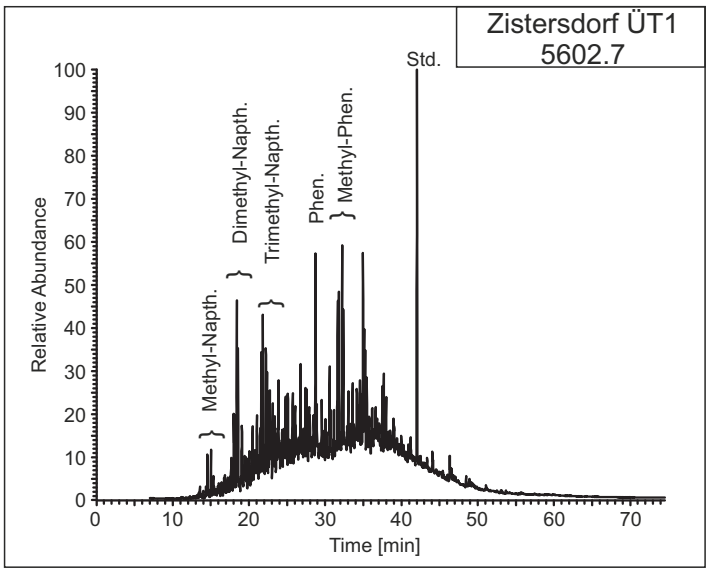
Zistersdorf ÜT1
5602.7
Std.
Methyl-Napth.
Dimethyl-Napth.
Trimethyl-Napth.
Phen.
Methyl-Phen.
Relative Abundance
Time [min]

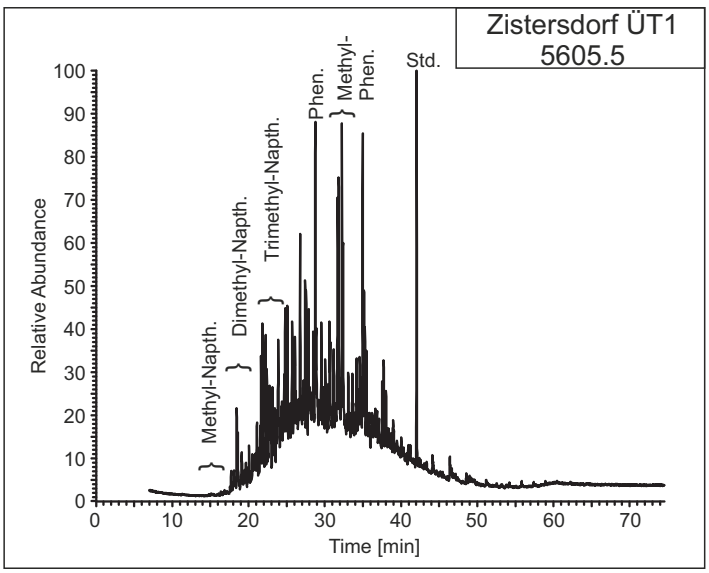
Zistersdorf ÜT1
5605.5
Std.
Methyl-Napth.
Dimethyl-Napth.
Trimethyl-Napth.
Phen.
Methyl-Phen.
Relative Abundance
Time [min]

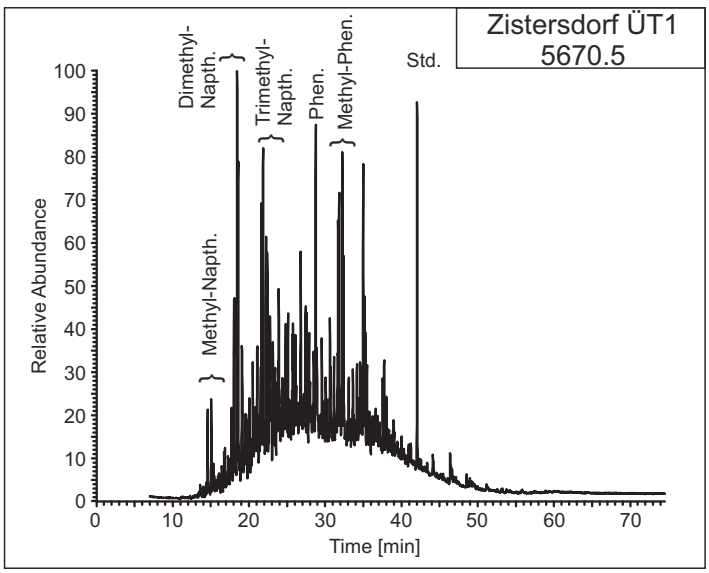
Zistersdorf ÜT1
5670.5
Std.
Methyl-Napth.
Dimethyl-Napth.
Trimethyl-Napth.
Phen.
Methyl-Phen.
Relative Abundance
Time [min]

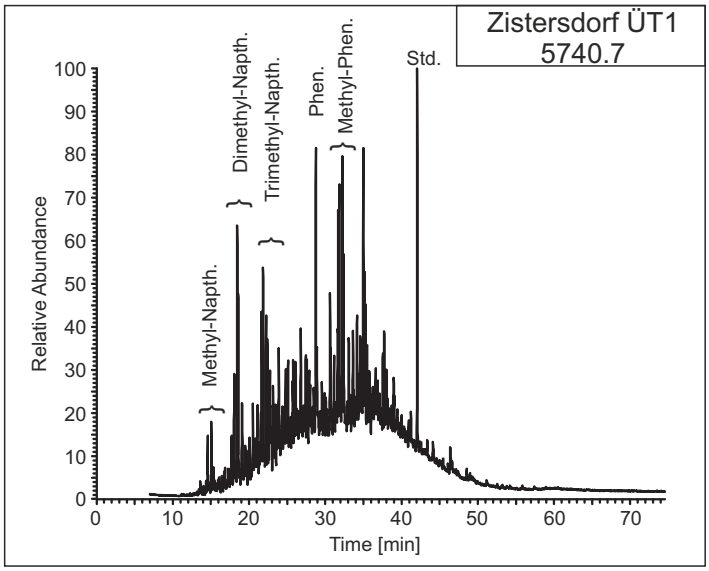
Zistersdorf ÜT1
5740.7
Relative Abundance
Time [min]
Methyl-Napth.
Dimethyl-Napth.
Trimethyl-Napth.
Phen.
Methyl-Phen.
Std.

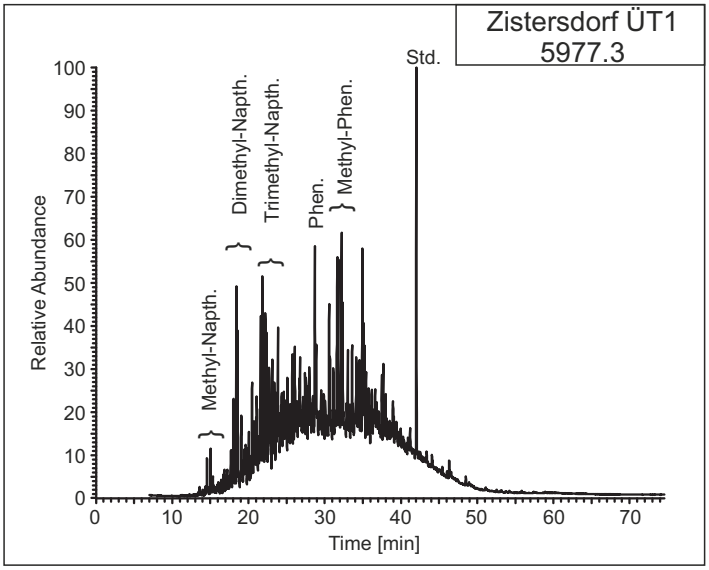
Zistersdorf ÜT1
5977.3
Relative Abundance
Time [min]
Methyl-Napth.
Dimethyl-Napth.
Trimethyl-Napth.
Phen.
Methyl-Phen.
Std.

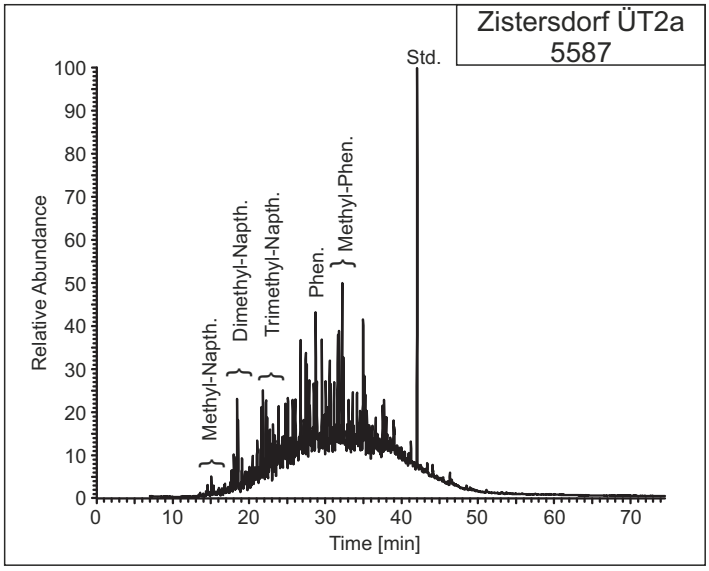
Zistersdorf ÜT2a
5587
Relative Abundance
Time [min]
Methyl-Napth.
Dimethyl-Napth.
Trimethyl-Napth.
Phen.
Methyl-Phen.
Std.

Oils

Whole Oil

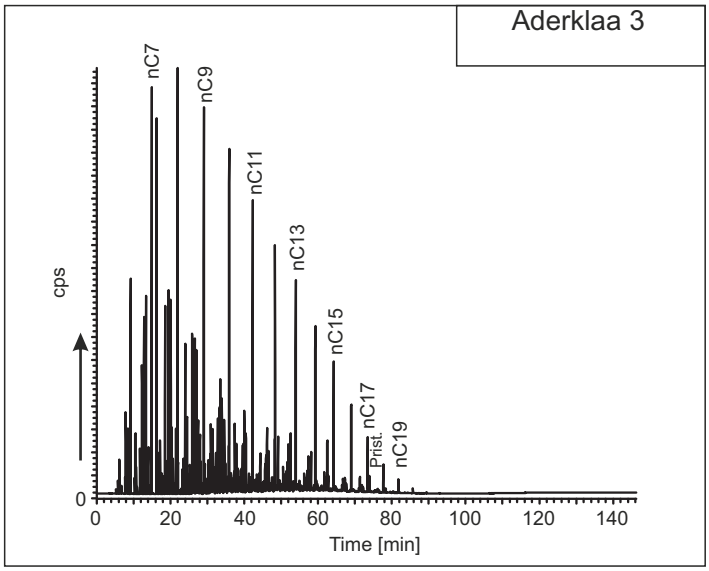
Aderklaa 3
cps
nC7
nC9
nC11
nC13
nC15
nC17
Prist.
nC19
0
0 20 40 60 80 100 120 140
Time [min]

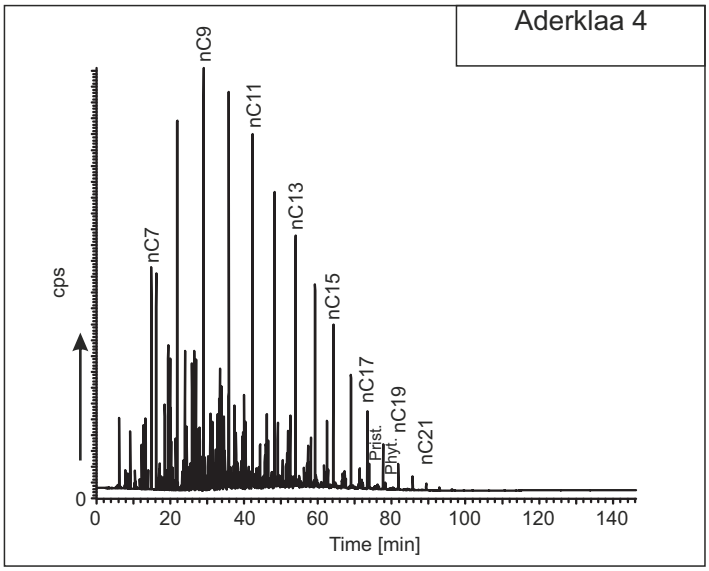
Aderklaa 4
cps
nC7
nC9
nC11
nC13
nC15
nC17
Prist.
Phyt.
nC19
nC21
0
0 20 40 60 80 100 120 140
Time [min]

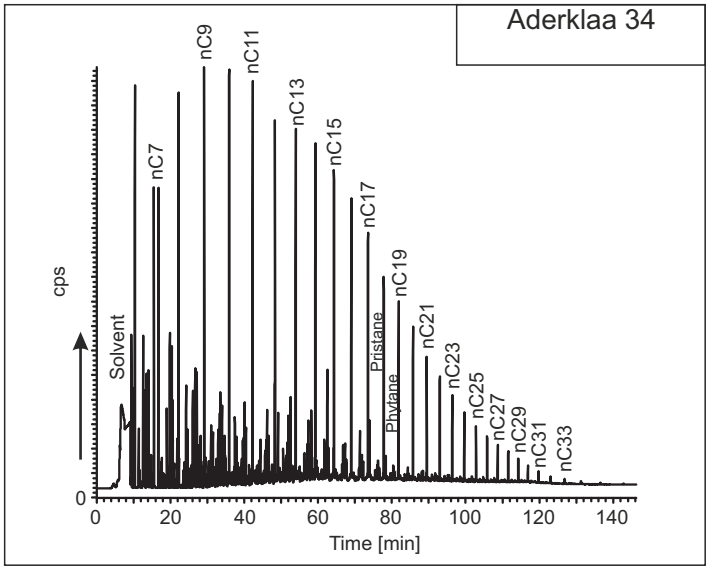
Aderklaa 34
cps
Solvent
nC7
nC9
nC11
nC13
nC15
nC17
Pristane
nC19
Phytane
nC21
nC23
nC25
nC27
nC29
nC31
nC33
0
0 20 40 60 80 100 120 140
Time [min]

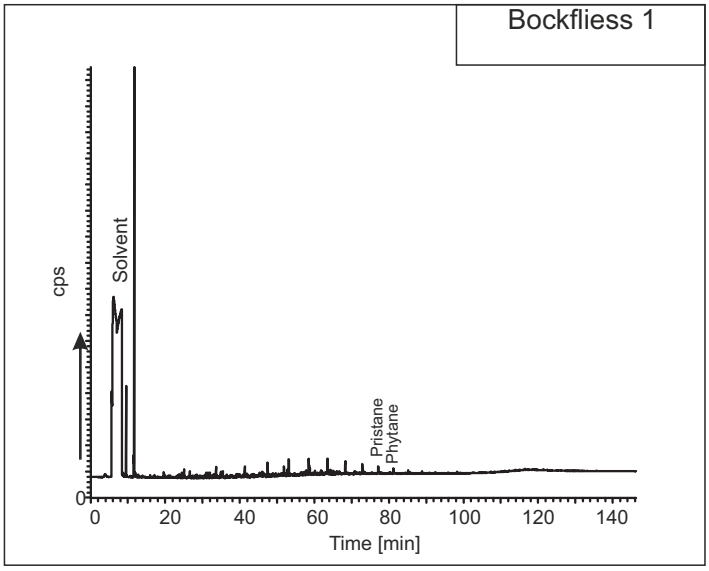
Bockfliess 1
cps
Solvent
Pristane
Phytane
0
0 20 40 60 80 100 120 140
Time [min]

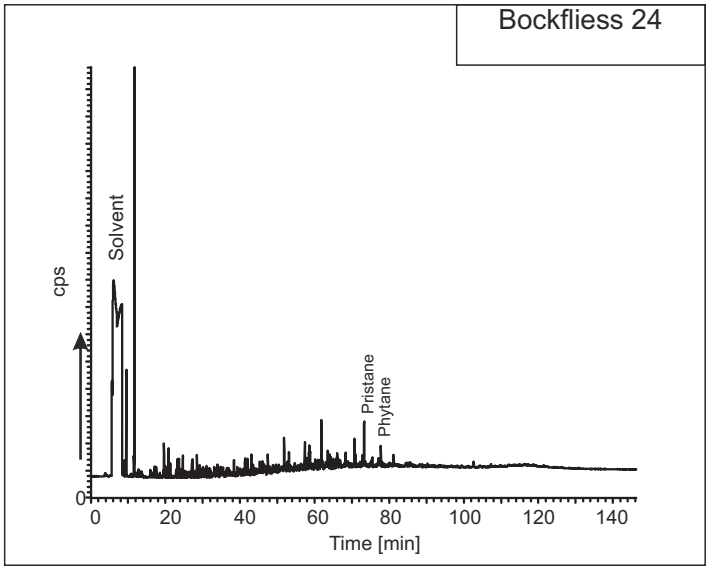
Bockfliess 24
cps
Solvent
Pristane
Phytane
0
0 20 40 60 80 100 120 140
Time [min]

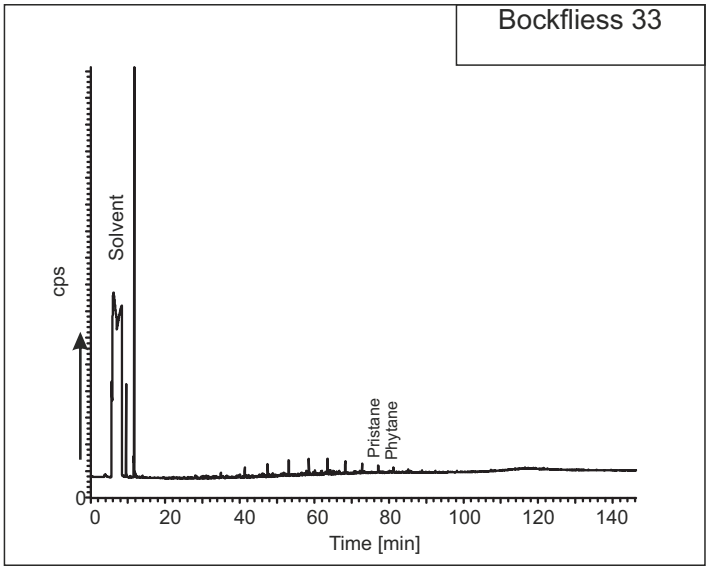
Bockfliess 33
cps
Solvent
Pristane
Phytane
0
0 20 40 60 80 100 120 140
Time [min]

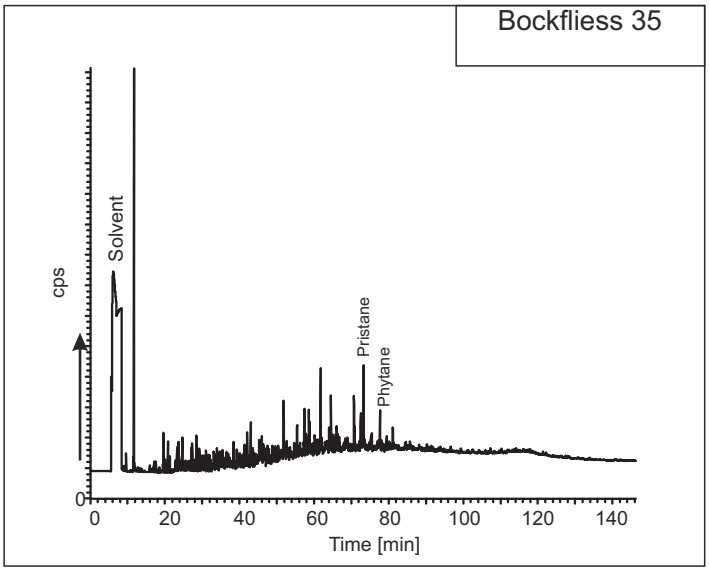
Bockfliess 35
cps
Solvent
Pristane
Phytane
0
0 20 40 60 80 100 120 140
Time [min]

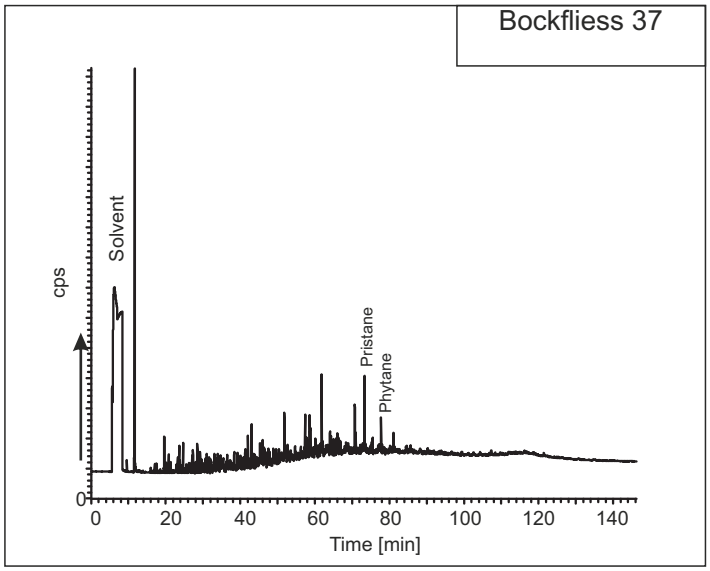
Bockfliess 37
cps
Solvent
Pristane
Phytane
0
0 20 40 60 80 100 120 140
Time [min]

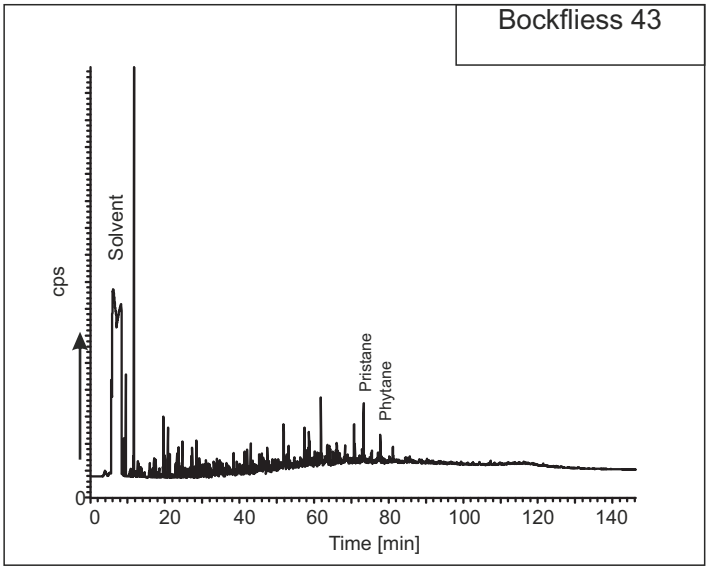
Bockfliess 43
cps
Solvent
Pristane
Phytane
0
0 20 40 60 80 100 120 140
Time [min]

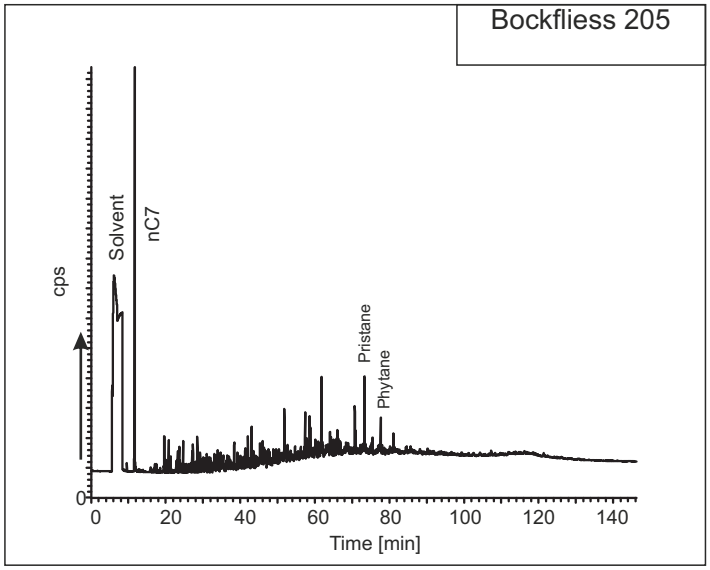
Bockfliess 205
cps
Solvent
nC7
Pristane
Phytane
0
0 20 40 60 80 100 120 140
Time [min]

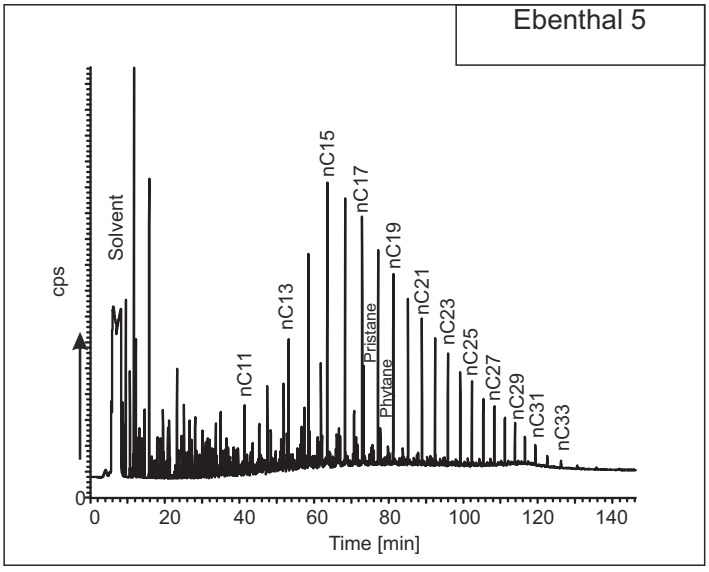
Ebenthal 5
cps
Solvent
nC11
nC13
nC15
nC17
Pristane
Phytane
nC19
nC21
nC23
nC25
nC27
nC29
nC31
nC33
0
0 20 40 60 80 100 120 140
Time [min]

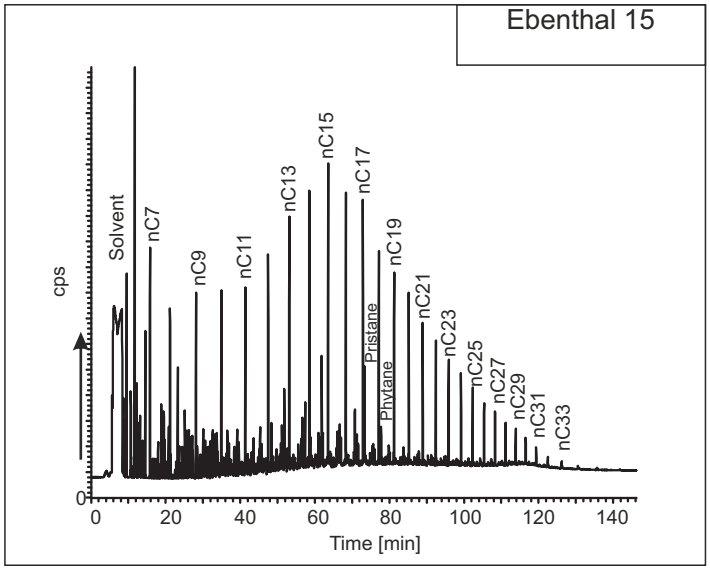
Ebenthal 15
cps
Solvent
nC7
nC9
nC11
nC13
nC15
nC17
Pristane
Phytane
nC19
nC21
nC23
nC25
nC27
nC29
nC31
nC33
0
0 20 40 60 80 100 120 140
Time [min]

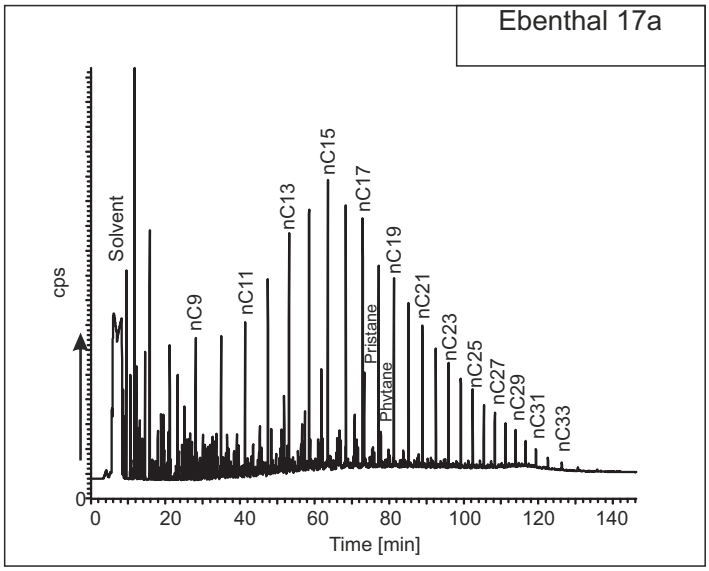
Ebenthal 17a
cps
Solvent
nC9
nC11
nC13
nC15
nC17
Pristane
Phytane
nC19
nC21
nC23
nC25
nC27
nC29
nC31
nC33
0
0 20 40 60 80 100 120 140
Time [min]

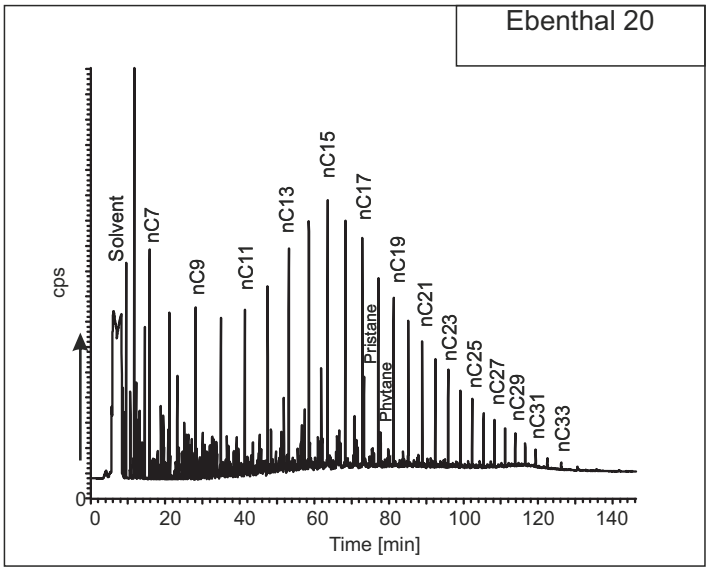
Ebenthal 20
cps
Solvent
nC7
nC9
nC11
nC13
nC15
nC17
nC19
Pristane
Phytane
nC21
nC23
nC25
nC27
nC29
nC31
nC33
0
0 20 40 60 80 100 120 140
Time [min]

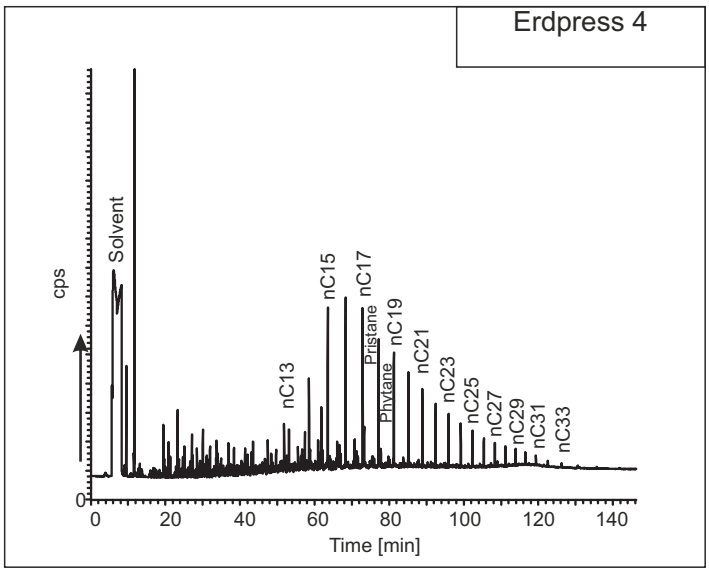
Erdpress 4
cps
Solvent
nC13
nC15
nC17
Pristane
Phytane
nC19
nC21
nC23
nC25
nC27
nC29
nC31
nC33
0
0 20 40 60 80 100 120 140
Time [min]

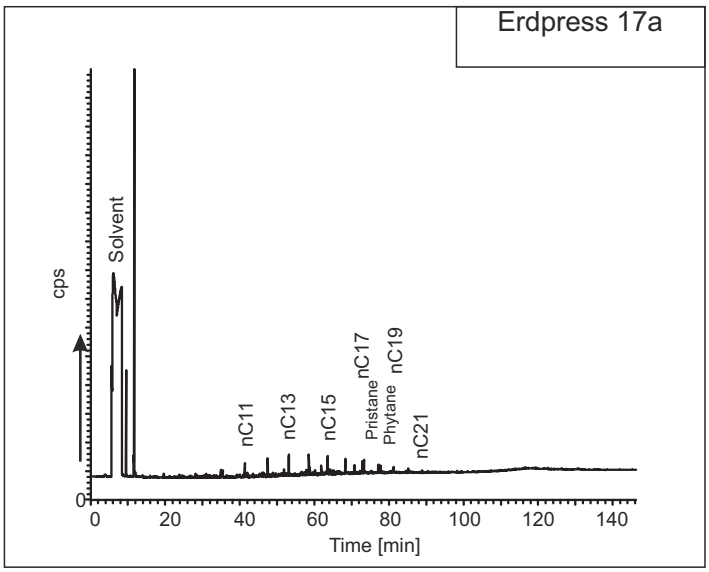
Erdpress 17a
cps
Solvent
nC11
nC13
nC15
nC17
Pristane
Phytane
nC19
nC21
0
0 20 40 60 80 100 120 140
Time [min]

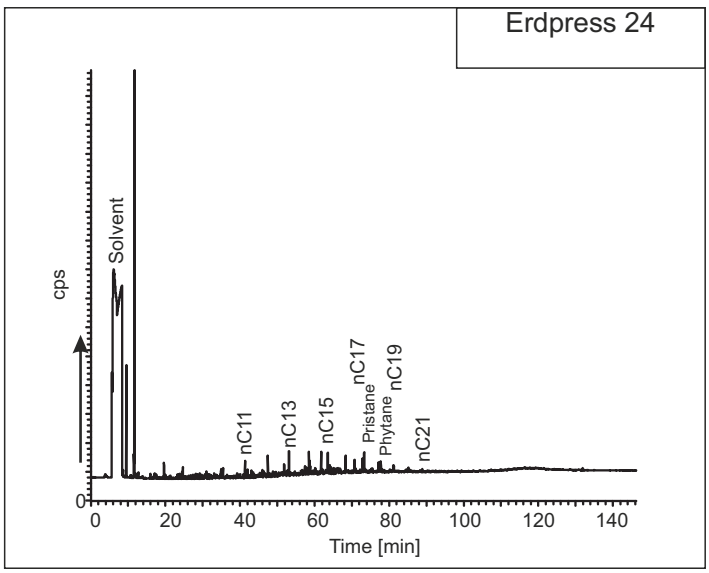
Erdpress 24
cps
Solvent
nC11
nC13
nC15
nC17
Pristane
Phytane
nC19
nC21
0
0 20 40 60 80 100 120 140
Time [min]

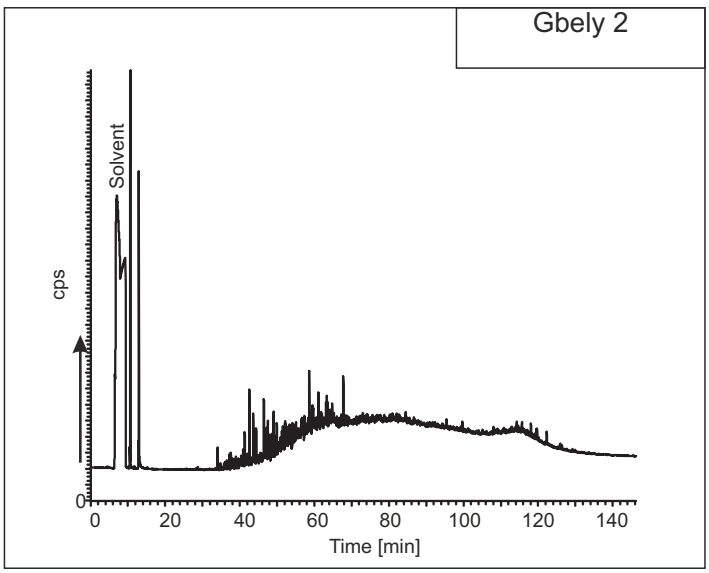
Gbely 2
cps
Solvent
0
0 20 40 60 80 100 120 140
Time [min]

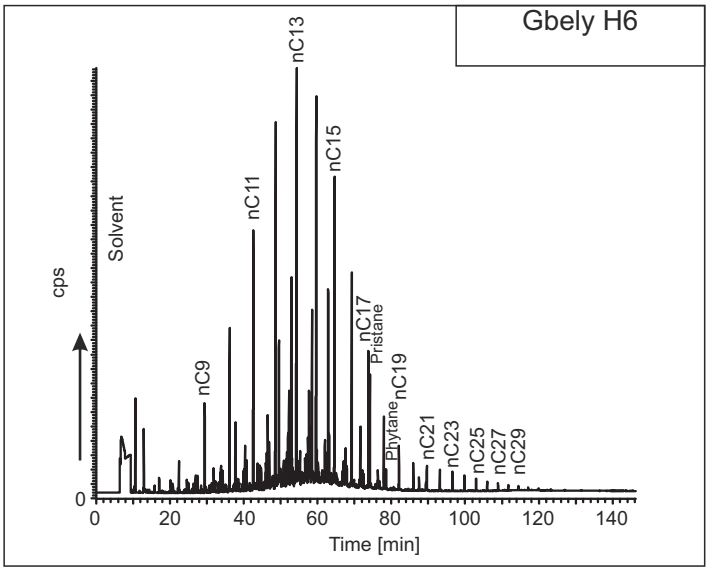
Gbely H6
Solvent
nC9
nC11
nC13
nC15
nC17
Pristane
Phytane
nC19
nC21
nC23
nC25
nC27
nC29
cps
0
0 20 40 60 80 100 120 140
Time [min]

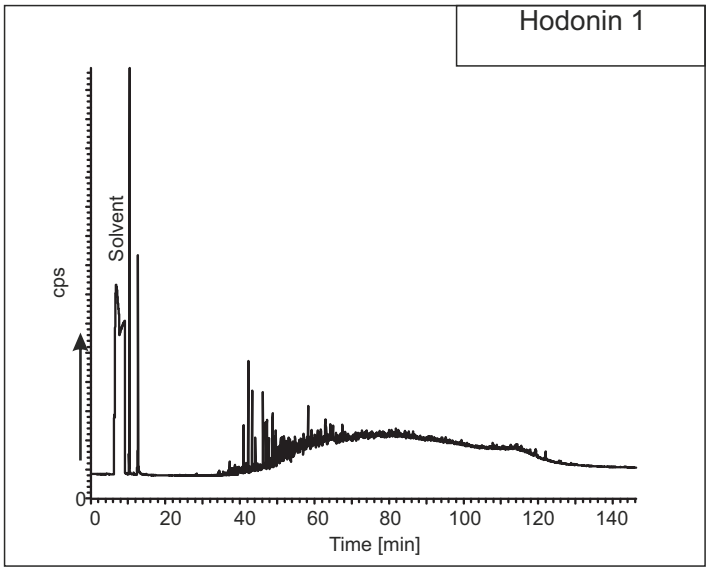
Hodonin 1
Solvent
cps
0
0 20 40 60 80 100 120 140
Time [min]

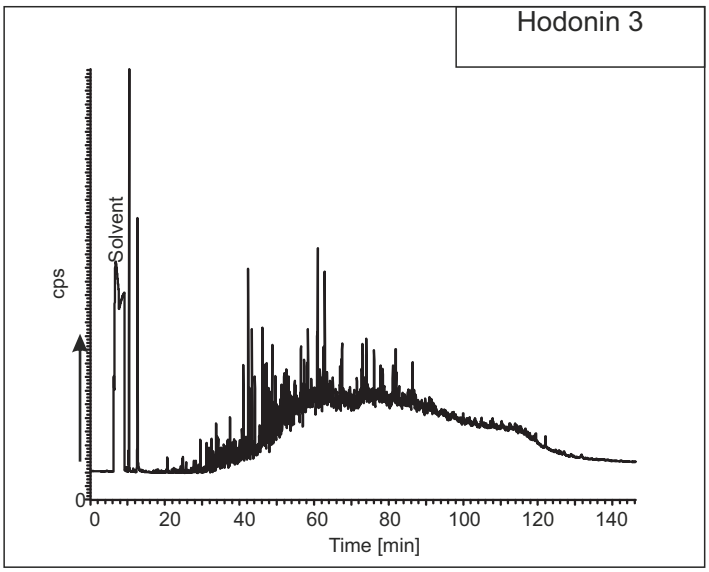
Hodonin 3
Solvent
cps
0
0 20 40 60 80 100 120 140
Time [min]

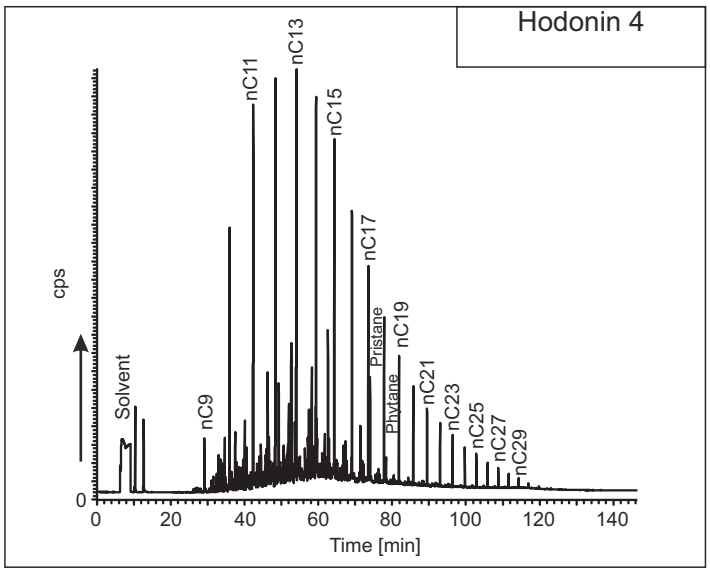
Hodonin 4
Solvent
nC9
nC11
nC13
nC15
nC17
Pristane
Phytane
nC19
nC21
nC23
nC25
nC27
nC29
cps
0
0 20 40 60 80 100 120 140
Time [min]

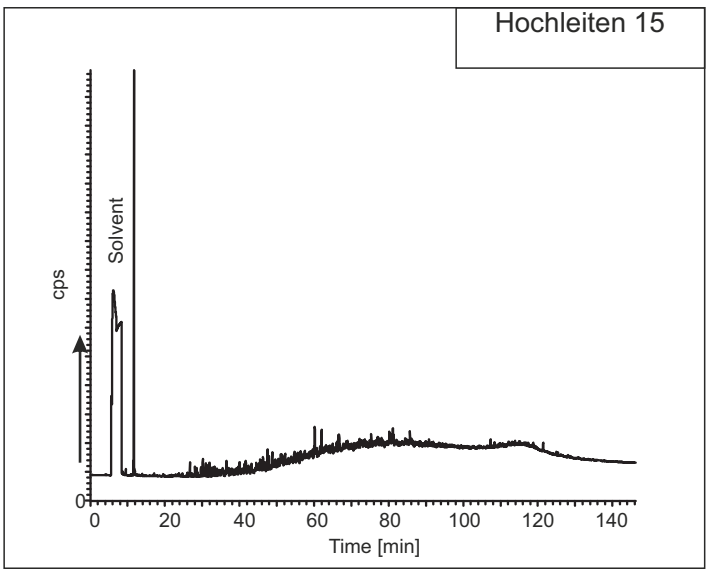
Hochleiten 15
Solvent
cps
0
0 20 40 60 80 100 120 140
Time [min]

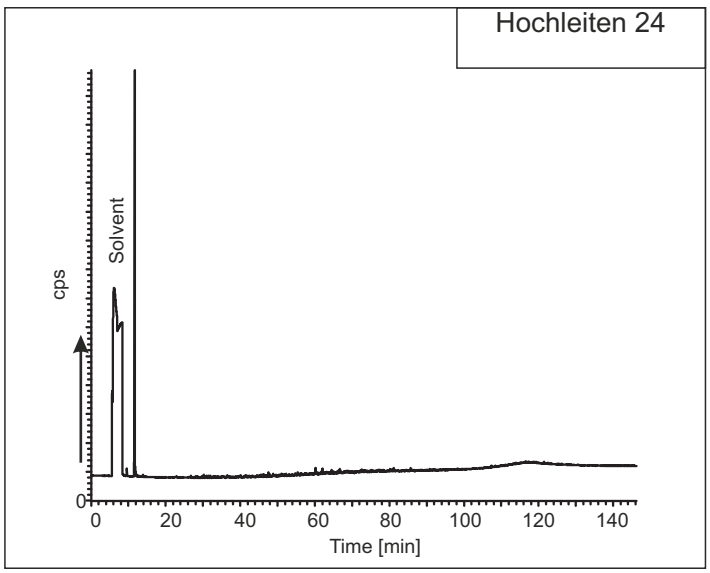
Hochleiten 24
Solvent
cps
0
0 20 40 60 80 100 120 140
Time [min]

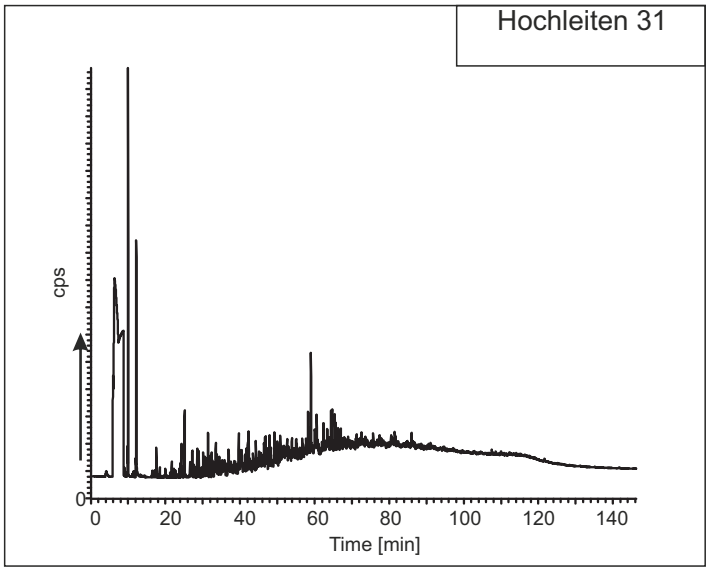
Hochleiten 31
cps
0
0 20 40 60 80 100 120 140
Time [min]

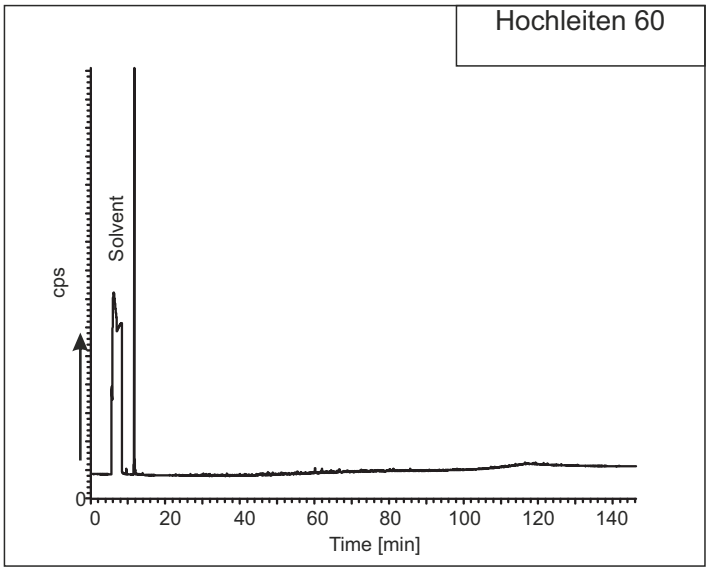
Hochleiten 60
Solvent
cps
0
0 20 40 60 80 100 120 140
Time [min]

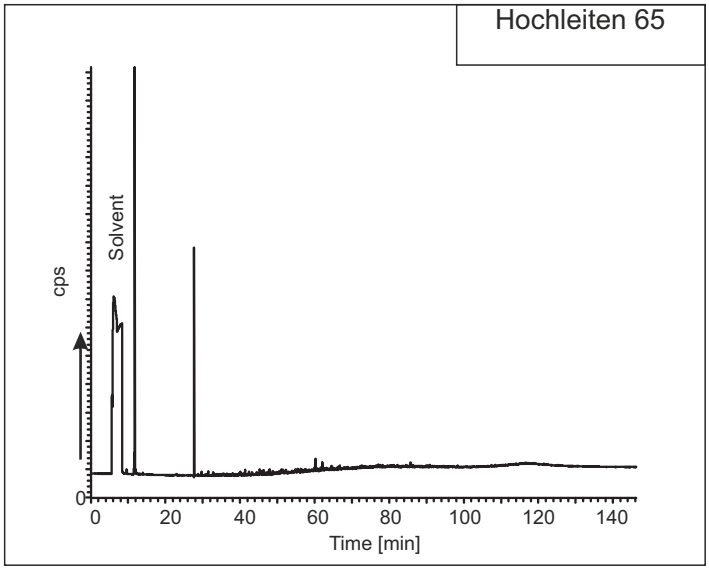
Hochleiten 65
Solvent
cps
0
0 20 40 60 80 100 120 140
Time [min]

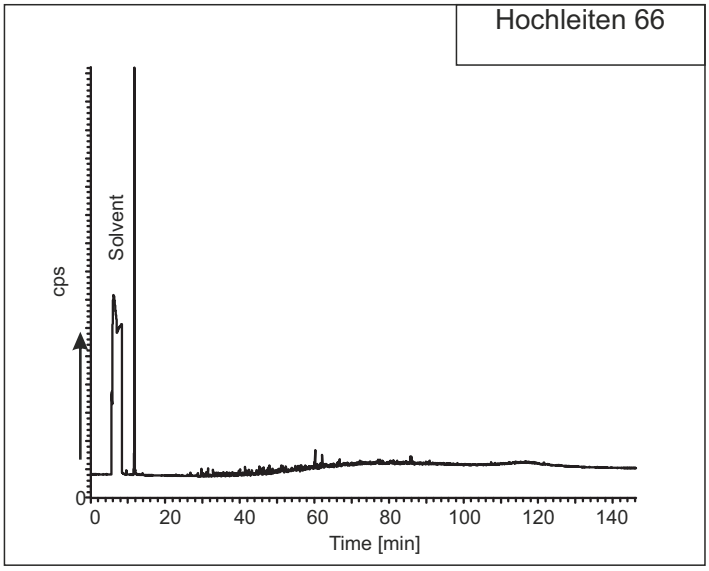
Hochleiten 66
Solvent
cps
0
0 20 40 60 80 100 120 140
Time [min]

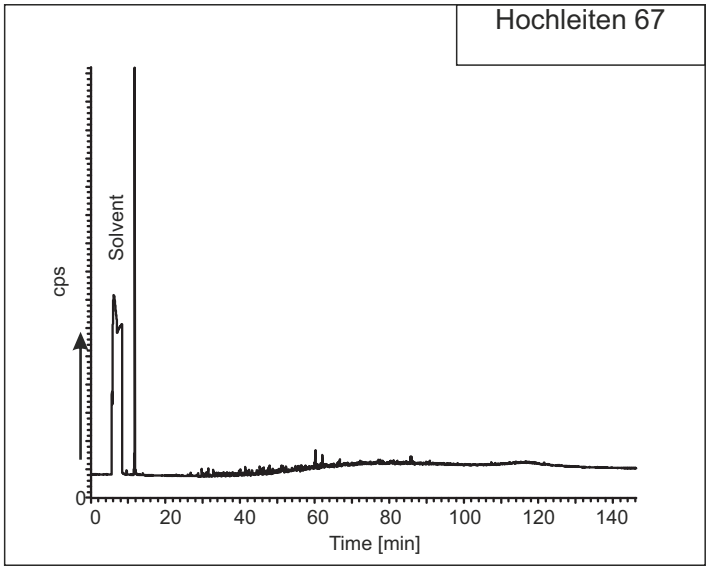
Hochleiten 67
Solvent
cps
0
0 20 40 60 80 100 120 140
Time [min]

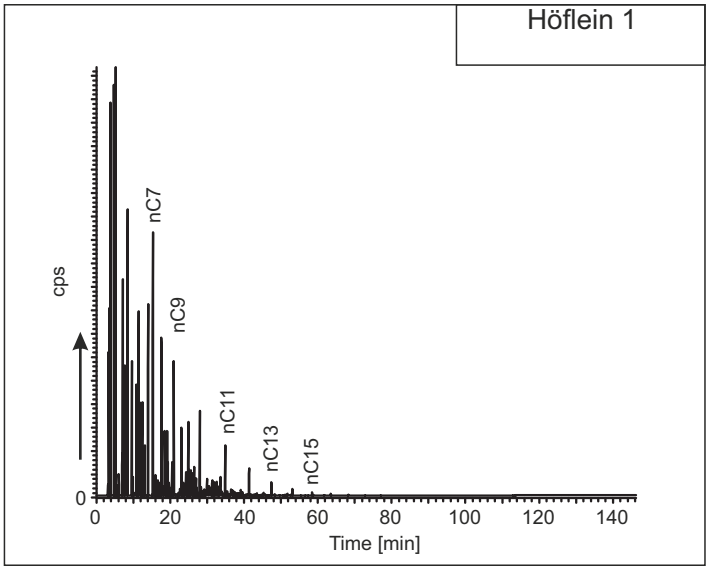
Höflein 1
nC7
nC9
nC11
nC13
nC15
cps
0
0 20 40 60 80 100 120 140
Time [min]

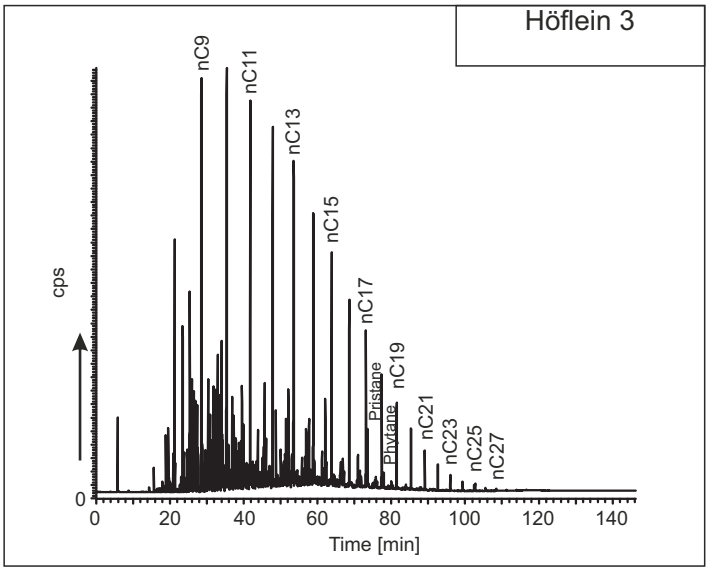
Höflein 3
nC9
nC11
nC13
nC15
nC17
Pristane
Phytane
nC19
nC21
nC23
nC25
nC27
cps
0
0 20 40 60 80 100 120 140
Time [min]

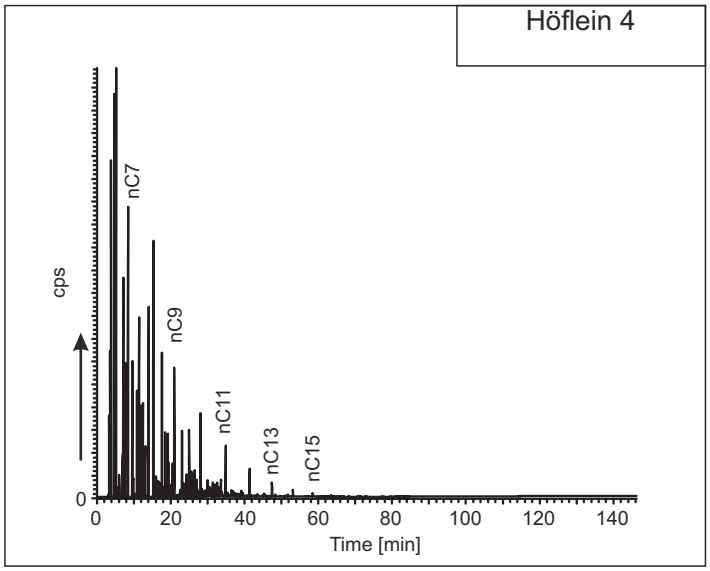
Höflein 4
nC7
nC9
nC11
nC13
nC15
cps
0
0 20 40 60 80 100 120 140
Time [min]

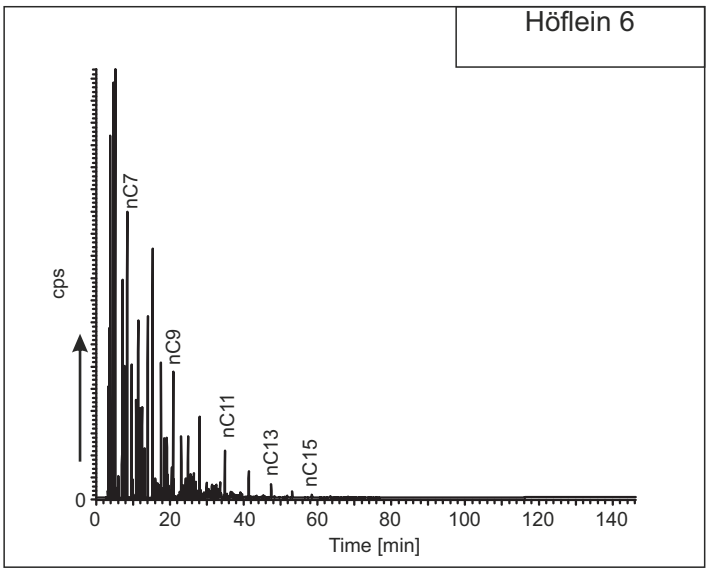
Höflein 6
nC7
nC9
nC11
nC13
nC15
cps
0
0 20 40 60 80 100 120 140
Time [min]

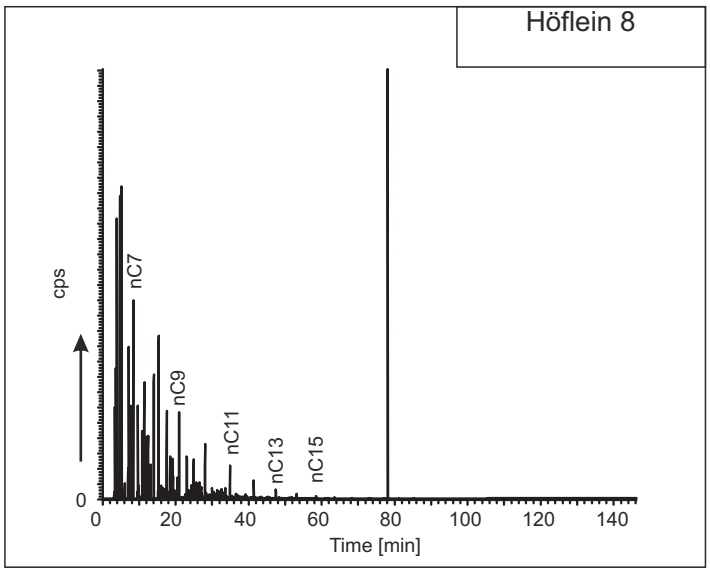
Höflein 8
nC7
nC9
nC11
nC13
nC15
cps
0
0 20 40 60 80 100 120 140
Time [min]

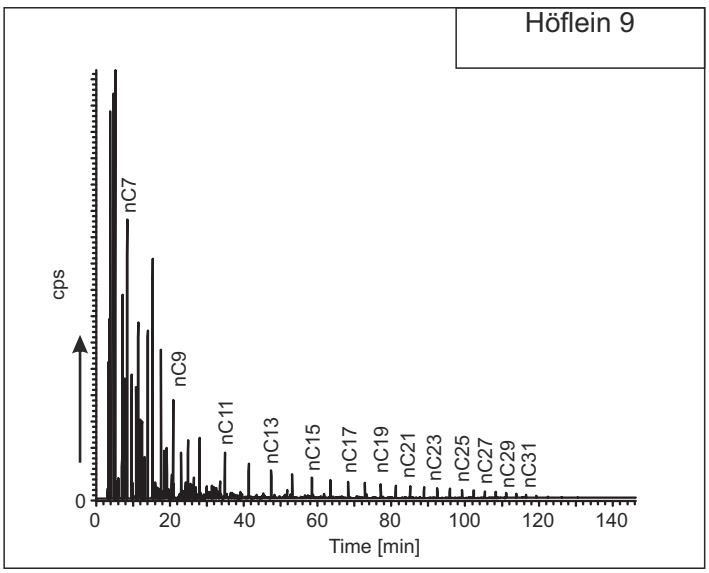
Höflein 9
nC7
nC9
nC11
nC13
nC15
nC17
nC19
nC21
nC23
nC25
nC27
nC29
nC31
cps
0
0 20 40 60 80 100 120 140
Time [min]

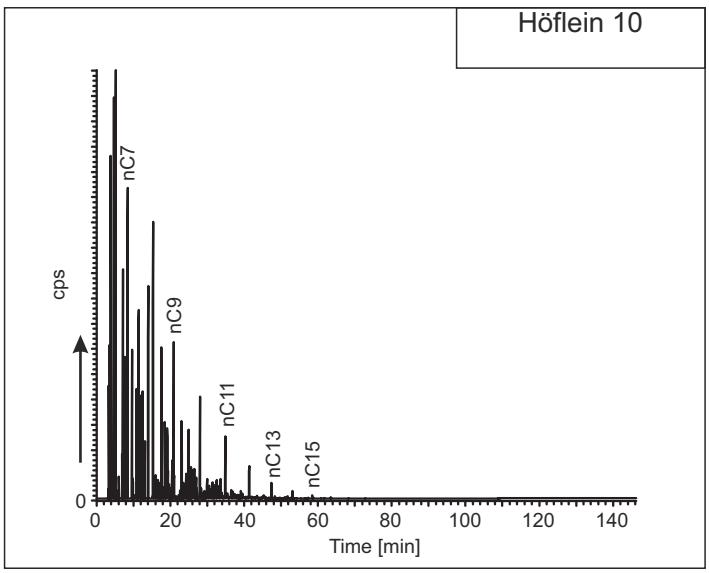
Höflein 10
nC7
nC9
nC11
nC13
nC15
cps
0
0 20 40 60 80 100 120 140
Time [min]

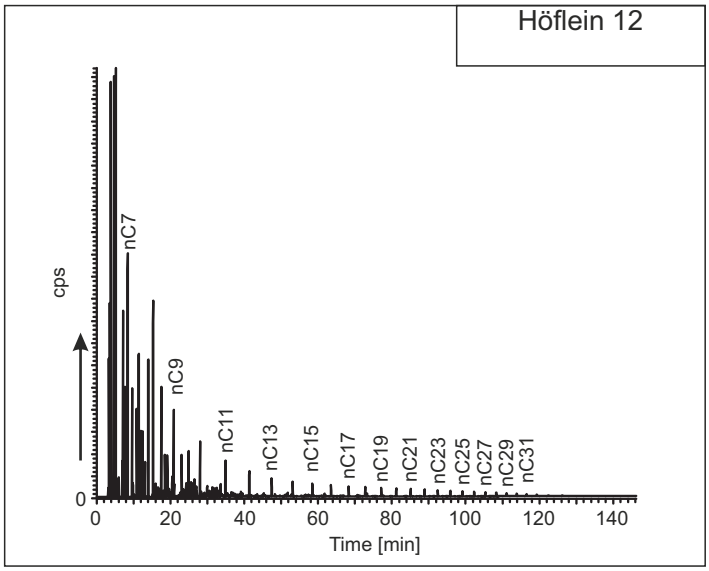
Höflein 12
cps
0
nC7
nC9
nC11
nC13
nC15
nC17
nC19
nC21
nC23
nC25
nC27
nC29
nC31
0 20 40 60 80 100 120 140
Time [min]

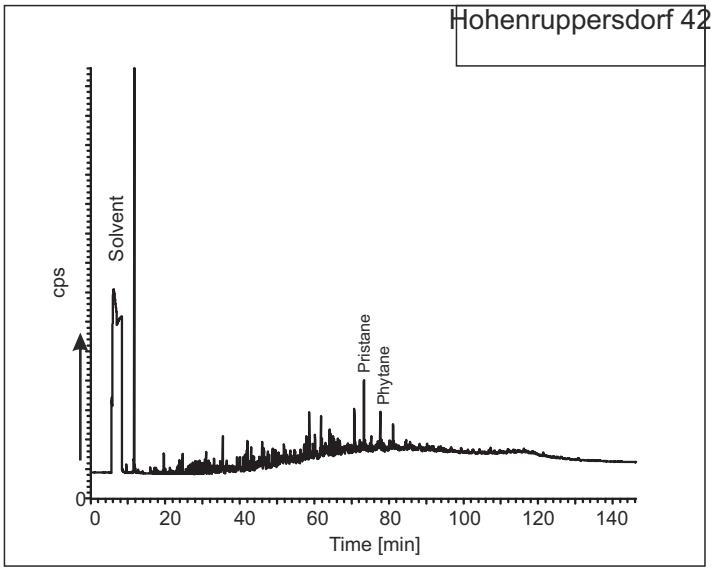
Hohenruppersdorf 42
cps
0
Solvent
Pristane
Phytane
0 20 40 60 80 100 120 140
Time [min]

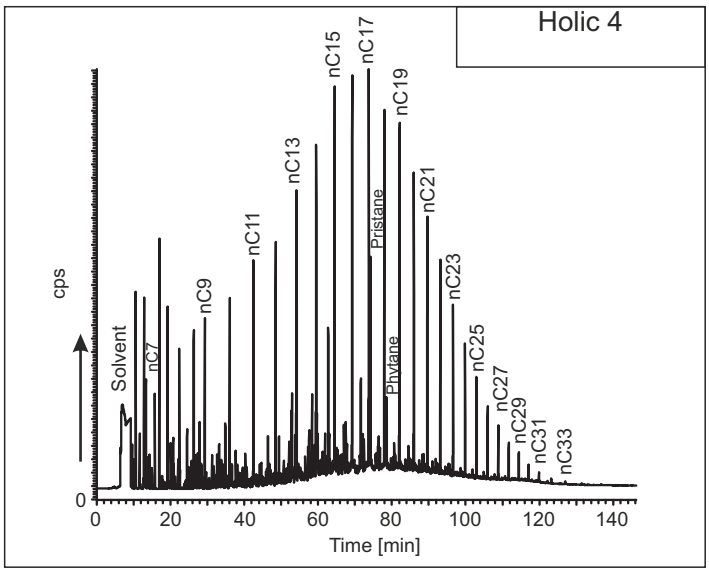
Holic 4
cps
0
Solvent
nC7
nC9
nC11
nC13
nC15
nC17
nC19
Pristane
Phytane
nC21
nC23
nC25
nC27
nC29
nC31
nC33
0 20 40 60 80 100 120 140
Time [min]

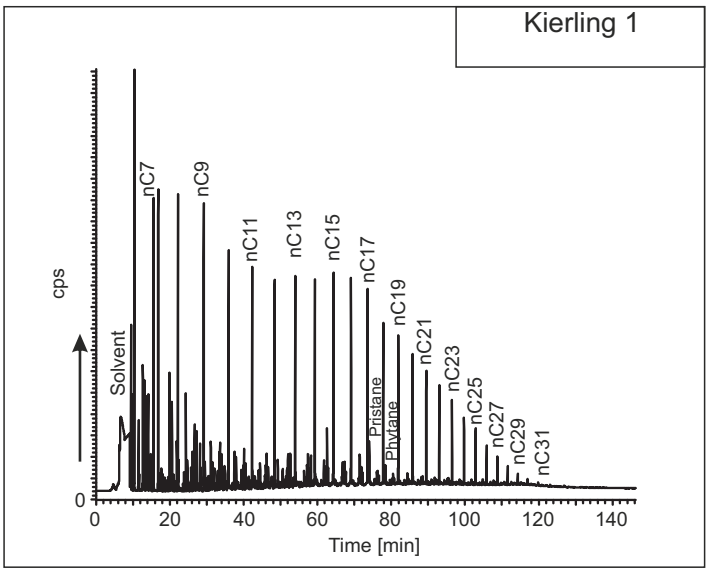
Kierling 1
cps
0
Solvent
nC7
nC9
nC11
nC13
nC15
nC17
nC19
Pristane
Phytane
nC21
nC23
nC25
nC27
nC29
nC31
0 20 40 60 80 100 120 140
Time [min]

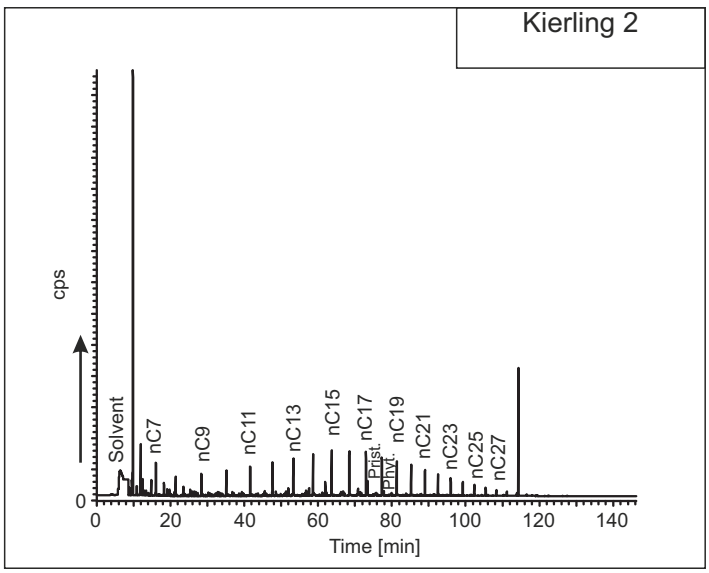
Kierling 2
cps
0
Solvent
nC7
nC9
nC11
nC13
nC15
nC17
Pist.
Phyt.
nC19
nC21
nC23
nC25
nC27
0 20 40 60 80 100 120 140
Time [min]

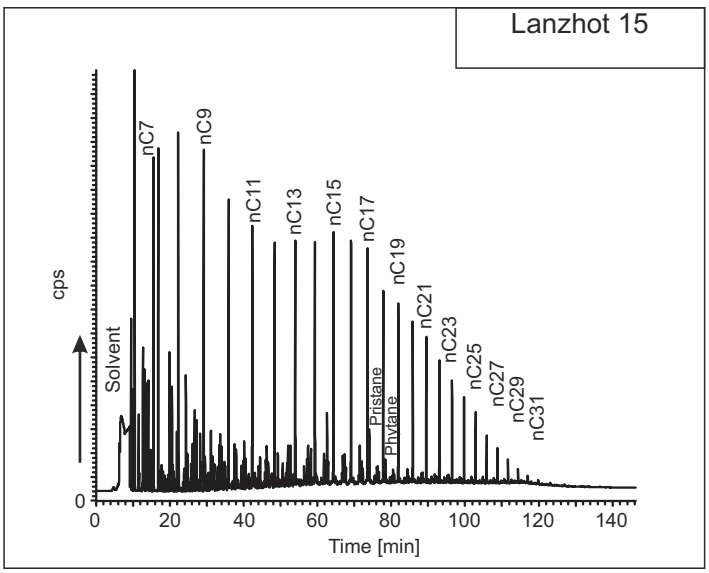
Lanzhot 15
cps
0
Solvent
nC7
nC9
nC11
nC13
nC15
nC17
nC19
Pristane
Phytane
nC21
nC23
nC25
nC27
nC29
nC31
0 20 40 60 80 100 120 140
Time [min]

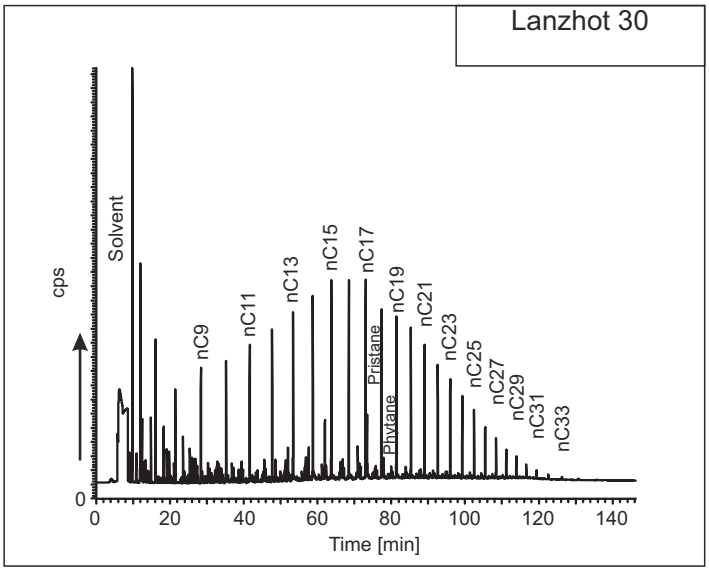
Lanzhot 30
cps
Solvent
nC9
nC11
nC13
nC15
nC17
Pristane
Phytane
nC19
nC21
nC23
nC25
nC27
nC29
nC31
nC33
0
0 20 40 60 80 100 120 140
Time [min]

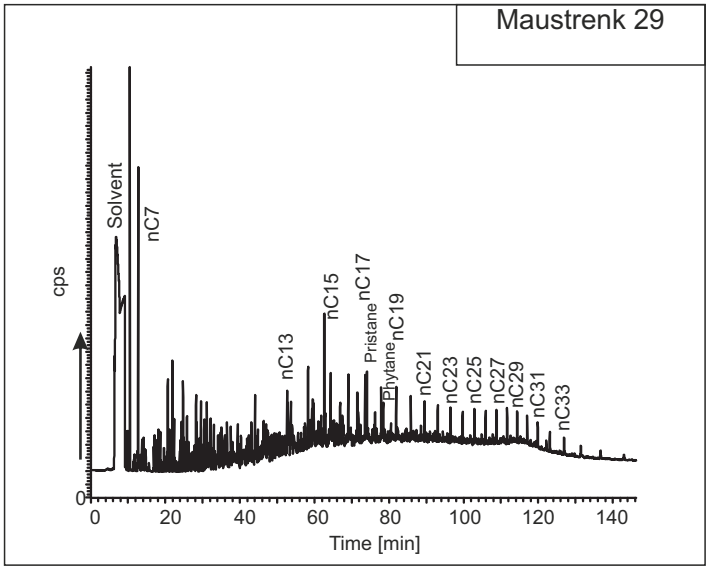
Maustrenk 29
cps
Solvent
nC7
nC13
nC15
nC17
Pristane
Phytane
nC19
nC21
nC23
nC25
nC27
nC29
nC31
nC33
0
0 20 40 60 80 100 120 140
Time [min]

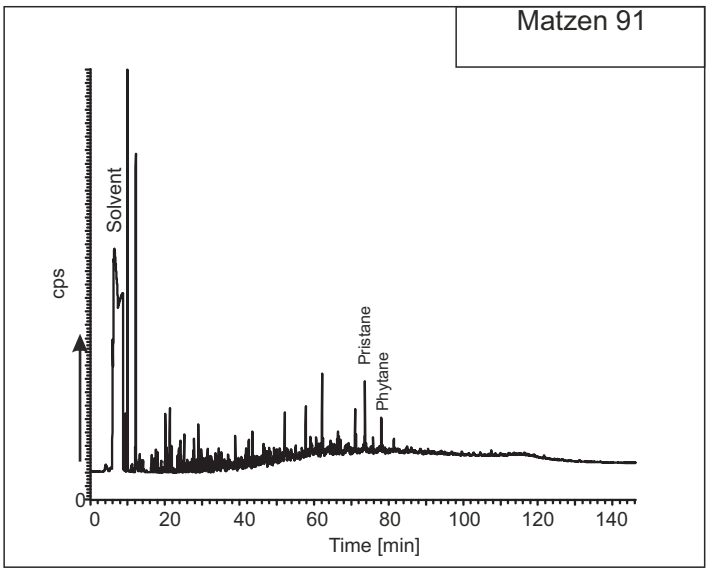
Matzen 91
cps
Solvent
Pristane
Phytane
0
0 20 40 60 80 100 120 140
Time [min]

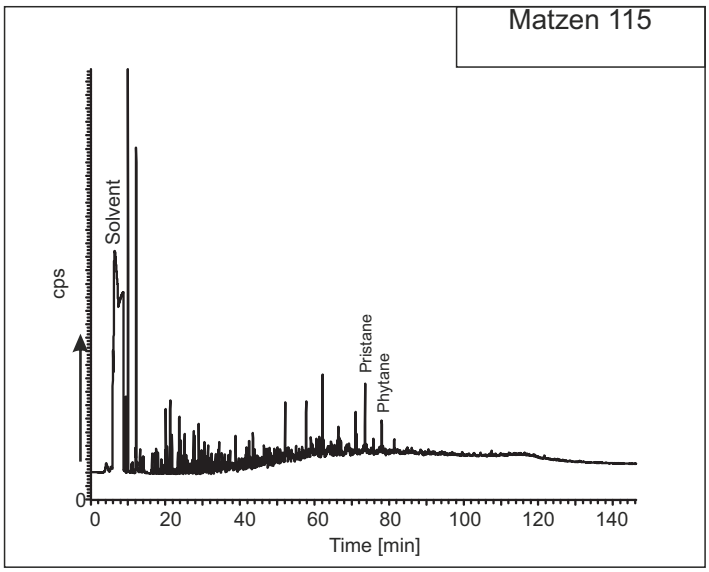
Matzen 115
cps
Solvent
Pristane
Phytane
0
0 20 40 60 80 100 120 140
Time [min]

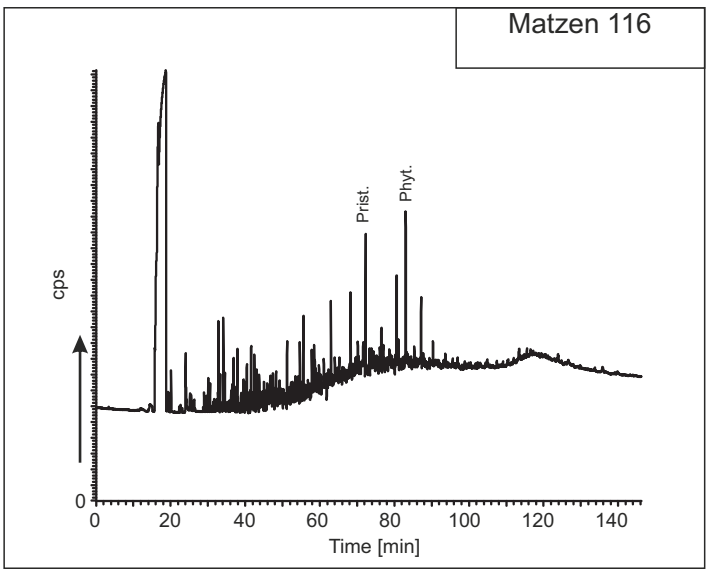
Matzen 116
cps
Prist.
Phyt.
0
0 20 40 60 80 100 120 140
Time [min]

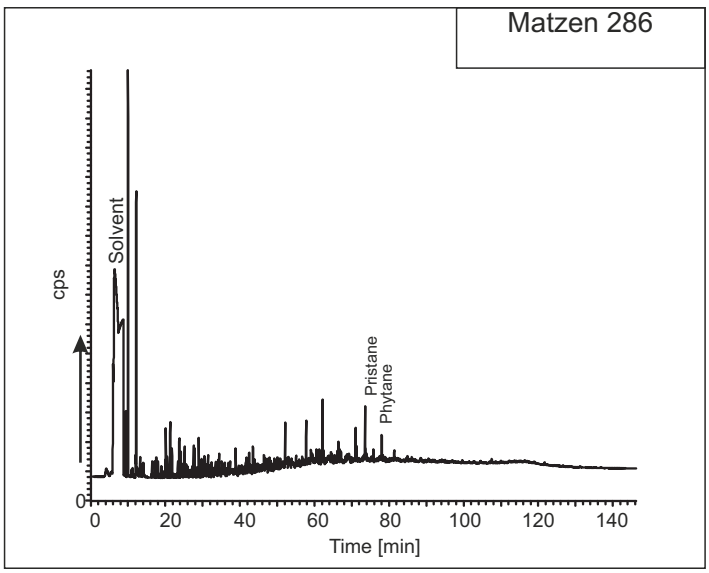
Matzen 286
cps
Solvent
Pristane
Phytane
0
0 20 40 60 80 100 120 140
Time [min]

Matzen 322

File unfortunatly corrupted

Matzen 390y

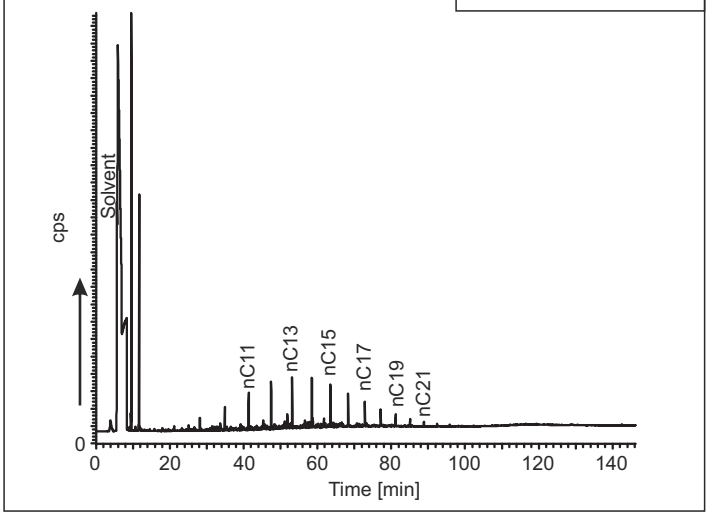

Matzen H 703b

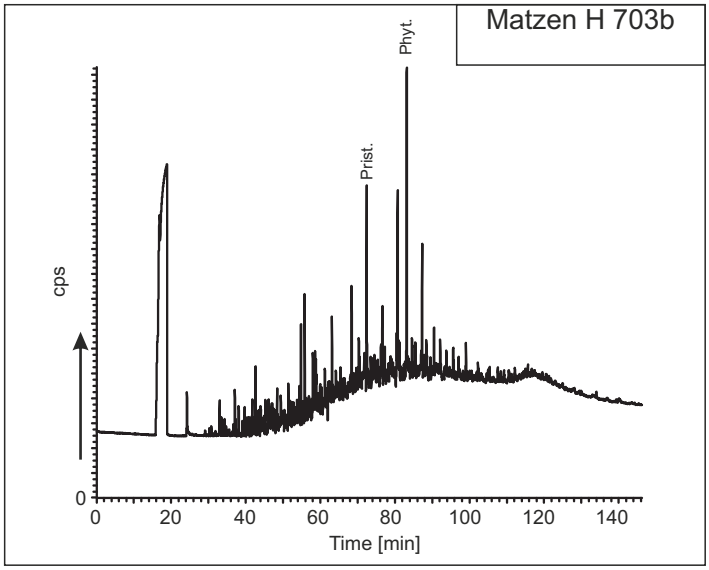

Mühlberg 15

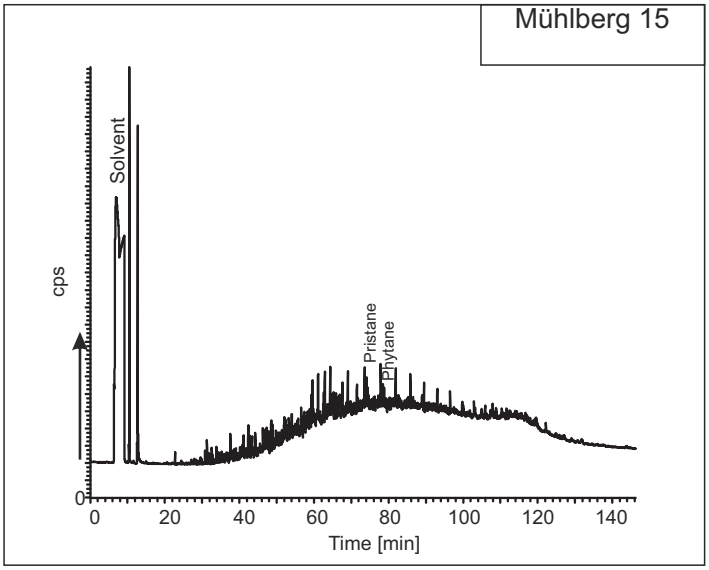

Neusiedl 1

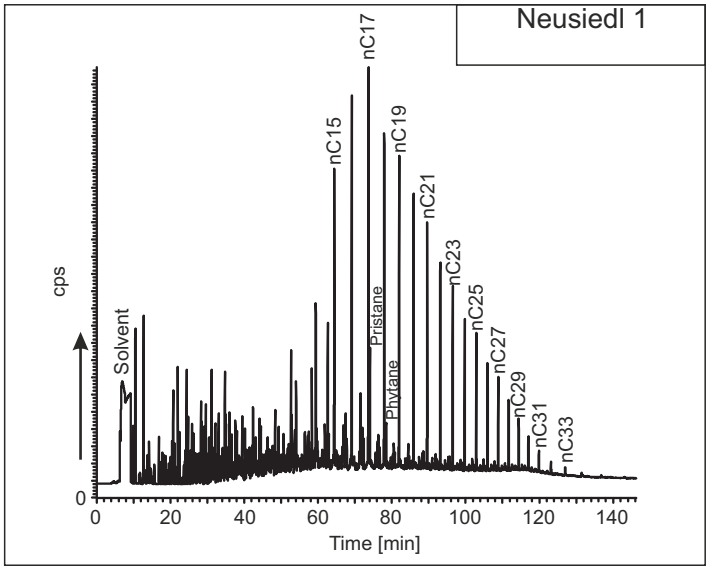

Neusiedl 3

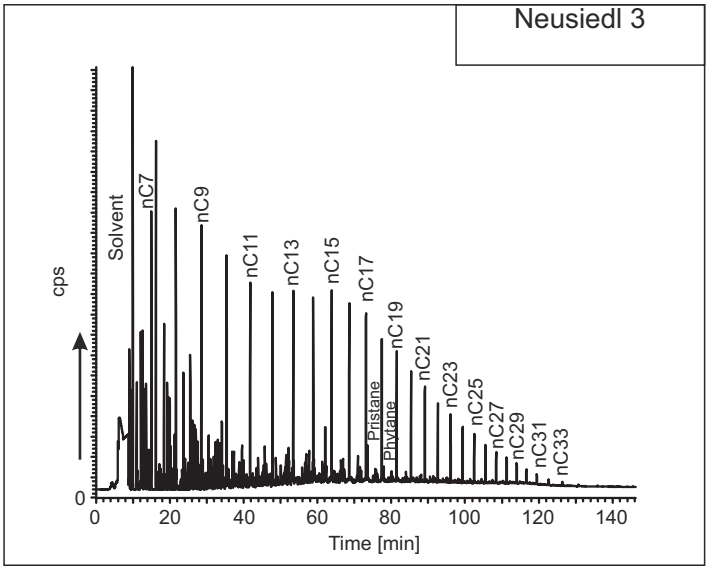

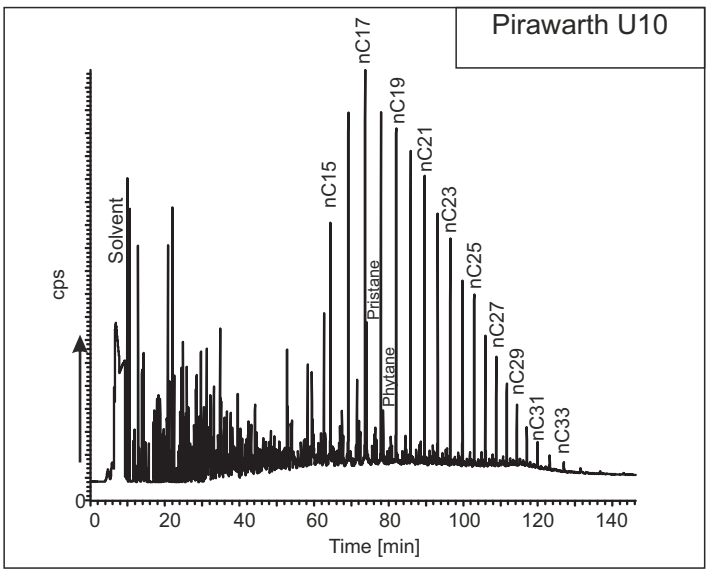
Pirawarth U10
Solvent
nC15
nC17
Pristane
nC19
Phytane
nC21
nC23
nC25
nC27
nC29
nC31
nC33
cps
0
0 20 40 60 80 100 120 140
Time [min]

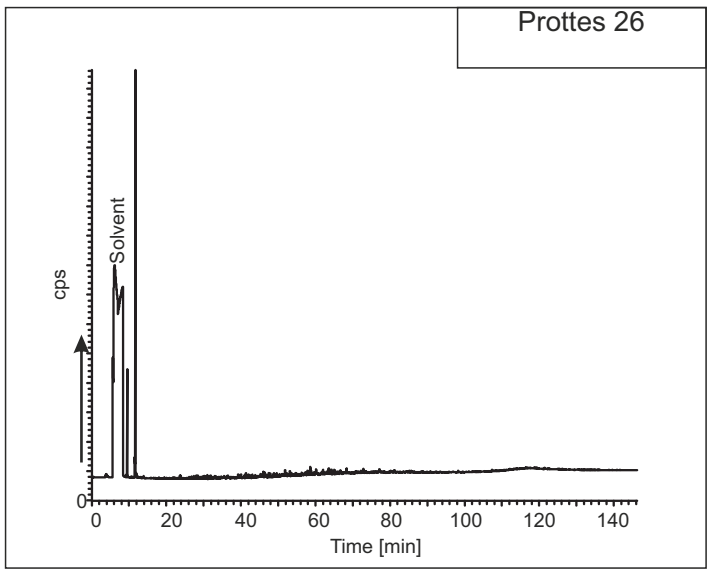
Prottes 26
Solvent
cps
0
0 20 40 60 80 100 120 140
Time [min]

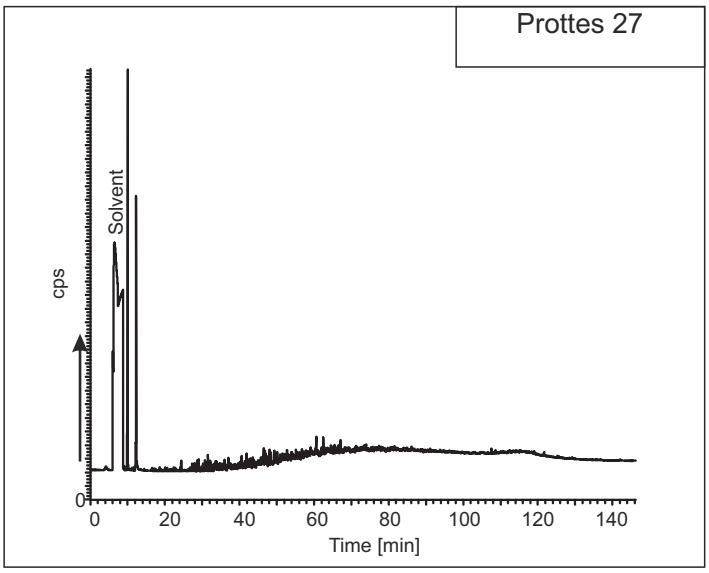
Prottes 27
Solvent
cps
0
0 20 40 60 80 100 120 140
Time [min]

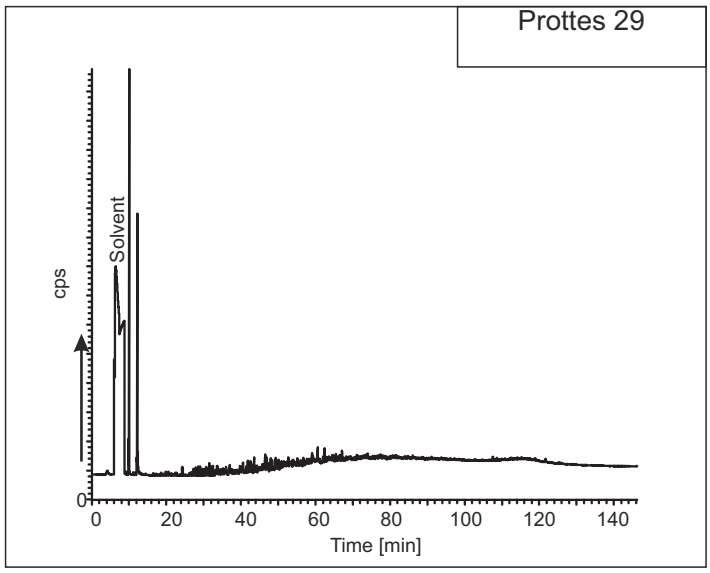
Prottes 29
Solvent
cps
0
0 20 40 60 80 100 120 140
Time [min]

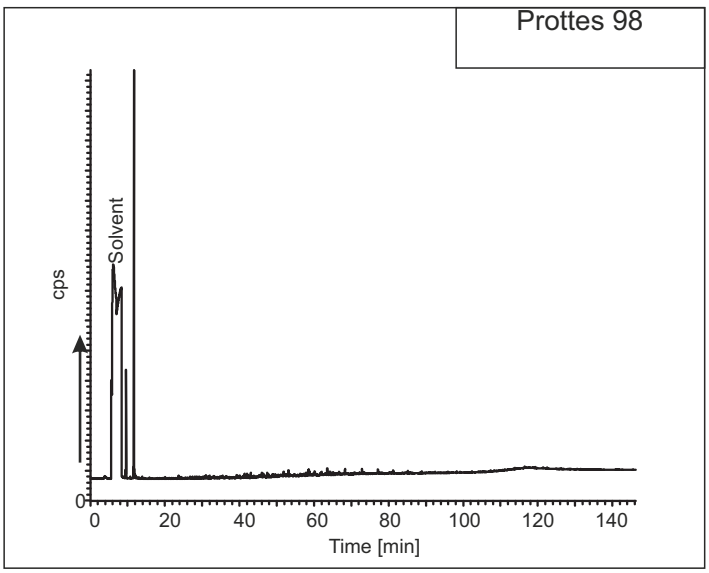
Prottes 98
Solvent
cps
0
0 20 40 60 80 100 120 140
Time [min]

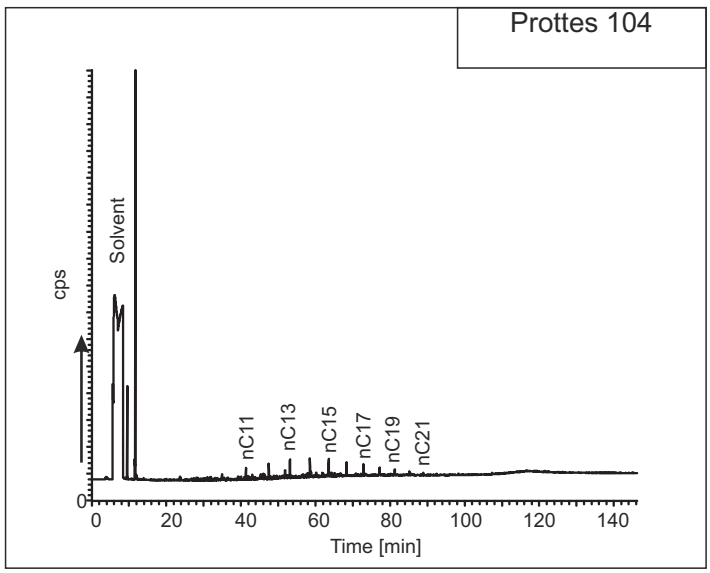
Prottes 104
Solvent
nC11
nC13
nC15
nC17
nC19
nC21
cps
0
0 20 40 60 80 100 120 140
Time [min]

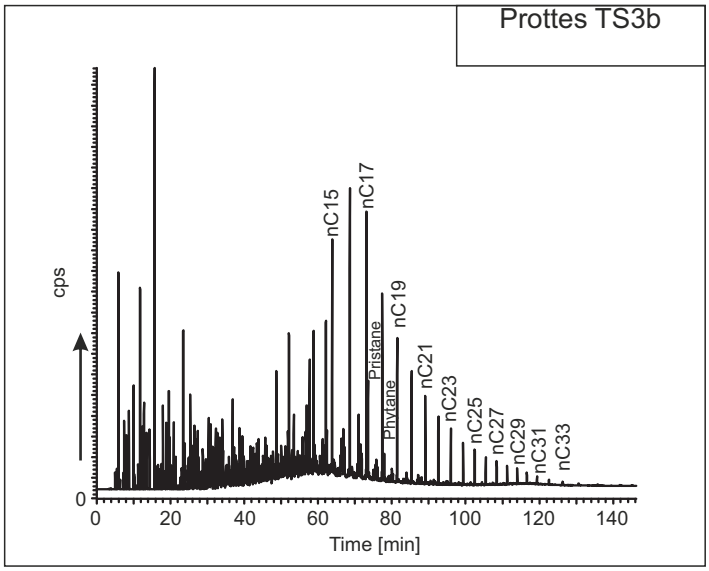
Prottes TS3b
cps
0
nC15
nC17
nC19
Pristane
Phytane
nC21
nC23
nC25
nC27
nC29
nC31
nC33
0 20 40 60 80 100 120 140
Time [min]

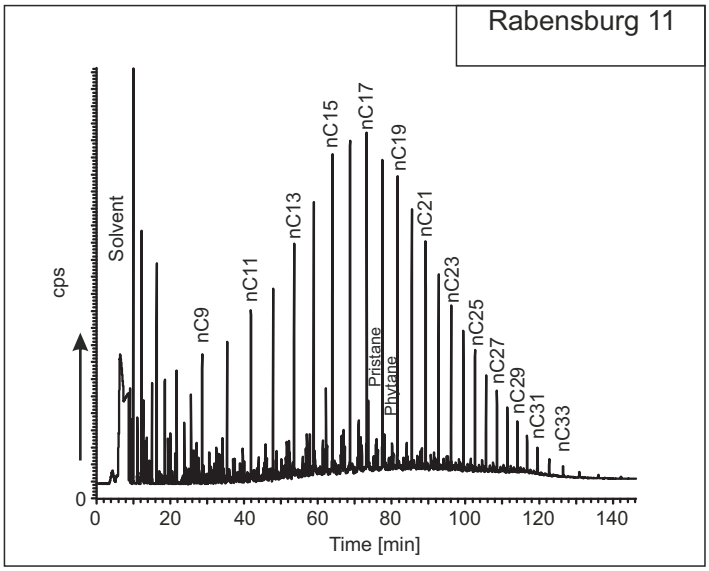
Rabensburg 11
cps
0
Solvent
nC9
nC11
nC13
nC15
nC17
nC19
Pristane
Phytane
nC21
nC23
nC25
nC27
nC29
nC31
nC33
0 20 40 60 80 100 120 140
Time [min]

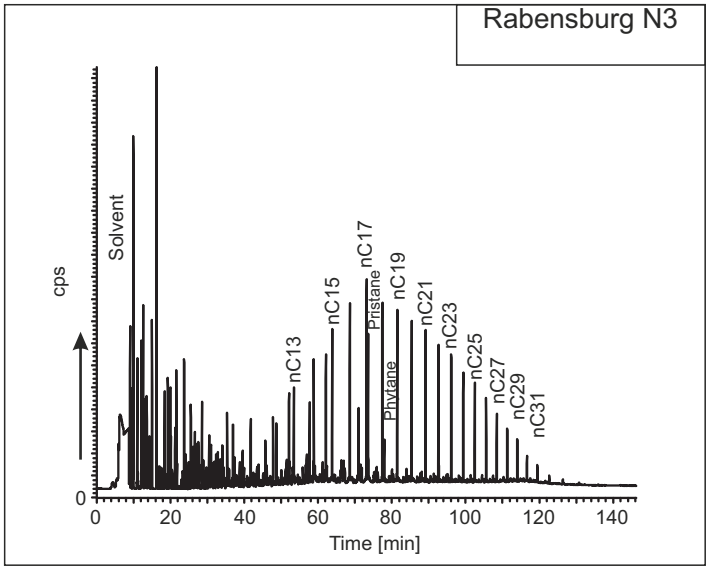
Rabensburg N3
cps
0
Solvent
nC13
nC15
nC17
Pristane
nC19
Phytane
nC21
nC23
nC25
nC27
nC29
nC31
0 20 40 60 80 100 120 140
Time [min]

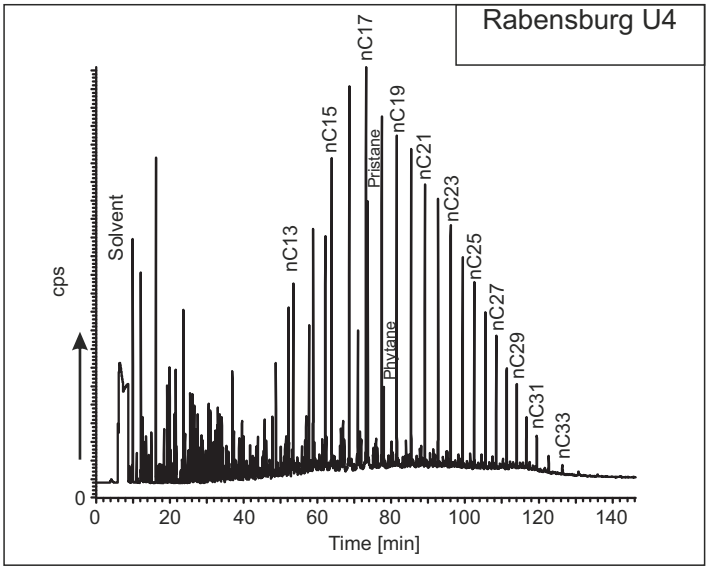
Rabensburg U4
cps
0
Solvent
nC13
nC15
nC17
Pristane
nC19
Phytane
nC21
nC23
nC25
nC27
nC29
nC31
nC33
0 20 40 60 80 100 120 140
Time [min]

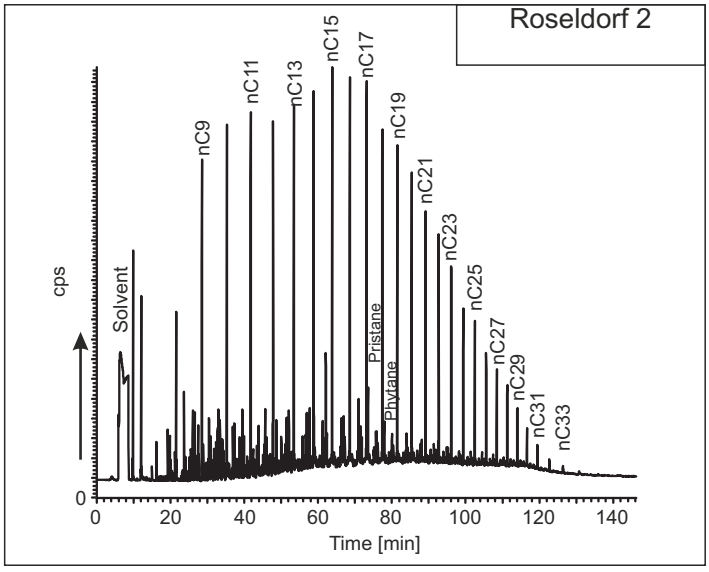
Roseldorf 2
cps
0
Solvent
nC9
nC11
nC13
nC15
nC17
nC19
nC21
nC23
nC25
Pristane
nC27
Phytane
nC29
nC31
nC33
0 20 40 60 80 100 120 140
Time [min]

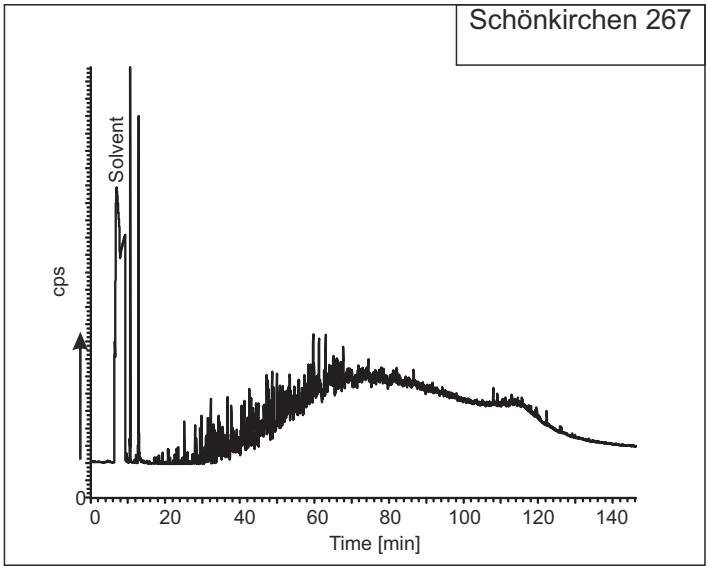
Schönkirchen 267
cps
0
Solvent
0 20 40 60 80 100 120 140
Time [min]

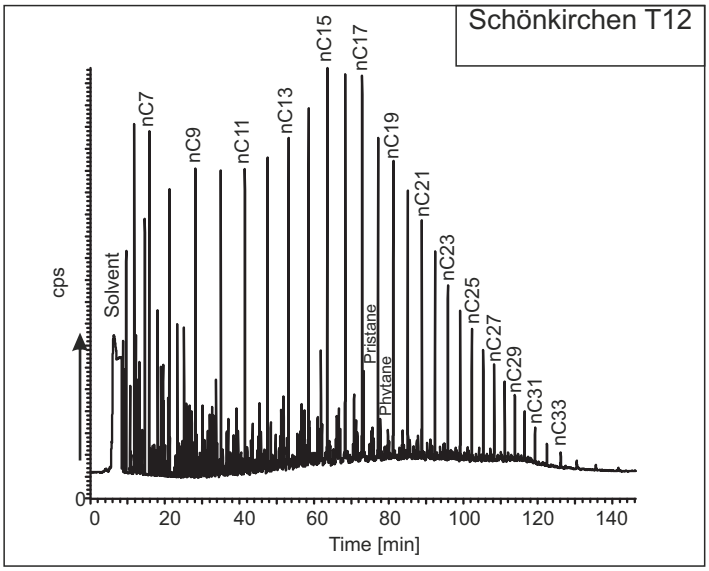
Schönkirchen T12
cps
Solvent
nC7
nC9
nC11
nC13
nC15
nC17
Pristane
nC19
Phytane
nC21
nC23
nC25
nC27
nC29
nC31
nC33
0
0 20 40 60 80 100 120 140
Time [min]

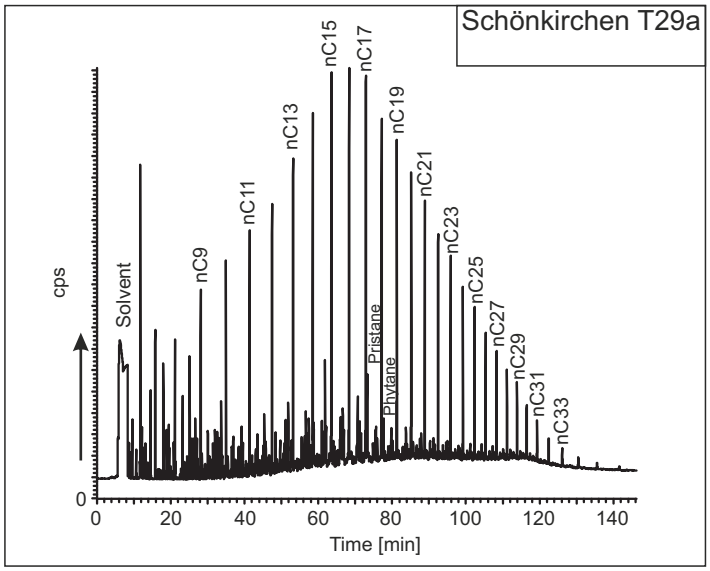
Schönkirchen T29a
cps
Solvent
nC9
nC11
nC13
nC15
nC17
Pristane
nC19
Phytane
nC21
nC23
nC25
nC27
nC29
nC31
nC33
0
0 20 40 60 80 100 120 140
Time [min]

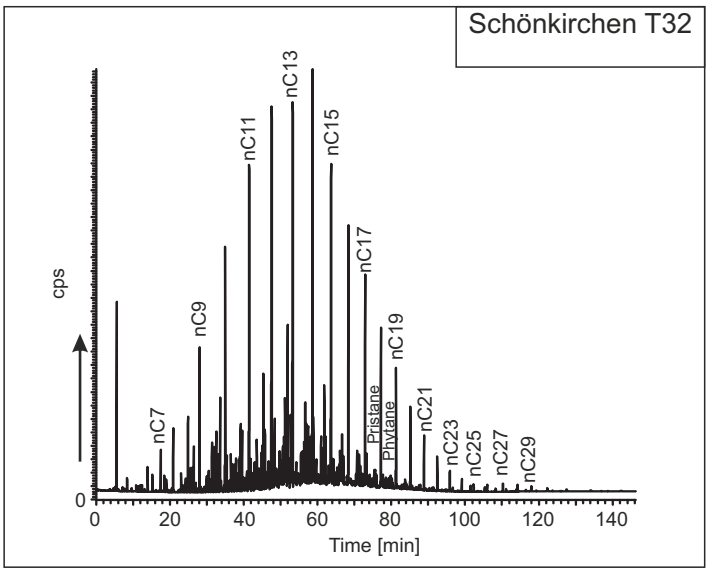
Schönkirchen T32
cps
nC7
nC9
nC11
nC13
nC15
nC17
Pristane
nC19
Phytane
nC21
nC23
nC25
nC27
nC29
0
0 20 40 60 80 100 120 140
Time [min]

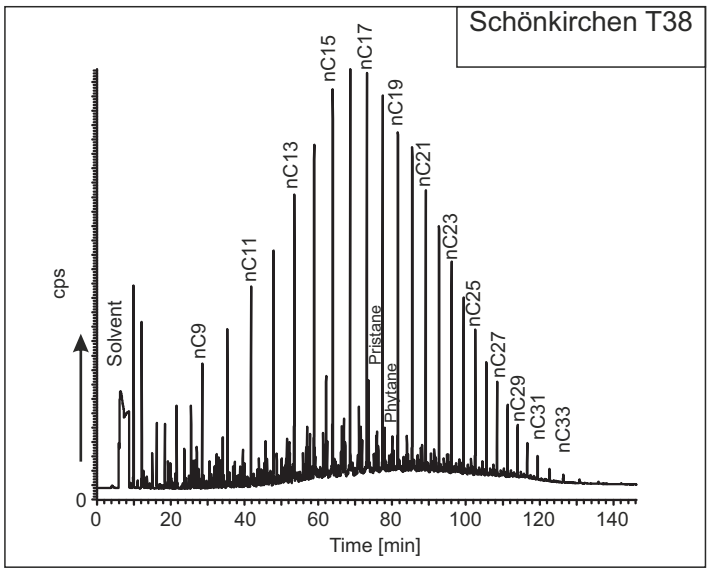
Schönkirchen T38
cps
Solvent
nC9
nC11
nC13
nC15
nC17
Pristane
nC19
Phytane
nC21
nC23
nC25
nC27
nC29
nC31
nC33
0
0 20 40 60 80 100 120 140
Time [min]

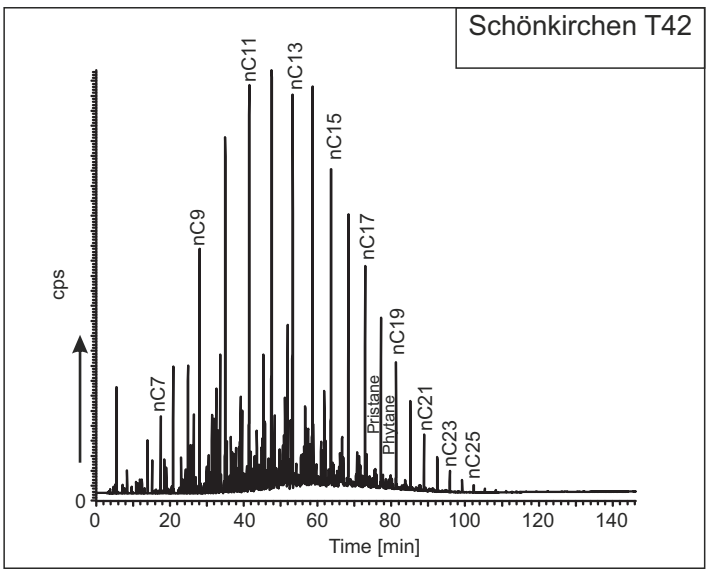
Schönkirchen T42
cps
nC7
nC9
nC11
nC13
nC15
nC17
Pristane
nC19
Phytane
nC21
nC23
nC25
0
0 20 40 60 80 100 120 140
Time [min]

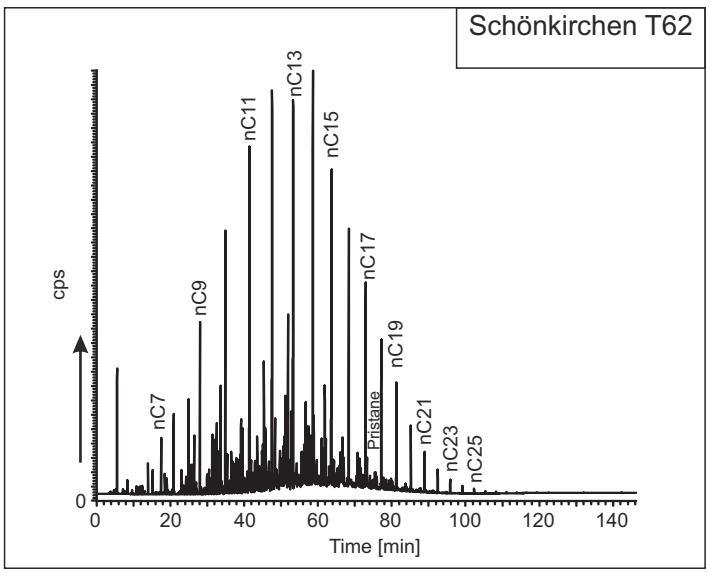
Schönkirchen T62
cps
nC7
nC9
nC11
nC13
nC15
nC17
Pristane
nC19
nC21
nC23
nC25
0
0 20 40 60 80 100 120 140
Time [min]

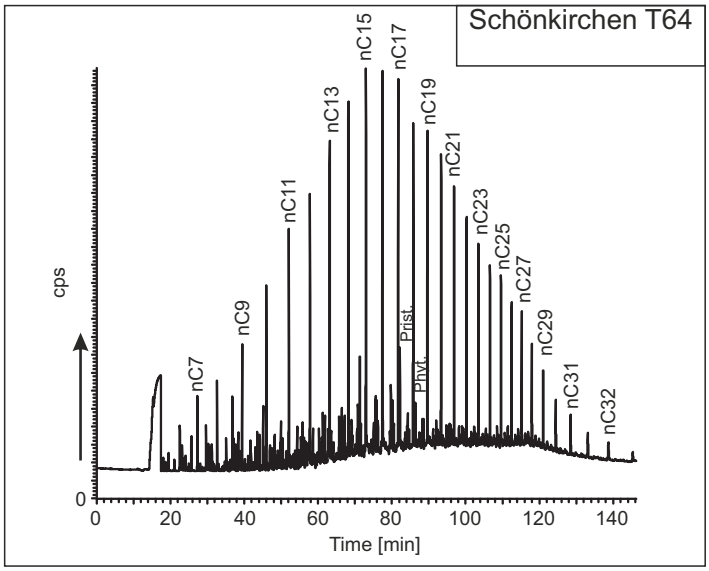
Schönkirchen T64
cps
0
nC7
nC9
nC11
nC13
nC15
nC17
nC19
nC21
nC23
nC25
nC27
nC29
nC31
nC32
Prist.
Phyt.
0 20 40 60 80 100 120 140
Time [min]

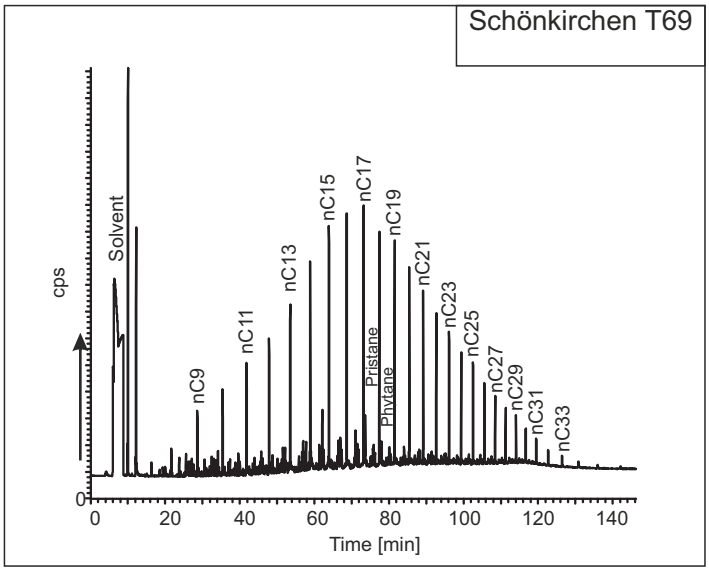
Schönkirchen T69
cps
0
Solvent
nC9
nC11
nC13
nC15
nC17
nC19
nC21
nC23
nC25
nC27
nC29
nC31
nC33
Pristane
Phytane
0 20 40 60 80 100 120 140
Time [min]

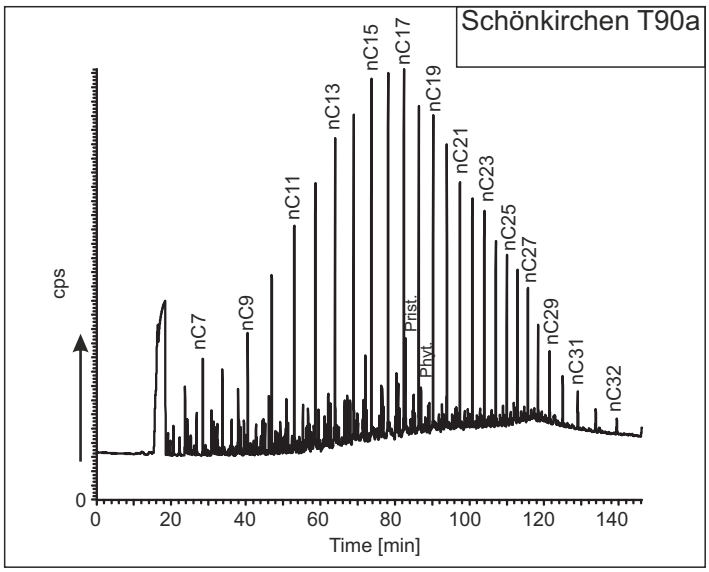
Schönkirchen T90a
cps
0
nC7
nC9
nC11
nC13
nC15
nC17
nC19
nC21
nC23
nC25
nC27
nC29
nC31
nC32
Prist.
Phyt.
0 20 40 60 80 100 120 140
Time [min]

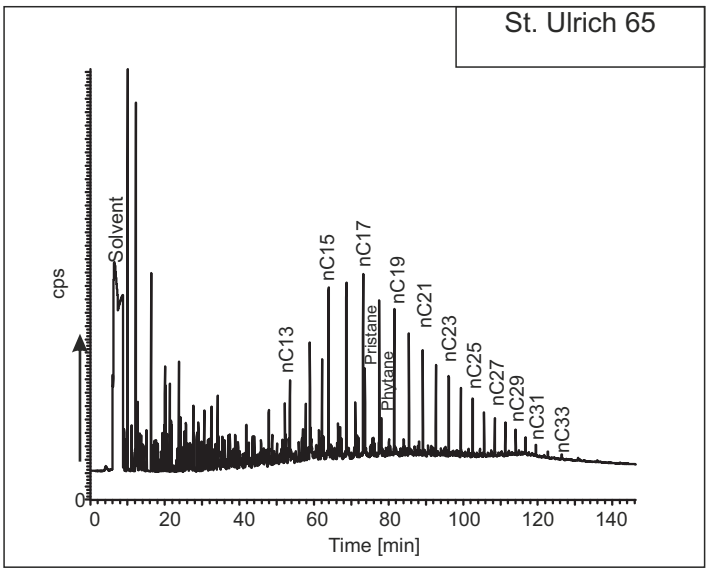
St. Ulrich 65
cps
0
Solvent
nC13
nC15
nC17
nC19
nC21
nC23
nC25
nC27
nC29
nC31
nC33
Pristane
Phytane
0 20 40 60 80 100 120 140
Time [min]

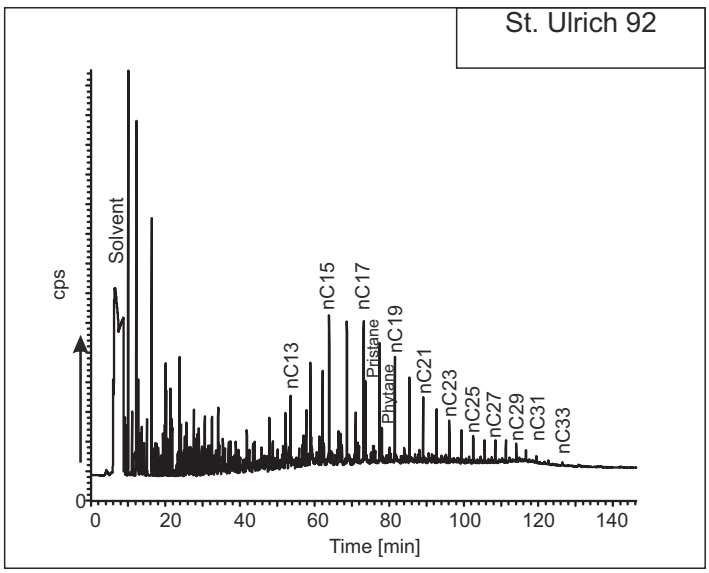
St. Ulrich 92
cps
0
Solvent
nC13
nC15
nC17
nC19
nC21
nC23
nC25
nC27
nC29
nC31
nC33
Pristane
Phytane
0 20 40 60 80 100 120 140
Time [min]

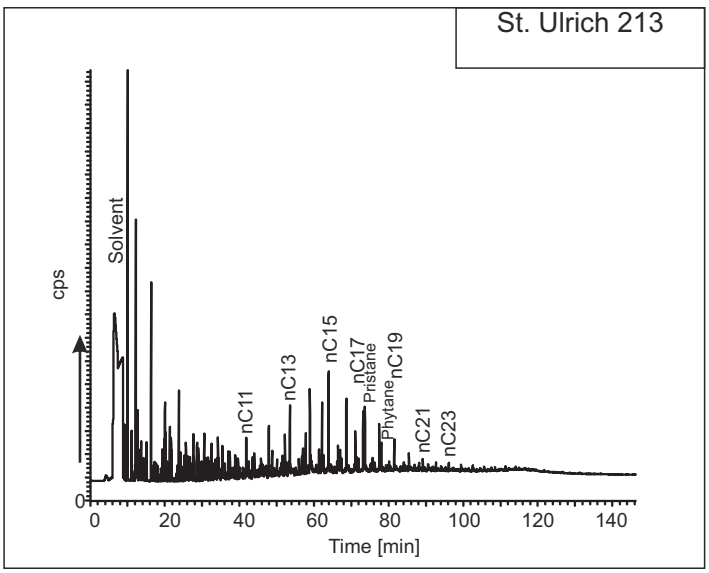
St. Ulrich 213
cps
0
Solvent
nC11
nC13
nC15
nC17
nC19
nC21
nC23
Pristane
Phytane
0 20 40 60 80 100 120 140
Time [min]

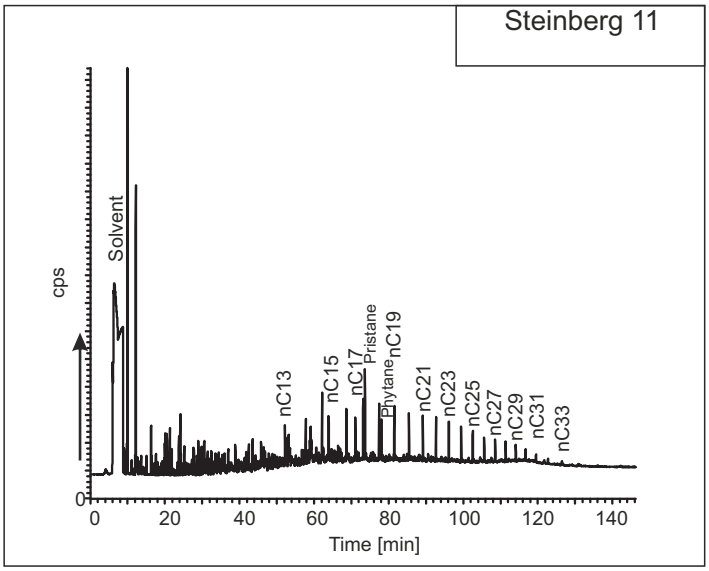
Steinberg 11
cps
Solvent
nC13
nC15
nC17
Pristane
Phytane
nC19
nC21
nC23
nC25
nC27
nC29
nC31
nC33
0
0 20 40 60 80 100 120 140
Time [min]

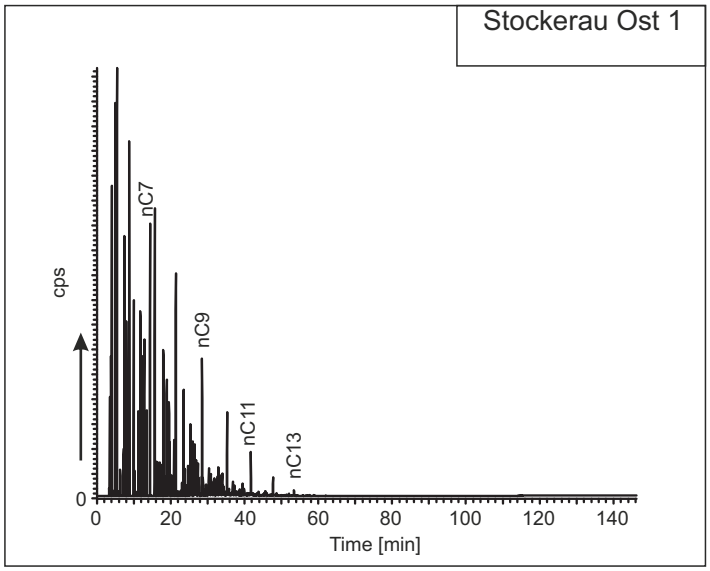
Stockerau Ost 1
cps
nC7
nC9
nC11
nC13
0
0 20 40 60 80 100 120 140
Time [min]

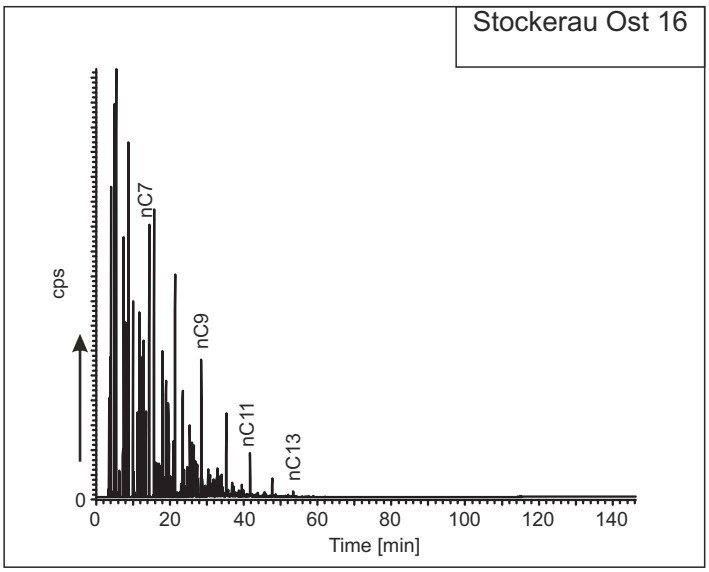
Stockerau Ost 16
cps
nC7
nC9
nC11
nC13
0
0 20 40 60 80 100 120 140
Time [min]

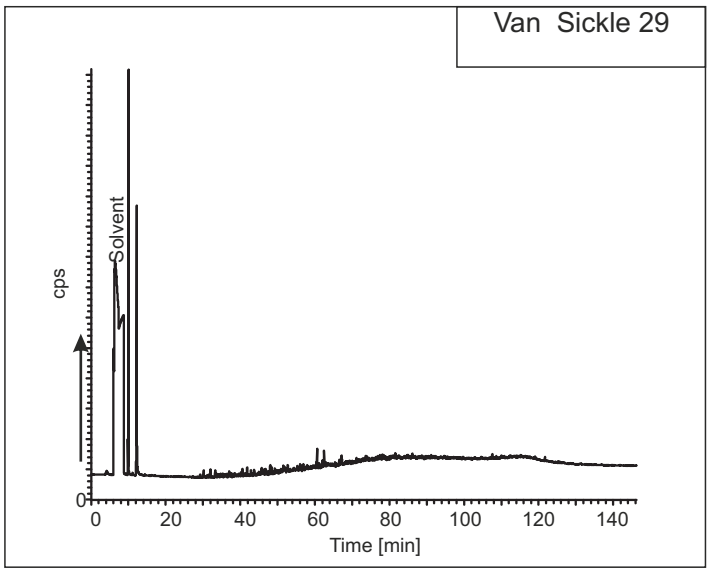
Van Sickle 29
cps
Solvent
0
0 20 40 60 80 100 120 140
Time [min]

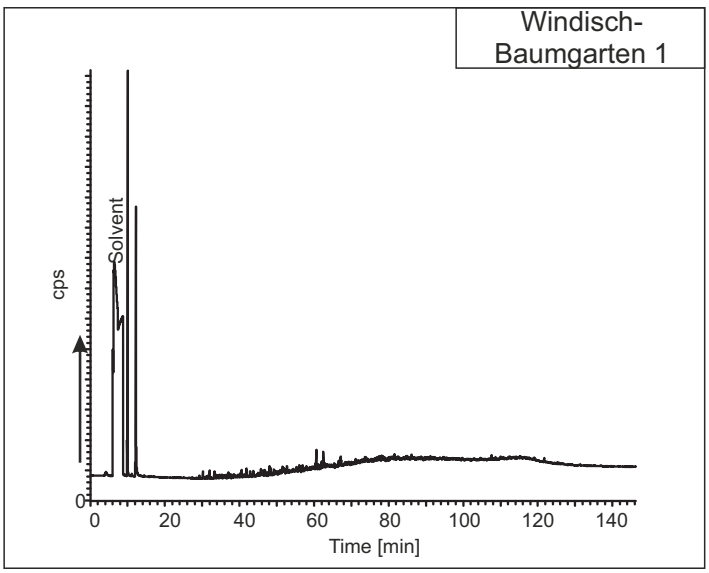
Windisch-
Baumgarten 1
cps
Solvent
0
0 20 40 60 80 100 120 140
Time [min]

Oils

Aliphatic Fraction

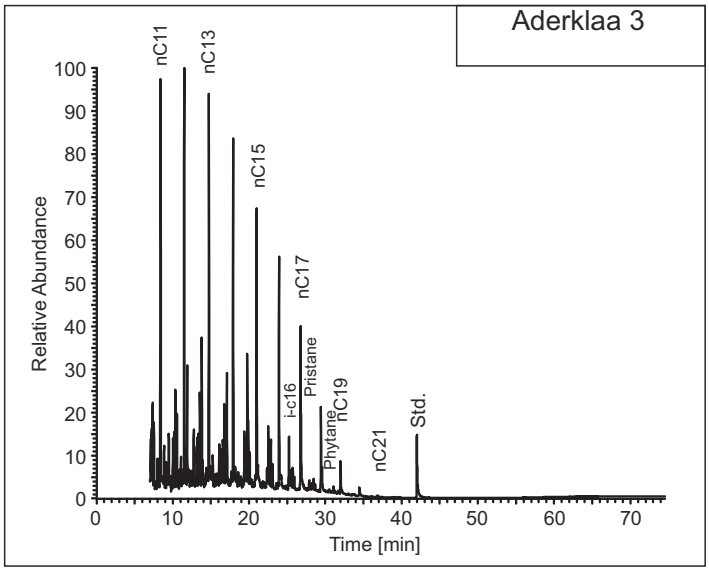
Aderklaa 3
nC11
nC13
nC15
nC17
i-c16
Pristane
Phytane
nC19
nC21
Std.
Relative Abundance
Time [min]

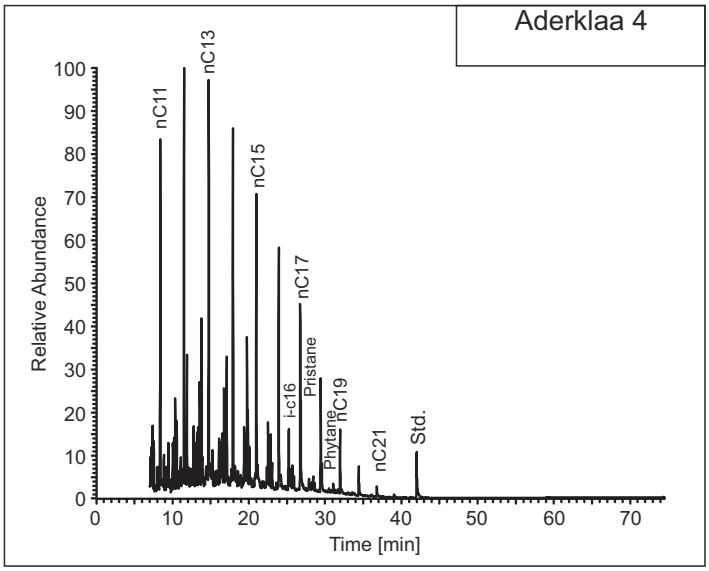
Aderklaa 4
nC11
nC13
nC15
nC17
i-c16
Pristane
Phytane
nC19
nC21
Std.
Relative Abundance
Time [min]

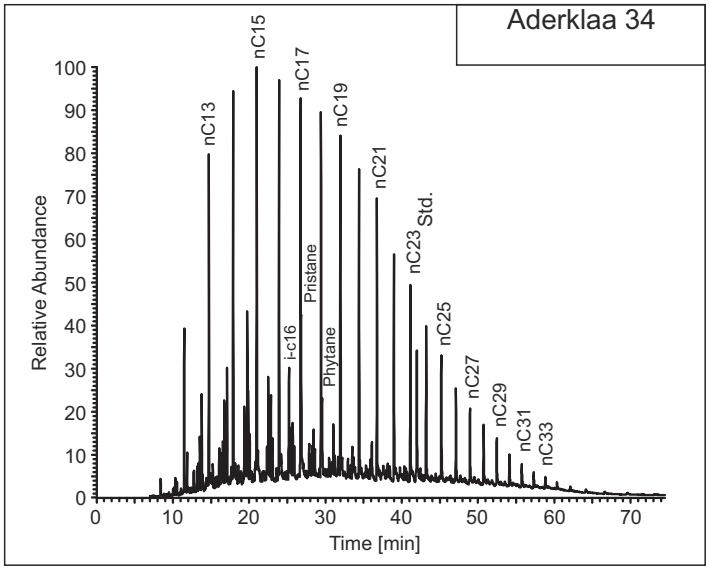
Aderklaa 34
nC13
nC15
nC17
nC19
nC21
Std.
nC23
nC25
nC27
nC29
nC31
nC33
i-c16
Pristane
Phytane
Relative Abundance
Time [min]

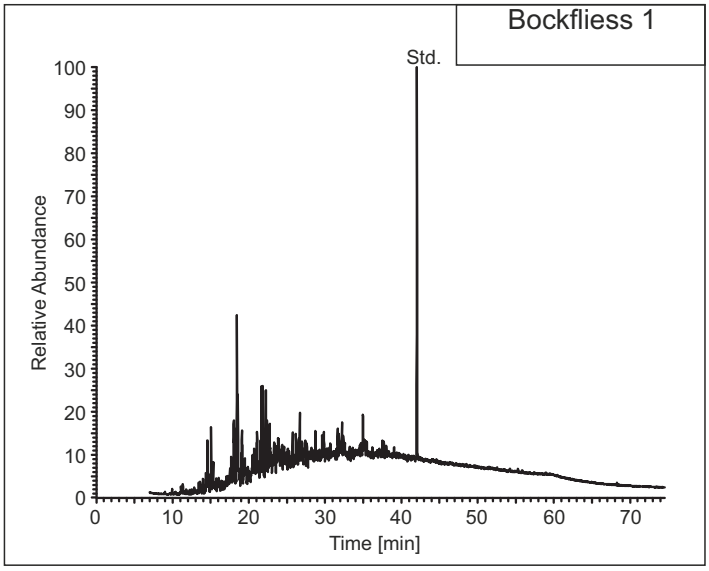
Bockfliess 1
Std.
Relative Abundance
Time [min]

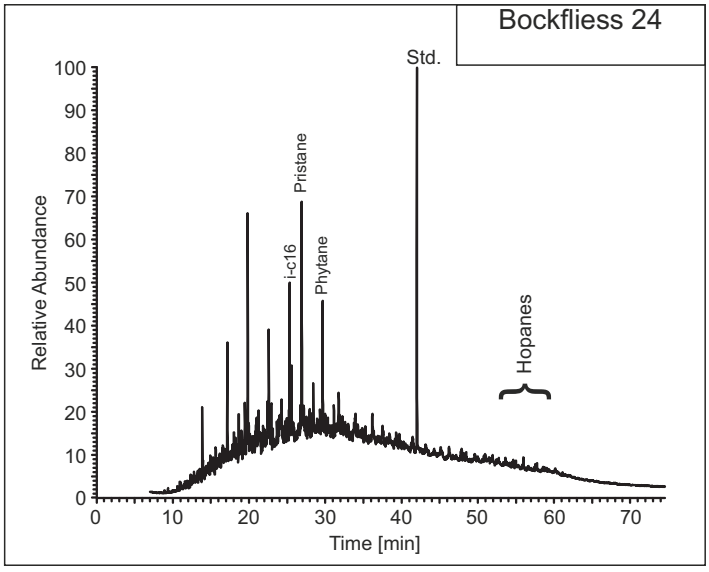
Bockfliess 24
Std.
Pristane
i-c16
Phytane
Hopanes
Relative Abundance
Time [min]

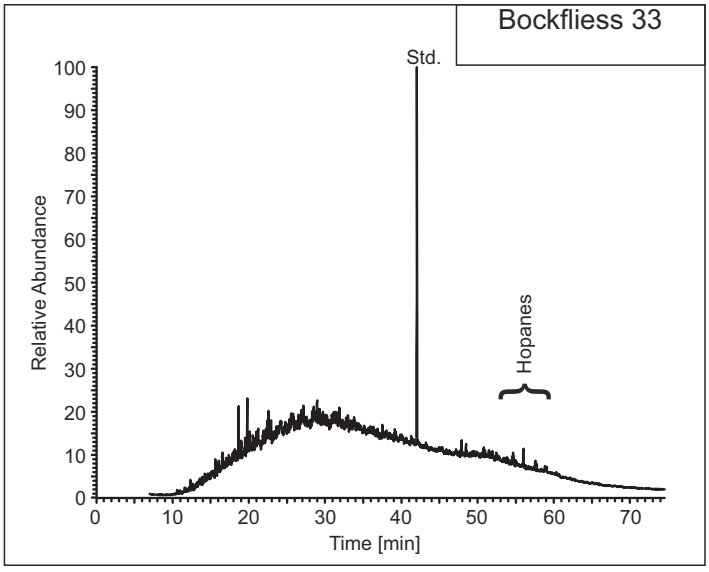
Bockfliess 33
Std.
Hopanes
Relative Abundance
Time [min]

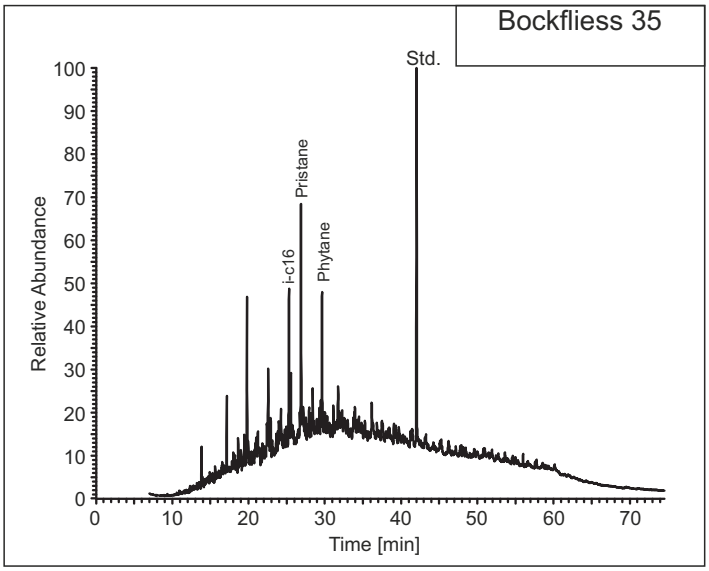
Bockfliess 35
Std.
Pristane
i-c16
Phytane
Relative Abundance
Time [min]

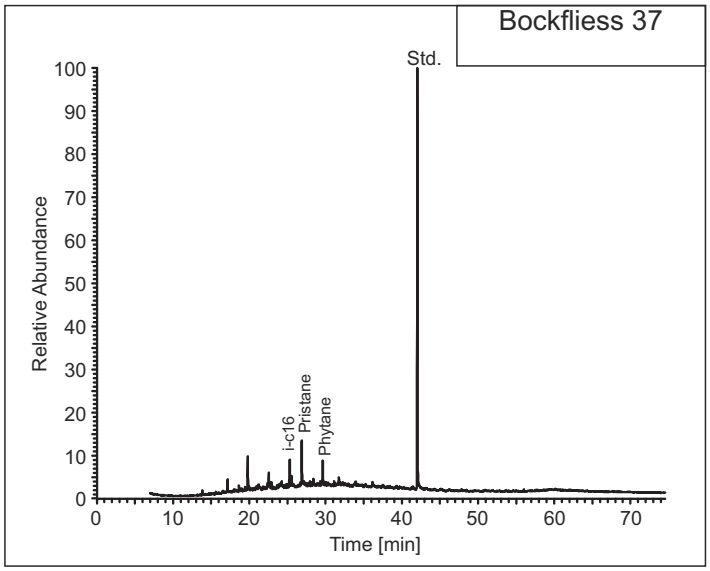
Bockfliess 37
Std.
i-c16
Pristane
Phytane
Relative Abundance
Time [min]

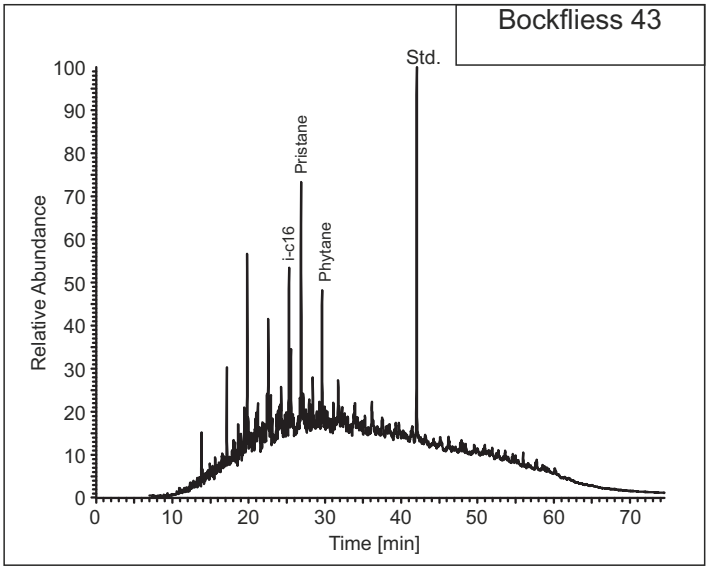
Bockfliess 43
Std.
Pristane
i-c16
Phytane
Relative Abundance
Time [min]

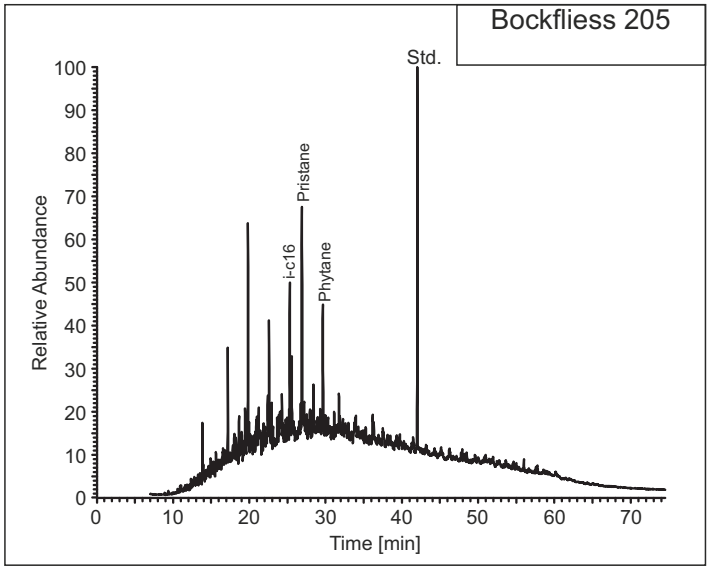
Bockfliess 205
Std.
Pristane
i-c16
Phytane
Relative Abundance
Time [min]

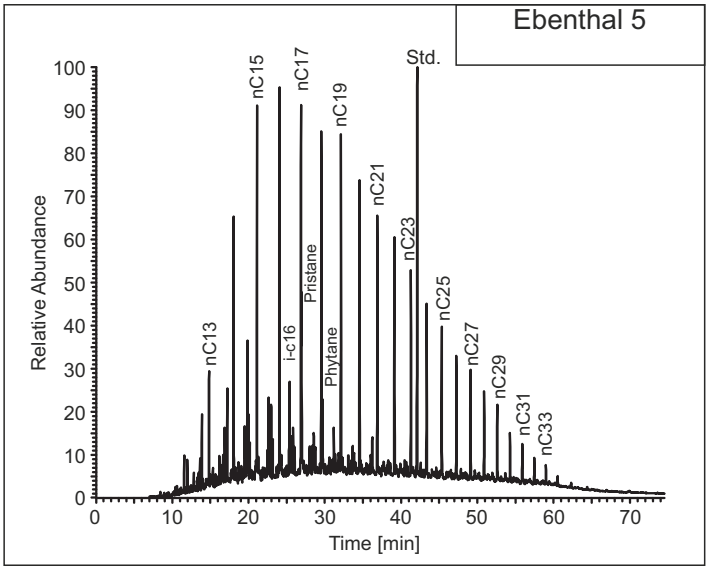
Ebenthal 5
Std.
nC13
nC15
nC17
nC19
nC21
nC23
nC25
nC27
nC29
nC31
nC33
i-c16
Pristane
Phytane
Relative Abundance
Time [min]

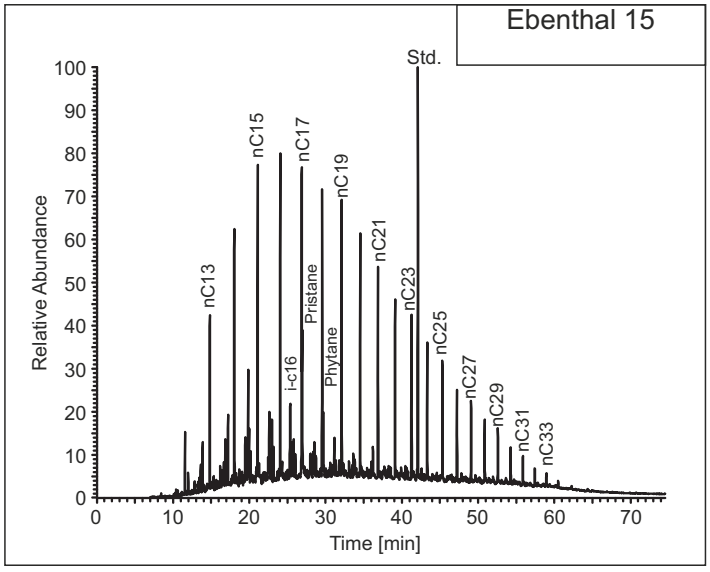
Ebenthal 15
Std.
nC13
nC15
nC17
nC19
nC21
nC23
nC25
nC27
nC29
nC31
nC33
i-c16
Pristane
Phytane
Relative Abundance
Time [min]

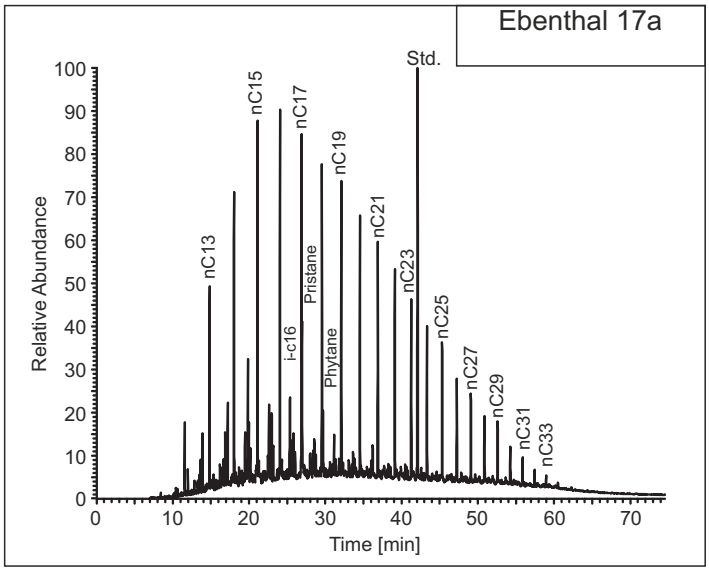
Ebenthal 17a
Relative Abundance
Time [min]
Std.
nC13
nC15
nC17
nC19
nC21
nC23
nC25
nC27
nC29
nC31
nC33
i-c16
Pristane
Phytane

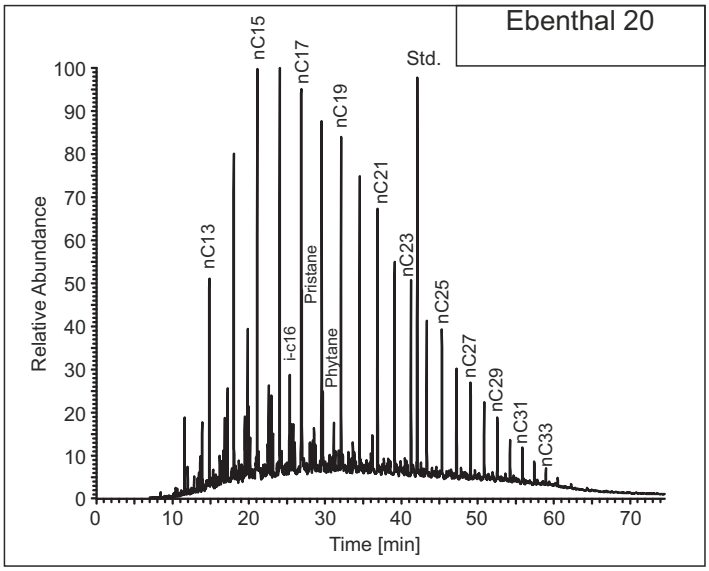
Ebenthal 20
Relative Abundance
Time [min]
Std.
nC13
nC15
nC17
nC19
nC21
nC23
nC25
nC27
nC29
nC31
nC33
i-c16
Pristane
Phytane

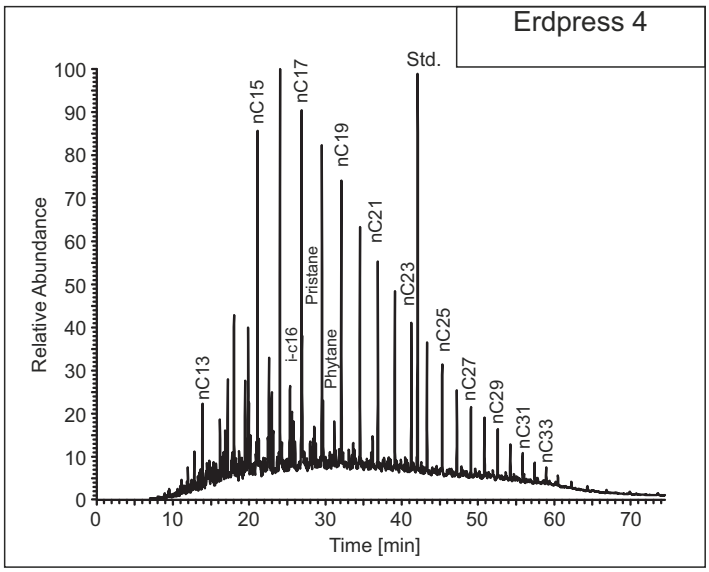
Erdpress 4
Relative Abundance
Time [min]
Std.
nC13
nC15
nC17
nC19
nC21
nC23
nC25
nC27
nC29
nC31
nC33
i-c16
Pristane
Phytane

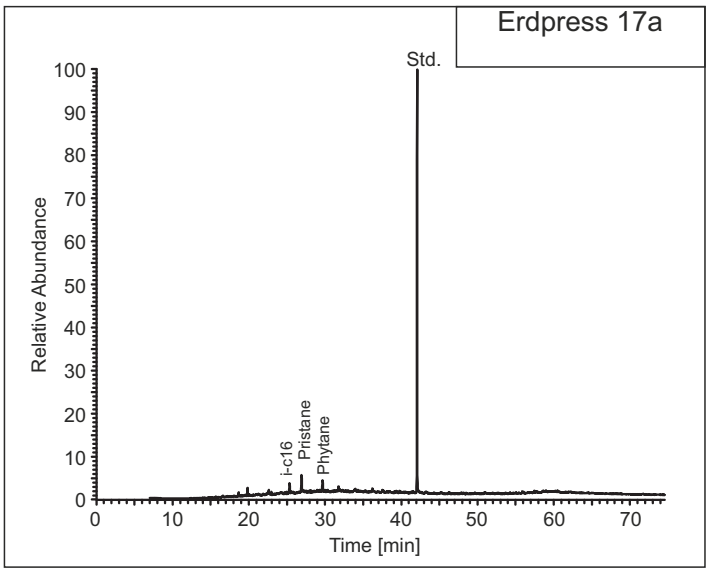
Erdpress 17a
Relative Abundance
Time [min]
Std.
i-c16
Pristane
Phytane

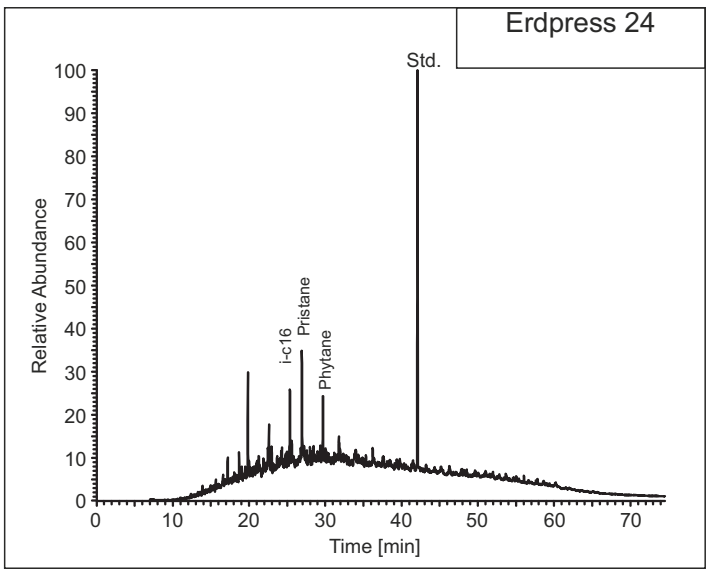
Erdpress 24
Relative Abundance
Time [min]
Std.
i-c16
Pristane
Phytane

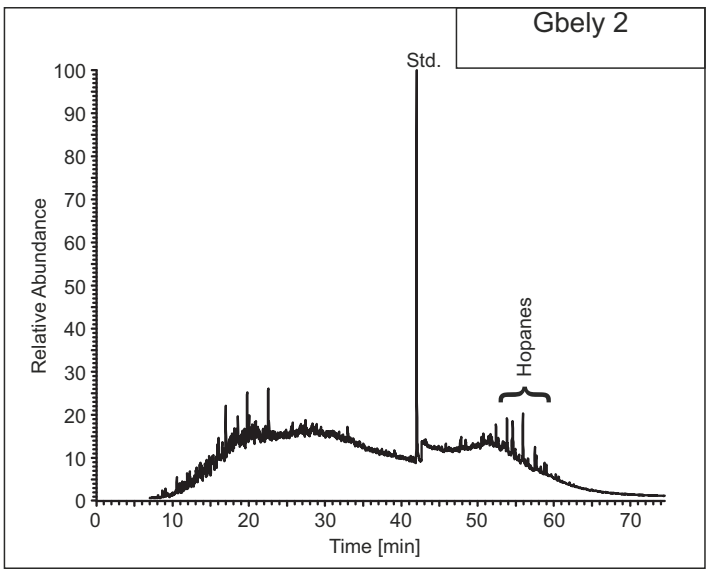
Gbely 2
Relative Abundance
Time [min]
Std.
Hopanes

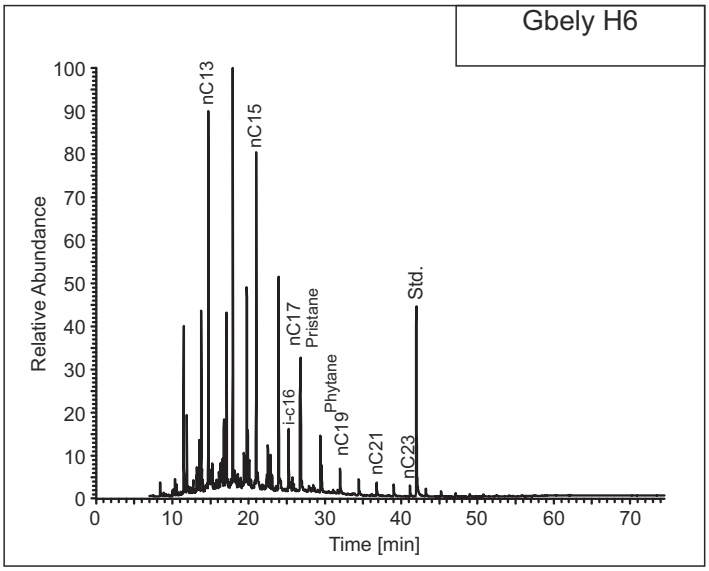
Gbely H6
nC13
nC15
nC17
Pristane
i-c16
Phytane
nC19
nC21
nC23
Std.
Relative Abundance
Time [min]

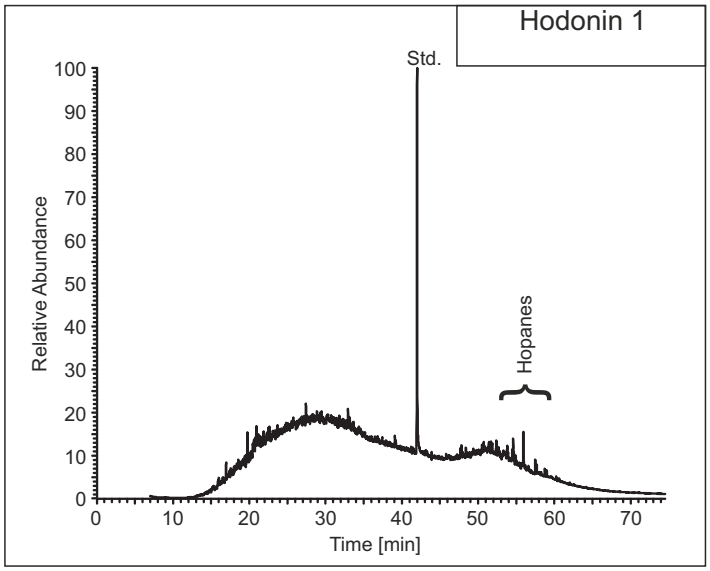
Hodonin 1
Std.
Hopanes
Relative Abundance
Time [min]

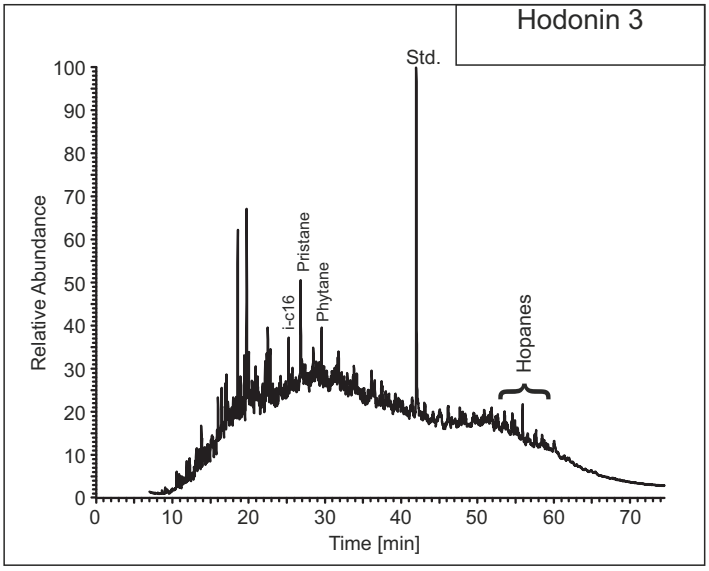
Hodonin 3
Std.
Pristane
i-c16
Phytane
Hopanes
Relative Abundance
Time [min]

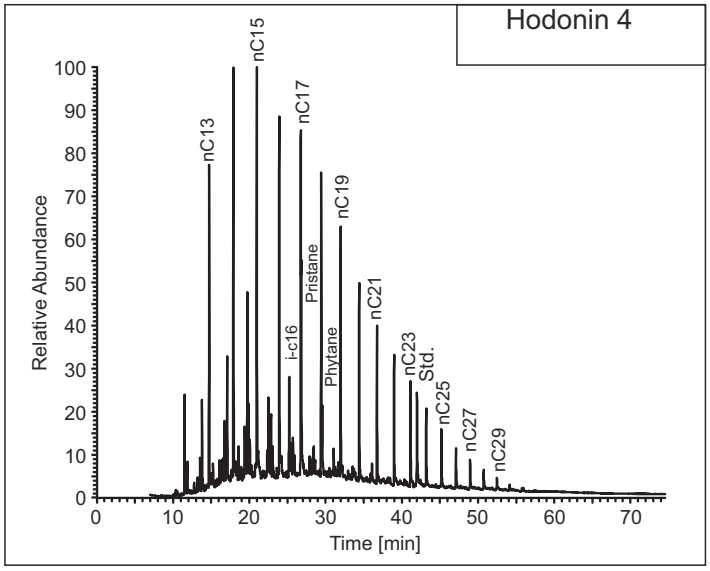
Hodonin 4
nC13
nC15
nC17
nC19
nC21
nC23
Std.
nC25
nC27
nC29
Pristane
i-c16
Phytane
Relative Abundance
Time [min]

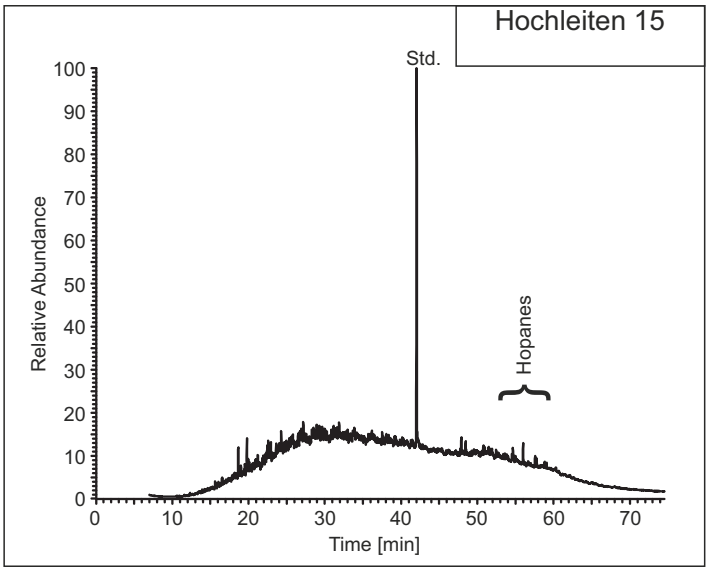
Hochleiten 15
Std.
Hopanes
Relative Abundance
Time [min]

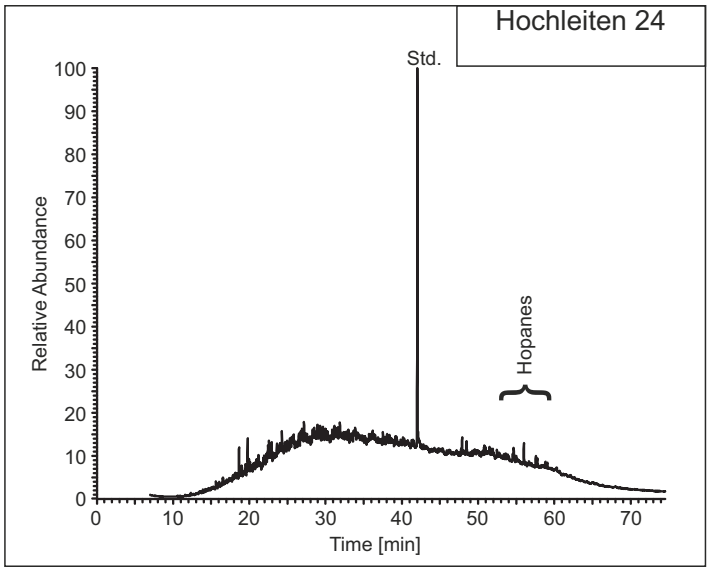
Hochleiten 24
Std.
Hopanes
Relative Abundance
Time [min]

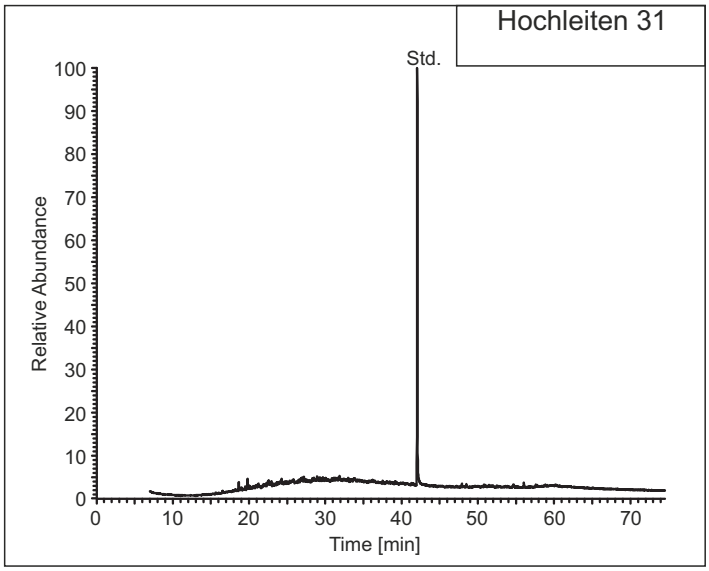
Hochleiten 31
Std.
Relative Abundance
Time [min]

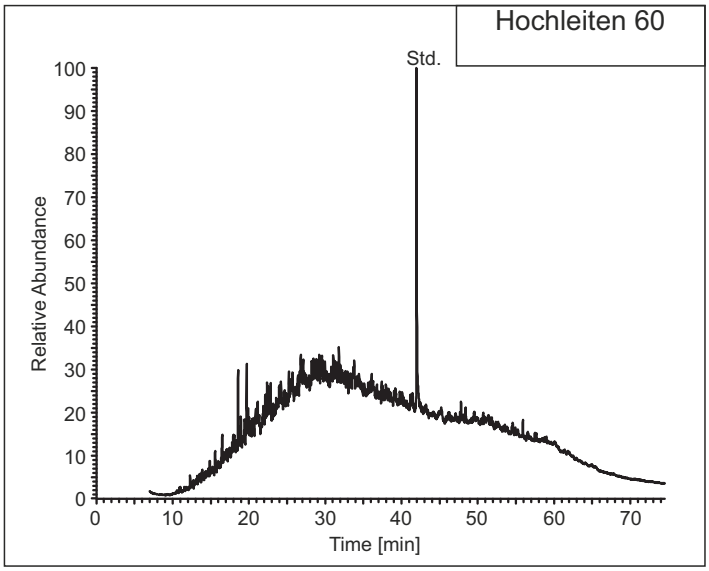
Hochleiten 60
Std.
Relative Abundance
Time [min]

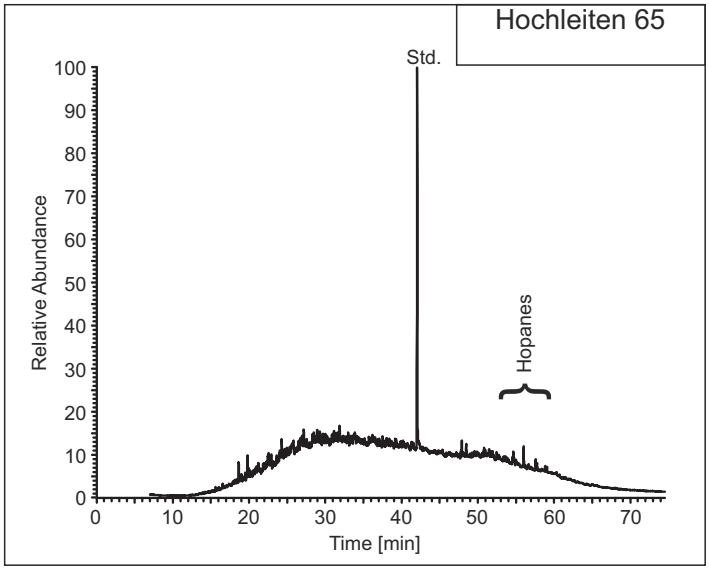
Hochleiten 65
Std.
Hopanes
Relative Abundance
Time [min]

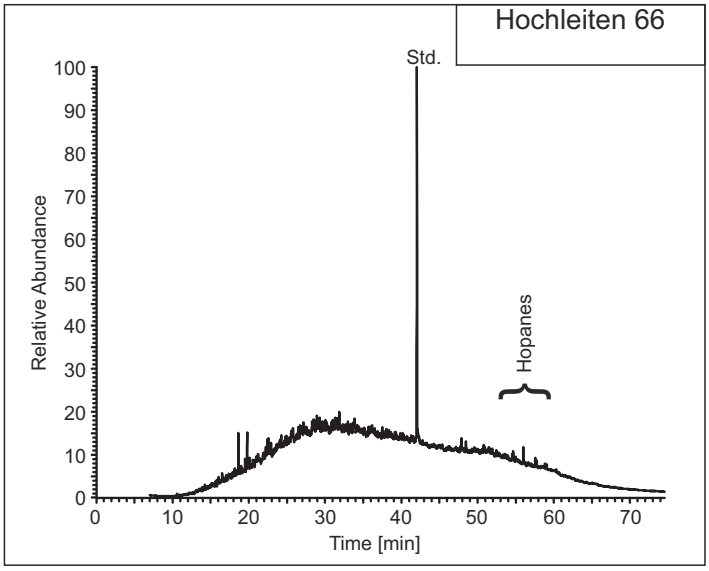
Hochleiten 66
Std.
Hopanes
Relative Abundance
Time [min]

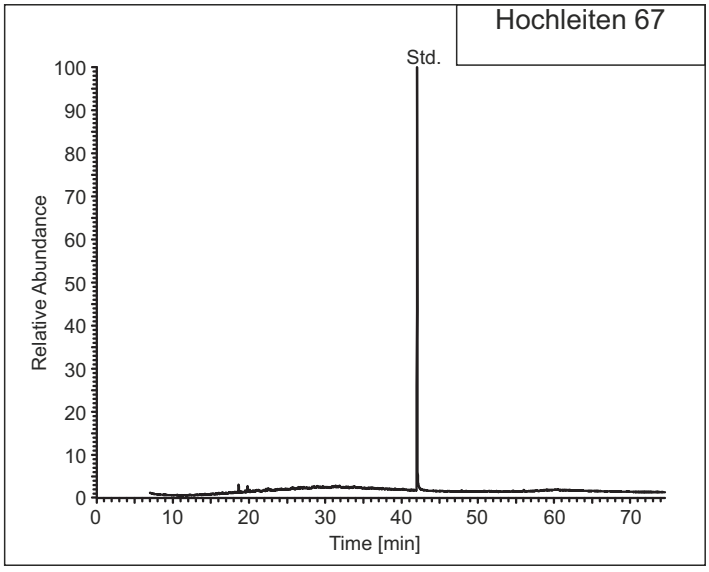
Hochleiten 67
Std.
Relative Abundance
Time [min]

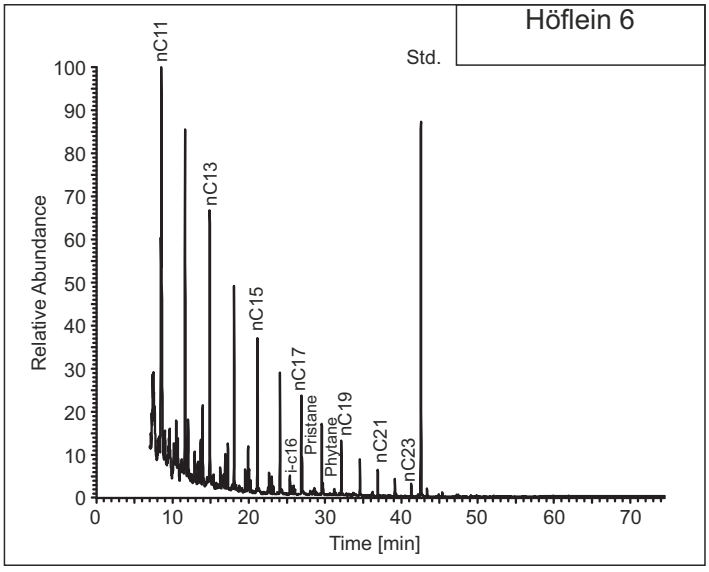
Höflein 6
nC11
Std.
nC13
nC15
nC17
i-c16
Pristane
Phytane
nC19
nC21
nC23
Relative Abundance
Time [min]

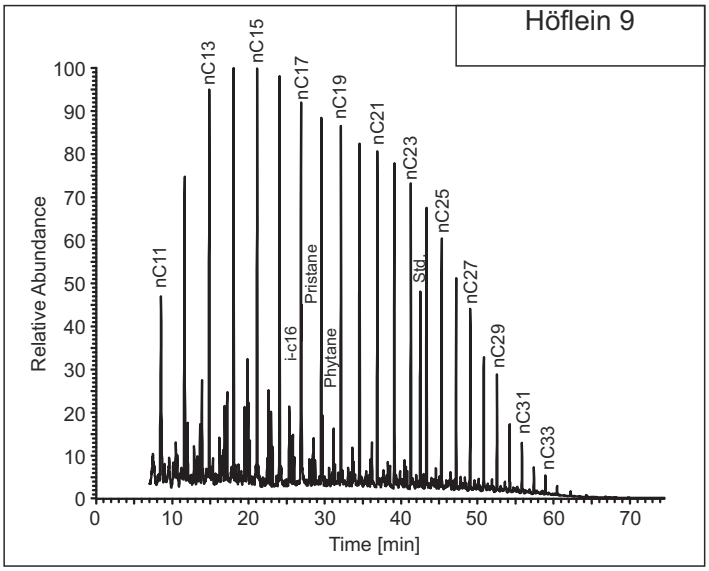
Höflein 9
Relative Abundance
Time [min]
nC11
nC13
nC15
nC17
nC19
nC21
nC23
nC25
nC27
nC29
nC31
nC33
i-c16
Pristane
Phytane
Std.

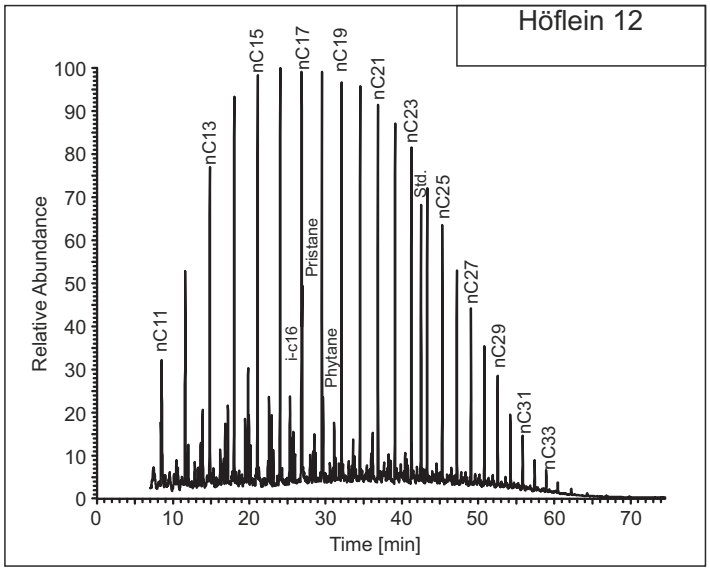
Höflein 12
Relative Abundance
Time [min]
nC11
nC13
nC15
nC17
nC19
nC21
nC23
nC25
nC27
nC29
nC31
nC33
i-c16
Pristane
Phytane
Std.

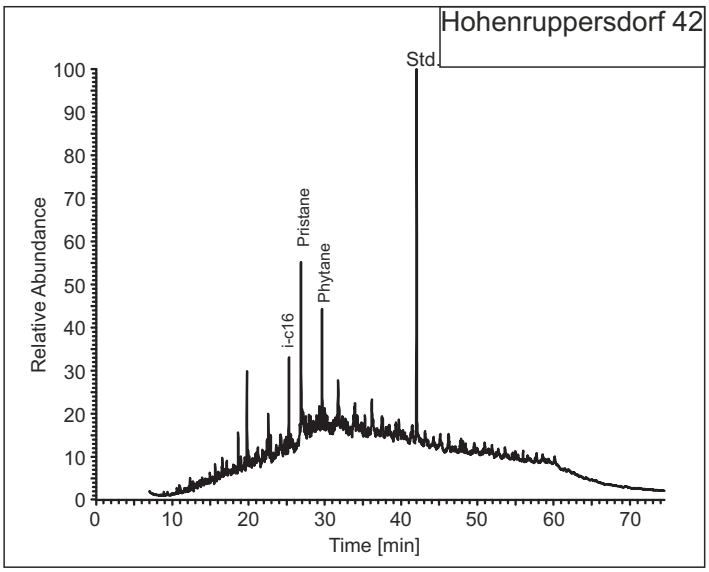
Hohenruppersdorf 42
Relative Abundance
Time [min]
nC13
nC15
nC17
nC19
nC21
nC23
nC25
nC27
nC29
nC31
i-c16
Pristane
Phytane
Std.

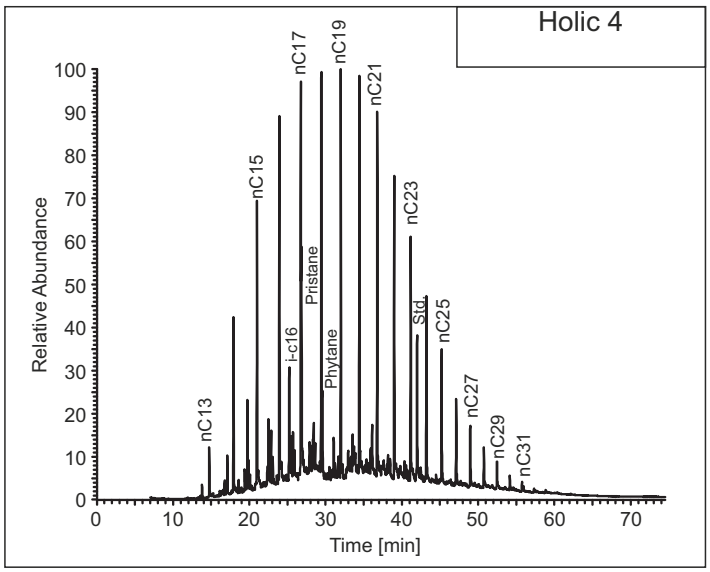
Holic 4
Relative Abundance
Time [min]
nC13
nC15
nC17
nC19
nC21
nC23
nC25
nC27
nC29
nC31
i-c16
Pristane
Phytane
Std.

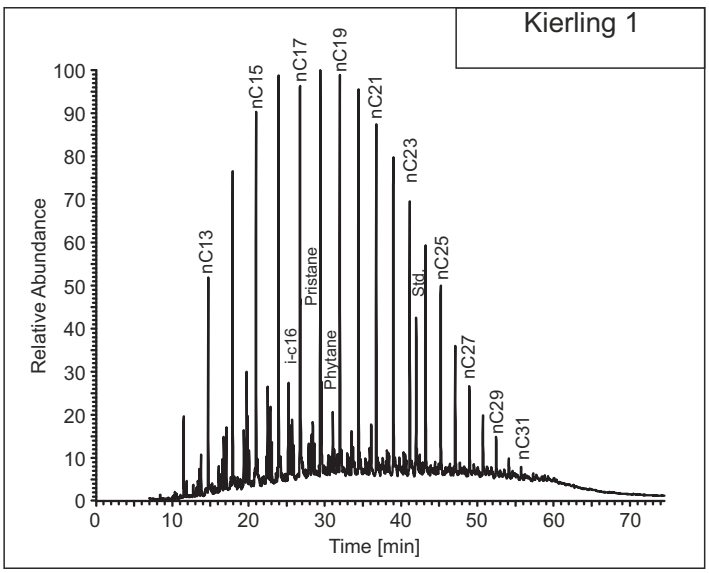
Kierling 1
Relative Abundance
Time [min]
nC13
nC15
nC17
nC19
nC21
nC23
nC25
nC27
nC29
nC31
i-c16
Pristane
Phytane
Std.

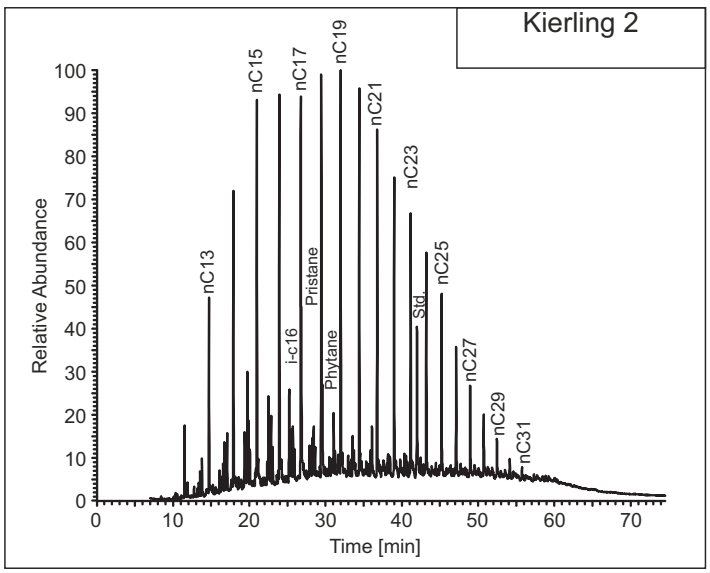
Kierling 2
Relative Abundance
Time [min]
nC13
nC15
nC17
nC19
nC21
nC23
nC25
nC27
nC29
nC31
i-c16
Pristane
Phytane
Std.

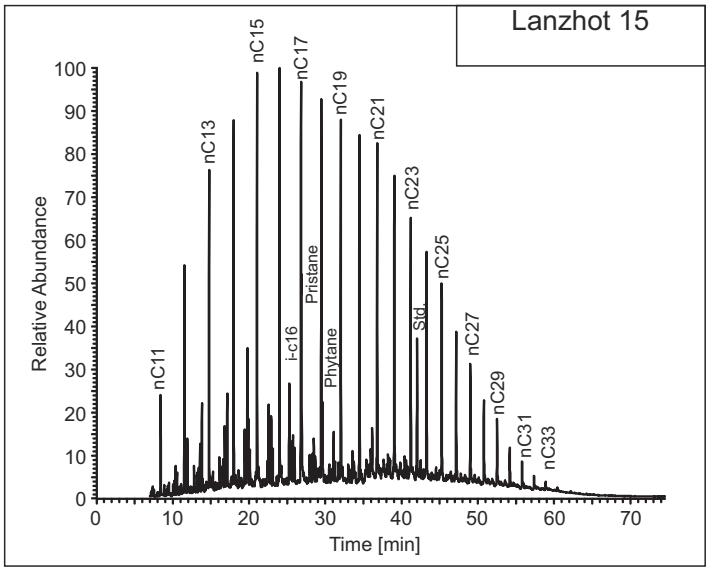
Lanzhot 15
Relative Abundance
Time [min]
nC11
nC13
nC15
nC17
nC19
nC21
nC23
nC25
nC27
nC29
nC31
nC33
i-c16
Pristane
Phytane
Std.

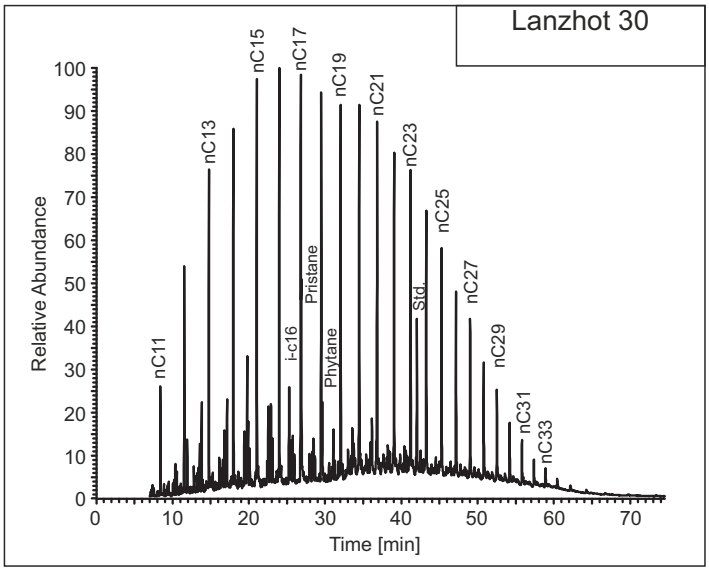
Lanzhot 30
Relative Abundance
Time [min]
nC11
nC13
nC15
nC17
nC19
nC21
nC23
nC25
nC27
nC29
nC31
nC33
i-c16
Pristane
Phytane
Std.

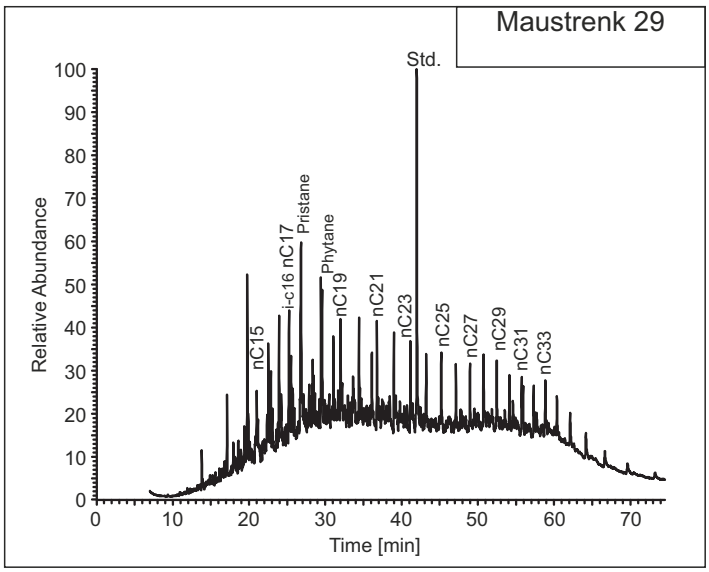
Maustrenk 29
Relative Abundance
Time [min]
nC15
i-c16
nC17
Pristane
Phytane
nC19
nC21
nC23
Std.
nC25
nC27
nC29
nC31
nC33

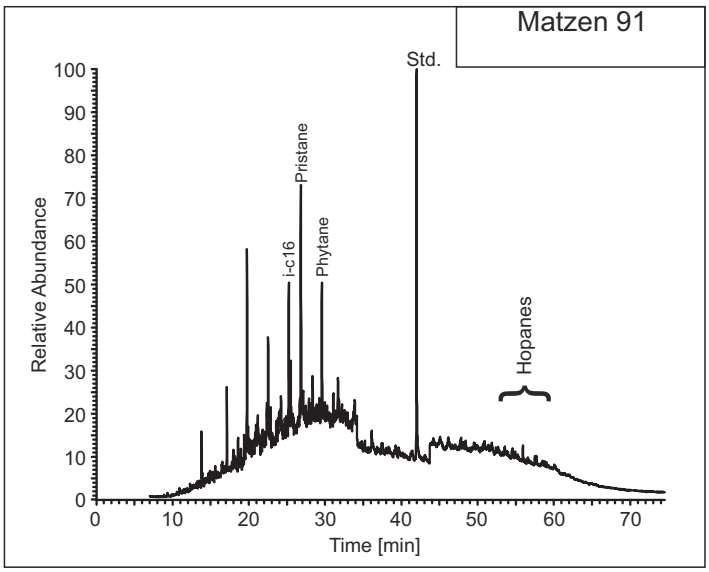
Matzen 91
Relative Abundance
Time [min]
Pristane
i-c16
Phytane
Std.
Hopanes

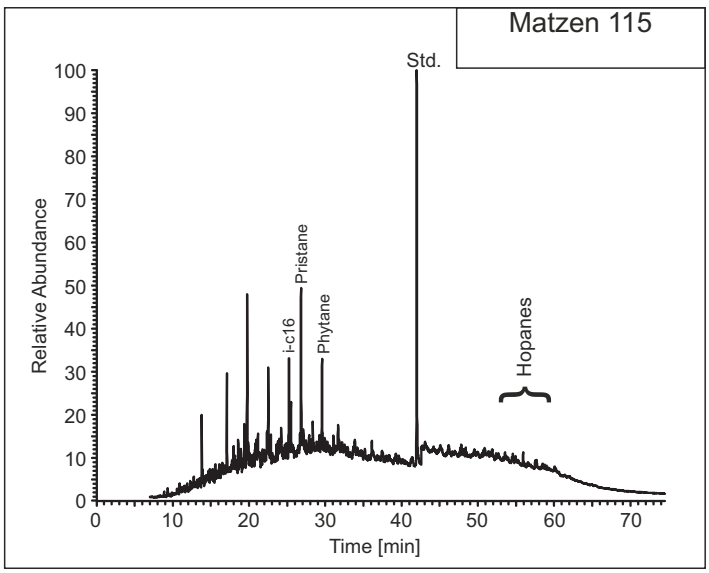
Matzen 115
Relative Abundance
Time [min]
i-c16
Pristane
Phytane
Std.
Hopanes

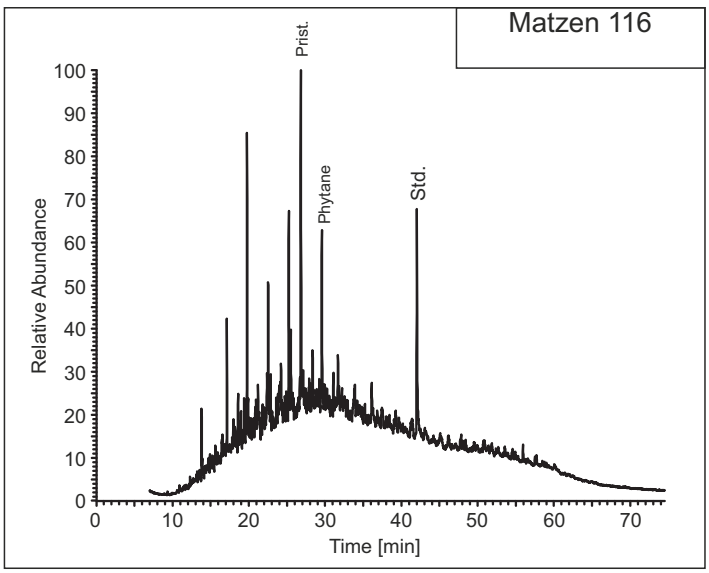
Matzen 116
Relative Abundance
Time [min]
Prist.
Phytane
Std.

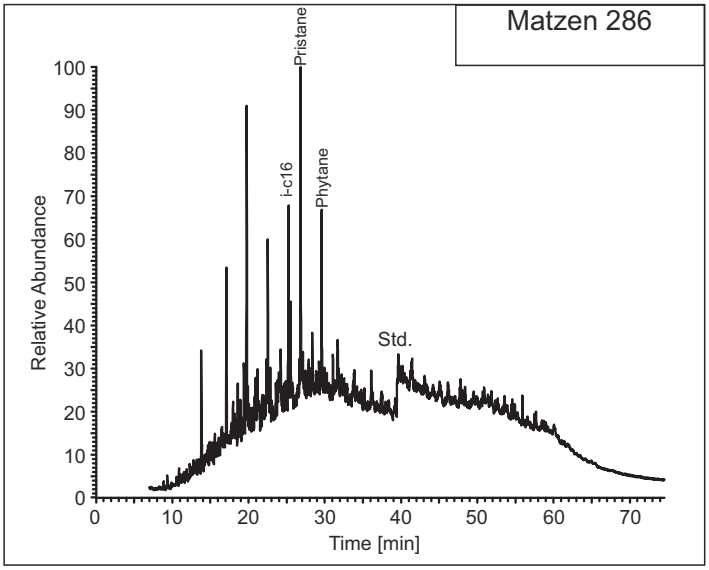

Matzen 322

File unfortunatly corrupted

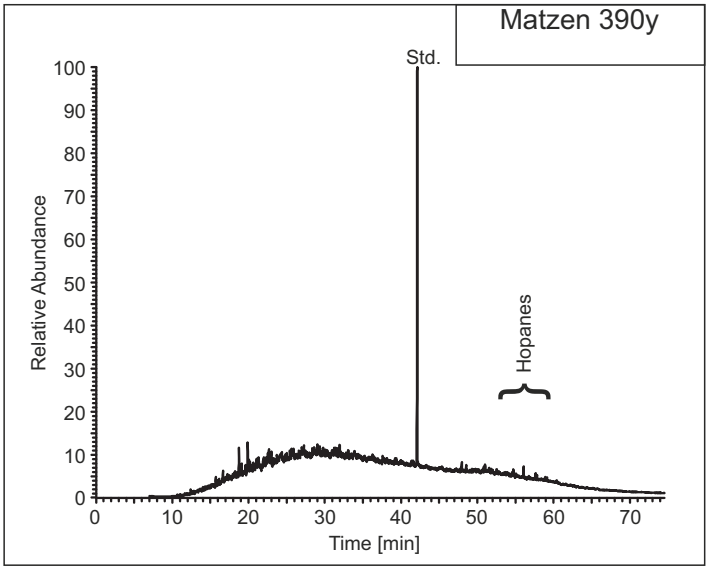

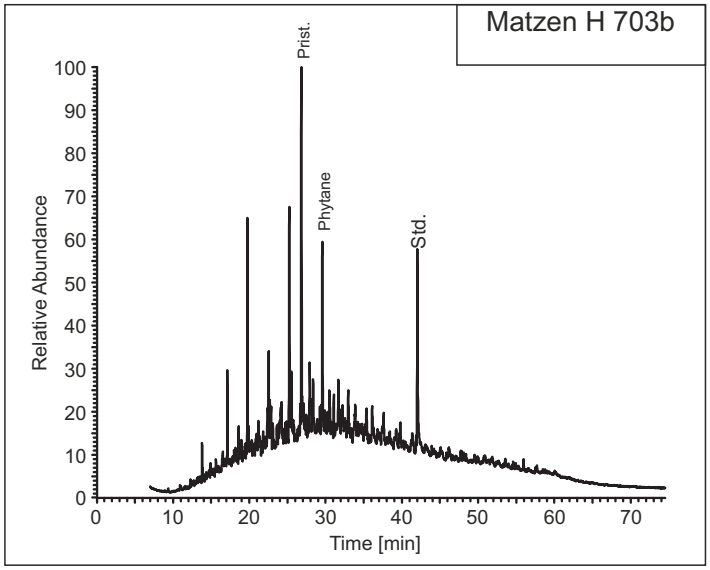

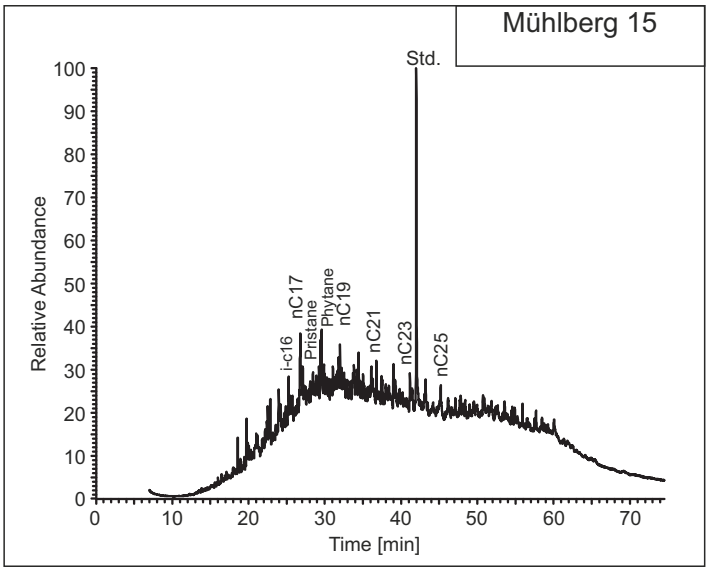

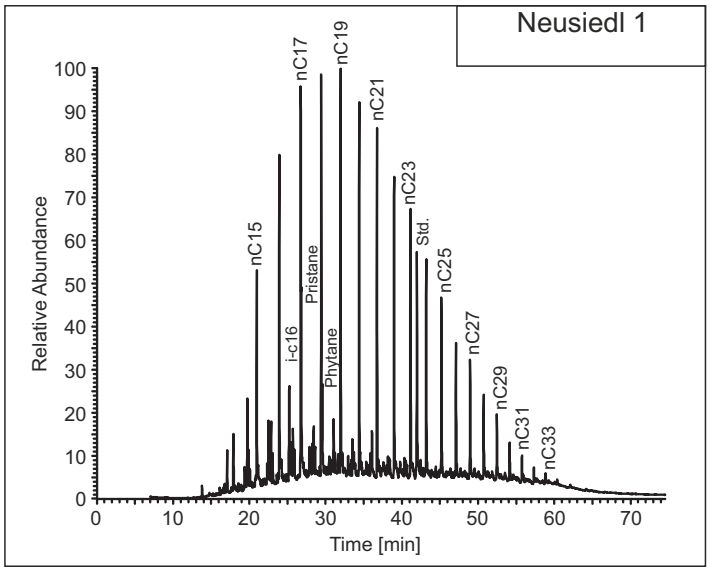

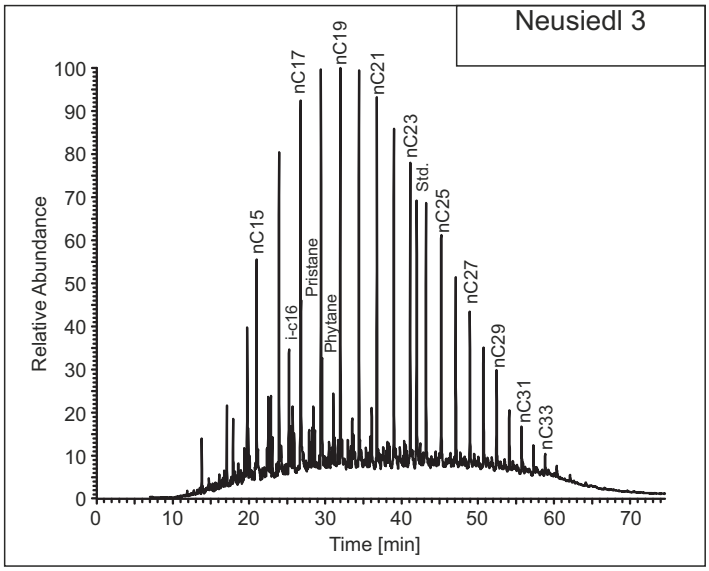
Neusiedl 3
Relative Abundance
Time [min]
nC15
nC17
nC19
nC21
nC23
Std.
nC25
nC27
nC29
nC31
nC33
i-c16
Pristane
Phytane

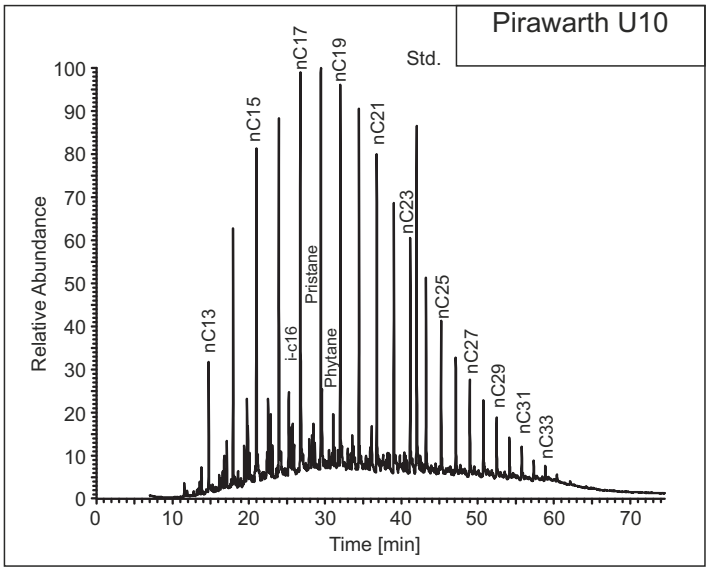
Pirawarth U10
Relative Abundance
Time [min]
nC13
nC15
nC17
nC19
Std.
nC21
nC23
nC25
nC27
nC29
nC31
nC33
i-c16
Pristane
Phytane

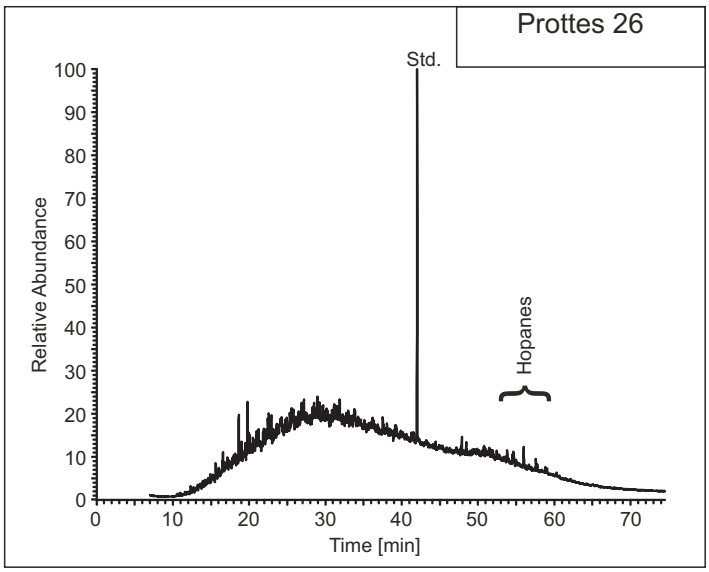
Prottes 26
Relative Abundance
Time [min]
Std.
Hopanes

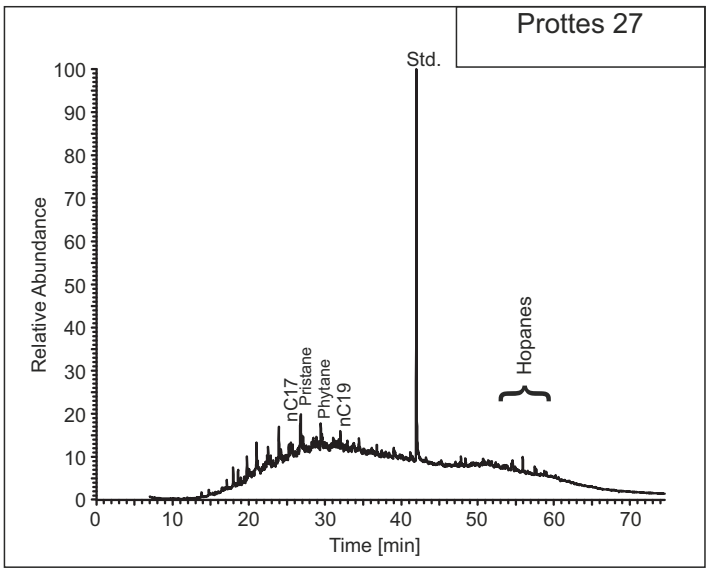
Prottes 27
Relative Abundance
Time [min]
Std.
Hopanes
nC17
Pristane
Phytane
nC19

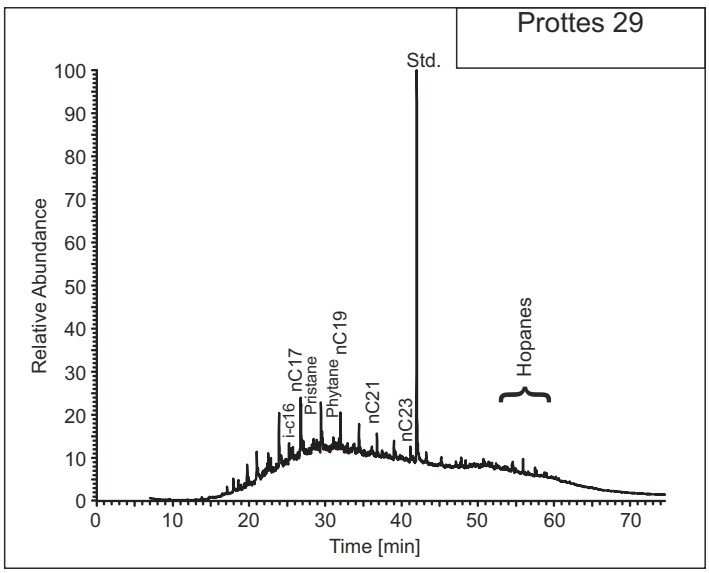
Prottes 29
Relative Abundance
Time [min]
Std.
Hopanes
i-c16
nC17
Pristane
Phytane
nC19
nC21
nC23

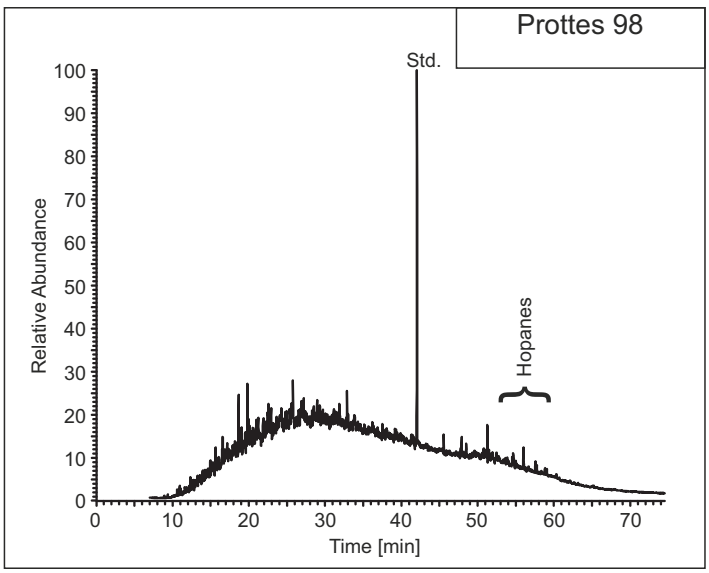
Prottes 98
Relative Abundance
Time [min]
Std.
Hopanes

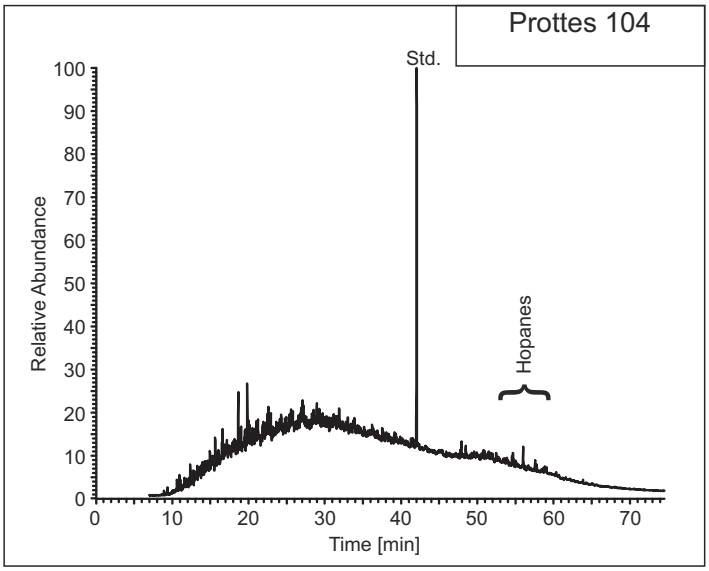
Prottes 104
Std.
Hopanes
Relative Abundance
Time [min]

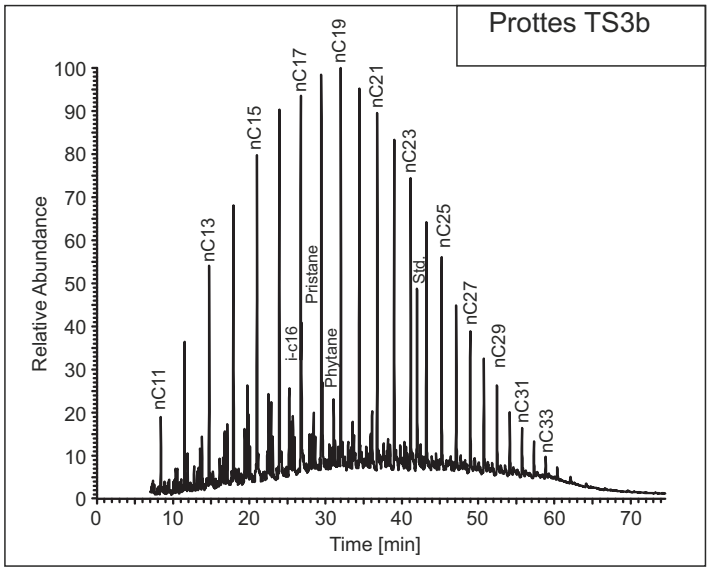
Prottes TS3b
nC11
nC13
nC15
nC17
nC19
nC21
nC23
nC25
nC27
nC29
nC31
nC33
i-c16
Pristane
Phytane
Std.
Relative Abundance
Time [min]

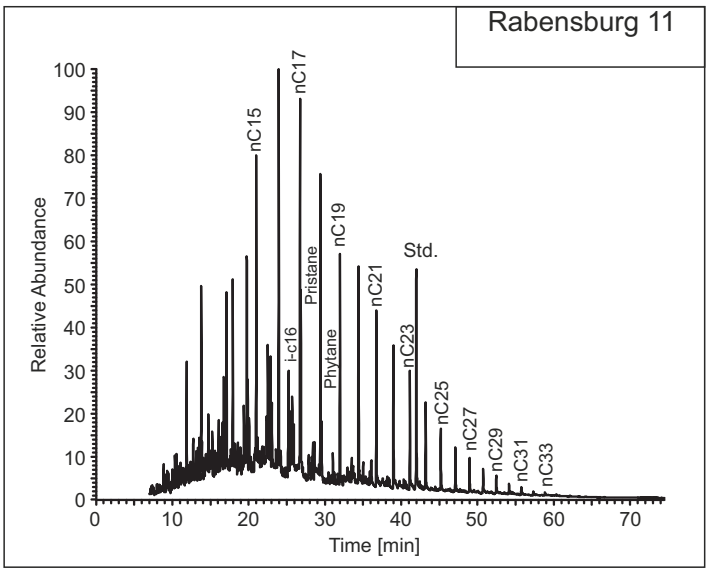
Rabensburg 11
nC13
nC15
nC17
nC19
nC21
nC23
nC25
nC27
nC29
nC31
nC33
i-c16
Pristane
Phytane
Std.
Relative Abundance
Time [min]

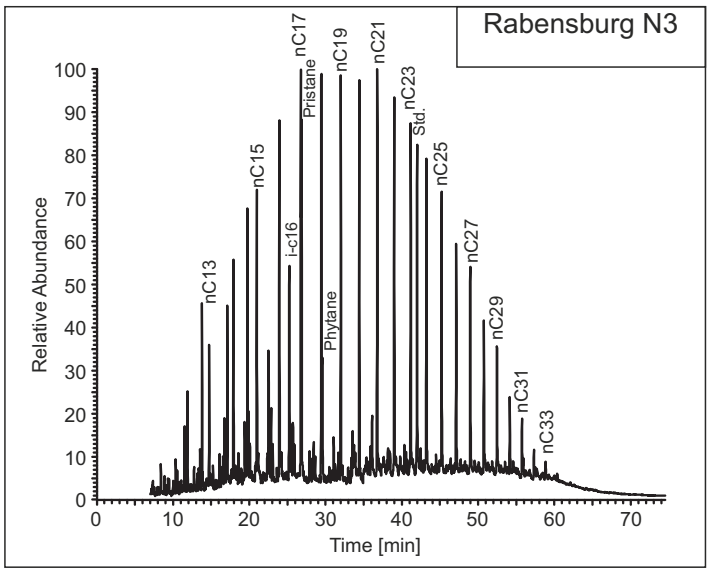
Rabensburg N3
nC13
nC15
nC17
nC19
nC21
nC23
nC25
nC27
nC29
nC31
nC33
i-c16
Pristane
Phytane
Std.
Relative Abundance
Time [min]

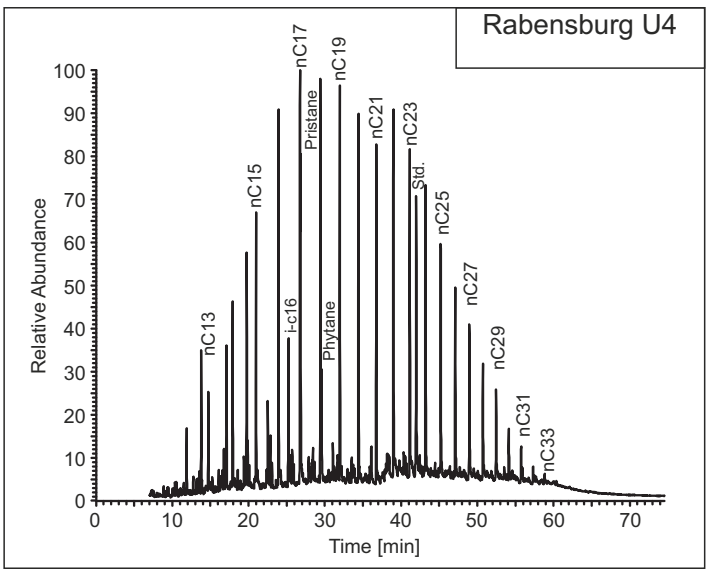
Rabensburg U4
nC13
nC15
nC17
nC19
nC21
nC23
nC25
nC27
nC29
nC31
nC33
i-c16
Pristane
Phytane
Std.
Relative Abundance
Time [min]

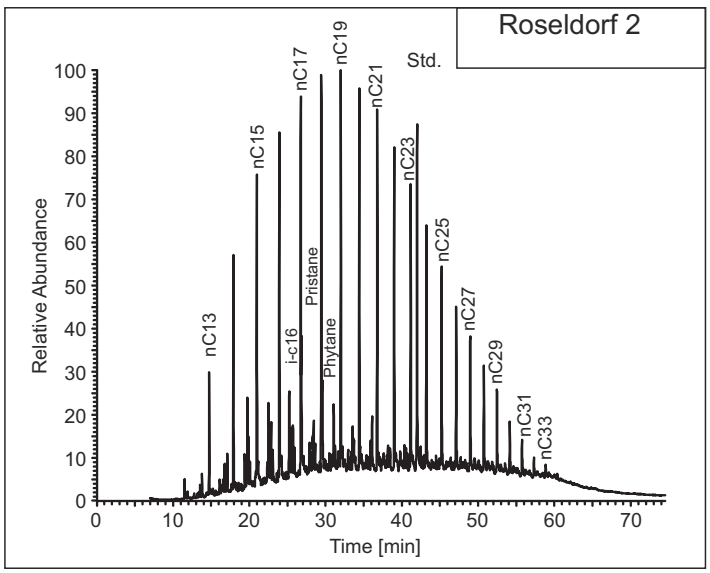
Roseldorf 2
nC13
nC15
nC17
nC19
nC21
nC23
nC25
nC27
nC29
nC31
nC33
i-c16
Pristane
Phytane
Std.
Relative Abundance
Time [min]

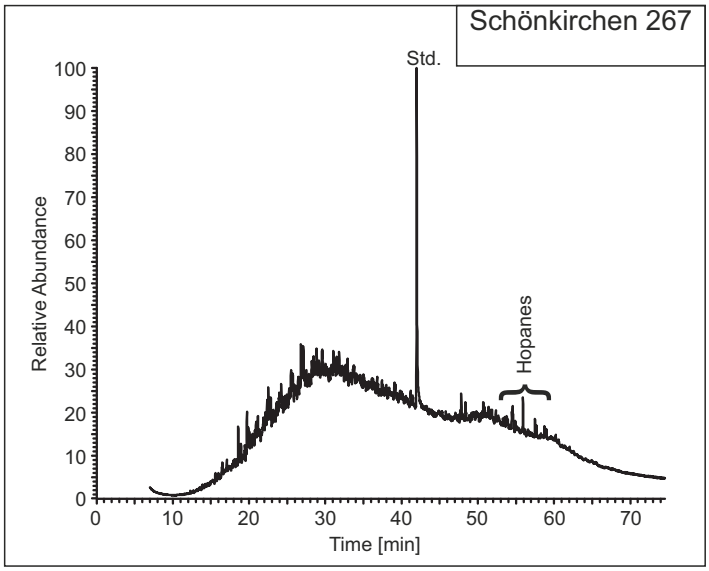
Schönkirchen 267
Std.
Hopanes
Relative Abundance
Time [min]

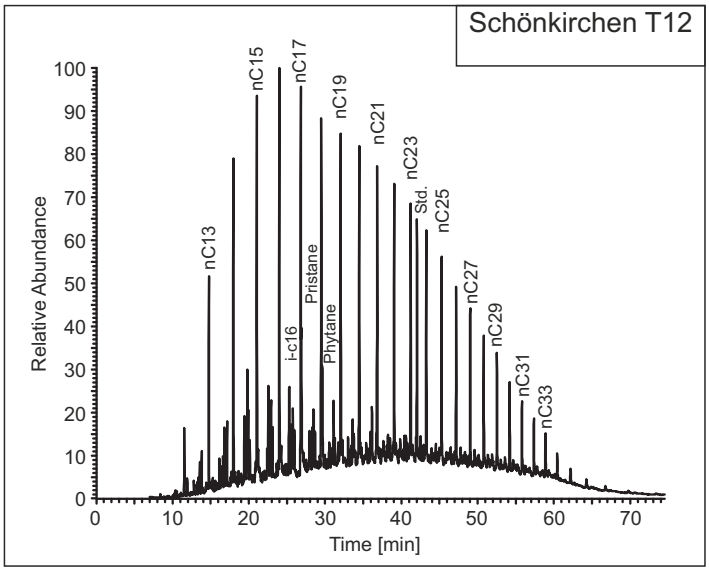
Schönkirchen T12
nC13
nC15
nC17
nC19
nC21
nC23
Std.
nC25
nC27
nC29
nC31
nC33
i-c16
Pristane
Phytane
Relative Abundance
Time [min]

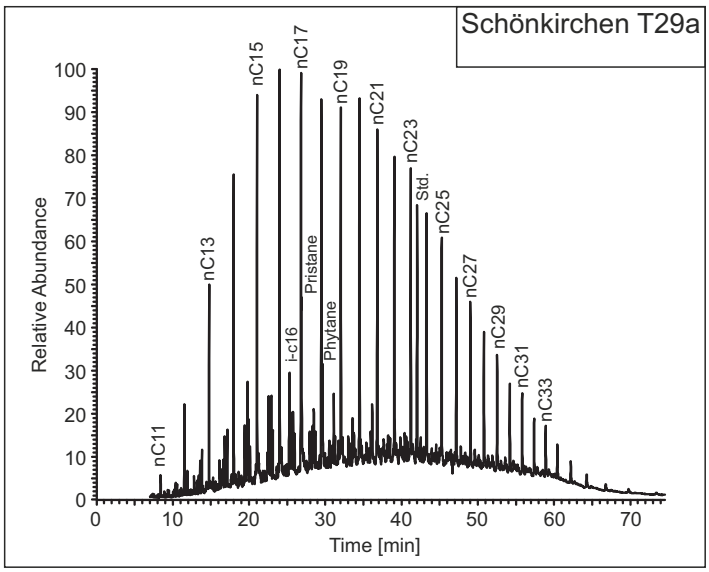
Schönkirchen T29a
nC11
nC13
nC15
nC17
nC19
nC21
nC23
Std.
nC25
nC27
nC29
nC31
nC33
i-c16
Pristane
Phytane
Relative Abundance
Time [min]

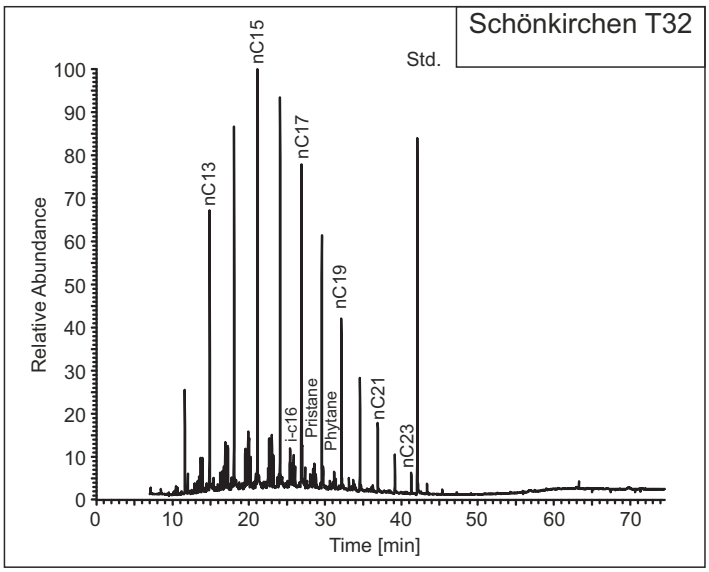
Schönkirchen T32
Std.
nC13
nC15
nC17
nC19
nC21
nC23
i-c16
Pristane
Phytane
Relative Abundance
Time [min]

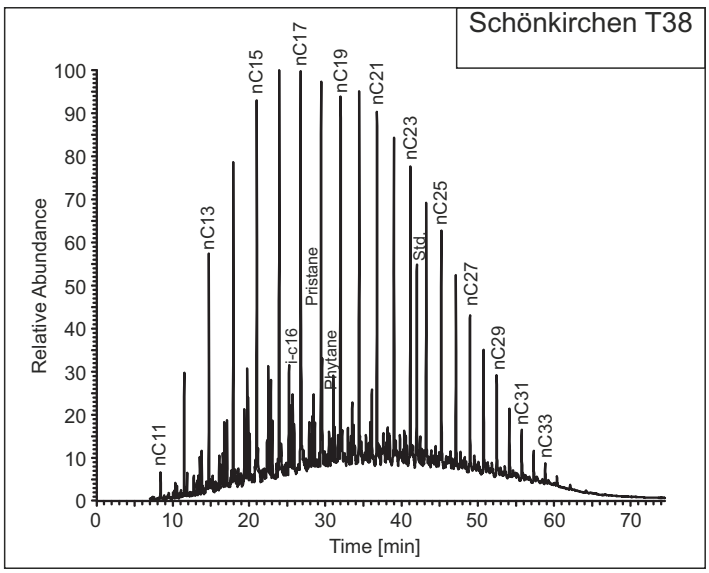
Schönkirchen T38
nC11
nC13
nC15
nC17
nC19
nC21
nC23
Std.
nC25
nC27
nC29
nC31
nC33
i-c16
Pristane
Phytane
Relative Abundance
Time [min]

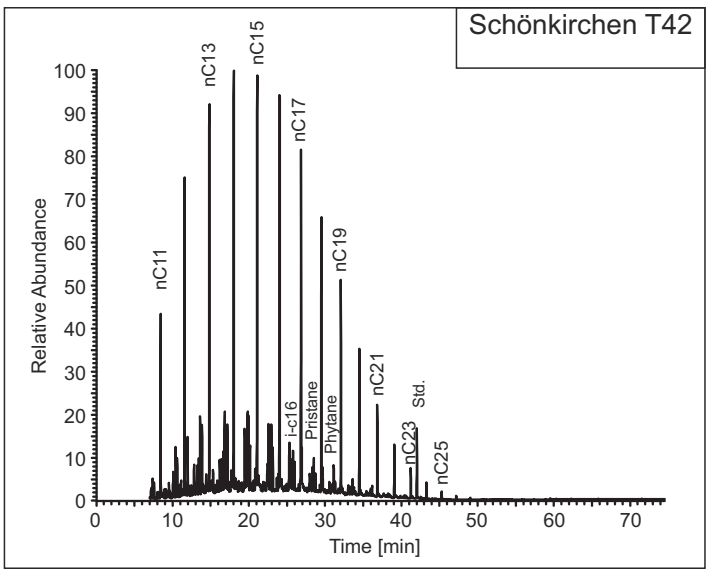
Schönkirchen T42
nC11
nC13
nC15
nC17
nC19
nC21
nC23
Std.
nC25
i-c16
Pristane
Phytane
Relative Abundance
Time [min]

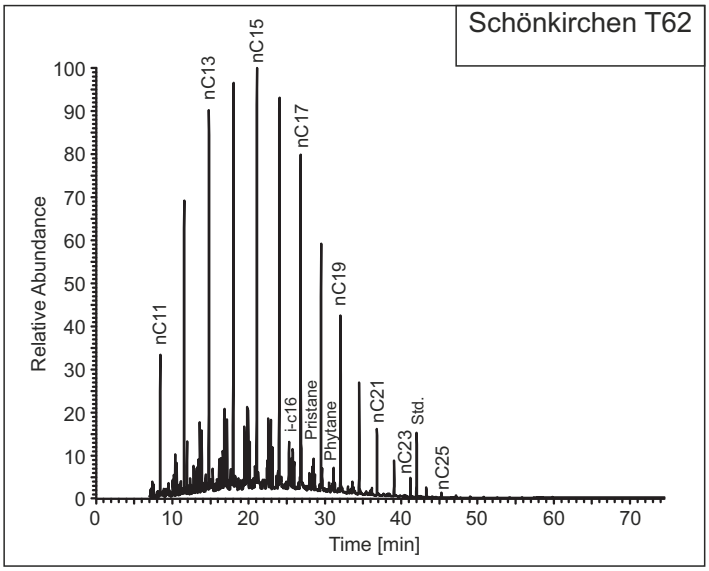
Schönkirchen T62
Relative Abundance
Time [min]
nC11
nC13
nC15
nC17
nC19
nC21
nC23
nC25
i-c16
Pristane
Phytane
Std.

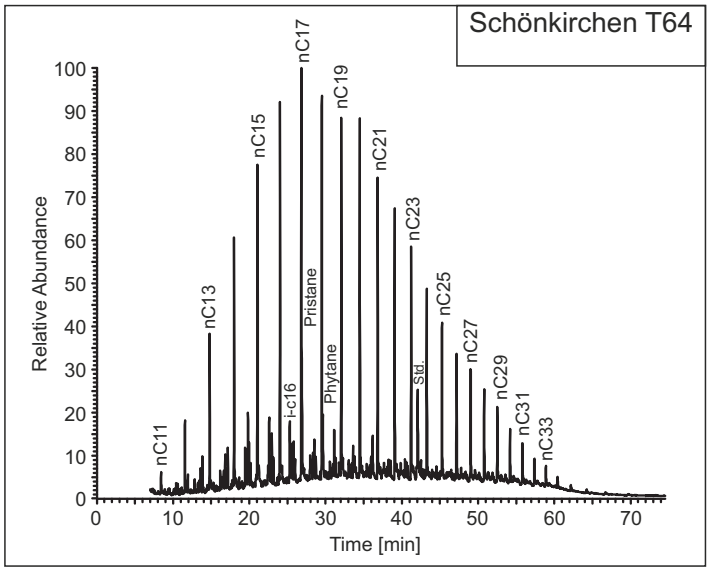
Schönkirchen T64
Relative Abundance
Time [min]
nC11
nC13
nC15
nC17
nC19
nC21
nC23
nC25
nC27
nC29
nC31
nC33
i-c16
Pristane
Phytane
Std.

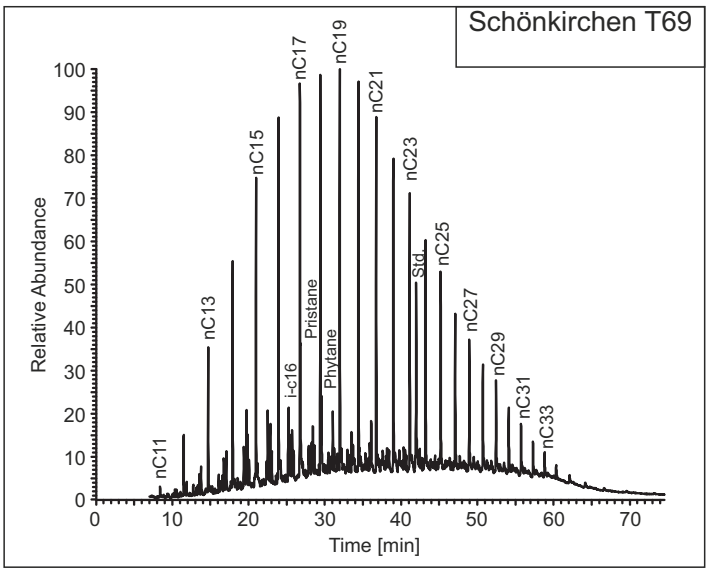
Schönkirchen T69
Relative Abundance
Time [min]
nC11
nC13
nC15
nC17
nC19
nC21
nC23
nC25
nC27
nC29
nC31
nC33
i-c16
Pristane
Phytane
Std.

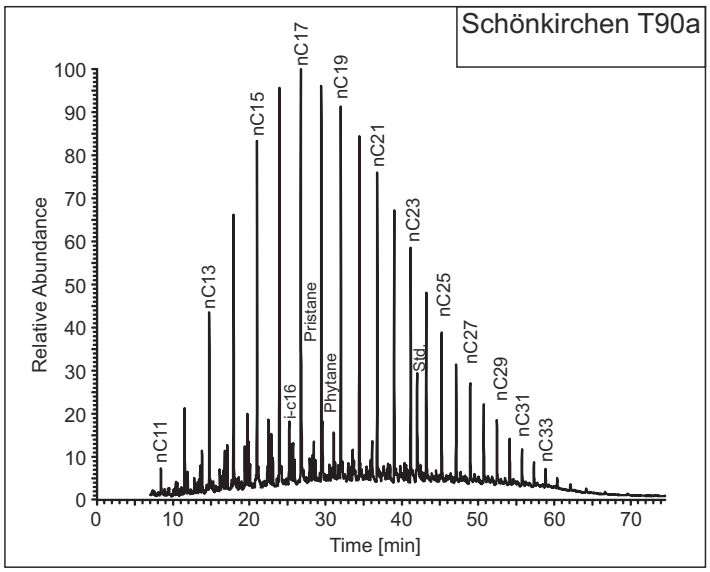
Schönkirchen T90a
Relative Abundance
Time [min]
nC11
nC13
nC15
nC17
nC19
nC21
nC23
nC25
nC27
nC29
nC31
nC33
i-c16
Pristane
Phytane
Std.

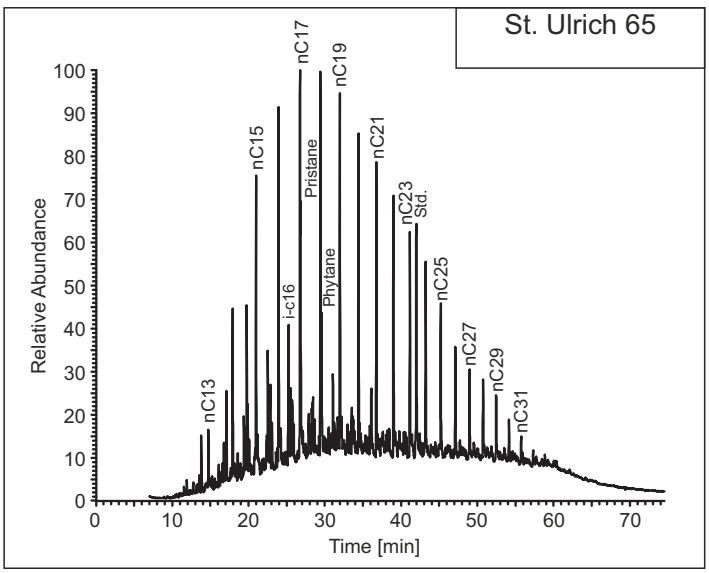
St. Ulrich 65
Relative Abundance
Time [min]
nC13
nC15
nC17
nC19
nC21
nC23
nC25
nC27
nC29
nC31
i-c16
Pristane
Phytane
Std.

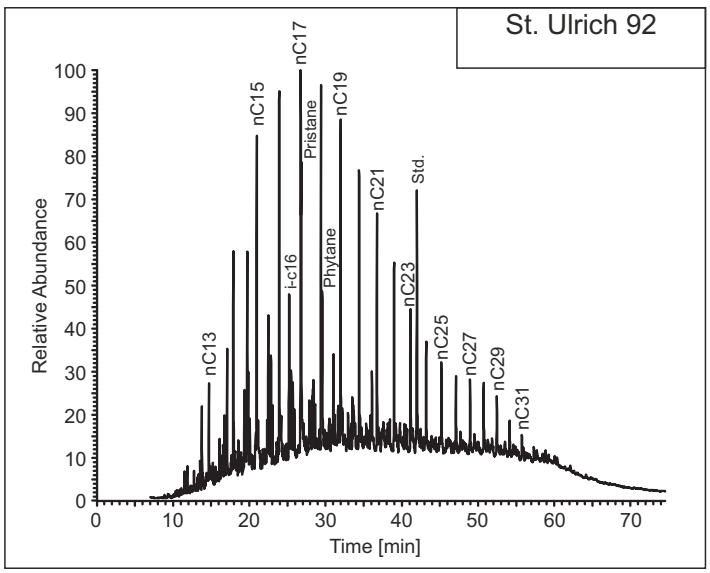
St. Ulrich 92
Relative Abundance
Time [min]
nC13
nC15
nC17
nC19
nC21
nC23
nC25
nC27
nC29
nC31
i-c16
Pristane
Phytane
Std.

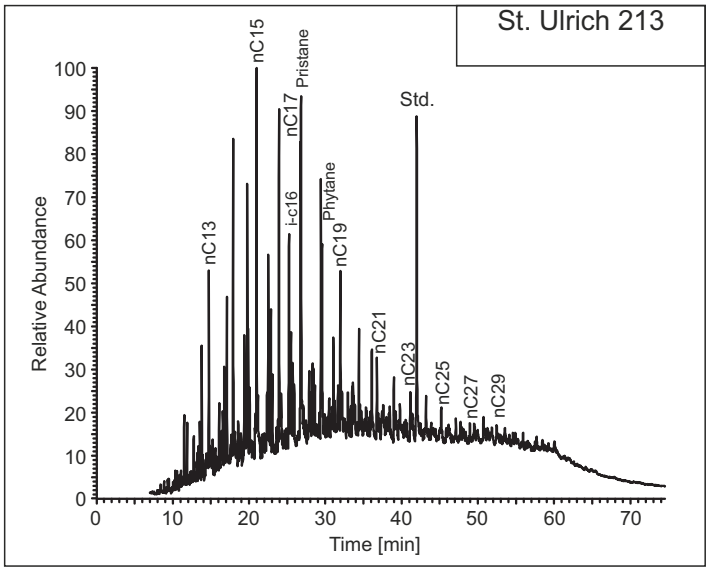
St. Ulrich 213
Relative Abundance
Time [min]
nC13
nC15
i-c16
nC17
Pristane
Phytane
nC19
nC21
nC23
Std.
nC25
nC27
nC29

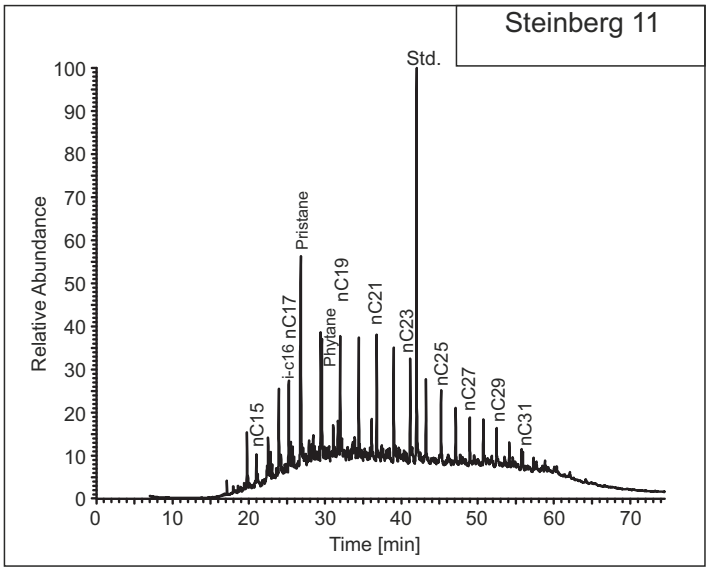
Steinberg 11
Relative Abundance
Time [min]
nC15
i-c16
nC17
Pristane
Phytane
nC19
nC21
nC23
Std.
nC25
nC27
nC29
nC31

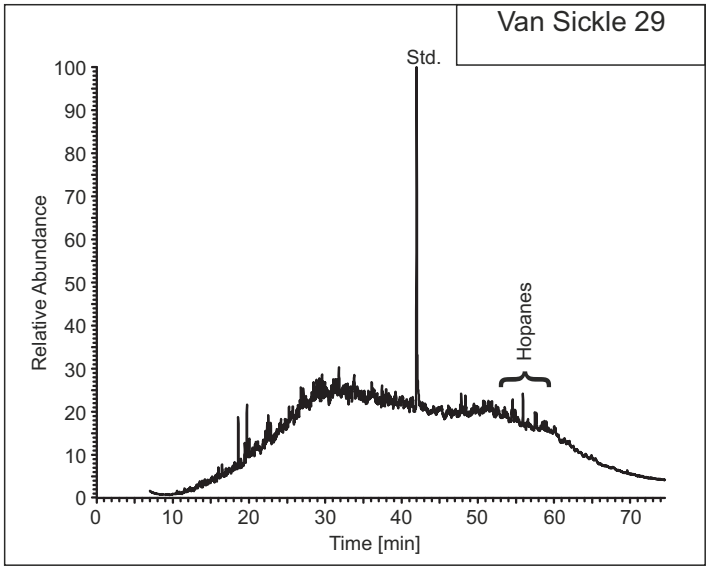
Van Sickle 29
Relative Abundance
Time [min]
Std.
Hopanes

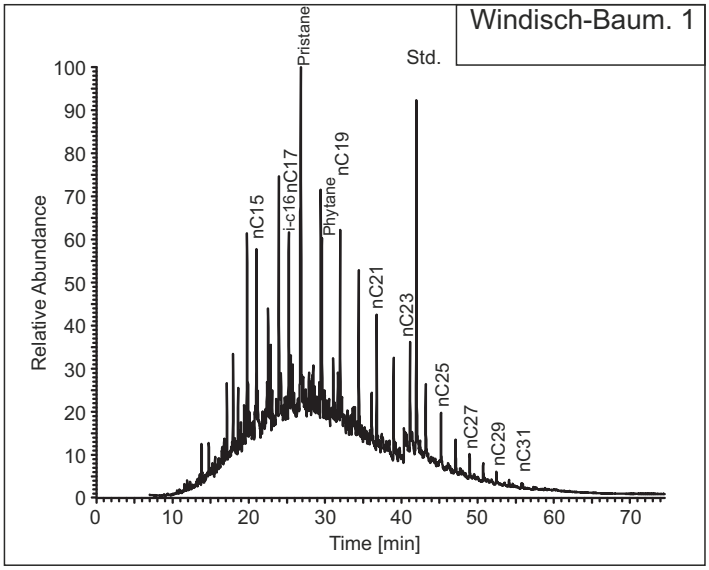
Windisch-Baum. 1
Relative Abundance
Time [min]
Pristane
Std.
nC15
i-c16
nC17
Phytane
nC19
nC21
nC23
nC25
nC27
nC29
nC31

Oils

Aromatic Fraction

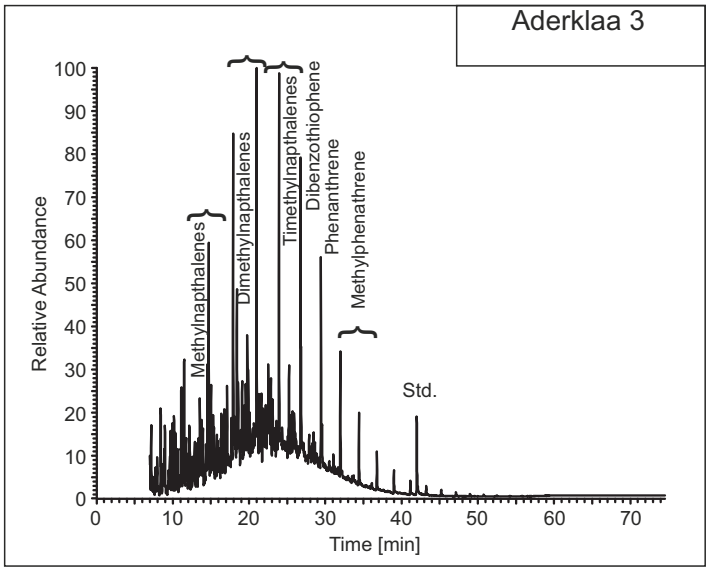
Aderklaa 3
Relative Abundance
Time [min]
Methylnapthalenes
Dimethylnapthalenes
Timethylnapthalenes
Dibenzothiophene
Phenanthrene
Methylphenathrene
Std.

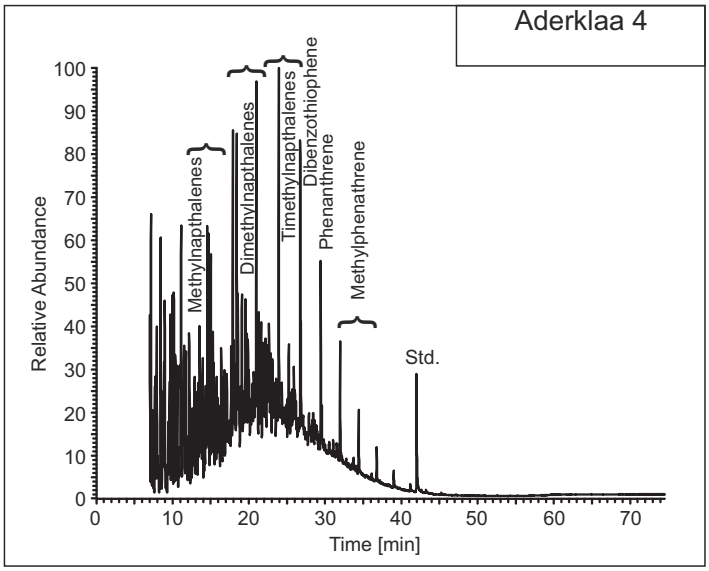
Aderklaa 4
Relative Abundance
Time [min]
Methylnapthalenes
Dimethylnapthalenes
Timethylnapthalenes
Dibenzothiophene
Phenanthrene
Methylphenathrene
Std.

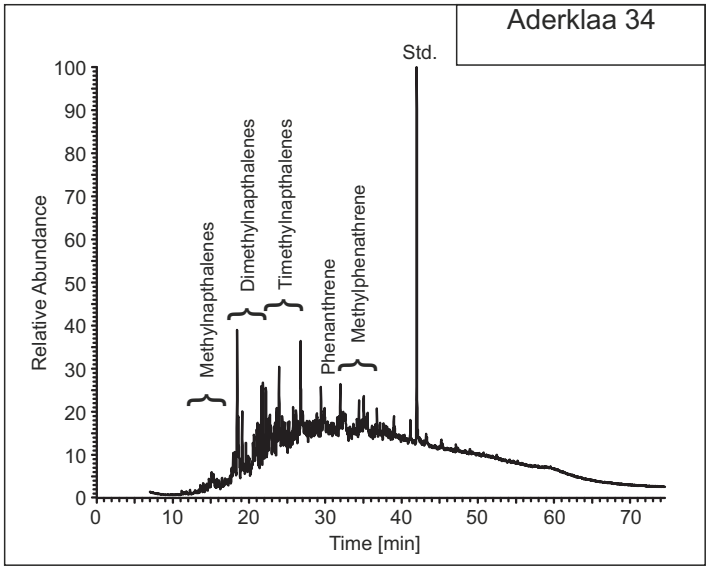
Aderklaa 34
Relative Abundance
Time [min]
Methylnapthalenes
Dimethylnapthalenes
Timethylnapthalenes
Phenanthrene
Methylphenathrene
Std.

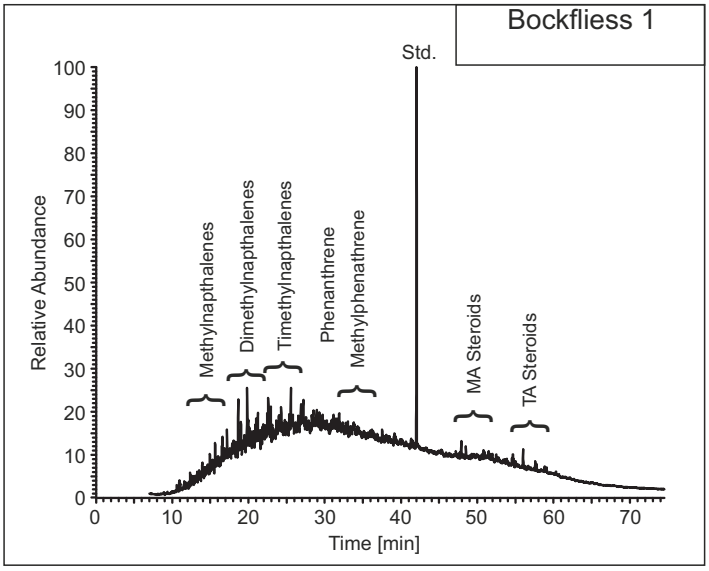
Bockfliess 1
Relative Abundance
Time [min]
Methylnapthalenes
Dimethylnapthalenes
Timethylnapthalenes
Phenanthrene
Methylphenathrene
MA Steroids
TA Steroids
Std.

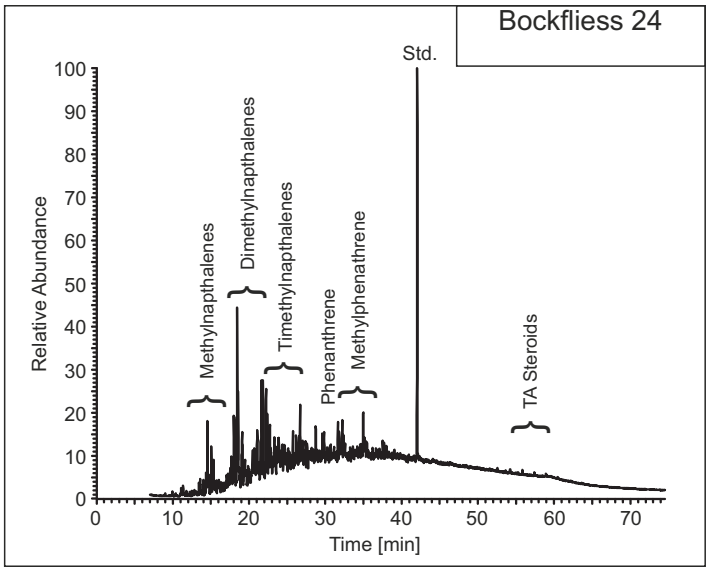
Bockfliess 24
Relative Abundance
Time [min]
Methylnapthalenes
Dimethylnapthalenes
Timethylnapthalenes
Phenanthrene
Methylphenathrene
TA Steroids
Std.

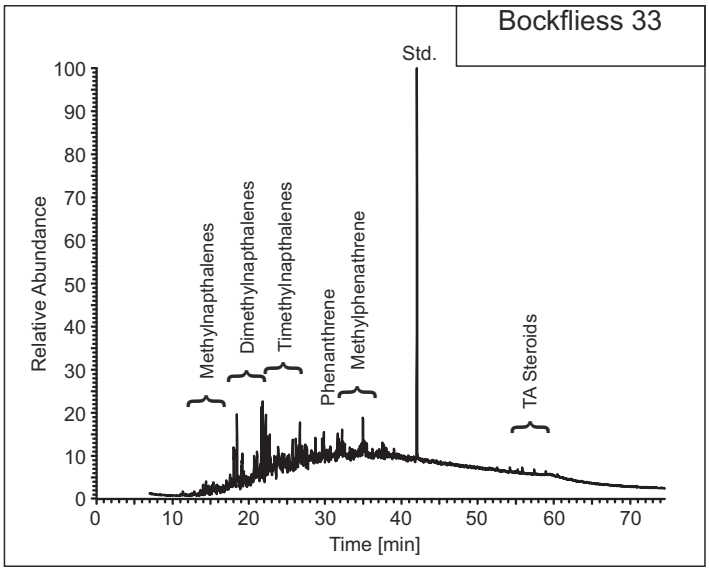
Bockfliess 33
Relative Abundance
Time [min]
Methylnapthalenes
Dimethylnapthalenes
Timethylnapthalenes
Phenanthrene
Methylphenathrene
TA Steroids
Std.

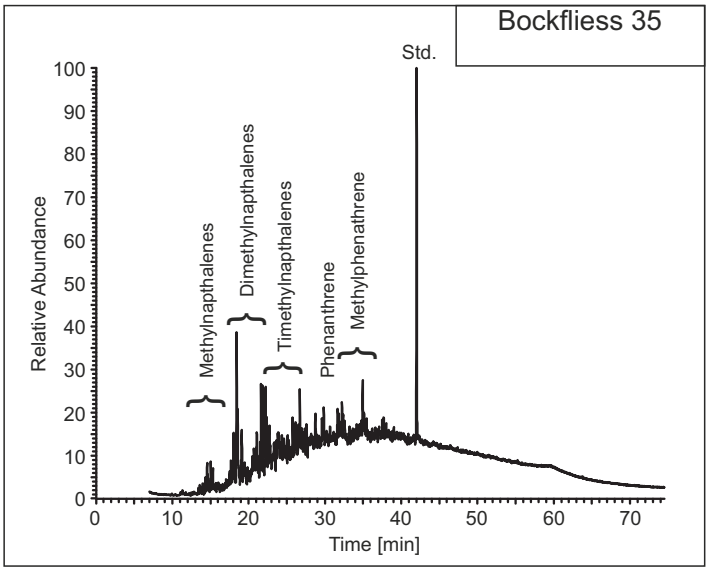
Bockfliess 35
Std.
Methylnapthalenes
Dimethylnapthalenes
Timethylnapthalenes
Phenanthrene
Methylphenathrene
Relative Abundance
Time [min]

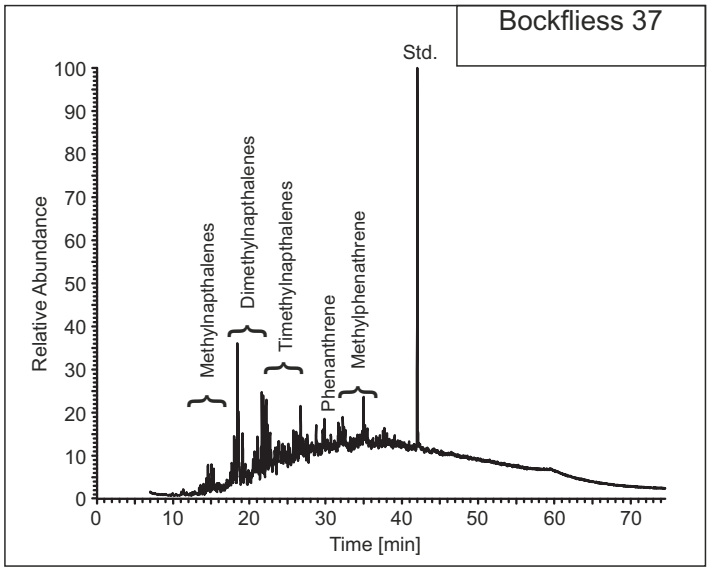
Bockfliess 37
Std.
Methylnapthalenes
Dimethylnapthalenes
Timethylnapthalenes
Phenanthrene
Methylphenathrene
Relative Abundance
Time [min]

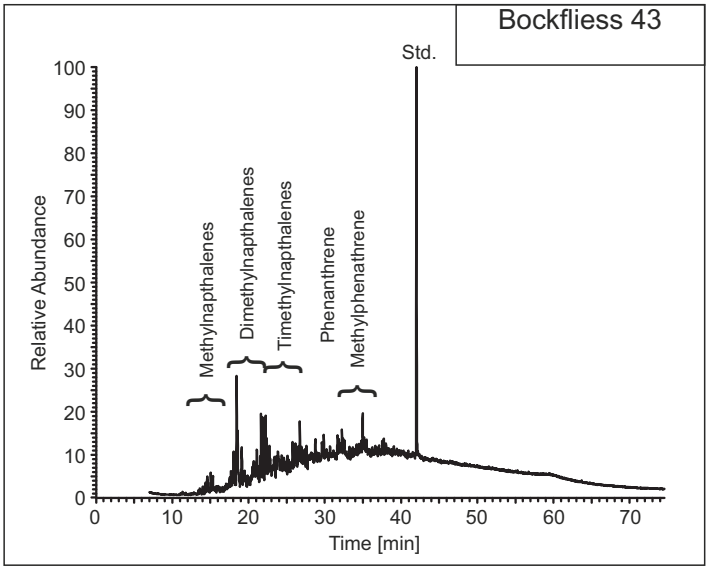
Bockfliess 43
Std.
Methylnapthalenes
Dimethylnapthalenes
Timethylnapthalenes
Phenanthrene
Methylphenathrene
Relative Abundance
Time [min]

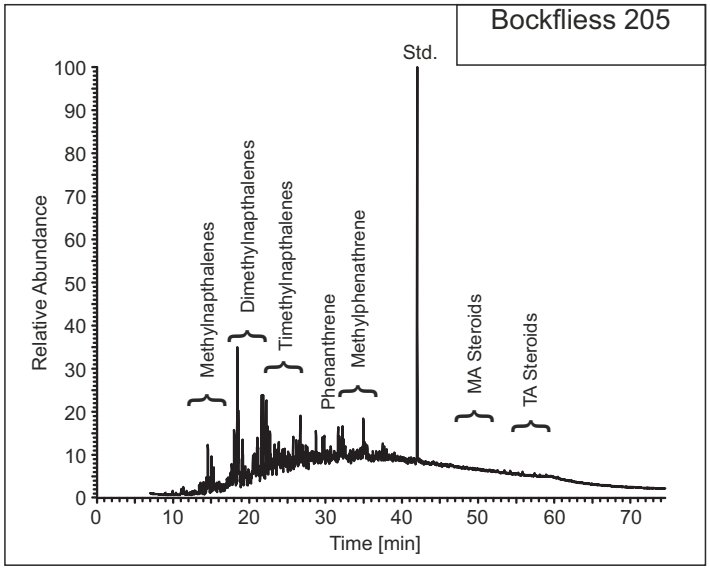
Bockfliess 205
Std.
Methylnapthalenes
Dimethylnapthalenes
Timethylnapthalenes
Phenanthrene
Methylphenathrene
MA Steroids
TA Steroids
Relative Abundance
Time [min]

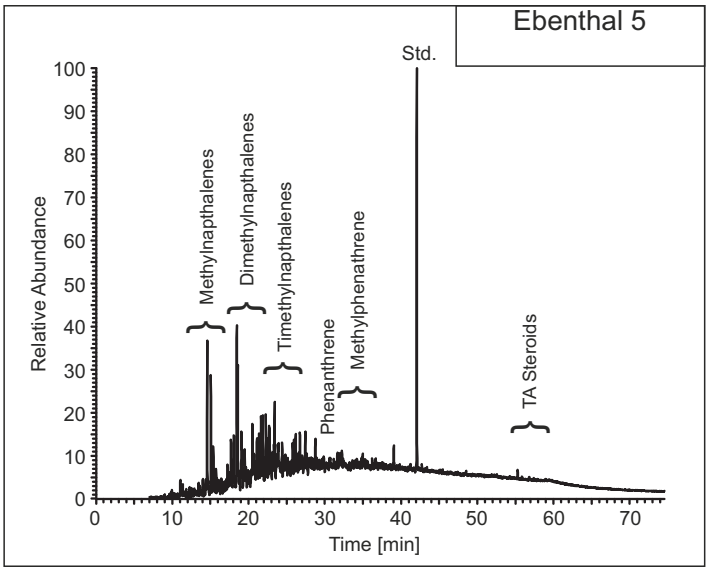
Ebenthal 5
Std.
Methylnapthalenes
Dimethylnapthalenes
Timethylnapthalenes
Phenanthrene
Methylphenathrene
TA Steroids
Relative Abundance
Time [min]

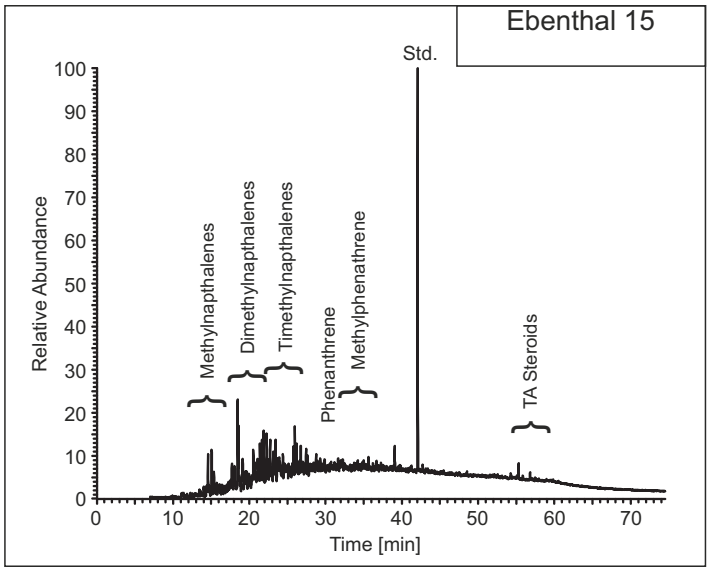
Ebenthal 15
Std.
Methylnapthalenes
Dimethylnapthalenes
Timethylnapthalenes
Phenanthrene
Methylphenathrene
TA Steroids
Relative Abundance
Time [min]

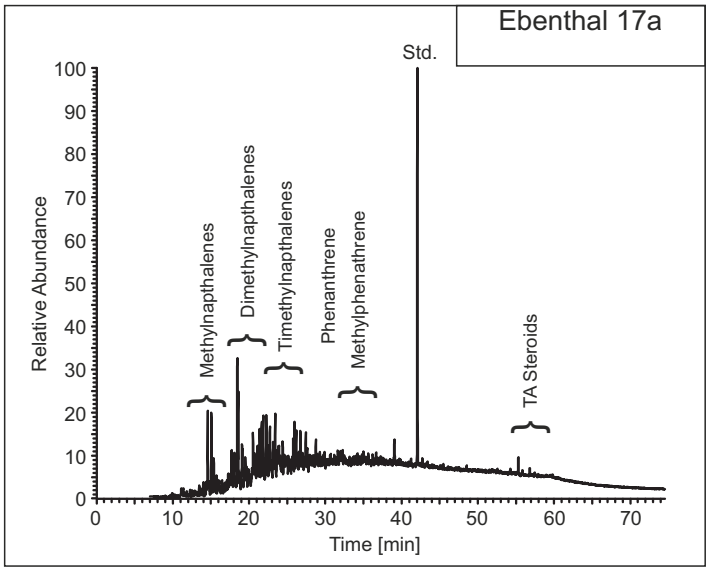
Ebenthal 17a
Std.
Methylnapthalenes
Dimethylnapthalenes
Timethylnapthalenes
Phenanthrene
Methylphenathrene
TA Steroids
Relative Abundance
Time [min]

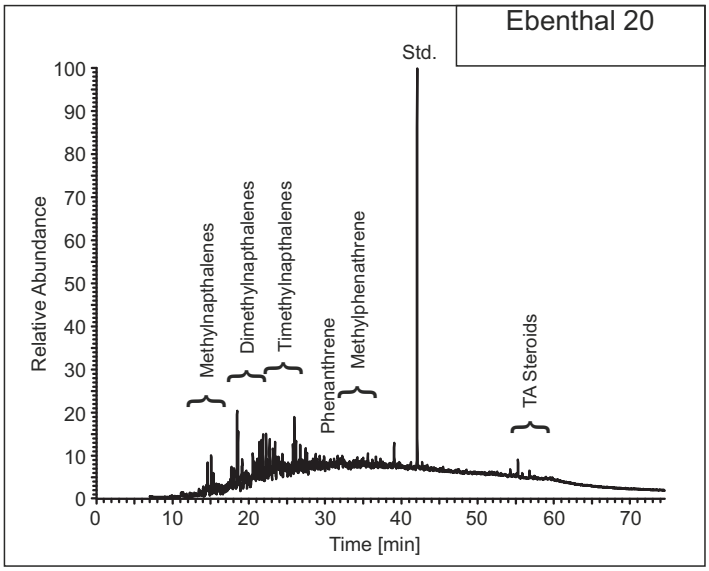
Ebenthal 20
Std.
Methylnapthalenes
Dimethylnapthalenes
Timethylnapthalenes
Phenanthrene
Methylphenathrene
TA Steroids
Relative Abundance
Time [min]

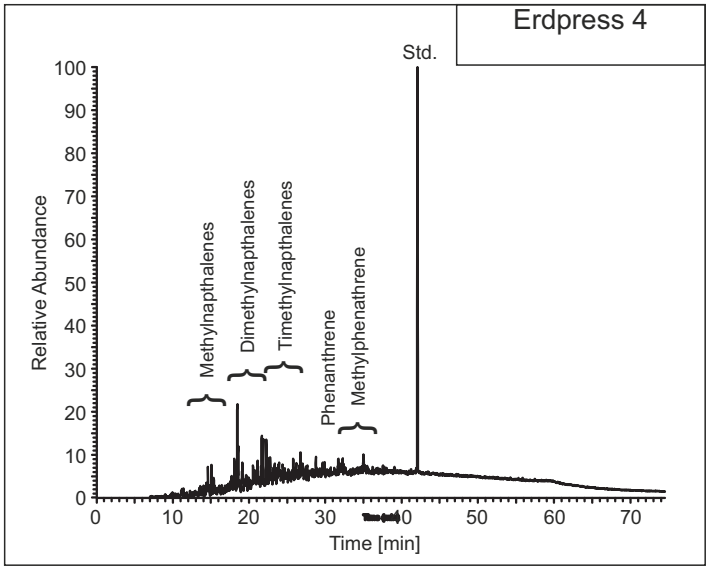
Erdpress 4
Std.
Methylnapthalenes
Dimethylnapthalenes
Timethylnapthalenes
Phenanthrene
Methylphenathrene
Relative Abundance
Time [min]

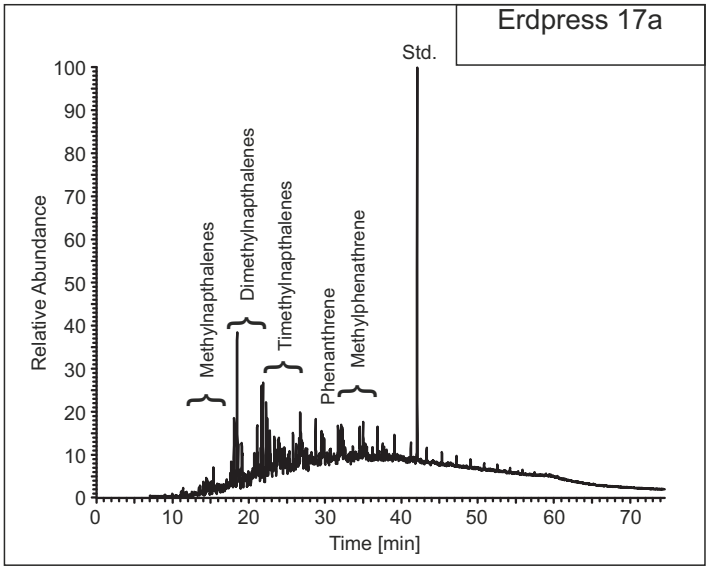
Erdpress 17a
Std.
Methylnapthalenes
Dimethylnapthalenes
Timethylnapthalenes
Phenanthrene
Methylphenathrene
Relative Abundance
Time [min]

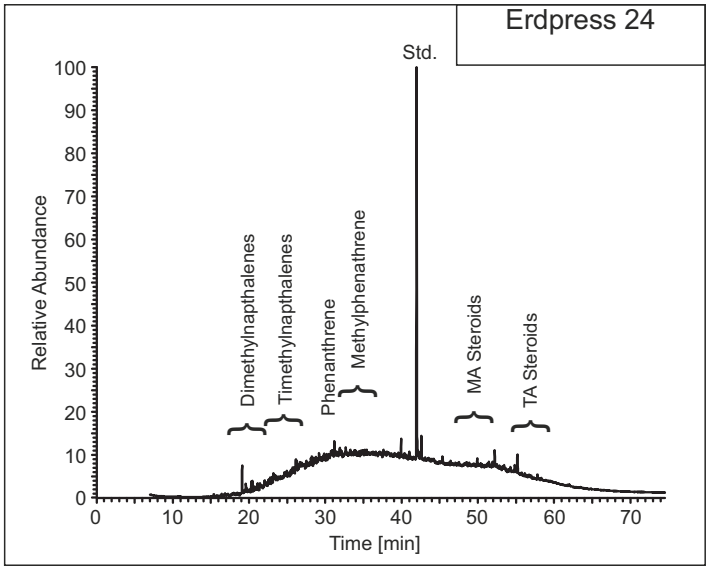
Erdpress 24
Std.
Dimethylnapthalenes
Timethylnapthalenes
Phenanthrene
Methylphenathrene
MA Steroids
TA Steroids
Relative Abundance
Time [min]

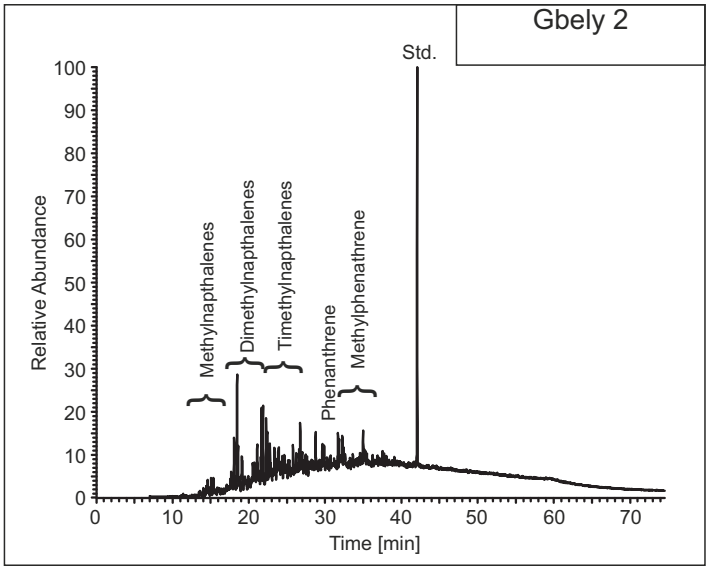
Gbely 2
Std.
Methylnapthalenes
Dimethylnapthalenes
Timethylnapthalenes
Phenanthrene
Methylphenathrene
Relative Abundance
Time [min]

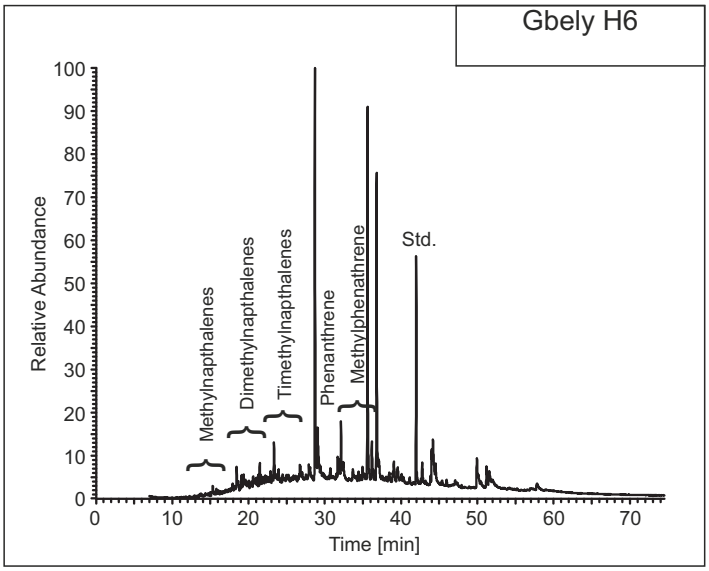
Gbely H6
Relative Abundance
Time [min]
Methylnapthalenes
Dimethylnapthalenes
Timethylnapthalenes
Phenanthrene
Methylphenathrene
Std.

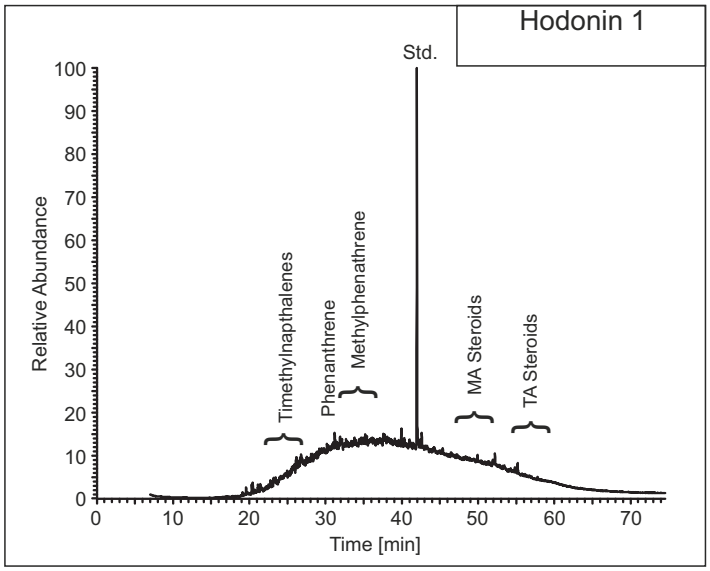
Hodonin 1
Relative Abundance
Time [min]
Timethylnapthalenes
Phenanthrene
Methylphenathrene
Std.
MA Steroids
TA Steroids

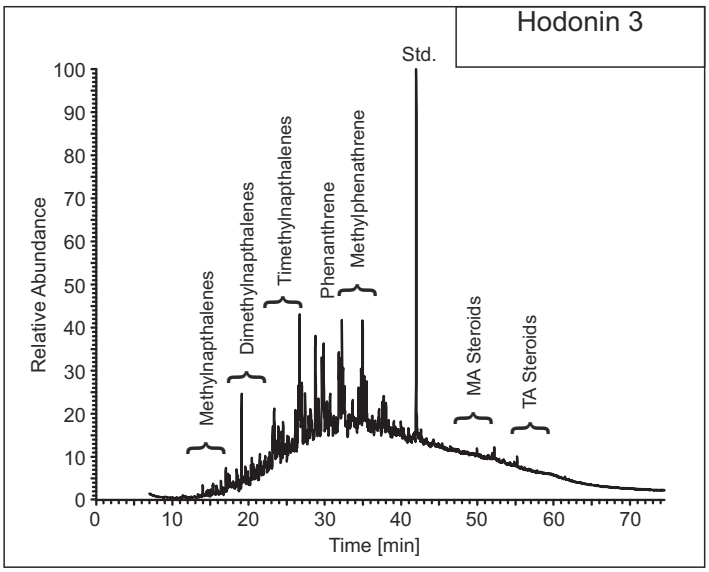
Hodonin 3
Relative Abundance
Time [min]
Methylnapthalenes
Dimethylnapthalenes
Timethylnapthalenes
Phenanthrene
Methylphenathrene
Std.
MA Steroids
TA Steroids

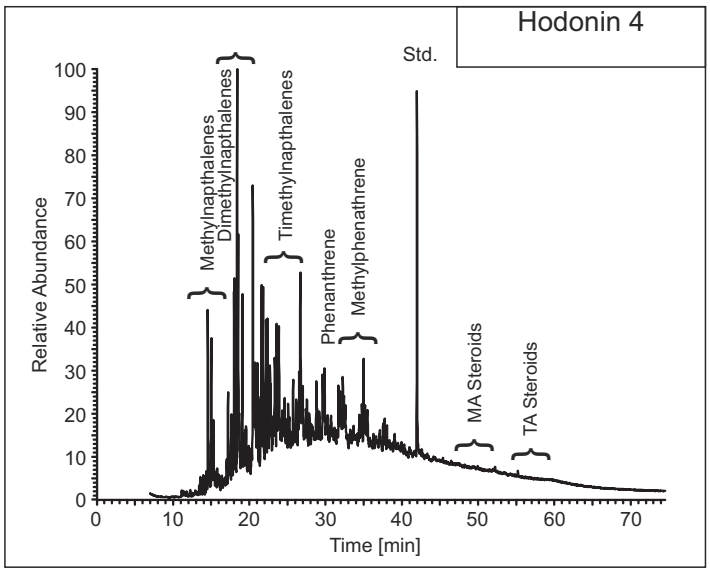
Hodonin 4
Relative Abundance
Time [min]
Methylnapthalenes
Dimethylnapthalenes
Timethylnapthalenes
Phenanthrene
Methylphenathrene
Std.
MA Steroids
TA Steroids

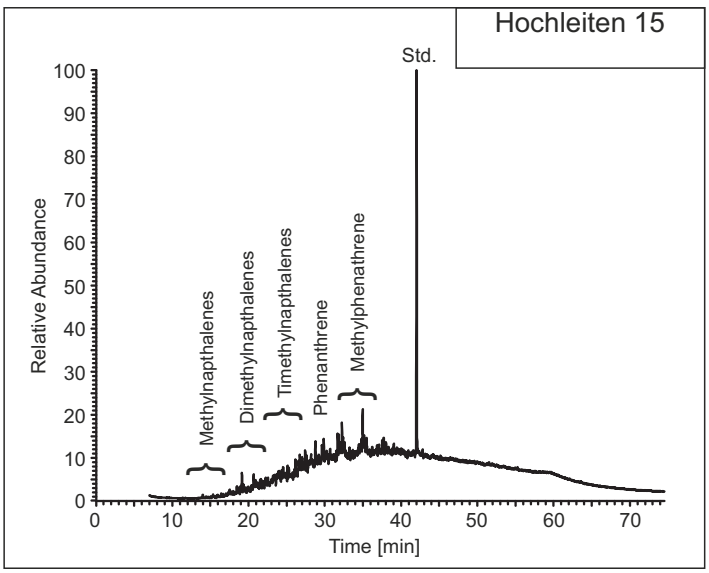
Hochleiten 15
Relative Abundance
Time [min]
Methylnapthalenes
Dimethylnapthalenes
Timethylnapthalenes
Phenanthrene
Methylphenathrene
Std.

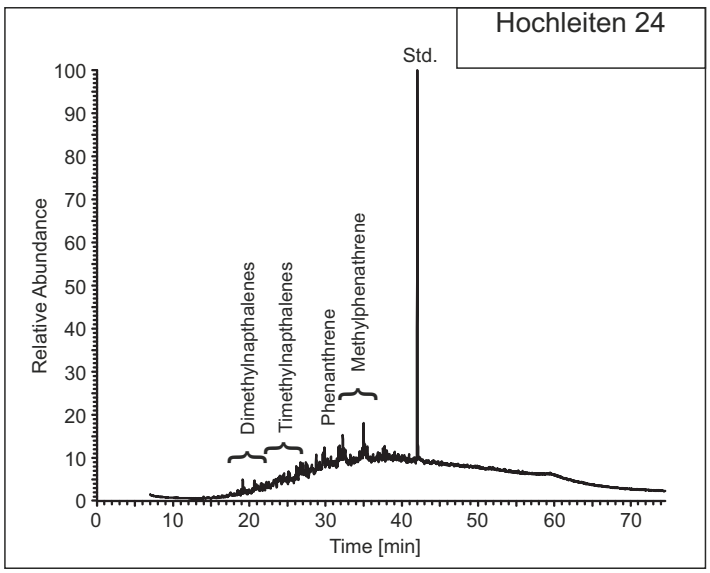
Hochleiten 24
Relative Abundance
Time [min]
Dimethylnapthalenes
Timethylnapthalenes
Phenanthrene
Methylphenathrene
Std.

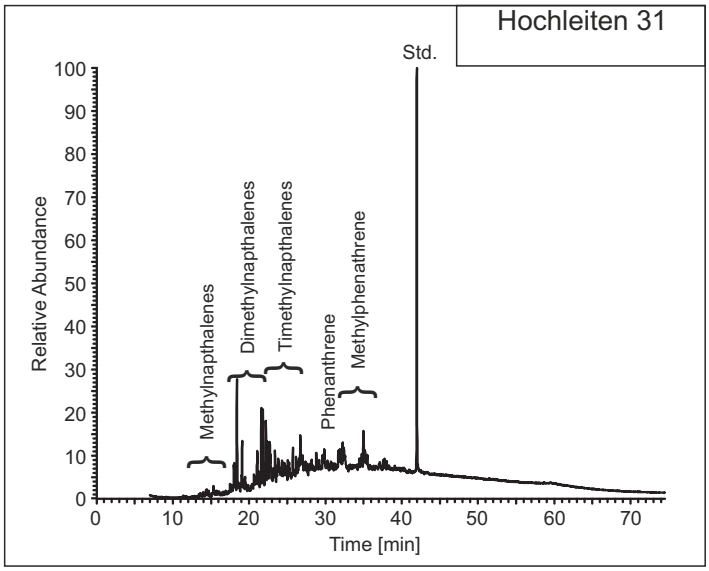
Hochleiten 31
Std.
Methylnapthalenes
Dimethylnapthalenes
Timethylnapthalenes
Phenanthrene
Methylphenathrene
Relative Abundance
Time [min]

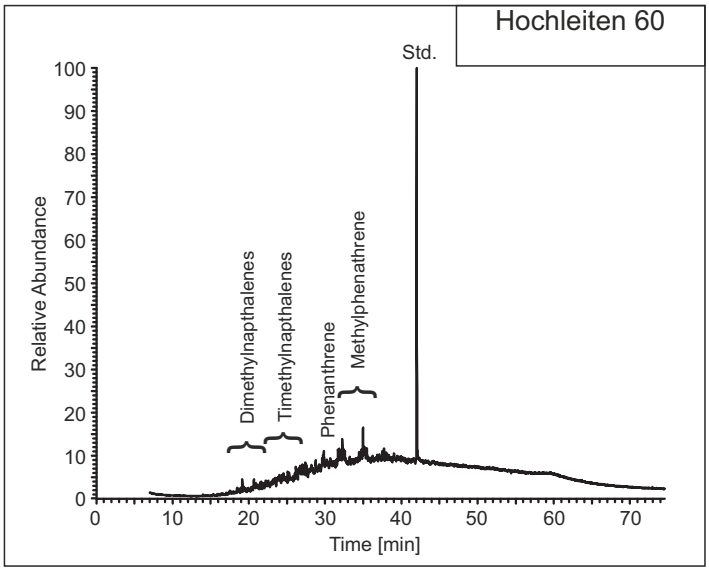
Hochleiten 60
Std.
Dimethylnapthalenes
Timethylnapthalenes
Phenanthrene
Methylphenathrene
Relative Abundance
Time [min]

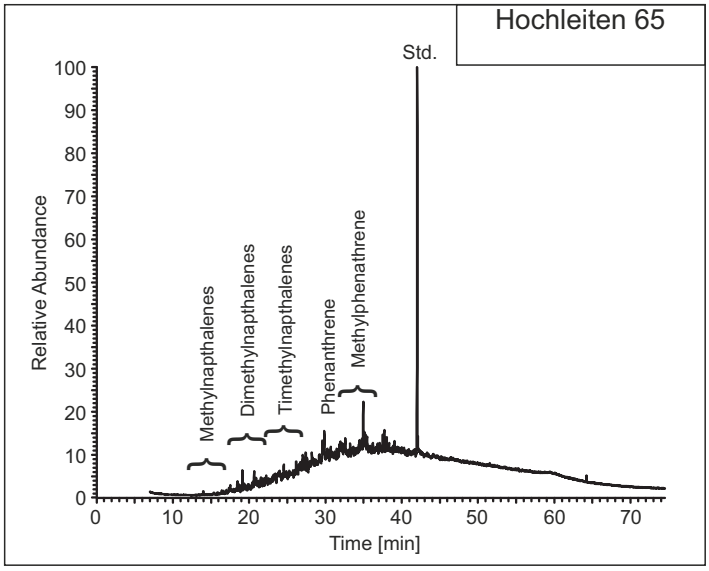
Hochleiten 65
Std.
Methylnapthalenes
Dimethylnapthalenes
Timethylnapthalenes
Phenanthrene
Methylphenathrene
Relative Abundance
Time [min]

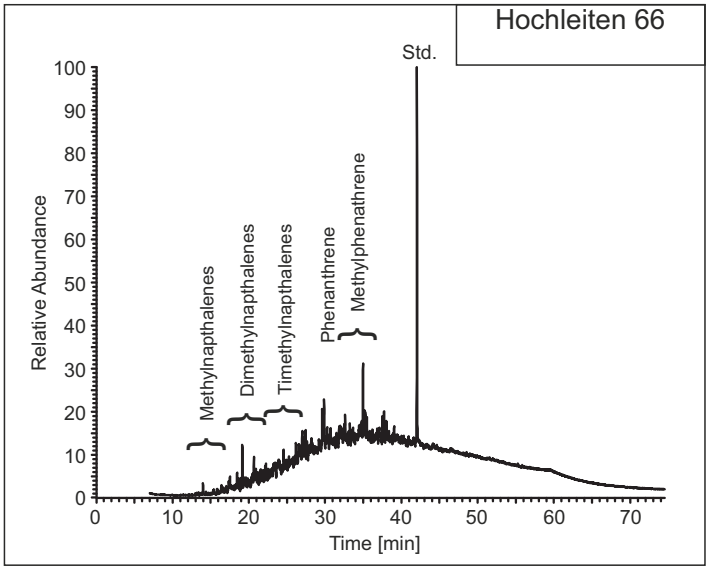
Hochleiten 66
Std.
Methylnapthalenes
Dimethylnapthalenes
Timethylnapthalenes
Phenanthrene
Methylphenathrene
Relative Abundance
Time [min]

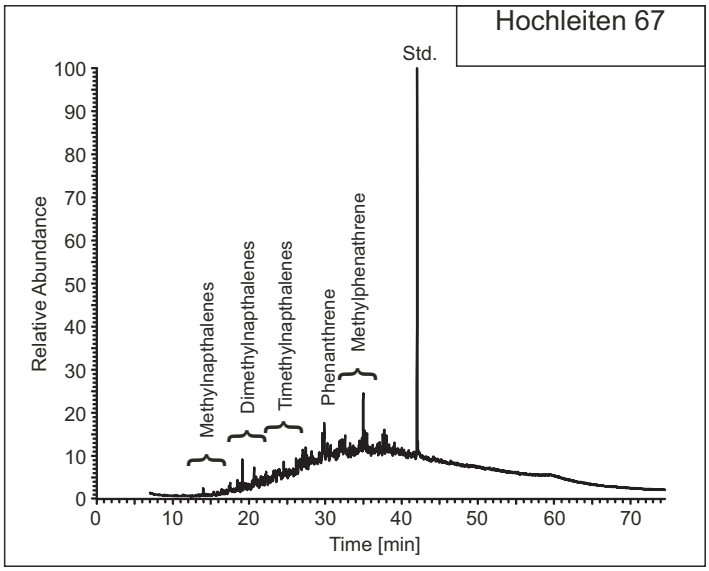
Hochleiten 67
Std.
Methylnapthalenes
Dimethylnapthalenes
Timethylnapthalenes
Phenanthrene
Methylphenathrene
Relative Abundance
Time [min]

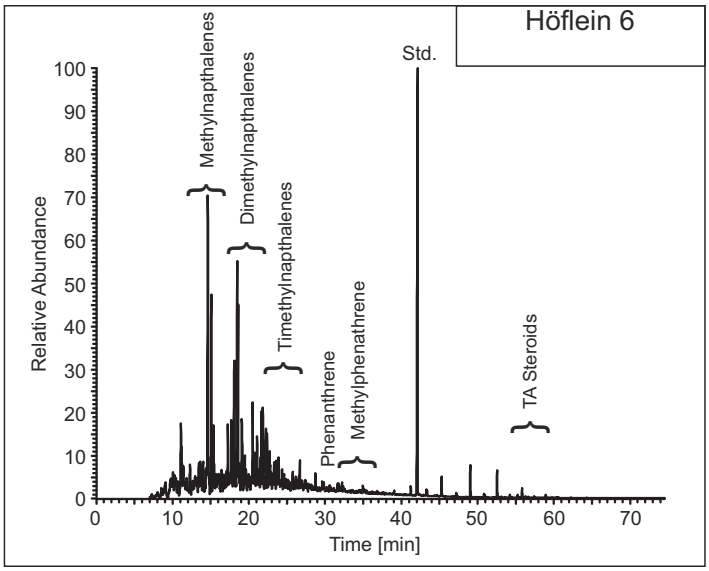
Höflein 6
Std.
Methylnapthalenes
Dimethylnapthalenes
Timethylnapthalenes
Phenanthrene
Methylphenathrene
TA Steroids
Relative Abundance
Time [min]

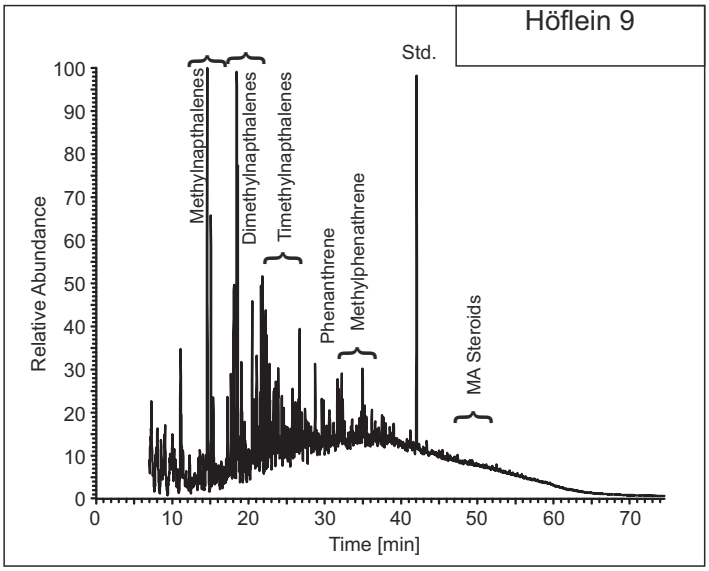
Höflein 9
Std.
Methylnapthalenes
Dimethylnapthalenes
Timethylnapthalenes
Phenanthrene
Methylphenathrene
MA Steroids
Relative Abundance
Time [min]

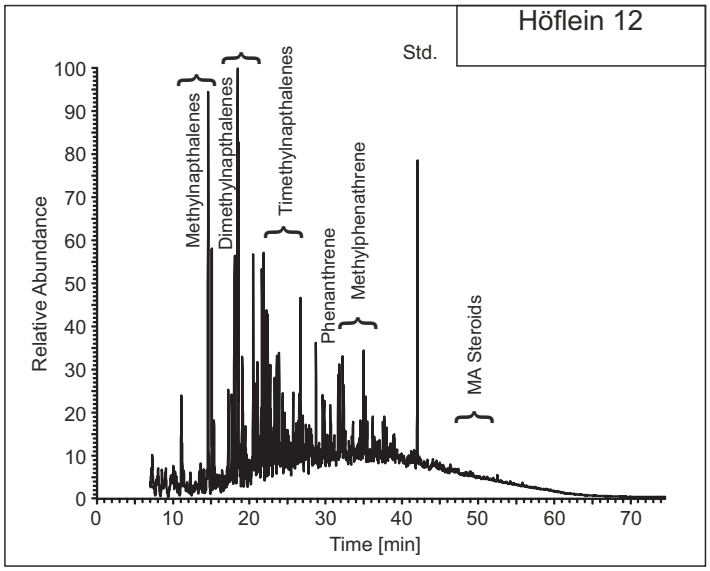
Höflein 12
Std.
Methylnapthalenes
Dimethylnapthalenes
Timethylnapthalenes
Phenanthrene
Methylphenathrene
MA Steroids
Relative Abundance
Time [min]

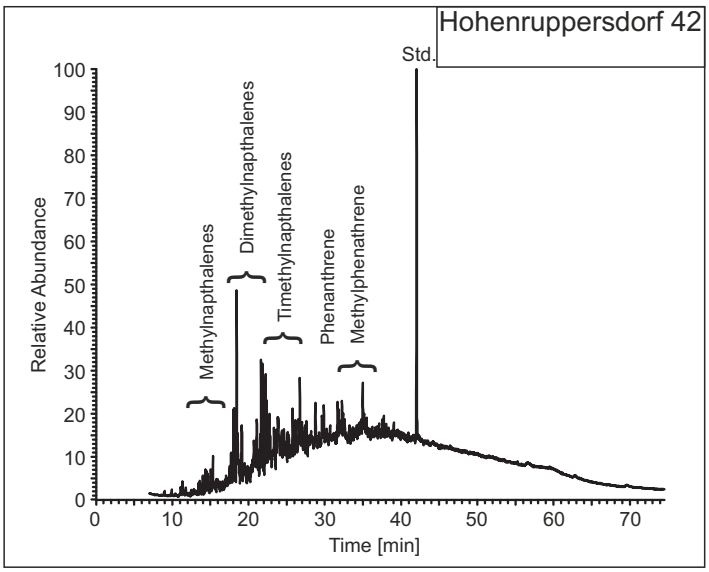
Hohenruppersdorf 42
Std.
Methylnapthalenes
Dimethylnapthalenes
Timethylnapthalenes
Phenanthrene
Methylphenathrene
Relative Abundance
Time [min]

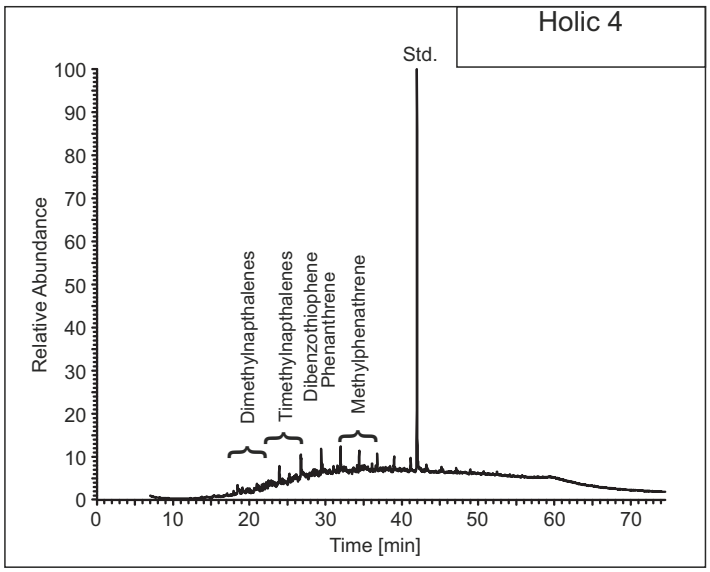
Holic 4
Std.
Dimethylnapthalenes
Timethylnapthalenes
Dibenzothiophene
Phenanthrene
Methylphenathrene
Relative Abundance
Time [min]

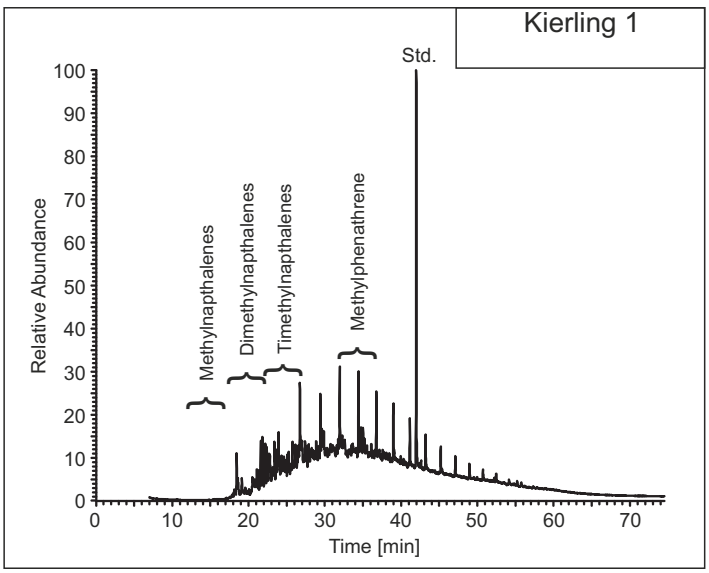
Kierling 1
Std.
Methylnapthalenes
Dimethylnapthalenes
Timethylnapthalenes
Methylphenathrene
Relative Abundance
Time [min]

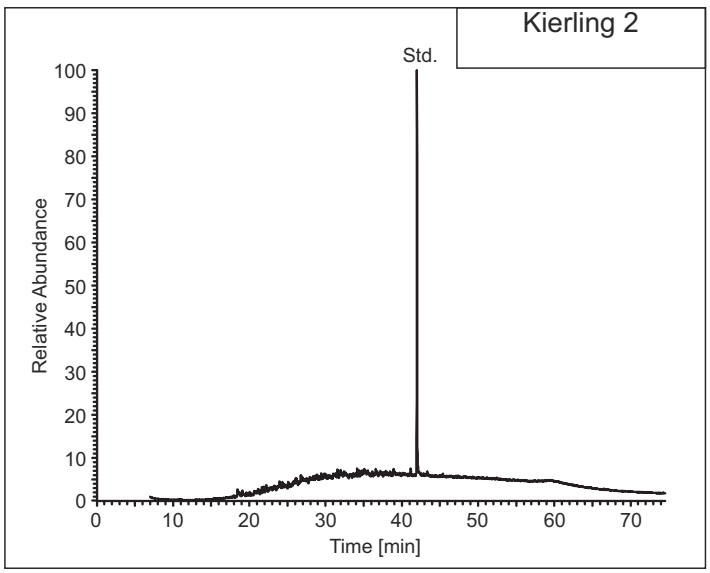
Kierling 2
Std.
Relative Abundance
Time [min]

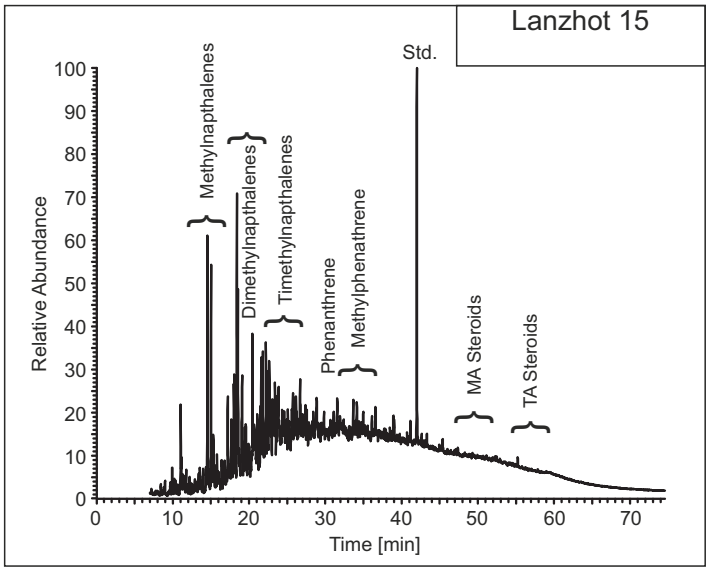
Lanzhot 15
Relative Abundance
Time [min]
Std.
Methylnapthalenes
Dimethylnapthalenes
Timethylnapthalenes
Phenanthrene
Methylphenathrene
MA Steroids
TA Steroids

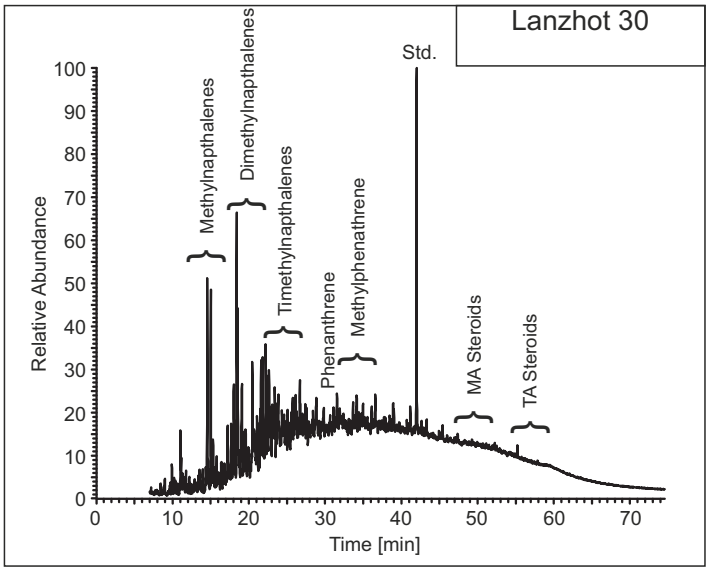
Lanzhot 30
Relative Abundance
Time [min]
Std.
Methylnapthalenes
Dimethylnapthalenes
Timethylnapthalenes
Phenanthrene
Methylphenathrene
MA Steroids
TA Steroids

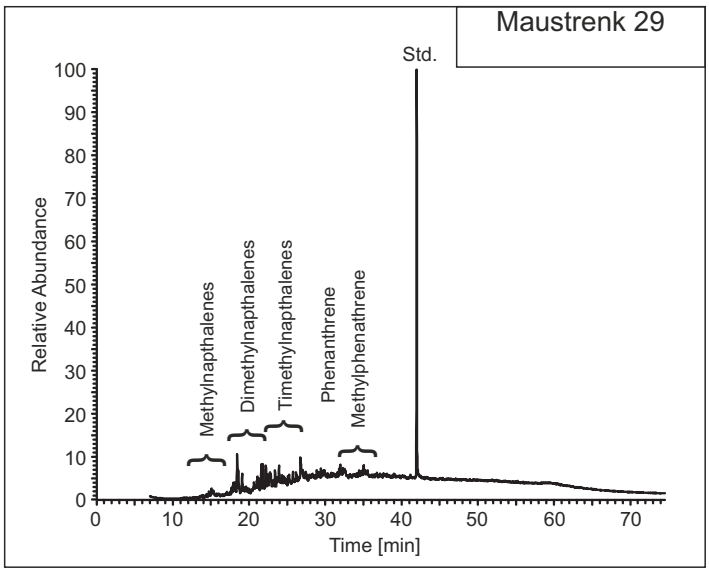
Maustrenk 29
Relative Abundance
Time [min]
Std.
Methylnapthalenes
Dimethylnapthalenes
Timethylnapthalenes
Phenanthrene
Methylphenathrene

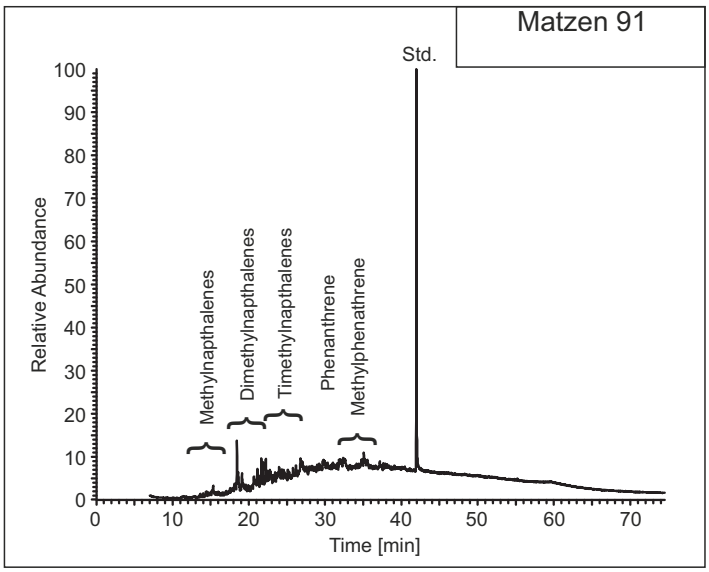
Matzen 91
Relative Abundance
Time [min]
Std.
Methylnapthalenes
Dimethylnapthalenes
Timethylnapthalenes
Phenanthrene
Methylphenathrene

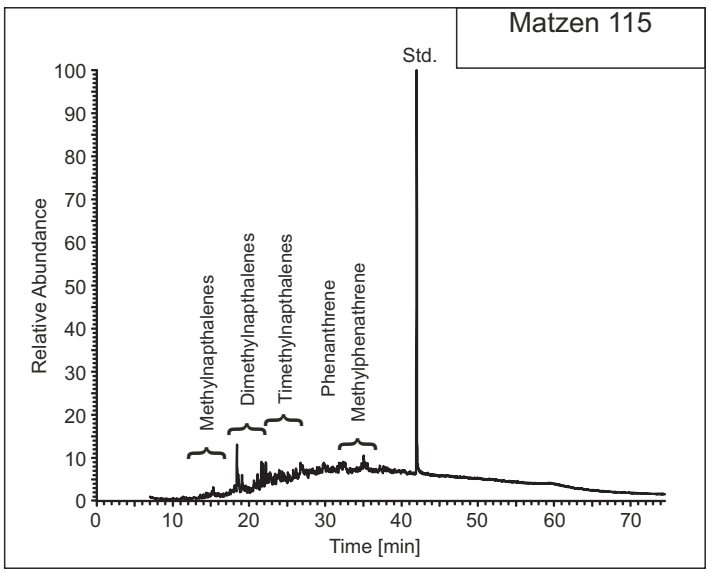
Matzen 115
Relative Abundance
Time [min]
Std.
Methylnapthalenes
Dimethylnapthalenes
Timethylnapthalenes
Phenanthrene
Methylphenathrene

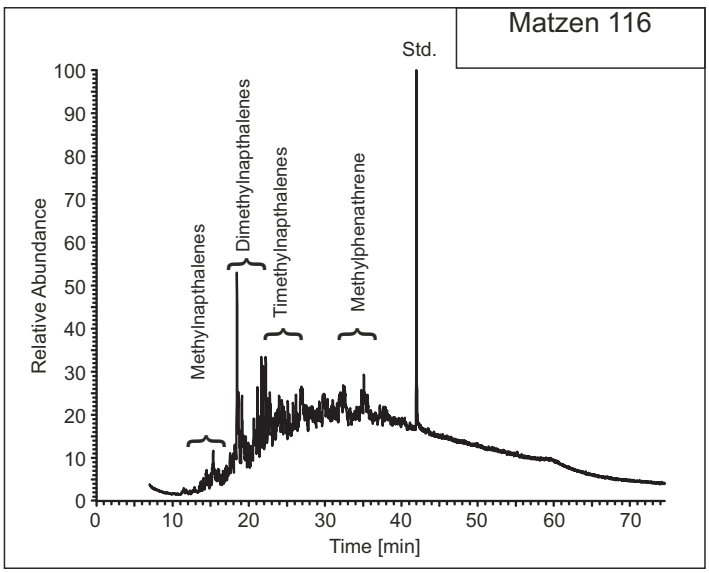
Matzen 116
Relative Abundance
Time [min]
Std.
Methylnapthalenes
Dimethylnapthalenes
Timethylnapthalenes
Methylphenathrene

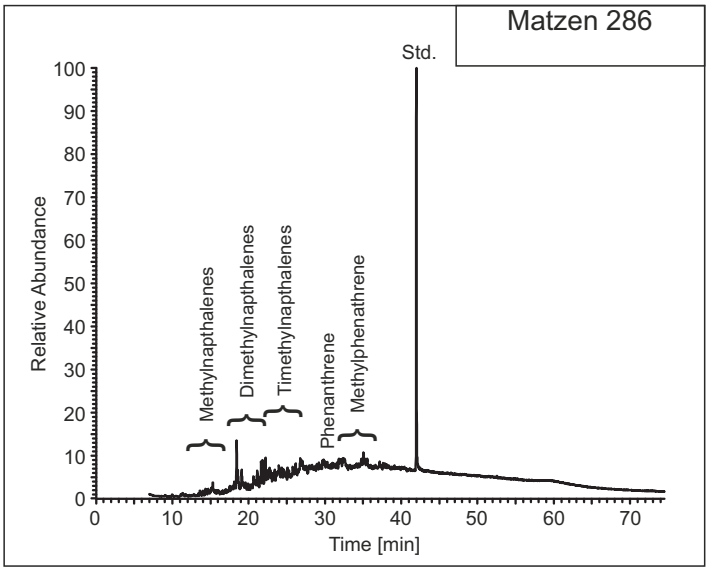

Matzen 322

File unfortunatly corrupted

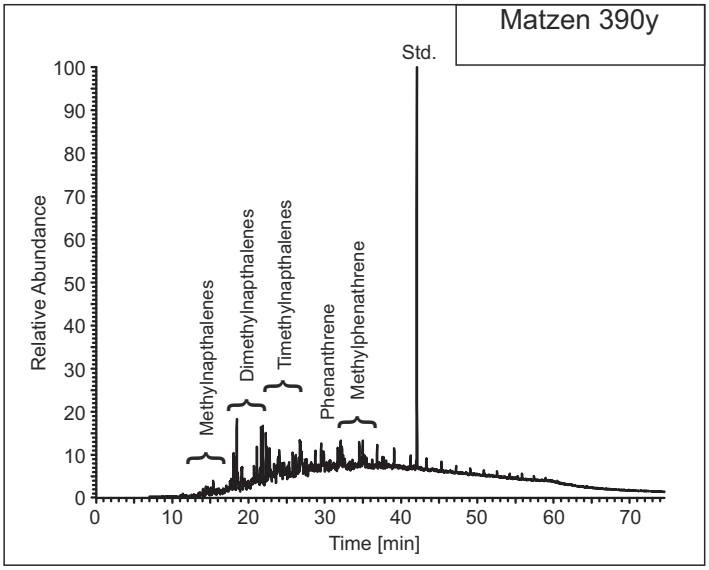

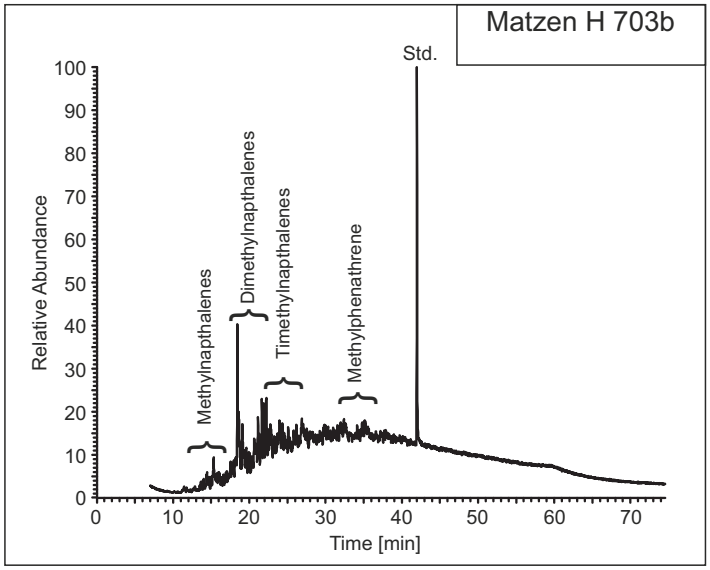

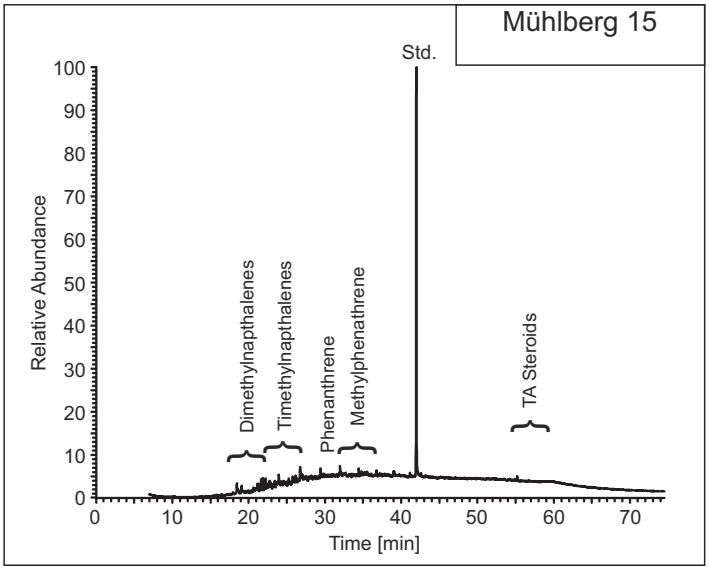

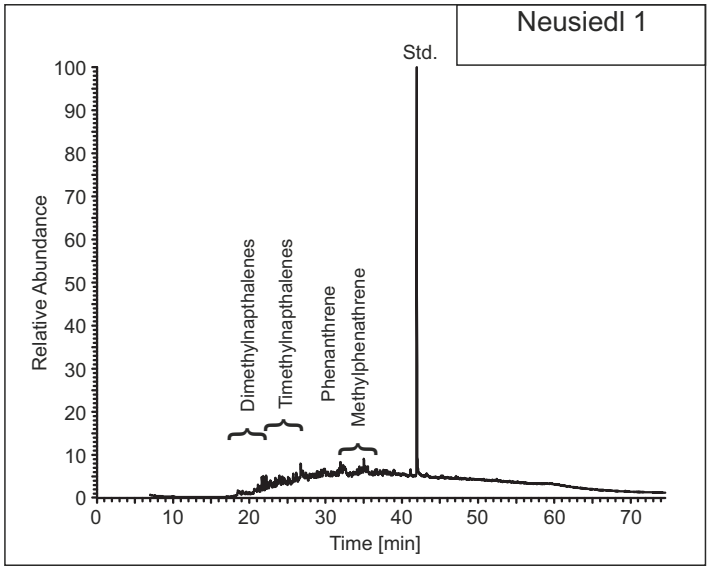

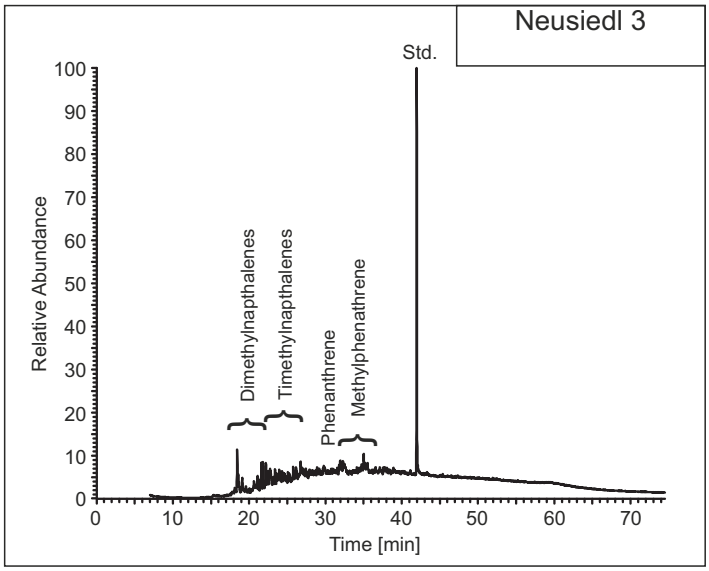
Neusiedl 3
Std.
Dimethylnapthalenes
Timethylnapthalenes
Phenanthrene
Methylphenathrene
Relative Abundance
Time [min]

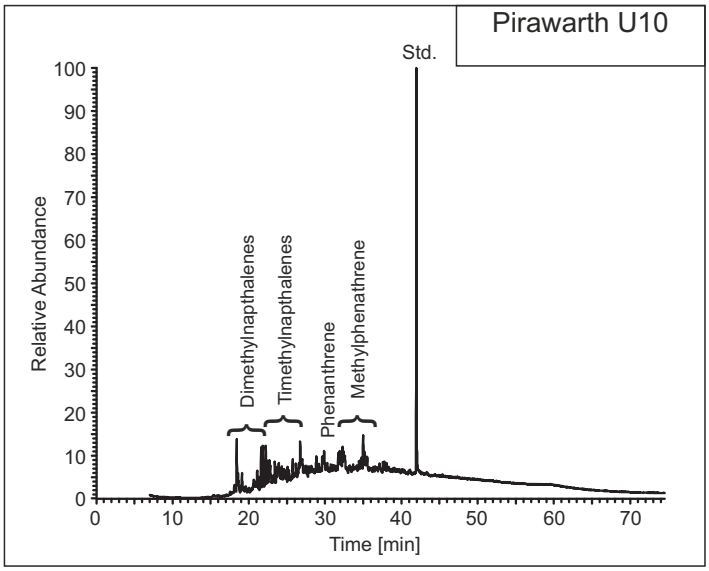
Pirawarth U10
Std.
Dimethylnapthalenes
Timethylnapthalenes
Phenanthrene
Methylphenathrene
Relative Abundance
Time [min]

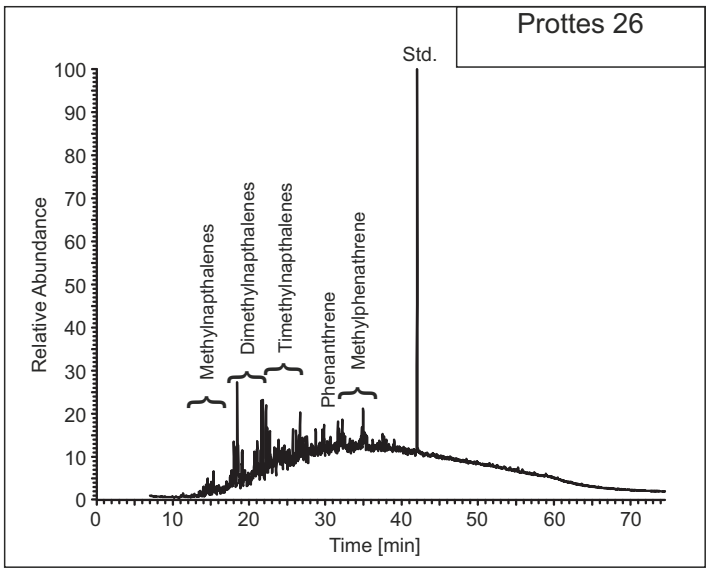
Prottes 26
Std.
Methylnapthalenes
Dimethylnapthalenes
Timethylnapthalenes
Phenanthrene
Methylphenathrene
Relative Abundance
Time [min]

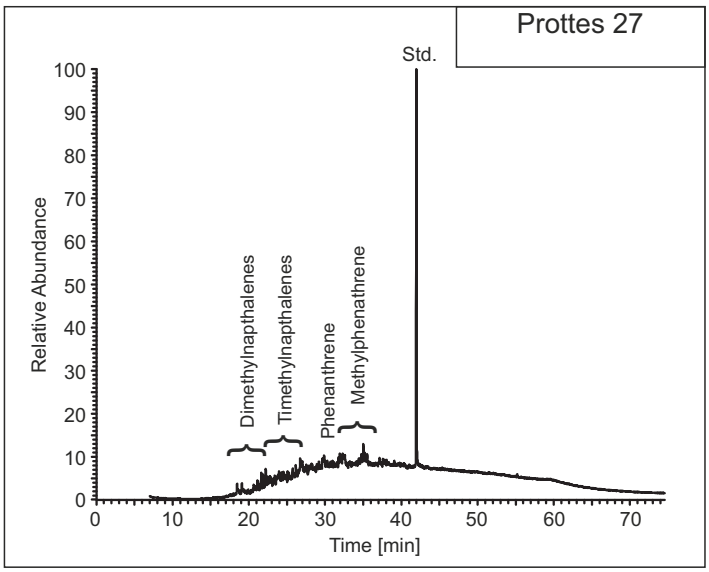
Prottes 27
Std.
Dimethylnapthalenes
Timethylnapthalenes
Phenanthrene
Methylphenathrene
Relative Abundance
Time [min]

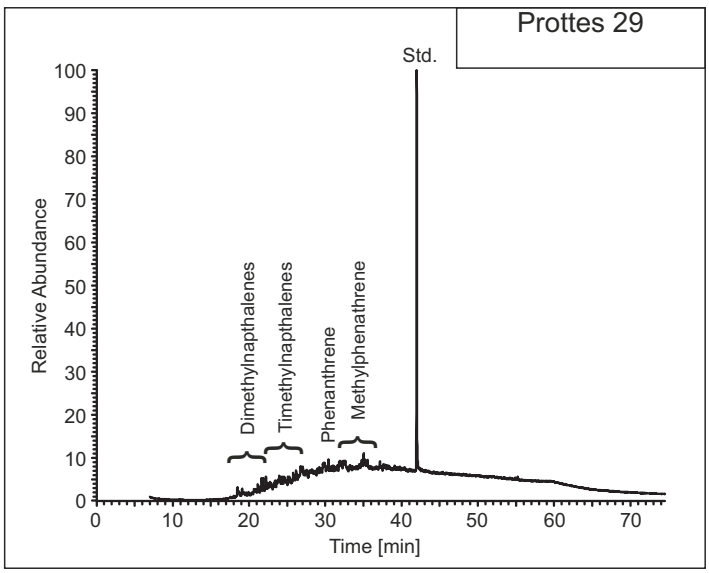
Prottes 29
Std.
Dimethylnapthalenes
Timethylnapthalenes
Phenanthrene
Methylphenathrene
Relative Abundance
Time [min]

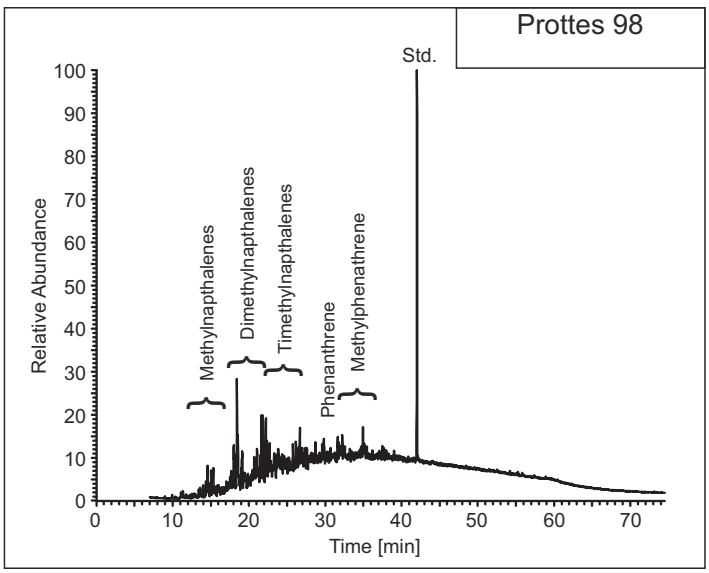
Prottes 98
Std.
Methylnapthalenes
Dimethylnapthalenes
Timethylnapthalenes
Phenanthrene
Methylphenathrene
Relative Abundance
Time [min]

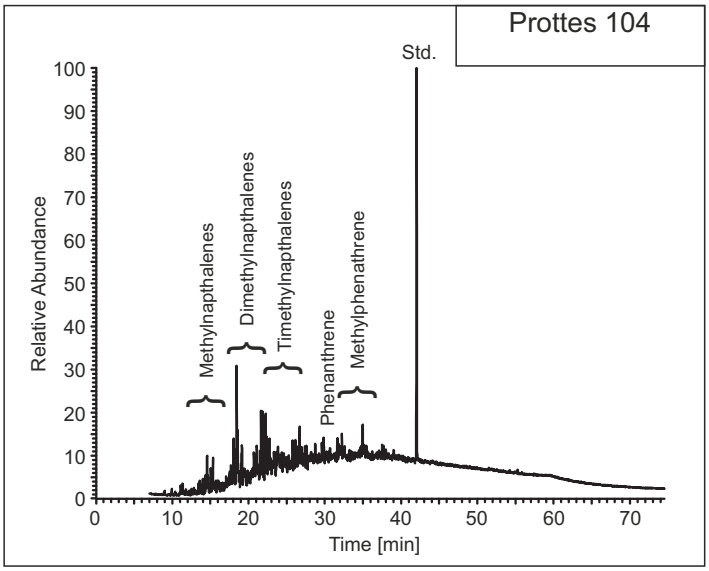
Prottes 104
Std.
Methylnapthalenes
Dimethylnapthalenes
Timethylnapthalenes
Phenanthrene
Methylphenathrene
Relative Abundance
Time [min]

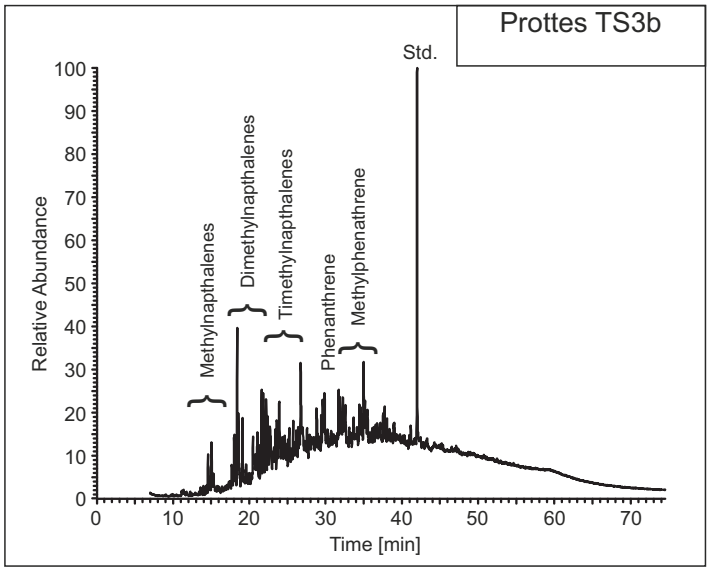
Prottes TS3b
Std.
Methylnapthalenes
Dimethylnapthalenes
Timethylnapthalenes
Phenanthrene
Methylphenathrene
Relative Abundance
Time [min]

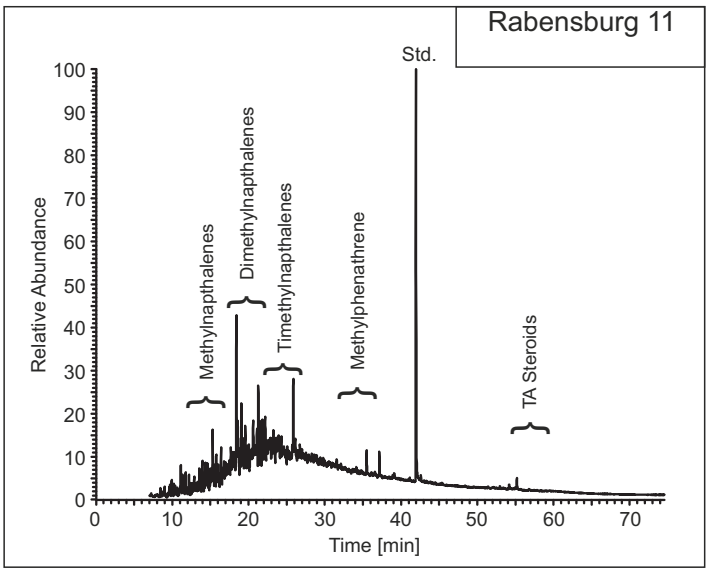
Rabensburg 11
Std.
Methylnapthalenes
Dimethylnapthalenes
Timethylnapthalenes
Methylphenathrene
TA Steroids
Relative Abundance
Time [min]

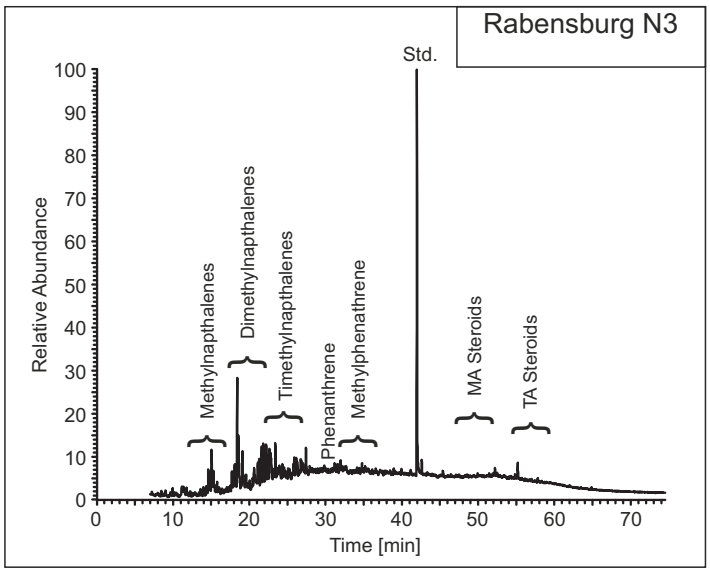
Rabensburg N3
Std.
Methylnapthalenes
Dimethylnapthalenes
Timethylnapthalenes
Phenanthrene
Methylphenathrene
MA Steroids
TA Steroids
Relative Abundance
Time [min]

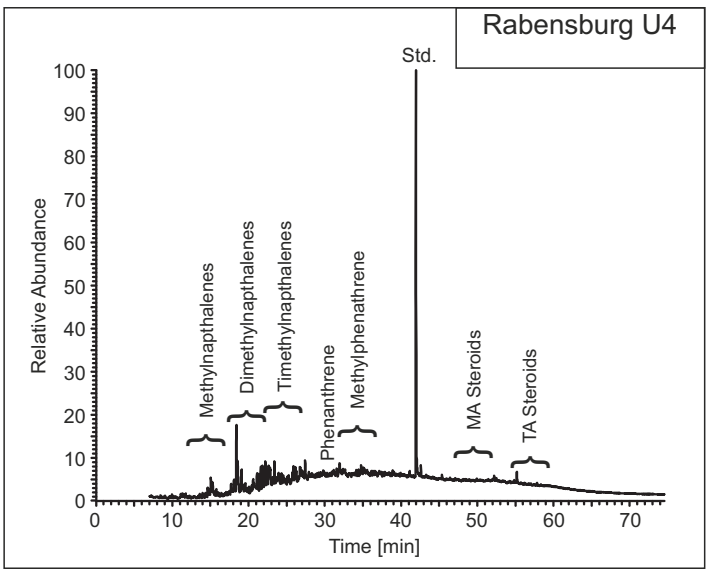
Rabensburg U4
Std.
Methylnapthalenes
Dimethylnapthalenes
Timethylnapthalenes
Phenanthrene
Methylphenathrene
MA Steroids
TA Steroids
Relative Abundance
Time [min]

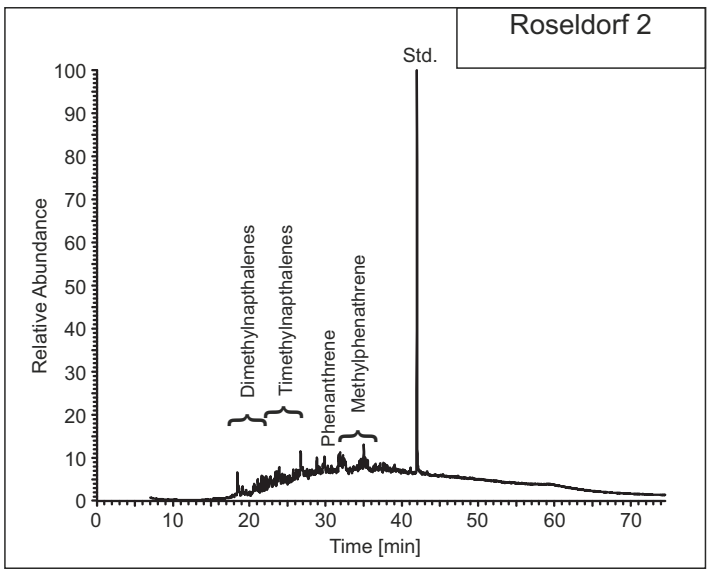
Roseldorf 2
Std.
Dimethylnapthalenes
Timethylnapthalenes
Phenanthrene
Methylphenathrene
Relative Abundance
Time [min]

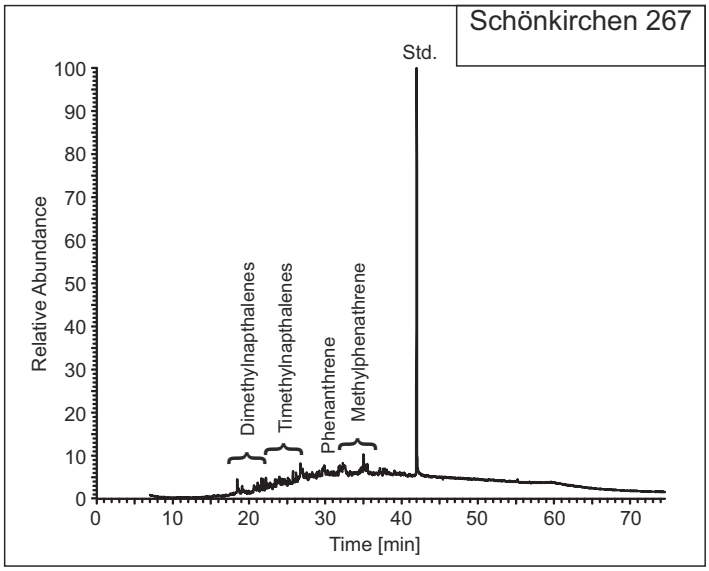
Schönkirchen 267
Std.
Dimethylnapthalenes
Timethylnapthalenes
Phenanthrene
Methylphenathrene
Relative Abundance
Time [min]

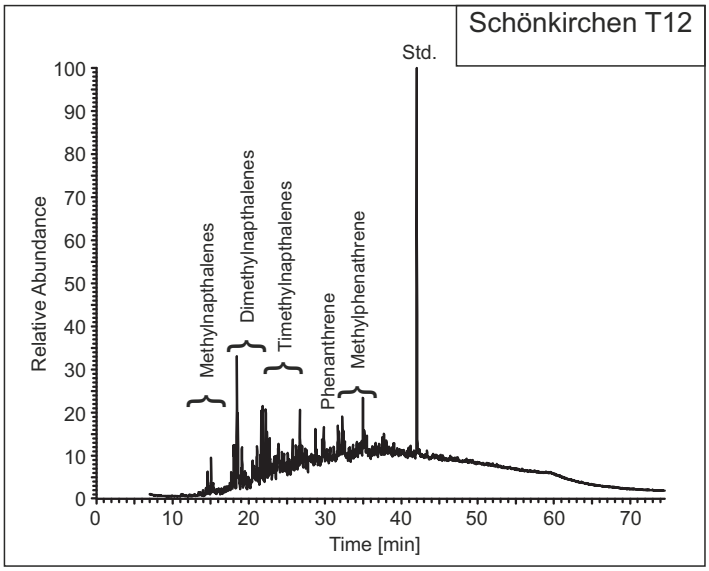
Schönkirchen T12
Std.
Methylnapthalenes
Dimethylnapthalenes
Timethylnapthalenes
Phenanthrene
Methylphenathrene
Relative Abundance
Time [min]

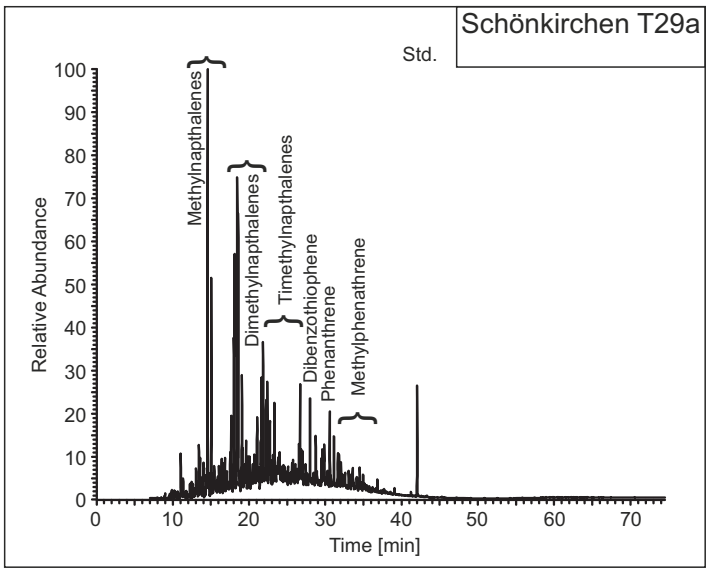
Schönkirchen T29a
Std.
Methylnapthalenes
Dimethylnapthalenes
Timethylnapthalenes
Dibenzothiophene
Phenanthrene
Methylphenathrene
Relative Abundance
Time [min]

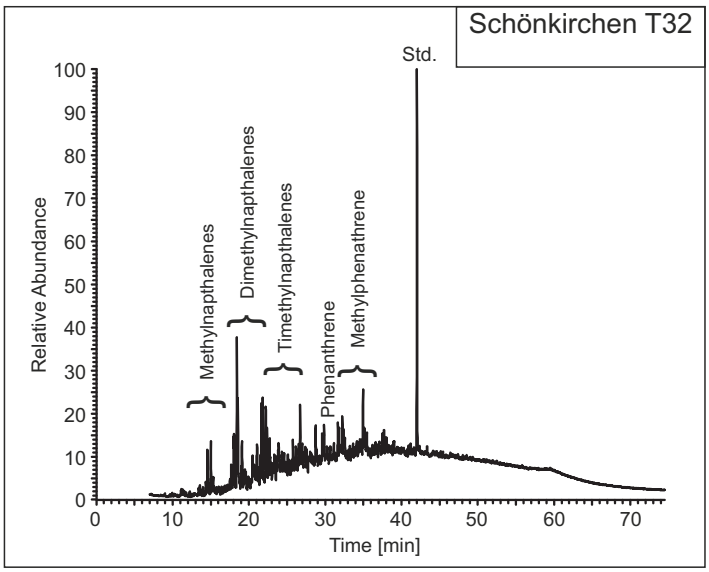
Schönkirchen T32
Std.
Methylnapthalenes
Dimethylnapthalenes
Timethylnapthalenes
Phenanthrene
Methylphenathrene
Relative Abundance
Time [min]

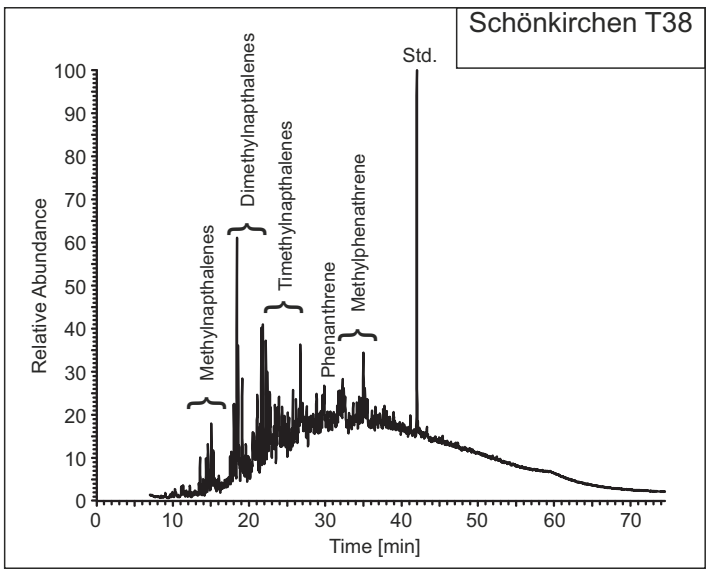
Schönkirchen T38
Std.
Methylnapthalenes
Dimethylnapthalenes
Timethylnapthalenes
Phenanthrene
Methylphenathrene
Relative Abundance
Time [min]

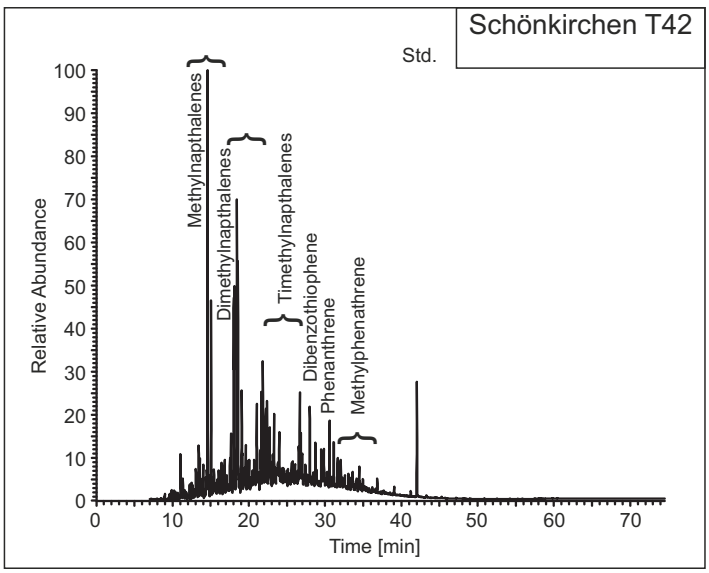
Schönkirchen T42
Std.
Methylnapthalenes
Dimethylnapthalenes
Timethylnapthalenes
Dibenzothiophene
Phenanthrene
Methylphenathrene
Relative Abundance
Time [min]

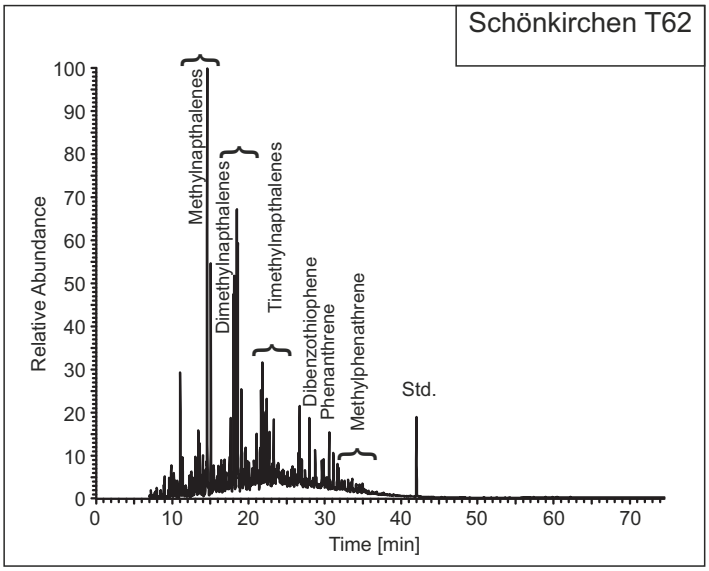
Schönkirchen T62
Relative Abundance
Time [min]
Methylnapthalenes
Dimethylnapthalenes
Timethylnapthalenes
Dibenzothiophene
Phenanthrene
Methylphenathrene
Std.

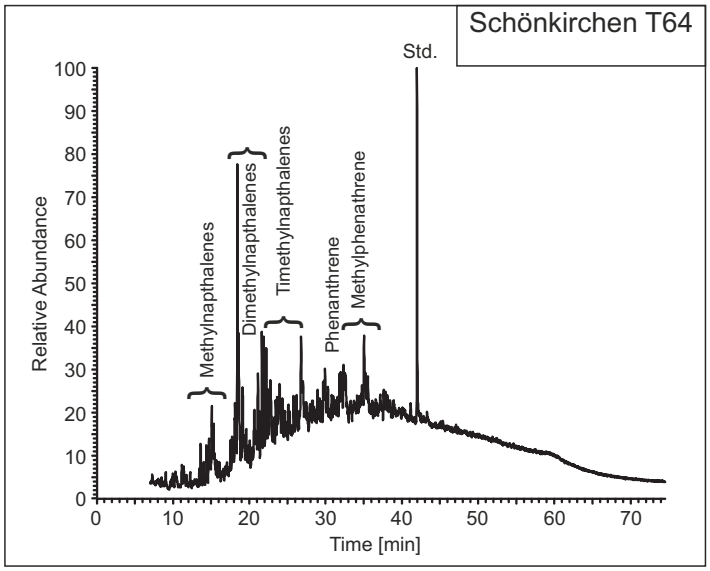
Schönkirchen T64
Relative Abundance
Time [min]
Std.
Methylnapthalenes
Dimethylnapthalenes
Timethylnapthalenes
Phenanthrene
Methylphenathrene

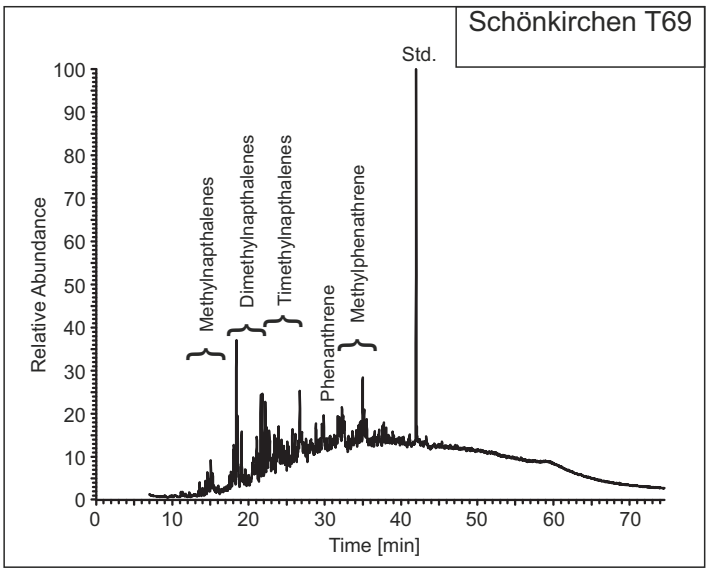
Schönkirchen T69
Relative Abundance
Time [min]
Std.
Methylnapthalenes
Dimethylnapthalenes
Timethylnapthalenes
Phenanthrene
Methylphenathrene

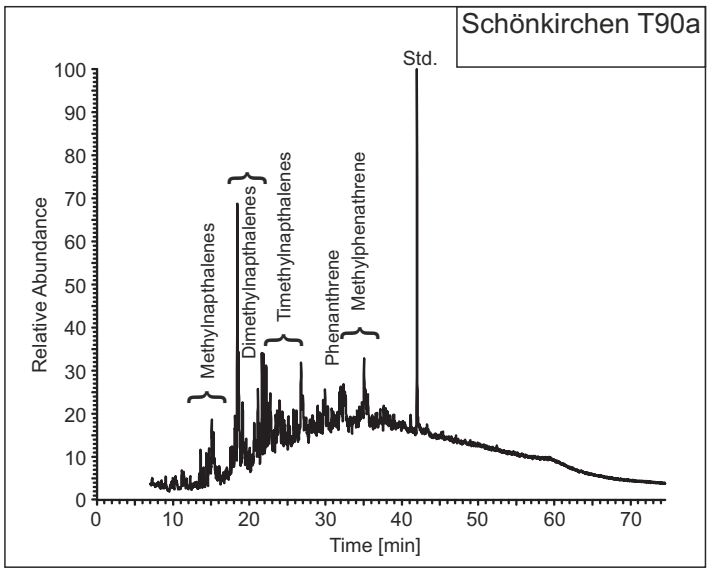
Schönkirchen T90a
Relative Abundance
Time [min]
Std.
Methylnapthalenes
Dimethylnapthalenes
Timethylnapthalenes
Phenanthrene
Methylphenathrene

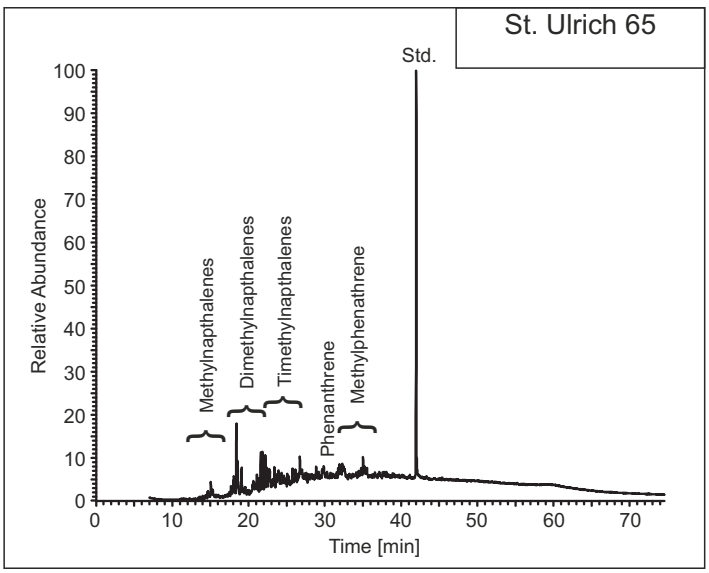
St. Ulrich 65
Relative Abundance
Time [min]
Std.
Methylnapthalenes
Dimethylnapthalenes
Timethylnapthalenes
Phenanthrene
Methylphenathrene

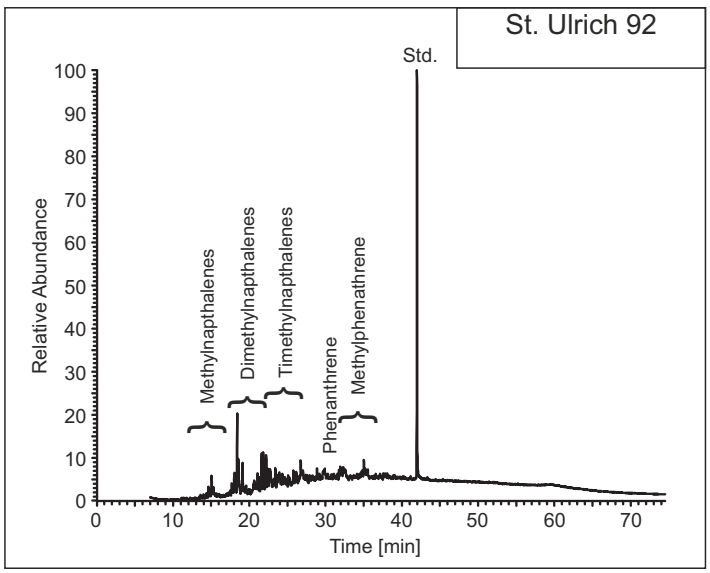
St. Ulrich 92
Relative Abundance
Time [min]
Std.
Methylnapthalenes
Dimethylnapthalenes
Timethylnapthalenes
Phenanthrene
Methylphenathrene

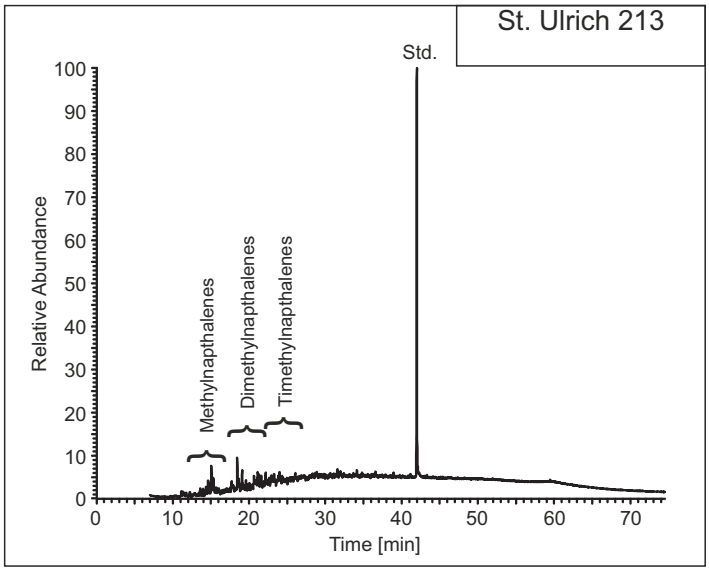
St. Ulrich 213
Std.
Relative Abundance
Time [min]
Methylnapthalenes
Dimethylnapthalenes
Timethylnapthalenes

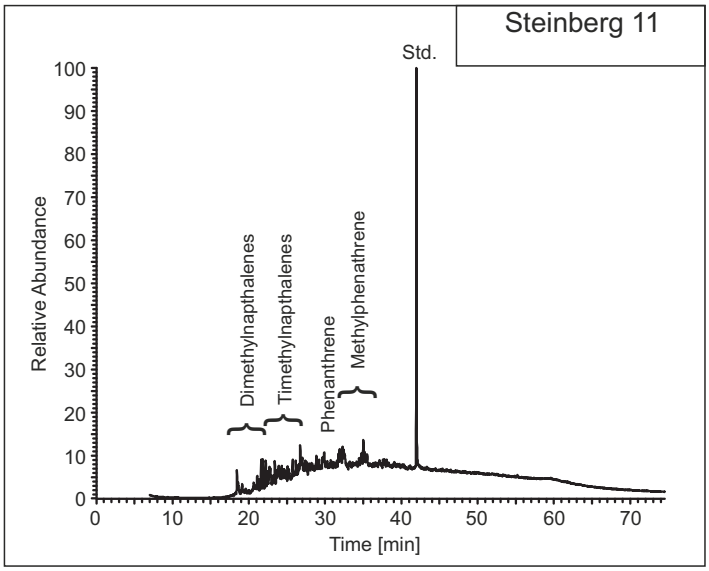
Steinberg 11
Std.
Relative Abundance
Time [min]
Dimethylnapthalenes
Timethylnapthalenes
Phenanthrene
Methylphenathrene

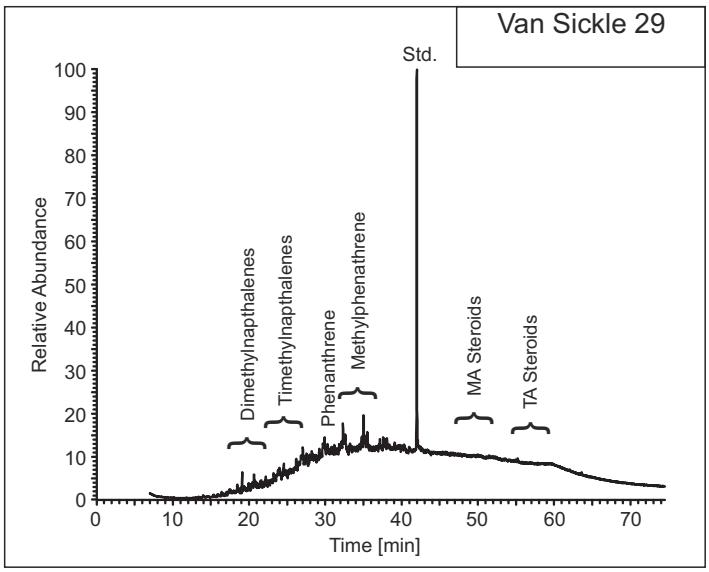
Van Sickle 29
Std.
Relative Abundance
Time [min]
Dimethylnapthalenes
Timethylnapthalenes
Phenanthrene
Methylphenathrene
MA Steroids
TA Steroids

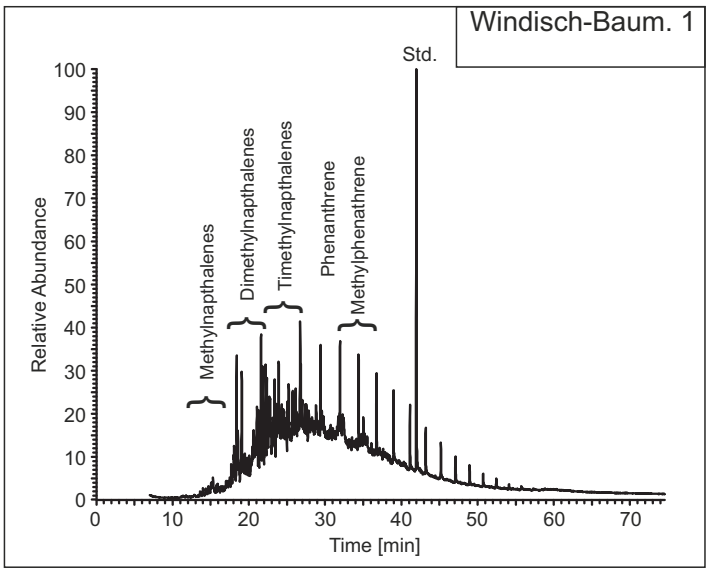
Windisch-Baum. 1
Std.
Relative Abundance
Time [min]
Methylnapthalenes
Dimethylnapthalenes
Timethylnapthalenes
Phenanthrene
Methylphenathrene

Rocks and Oils

Low Polarity Fraction

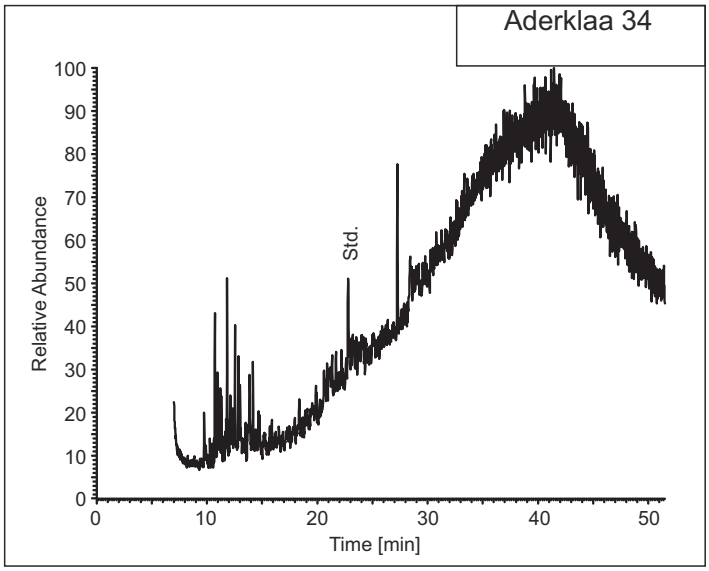
Aderklaa 34
Relative Abundance
Time [min]
Std.

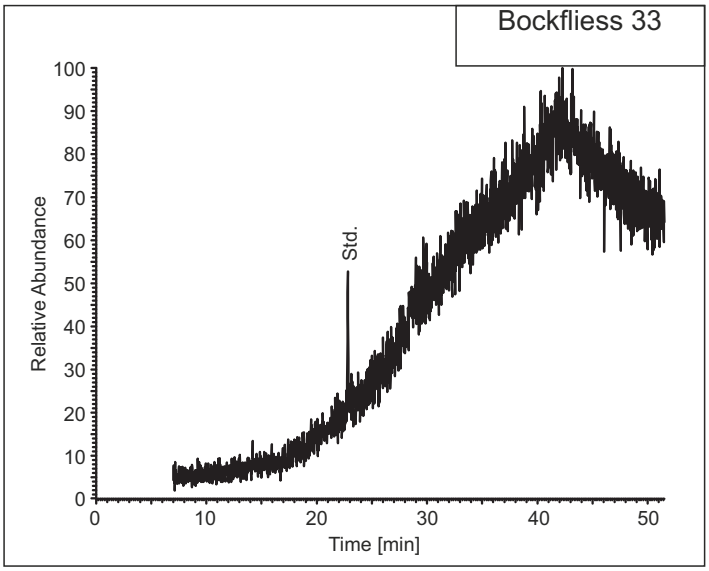
Bockfliess 33
Relative Abundance
Time [min]
Std.

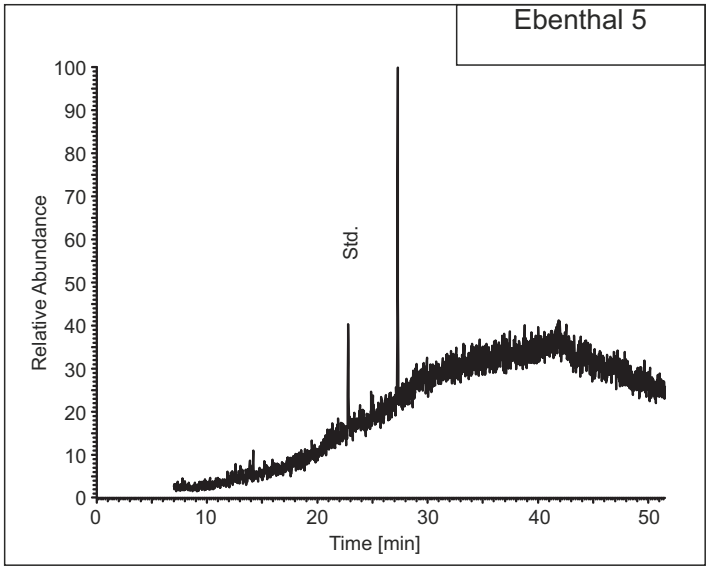
Ebenthal 5
Relative Abundance
Time [min]
Std.

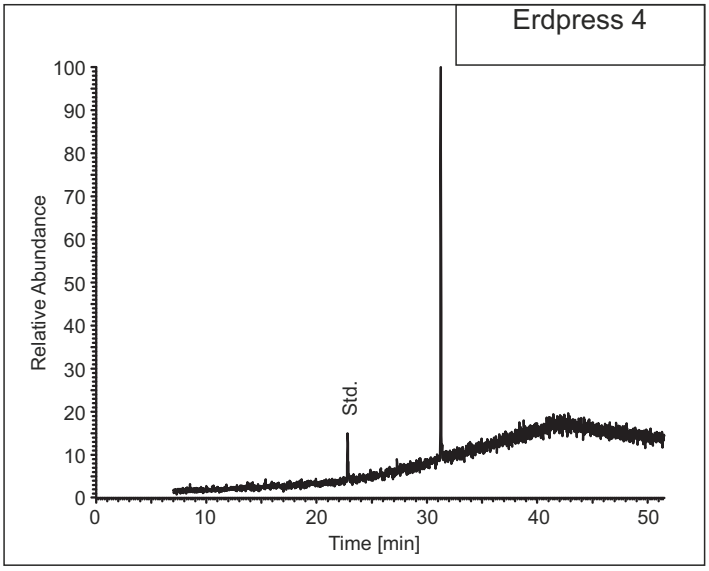
Erdpress 4
Relative Abundance
Time [min]
Std.

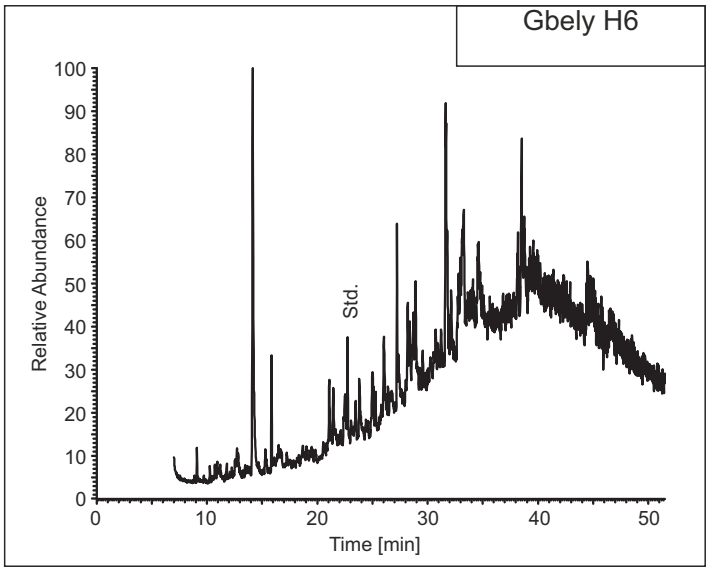
Gbely H6
Relative Abundance
Time [min]
Std.

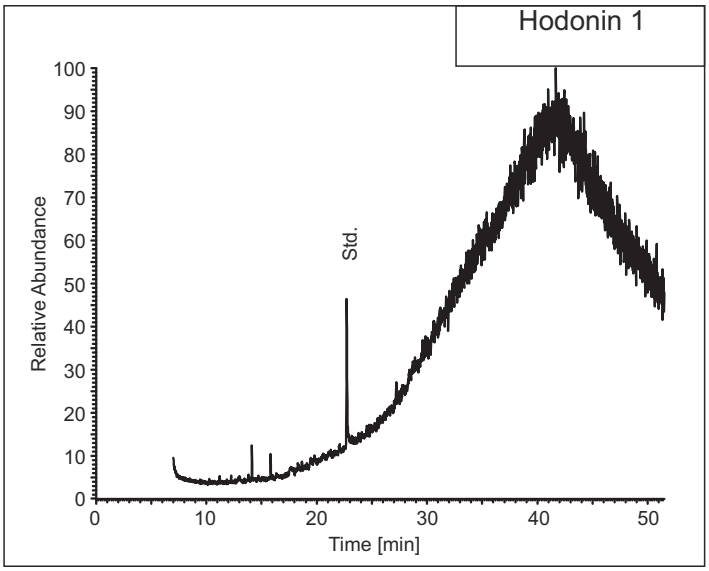
Hodonin 1
Relative Abundance
Time [min]
Std.

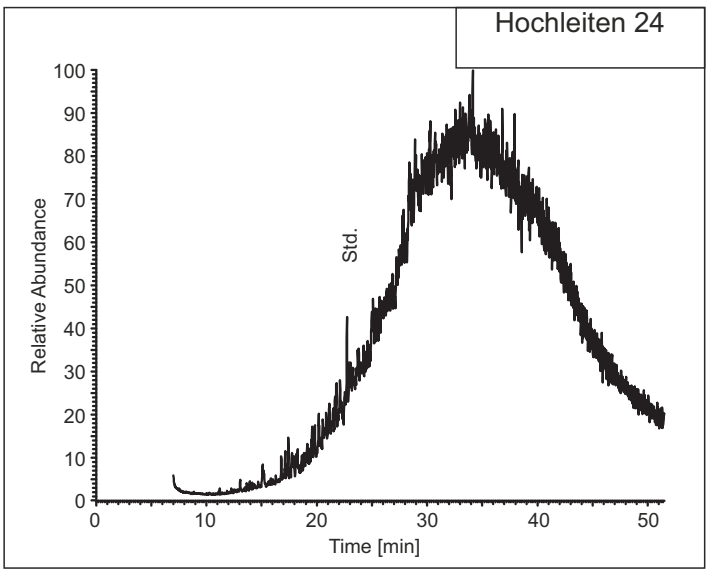
Hochleiten 24
Relative Abundance
Time [min]
Std.

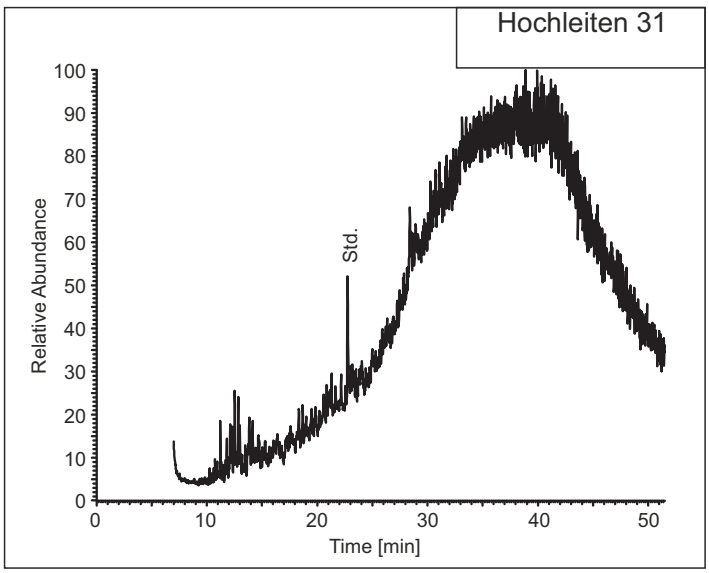
Hochleiten 31
Relative Abundance
Time [min]
Std.

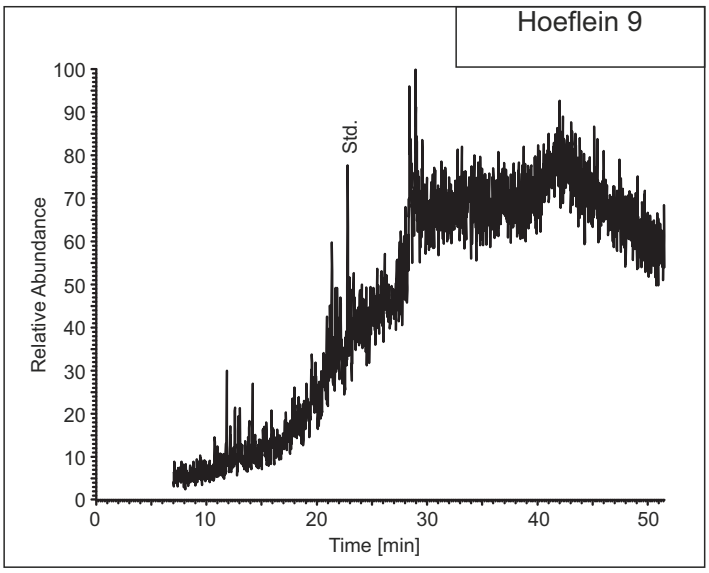
Hoeflein 9
Relative Abundance
Time [min]
Std.

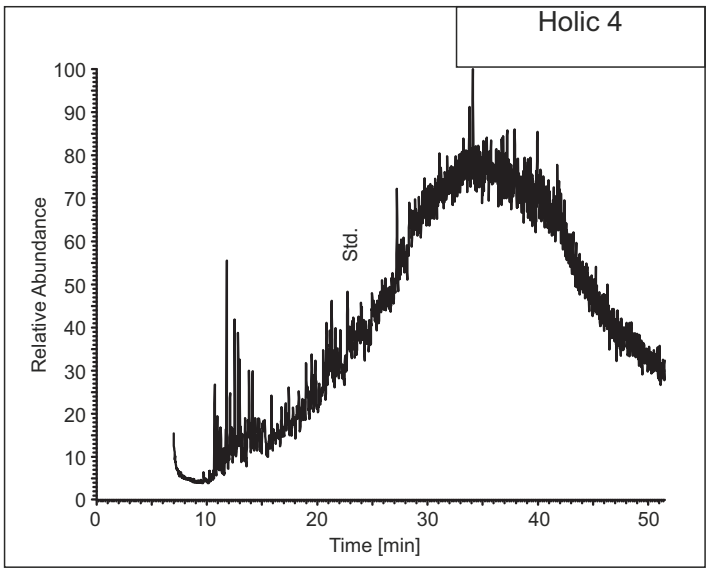
Holic 4
Relative Abundance
Time [min]
Std.

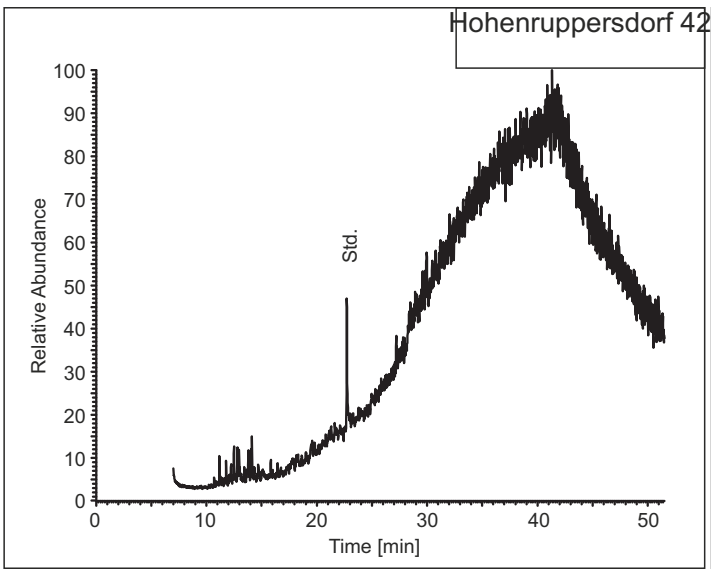
Hohenruppersdorf 42
Relative Abundance
Time [min]
Std.

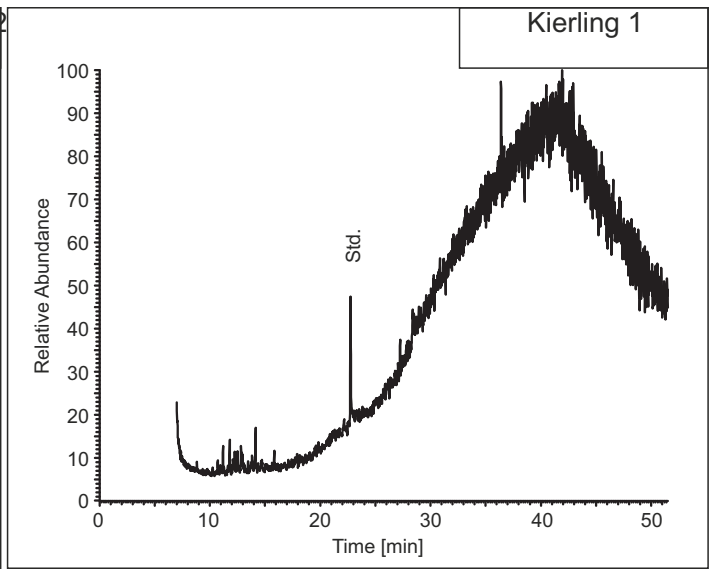
Kierling 1
Relative Abundance
Time [min]
Std.

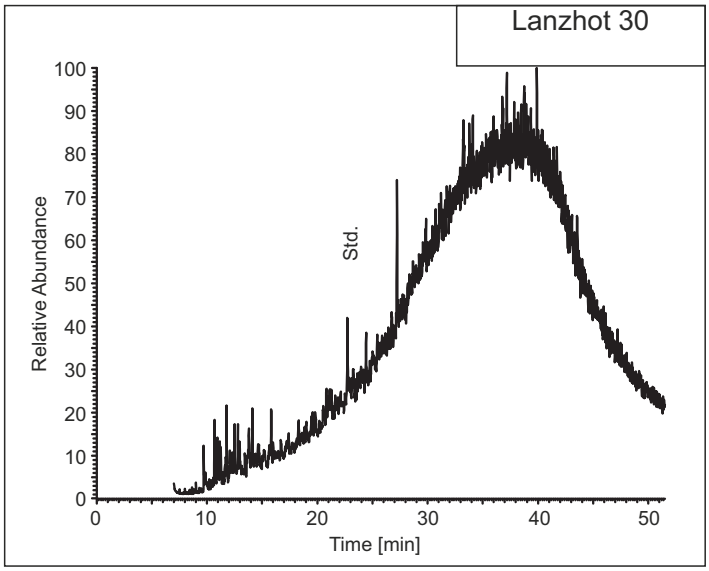
Lanzhot 30
Relative Abundance
Time [min]
Std.

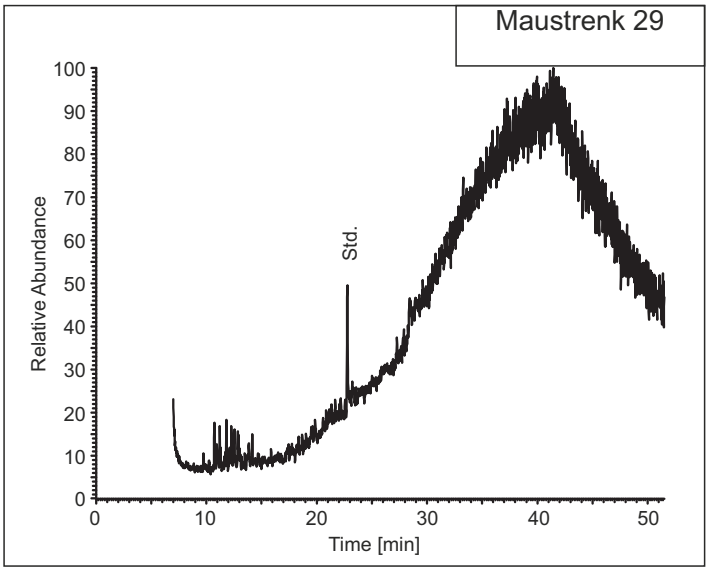
Maustrenk 29
Relative Abundance
Time [min]
Std.

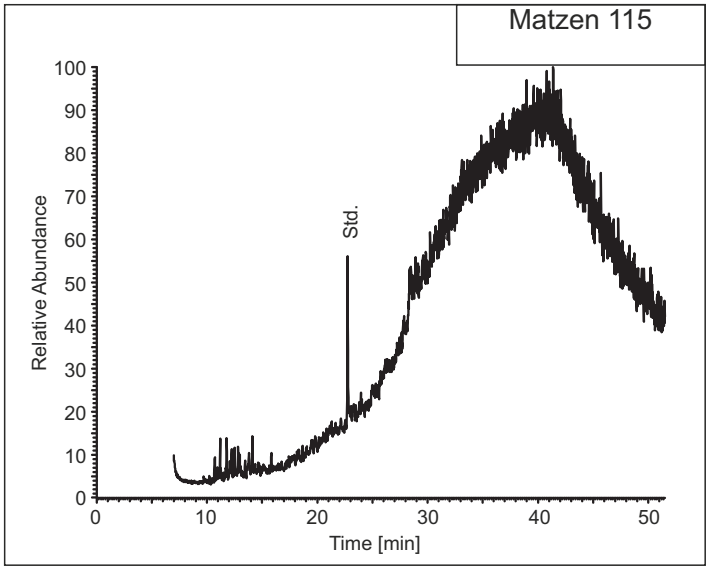
Matzen 115
Relative Abundance
Time [min]
Std.

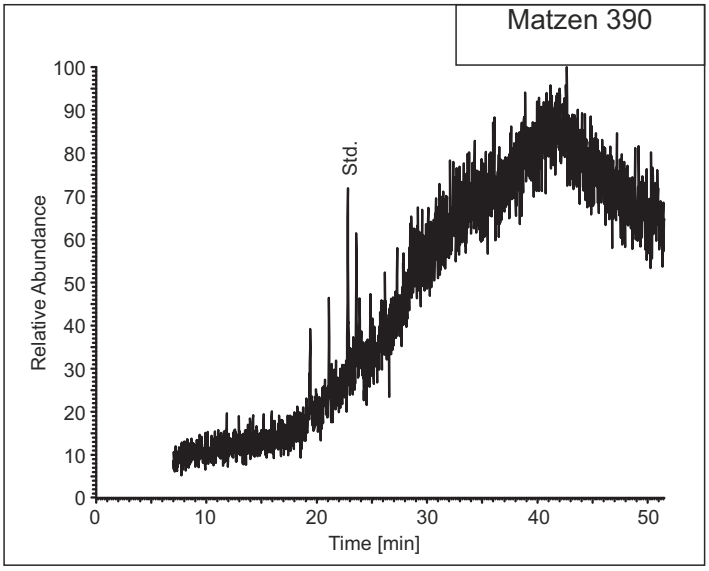
Matzen 390
Relative Abundance
Time [min]
Std.

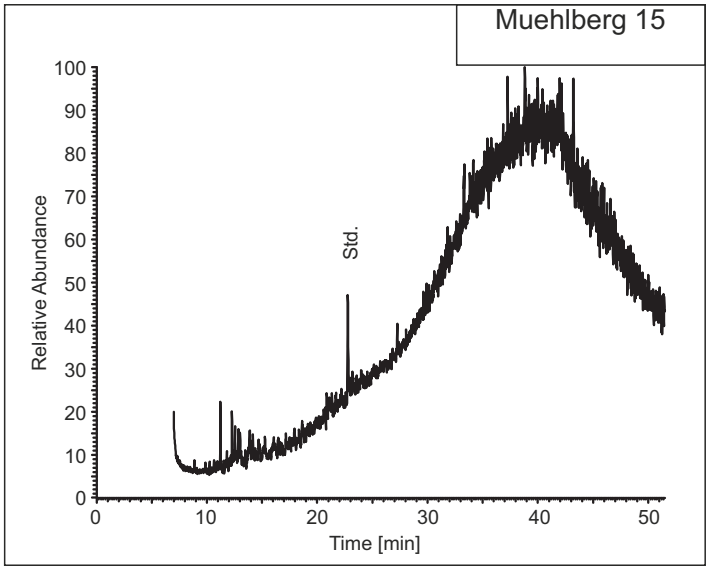
Muehlberg 15
Relative Abundance
Time [min]
Std.

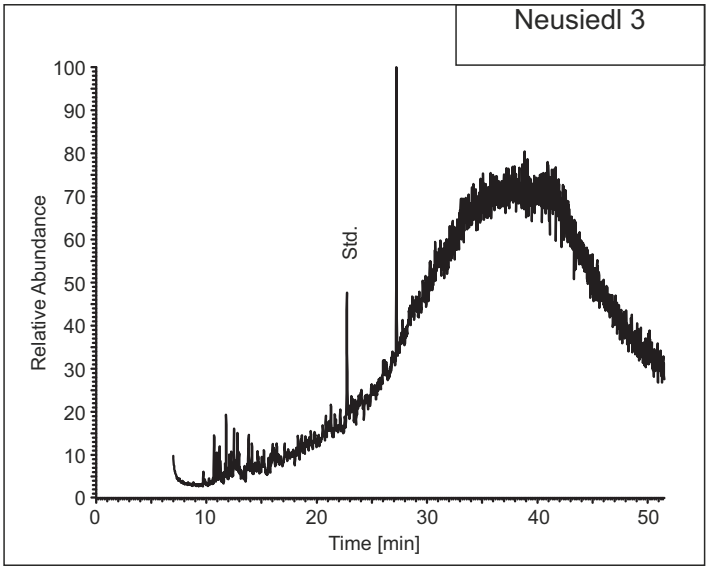
Neusiedl 3
Relative Abundance
Time [min]
Std.

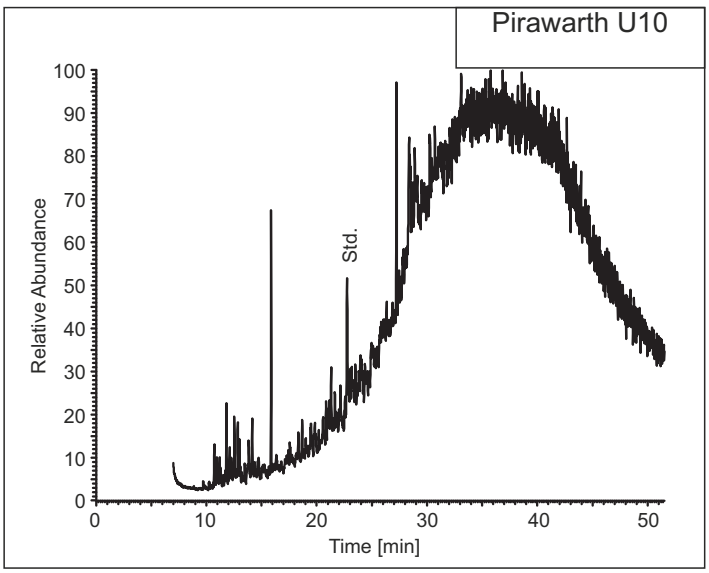
Pirawarth U10
Relative Abundance
Time [min]
Std.

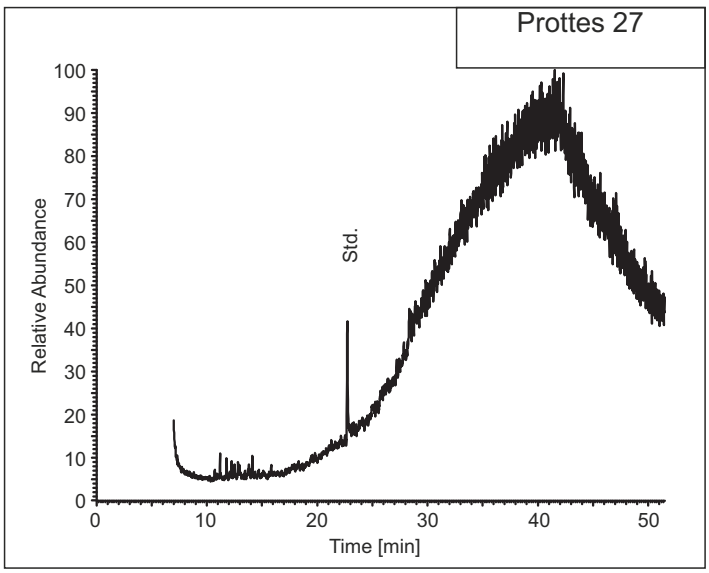
Prottes 27
Relative Abundance
Time [min]
Std.

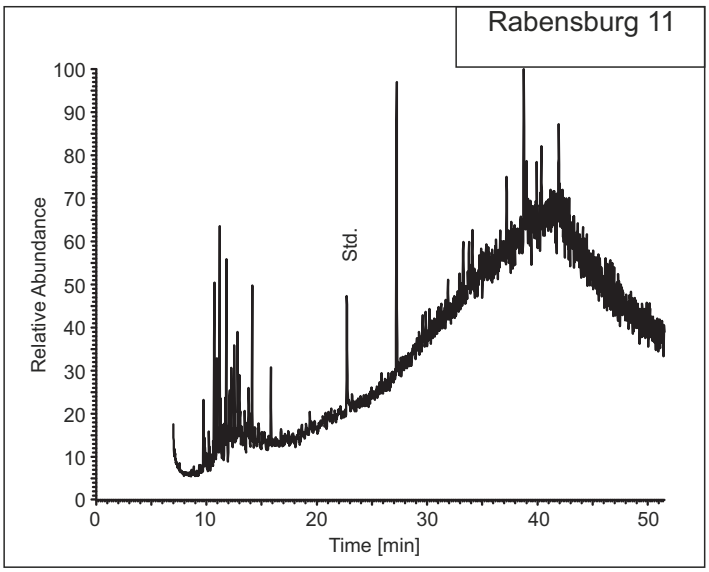
Rabensburg 11
Relative Abundance
Time [min]
Std.

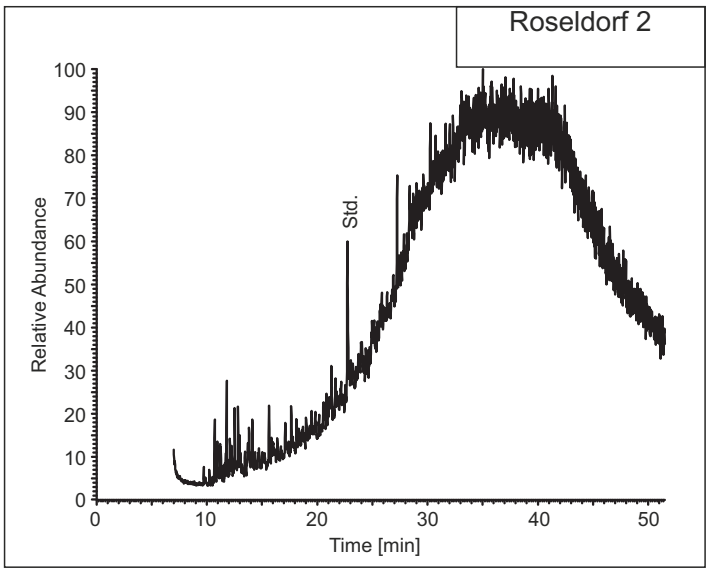
Roseldorf 2
Relative Abundance
Time [min]
Std.

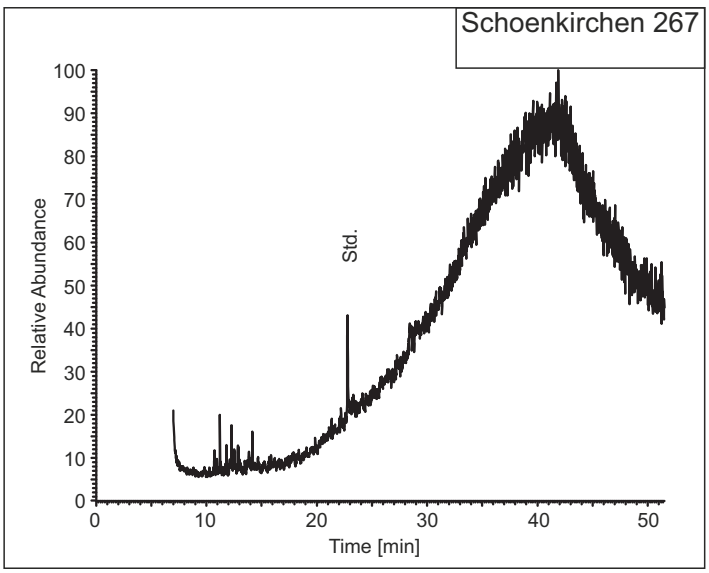
Schoenkirchen 267
Relative Abundance
Time [min]
Std.

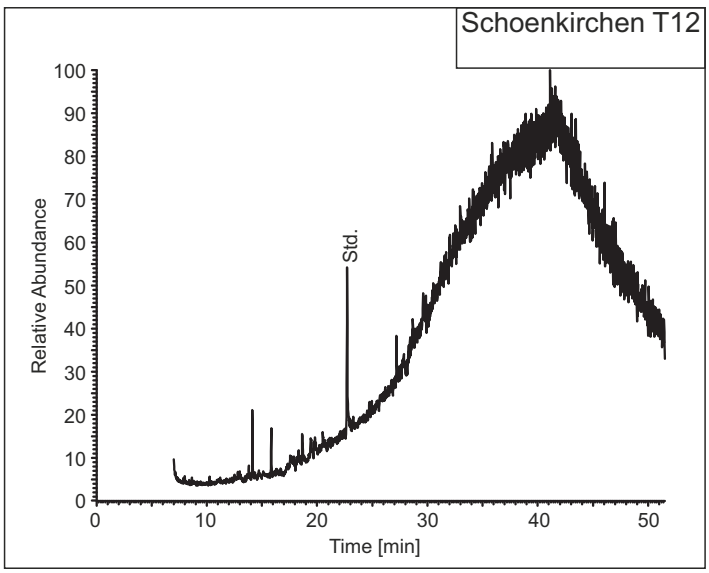
Schoenkirchen T12
Relative Abundance
Time [min]
Std.

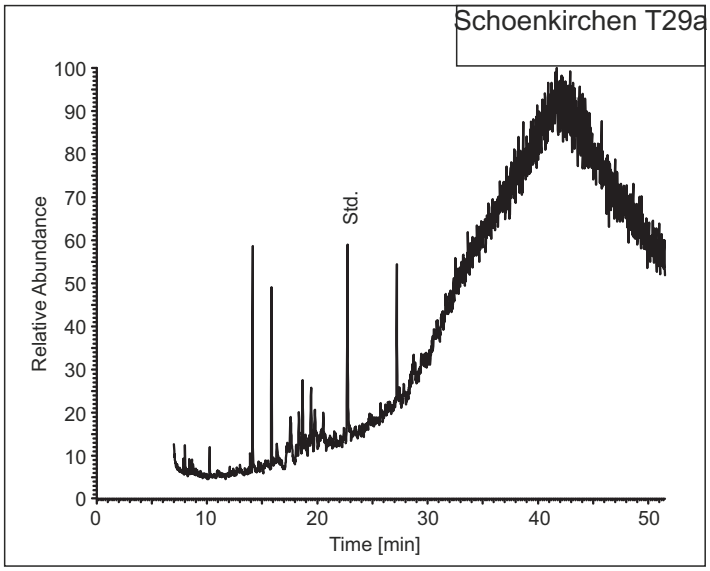
Schoenkirchen T29a
Relative Abundance
Time [min]
Std.

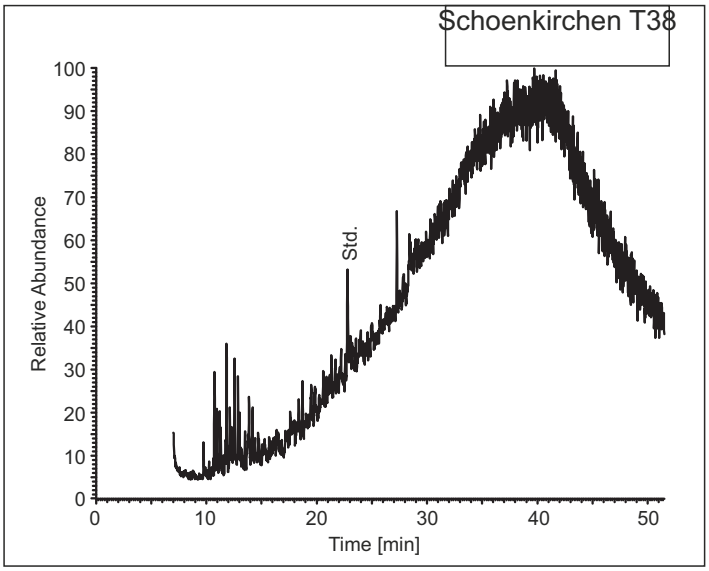
Schoenkirchen T38
Relative Abundance
Time [min]
Std.

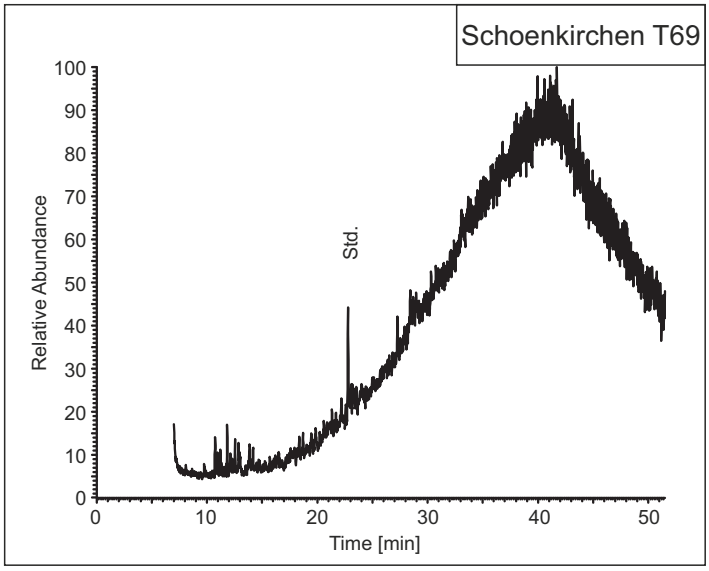
Schoenkirchen T69
Relative Abundance
Time [min]
Std.

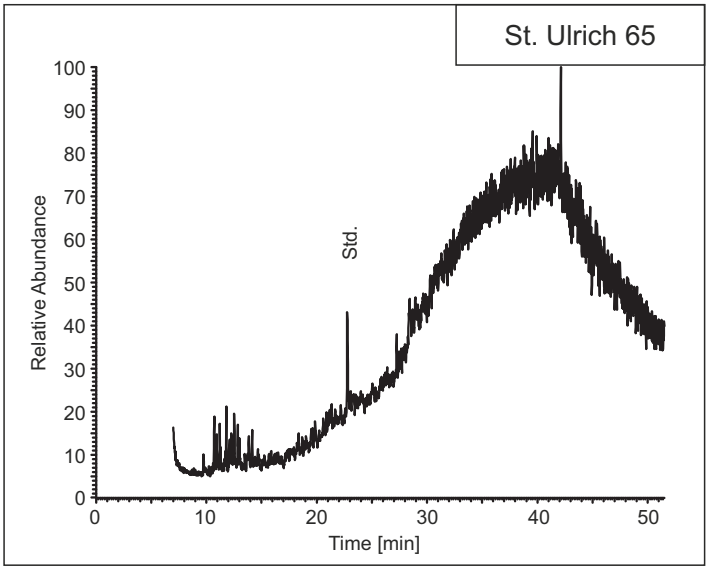
St. Ulrich 65
Relative Abundance
Time [min]
Std.

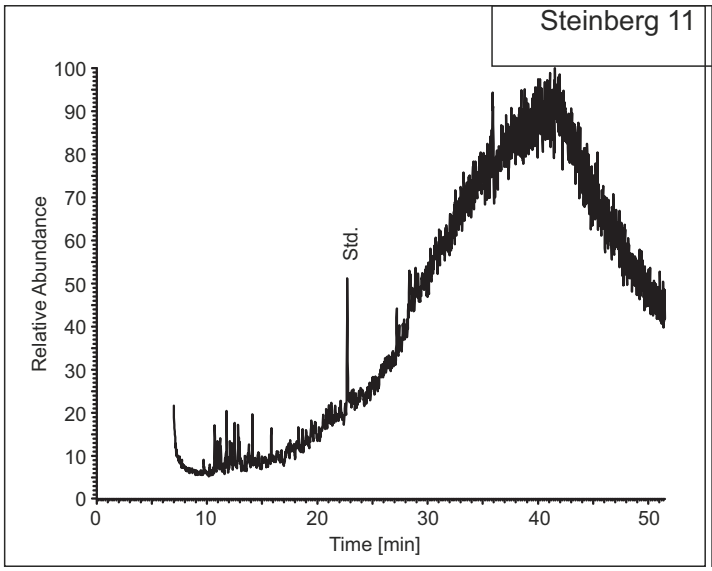
Steinberg 11
Relative Abundance
Time [min]
Std.

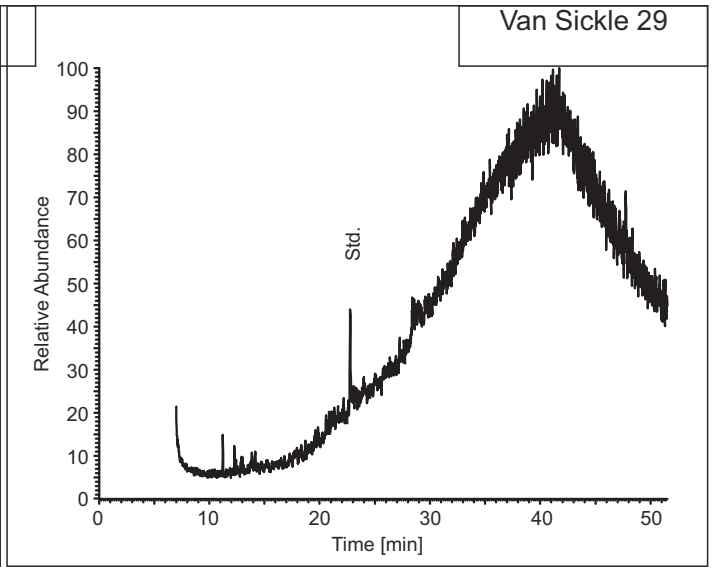
Van Sickle 29
Relative Abundance
Time [min]
Std.

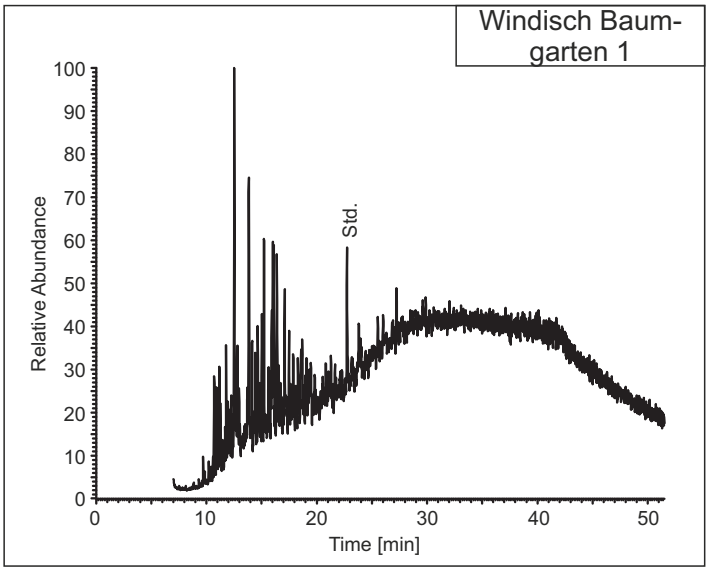
Windisch Baum-
garten 1
Relative Abundance
Time [min]
Std.

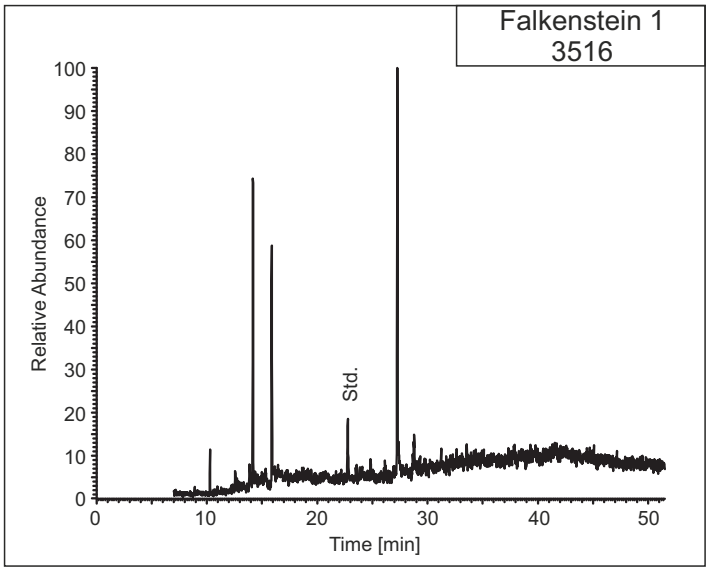
Falkenstein 1
3516
Relative Abundance
Time [min]
Std.

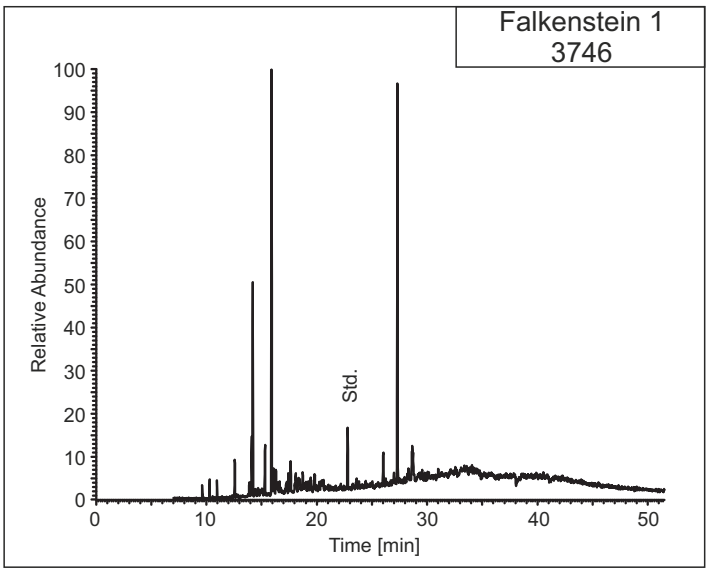
Falkenstein 1
3746
Relative Abundance
Time [min]
Std.

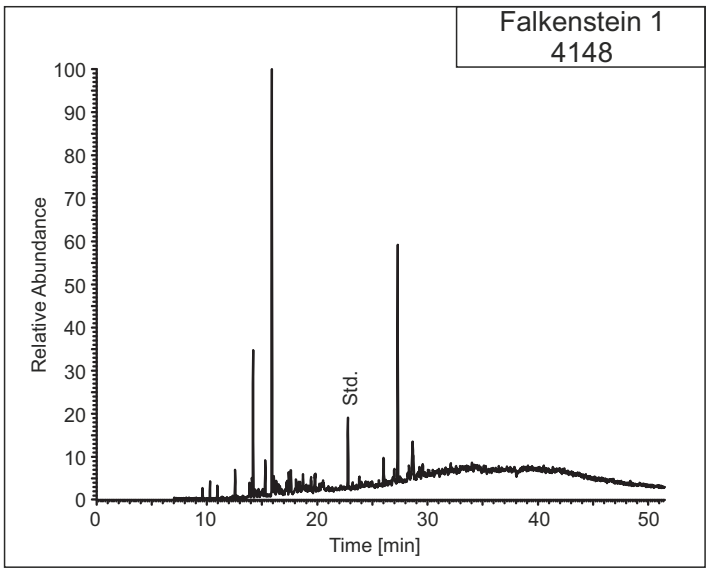
Falkenstein 1
4148
Relative Abundance
Time [min]
Std.

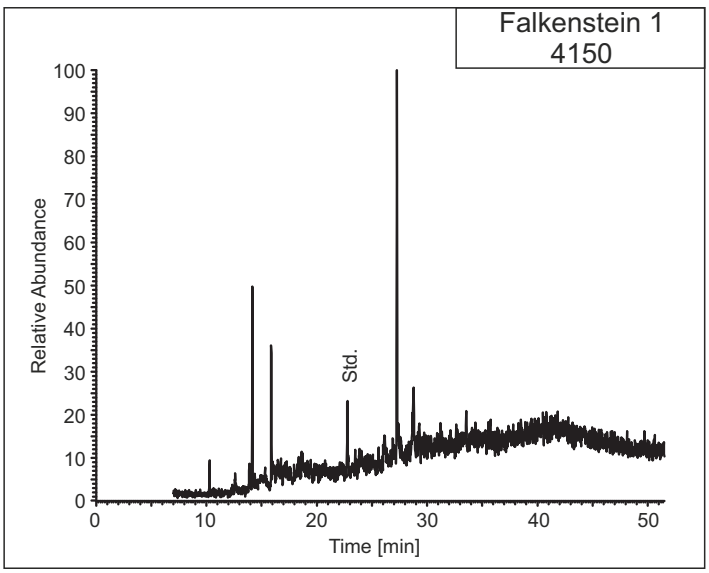
Falkenstein 1
4150
Relative Abundance
Time [min]
Std.

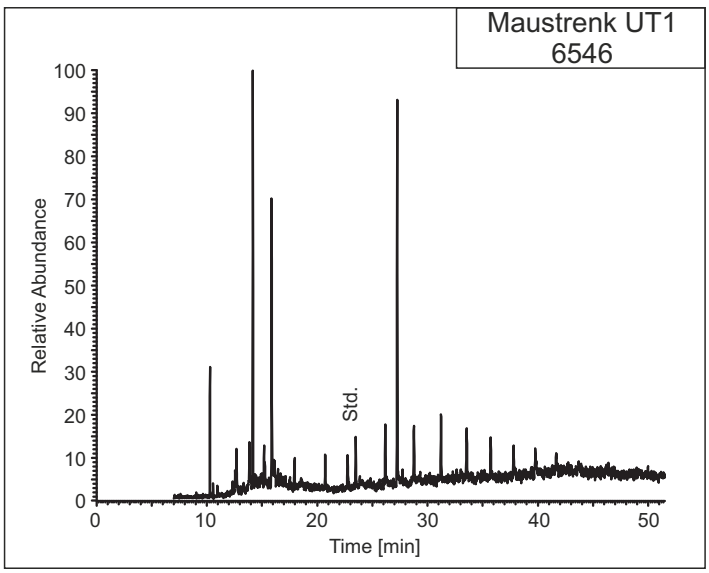
Maustrenk UT1
6546
Relative Abundance
Time [min]
Std.

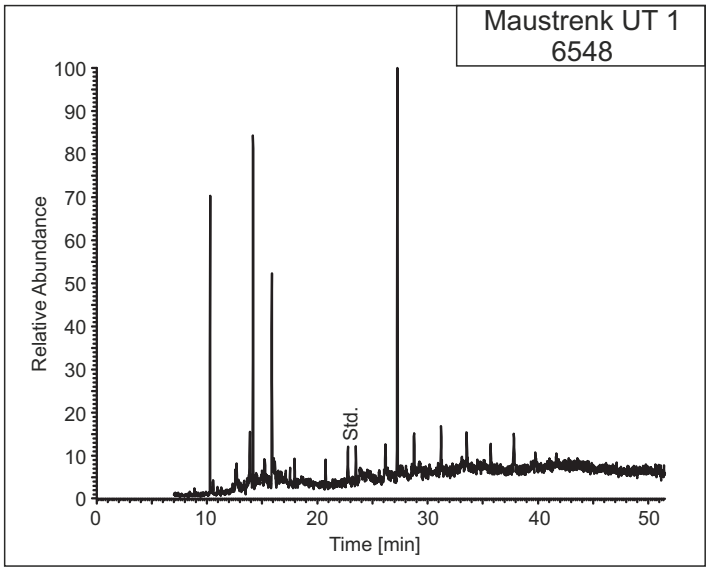
Maustrenk UT 1
6548
Relative Abundance
Time [min]
Std.

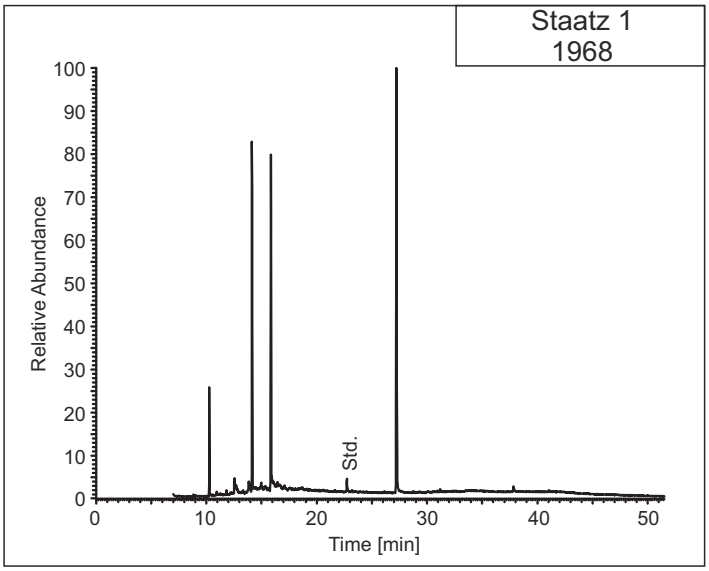
Staatz 1
1968
Relative Abundance
Time [min]
Std.

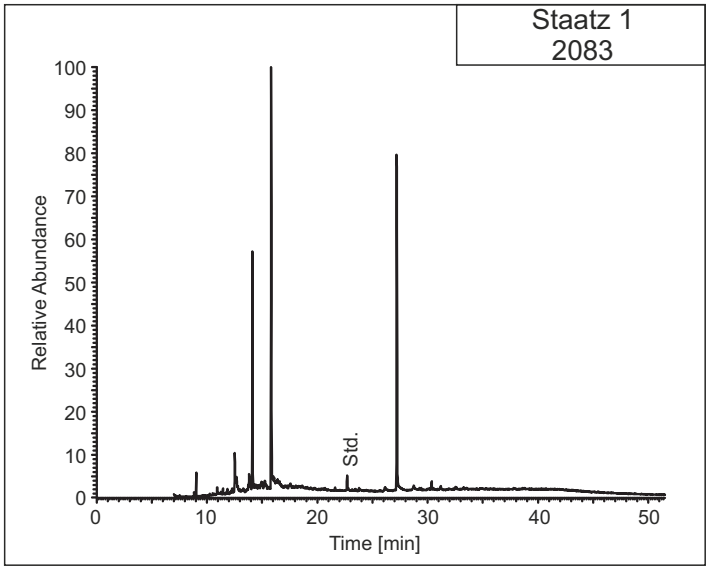
Staatz 1
2083
Relative Abundance
Time [min]
Std.

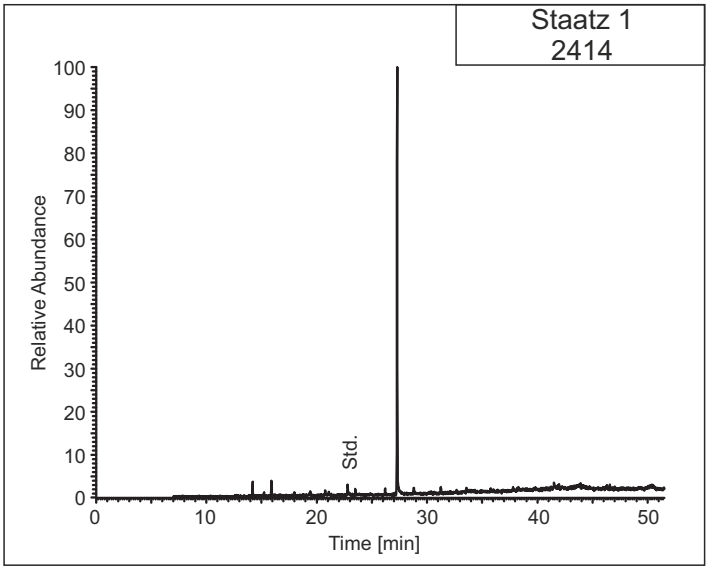
Staatz 1
2414
Relative Abundance
Time [min]
Std.

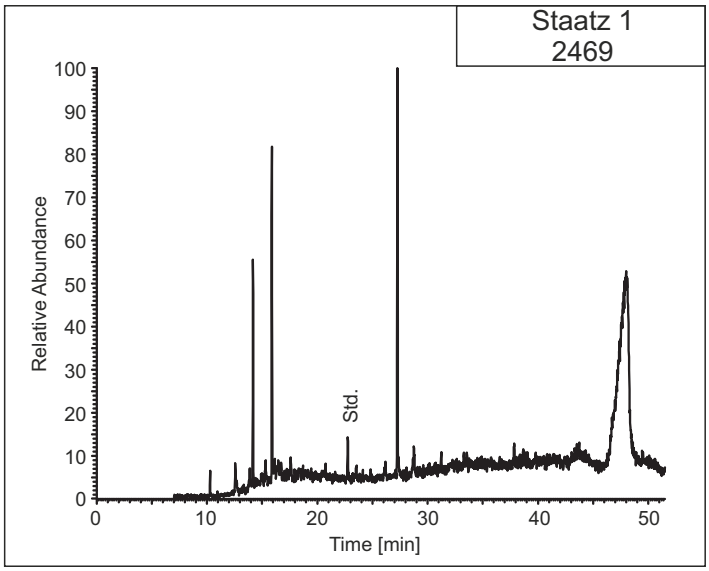
Staatz 1
2469
Relative Abundance
Time [min]
Std.

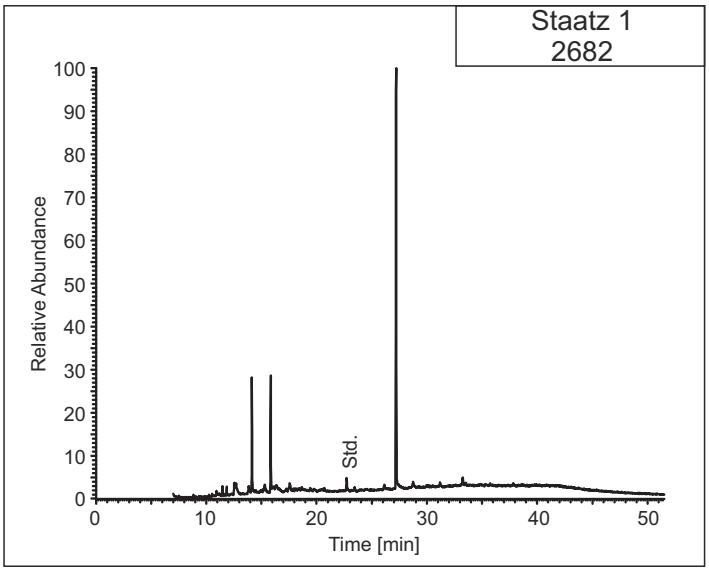
Staatz 1
2682
Relative Abundance
Time [min]
Std.

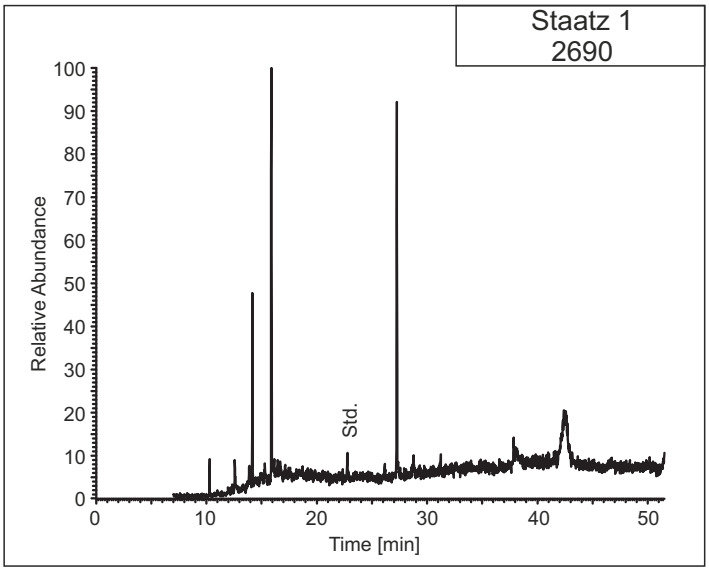
Staatz 1
2690
Relative Abundance
Time [min]
Std.

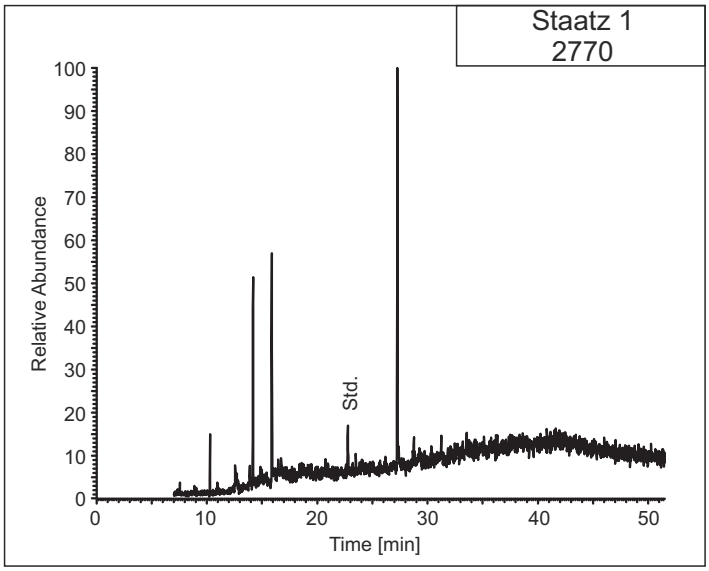
Staatz 1
2770
Relative Abundance
Time [min]
Std.

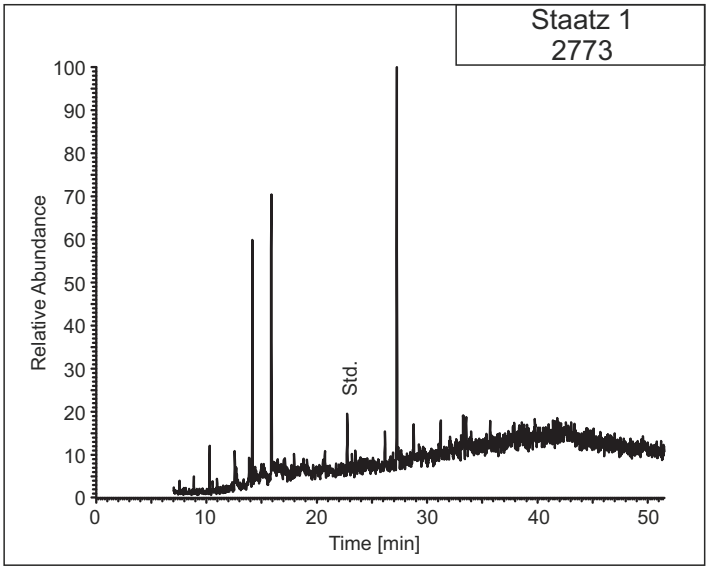
Staatz 1
2773
Relative Abundance
Time [min]
Std.

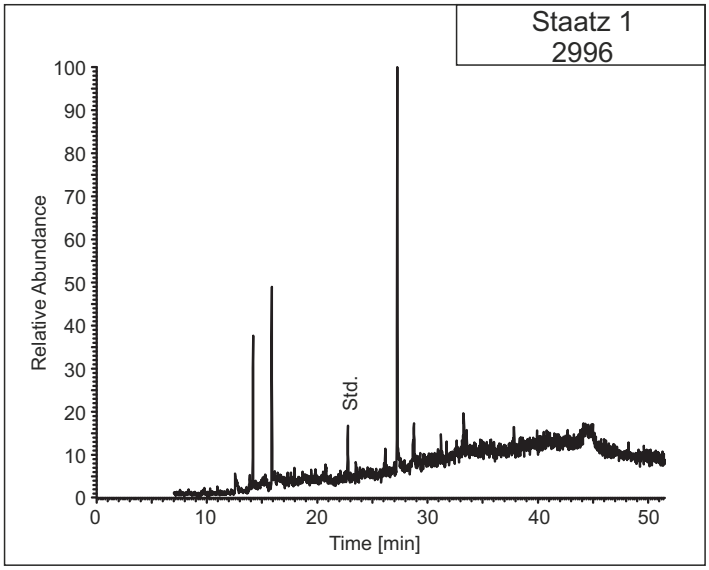
Staatz 1
2996
Relative Abundance
Time [min]
Std.

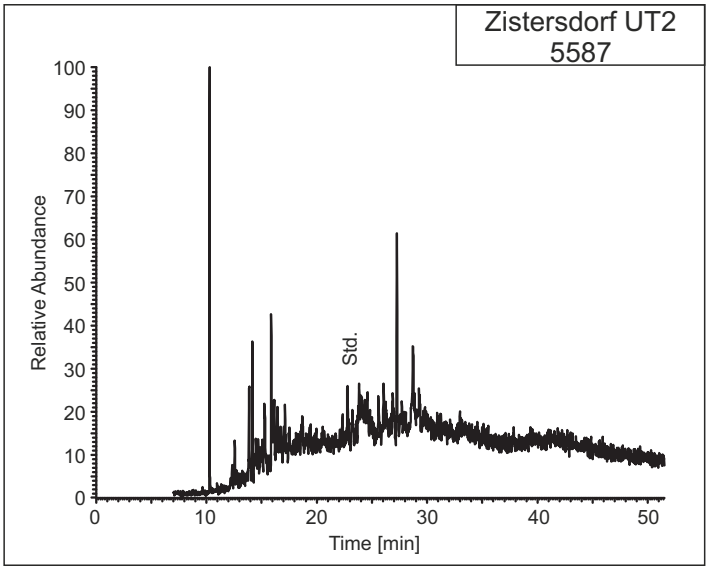
Zistersdorf UT2
5587
Relative Abundance
Time [min]
Std.

Rocks and Oils

Medium Polarity Fraction

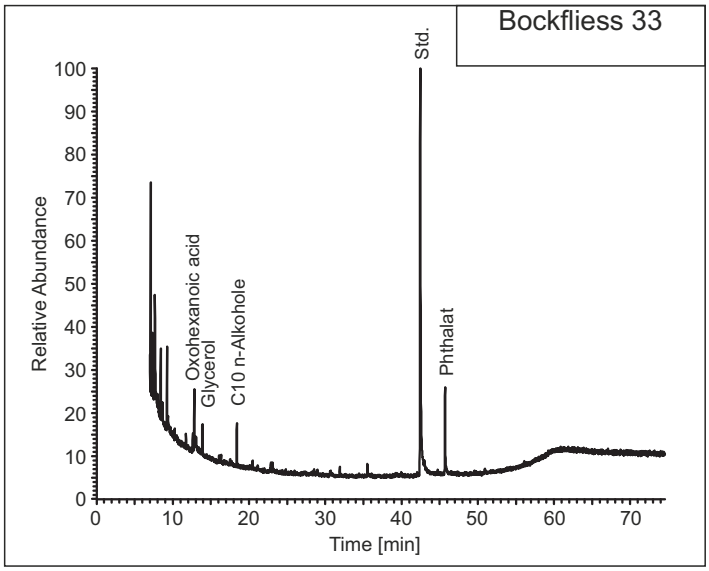
Bockfliess 33
Relative Abundance
Time [min]
Std.
Oxohexanoic acid
Glycerol
C10 n-Alkohole
Phthalat

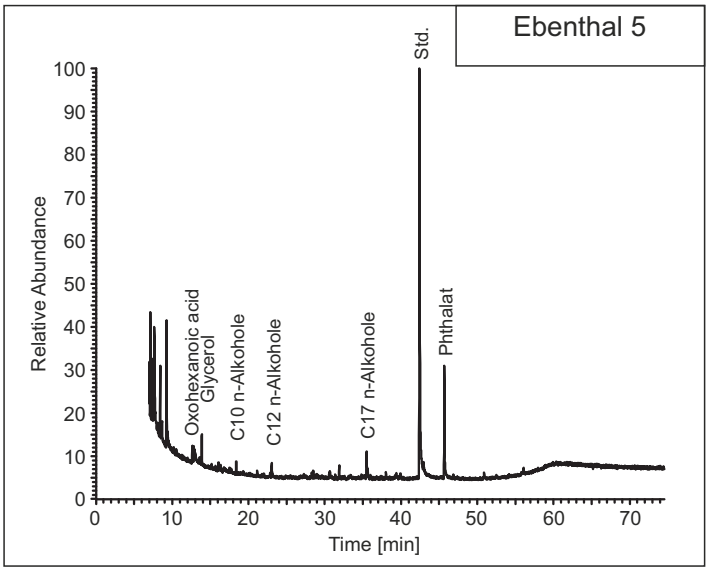
Ebenthal 5
Relative Abundance
Time [min]
Std.
Oxohexanoic acid
Glycerol
C10 n-Alkohole
C12 n-Alkohole
C17 n-Alkohole
Phthalat

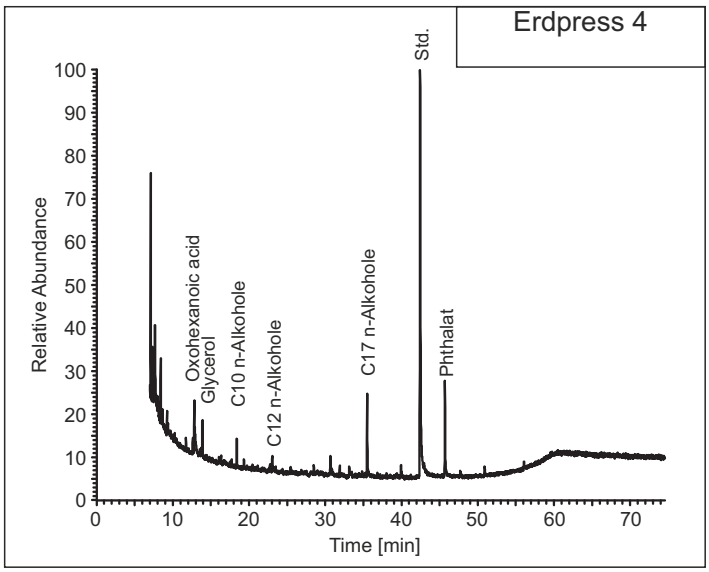
Erdpress 4
Relative Abundance
Time [min]
Std.
Oxohexanoic acid
Glycerol
C10 n-Alkohole
C12 n-Alkohole
C17 n-Alkohole
Phthalat

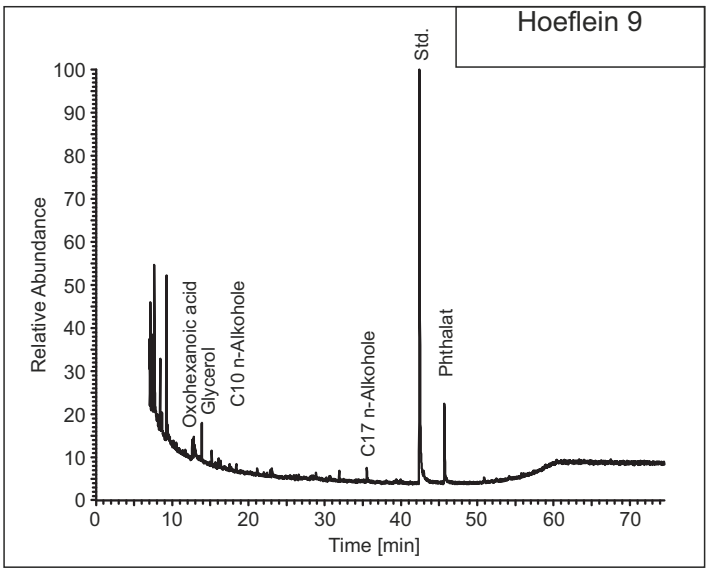
Hoeflein 9
Relative Abundance
Time [min]
Std.
Oxohexanoic acid
Glycerol
C10 n-Alkohole
C17 n-Alkohole
Phthalat

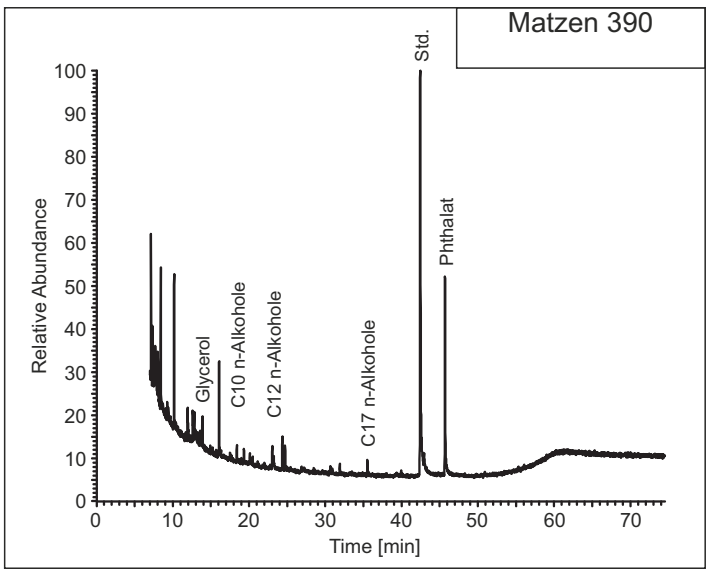
Matzen 390
Relative Abundance
Time [min]
Std.
Glycerol
C10 n-Alkohole
C12 n-Alkohole
C17 n-Alkohole
Phthalat

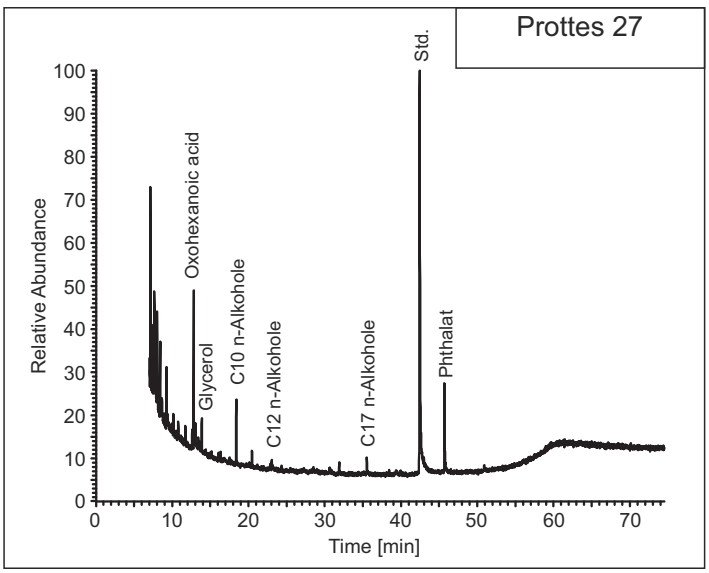
Prottes 27
Relative Abundance
Time [min]
Std.
Oxohexanoic acid
Glycerol
C10 n-Alkohole
C12 n-Alkohole
C17 n-Alkohole
Phthalat

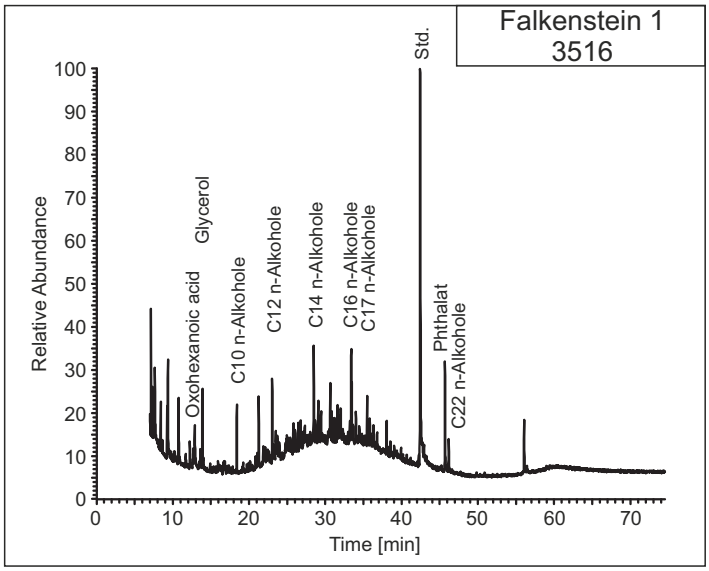
Falkenstein 1
3516
Relative Abundance
Time [min]
Oxohexanoic acid
Glycerol
C10 n-Alkohole
C12 n-Alkohole
C14 n-Alkohole
C16 n-Alkohole
C17 n-Alkohole
Std.
Phthalat
C22 n-Alkohole

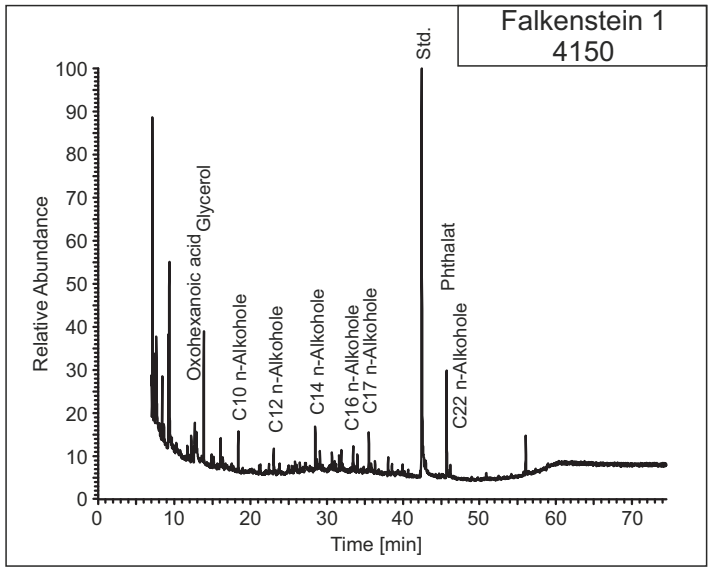
Falkenstein 1
4150
Relative Abundance
Time [min]
Oxohexanoic acid
Glycerol
C10 n-Alkohole
C12 n-Alkohole
C14 n-Alkohole
C16 n-Alkohole
C17 n-Alkohole
Std.
Phthalat
C22 n-Alkohole

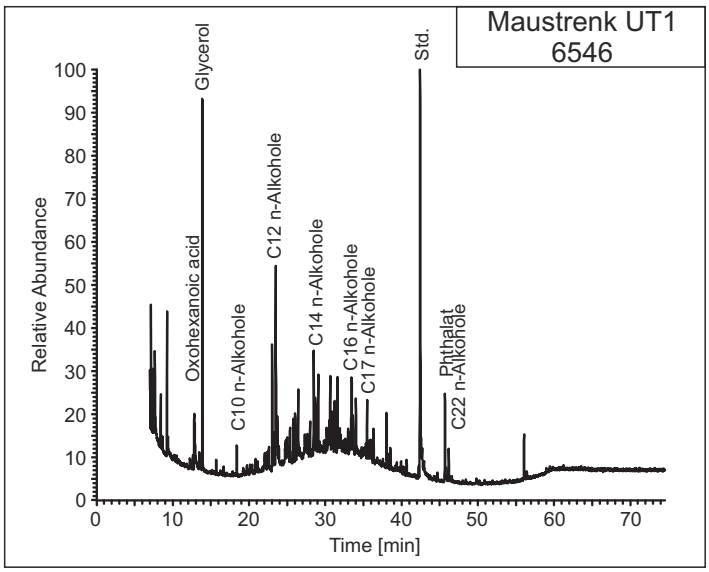
Maustrenk UT1
6546
Relative Abundance
Time [min]
Glycerol
Oxohexanoic acid
C10 n-Alkohole
C12 n-Alkohole
C14 n-Alkohole
C16 n-Alkohole
C17 n-Alkohole
Std.
Phthalat
C22 n-Alkohole

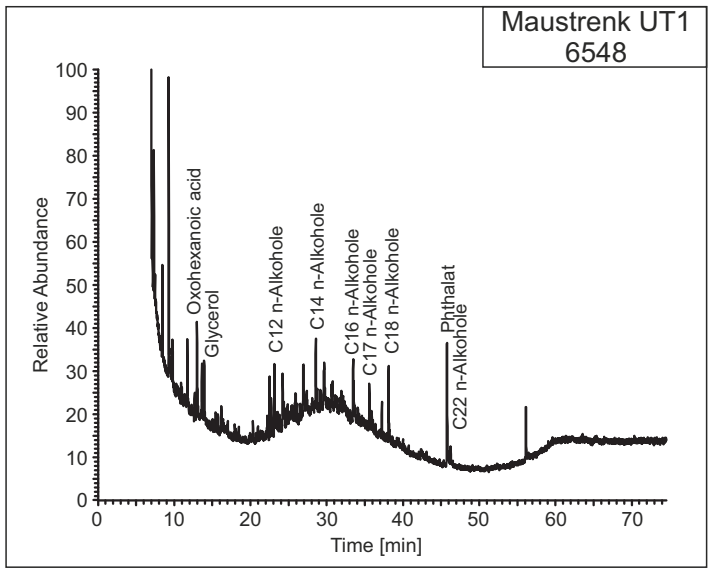
Maustrenk UT1
6548
Relative Abundance
Time [min]
Oxohexanoic acid
Glycerol
C12 n-Alkohole
C14 n-Alkohole
C16 n-Alkohole
C17 n-Alkohole
C18 n-Alkohole
Phthalat
C22 n-Alkohole

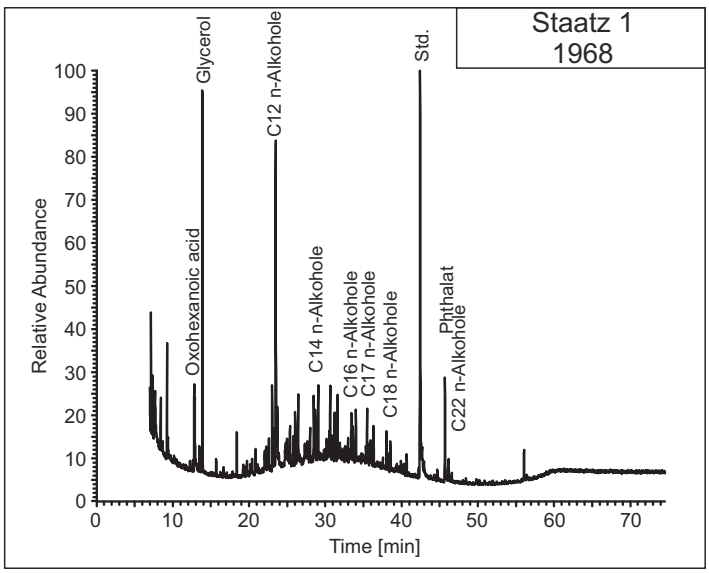
Staatz 1
1968
Relative Abundance
Time [min]
Glycerol
Oxohexanoic acid
C12 n-Alkohole
C14 n-Alkohole
C16 n-Alkohole
C17 n-Alkohole
C18 n-Alkohole
Std.
Phthalat
C22 n-Alkohole

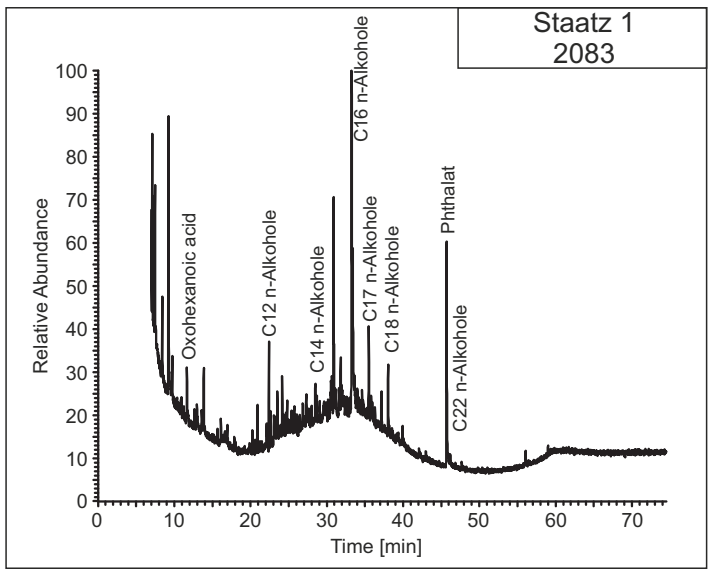
Staatz 1
2083
Relative Abundance
Time [min]
Oxohexanoic acid
C12 n-Alkohole
C14 n-Alkohole
C16 n-Alkohole
C17 n-Alkohole
C18 n-Alkohole
Phthalat
C22 n-Alkohole

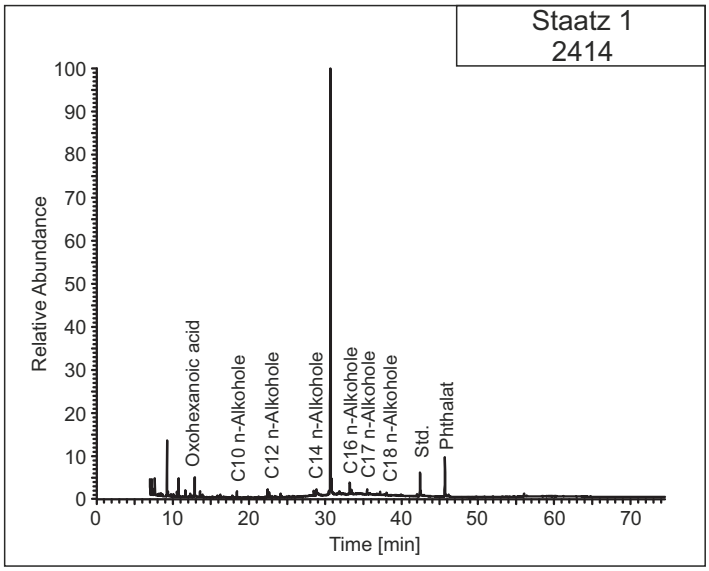

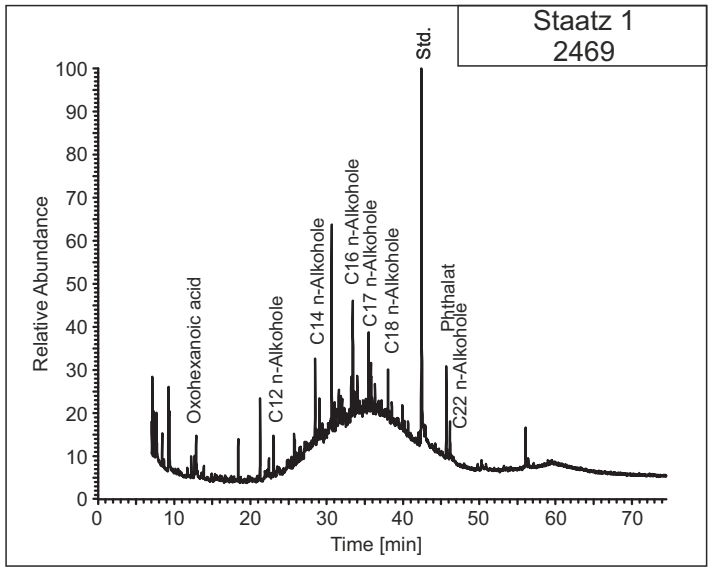

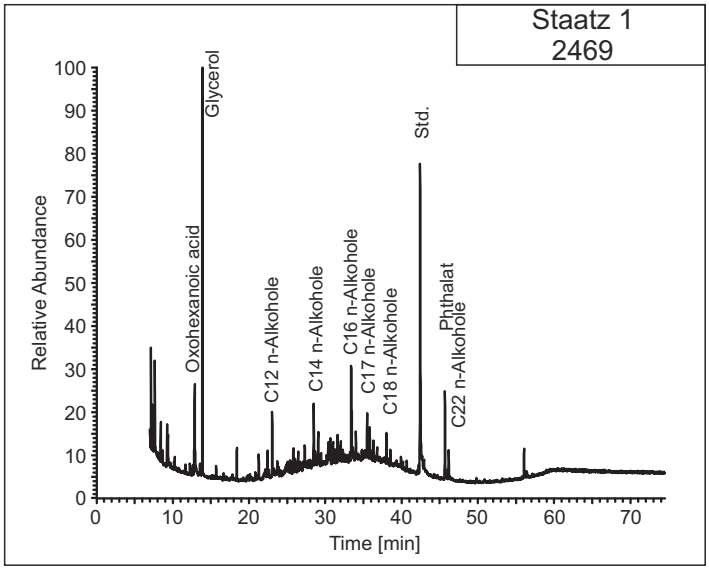

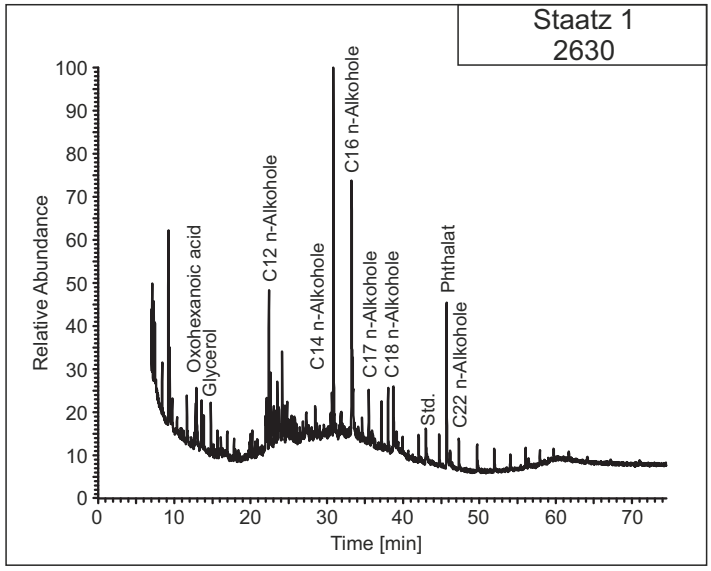

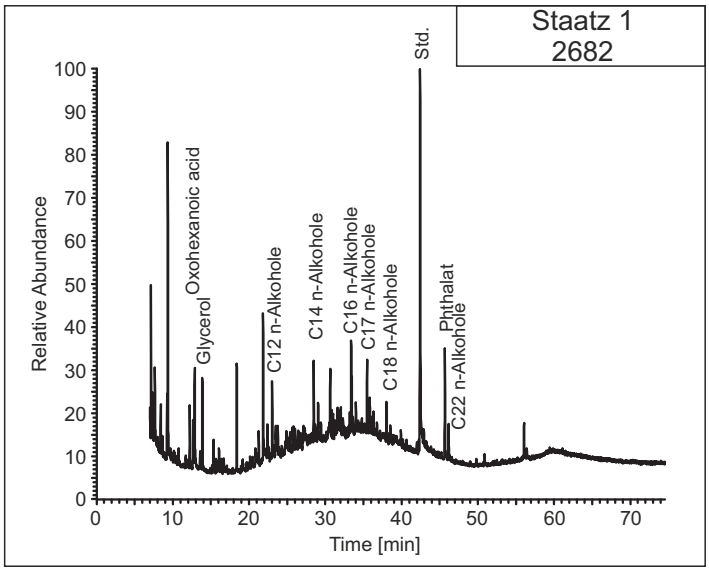

Staatz 1
2770

Unfortunately File Corrupted

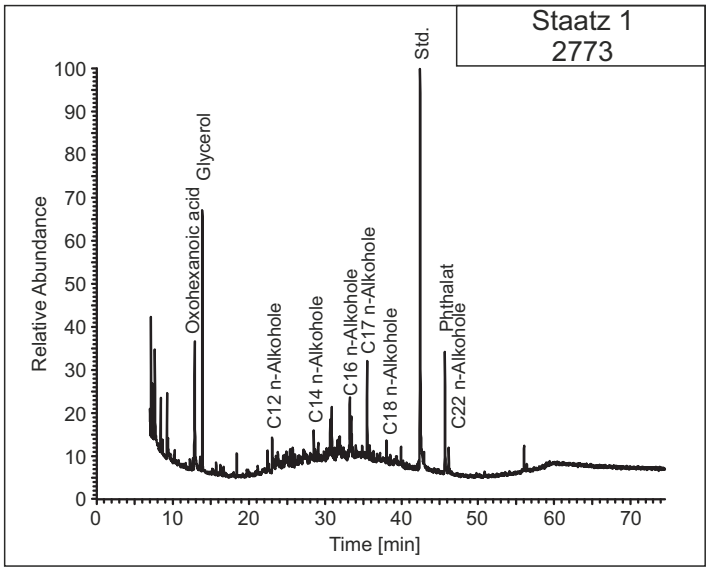
Staatz 1
2773
Relative Abundance
Time [min]
Oxohexanoic acid
Glycerol
C12 n-Alkohole
C14 n-Alkohole
C16 n-Alkohole
C17 n-Alkohole
C18 n-Alkohole
Std.
Phthalat
C22 n-Alkohole

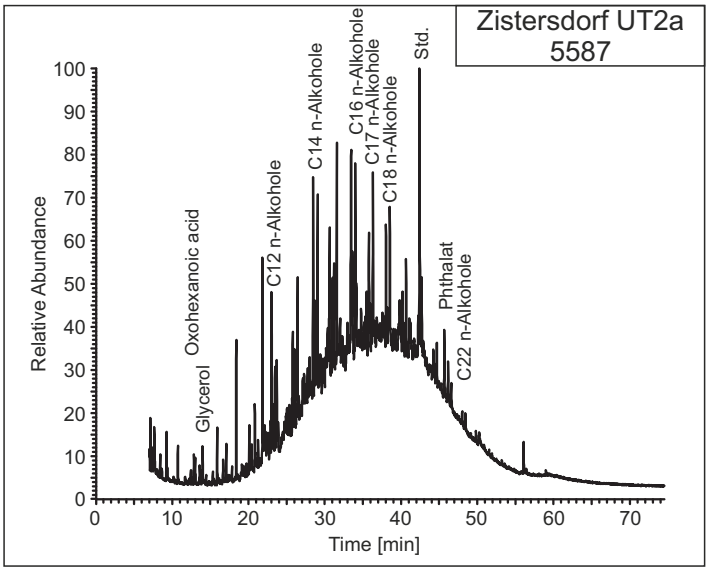
Zistersdorf UT2a
5587
Relative Abundance
Time [min]
Oxohexanoic acid
Glycerol
C12 n-Alkohole
C14 n-Alkohole
C16 n-Alkohole
C17 n-Alkohole
C18 n-Alkohole
Std.
Phthalat
C22 n-Alkohole

Appendix IX
Gas composition

Well	Depth	i/n C_4H_{10}	Wetness	CH_4	C_2H_6	C_3H_8	iC_4H_{10}	nC_4H_{10}	iC_5H_{12}	nC_5H_{12}	C_6+	CO_2	N_2	H_2S
	[m ss]	[-]	$C_1/(C_2+C_3)$					[Vol.%]						[ppm]
Aderklaa 98	2408	0.77	13	90.08	5.49	1.60	0.40	0.52	0.23	0.19	0.40	0.65	0.44	
Baumgarten 1	830	1.00	994	99.42	0.09	0.01	0.01	0.01	0.01	0.01	0.01	0.16	0.33	
Bockfliess 1	1177.38	5.33	43	96.52	2.04	0.22	0.16	0.03	0.02	0.01	0.01	0.85	0.15	1
Bockfliess 24	1436.21	2.18	41	92.67	2.08	0.20	0.24	0.11	0.17	0.01	0.16	4.28	0.08	5
Bockfliess 33	1181.24	1.50	106	96.23	0.86	0.05	0.06	0.04	0.06	0.01	0.05	2.52	0.13	3
Bockfliess 35	1460.64		49	63.91	1.31	0.00	0.08	0.00				4.99	0.49	
Bockfliess 37	1463.4		37	91.11	2.45	0.00	0.17	0.00	0.09			5.57	0.44	
Bockfliess 43	1428.71		29	91.37	3.19	0.00	0.15	0.00	0.07			3.92	0.35	
Bockfliess 205	1627		32	63.22	1.97	0.00	0.10	0.00	0.16			2.29	0.03	
Breitenlee 15	990	0.50	319	99.04	0.30	0.01	0.01	0.01	0.01	0.01	0.01	0.19	0.45	
Breitenlee 17	1217	1.00	65	97.74	1.42	0.09	0.03	0.03	0.01	0.01	0.05	0.39	0.24	
Ebenthal Tief 1	3300	0.63	26	93.38	2.68	0.98	0.19	0.30	0.10	0.10	0.27	1.61	0.39	
Erdpress 4	1787.51	0.79	41	96.07	1.74	0.59	0.22	0.28	0.15	0.01	0.10	0.71	0.13	45
Erdpress 17a	1424.18	1.00	59	94.89	1.57	0.03	0.01	0.01	0.01	0.01	0.01	3.32	0.16	2
Erdpress 24	1419.12	1.00	59	97.77	1.62	0.03	0.01	0.01	0.01	0.01	0.01	0.39	0.16	0.5
Fischamend 6	278	1.00	3299	98.96	0.02	0.01	0.01	0.01	0.01	0.01	0.01	0.28	0.74	
Ginzersdorf 4	776	1.00	65	97.40	1.49	0.01	0.01	0.01	0.01	0.01	0.01	0.06	1.05	
Hauskirchen 86	910		27	95.80	3.36	0.17		0.02				0.42	0.23	
Hirschstetten 7a	1875	0.85	66	97.04	1.12	0.35	0.11	0.13	0.07	0.05	0.17	0.36	0.60	1
Hochleiten 15	737.58		123	93.14	0.76	0.00	0.00	0.00				4.45	0.16	
Hochleiten 24	748.74		113	83.80	0.74	0.00	0.00	0.00				2.73	0.07	
Hochleiten 60	759.31		12	84.67	7.02	0.17	0.22	0.00				9.17	0.03	
Hochleiten 65	851.09		n.c.	90.38	0.00	0.00	0.00	0.00				9.84	0.12	
Hochleiten 66	911.32		389	91.14	0.23	0.00	0.00	0.00				8.17		
Hochleiten 67	786.44		502	90.08	0.18	0.00	0.00	0.00				5.99		
Hoeflein 1	2580	0.78	9	71.61	5.36	2.54	1.32	0.58	0.25	0.21	0.34	16.18	2.19	3
Hoeflein 4	2591	0.77	9	71.81	5.09	2.41	1.26	0.55	0.23	0.19	0.33	16.39	2.29	2
Hoeflein 6	2607	0.79	9	70.54	4.96	2.36	1.22	0.54	0.22	0.18	0.3	17.99	2.23	2
Hoeflein 8	2550	0.77	9	70.22	4.61	2.21	1.17	0.51	0.22	0.18	0.32	18.78	2.29	1
Hoeflein 9	2631	0.81	9	72.2	5.63	2.57	1.23	0.55	0.21	0.17	0.28	15.62	2.09	2
Hoeflein 10	2550	0.76	9	70.95	4.61	2.19	1.18	0.51	0.23	0.19	0.37	17.96	2.32	2
Hoeflein 12	2665	0.82	9	72.51	5.2	2.35	1.11	0.5	0.17	0.13	0.19	16.1	2.24	2
Hohenruppersdorf 42	1412.35		46	95.70	2.10	0.00	0.00	0.00				1.06	0.07	
Matzen 115	1472	1.34	26	90.94	2.76	0.79	0.47	0.35	0.34	0.01	0.25	3.98	0.11	113
Matzen 116	1449	2.63	47	93.58	1.84	0.17	0.21	0.08	0.14	0.01	0.08	2.91	0.99	64
Matzen 286	1467	1.30	27	90.97	2.63	0.79	0.43	0.33	0.28	0.01	0.17	4.28	0.11	387
Matzen 322	1458	1.50	63	95.93	1.29	0.23	0.12	0.08	0.07	0.01	0.03	2.00	0.25	124
Matzen H 703b	1523	2.00	47	91.27	1.89	0.04	0.02	0.01			0.03	6.55	0.19	58
Moosbrunn Ost 1	820	1.00	551	99.18	0.17	0.01	0.01	0.01	0.01	0.01	0.01	0.30	0.34	1
Moosbrunn West 1	950	2.00	451	99.18	0.16	0.06	0.02	0.01	0.01	0.01	0.01	0.23	0.34	
Niedersulz 12	1281		292	99.31	0.34	0.00	0.00	0.00	0.00	0.00	0.00	0.16	0.19	
Oberweiden West 1	647	1.00	3211	99.55	0.03	0.00	0.00	0.00	0.00	0.00	0.00	0.12	0.30	
Orth 2	708	1.00	432	99.33	0.22	0.01	0.00	0.00	0.00	0.00	0.00	0.20	0.24	
Prottes 27	1150	3.00	52	96.45	1.83	0.03	0.03	0.01	0.01	0.01	0.01	1.33	0.31	
Prottes 29	1152	5.00	54	96.01	1.74	0.04	0.10	0.02	0.02	0.01	0.02	1.86	0.19	
Rabensburg 12	964.78		n.c.	97.99	0.00	0.00	0.00	0.00				0.34	0.27	
Rabensburg 13	1733.35	0.91	39	95.84	1.83	0.62	0.16	0.17	0.10			0.16	0.16	
Rabensburg 14	1097.04		215	97.80	0.46	0.00	0.00	0.00				0.12	0.12	
Rabensburg West 4	1062		1245	99.62	0.08							0.05	0.25	
Roseldorf 4	532	1.00	242	99.33	0.36	0.05	0.01	0.01	0.00	0.00	0.00	0.03	0.21	
Roseldorf 6	760		343	99.45	0.26	0.03	0.01	0.00	0.00	0.00	0.00	0.06	0.19	
Roseldorf 20	380		398	99.50	0.23	0.02	0.01	0.00	0.00	0.00	0.00	0.03	0.21	
Roseldorf Tief 2	500	1.00	231	99.32	0.37	0.06	0.01	0.01	0.00	0.00	0.00	0.03	0.20	
Sankt Ulrich 65	875	1.57	21	76.27	3.01	0.56	0.36	0.23	0.15	0.08	0.58	16.55	2.21	7
Sankt Ulrich 92	1050	1.31	59	85.20	1.15	0.29	0.17	0.13	0.09	0.05	0.26	11.17	1.49	36
Sankt Ulrich 213	812	0.70	38	81.39	1.22	0.93	0.35	0.50	0.25	0.15	0.52	14.45	0.24	6
Schoenkirchen T32	4873.01	1.25	98	83.13	0.68	0.17	0.05	0.04	0.04	0.04	0.23	13.19	0.71	30710
Schoenkirchen T38	2892	0.50	159	88.85	0.46	0.10	0.02	0.04	0.02	0.02	0.13	7.98	0.73	16500
Schoenkirchen T42	5386.79	0.57	109	83.07	0.61	0.15	0.04	0.07	0.03	0.03	0.22	13.05	0.73	32092
Schoenkirchen T62	5119.25	0.63	92	83.23	0.72	0.18	0.05	0.08	0.04	0.04	0.19	13.09	0.71	29942
Schoenkirchen T 64	2542	0.60	36	90.11	1.83	0.66	0.15	0.25	0.09	0.08	0.18	6.19	0.46	26

Well	Depth [m ss]	i/n C_4H_{10} [-]	Wetness $C_1/(C_2+C_3)$	CH_4	C_2H_6	C_3H_8	iC_4H_{10}	nC_4H_{10} [Vol.%]	iC_5H_{12}	nC_5H_{12}	C_6+	CO_2	N_2	H_2S [ppm]
Schoenkirchen T 90a	2590	0.64	34	94.02	2.06	0.67	0.14	0.22	0.08	0.07	0.18	2.11	0.45	7
Steinberg 21	950	1.66	25	93.09	3.56	0.13	0.05	0.03	0.01	0.01	0.04	3.01	0.07	
Stockerau Ost 7	1980	1.75	23	93.79	3.72	0.30	0.28	0.16	0.14	0.10	0.33	0.16	1.02	
Stockerau Ost 13	1792	1.94	22	93.65	3.83	0.35	0.33	0.17	0.15	0.12	0.26	0.14	1.00	
Stockerau Ost 16	2101	0.72	17	88.64	3.70	1.53	0.39	0.54	0.21	0.17	0.34	1.02	3.46	
VanSickle 29	762	0.50	260	96.06	0.36	0.01	0.01	0.02			0.01	3.46	0.08	
Wildendürnbach 5	540		473	99.40	0.19	0.02	0.00	0.00	0.00	0.00	0.00	0.10	0.29	
Wildendürnbach 10	550		711	99.50	0.13	0.01	0.00	0.00	0.00	0.00	0.00	0.09	0.27	
Wildendürnbach 16	560		414	99.32	0.21	0.03	0.00	0.00	0.00	0.00	0.00	0.10	0.34	

Appendix X

Trace metal concentration

Well		Bockfliess 1	Ebenthal 5	Ebenthal 15	Erdpress 4	Erdpress 17a	Hochleiten 15	Hochleiten 24	Hochleiten 31	Hochleiten 60	Hohenruppersdorf 42	Matzen 390	Prottes 26	St. Ulrich 92	Schoenkirchen T29a	Schoenkirchen T 38	Schoenkirchen T62	Staatz 1	Zistersdorf ÜT 1
Depth	**[m]**	**1177.38**	**1614.4**	**1636**	**1787.51**	**1424.18**	**737.58**	**748.74**	**982**	**759.31**	**1412.35**	**1139.7**	**1140.44**	**1050**	**2725.54**	**2726**	**5119.25**	**2825.7**	**5602.7**
Mg	[ppb]	2730	161	288	520	921	1120	511	247	493	207	1140	2530	729	5680	210	162	276582	82205
P	[ppb]	1300	1060	107	1230	214	176	116	2470	188	620	46.9	52.4	5021	268	80	74.9	167221	34442
S	[ppm]	2090	783	915	1590	1620	2191	2401	1054	2620	1590	2090	2110	1203	1700	955	1290	46230	8237
K	[ppb]	1570	692	661	1820	1500	674	486	190	653	850	465	1280	859	6220	347	344	885144	105684
Ti	[ppb]	208	12.2	26.5	81.7	28.9	74	65	45	20.7	30.8	198	182	92	54	57	9.09	21303	29307
V	[ppb]	48.8	9.44	8.93	19.6	13.5	57	57	25	55.4	12.4	57.1	57.2	38	58.3	304	0.815	2282	587
Cr	[ppb]	80.5	66	41.2	255	57.3	26	-	-	47	29.7	34.7	102	23	38.9	5	17.4	52027	31320
Mn	[ppb]	38.1	6.72	34.9	397	92.2	39	-	-	11.8	39.1	30.5	627	60	71.1	-	106	27194	9321
Fe	[ppb]	5480	698	1300	53800	14800	7477	949	2673	1180	5460	2240	38300	12195	1270	392	763	409419	217921
Co	[ppb]	53.6	13	26.1	57.1	29.4	92	87	31	104	28.4	61.2	63.4	45	24.5	7	0.45	692	377
Ni	[ppb]	5480	585	803	2910	1800	8480	8323	2078	9920	1750	4720	5260	2607	2120	555	10.4	164339	14966
Cu	[ppb]	32.8	75.1	26.9	188	30.7	-	-	-	57	34.1	506	99.1	917	30.1	-	16.7	n.a.	n.a
Zn	[ppb]	2770	287	2620	2750	1390	396	419	433	2280	2700	1730	942	6537	555	2794	271	99596	11243
As	[ppb]	26	6.9	23.9	44.2	10.8	74	59	39	69.5	15.3	28.1	26.7	68	2.04	5	14.3	1149	255
Se	[ppb]	19	4.86	10.9	20.2	12.8	20	20	14	14.5	11.7	15.3	15.8	-	3.57	-	28.2	43191	7939
Rb	[ppb]	1.41	0.573	1.08	1.87	2.05	0.4	0.3	-	0.683	0.927	0.674	1.48	0.8	2.4	0.3	0.304	886	507
Sr	[ppb]	521	14.9	60.3	404	323	226.4	67.5	18	116	159	3300	1180	44.9	556	6.7	14.3	4964	1465
Ag	[ppb]	18.1	33	10.7	1.55	16.2	20	16	14	8.15	7.39	6.42	5.17	4	57.7	69491	2.69	9606	379
Cd	[ppb]	0.581	0.585	0.73	0.27	0.46	-	-	-	0.372	0.567	0.688	0.414	-	0.311	6.5	0.584	122	33
Ba	[ppb]	255	151	218	516	414	247	106	310	390	391	556	586	384	327	138	417	9466	8764
Re	[ppb]	0.254	0.0477	0.0962	0.0315	0.102	0.7	0.9	0.6	0.0619	0.0604	0.257	0.341	-	0.0807	0.5	0.113	n.d.	n.d.
Pb	[ppb]	2.82	22.7	11.2	55.3	18.9	26	10	6	11.7	7.76	25.7	16.2	927	15.9	1446	7.09	35389	706
U	[ppb]	0.244	0.031	0.0206	0.0825	0.0476	0.07	0.04	-	0.0369	0.0382	0.0539	0.0579	0.1	0.0257	0.06	0.059	43	25

n.d	not detected
n.a.	not applicable

Oil samples refer to ppb per g whole oil
Rock samples refer to ppb per g TOC

	Oil
	Rock extract

Copper in Source Rock extracts not applicable due to contamination during extraction

Appendix XI

Stable isotope ratios

Rock Samples

Well	Depth [m]	Stratigraphic Unit	Ker.	Sat	Aro	nC_{14}	nC_{15}	nC_{16}	nC_{17}	Pr	nC_{18}	Phy	nC_{19}	nC_{20}	nC_{21}	nC_{22}	nC_{23}	nC_{24}	nC_{25}	nC_{26}	nC_{27}	nC_{28}
													[‰ δ^{13}C V-PDB]									
Altenmarkt 1	2641.6	Lower ShMb.		-27.3	-26.0																	
Falkenst. 1	3378.7	Mikulov Fm.		-28.2	-28.2																	
Falkenst. 1	3516	Mikulov Fm.		-28.0	-26.8																	
Falkenst. 1	3748.4	Mikulov Fm.		-29.7	-27.7																	
Falkenst. 1	4150.4	Flknstn. Fm.		-28.5	-27.4																	
Falkenst. 1	4495.5	Lower ShMb.		-27.6	-25.1																	
Falkenst. 1	4498.3	Lower ShMb.		-27.4	-25.7																	
Hoeflein 7a	2761.5	Mikulov Fm.		-28.4	-27.2																	
Hoeflein 7a	2762.2	Mikulov Fm.		-28.1	-27.7																	
Maustr. ÜT 1	6546.7	Mikulov Fm.		-27.8	-27.1				-29.3		-28.6		-28.3	-28.5	-29.0	-27.7						
Maustr. ÜT 1	6548.8	Mikulov Fm.		-27.6	27.9	-30.4	-30.4	-29.9	-29.6	-39.1	-30.0	-33.8	-30.0	-30.5	-30.7	-30.5	-30.4	-30.4	-30.7	-30.3	-30.8	-31.2
Porrau 2	2166.8	Lower ShMb.		-25.6	-25.4																	
Porrau 2	2495	Lower QaMb.		-26.5	-25.9																	
Staatz 1	1968	Mikulov Fm.	-26.8	-25.7	-25.8																	
Staatz 1	2022.7	Mikulov Fm.	-26.8																			
Staatz 1	2026.5	Mikulov Fm.	-26.6	-28.2	-28.7																	
Staatz 1	2045.5	Mikulov Fm.	-26.8																			
Staatz 1	2083	Mikulov Fm.	-27.5	-27.1	-25.3																	
Staatz 1	2109.3	Mikulov Fm.	-27.2																			
Staatz 1	2113.1	Mikulov Fm.	-26.5	-27.3	-28.8																	
Staatz 1	2140.5	Mikulov Fm.	-26.1																			
Staatz 1	2141.3	Mikulov Fm.	-26.3	-27.0	-26.5																	
Staatz 1	2176.3	Mikulov Fm.	-25.9	-27.3	-26.7																	
Staatz 1	2178	Mikulov Fm.	-26.4	-27.4	-26.3																	
Staatz 1	2211.2	Mikulov Fm.	-26.0																			
Staatz 1	2213.2	Mikulov Fm.		-28.9	-28.8																	
Staatz 1	2250.5	Mikulov Fm.	-24.9																			
Staatz 1	2251.5	Mikulov Fm.	-23.5	-24.9	-25.6																	
Staatz 1	2284.5	Mikulov Fm.	-25.7	-26.9	-26.6																	
Staatz 1	2322.5	Mikulov Fm.	-27.2	-27.8	-26.5																	
Staatz 1	2324.5	Mikulov Fm.		-29.8	-25.8																	
Staatz 1	2359.5	Mikulov Fm.	-26.7																			
Staatz 1	2414.5	Mikulov Fm.	-26.6	-28.6	-27.6																	
Staatz 1	2467.8	Mikulov Fm.	-25.3																			
Staatz 1	2469.5	Mikulov Fm.		-27.0	-28.0																	
Staatz 1	2522.5	Mikulov Fm.	-27.0																			
Staatz 1	2524.5	Mikulov Fm.	-26.5	-27.5	-29.0																	
Staatz 1	2574.5	Mikulov Fm.	-26.7																			
Staatz 1	2575.5	Mikulov Fm.	-26.4	-29.4	-27.6																	
Staatz 1	2630.5	Mikulov Fm.		-27.9	-27.8																	
Staatz 1	2634.5	Mikulov Fm.		-28.1	-27.9																	

Well	Depth [m]	Stratigraphic Unit	Ker.	Sat	Aro	nC_{14}	nC_{15}	nC_{16}	nC_{17}	Pr	nC_{18}	Phy	nC_{19}	nC_{20}	nC_{21}	nC_{22}	nC_{23}	nC_{24}	nC_{25}	nC_{26}	nC_{27}	nC_{28}
			[‰ $\delta^{13}C$ V-PDB]																			
Staatz 1	2682.5	Mikulov Fm.	-25.9	-25.7	-26.5																	
Staatz 1	2685.5	Mikulov Fm.	-25.1																			
Staatz 1	2740.5	Mikulov Fm.	-26.2	-30.3	-27.3																	
Staatz 1	2743.5	Mikulov Fm.	-26.2	-27.8	-27.2																	
Staatz 1	2770.2	Mikulov Fm.	-26.1	-28.7	-27.3																	
Staatz 1	2773.5	Mikulov Fm.	-26.1	-29.1																		
Staatz 1	2774.5	Mikulov Fm.	-26.6	-27.2	-27.3																	
Staatz 1	2822.5	Mikulov Fm.	-26.4																			
Staatz 1	2825.7	Mikulov Fm.	-26.2	-24.8	-24.5																	
Staatz 1	2936	Flknstn. Fm.	-25.6																			
Staatz 1	2938.2	Flknstn. Fm.	-25.4																			
Staatz 1	2993.8	Flknstn. Fm.	-27.3																			
Staatz 1	2996.5	Flknstn. Fm.		-28.6	-28.6																	
Staatz 1	3096.6	Flknstn. Fm.	-26.4																			
Staatz 1	3098.5	Flknstn. Fm.	-27.1	-24.5	-25.2																	
Thomasl 1	2302.6	Mikulov Fm.		-27.9	-27.0																	
Thomasl 1	2304	Mikulov Fm.		-28.3	-28.0																	
Thomasl 1	3006.7	Mikulov Fm.		-27.7	-27.3																	
Waschberg 1	2536.1	Flknstn. Fm.		-28.2	-27.4																	
Waschberg 1	2538.8	Flknstn. Fm.		-28.7	-28.2																	
Zistersd. ÜT 1	5602.7	Mikulov Fm.		-27.9	-28.2																	
Zistersd. ÜT 1	5605.5	Mikulov Fm.		-28.8	-26.8			-30.3	-28.8	-34.2	-29.4	-33.6	-29.2	-29.5	-29.8	-29.3	-29.2	-28.5				
Zistersd. ÜT 1	5670.5	Mikulov Fm.		-29.3	-26.4																	
Zistersd. ÜT 1	5674.6	Mikulov Fm.			-26.1																	
Zistersd. ÜT 1	5740.7	Mikulov Fm.				-29.5	-29.8	-29.7	-31.3	-35.5	-33.5	-33.4	-33.4	-32.7	-31.9	-31.7	-31.6	-31.0	-31.9	-30.7	-31.9	-31.5
Zistersd. ÜT 1	5977.3	Mikulov Fm.		-31.1	-28.7																	
Zistersd.ÜT 2	5587	Mikulov Fm.		-29.1	-31.0																	

Oil Samples

Well	Depth [m ss]	Sat	Aro	nC_{14}	nC_{15}	nC_{16}	nC_{17}	Pr	nC_{18}	Phy	nC_{19}	nC_{20}	nC_{21}	nC_{22}	nC_{23}	nC_{24}	nC_{25}	nC_{26}	nC_{27}	nC_{28}	nC_{29}	nC_{30}	nC_{31}
		[‰ δ^{13}C V-PDB]																					
Aderklaa 3	2351	-24.0	-24.6																				
Aderklaa 4	2515	-24.8	-23.9																				
Aderklaa 34	1715	-26.0	-24.8	-26.8	-27.7	-27.9	-28.3		-28.2		-28.7	-28.1	-28.3	-27.4	-28.3	-28.1	-28.0	-29.7					
Bockfliess 1	1177.38	-25.9	-25.0																				
Bockfliess 24	1436.21	-26.0	-24.9					-31.3		-31.7													
Bockfliess 33	1181.24	-26.0	-25.3																				
Bockfliess 35	1460.64	-25.1	-25.2					-29.8		-26.9													
Bockfliess 37	1463.4	-25.9	-24.2																				
Bockfliess 43	1428.71	-25.7	-24.0					-31.4		-23.5													
Bockfliess 205	1627	-25.9	-25.0					-29.7		-29.2													
Ebenthal 5	1614.4	-26.3	-25.4	-28.2	-28.6	-28.4	-29.1	-49.6	-28.4	-34.1	-29.4	-29.4	-29.2	-29.1	-29.3	-29.4	-30.0	-30.1	-30.7	-31.4	-31.7	-33.0	
Ebenthal 15	1636	-26.4	-25.4	-28.8	-28.8	-28.9	-28.8	-37.8	-28.5	-34.1	-29.5	-29.4	-29.2	-29.2	-29.4	-29.5	-30.3	-30.5	-31.0	-31.8	-33.3		
Ebenthal 17a	1614	-26.5	-25.4	-28.9	-29.4	-29.2	-29.8	-36.7	-29.1	-34.2	-29.7	-29.7	-29.6	-29.5	-29.6	-29.7	-30.3	-30.4	-30.7	-31.1	-32.3		
Ebenthal 20	1614.4	-26.7	-25.6	-28.6	-28.6	-29.2	-29.2	-31.0	-31.2	-31.2	-29.6	-30.4	-31.5	-31.8	-32.3	-32.6	-33.2	-33.6	-34.0	-33.7	-34.2		
Erdpress 4	1787.51	-26.4	-25.0		-29.6	-29.3	-29.0	-44.4	-28.8	-34.0	-29.2	-29.2	-28.9	-29.2	-28.8	-29.2	-29.7	-28.8	-29.7	-28.3			
Erdpress 17a	1424.18	-25.5	-25.5																				
Erdpress 24	1419.12	-26.1	-25.2																				
Gbely 2		-25.9	-24.7																				
Gbely H6		-23.2	-24.7																				
Hochleiten 15	737.58	-25.4	-24.8																				
Hochleiten 24	748.74	-24.4	-24.8																				
Hochleiten 31	982	-25.5	-24.9																				
Hochleiten 60	759.31	-25.4	-24.6																				
Hochleiten 65	851.09	-25.9	-23.7																				
Hochleiten 66	911.32	-23.7	-24.8																				
Hochleiten 67	786.44	-26.0	-24.6																				
Hodonin 1		-25.9	-24.8																				
Hodonin 3		-25.8	-24.6																				
Hodonin 4		-25.5	-24.7																				
Hoeflein 6	2663	-26.7	-24.3																				
Hoeflein 9	2685	-25.5	-24.1																				
Hoeflein 12	2670.29	-26.4	-25.0																				
HRPD 42	1412.35	-25.4	-24.8					-32.6		-31.4													
Holic 4		-26.0	-24.8		-27.1	-26.9	-27.2		-27.2		-27.4	-27.5	-27.5	-27.8	-27.9	-27.2	-27.6	-26.1					
Kierling 1	60	-26.3	-24.9																				
Kierling 2		-26.1	-24.9	-29.2	-28.9	-29.0	-28.9		-28.5		-28.6	-28.4	-28.0	-27.9	-27.6	-28.3	-28.3	-29.0					
Klement 1	3539	-27.0	-24.9		-26.6	-27.0	-26.7		-26.4		-27.1	-27.5	-27.3	-27.4	-27.7	-27.4	-27.3	-27.4	-27.6	-27.9	-27.8	-28.0	-28.3
Lanzhot 15		-26.0	-25.3			-28.1	-28.2	-33.0	-27.0	-30.5	-27.9	-27.9	-28.2	-27.9	-28.1	-28.5							
Lanzhot 30		-26.4	-25.5				-27.2	-29.8	-27.1	-42.4	-27.6	-28.0	-28.1	-28.3	-27.9	-26.6	-28.3						
Mank 1	157	-28.5	-26.5																				
Matzen 91	1464	-25.6	-24.3					-29.5		-30.2													

Well	Depth	Sat	Aro	nC_{14}	nC_{15}	nC_{16}	nC_{17}	Pr	nC_{18}	Phy	nC_{19}	nC_{20}	nC_{21}	nC_{22}	nC_{23}	nC_{24}	nC_{25}	nC_{26}	nC_{27}	nC_{28}	nC_{29}	nC_{30}	nC_{31}
	[m ss]	[‰ δ^{13}C V-PDB]																					
Matzen 115	1472	-25.7	-24.5																				
Matzen 116	1449	-27.0	-25.9																				
Matzen 390	1139.7	-26.1	-25.3																				
Matzen H 703b	1523	-27.5	-26.2																				
Maustrenk 29	900	-26.1	-25.2				-29.4		-29.1		-28.3	-29.5	-28.3	-27.4									
Mühlberg 15	1480	-25.7	-24.8																				
Neusiedl 1	1180	-26.2	-24.8																				
Neusiedl 3	1100	-26.6	-24.5																				
Pirawarth U10	707	-26.0	-24.7																				
Prottes 26	1140.44	-25.7	-24.9																				
Prottes 27	1151	-25.6	-25.2																				
Prottes 29	1153	-25.5	-24.4																				
Prottes 98	1157.63	-25.8	-25.3																				
Prottes 104	1156.78	-25.8	-24.8																				
Prottes T S 3b	2653	-26.1	-24.6	-28.3	-29.2	-28.9	-29.0		-29.0		-29.0	-29.1	-29.4	-29.4	-29.1	-28.8	-29.7	-30.1	-30.5	-30.9	-30.4		
Rabensburg 11	1742	-25.7	-24.2		-26.9	-27.2	-27.8		-27.5		-27.4	-27.1	-27.2	-26.9	-27.3								
Rabensburg N3	1718	-26.2	-24.7	-27.6	-28.2	-28.6	-29.0		-28.8		-28.9	-29.3	-29.5	-29.1	-28.7	-29.3	-29.0	-29.6	-29.9	-32.6			
Rabensburg U4		-25.9	-24.7		-28.0	-28.5	-28.9	-31.4	-29.0	-32.9	-28.8	-29.1	-28.7	-29.2	-28.9	-29.1	-31.0	-29.4	-30.7	-30.2			
Roseldorf 2	1383	-25.8	-24.3																				
Roseldorf 2	1383	-25.6	-24.4																				
Sankt Ulrich 65	875	-26.0	-24.9	-27.8	-28.6	-29.1	-29.2		-28.7	-36.0	-28.8	-29.4	-28.6	-28.7	-28.9	-28.0							
Sankt Ulrich 92	1050	-26.0	-24.9		-28.4	-28.9	-28.6	-25.2	-28.7	-36.0	-28.8	-29.4	-28.6	-28.7	-28.9	-28.0							
Sankt Ulrich 213	812	-26.2	-24.9																				
Schönkir. 267	1260	-25.9	-23.8																				
Schönkir. T12	2709.73	-27.0		-28.7	-28.9	-28.7	-29.3	-17.6	-30.5	-29.1	-31.3	-31.8	-31.4	-31.3	-31.4	-31.3	-31.9	-32.1	-32.0	-31.9	-34.6		
Schönkir. T29	2725.54	-26.7	-24.4	-28.5	-29.2	-31.5	-33.7	-35.2	-33.0	-39.8	-32.4	-31.3	-30.9	-30.5	-30.2	-30.3	-31.2	-31.6	-31.9	-32.8	-33.4	-32.3	-32.2
Schönkir. T32	4873.01	-24.4	-23.6																				
Schönkir. T38	2726	-26.7	-24.7	-28.4	-28.5	-28.3	-28.4		-28.6		-29.0	-28.9	-28.9	-28.9	-28.9	-28.4	-29.0	-29.2	-29.6	-30.7	-30.6		
Schönkir. T42	5386.79	-25.4	-23.9				-27.5	-52.3	-28.1	-30.0	-28.6	-28.5	-28.2	-28.4	-28.5								
Schönkir. T62	5119.25	-25.4	-23.4					-27.5		-27.9													
Schönkir. T64	2542	-27.6	-26.6																				
Schönkir. T69	2815	-26.1	-24.7	-27.5	-27.9	-27.9	-28.0		-27.9		-28.0	-28.0	-27.7	-27.6	-27.7	-28.5	-28.0	-27.4	-27.8	-28.9	-27.4		
Schönkir. T90	2590	-28.3	-26.3																				
Steinberg 11	950	-26.6	-25.2			-28.5	-27.6	-32.8	-28.4	-30.9	-28.6	-28.8	-29.3	-29.5	-29.5	-29.2	-30.1	-31.2	-30.4	-32.6			
Urmansau 1	152	-28.5	-26.8																				
Urmansau 1	758	-28.5	-27.5																				
VanSickle 29	762	-25.7	-25.0																				
Wind. Baumg. 1	700	-25.8	-24.2		-28.6	-29.0	-28.8	-32.4	-28.7	-30.4	-29.2	-30.1	-30.1	-30.6	-30.5	-30.9	-31.8	-30.9	-32.2	-31.9	-33.2	-32.0		
Wind. Baumg. 1	700	-26.1	-24.9																				

Gas Samples

Well	Depth	CH_4	C_2H_6	nC_3H_8	iC_4H_{10}	nC_4H_{10}	CO_2	CH_4	C_2H_6	H_2S
	[m ss]			[‰ δ^{13}C V-PDB]				[‰ δD V-SMOW]		[‰ δ^{34}S V-CDT]
Aderklaa 98	2408	-36.9	-25.0	-22.4	-23.2	-21.7	-1.9	-120.2	-77.4	
Baumgarten 1	830	-57.9						-219.9		
Bockfliess 1	1177.38	-54.2	-24.4				6.1	-178.8	-103.8	
Bockfliess 24	1436.21	-40.5	-23.9				8.0	-181.1	-128.6	
Bockfliess 33	1181.24	-41.7	-21.9				12.0	-178.3		
Bockfliess 35	1460.64	-41.4	-23.6				10.8		-149.8	
Bockfliess 37	1463.4	-41.6	-23.5				12.2		-152.8	
Bockfliess 43	1428.71	-38.3	-23.8				11.2		-148.1	
Breitenlee 15	990	-41.8	-14.4					-232.0		
Breitenlee 17	1217	-43.1	-24.1				1.0	-226.3		
Bockfliess 205	1627	-38.6	-23.7				13.5	-174.0	-122.5	
Ebenthal Tief 1	3300	-33.0	-26.0	-24.1		-24.3	-3.3	-113.9	-104.8	
Erdpress 4	1787.51	-44.8	-25.9	-22.6			3.2	-171.9	-129.0	
Erdpress 17a	1424.18	-39.3	-23.8				13.4	-180.2		
Erdpress 24	1419.12	-43.4	-24.0					-176.0		
Fischamend 6	278	-62.9						-236.3		
Ginzersdorf 4	776	-51.4	-27.4					-229.8		
Hauskirchen 86	910	-39.8	-26.2	-15.2			23.5	-200.0	-56.2	
Hirschstetten 7a	1875	-35.0	-24.7	-22.1			-1.6	-182.7		
Hochleiten 15	737.58	-41.9	-23.4				18.3			
Hochleiten 24	748.74	-48.9	-23.1				8.0			
Hochleiten 60	759.31	-43.5	-25.5				13.5		-163.9	
Hochleiten 65	851.09	-45.9					15.2			
Hochleiten 66	911.32	-42.9					16.3			
Hochleiten 67	786.44	-31.1					16.3			
Hoeflein 1	2605.37	-39.1	-26.0	-23.5	-22.8	-22.9	-7.2	-161.4	-174.9	
Hoeflein 4	2618.1	-38.2	-25.9	-23.3	-23.1	-22.4	-7.3	-153.4	-183.9	
Hoeflein 6	2614.04	-38.8	-26.0	-23.6	-22.6	-23.0	-7.3	-158.8	-182.8	
Hoeflein 8	2629.55	-38.4	-26.0	-23.4		-22.8	-7.2	-156.8	-168.4	
Hoeflein 9	2633.63	-37.4	-25.2	-23.1		-21.2	-6.7	-162.2	-173.6	
Hoeflein 10	2613.33	-37.7	-25.5	-23.1		-21.0	-6.8	-156.0	-187.2	
Hoeflein 12	2670.29	-37.9	-25.6	-23.6		-21.5	-7.4	-157.5	-169.9	
HRPD 42	1412.35	-41.9	-23.8				8.9		-115.9	
Matzen 115	1472	-24.0	-20.2	-19.4	-24.4		9.3	-189.3		
Matzen 116	1449	-44.6	-24.9	-19.7		-24.6	2.6	-210.0	-49.0	
Matzen 286	1467	-42.2	-25.4	-21.5	-23.9	-19.8	0.8	-236.0		
Matzen 322	1458	-41.4	-25.3	-23.2			-1.6	-204.5	-52.9	
Matzen H 703b	1523	-36.9	-26.7				14.5	-185.9	-70.4	
Moosbrunn O 1	820	-62.8						-232.2		
Moosbrunn W 1	950	-62.5						-235.9		
Niedersulz 12	1281	-43.1	-17.2					-158.8		
Oberweiden W 1	647	-60.6						-228.0		
Orth 2	708	-59.9						-233.1		
Prottes 27	1151	-47.1	-26.2				8.1	-159.4	-49.4	
Prottes 29	1153	-45.0	-25.5				-1.7	-158.8	-56.7	
Rabensburg 12	964.78	-56.1						-189.5		
Rabensburg 13	1733.35	-48.2	-25.5	-23.9				-168.8	-157.1	
Rabensburg 14	1097.04	-55.1	-26.8					-185.2		
Rabensburg W 4	1062	-49.6						-198.3		
Roseldorf 4	532	-59.3	-41.6					-181.1		
Roseldorf 6	760	-59.0	-52.6					-175.3		
Roseldorf 20	380	-61.7	-57.3					-173.5		
Roseldorf Tief 2	500	-57.7	-39.6					-178.6		
Sankt Ulrich 65	875	-38.7	-24.7	-12.2	-20.4		13.2	-286.8		
Sankt Ulrich 92	1050	-39.5	-25.3	-15.5			15.9	-282.2		
Sankt Ulrich 213	812	-38.2	-27.0	-21.0	-24.2	-21.5	9.3	-287.8		
Schönkir. T32	4873.01	-29.3	-24.1	-22.1	-22.8	-23.2	-0.8	-165.0		15.6
Schönkir. T38a	2809	-26.4	-25.6	-25.4	-23.4	-23.4	-2.2	-128.0		
Schönkir. T42	5386.79	-29.0	-20.6	-23.2	-22.7	-22.7	0.6	-132.0		16.0

Well	Depth	CH_4	C_2H_6	nC_3H_8	iC_4H_{10}	nC_4H_{10}	CO_2	CH_4	C_2H_6	H_2S
	[m ss]	[‰ $\delta^{13}C$ V-PDB]						[‰ δD V-SMOW]		[‰ $\delta^{34}S$ V-CDT]
Schönkir. T62	5119.25	-29.8	-24.3	-22.5	-22.8	-22.8	0.5	-156.0		15.6
Schönkir. T64	2542	-33.6	-26.6	-25.6		-23.6	-5.1	-149.2	-66.7	
Schönkir. T90	2590	-34.2	-26.8	-25.6		-25.2	-6.1	-160.5	-59.0	
Steinberg 21	960	-41.7	-25.0				8.2	-210.1		
Stockerau Ost 7	1980	-46.7	-26.4	-18.3	-25.5	-21.3		-145.0	-59.6	
Stockerau Ost 13	1792	-44.5	-25.4	-18.1	-25.5			-143.4	-115.7	
Stockerau Ost 16	2101	-41.8	-26.0	-24.9	-25.7	-24.1	-3.1	-128.1	-71.4	
VanSickle 29	762	-48.5	-27.2				9.6	-237.0		
Wildendürnb. 5	540	-61.8						-156.1		
Wildendürnb. 10	550	-63.7	-37.3					-156.7		
Wildendürnb. 16	560	-56.4						-151.6		